Birth, evolution and demise of the Mediterranean Lago-Mare

A biogeochemical perspective on water level and connectivity changes during the final phase of the Messinian Salinity Crisis

Federico Andreetto

Utrecht Studies in Earth Sciences
No. 265

This research was part of the SALTGIANT (Uncovering the Mediterranean Salt Giant) project, which has received funding from the European Union's Horizon 2020 research and innovation program, under the Marie Skłodowska-Curie grant agreement No. 765256.

ISBN/EAN: 978-90-6266-634-8

Printed by: Ipskamp, the Netherlands. Cover by: Margot Stoete.
Author contact: f.andreetto@outlook.it

Front cover: The steep cliff of Capo Bianco (Sicily, Italy) with (folded) outcrops of the late Messinian-early Zanclean.

Birth, evolution and demise of the Mediterranean Lago-Mare

A biogeochemical perspective on water level and connectivity changes during the final phase of the Messinian Salinity Crisis

Ontstaan, evolutie en ondergang van de Lago-Mare in het Middellandse Zeegebied

Een biogeochemisch perspectief op veranderingen in waterniveau en connectiviteit tijdens de laatste fase van de Messiniaanse zoutcrisis
(met een samenvatting in het Nederlands)

Nascita, evoluzione e scomparsa del Lago-Mare Mediterraneo

Un punto di vista biogeochimico sui cambiamenti del livello dell'acqua e della connettività durante la fase finale della Crisi di Salinitá del Messiniano
(con riassunto in Italiano)

Proefschrift

ter verkrijging van de graad van doctor aan de Universiteit Utrecht op gezag van de rector magnificus, prof.dr. H.R.B.M. Kummeling, ingevolge het besluit van het college voor promoties in het openbaar te verdedigen op maandag 16 januari 2023 des ochtends te 10.15 uur

door

Federico Andreetto

geboren op maandag 02 augustus 1993
te Imperia, Italië

Promotoren: Prof.dr. Wout Krijgsman
Prof.dr. Rachel Flecker

Beoordelingscommissie:

Prof. dr. Lucas J. Lourens
Department of Earth Sciences, Utrecht University - Utrecht, The Netherlands

Dr. Mariette Wolthers
Department of Earth Sciences, Utrecht University - Utrecht, The Netherlands

Prof. dr. Elsa Gliozzi
Dipartimento di Scienze, Università degli Studi Roma Tre - Rome, Italy

Prof. dr. Gareth R. Davies
Geology & Geochemistry, VU University - Amsterdam, the Netherlands

Prof. dr. Christian Gorini
Sorbonne Université-Institut des Sciences de la Terre de Paris (ISTeP) - Paris, France

To my grandparents, in loving memory.

C

Contents

A-EN

Abstract

The Mediterranean Sea is a large sea almost completely enclosed by Europe, Africa, and SW Asia. Today, the continuous flow of Atlantic seawater through the Strait of Gibraltar balances the net water loss due to the excess of evaporation over input from rain and rivers and keeps the Mediterranean a marine basin with the water level equal to the global ocean level. In the late Miocene, the input of Atlantic seawater was through shallow gateways in southern Spain and northern Morocco. The exhumation of the Betic and Rif Cordilleras and orbitally-controlled regional climate change contributed to the step-by-step close these marine gateways and transformed the Mediterranean into an inhospitable evaporitic sea, starting at 5.96±0.02 Ma. The environmental and hydrological crisis that followed, known as the Messinian Salinity Crisis, peaked at ~5.55 Ma, when a 1.5-2 km-thick salt layer precipitated on the sea floor, and terminated at ~5.332 Ma, when normal marine conditions were re-established, perhaps as a consequence of catastrophic flooding at Gibraltar. The transitional interval from the giant salina to Mediterranean Sea that resembles what we know today is known as the Lago-Mare phase. Gypsum and brackish water biota from the Central Paratethys (approximately coinciding with the present-day Hungary-Slovenia) are both characteristic of Lago-Mare successions. This sedimentary and paleontological evidence suggest that the Mediterranean, during the Lago-Mare phase, experienced a complex history of inter- and extrabasinal connections, base-level fluctuations and extreme environmental and biological changes. This thesis aims to reconstruct the fiercely debated Mediterranean water level changes and identify the hydrological fluxes responsible for these Lago-Mare environmental and biological turnover events. It focuses on key sections exposed on-land and recovered from deep sea cores along an E-W transect across the Mediterranean with a multi-disciplinary approach that integrates biocyclostratigraphic analyses with high-resolution Sr-isotope ratios. The new data show that the Lago-Mare phase was a far more dynamic period of the Mediterranean history than previously thought. Large areas of the Mediterranean were occupied by an anomalohaline water mass predominantly formed by low-salinity waters from the Eastern Paratethys (i.e. the present-day Black-Caspian seas) and from the larger circum-Mediterranean rivers such as the Nile, the Rhône and currently dried North-African rivers. A small and possibly episodic Atlantic flux was a minor contributor. The regular variability of the Mediterranean's freshwater budget with the astronomic precession combined

with fluctuating Atlantic inflow and negligible outflow resulted in a Mediterranean base level that oscillated dramatically, but consistently below eustatic sea level. These precession-paced fluctuations caused the low-salinity Paratethyan biota to colonize the marginal areas of the Mediterranean at times of high base level and central areas during phases of low base level, gypsum to precipitate only in the deeper basins during the regressive phases and silled regions such as the Adriatic and the North Aegean to exist for long as some of the largest endorheic lakes.

A-NL

Samenvatting

De Middellandse Zee is een grote, intercontinentale zee tussen Europa, Afrika en Zuid-West Azië met een negatief hydrologisch budget. Toen de Indiase verbinding aan het einde van het vroege Mioceen dicht ging, werd dit watertekort voornamelijk gecompenseerd door de toevoer vanuit de Atlantische Oceaan via ondiepe zeestraten in Zuid-Spanje en Noord-Marokko tot aan het late Mioceen en via de straat van Gibraltar vanaf het Plioceen (of mogelijk al daarvoor). Opheffing van de Betische en Rif Cordillera's gecombineerd met regionale klimaatverandering zorgden vooreen stapsgewijze beperking van de verbindingen tussen de Middellandse Zee en de Atlantische Oceaan in het laatste Mioceen. Hierdoor transformeerde de Middellandse Zee in een super zoute, geïsoleerde en verdampte zee. Deze fase begon 5.96±0.02 miljoen jaar geleden (Ma) en staat bekend als de Messiniaanse zoutcrisis. Deze milieu- en hydrologische crisis bereikte een hoogtepunt op ~5.55 Ma, toen een 1.5-2 km dikke zoutlaag op de zeebodem vormde, en eindigde op ~5.332 Ma, toen de normale zee-omstandigheden werden hersteld. Dit laatste was waarschijnlijk het gevolg was van een catastrofale doorbraak van de Straat van Gibraltar. Het overgangsinterval van de reusachtige zoutvlakte naar de Middellandse Zee staat bekend als de Lago-Mare fase. Gips en zoetwater-biota uit de oostelijke Paratethyszee (de huidige Zwarte en Kaspische zeeën) zijn beide kenmerkend voor Lago-Mare-afzettingen. Deze sedimentaire en paleontologische observaties tonen aan dat de Middellandse Zee tijdens de Lago-Mare fase een complexe geschiedenis heeft meegemaakt van inter- en extrabekken verbindingen, schommelingen van het waterniveau en extreme milieu veranderingen. Dit proefschrift richt zich op de reconstructie van de fel bediscussieerde veranderingen in het waterpeil in de Middellandse Zee en de identificatie van hydrologische fluxen die verantwoordelijk zijn voor de milieuveranderingen tijdens Lago-Mare. Het behandelt de onderzoeksresultaten van de meest prominente secties op land, en kernen uit diepe wateren (DSDP-ODP), langs een oost-westelijke doorsnede in de Middellandse Zee. Met behulp van een multidisciplinaire aanpak waarin bio- en cyclostratigrafische analyses geïntegreerd worden met hoge-resolutie Sr-isotoop ratio's blijkt dat de Lago-Mare fase een veel dynamischer periode van de mediterrane geschiedenis beslaat dan voorheen gedacht. Grote gebieden van de Middellandse Zee werden bedekt door een watermassa met een bijzonder zoutgehalte. Deze werd voornamelijk gevormd uit diep pekelachtig water, plus ondiep rivier water met

in het Tsjaadmeer dat momenteel droog is) en de oostelijke Paratethyszee. Een minimale, en mogelijk episodische, Atlantische bijdrage leverde waarschijnlijk ook een kleine zoutwater component. In het late Mioceen wordt de zoetwatertoevoer van de Middellandse Zee bepaald door klimaatsveranderingen die gerelateerd zijn aan de astronomische precessie van de aardas. Deze regelmatige variabiliteit in combinatie met fluctuerende Atlantische instroom en verwaarloosbare uitstroom resulteerde in een mediterraan basisniveau dat dramatisch schommelde, maar zich constant onder de globale zeespiegel bevond. Deze fluctuaties in mediterraan klimaat hebben ervoor gezorgd dat de brak-water Paratethys biota de marginale gebieden van de Middellandse Zee koloniseerden in tijden van een hoog waterniveau en centrale diepe gebieden tijdens fasen van een laag waterniveau. Het zorgde er ook voor dat gips enkel precipiteerde in de diepere bekkens tijdens de regressieve fasen, terwijl de ondiepe bekkens zoals de Adriatische en de Noord-Egeïsche zee lange tijd afgesloten meren bleven.

A-IT

Riassunto

Il Mar Mediterraneo è un grande mare intracontinentale quasi interamente racchiuso tra le coste dell'Europa meridionale, del Nord Africa e dell'Asia sud-occidentale. La sua esistenza come un mare brulicante di vita al livello medio degli oceani è assicurata dall'incessante afflusso d'acqua marina dall'Atlantico attraverso lo Stretto di Gibilterra, che compensa il deficit idrico causato dall'eccesso di evaporazione rispetto agli apporti di acqua dolce dalle precipitazioni e dai fiumi. Durante il Miocene superiore, l'Atlantico defluiva verso il Mediterraneo attraverso corridoi marini stretti e poco profondi che attraversavano la Spagna sud-orientale ed il Marocco settentrionale. Insieme, l'esumazione delle catene Betica (Spagna) e del Rif (Marocco) come risultato della continua collisione tra le placche africana ed euroasiatica e l'azione di cambiamenti climatici controllati dalle variazioni dei parametri astronomici causarono la graduale chiusura di questi corridoi marini e la conseguente trasformazione, a 5.96±0.02 milioni di anni, del Mediterraneo in un mare inospitale ed incline alla precipitazione di evaporiti (gesso e salgemma). La crisi idrologica ed ambientale che ne è scaturita, nota come Crisi di Salinità del Messiniano, ha raggiunto l'apice a ~5.55 Ma, quando uno strato di sale spesso 1.5-2 chilometri è precipitato sul fondale del Mediterraneo, ed è terminata a ~5.332 Ma, quando le acque dell'Atlantico si riversarono nel Mediterraneo in grande quantità, verosimilmente creando imponenti cascate a Gibilterra. L'intervallo di tempo che intercorre tra la formazione del gigante salino ed il ripristino delle normali condizioni marine che persistono fino ad oggi è conosciuto come la fase Lago-Mare. La presenza, nelle successioni di Lago-Mare, sia di gesso che di organismi di acqua salmastra endemici della Paratetide centrale (all'incirca corrispondente all'attuale Ungheria-Slovenia) suggerisce che il Mediterraneo, durante questa fase, ha vissuto una complessa storia di cambiamenti della connettività intra- ed extrabacinale, di fluttuazioni del livello di base e di mutamenti ambientali e biologici estremi. Il presente lavoro di tesi si propone di ricostruire i cambiamenti del livello di base del Mediterraneo e la provenienza dei flussi idrologici durante la fase Lago-Mare mediante lo studio multidisciplinare delle sezioni chiave esposte sulla terraferma e di carote che hanno recuperato il record sedimentario sepolto al di sotto delle piane abissali lungo un transetto E-W attraverso il Mediterraneo. Allo scopo, sono state integrate analisi sedimentologiche e biociclostratigrafiche con misure ad alta risoluzione dei rapporti radiogenici degli isotopi dello stronzio. I nuovi dati

mostrano che il Lago-Mare è stato un periodo della storia mediterranea molto più dinamico di quanto si pensasse in precedenza. Vaste aree del Mediterraneo erano occupate da una massa d'acqua con salinità anomala formata prevalentemente dall'afflusso di acque dolci e/o poco salate dalla Paratetide orientale e dai principali fiumi tributari del Mediterraneo quali il Nilo, il Rodano e fiumi africani non più esistenti (es. l'Eosahabi), ed in misura minore, e forse episodica, dall'afflusso di acqua marina dall'Atlantico. La variazione, compiuta su un ciclo precessionale, dell'apporto di acque dolce dai grandi fiumi combinata con l'incostante afflusso marino e l'assenza di un deflusso del Mediterraneo verso l'Atlantico hanno fatto sì che il livello di base del Mediterraneo oscillasse drammaticamente durante tutta la fase Lago-Mare, ma sempre al di sotto del livello medio dei mari e oceani. Tra le tante conseguenze, queste oscillazioni avrebbero causato la colonizzazione delle aree marginali da parte degli organismi di derivazione paratetidea durante le fasi di stazionamento alto del livello di base e delle aree più profonde durante le fasi di stazionamento basso, la precipitazione di gesso nei bacini profondi durante le fasi regressive e l'instaurazione di grandi laghi endoreici in regioni che erano isolate dal resto del Mediterraneo da alti strutturali come il bacino Adriatico ed il Mar Egeo settentrionale.

P-EN

Prologue

0.1 Can a sea cease to exist?

Water covers approximately 71% of the earth's surface, today. 97% of the earth's water volume is in the oceans and seas. The remaining 3% is in ice caps and glaciers (mostly in Antarctica and Greenland; 2%), freshwater/salt lakes, inland seas (0.017%) and in the atmosphere (0.001%), is stored underground (0.62%) or flows in rivers (0.0001%). Our survival is intimately linked to the existence and endurance of healthy aquatic ecosystems. We eat fish from the ocean, we breathe the oxygen its plant life gives off, we feel the warmth of its currents, we irrigate agricultural fields and run factories with lake, river and aquifer water. These ecosystems can change rapidly, even to the point of disappearing, due to the most diverse range of natural and, with the advent of the industrial era, anthropogenic factors. With a quick scour on any search engine, it is easy to find tens of lakes that are currently shrinking and drying up. A prime example is the Aral Sea in Central Asia-Eastern Europe (between Kazakhstan in the north and Uzbekistan in the south), that went from being the fourth-largest lake on Earth in the 1960s, covering 68.000 km^2, to be now 85% smaller (Figs. 0.1a-b). The Syr Darya and Amu Darya rivers, the Aral Sea's primary fresh water sources, were diverted and used for irrigating the Soviet Union's cotton fields. Once the lake was deprived of its main water supplies, the lake-level lowered quickly and dramatically to the point of near-desiccation. To name a more recent example of lakes that have disappeared due to natural causes: a natural pearl in the heart of the Western Alps, the Ceresole Lake (Province of Turin, Piedmont, northern Italy), existing since 1931 as a consequence of the damming of the Orco river is since the winter season 2021-2022 mostly dried up due to a drought period (Figs. 0.1c-d). Finally, given its relevance for the hydrological budget of the Mediterranean during the late Messinian, of which this thesis is the subject, we cannot fail to mention the Lake Chad, an economically important endorheic lake in Central Africa that has greatly varied in size over the centuries due to climate change. According to Griffin (2002, 2006), the Messinian Lake Chad covered an area of approximately 1-2 Mkm^2, shrinking and expanding following orbitally-driven changes in the Intertropical Convergence Zone, and was the source of a river, the Eosahabi, that flowed to the Mediterranean in the Gulf of Sirt (Fig. 0.1e). Today, the Eosahabi river no longer flows and the Lake Chad is four-seven times smaller (~300 km^2) than it used to be in the Messinian (Fig. 0.1f).

Oceans and seas can also disappear despite their larger volumes. Through the movement of plate tectonics, the surface of the Earth is in constant motion and the shape and location of continents and oceans forever changing. Oceans that once existed have been slowly swallowed up in subduction zones, where one tectonic plate plunges beneath another, and are now digested in the mantle. Compared to smaller-size endorheic lakes, the vanishing of an ocean as a result of the collision between two or more tectonic plates is an invisible process for the human being, as it takes up some hundreds of million years for each plate to disappear in the bowels of the Earth. Nowhere in Quaternary depositional systems there is proof that an ocean basin or epicontinental sea ceased to exist (Warren, 2016). Yet, there are a number of geological features buried beneath the abyssal plains of the Mediterranean Sea and exposed along its coastlines and mountain valleys suggesting that this up to 5.267 m deep sea teeming with life was transformed, for a short period of its existence (~640.000 years), into a giant salt pan deprived of life (Hsü et al., 1973a). The alleged disappearance of the Mediterranean Sea is relatively recent geological history, having occurred only ~6-5 million years ago, and constitutes one of the most fascinating scientific puzzles. It is known as Messinian Salinity Crisis.

0.2 History of the Messinian Salinity Crisis of the Mediterranean Basin

As early as the 1950s, field geologists documented the widespread occurrence of evaporites between marine sequences of some Spanish and Italian basins (e.g. Selli, 1954, 1960; Ogniben, 1955). Evaporites are chemical sedimentary rocks including a wide array of minerals, of which halite (NaCl) and gypsum ($CaSO_4*2H_2O$) are the highest volumes, that crystallize in a predictable order as seawater volume decreases and density and salinity increase (Fig. 0.2;

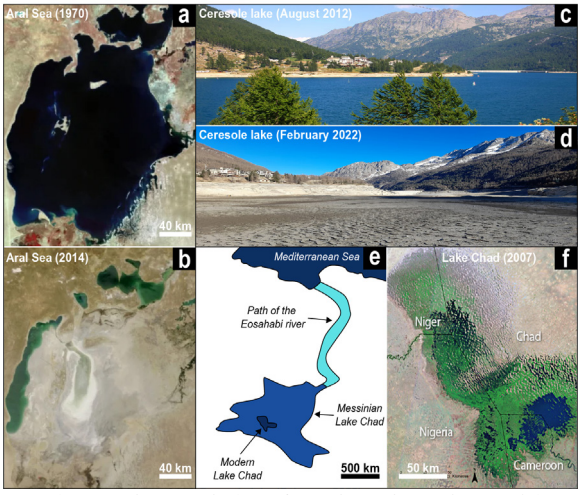

Fig. 0.1. *Comparison between images of the Aral Sea (***a-b***, credit: NASA), Ceresole Lake (***c-d***, credit for c: Alessandro Vecchi) and Lake Chad (***e***: re-drawn after Griffin, 2006;* **f***: UNEP Atlas of Our Changing Environment) taken at different times. | Vergelijking van afbeeldingen van het Aral meer (***a-b***, bron: NASA), het Ceresole meer (***c-d***, bron voor c: Alessandro Vecchi) en het Tsjaadmeer (***e***, nagemaakt van Griffin; 2006;* **f***, UNEP Atlas of Our Changing Environment). | Messa a confronto di immagini del Lago d'Aral (***a-b***, fonte: NASA), Lago di Ceresole (***c-d***, fonte di c: Alessandro Vecchi) e Lago Chad (***e***: modificata da Griffin, 2006;* **f***: UNEP Atlas of Our Changing Environment) in tempi diversi.*

Usiglio, 1849). Typically, evaporite precipitation occurs in closed, standing bodies of seawater (marine evaporites) or lake-waters (nonmarine evaporites) where evaporation exceeds inflow (Warren, 2016). Evaporite precipitation therefore requires peculiar conditions to initiate that only a few places on the Earth meet (for instance, modern evaporites are limited to arid regions). This is why evaporites are not common in the geologic record, constituting less than 5 percent of the volume of sedimentary rocks, and where they are present indicate the (past) existence of harsh environmental conditions (see Warren, 2016 for insights).

The sudden interruption of million years of marine sedimentation by precipitation of evaporites therefore brought to the attention of the scientific community that the periphery of the Mediterranean Basin underwent a salinity crisis at the end of the Miocene. The isolation of the Mediterranean from the Atlantic had been postulated as the underlying cause of this salinity crisis (Ogniben, 1955). This is an apocalyptic scenario. We know from studies of the pre- and post-Messinian deep-sea sediments that the Mediterranean was, already during the late Miocene, a basin with maximum depths exceeding thousands of meters (Hsü et al., 1978a). Owing to its mid-latitude position, the Mediterranean is subjected, on annual basis, to negative surface heat and freshwater budgets, meaning that it loses more water (and heat) to the atmosphere by evaporation than it gains from rainfall and surficial/underground continental input (e.g. Skliris et al., 2018). Today, the water exchange that occurs through the 13 km wide and 320 m deep Strait of Gibraltar, with relatively warm and fresh Atlantic water (15.4°C, 36.2 g/kg) that makes its way into the Mediterranean at the surface, while relatively cooler and saltier (13°C, 38.4 g/kg) Mediterranean water makes its way out at depth (e.g. Tsimplis and Bryden 2000), compensates for this net water loss and allows the Mediterranean to remain filled at the Atlantic level. Should this connection go missing or restrict substantially, as a result of the negative freshwater budget the Mediterranean sea level would drop by more than 2000 meters in 3000-8000 years and a salt desert would establish (Meijer and Krijgsman, 2005). However, since during the '60s and earlier these evaporites were known only from marginal basins, something less catastrophic could equally provide a plausible explanation. Local tectonic movements and/or minor glacio-eustatic sea-level falls could have easily caused a Mediterranean sea level drop of few meters/tens of meters, which would be enough to temporary cut the Mediterranean coastal areas off from the global ocean circulation. Then, evaporation would take over the hydrology of these now endorheic basins, causing the water level of the residual marine water mass to progressively fall, salts in solution to concentrate and evaporitic minerals to precipitate (Fig. 0.2). This is possibly the reason why the discovery of Messinian evaporites in marginal Mediterranean locations did not draw too much curiosity among scientists.

In the late '60s-'70s, oceanographic campaigns unveiled that evaporites in the Mediterranean were not only confined to its periphery. Well portrayed in the seismic profiles was a salt layer up to 2 km thick with diapiric structures rooted in it (e.g. Hersey, 1965; Cornet, 1968; Ryan et al., 1971; see Roveri et al., 2014a for further references). The existence of halite

under the deep Mediterranean floor was confirmed by the Deep Sea Drilling Campaign (DSDP) from Glomar Challenger in 1970 (Ryan et al., 1973). Not only halite, but also gypsum, anhydrite and dolomite were proven to be present by DSDP drilling. Seismic acquisitions also

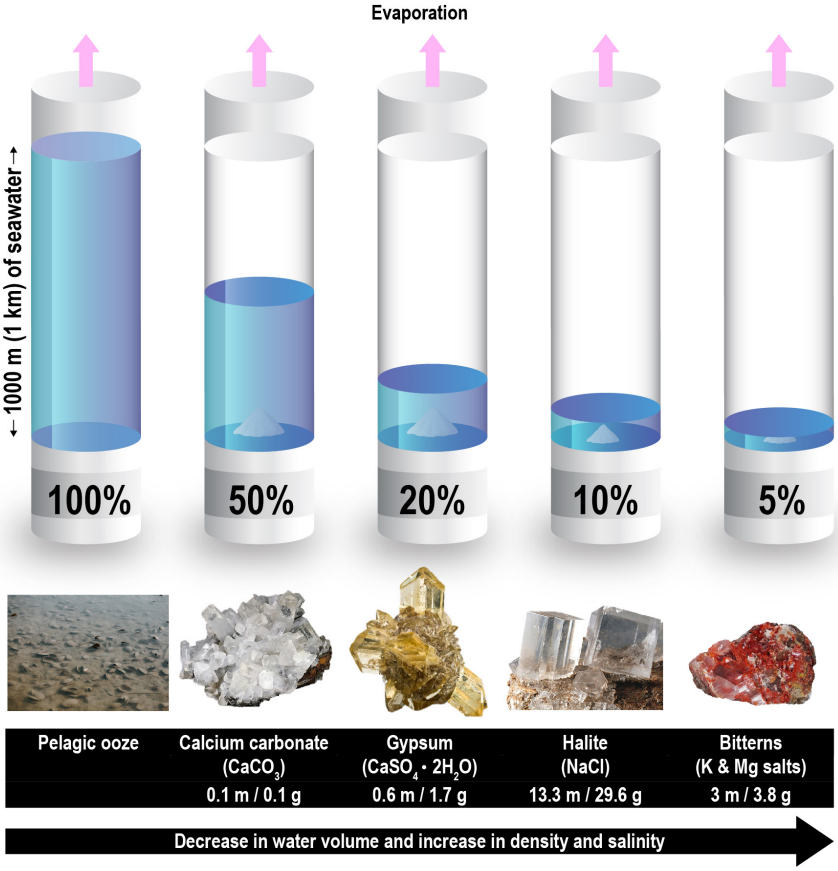

Fig. 0.2. *Sequence of salts that precipitates from an evaporating (fixed) volume of seawater. If a 1000 m tall seawater column evaporates, 17 m and 35.2 g of salts would be deposited.* | *Volgorde van zouten welke neerslaan door indamping van een vast volume zeewater. Als een 1000 m diepe zeewater kolom indampt dan wordt er 17 m en 35.2 g zout afgezet.* | *Sequenza di deposizione dei sali per evaporazione di acqua marina. Se si facesse evaporare una colonna d'acqua di mare alta 1000 m, si deporrebbero 17 m e 35.2 g di sali.*

documented several canyons underlying current fluvial valleys, such as in the Nile, Rhône, Var and Ebro valleys (e.g. Chumakov, 1973; Clauzon, 1982). Kenneth J. Hsü, Maria Bianca Cita and William B.F. Ryan were convinced that the presence of evaporites on the bottom of a more than 4 km deep basin that up to the first evaporite was depositing pelagites in a sea bursting of life hinted at something catastrophic. As they state in the conclusion of the Nature publication where they present for the first time their "deep-basin, shallow-water" or "deep desiccated basin"

model (Hsü et al., 1973a, p. 244), "*the improbable fact that the Mediterranean Sea is underlain by a salt deposit demands an improbable explanation*". Their idea was that tectonics and/or eustatic sea-level changes shut or repeatedly opened and closed the marine exchange(s) between the Atlantic Ocean and the Mediterranean Basin, perennially or intermittently transforming the Mediterranean into a desert with scattered saline ponds (Fig. 0.3). As much biblical is the scenario envisaged for the restoration of the marine conditions that persist up until now, which foresees the collapse of a proto-Gibraltar Strait (back then a sill) followed by a megaflood. This scenario was greeted with disbelief both among the shipboard staff, with several alternative interpretations that were given (Volume 13, Initial Reports), and other scientists that did not participate to the sea expedition (see Drooger, 1973, which is a collection of papers following the first Messinian colloquium in Utrecht in 1973 post desiccated theory). However, as shocking and improbable the scenario depicted by Hsü et al. (1973a) may seem (the same authors, in Hsü et al., 1973b, p. 1203, admitted that "*the idea that an ocean the size of the Mediterranean could actually dry up and leave a big hole thousands of meters below worldwide sea level seems*

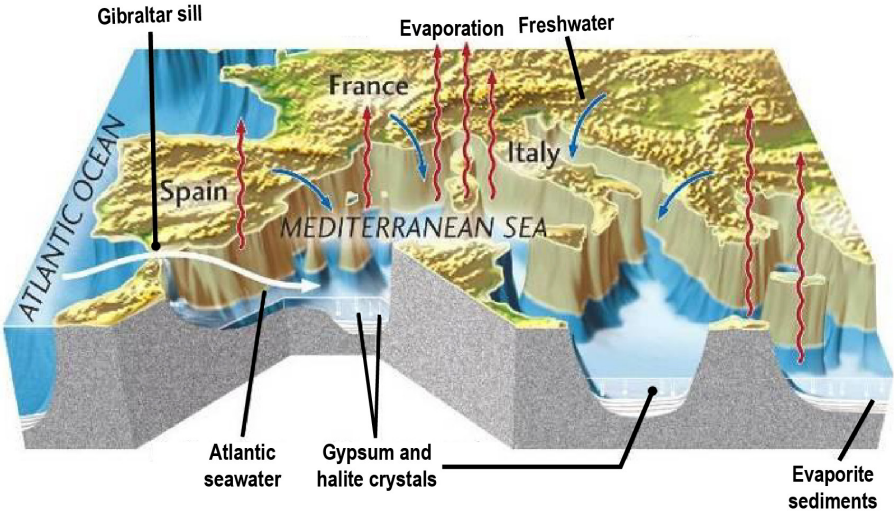

Fig. 0.3. *The Mediterranean Sea during the Messinian Salinity Crisis according to the "Deep desiccated basin" model. | De Middellandse Zee tijdens de saliniteitscrisis in het Messinien volgens het "diep drooggevallen bekken" model| Il Mar Mediterraneo durante la Crisi di Salinitá del Messiniano secondo il modello del "Bacino profondo disseccato".*

preposterous indeed"), it has gained momentum in the following decades because it was the only one able to provide an explanation for most of the data available and being acquired. The "deep-basin shallow-water" model thus became the paradigm of the Messinian Salinity Crisis, raising it to the status of one of the most dramatic paleoceanographic events in Earth's history and

generating an explosion of scientific and public interest. What makes the MSC an even more extraordinary geological event is its extremely short duration. In fact, only ~640 kyr separates the deposition of the first gypsum in marginal Spanish and Italian successions at 5.96±0.02 Ma (Krijgsman et al., 1999a) and the return of the sea at 5.332 Ma (Van Couvering et al., 2000). What really happened in between is still a beautiful mystery.

0.3 The up-to-date knowledge on the Messinian Salinity Crisis

Despite the broad consensus that supported the "deep-basin, shallow-water" model during the '80s-'90s and still today, over the years there has been increased evidence that the Mediterranean never did dry up and that, at least for certain periods during the MSC, was not isolated (e.g. McCulloch and De Deckker, 1989; Roveri et al., 2001; Hardie and Lowenstein, 2004; Lugli et al., 2015). Instead, a number of other aspects remained contentious among different research groups, such as:

- the main trigger of the MSC (tectonics vs climate);
- the timing of the paleohydrological and paleoenvironmental changes recognized in the sedimentary record (i.e. the stages of Roveri et al., 2014a; see below);
- the provenance of the water fluxes (i.e. Mediterranean connections with the neighbouring Atlantic, Red Sea and Paratethys);
- the exact position of the Mediterranean base-level;
- the onshore-offshore equivalence of evaporite units.

These and many more controversial arguments are described (and referenced) in a comprehensive way in the work of Roveri et al. (2014a). In addition to providing an overview of the history and controversies of the MSC, Roveri et al. (2014a) brings order in the understanding of the events leading to, happening during and following the MSC. Below we provide a summary of the progress of the MSC according to Roveri et al. (2014a).

The triggering factor of the MSC is widely considered to be the reduction in exchange between the Atlantic and the Mediterranean. Unlike today, during the late Miocene the link between the Atlantic Ocean and the Mediterranean Sea was provided by a series of gateways cutting through the uplifting Betic and Rifian Cordilleras in Southern Spain and Northern Morocco, respectively (Fig. 0.4; Flecker et al., 2015; Capella et al. 2017, 2018; Krijgsman et al., 2018). As the mountain belts uplifted during the Alpine orogeny, these gateways closed one by one, leaving (perhaps) only a narrow passage through the present-day Strait of Gibraltar (Fig. 0.4; Krijgsman et al., 2018). The first evidence of ecological changes related with the progressive restriction of the Mediterranean-Atlantic connections have been documented close to the Tortonian/Messinian boundary in the benthic foraminifera population, which indicate an enhanced sensitivity of the Mediterranean to the continental runoff and an increase in the water column stratification that led to less oxygenated bottom water conditions (e.g. Kouwenhoven et al. 1999, 2003; Bulian et al., 2021). The Mediterranean's response to this restriction was non-

linear, with major steps recognized at 6.72, 6.35 Ma and 5.96 Ma (see Corbí et al., 2020 and references therein). The precipitation of the first gypsum beds at 5.96±0.02 Ma, which marks the beginning of MSC Stage 1 (sensu Roveri et al., 2014a), is though to reflect an exacerbation of water column stratification, possibly related to the combined effect of persistent freshwater inflow in an increasingly isolated basin (e.g. Natalicchio et al., 2019; Sabino et al., 2020, 2021). Gypsum precipitated mainly in shallow-water marginal basins, while organic-rich shales accumulated in deeper-water areas (Roveri et al., 2003; Manzi et al., 2005; Lugli et al., 2010; Dela Pierre et al., 2011; Natalicchio et al., 2019; Sabino et al., 2020, 2021). During Stage 1, a continuous, albeit restricted, Mediterranean outflow to the Atlantic is thought to have persisted (Krijgsman et al., 2018). During Stage 2 (5.59-5.55 Ma), tectonics and/or glacio-eustacy terminated the Mediterranean outflow to the Atlantic (e.g. Krijgsman and Meijer, 2008; Krijgsman et al., 2018) and the Mediterranean base level dropped of hundreds/thousands

Fig. 0.4. *Late Miocene-Pliocene palaeogeographic evolution of the Mediterranean- Atlantic gateways (Krijgsman et al., 2018).* | *Paleogeografische evolutie van de Middellandse Zee-Atlantische Oceaan connectie gedurende het Laat Mioceen-Plioceen (Krijgsman et al., 2018).* | *Evoluzione paleogeografica della connessione tra l'Atlantico ed il Mediterraneo nel tardo Miocene-Pliocene (Krijgsman et al., 2018).*

of meters (e.g. Roveri et al., 2014a). As a consequence, the Mediterranean periphery became isolated and underwent an important phase of erosion of pre-MSC and Stage 1 successions. Chaotic, mass-transport units indicate downslope resedimentation, and evaporite deposition shifted to the deeper basins, which mostly accumulated halite and, to a lesser degree, bitter salts (e.g. Hsü et al., 1978a; Lugli et al., 1999). Gypsum precipitation resumed in Stage 3 (5.55-5.332) in the same deep water settings that had accumulated halite during Stage 2. At the same time, gypsum-free terrigenous successions accumulated in the marginal basins. Similarly to Stage 1, the gypsum beds alternate with marl horizons and these alternations register dry-wet cycles controlled by changes in the orbital parameters of eccentricity and precession (Hilgen et al., 2007; Manzi et al., 2009). Unlike Stage 1, however, many of the Stage 3 marl interbeds in both marginal and deep-basin Stage 3 sequences contain ostracods, mollusks and dinoflagellate cysts endemic to the Eastern Paratethys region. This was a vast, brackish water lake (Grothe et al., 2020 and references therein) of which the present-day Black, Caspian and Aral seas are relict areas. These Paratethyan-derived organisms are largely thought to have migrated and spread in the Mediterranean following the sudden establishment of a more efficient intra-basinal connections and water exchanges with the Paratethys (Roveri et al., 2008a, 2014a), possibly following the rising of the Mediterranean base-level above the Mediterranean-Paratethys sill and the consequent enhancement of the Mediterranean outflow (Marzocchi et al., 2016). This hydrological change is thought to have occurred synchronously at 5.42 Ma (Roveri et al., 2008a, 2014). This led Roveri et al. (2014a) to split the Stage 3 into a substage 3.1 largely barren of biota and a substage 3.2 (or Lago-Mare phase) rich of Paratethyan biota. These sediments are capped by fine-grained lithologies devoid of Paratethys elements and rich in open marine biota that testify the definitive, possibly catastrophic (Micallef et al., 2018; Garcia-Castellanos et al., 2020), return of the sea in the Mediterranean in the early Pliocene.

0.4 Thesis objectives and outline

The publication from Roveri et al. (2014a) provides an evolutionary scenario for the MSC and a reconstruction of the Mediterranean paleoenvironment and paleohydrology during this event that agrees with many existing data. However, several aspects of the Roveri et al. (2014a)'s publication have been challenged by more recent studies (e.g. Meilijson et al., 2018, 2019; Aloisi et al., 2022) and many questions remain contested for each of the three stages. The Stage 3 is possibly the most ambiguous of all the phases, with several different scenarios that have been presented. These scenarios are distinguished by the provenance of the water fluxes, the position of the base-level and the connectivity between basins within the Mediterranean and with the neighbouring Atlantic Ocean, Red Sea and Eastern Paratethys. As reported by Ryan (2009), many of these debates arise from the different perspectives and methods used by the sea-going scientist, who approached the MSC with geophysical tools and DSDP cores and largely overlooked the data from the outcrops, and by the land geologists, who measured and described

sections in outcrops and largely ignored the deep basins' sedimentary archive. This PhD thesis aims to reconstruct Mediterranean water level and hydrological fluxes during the final Stage 3 of the Messinian Salinity Crisis by studying both the key sections on-land and in the deep sea (DSDP-ODP cores) on an E-W transect across the Mediterranean. These sections/cores are approached with a multi-disciplinary strategy combining integrated biocyclostratigraphic analyses with high-resolution radiogenic strontium isotope records ($^{87}Sr/^{86}Sr$ ratios).

The Stage 3 sediments yield mainly brackish, Paratethys-derived fossils. In this thesis, the main biological focus is the ostracods, small crustaceans (typically ≤1 mm in size) protected by two chitinous or calcareous valves. The reasons for this choice include: (I) the recognized species are certainly autochtonous because nowhere in the Mediterranean they are reported in pre-MSC sediments. This means that they reflect the time of deposition of the sediments they are embedded in; (II) they are a reliable archive for the $^{87}Sr/^{86}Sr$ ratio of the water in which they dwelt because their valves are made of low-Mg calcite, which is subject to minimal diagenesis (e.g. Marcano et al., 2015), and they do not fractionate the different isotopes of Sr (e.g. Bista et al., 2021); (III) unlike, for instance, the mollusks, which are only sporadically found, ostracods are known to occur throughout the Mediterranean, from Malaga (Guerra-Merchán et al., 2010) to Cyprus (Rouchy et al., 2001), from the Piedmont Basin in the north (Trenkwalder et al., 2008) to African localities to the south (Temani et al., 2020) and even in relatively deeper settings (Iaccarino and Bossio, 1999; Grossi et al., 2015). Therefore, their ubiquitous presence allows the reconstruction of a high-resolution $^{87}Sr/^{86}Sr$ isotope record both in space and time.

Sr isotopes are the preferred geochemical tool for this work because they can be used to trace the provenance of water in specific sedimentary environments, owing to the different $^{87}Sr/^{86}Sr$ isotopic signatures that water sources of different origin (mostly continental vs marine) yield. The $^{87}Sr/^{86}Sr$ signature of the global ocean and Eastern Paratethys for the Stage 3 interval are derived from measurements on calcareous material from time-equivalent sedimentary successions located around and at depth in the oceans (McArthur et al., 2012) and in the Black-Caspian seas (Grothe et al., 2020), respectively. $^{87}Sr/^{86}Sr$ data for Messinian rivers are not available, but can be reliably approximated assuming that the paleorivers had similar $^{87}Sr/^{86}Sr$ ratios to those of the present-day rivers. If $^{87}Sr/^{86}Sr$ measurements of present-day rivers are not available in the literature, then they can be reconstructed, with the aid of mass-balance calculations, using the $^{87}Sr/^{86}Sr$ ratios of the lithologies forming the rivers' catchments. In fact, the $^{87}Sr/^{86}Sr$ values of river water largely depends on the drained bedrock material, which has a highly variable $^{87}Sr/^{86}Sr$ signature (e.g. ophiolites are typified by $^{87}Sr/^{86}Sr$ ratios <0.7060, whereas plutonic and metamorphic acid rocks yield $^{87}Sr/^{86}Sr$ ratios >0.7071; e.g. Hajj et al., 2017) and solubility (evaporites and carbonates are more soluble relative to igneous and metamorphic basement rocks).

The results of this cross-disciplinary, Mediterranean-wide study are presented in 6 chapters (Fig. 0.5). **Chapter 1** is a comprehensive literature review of the state-of-the-art knowledge on

the Stage 3 (seismo)stratigraphic, sedimentological, paleontological and (bio)geochemical data from the key onshore and offshore domains. We then discuss the arguments for and against the two prevailing, and apparently mutually exclusive, paleoenvironmental scenarios:

I. that during Stage 3 the Mediterranean was isolated from the Atlantic and contained shallow endorheic lakes;

II. the Mediterranean during Stage was filled with water derived from the Atlantic, Paratethys and large river waters.

Finally, we highlight the working principles of some methods and proxies that may be of help to reconstruct base-level and connectivity changes and we address the direction that future research should take in order to come to an agreement. To tackle this controversy, we start by investigating the sub-basins at the periphery of the Mediterranean Basin. The so-called marginal basins are, in fact, a good location for testing the isolated/connected (or empty/full) dispute, since evidence of connectivity with the Atlantic and/or Eastern Paratethys requires the Mediterranean Basin to have been relatively full. We therefore start from three marginal basins (Sorbas, Nijar and Vera) in SE Spain (**chapter 2**) and from the deeper, but more remote, Piedmont Basin (N Italy) at the northernmost offshoot of the Mediterranean (**chapter 3**), which we investigate with a multi-disciplinary approach combining integrated sedimentological and paleontological analyses with high-resolution Sr-isotope records. The search for a unifying scenario necessarily hinges on the deepest basins. What works to explain the deposits around the Mediterranean's periphery and at the northernmost tip of the Adriatic Basin must also explain the coeval deposits in the Balearic, Sicily, Ionian and Cyprus basins and in the Northern-Central Apennines. The Eraclea Minoa section (Caltanissetta Basin, Sicily), having an intermediate position, during the Messinian, between the Spanish and deep basins, is the focus of **chapter 4**. We investigated the sedimentology, paleontology and strontium isotope geochemistry of its beautifully exposed gypsum-marl cycles and we propose a paleoenvironmental and paleohydrological model that favours an oscillating high-low Mediterranean base-level during Stage 3. In **chapter 5** we investigate an aftermath of the scenario proposed in chapter 4, namely the possibility that, during at least part of Stage 3, the Adriatic region existed as an endorheic lake separated from the Mediterranean by the Gargano sill, where a mountain ridge was elevated offshore. This region has been subject to extensive studies, but the chronology and nature of its paleoenvironmental and paleohydrological changes need to be better constrained. Finally, **chapter 6** collects $^{87}Sr/^{86}Sr$ ratios recently acquired from the three other gypsum-bearing locations across a W-E transect in the Mediterranean Basin. These are: ODP Site 975B drilled on the South Balearic Margin between the Balearic Promontory (Menorca and Mallorca Islands) and the Algerian Basin; ODP Site 654A located on the upper Sardinia margin (Tyrrhenian Basin); the Polemi Basin (Cyprus), which is the only other place, besides Sicily, where Stage 3 gypsum-marl cycles are exposed onland. These data add a Mediterranean-wide and deep basin perspective to the hypothesis put forward with the

Eraclea Minoa study that Stage 3 gypsum across the Mediterranean precipitated synchronously from the same water mass.

0.5 The SALTGIANT ETN

This thesis was carried out as part of the SALTGIANT ETN project, an EU-funded, Marie Curie Initial Training Network (grant agreement number 765256) that brought together natural and social scientists. More specifically, SALTGIANT brings together 30 academic organizations (13 beneficiaries, 17 partners), 6 private sector Oil&Gas companies, 2 mining sector companies, 1 biotechnology company, 1 geotechnical institute, 1 museum and 1 specialist in transferable skills training from 12 countries. The scientific goal of SALTGIANT is the understanding of the formation of the Mediterranean Salt Giant (MSG), one of the largest salt deposits on Earth, and its implications for sub-seafloor microbial life, risk assessment in the oil industry, geo-economics of the Mediterranean region and the history of oceanography. The non-scientific goal is to stimulate interdisciplinary and intersectorial knowledge exchange between experts of various disciplines, including geologists, geophysicists, geochemists, microbiologist, geographers and historians. Dr. Giovanni Aloisi (Institut de Physique du Globe de Paris,

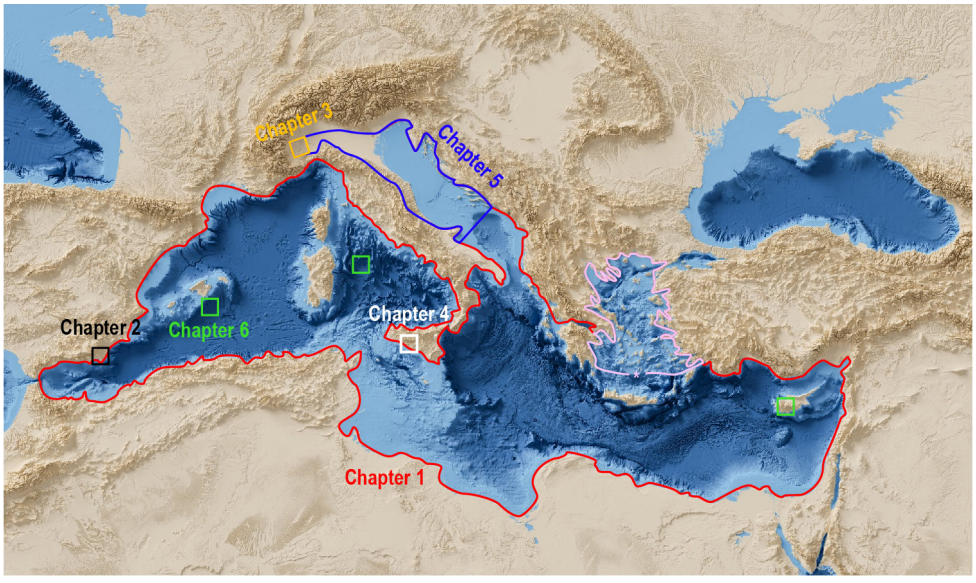

Fig. 0.5. *Map of the Mediterranean Sea showing the geographical distribution of the thesis' chapters. The pink line refers to the Aegean Sea, which has been studied and the results published in Krijgsman et al. (2020a).* | *Map of the Mediterranean Sea showing the geographical distribution of the thesis' chapters. The pink line refers to the Aegean Sea, which has been studied and the results published in Krijgsman et al. (2020a).* | *Mappa del Mar Mediterraneo che mostra la distribuzione geografica dei capitoli di questa tesi. La linea rosa si riferisce al Mar Egeo, che è stato studiato ed i risultati pubblicati in Krijgsman et al. (2020a).*

-CNRS-University of Paris) has brilliantly coordinated the project. 15 PhD students constituted the core of the project. Individual PhD projects were grouped in four work packages (WP). WP1, which this thesis is part of, aimed at the development of a unified model that explains the formation of the MSG. WP2 was dedicated to the study of the deep microbial biosphere in the MSG, which provides a terrestrial analogue for the hypersaline environments of Mars, where life forms might have been preserved. WP3 aimed to develop a mechanistic and quantitative understanding of early salt deformation and sub-salt overpressure development that can be used by the oil industry to mitigate the risks associated with drilling in salt-capped hydrocarbon provinces. WP4 had the twofold goal to provide an integrated history of the discovery of the MSG and to study the economic and geopolitical implications of the mapping of big salt deposits because of their association with natural gas fields.

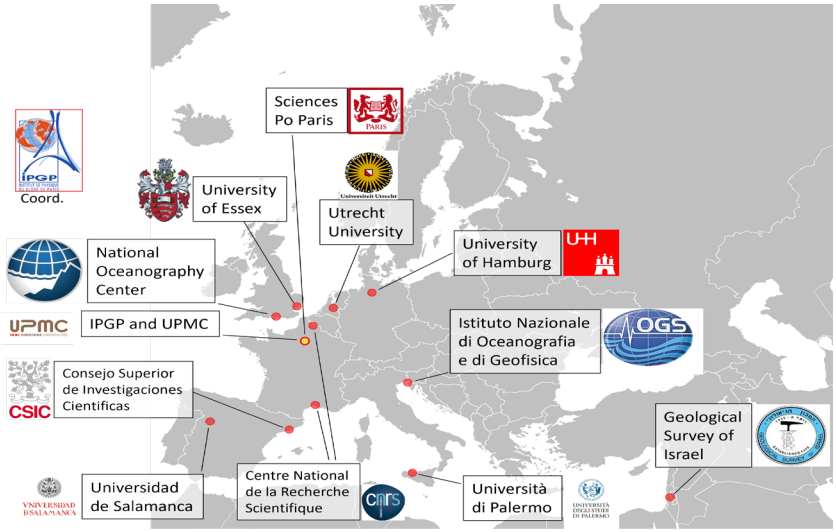

Fig. 0.6. *Map of Europe showing the distribution of the 12 academic organizations hosting the 15 PhD students of the SALTGIANT ETN (designed from Fadl Raad).* | *Kaart van Europa met de locaties van alle academische organizaties die de 15 PhD studenten van de SALTGIANT ETN huisvesten.* | *Cartina dell'Europa dove viene mostrata la distribuzione delle 12 organizzazioni accademiche che hanno ospitato i 15 dottorandi del progetto SALTGIANT ETN.*

P-NL

Proloog

0.1 Kan een zee ophouden te bestaan?

Vandaag de dag is ongeveer 71% van het aardoppervlak bedekt met water. 97% van het watervolume op aarde bevindt zich in de oceanen en zeeën. De resterende 3% zit in ijskappen en gletsjers (voornamelijk op Antarctica en Groenland; 2%), zoet- en zoutwater meren, binnenzeeën (0.017%), in de atmosfeer (0.001%), wordt ondergronds opgeslagen (0.62%) of stroomt in rivieren (0.0001%). Onze overleving is nauw verbonden met het voortbestaan van gezonde aquatische ecosystemen. We eten vis uit de oceaan, we ademen de zuurstof die het plantenleven afgeeft, we voelen de warmte van de zee- en luchtstromen, we irrigeren landbouwvelden en we runnen fabrieken met water uit de meren, rivieren en watervoerende lagen. Deze ecosystemen kunnen snel veranderen, zelfs tot het punt van verdwijning, als gevolg van de meest uiteenlopende natuurlijke en, met de komst van het industriële tijdperk, antropogene factoren. Met een snelle zoekopdracht op een willekeurige zoekmachine is het gemakkelijk om tientallen meren te vinden die momenteel krimpen en opdrogen. Een goed voorbeeld is het Aralmeer in Centraal-Azië (tussen Kazachstan en Oezbekistan), wat in de jaren zestig het vierde grootste meer op aarde was (68.000 km^2) en nu 85% kleiner is geworden (afb. 0.1a-b). De Syr Darja en Amu Darja rivieren, de primaire zoetwaterbronnen van het Aralmeer, werden omgeleid en gebruikt voor de irrigatie van de katoenvelden van de voormalige Sovjet-Unie. Zodra het meer van zijn belangrijkste watervoorraden werd beroofd, verminderde het meer-niveau drastisch tot het punt van bijna-opdroging. Om een recenter voorbeeld te noemen van meren die zijn verdwenen als gevolg van natuurlijke oorzaken: Een natuurlijke parel in het hart van de westelijke Alpen, het Ceresole-meer (Provincie Turijn, Piëmont, Noord-Italië) dat sinds 1931 bestond als gevolg van de afdamming van de Orco rivier, maar sinds het winterseizoen 2021-2022 grotendeels is opgedroogd door een droogteperiode (afb. 0.1c-d). Tenslotte, gezien de relevantie voor het watervolume van de Middellandse Zee aan het einde van het Messiniaanse tijdperk, waar dit proefschrift over gaat, kunnen we niet om het Tsjaadmeer heen. Dit was een enorm groot endoreïsch meer in Centraal-Afrika dat door de eeuwen heen enorm in omvang is veranderd als gevolg van klimaatverandering. Volgens Griffin (2002, 2006) bedekte het Messiniaanse Tsjaadmeer een gebied van ongeveer 1-2 Mkm^2, waarna het kromp en zich uitbreidde door cyclische veranderingen in de intertropische

Zee stroomde in de golf van Sidra (afb. 0.1e). Tegenwoordig bestaat de Eosahabi rivier niet meer en is het Tsjaadmeer vier tot zeven keer zo klein (~300 km2) als vroeger in het Messiniaanse tijdperk (Afb. 0.1f).

Oceanen en zeeën kunnen ook verdwijnen, ondanks hun grotere volumes. Door plaattektoniek is het oppervlak van de aarde constant in beweging en verandert de vorm en locatie van continenten en oceanen voorgoed. Oceanen die ooit bestonden zijn langzaam opgeslokt in subductiezones, waar de ene tektonische plaat onder de andere duikt en opgaat in de aardmantel. In vergelijking met kleinere endoreïsche meren is het verdwijnen van een oceaan als gevolg van een botsing tussen twee of meer tektonische platen een onzichtbaar proces voor de mens, omdat het honderden miljoenen jaar duurt voordat elke plaat in de diepte van de aarde verdwijnt. Nergens in de recente sedimentarchieven is er bewijs dat een oceaanbekken of binnenzee ophield te bestaan (Warren, 2016). Toch zijn er een aantal geologische kenmerken te vinden onder de abyssale vlaktes van de Middellandse Zee en langs kustlijnen en bergdalen. Dit suggereert dat de max. 5.267 m diepe Middellandse Zee gedurende een korte tijd van zijn bestaan (~640.000 jaren) veranderende in een gigantische zout vlakte (Hsü et al. 1973a). De vermeende verdwijning van de Middellandse Zee vond plaats in vrij recente geologische geschiedenis, zo'n 6 tot 5 miljoen jaar geleden, en vormt een van de meest fascinerende wetenschappelijke puzzels. Het staat dan ook bekend als de Messiniaanse saliniteitscrisis (MSC) of zoutcrisis.

0.2 Geschiedenis van de Messiniaanse saliniteitscrisis van het Middellandse Zeegebied

Al in de jaren vijftig documenteerden geologen het wijdverbreide voorkomen van verdampingsgesteente, genaamd evaporieten, tussen normale zeeafzettingen in een aantal Spaanse en Italiaanse bekkens (bv. Selli, 1954, 1960; Ogniben, 1957). Evaporieten zijn chemische sedimentaire gesteenten die een scala aan mineralen bevatten, waarvan het grootste volume bestaat uit haliet (NaCl) en gips ($CaSO_4*2H_2O$). Deze mineralen kristalliseren in een voorspelbare volgorde als het zeewatervolume afneemt en het zoutgehalte en de dichtheid toeneemt (Afb. 0.2; Usiglio, 1849). Doorgaans treedt verdamping in afgebakende, stilstaande waterlichamen van zeewater (mariene verdamping) of zoetwater (niet-mariene verdamping) waar de verdampingssnelheid hoger is dan de water instroom (Warren, 2016). De afzetting van evaporieten vereist daarom een bijzondere combinatie van omstandigheden, wat slechts op enkele plaatsen op aarde te vinden is (moderne evaporieten zijn bijvoorbeeld gelimiteerd tot droge regio's). Hierom zijn evaporieten niet gebruikelijk en vormen ze minder dan 5 procent van het volume van sedimentaire gesteente op aarde. Op de plaatsen waar ze wel aanwezig zijn duidt dit op de (vroegere) aanwezigheid van extreme ecologische omstandigheden (zie Warren, 2016 voor meer inzichten). De plotselinge onderbreking van mariene sedimentatie door evaporiet afzetting geeft daarom aan dat er een saliniteitscrisis plaats vond in het Middellandse Zee bekken. Het wordt verondersteld dat het isoleren van de Middellandse Zee

door de sluiting van de zeestraat naar de Atlantische Oceaan de onderliggende oorzaak is van deze saliniteitscrisis (Ogniben, 1957). We weten uit diepzee sediment studies van voor en na het Messiaanse tijdperk dat de Middellandse Zee al aan het einde van het Mioceen tijdperk een bekken was met een maximale diepte van meer dan duizenden meters (Hsü et al., 1978a). Door zijn positie op de middelste breedtegraad wordt de Middellandse Zee op jaarbasis blootgesteld aan negatieve oppervlaktewarmte en zoetwater volume, wat inhoudt dat er meer water en warmte verloren gaat aan de atmosfeer door verdamping dan dat er toename is door regenval en via oppervlakte en ondergrondse continentale aanvoer (bijv. Skliris et al., 2018). Tegenwoordig vindt de wateruitwisseling plaats via de 13 km brede en 320 m diepe straat van Gibraltar, waar relatief warm en minder zout Atlantisch water (15.4°C, 36.2 g/kg) aan het oppervlak de Middellandse Zee binnenstroomt, terwijl er via de diepte relatief koeler en zouter water terugstroomt naar de Atlantische Oceaan (Bryden et al., 1994; Tsimplex en Bryden 2000). Dit compenseert voor het waterverlies en zorgt er voor dat de Middellandse Zee op hetzelfde niveau blijft als de Atlantische Oceaan. Mocht deze verbinding verdwijnen of substantieel krimpen, dan zou het niveau van de Middellandse Zee in 3000 tot 8000 jaar met meer dan 2000 m dalen, waardoor er een zoutwoestijn zou ontstaan op delen van de bodem (Meijer en Krijgsman, 2005). De Messiniaanse evaporieten zijn echter enkel bekend van ondiepe wateren, dus een minder catastrofale gebeurtenis zou eveneens een plausibele verklaringen kunnen vormen. Lokale plaattektoniek en/of kleine glacio-eustatisch gecontroleerde zeespiegelfluctuaties zouden gemakkelijk een niveaudaling van enkele tot tientallen meters kunnen veroorzaken, wat voldoende zou zijn om de kustgebieden van de Middellandse Zee tijdelijk af te snijden van de mondiale oceaancirculatie. In dat geval zou verdamping de overhand krijgen waardoor het waterniveau progressief zou afnemen, de zouten in oplossing zouden concentreren en evaporiet mineralen precipiteren (afb. 0.2). Dit is wellicht de reden dat de ontdekking van Messiaanse evaporieten in het Middellandse Zeegebied in de jaren 60 weinig aandacht trok van onderzoekers. In eind jaren 60 en begin jaren 70 onthulden oceanografische studies echter dat de evaporieten niet enkel beperkt bleven tot de randen van de Middellandse Zee. Dit is goed terug te zien in de seismische profielen, waarin een zoutlaag tot 2 km dikte met diepgewortelde diapier structuren zichtbaar is (bijv. Alinat en Cousteau, 1962; Cornet, 1968). Het bestaan van haliet onder de diepe mediterrane zeebodem werd bevestigd door de Deep Sea Drilling Campaign (DSDP) van Glomar Challenger in de 70er jaren (Ryan et al., 1973), maar ook gips, anhydriet en dolomiet bleken aanwezig te zijn. Kenneth J. Hsü, Maria Bianca Cita en William B.F. Ryan waren overtuigd dat de aanwezigheid van evaporieten op de bodem van een meer dan 4 km diep bekken een teken was van een catastrofale gebeurtenis. Zoals zij concludeerden in hun Nature publicatie, waarin zij voor het eerst het model "diep-bekken, ondiep water" ofwel "diep uitgedroogd bekken" presenteerden, "het onwaarschijnlijke feit dat een zoutafzetting onder de Middellandse Zee ligt, vereist een onwaarschijnlijke verklaring". Hun idee was dat tektoniek en/of eustatische zeespiegelschommelingen herhaaldelijk de uitwisseling

tussen de Middellandse Zee en de Atlantische Oceaan verhinderde, waardoor het Middellandse Zeegebied herhaaldelijk werd veranderd in een woestijn met wijd verspreide zout meren (Fig. 0.3). Net zo bijbels is het scenario dat wordt overwogen voor het herstel van de tot nu toe aanhoudende mariene omstandigheden, die de instorting van een voormalige Gibraltar straat beschrijft, gevolgd door een gigantische vloedgolf. Dit scenario werd vol ongeloof ontvangen en veel alternatieve interpretaties werden gegeven (Volume 13, Initial Reports) door personeel en andere wetenschappers die niet deelnamen aan de expedities (zie Drooger, 1973). Hoe schokkend en onwaarschijnlijk het scenario uitgebeeld door Hsü et al. (1973a) ook lijkt, nam de geloofwaardigheid door de tijd toch toe doordat er geen enkele andere verklaring voor de meeste observaties voorhanden was. Het "diepe bekken, ondiep water" model is dus een paradigma geworden van de Messiniaanse saliniteitscrisis, waardoor de status is gestegen naar een van de meest dramatische paleo-oceanografische gebeurtenissen in de geschiedenis der aarde, met een explosieve toename in wetenschappelijke en publieke interesse. Wat de MSC een nog bijzondere geologische gebeurtenis maakt, is dat het van extreme korte duur was. De oudste afzettingen van gips in de Spaanse en Italiaanse bekkens zijn van 5.96±0.02 miljoen jaar geleden en de terugkeer van de zee van 5.332 Ma worden dus door slechts ~640 kyr gescheiden (van Couvering et al., 2000). Wat er in de tussentijd werkelijk gebeurde blijft een wonderlijk mysterie.

0.3 De actuele kennis over de Messiaanse Saliniteitscrisis

Ondanks dat er over de jaren heen een consensus heerst over het "diep bassin, ondiep water" model, zijn er ook aanwijzingen dat de Middellandse Zee nooit echt is opgedroogd en dat, in ieder geval voor bepaalde periodes in de MSC, het niet geïsoleerd was (bv. McCulloch en de Deckker, 1989; Roveri et al., 2001; Hardie en Lowenstein, 2004; Lugli et al., 2015). Ook bleken een aantal andere aspecten controversieel tussen verschillende onderzoeksgroepen, zoals: De belangrijkste oorzaak van de MSC (tektoniek versus klimaat); De timing van de paleo-hydrologische en paleo-ecologische veranderingen die in het sedimentaire archief worden gevonden; de herkomst van de waterstromen (bijv. Mediterrane verbindingen met de naburige Atlantische Oceaan, Rode Zee en Paratethyszee); De exacte positie van het Middellandse Zeegebied; de land naar diep zee correlatie van evaporiet afzettingen . Deze en nog veel meer controversiële aspecten worden in het werk van Roveri et al. beschreven (en gerefereerd) (2014a). Naast het geven van een overzicht van de geschiedenis en controverses van de MSC, geeft dit werk ook duidelijkheid in de gebeurtenissen die leidden tot, en gebeurden tijdens en na de MSC. Hieronder wordt een samenvatting gegeven van het verloop van de MSC volgens Roveri et al. (2014a).

De verminderde uitwisseling tussen de Atlantische Oceaan en de Middellandse Zee wordt algemeen beschouwd als hoofd factor van de MSC. In tegenstelling tot de huidige situatie bestond de verbinding in het Mioceen tijdperk uit verschillende zeestraten tussen

de Atlantische Oceaan en de Middellandse Zee, die tussen de pieken van de Betische en Rif gebergten in zuid-Spanje en noord-Marokko stroomden (Fig. 0.4; Flecker et al., 2015; Capella et al. 2017, 2018; Krijgsman et al., 2018). Toen deze bergketens omhoog kwam tijdens de Alpiene orogenese, sloten deze zeestraten één voor één, waarbij mogelijk enkel een nauwe opening overbleef in de hedendaagse straat van Gibraltar (Fig. 0.4; Krijgsman et al., 2018). Het eerste bewijs van ecologische veranderingen die verband houden met de geleidelijke verkleining van de verbindingen tussen de Middellandse Zee en de Atlantische Oceaan, is gedocumenteerd rond de grens tussen de Tortoon en Messien tijdperken. Daar laten fossielen benthische foraminifera soorten een grote verandering zien, wat duidt op een verhoogde gevoeligheid van de Middellandse Zee voor zoetwater toevoer en een toename van de waterkolom stratificatie die leidde tot minder zuurstofrijk bodemwater (bv. Kouwenhoven et al. 1999, 2003; Bulian et al., 2021). De reactie van de Middellandse Zee op deze beperking was niet lineair in tijd, en belangrijke stappen zijn herkend op 6.72, 6.35 Ma en 5.96 Ma (zie Corbí et al., 2020). De precipitatie van de eerste gips lagen op 5.96±0.02 Ma markeert het begin van MSC fase 1 (sensu Roveri et al., 2014a) en weerspiegelt een toename in de waterkolom stratificatie, wat mogelijk gerelateerd is aan het gecombineerde effect van aanhoudende zoetwaterinstroom in een steeds meer geïsoleerd bekken (bijv. Natalicchio et al., 2019; Sabino et al., 2020, 2021). Gips precipiteerde voornamelijk in ondiepe wateren in de randbekkens van de Middellandse Zee, terwijl organisch rijk schalie accumuleerde in de diepzee (Roveri et al., 2003; Manzi et al., 2005; Lugli et al., 2010; Dela Pierre et al., 2011; Natalicchio et al., 2019; Sabino et al., 2020, 2021). Tijdens fase 1 zou een voortdurende, zij het beperkte, mediterrane uitstroom naar de Atlantische Oceaan hebben plaatsgevonden (Krijgsman et al., 2018). Tijdens fase 2 (5.59-5.55 Ma) hebben tektoniek en/of glacio-eustatisch gecontroleerde zeespiegelfluctuaties de uitstroom van de Middellandse Zee naar de Atlantische Oceaan verhinderd (bijv. Krijgsman en Meijer, 2008; Krijgsman et al., 2018) waardoor de zeespiegel van de Middellandse-Zee daalde met honderden tot enkele duizenden meters (bijv. Roveri et al., 2014a). Als gevolg daarvan werden de randbekkens van de Middellandse Zee geïsoleerd en vond er een belangrijke erosie fase plaats. Ongeordende massatransport eenheden zijn aangetroffen die duiden op een gravitatief afglijden waarbij evaporiet afzettingen uit fase 1 zich verplaatsten naar dieper gelegen delen, waar voornamelijk haliet accumuleerde en in mindere mate ook bitter zouten (bijv. Hsü et al., 1978a; Lugli et al., 1999). In fase 3 (5.55-5.332) werd de precipitatie van gips weer vervolgd. Tegelijkertijd vond er ook accumulatie van gips-vrije sedimenten plaats in ondiepe wateren. Net zoals in fase 1, worden de fase 3 gipslagen afgewisseld met mergelafzettingen, wat een aanwijzing is voor natte-droge cyclische klimaatsveranderingen, de zogenaamde Milanković-parameters (excentriciteit en precessie; Hilgen et al., 2007; Manzi et al., 2009). In tegenstelling tot fase 1, bevatten veel van de mergellagen (zowel afkomstig uit ondiepe als diepe bekkens) in fase 3 fossielen van mosselkreeften, weekdieren en dinoflagellaten cysten, welke inheems zijn voor de oostelijke regio van de Paratethyszee. Dit was een uitgestrekt zoetwater meer (Grothe

et al., 2020 en referenties) waarvan de huidige Zwarte, Kaspische en Aral zeeën relicten zijn. Deze Paratethys organismen zouden vermoedelijk gemigreerd naar en verspreid over de hele Middellandse Zee zijn na de plotselinge totstandkoming van nieuwe verbindingen en wateruitwisseling met de Paratethys zee. Dit werd mogelijk teweeg werd gebracht door de stijging van het Middellandse Zee bodemniveau boven de Middellandse Zee-Paratethys-drempel en de daaruit voortvloeiende verbetering van de Middellandse Zee uitstroom (Marzocchi et al., 2016). Deze hydrologische verandering zou hebben plaatsgevonden rond 5.42 Ma (Roveri et al., 2008a, 2014) en leidde er toe dat fase 3 opgesplitst kon worden in twee subfases: de grotendeels fossielloze fase 3.1 en fase 3.2 (ook wel Lago-Mare fase genoemd) die rijk is aan Paratethische biota. Deze sedimentlagen worden vervolgens abrupt opgevolgd door fijnkorrelige gesteentes met marine biota afkomstig van een open zee en waar geen enkele biota uit de Paratethyszee is terug te vinden. Dit getuigt van de, mogelijk catastrofale (Micallef et al., 2018; Garcia-Castellanos et al., 2020), terugkeer van Atlantische Oceaan water in de Middellandse Zee tijdens het vroeg Plioceen.

0.4 Doelstellingen en hoofdlijnen van het proefschrift

De publicatie van Roveri et al. (2014a) biedt een evolutionair scenario voor de MSC en een reconstructie van het mediterrane paleo-milieu en paleo-hydrologie tijdens deze. Echter, verschillende aspecten van deze publicatie werden betwist in recentere studies (bv. Meilijson et al., 2018, 2019; Aloisi et al., 2022) en veel aspecten van elk van de drie fasen blijven onduidelijk. Fase 3 is mogelijk de meest onduidelijke van alle fasen, waarbij geheel verschillende scenario's zijn gepresenteerd. Deze scenario's onderscheiden zich vooral door de herkomst van de waterstromen, de positie van het waterniveau en de connectiviteit tussen de bekkens binnen de Middellandse Zee en met de naburige Atlantische Oceaan en de oostelijke Paratethyszee. Zoals gerapporteerd door Ryan (2009) komen veel van deze discussies voort uit de verschillende perspectieven en de gebruikte methodes. Om het MSC te benaderen gebruiken zeegaande geologen namelijk voornamelijk geofysische hulpmiddelen en DSDP-kernen waarmee gegevens van de verschillende aardlagen op land grotendeels over het hoofd werden gezien. Landgeologen hebben echter alleen secties van randbekkens gemeten en beschreven, waarbij het sedimentaire archief van diepe bekkens grotendeels genegeerd is. Dit proefschrift heeft als doel het waterniveau van de Middellandse Zee en de hydrologische stromen tijdens de derde fase van de Messiniaanse saliniteitscrisis te reconstrueren, door zowel de belangrijkste secties op het land en in de diepe zee (DSDP-ODP kernen) te bestuderen op een oost-westelijke doorsnede van de Middellandse Zee. Deze secties en kernen worden benaderd met een multidisciplinaire strategie die geïntegreerde bio-cyclostratigrafische analyses combineert met radiogene strontium isotoop-records met hoge resolutie ($^{87}Sr/^{86}Sr$).

De sedimenten in fase 3 bevatten voornamelijk zoetwater fossielen, die afkomstig zijn van de Paratethyszee. In dit proefschrift zijn de belangrijkste organismen, mosselkreeften,

beschreven wat kleine schaaldieren zijn (≤1 mm in grootte) die zich beschermen met twee chitine of kalkhoudende kleppen. De keuze is gevallen op deze organismen omdat (I) het vast staat dat de erkende soorten autochtoon zijn, omdat ze nergens in de Middellandse Zee worden vermeld in sedimenten vóór de MSC. Dit betekent dat zij de tijd weerspiegelen van depositie van de sedimenten waarin zij ingebed zijn. (II) de $^{87}Sr/^{86}Sr$-verhoudingen die zijn vastgelegd in deze organismen zijn betrouwbaar voor de wateren waarin ze leefden, omdat hun kleppen gemaakt zijn van calciet laag in Mg, wat onderhevig is aan minimale diagenese (bijv. Marcano et al., 2015), en ze fractioneren de verschillende isotopen van Sr niet (bv. Bista et al., 2021); III) in tegenstelling tot bijvoorbeeld weekdieren, die slechts sporadisch worden aangetroffen. Het is bekend dat mosselkreeften voorkomen in de gehele Middellandse Zee, van Malaga (Guerra-Merchán et al., 2010) tot Cyprus (Rouchy et al., 2001), van het Piëmont bekken in het noorden (Trenkwalder et al., 2008) tot Afrikaanse bekkens in het zuiden (Temani et al., 2020) en zelfs in relatief diepere delen van de Middellandse Zee (Iaccarino en Bossio, 1999; Grossi et al., 2015). Doordat zij overal aanwezig zijn, maakt het gebruik van deze organismen de reconstructie van een hoog resolutie $^{87}Sr/^{86}Sr$ record mogelijk, zowel in ruimte als in tijd.

De analyse van Sr-isotopen is de aangewezen geochemische techniek voor dit proefschrift, omdat dit kan worden gebruikt om de herkomst van water te traceren in specifieke sedimentaire omgevingen dankzij de verschillende isotopenverhouding van $^{87}Sr/^{86}Sr$ die waterbronnen van verschillende herkomst (meestal continentaal of marien) hebben. De karakteristieke Sr-verhouding van de mondiale oceaan en de oostelijke Paratethyszee van het fase 3 interval zijn afgeleid van metingen van kalkhoudend materiaal, afkomstig van tijd-equivalente sedimentaire opeenvolgingen die zich rond en in de diepte van oceanen (McArthur et al., 2012) en in de Zwarte-Kaspische zee bevinden (Grothe et al., 2020). $^{87}Sr/^{86}Sr$-verhoudingen voor de rivieren in het Messiniaanse tijdperk zijn niet beschikbaar, maar kunnen betrouwbaar worden benaderd door er vanuit te gaan dat paleo-rivieren dezelfde $^{87}Sr/^{86}Sr$-verhoudingen hadden als de hedendaagse rivieren. Als er geen $^{87}Sr/^{86}Sr$-verhoudingen van de hedendaagse rivieren beschikbaar zijn in de literatuur, dan kunnen ze met behulp van massabalans berekeningen worden gereconstrueerd door $^{87}Sr/^{86}Sr$-ratios van lithologieën die stroomgebieden van de rivieren vormen. De $^{87}Sr/^{86}Sr$-waarden van rivierwater hangt grotendeels af van het gesteentemateriaal in het stroomgebied, wat zeer variabele $^{87}Sr/^{86}Sr$-waarden kan hebben (bijvoorbeeld: ofiolieten worden gekenmerkt door $^{87}Sr/^{86}Sr$-ratios <0.7060, terwijl plutonische en metamorfe gesteentes $^{87}Sr/^{86}Sr$-ratios >0.7071 geven; Hajj et al. 2017) en oplosbaarheid (evaporieten en carbonaten zijn beter oplosbaar in verhouding tot stollingsgesteente en metamorf gesteente).

De resultaten van deze interdisciplinaire studie wordt in 6 hoofstukken gepresenteerd (Fig. 0.5). **Hoofdstuk 1** is een uitgebreide literatuurstudie van de state-of-the-art kennis van fase 3 (seismische)stratigrafische, sedimentologische, paleontologische en (bio)geochemische data uit de belangrijkste on- en offshore domeinen. Vervolgens worden de voor- en tegenargumenten

besproken van de twee heersende en tegenstrijdige paleo-milieu scenario's:

I. In de derde fase was de Middellandse Zee geïsoleerd van de Atlantische Oceaan en bestonden er ondiepe, endoreïsche bekkens.

II. In de derde fase was de Middellandse Zee gevuld met water afkomstig uit de Atlantische Oceaan, de Paratethyszee en grote rivieren.

Tot slot worden de principes uitgelegd van sommige methodes en proxies die van belang kunnen zijn voor de reconstructie van veranderingen in het bodemniveau en de verbindingen met de oceaan, en zal er een aanbeveling worden gedaan voor de richting van toekomstig onderzoek.

Om deze controverse te tackelen, wordt er begonnen met het onderzoeken van de sub-bekkens die zich aan de periferie van de Middellandse Zee bevonden. Deze zogenaamde marginale bekkens zijn een goede locatie om de isolatie/verbinding (of leeg/vol) te testen, omdat mogelijke verbindingen van de Atlantische Oceaan en/of de oostelijke Paratethyszee vereisen dat het Middellandse Zee bekken relatief vol water was. Hierom wordt er begonnen met drie marginale bekkens (Sorbas, Nijar en Vera) in zuidoost Spanje (**hoofdstuk 2**) en met het diepere, maar meer afgelegen Piëmont bekken (noord Italië), de meest noordelijke zijtak van de Middellandse Zee (**hoofdstuk 3**). Deze bekkens worden onderzocht met een multidisciplinaire aanpak waarbij geïntegreerde sedimentologische en paleontologische analyses worden gecombineerd met hoge resolutie Sr-isotoop documentaties. De zoektocht naar een eenduidig scenario hangt noodzakelijk af van de diepste bekkens. Wat de afzettingen in de randbekkens verklaart, moet ook een verklaring kunnen geven voor de relatief diepe bekkens van de Balearen, Sicilië, Cyprus, Adriatische Zee en noord-centrale Apennijnen. De Eraclea Minoa sectie (Caltanissetta bekken, Sicilië) had tijdens het Messiniaanse tijdperk een intermediaire diepte, en vormt de focus in **hoofdstuk 4**. De sedimentologie, paleontologie en strontium isotoop geochemie van de ontsloten gips-mergelcycli worden onderzocht wat tot een nieuw paleoecologisch en paleohydrologisch model leidt dat een oscillerend hoog-laag waterniveau in de Middellandse Zee schetst tijdens fase 3. In **hoofdstuk 5** wordt de nasleep van dit scenario onderzocht. Namelijk, de mogelijkheid dat de Adriatische regio gedurende (minstens een gedeelte van) fase 3 heeft bestaan als een endoreïsch meer, wat gescheiden was van de Middellandse Zee door een ondiepe drempel ter hoogte van het Gargano schiereiland. Deze regio is onderworpen aan uitgebreide studies, waarbij de chronologie en de aard van de paleoecologische en paleohydrologische veranderingen zijn verbeterd. Tot slot worden in **hoofdstuk 6** de $^{87}Sr/^{86}Sr$-ratios verzameld die onlangs zijn verworven van de drie gips bevattende locaties op een oost-west doorsnede in het Middellandse Zee bassin. Dit zijn: ODP locatie 975B, geboord op de zuidelijke Balearische grens, tussen het Balearische uitsteeksel (Menorca en Mallorca eilanden) en het Algerijnse bekken; ODP locatie 654A, gelegen bij de bovenste grens van Sardinië (Tyrreense bassin); het Polemi bassin (Cyprus), wat de enige plaats naast Sicilië is waar fase 3 gips-mergel cycli op het land zijn ontsloten. Deze gegevens leiden tot

de hypothese dat gips afkomstig uit fase 3 tegelijkertijd uit hetzelfde water precipiteerde door het gehele Middellandse Zeegebied.

0.5 SaltGiant ETN

Dit proefschrift werd uitgevoerd als onderdeel van het SALTGIANT ETN-project, een door de EU gefinancieerd Marie Curie European Training Network (subsidieovereenkomst nummer 765256) dat natuur- en sociale wetenschappers samenbrengt. SALTGIANT brengt 30 academische organisaties (13 begunstigden, 17 partners), 6 particuliere olie- en gasbedrijven, 2 mijnbouwbedrijven, 1 biotechnologiebedrijf, 1 geotechnisch instituut, 1 museum en 1 specialist in overdraagbare vaardigheidstraining uit 12 landen samen. Het wetenschappelijk doel van SALTGIANT is het begrijpen van de vorming van Mediterrane zoutgigant (MSG), wat een van de grootste zoutafzettingen op aarde is, en de implicaties daarvan voor het microbiële leven op/in de zeebodem, de risicobeoordeling in de olie-industrie, de geo-economie van het Middellandse Zeegebied en de geschiedenis van de oceanografie. Het niet-wetenschappelijke doel is het stimuleren van interdisciplinaire en intersectorale kennisuitwisseling tussen deskundigen uit verschillende disciplines, waaronder geologen, geofysici, geochemici, microbiologen, geografen en historici. Dr. Giovanni Aloisi (Institut de Physique du Globe de Paris-CNRS-Universiteit van Parijs) heeft het project gecoördineerd. 15 promovendi vormden de kern van het project. Individuele PhD-projecten werden gegroepeerd in vier werkpakketten (WP). WP1, waar dit proefschrift deel van uitmaakt, is gericht op de ontwikkeling van een uniform model dat de vorming van de MSG verklaart. WP2 was gewijd aan de studie van de diepe microbiële biosfeer in de MSG, die een terrestrische analoog levert voor de hypersaline omgevingen op Mars, waar levensvormen bewaard zouden kunnen zijn gebleven. WP3 had als doel een mechanistisch en kwantitatief inzicht te ontwikkelen in de vroege zoutvervorming en de ontwikkeling van sub-zout overdruk, die door de olie-industrie kan worden gebruikt om de risico's die verbonden zijn aan het boren in de met zout bedekte koolwaterstof landschappen te beperken. WP4 had het tweeledige doel om een geïntegreerde geschiedenis van de ontdekking van de MSG te definiëren en de economische en geopolitieke implicaties te bestuderen.

P-IT

Prologo

0.1 Può un mare cessare di esistere?

L'acqua copre circa il 71% della superficie terrestre. Il 97% del volume d'acqua sulla Terra si trova negli oceani e nei mari. Il rimanente 3% è immagazzinato nelle calotte glaciali e nei ghiacciai (principalmente in Antartide e Groenlandia; 2%), in laghi freschi/salati, mari epicontinentali come il Mar Caspio (0.017%), in atmosfera (0.001%) e nel sottosuolo (0.62%) o scorre nei fiumi (0.0001%). La nostra sopravvivenza è intimamente legata all'esistenza ed alla persistenza di sani ecosistemi aquatici. Ci nutriamo delle forme di vita che abitano oceani, laghi e fiumi, respiriamo l'ossigeno che emanano le forme di vita vegetali che abitano questi ecosistemi, sentiamo il calore delle correnti oceaniche, irrighiamo campi agricoli e gestiamo fabbriche con l'acqua dei laghi, dei fiumi e degli acquiferi. Questi ecosistemi sono in continuo e rapido mutamento e se,[re sul punto di scomparire, a causa dei più disparati fattori naturali e, con l'avvento dell'era industriale, antropogenici. Con una rapida ricerca su qualsiasi motore di ricerca è facile trovare decine di laghi che attualmente si stanno restringendo e prosciugando. L'esempio più calzante è il Mare d'Aral nell'Asia centrale-Europa orientale (compreso tra il Kazakistan a nord e l'Uzbekistan a sud), che è passato dall'essere il quarto lago più grande della Terra negli anni '60, coprendo 68.000 km^2, ad essere l'85% più piccolo nel XXI secolo (Figs. 0.1a-b). I fiumi Syr Darya e Amu Darya, che sono le principali fonti d'approvigionamento del Mare d'Aral, furono deviati ed utilizzati per irrigare i campi di cotone dell'Unione Sovietica. Una volta che il lago fu privato delle sue principali riserve idriche, il livello dell'acqua si abbassò rapidamente e drammaticamente fino al punto di quasi essiccazione. Per citare un esempio più recente di lago che è scomparso per cause naturali: una perla naturale nel cuore delle Alpi occidentali, il Lago di Ceresole (Provincia di Torino, Piemonte, Italia settentrionale), esistente sin dal 1931 come conseguenza dello sbarramento del fiume Orco è, a partire dall'inverno del 2021-2022, per lo più prosciugato a causa di un prolungato periodo di siccità (Figs. 0.1c-d). Infine, data la sua rilevanza per il bilancio idrologico del Mediterraneo durante il Messiniano superiore, di cui questa tesi è oggetto, non possiamo non citare il Lago Ciad, un lago endoreico economicamente importante per l'Africa centrale e le cui dimensioni sono variate notevolmente nel corso dei secoli a causa dei cambiamenti climatici. Secondo Griffin (2002, 2006), durante il Messiniano il Lago Chad, pur restringendosi ed espandendosi con frequenza orbitale a seguito

dello spostamento della Zona di Convergenza Intertropicale, copriva un'area di circa 1-2 Mkm^2 ed era la fonte di un fiume, l'Eosahabi, che drenava nel Mediterraneo nel Golfo di Sirte (Fig. 0.1e). Oggi il fiume Eosahabi non scorre più e il lago Ciad è quattro-sette volte più piccolo (~300 km^2) di quanto non fosse nel Messiniano (Fig. 0.1f). Anche oceani e mari, nonostante siano volumetricamente più grandi di qualsiasi lago, possono cessare di esistere. Attraverso lo spostamento delle placche tettoniche, la superficie della Terra è in costante movimento e la forma e posizione dei continenti e degli oceani in continuo mutamento. Gli oceani che esistevano in un tempo remoto sono stati lentamente inghiottiti nelle zone di subduzione, dove una placca tettonica si immerge sotto un'altra, e sono ora digeriti nel mantello terrestre. Rispetto alla scomparsa di un lago endoreico, la scomparsa di un oceano come risultato della collisione tra due o più placche tettoniche è un processo invisibile per l'essere umano, in quanto ci vogliono alcune centinaia di milioni di anni affinchè una placca scompaia nelle viscere della Terra. Da nessuna parte nei sistemi deposizionali più recenti vi è la prova che un bacino oceanico o un mare epicontinentale abbia completamente cessato di esistere (Warren, 2016). Eppure, ci sono diverse caratteristiche geologiche sepolte al di sotto delle pianure abissali del Mar Mediterraneo ed esposte lungo le sue coste e nelle sue valli montuose che suggeriscono che questo mare oggi brulicante di vita e profondo fino a 5.267 m si sia trasformato, per un breve periodo della sua esistenza (~640.000 anni), in una gigantesca salina priva di vita (Hsü et al., 1973a). La presunta scomparsa del Mar Mediterraneo è storia geologica relativamente recente, essendo avvenuta solo 6-5 milioni di anni fa circa, e costituisce uno tra i puzzle scientifici più affascinanti, conosciuto come Crisi di Salinità del Messiniano.

0.2 Storia della Crisi di Salinità del Messiniano del bacino Mediterraneo

Negli anni '50, era diffusa la conoscenza che presenza di rocce evaporitiche le sequenze marine del Messiniano superiore e del Pliocene preservate in alcuni bacini spagnoli ed italiani erano interrotte da spesse sequenze evaporitiche (es. Selli, 1954, 1960; Ogniben, 1957). Le evaporiti sono rocce sedimentarie chimiche comprendenti una vasta gamma di minerali, di cui l'alite (NaCl) ed il gesso ($CaSO_4$*$2H_2O$) costituiscono i volumi più grandi, che cristallizzano in ordine inverso rispetto alla loro solubilità al diminuire del volume d'acqua e all'aumento della densità e della salinità della salamoia (Fig. 0.2; Usiglio, 1849). Tipicamente, la precipitazione evaporitica si verifica in bacini endoreici costituiti da acqua di mare (evaporiti marine) o acque continentali (evaporiti non marine) dove l'evaporazione supera l'afflusso (Warren, 2016). La precipitazione evaporitica richiede quindi condizioni particolari per iniziare che si trovano solo in pochi luoghi sulla Terra (per esempio, le evaporiti moderne sono limitate alle regioni aride). Questo è possibilmente il motivo per cui le rocce evaporitiche non sono comuni nel record geologico, costituendo meno del 5% del volume delle rocce sedimentarie, e dove sono presenti indicano l'esistenza di condizioni ambientali estreme (vedi Warren, 2016 per approfondimenti). Sulla base di quanto sopra, quindi, l'improvvisa interruzione, in questi

ambienti marginali del Mar Mediterraneo, di milioni di anni di sedimentazione marina e l'improvviso inizio della formazione di evaporiti portò all'attenzione della comunità scientifica che la periferia del Mediterraneo subì una crisi di salinità alla fine del Miocene. La riduzione e/o interruzione degli interscambi idrologici tra il Mar Mediterraneo e l'oceano Atlantico, che è il più grande serbatoio di ioni e molecole che formano le evaporiti, era stato ipotizzato come la possibile causa di questa crisi di salinità (Ogniben, 1957). Questo è uno scenario apocalittico. Sappiamo dagli studi dei sedimenti oceanici pre- e post-Messiniani che il Mediterraneo era, già durante il Miocene superiore, un bacino con profondità massime superiori alle migliaia di metri (Hsü et al., 1978a). A causa della sua posizione alle medie latitudini, il bilancio idrologico del Mediterraneo è, su base annua, negativo. Il che significa che perde più acqua (e calore) verso l'atmosfera per evaporazione di quanto ne guadagni dalle precipitazioni e dagli afflussi continentali superficiali e sotterranei (e.g. Skliris et al., 2018). Oggi, lo scambio d'acqua che avviene attraverso lo Stretto di Gibilterra (largo 13 km e con profondità massima di 320 m), con la relativamente calda e poco salata (15.4°C, 36.2 g/kg) acqua atlantica che si fa strada nel Mediterraneo in superficie, mentre la relativamente più fredda e salata (13°C, 38.4 g/kg) acqua del Mediterraneo esce in direzione dell'Atlantico più in profondità (Bryden et al., 1994; Tsimplis e Bryden 2000), compensa questa perdita netta annua di acqua e permette al Mediterraneo di rimanere pieno al livello dell'Atlantico. Se questo collegamento dovesse scomparire o ridursi in maniera sostanziale, a causa del bilancio idrologico negativo il livello del mare nel Mediterraneo si abbasserebbe di oltre 2000 metri in 3000-8000 anni ed il bacino si trasformerebbe in un grande e profondo deserto di sale (Meijer e Krijgsman, 2005). Poiché fino agli anni '60 queste evaporiti erano conosciute solo in bacini marginali, qualcosa di meno catastrofico poteva fornire una spiegazione ugualmente plausibile. I movimenti tettonici locali e/o piccoli abbassamenti del livello degli oceani potrebbero aver facilmente causato un calo del livello del mare nel Mediterraneo di pochi metri/decine di metri, che sarebbe stato sufficiente ad isolare temporaneamente le sue aree costiere dalla circolazione oceanica globale. Poi, l'evaporazione avrebbe preso il sopravvento sul circuito idrologico di questi bacini endoreici, causando la progressiva caduta del livello dell'acqua marina residua, la concentrazione dei sali in soluzione e la precipitazione dei minerali evaporitici (Fig. 0.2). Questo è probabilmente il motivo per cui, fino agli anni '60 circa, la scoperta della presenza di evaporiti in località marginali del Mediterraneo non ha attirato troppa curiosità tra la comunità scientifica. Alla fine degli anni '60-'70, diverse campagne oceanografiche rivelarono che evaporiti messiniane nel Mediterraneo non erano solo confinate alla sua periferia. Le linee sismiche dei fondali del Mediterraneo evidenziarono come sia presente uno strato di sale spesso 1.5-2 chilometri in gran parte del bacino e da cui dipartono strutture diapiriche (es. Alinat e Cousteau, 1962; Cornet, 1968). L'esistenza di salgemma al di sotto delle piane abissali del Mediterraneo è stata confermata, nel 1970, dal progetto americano di ricerca oceanografica noto come "progetto di perforazione in mare profondo (acronimo inglese: DSDP)" realizzato per mezzo della nave oceanografica

da perforazione Glomar Challenger (Ryan et al., 1973). Oltre all'alite, tramite questo progetto di perforazione è stata individuata anche la presenza di gesso, anidrite e dolomite. Per mezzo di queste campagne oceanografiche, è stata anche documentata la presenza di numerosi canyon erosivi sottostanti le attuali valli fluviali di grandi fiumi come il Nilo, il Rodano, il Var e l'Ebro (Barber, 1981; Chumakov, 1973; Clauzon, 1982). Almeno tre degli scienziati a bordo della Glomar Challenger, vale a dire Kenneth J. Hsü, Maria Bianca Cita e William B.F. Ryan, erano convinti che la presenza di evaporiti sul fondo di un bacino oggi profondo più di 4 km e che fino alla precipitazione delle prime evaporiti stava depositando sedimenti pelagici in un mare che brulicava di vita fosse un indizio che qualcosa di catastrofico fosse accaduto. Come affermano nelle conclusioni della pubblicazione sulla rivista scientifica Nature in cui presentano per la prima volta il modello del " bacino profondo disseccato" (Hsü et al., 1973a, p. 244), "il fatto improbabile che sotto i fondali del Mar Mediterraneo si trovi un giacimento di sale richiede una spiegazione altrettanto improbabile". Secondo questa teoria, i movimenti tettonici nell'area di Gibilterra e/o l'abbassamento eustatico del livello marino globale avrebbero chiuso definitivamente il corridoio (o i corridoi marini) che assicurava gli scambi idrici tra l'Oceano Atlantico ed il Mediterraneo. Il conseguente bilancio idrologico negativo avrebbe provocato un abbassamento del livello del mare nel Mediterraneo di oltre 1 km, riducendo quest'ultimo ad una serie di laghi salati poco profondi all'interno dei quali sarebbe avvenuta la deposizione delle evaporiti (Fig. 0.3). Altrettanto biblico è lo scenario previsto da questa teoria per il ripristino delle condizioni di mare aperto analoghe al periodo pre-crisi di salinità e che persistono fino ad oggi e che prevede il crollo di un muro di roccia a Gibilterra (con la formazione dell'attuale stretto) seguito da una mega alluvione che avrebbe portato ad un rapido riempimento del Mediterraneo. Questo scenario è stato accolto con scetticismo sia tra gli scienziati a bordo della Glomar Challenger, con diverse interpretazioni alternative che sono state proposte (Volume 13, Rapporti iniziali), che da altri scienziati che non hanno partecipato alla spedizione (vedi Drooger, 1973, che è una raccolta di articoli successivi al primo convegno sul messiniano tenutosi ad Utrecht nel 1973). Tuttavia, per quanto scioccante ed improbabile lo scenario raffigurato da Hsü et al. (1973a) possa sembrare (gli stessi autori modello del " bacino profondo disseccato", in Hsü et al., 1973b, p. 1203, hanno ammesso che l'idea che un mare delle dimensioni del Mediterraneo possa effettivamente prosciugarsi e lasciare un grande buco a migliaia di metri sotto il livello del mare mondiale sembra davvero assurda"), ha registrato un importante successo nei decenni successivi perché era l'unico modello in grado di fornire una spiegazione plausibile alla maggior parte dei dati disponibili ed in fase di acquisizione. Il modello del "bacino profondo disseccato" divenne così il paradigma della crisi di salinità messiniana, elevandola allo status di uno degli eventi paleoceanografici più drammatici della storia della Terra e generando un'esplosione di interesse scientifico e pubblico. Ciò che rende la crisi di salinitá del Messiniano un evento geologico ancora più straordinario è la sua durata estremamente breve. Infatti, solo ~640.000 anni separano la deposizione del primo gesso nelle

successioni marginali spagnole e italiane a 5.96±0.02 milioni di anni (Krijgsman et al., 1999a) e il ritorno delle condizioni di mare aperto a 5.332 milioni di anni (Van Couvering et al., 2000). Ciò che è realmente accaduto nel mezzo è ancora un affascinante mistero.

0.3 Conoscenze aggiornate sulla Crisi di Salinità del Messiniano

Nonostante l'ampio consenso che il modello del "bacino profondo disseccato" ha ricevuto durante gli anni '80-'90 e che ancora oggi riceve, nel corso degli anni sono aumentate le evidenze che il Mediterraneo non si è mai totalmente prosciugato e che, almeno durante alcuni periodi della crisi, non era totalmente isolato (es. McCulloch e De Deckker, 1989; Roveri et al., 2001; Hardie and Lowenstein, 2004; Lugli et al., 2015). Invece, una serie di altri aspetti sono rimasti controversi tra i diversi gruppi di ricerca, come ad esempio:

(i) la principale causa scatenante della crisi di salinità (tettonica vs clima);

(ii) la durata dei cambiamenti paleoidrologici e paleoambientali riconosciuti nel record sedimentario (vale a dire l'inizio e la fine delle diverse fasi riconosciute da Roveri et al., 2014a; vedi sotto);

(iii) la provenienza geografica dei flussi d'acqua (ad es. la presenza, permanente o temporanea, di scambi idrici tra il Mediterraneo ed i vicini regni acquatici dell'Atlantico, Mar Rosso e Paratetide);

(iv) l'esatta posizione del livello di base nel Mediterraneo in ciascuna delle fasi menzionate sopra;

(v) l'equivalente in mare aperto delle unità evaporitiche definite sulla terraferma e viceversa.

Questi e molti altri argomenti controversi sono descritti (e citati) in modo completo nel lavoro di Roveri et al. (2014a). Oltre a fornire una panoramica della storia e delle controversie relative alla crisi di salinità messiniana, Roveri et al. (2014a) mette ordine nella comprensione degli eventi che hanno portato a, sono accaduti durante e si sono verificati successivamente alla crisi. Di seguito forniamo una sintesi dell'evoluzione della crisi di salinità del Messiniano secondo Roveri et al. (2014a).

La riduzione degli scambi idrici tra l'oceano Atlantico e il bacino Mediterraneo sono ampiamente considerati il fattore scatenante della crisi di salinità. A differenza di oggi, durante il Miocene superiore il collegamento tra l'oceano Atlantico e il Mar Mediterraneo era assicurato da una serie di corridoi marini che attraversavano la cordigliera Betica nel sud della Spagna e la cordigliera Rifiana nel nord del Marocco (Fig. 0.4; Flecker et al., 2015; Capella et al. 2017, 2018; Krijgsman et al., 2018). Mentre queste catene montuose si sollevavano nel contesto dell'orogenesi alpina, questi corridoi si chiudevano uno ad uno, lasciando (forse) solo uno stretto passaggio attraverso l'attuale Stretto di Gibilterra (Fig. 0.4; Krijgsman et al., 2018). Le prime evidenze di cambiamenti ecologici legati alla progressiva riduzione degli scambi idrici tra il Mediterraneo e l'Atlantico sono state documentate a cavallo del limite Tortoniano/Messiniano nelle popolazioni dei foraminiferi bentonici, le quali indicano una maggiore sensibilità del

Mediterraneo al deflusso continentale ed un aumento della stratificazione della colonna d'acqua con conseguente instaurazione di condizioni poco ossigenate sul fondale (es. Kouwenhoven et al. 1999, 2003; Bulian et al., 2021). La risposta del Mediterraneo a questa riduzione degli scambi idrici non è stata lineare; steps importanti, consistenti nell'instaurazione di diverse condizioni paleoceanografiche ed ecologiche, sono riconosciuti a 6.72, 6.35 Ma e 5.96 milioni di anni (vedi Corbí et al., 2020 e le referenze in esso contenute per maggiori dettagli). La precipitazione dei primi strati di gesso a 5.96±0.02 Ma, che segna l'inizio della fase 1 della crisi di salinità (sensu Roveri et al., 2014a), si pensa sia dovuta ad un'esacerbazione della stratificazione colonna d'acqua indotta dal continuo afflusso di acqua dolce in un bacino sempre più isolato (es. Natalicchio et al., 2019; Sabino et al., 2020, 2021). Il gesso è precipitato principalmente in bacini marginali poco profondi, mentre argilliti ricche di sostanze organica si sono deposte in acque più profonde (Roveri et al., 2003; Manzi et al., 2005; Lugli et al., 2010; Dela Pierre et al., 2011; Natalicchio et al., 2019; Sabino et al., 2020, 2021). È pensiero abbastanza comune che gli scambi idrici tra il Mediterraneo e l'Atlantico siano continuati per tutta la durata della fase 1, anche se in misura ridotta rispetto alla fase pre-crisi (Krijgsman et al., 2018). La transizione alla fase 2 (5.59-5.55 Ma) consisterebbe nella terminazione, per motivi legati ai movimenti tettonici e/o eustatici, del deflusso del Mediterraneo verso l'Atlantico (ad es. Krijgsman e Meijer, 2008; Krijgsman et al., 2018) e al conseguente abbassamento del livello di base del Mediterraneo di centinaia, se non migliaia, di metri (ad es. Roveri et al., 2014a). Durante questo stadio, considerato come l'acme della crisi di salinità, i margini continentali del Mediterraneo subirono un'importante erosione, testimoniata dalla presenza di unità caotiche ai piedi delle scarpate, mentre la deposizione evaporitica si è spostata verso i bacini più profondi, dove si sono accumulati grandi spessori di salgemma e, in misura minore, i sali di potassio (es. Hsü et al., 1978a; Lugli et al., 1999). La precipitazione di gesso è ripresa nella fase 3 (5.55-5.332 Ma) negli stessi bacini che durante la fase 2 avevano accumulato salgemma. Contemporaneamente, successioni prevalentemente terrigene e prive di gesso si depositavano nei bacini marginali. Analogamente allo stadio 1, gli strati di gesso accumulatisi nella fase 3 si alternano con orizzonti marnosi e si ritiene che questi cicli litologici siano l'espressione sedimentaria una ciclicità climatica ad alta frequenza (cicli arido-umido) controllati da cambiamenti nei parametri orbitali di eccentricità e precessione (Hilgen et al., 2007; Manzi et al., 2009). A differenza dello stadio 1, tuttavia, molti degli strati marnosi dello stadio 3, specialmente nei bacini marginali ed in misure minore nei bacini profondi, contengono ostracodi, molluschi e dinocisti endemiche della Paratetide orientale, un vasto lago di acqua salmastra (es. Grothe et al., 2020) di cui gli attuali Mar Nero, Mar Caspio e lago d'Aral sono le uniche tracce rimaste della sua esistenza. Si ritiene che questi organismi paratetidei siano migrati e si siano diffusi nel Mediterraneo a partire da 5.42 Ma in seguito all'improvvisa instaurazione di un più efficiente scambio idrico tra il Mediterraneo e la Paratetide (Roveri et al., 2008a, 2014a). È stato ipotizzato che questa "maggiore efficienza" della connessione Mediterraneo-Paratetide consista in un aumento del

flusso d'acqua salmastra dalla Paratetide a seguito dall'innalzamento del livello di base nel Mediterraneo al di sopra della soglia Mediterraneo-Paratetide (Marzocchi et al., 2016). Secondo Roveri et al. (2008a, 2014a) tale evento sarebbe sincrono a scala del Mediterraneo e datato a 5.42 Ma. Questo ha portato Roveri et al. (2014a) a suddividere la fase 3 in un sottostadio 3.1 per la maggior parte sterile di organismi e un sottostadio 3.2 (o fase Lago-Mare) ricco di organismi Paratetidei. I sedimenti dello stadio 3 sono ricoperti da sedimenti a grana fine prive di elementi della Paratetide e ricchi di organismi marini che testimoniano un definitivo, forse catastrofico (Micallef et al., 2018; Garcia-Castellanos et al., 2020), ritorno delle condizioni di mare aperto nel Mediterraneo all'inizio del Pliocene.

0.4 Obiettivi e struttura della tesi

La pubblicazione di Roveri et al. (2014a) propone uno scenario evolutivo per la crisi di salinità messiniana ed una ricostruzione del paleoambiente e della paleoidrologia del Mediterraneo durante questo evento che concordano con molti dati esistenti. Tuttavia, diversi aspetti della pubblicazione di Roveri et al. (2014a) sono stati messi in dubbio da studi più recenti (es. Meilijson et al., 2018, 2019; Aloisi et al., 2022) e molte domande rimangono dibattute per ciascuna delle tre fasi. La fase 3 rimane, forse, la più ambigua. Nel corso degli anni è stata presentata una moltitudine di modelli paleoambientali e paleoidrologici piú o meno diversi gli uni dagli altri per quanto concerne la provenienza dei flussi d'acqua, la posizione del livello di base nel Mediterraneo e la connettività tra bacini del Mediterraneo e con i vicini oceano Atlantico, Mar Rosso e Paratetide orientale. Come riportato da Ryan (2009), l'assenza di uno scenario comune e la presenza di molte controversie derivano dai diversi metodi utilizzati dagli scienziati di mare, che hanno approcciato e tutt'ora approcciano lo studio della MSC con strumenti geofisici ed i pozzi DSDP-ODP trascurando i dati provenienti dagli affioramenti, e dai geologi di terreno, che hanno posto particolare attenzione alle sezione stratigrafiche a terra e ignorando ampiamente l'archivio sedimentario dei bacini profondi.

Lo scopo principale di questo progetto di dottorato di ricerca è quello di ricostruire la posizione del livello dell'acqua nel Mar Mediterraneo e la provenienza geografica dei flussi idrologici durante la fase terminale della crisi di salinità messiniana attraverso lo studio delle principali successioni stratigrafiche affioranti sulla terraferma e rinvenute nei pozzi profondi disposte su un transetto E-W che attraversa tutto il bacino. Queste successioni sono state studiate mediante un'analisi multidisciplinare che integra analisi biociclostratigrafiche con analisi ad alta risoluzione degli isotopi radiogenici dello stronzio ($^{87}Sr/^{86}Sr$).

I sedimenti della fase 3 contengono principalmente fossili salmastri endemici della Paratetide. Tra i tanti organismi originari della Paratetide, in questo lavoro ci focalizziamo sugli ostracodi, che sono piccoli crostacei, tipicamente delle dimensioni di 1 millimetro, il cui corpo è protetto da una "conchiglia" in chitina o in calcare. Tre sono le ragioni principali di questa scelta: (I) le specie riconosciute sono certamente autoctone perché da nessuna parte nel

Mediterraneo sono riportate in sedimenti che pre-datano l'inizio della crisi. Ciò significa che la loro presenza e qualsiasi proxy ottenuto mediante la loro analisi riflettono le condizioni al tempo della deposizione dei sedimenti in cui sono incorporati; (ii) sono un archivio affidabile del rapporto isotopico $^{87}Sr/^{86}Sr$ dell'acqua in cui risiedevano, perché le loro valve sono fatte di calcite a basso contenuto di magnesio, che è poco soggetta a trasformazioni durante la diagenesi (ad es. Marcano et al., 2015), e non frazionano i diversi isotopi dello stronzio (es. Bista et al., 2021); (iii) a differenza, ad esempio, dei molluschi, che sono solo sporadicamente ritrovati nei sedimenti della fase 3, gli ostracodi sono presenti in tutto il Mediterraneo, da Malaga (Guerra-Merchán et al., 2010) a Cipro (Rouchy et al., 2001), dal bacino piemontese nella parte piú settentrionale del Mediterraneo (Trenkwalder et al., 2008) alle località africane a sud (Temani et al., 2020) e anche in ambienti relativamente più profondi (Iaccarino e Bossio, 1999; Grossi et al., 2015). Pertanto, la loro presenza ubiquitaria consente la ricostruzione di un record di $^{87}Sr/^{86}Sr$ ad alta risoluzione sia nello spazio che nel tempo. Il rapporto isotopico $^{87}Sr/^{86}Sr$ è lo strumento geochimico preferito per questo lavoro perché, a causa delle diverse firme isotopiche che caratterizzano le fonti d'acqua di diversa origine (per lo più continentali vs marine), possono essere utilizzati per tracciare la provenienza dell'acqua in specifici ambienti sedimentari. La firma isotopica dell'acqua marina e della Paratetide orientale durante la fase 3 della crisi di salinità sono note e derivano dalle analisi isotopiche effettuate su materiale calcareo contenuto in successioni sedimentarie tempo-equivalenti dei sedimenti della fase 3 nel Mediterraneo situate in profondità negli oceani (McArthur et al., 2012) e lungo le coste del Mar Nero e del Mar Caspio (Grothe et al., 2020). Le firma isotopiche dei fiumi Messiniani non sono disponibili, ma possono essere approssimate supponendo che i paleofiumi avessero un $^{87}Sr/^{86}Sr$ simile a quello dei fiumi attuali. Se gli $^{87}Sr/^{86}Sr$ dei fiumi attuali non sono disponibili in letteratura, allora la firma isotopica dello stronzio dei fiumi messiniani può essere ricostruita, con l'aiuto di calcoli del bilancio di massa, utilizzando i rapporti isotopici delle litologie che formano i bacini idrografici dei fiumi attuali. Infatti, i valori isotopici dello stronzio dell'acqua fluviale dipendono in gran parte dalle litologie che vengono drenate, le quali, a loro volta, hanno un $^{87}Sr/^{86}Sr$ altamente variabile (es. le ofioliti sono caratterizzate da $^{87}Sr/^{86}Sr<0.7060$, mentre le rocce acide plutoniche e metamorfiche producono $^{87}Sr/^{86}Sr>0.7071$; es. Hajj et al., 2017) e solubilità (evaporiti e carbonati sono più solubili rispetto alle rocce basiche ignee e metamorfiche).

I risultati di questo studio interdisciplinare su scala mediterranea sono presentati in 6 capitoli (Fig. 0.5). Il **capitolo 1** è una rassegna completa dello stato dell'arte delle conoscenze (sismo)stratigrafiche, sedimentologiche, paleontologiche e (bio)geochimiche dei domini onshore e offshore e degli argomenti a favore e contro i due scenari paleoambientali che più di tutti giustificano i dati esistenti:

(i) lo scenario in cui, durante lo stadio 3, il Mediterraneo era isolato dall'Atlantico e puntellato da laghi endoreici poco profondi;

(ii) Lo scenario di un Mediterraneo pieno di acqua dall'Atlantico, dalla Paratetide e dai

grandi sistemi fluviali.

Infine, evidenziamo i principi di funzionamento di alcuni metodi e proxy che possono essere di aiuto per ricostruire i cambiamenti del livello di base e della connettività del Mediterraneo e proponiamo la direzione che le ricerche future sul tema dovrebbero intraprendere per giungere ad uno scenario comune. Questa controversia viene inizialmente affrontata mediante lo studio dei bacini situati lungo la periferia del Mediterraneo. I cosiddetti bacini marginali si trovano, infatti, in una posizione batimetrica ideale per testare la disputa Mediterraneo vuoto ed isolato vs pieno e connesso, poiché evidenze dai bacini marginali di uno scambio idrico con l'Atlantico e/o le Paratetide orientale automaticamente implicano che il bacino del Mediterraneo fosse relativamente pieno. Abbiamo quindi cominciato da tre bacini marginali (Sorba, Nijar e Vera) nel sud-est della Spagna (**capitolo 2**) e dal più profondo, ma più remoto, bacino Piemontese (N Italia) alla propaggine più settentrionale del Mediterraneo (**capitolo 3**), combinando analisi sedimentologiche e paleontologiche con analisi ad alta risoluzione del rapporto isotopico $^{87}Sr/^{86}Sr$. La ricerca di uno scenario uniformante, però, dipende necessariamente anche dai bacini più profondi. Lo scenario che fornisce una spiegazione dei depositi situati intorno alla periferia del Mediterraneo e all'estremità settentrionale del bacino Adriatico deve anche provvedere a spiegare i depositi tempo-equivalenti che si sono accumulati nei bacini delle Baleari, della Sicilia, dello Ionio, di Cipro e nell'Appennino centro-settentrionale. La sezione di Eraclea Minoa (Bacino di Caltanissetta, Sicilia), avendo una posizione intermedia, durante il Messiniano, tra i bacini spagnoli e quelli profondi, rappresenta il fulcro del **capitolo 4**. Abbiamo studiato la sedimentologia, la paleontologia ed il rapporto isotopico $^{87}Sr/^{86}Sr$ dei cicli gesso-marna splendidamente esposti ad Eraclea Minoa e proponiamo un modello paleoambientale e paleoidrologico che favorisce lo scenario in cui il livello di base del Mediterraneo era soggetto ad ampie fluttuazioni durante la fase 3. Nel **capitolo 5** esaminiamo un'immediata conseguenza dello scenario proposto nel capitolo 4, vale a dire la possibilità che per almeno una parte della fase 3, la regione adriatica esistesse come un lago endoreico separato dal Mediterraneo dalla soglia del Gargano, dove un rilievo montuoso si elevava al largo. Questa regione è stata oggetto di numerosi studi approfonditi, ma la cronologia e la natura dei suoi cambiamenti paleoambientali e paleoidrologici devono essere meglio vincolate. Infine, il **capitolo 6** raccoglie i rapporti isotopici $^{87}Sr/^{86}Sr$ recentemente acquisiti da altre tre località, su un transetto E-W attraverso il Mediterraneo, in cui si trovano strati di gesso tempo-equivalenti a quelli affioranti in Sicilia. Queste località sono: il sito ODP 975B trivellato sul margine meridionale del Bacino Balearico tra il promontorio Balearico (vale a dire l'alto strutturale dove sono situate le isola Minorca e Mallorca) ed il bacino algerino; il sito ODP 654A situato sul margine superiore della Sardegna (bacino Tirrenico); il bacino di Polemi (Cipro), che è l'unico altro luogo, oltre alla Sicilia, dove affiorano i cicli litologici gesso-marna della fase 3 della crisi di salinità messiniana. Questi dati aggiungono una prospettiva piú "Mediterranean" e "profonda (in termini batimetrici)" all'ipotesi avanzata con lo studio di Eraclea Minoa che gli strati di gesso della fase

3 sono precipitati in maniera sincrona dalla stessa massa d'acqua.

0.5 Il progetto ETN SaltGiant

Questa tesi è stata realizzata come parte del progetto SALTGIANT ETN, un progetto Marie Curie per la formazione e la mobilità dei dottorandi finanziato dall'Unione Europea (accordo di sovvenzione numero 765256) che ha riunito scienziati naturali e sociali. Più specificamente, il progetto SALTGIANT ha riunito 30 organizzazioni accademiche (13 beneficiari, 17 partner), 6 aziende del settore privato Oil&Gas, 2 aziende del settore minerario, 1 società di biotecnologie, 1 istituto geotecnico, 1 museo e 1 specialista in formazione di competenze trasferibili da 12 paesi. L'obiettivo scientifico di SALTGIANT è stato la comprensione della formazione del gigante salino del Mediterraneo, uno dei più grandi giacimenti di sale sulla Terra, e le sue implicazioni per la vita microbica sub-marina, la valutazione del rischio nell'industria petrolifera, la geo-economia della regione mediterranea e la storia dell'oceanografia. L'obiettivo non scientifico è stato quello di stimolare lo scambio di conoscenze interdisciplinari e intersettoriali tra esperti di varie discipline, tra cui geologi, geofisici, geochimici, microbiologi, geografi e storici. Il Dr. Giovanni Aloisi (Institut de Physique du Globe de Paris-CNRS-University of Paris) ha coordinato brillantemente il progetto. 15 dottorandi hanno costituito la colonna portante del progetto. I singoli progetti di dottorato sono stati raggruppati in quattro pacchetti di lavoro (WP). WP1, di cui questa tesi fa parte, ha avuto come scopo principale quello di sviluppare un modello paleoambientale e paleoidrologico che fornisse una spiegazione comprensiva alla formazione del MSG. WP2 è stato dedicato allo studio della biosfera microbica presente nel MSG, il quale fornisce un analogo terrestre per gli ambienti ipersalini di Marte, dove forme di vita potrebbero essere state conservate. Il WP3 mirava a sviluppare una comprensione meccanicistica e quantitativa della deformazione del sale e dello sviluppo della sovrappressione sub-salina che può essere utilizzata dall'industria petrolifera per mitigare i rischi associati alle trivellazioni nelle province in cui ci sono riserve di idrocarburi ricoperte di sale. Il WP4 ha avuto il duplice obiettivo di ricostruire la storia della scoperta del MSG e di studiare le implicazioni economiche e geopolitiche della mappatura dei grandi giacimenti di sale a causa della loro associazione con serbatoi di gas naturale.

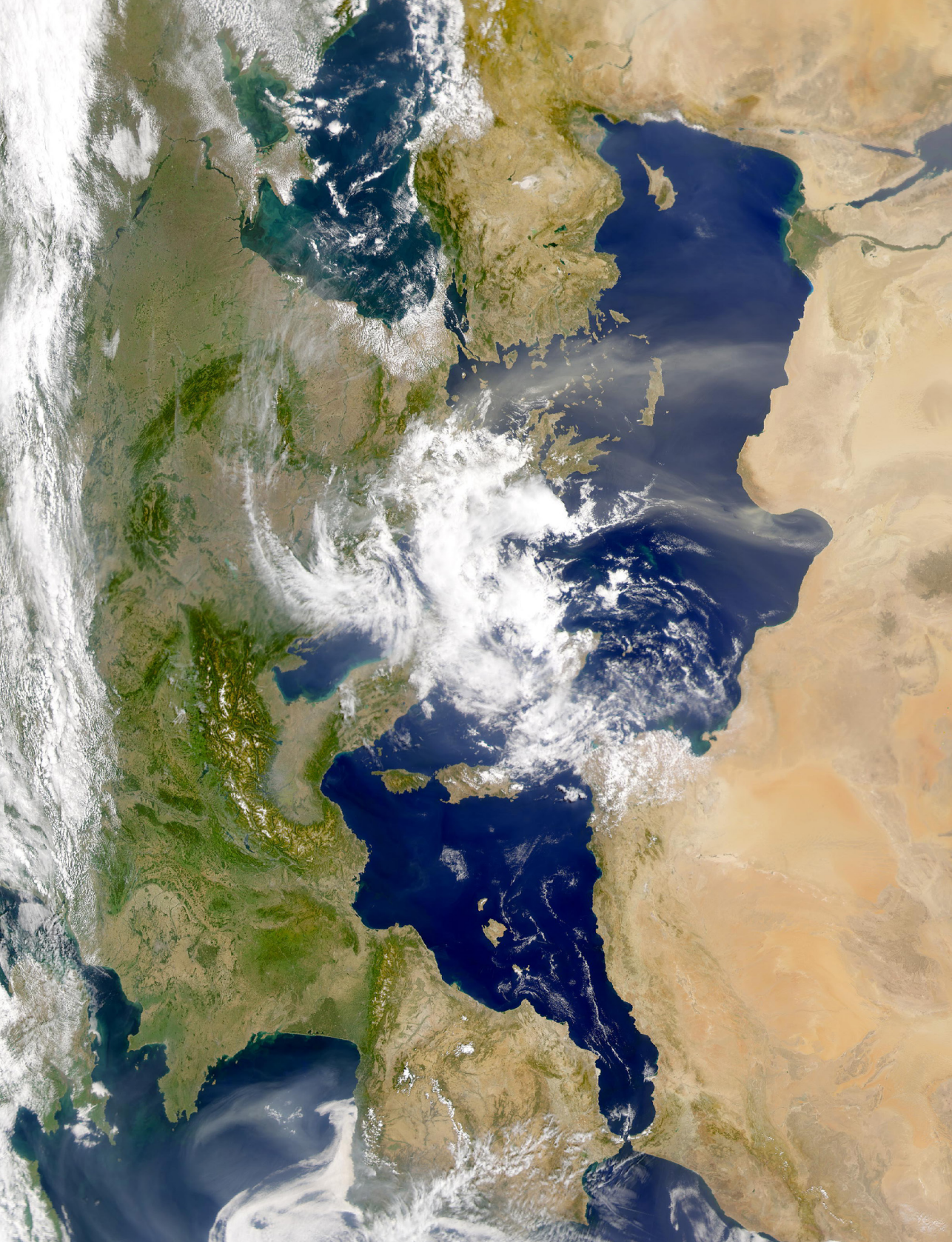

The Mediterranean Sea on September 10, 2000, ~6 million years after its alleged disappearance during the Messinian Salinity Crisis event (Credit: NASA).

1

FRESHENING OF THE MEDITERRANEAN SALT GIANT: CONTROVERSIES AND CERTAINTIES AROUND THE TERMINAL (UPPER GYPSUM AND LAGO-MARE) PHASES OF THE MESSINIAN SALINITY CRISIS

Andreetto, F., Aloisi, G., Raad, F., Heida, H., Flecker, R., Agiadi, K., Lofi, J., Blondel, S., Bulian, F., Camerlenghi, A., Caruso, A., Ebner, R., Garcia-Castellanos, D., Gaullier, V., Guibourdenche, L., Gvirtzman, Z., Hoyle, T.M., Meijer, P.T., Moneron, J., Sierro, F.J., Travan, G., Tzevahirtzian, A., Vasiliev, I., Krijgsman, W.

ABSTRACT

The late Miocene evolution of the Mediterranean Basin is characterized by major changes in connectivity, climate and tectonic activity resulting in unprecedented environmental and ecological disruptions. During the Messinian Salinity Crisis (MSC, 5.97-5.332 Ma) this culminated in most scenarios first in the precipitation of gypsum around the Mediterranean margins (Stage 1, 5.97-5.60 Ma) and subsequently >2 km of halite on the basin floor, which formed the so-called Mediterranean Salt Giant (Stage 2, 5.60-5.55 Ma). The final MSC Stage 3, however, was characterized by a "low-salinity crisis", when a second calcium-sulfate unit (Upper Gypsum; substage 3.1, 5.55-5.42 Ma) showing (bio)geochemical evidence of substantial brine dilution and brackish biota-bearing terrigenous sediments (substage 3.2 or Lago-Mare phase, 5.42-5.332 Ma) deposited in a Mediterranean that received relatively large amounts of riverine and Paratethys-derived low-salinity waters. The transition from hypersaline evaporitic (halite) to brackish facies implies a major change in the Mediterranean's hydrological regime. However, even after nearly 50 years of research, causes and modalities are poorly understood and the original scientific debate between a largely isolated and (partly) desiccated Mediterranean or a fully connected and filled basin is still vibrant. Here we present a comprehensive overview that brings together (chrono)stratigraphic, sedimentological, paleontological, geochemical and seismic data from all over the Mediterranean. We summarize the paleoenvironmental, paleohydrological and paleoconnectivity scenarios that arose from this cross-disciplinary dataset and we discuss arguments in favour of and against each scenario.

This chapter is peer-reviewed and published as:
Andreetto, F., Aloisi, G., Raad, F., Heida, H., Flecker, R., [...]., Krijgsman, W., 2021. Freshening of the Mediterranean Salt Giant: Controversies and certainties around the terminal (Upper Gypsum and Lago-Mare) phases of the Messinian Salinity Crisis. Earth-Science Reviews 216, 103577.

1.1 Introduction

At the end of the Miocene, orbital and tectonic drivers combined to alter the amount of water delivered to the Mediterranean Basin by the Atlantic Ocean from the west, the brackish Eastern Paratethys (i.e. Euxinic-Caspian Basin system) from the east and the major peri-Mediterranean freshwater drainage systems (e.g. African rivers and Rhône; Griffin, 2002; Gladstone et al., 2007; Van der Laan et al., 2006; Hilgen et al., 2007; Ryan, 2009; Flecker et al., 2015; Marzocchi et al., 2015, 2016, 2019; Simon et al., 2017; Krijgsman et al., 2018; Capella et al., 2020). The changes in extra and intrabasinal connectivity resulted in unprecedented paleoceanographic and paleohydrological budget changes that led to a relatively short-lived environmental and ecological crisis (approx. 660 kyr; 5.97-5.33 Ma), for which the term Messinian Salinity Crisis (MSC) was coined (Selli, 1954, 1960). Most conspicuous was the rapid accumulation of several kilometers of halite (i.e. ~1 million km^3) on the Mediterranean abyssal plains (e.g. Hsü, 1972; Ryan, 1973; Montadert et al., 1978; Haq et al., 2020). This happened within 50 kyr, from 5.60-5.55 Ma, according to Roveri et al. (2014a) and Manzi et al. (2018), or in >300 kyr, when starting at 5.97 Ma, as put forward by Meilijson et al. (2018, 2019).

During the ~200 kyr lapse (i.e. MSC Stage 3 following Roveri et al., 2014a; Fig. 1.1a) between the end of salt precipitation (5.55 Ma) and the restoration of the still enduring marine conditions (5.332 Ma), the Mediterranean underwent a sequence of paleohydrological and base-level changes that are the topic of intense and long-standing debates. The initial and still widely endorsed hypothesis was that the Mediterranean Sea, following the major drawdown event that led to halite deposition (i.e. Stage 2), maintained the isolated, deeply-desiccated geography containing a series of hypersaline (substage 3.1; 5.55-5.42 Ma) and hyposaline (substage 3.2; 5.42-5.33 Ma) ponds which only received water from local streams and were colonized by Black Sea organisms carried by aquatic migratory birds (Fig. 1.1b; e.g. Ruggieri, 1967; Decima and Sprovieri, 1973; Decima and Wezel, 1971, 1973; Cita et al., 1978; Müller et al., 1990; Benson and Rakic-El Bied, 1991; Benson et al., 1991; Müller and Mueller, 1991; Butler et al., 1995; Orszag-Sperber et al., 2000; Rouchy et al., 2001; Camerlenghi et al., 2019; Kartveit et al., 2019; Madof et al., 2019; Caruso et al., 2020; Raad et al., 2021). As morphological and seismic reflection studies at the Strait of Gibraltar documented a ~400 km long erosional trough connecting the Gulf of Cadiz (Atlantic Ocean) to the Mediterranean Sea, this scenario of a lowered Mediterranean Sea was promptly linked to the termination of the MSC (McKenzie, 1999; Blanc, 2002; García-Castellanos et al., 2009, 2020). This conclusion has recently been reinforced by the discovery of vast chaotic deposits sitting at the claimed Miocene/Pliocene transition in the area of the Malta Escarpment-Ionian Abyssal Plain (Micallef et al., 2018, 2019; Spatola et al., 2020).

In more recent years, the desiccated basin model was challenged by the observation of deposits that are uniform in terms of sedimentology and stratigraphic architecture (Roveri et al., 2008a), ostracod content (Gliozzi et al., 2007; Stoica et al., 2016) and geochemistry (McCulloch and De Dekker, 1989; García-Veigas et al., 2018; Andreetto et al., 2021) throughout

the Mediterranean marginal belt and of $\delta D_{n\text{-alkanes}}$ and $\delta D_{alkenones}$ sharing similarities with the coeval Atlantic Ocean and Black Sea, respectively (Vasiliev et al., 2017). A model of a (relatively) full Mediterranean Sea developed (Fig. 1.1c), where the debate mainly concerns the provenance of the hydrological fluxes and the resultant hydrochemical composition of the water mass. In this scenario, the Mediterranean was first, during substage 3.1, transformed into a new gypsum-precipitating basin filled with marine and continent-derived waters (e.g. Manzi et al., 2009; Roveri et al., 2014c; Flecker et al., 2015; Vasiliev et al., 2017; García-Veigas et al., 2018; Grothe et al., 2020). Then, during substage 3.2, it became a brackish lake-sea comparable to the present-day Black Sea or Caspian Sea (Roveri et al., 2008a; Stoica et al., 2016; Andreetto et al., 2021b), depending on whether a marine connection with the Atlantic was active (Manzi et al., 2009; Roveri et al., 2014b, c; Flecker et al., 2015; Marzocchi et al., 2016; Vasiliev et al., 2017; García-Veigas et al., 2018) or not (e.g. McCulloch and De Deckker, 1989; Roveri et al., 2008a), and with a base-level fluctuating by hundreds of meters with precessional periodicity (Fortuin and Krijgsman, 2003; Ben Moshe et al., 2020; Andreetto et al., 2021b). In the relatively full scenario, the revival of marine conditions is ascribed to either connectivity changes (Marzocchi et al., 2016) or to a moderate sea-level rise (Andreetto et al., 2021b). In contrast, Carnevale et al. (2006a, b, 2008, 2018) and Grunert et al. (2016), based on the recovery of fish remains ascribed to marine species, proposed that fully marine conditions were in force in the Mediterranean already at the end of substage 3.1.

After nearly 50 years of research on both onshore and offshore localities (Fig. 1.2), the observations backing up the competing desiccated and full basin Mediterranean models remain extremely difficult to reconcile. Uncertainties regarding the chronostratigraphic framework of Stage 3 deposits, the origin and migration of its characteristic biota, the meaning of the data derived from the applied geochemical techniques and the relationship between the Mediterranean and its surrounding water bodies (i.e. Atlantic Ocean, Indian Ocean and Paratethys) all inhibit a clear understanding of the Mediterranean base level and its hydrochemical structure.

In this paper we attempt to summarize all the existing, but heavily scattered, data resulting from ~50 years of cross-disciplinary studies with the aim of providing a comprehensive overview of the stratigraphic arrangement of Stage 3 onshore and offshore deposits, as well as of their sedimentological, paleontological, geochemical and seismic properties. Subsequently, we assemble the observations favoring both end-member scenarios of a relatively desiccated and relatively full Mediterranean. Finally, we focus on novel future analytical techniques and approaches that have the potential to constrain Mediterranean base-level during MSC Stage 3 as well as the changing hydrological fluxes and connectivity phases between the intra-Mediterranean basins and the neighboring Atlantic Ocean and Paratethyan domains as a mean of reconstructing the state of the art of the complex history of this enigmatic period of the Mediterranean history once and for all.

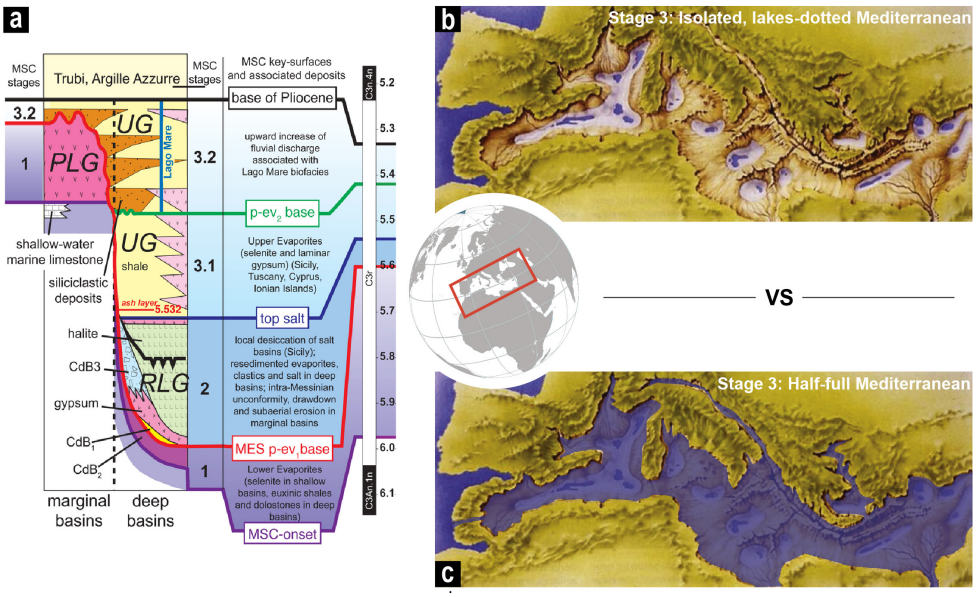

Fig. 1.1. (a) *Consensus chronostratigraphic model for the MSC events (Roveri et al., 2014a). Stage 3, here of interest, spans between 5.55 Ma and 5.332 Ma, the astronomical ages of the base of the Upper Gypsum Unit (following Manzi et al., 2009) and Trubi Formation (Van Couvering et al., 2000) in the Sicilian Eraclea Minoa section, respectively. CdB: Calcare di Base; PLG: Primary Lower Gypsum; RLG: Resedimented Lower Gypsum; UG: Upper Gypsum.* **(b), (c)** *Map of the Mediterranean region showing the two extreme and mutually exclusive paleoenvironmental scenarios proposed to have featured the Mediterranean during Stage 3 (see discussion in Chapter 7; modified after Krijgsman et al., 2018).*

1.2 The terminal Stage 3 of the MSC

1.2.1 Historic overview of nomenclature and concepts

The final phase of the MSC (i.e. substage 3.2), also known as "Lago-Mare", finds its sedimentary expression in cyclically-arranged terrigenous and evaporitic sediments hosting unique faunal assemblages of ostracods, mollusks and dinoflagellate cysts (dinocysts). They are related, at species level, to those inhabiting, during the Miocene, the brackish basins of the Paratethys realm (e.g. Gliozzi et al., 2007; Stoica et al., 2016). But what exactly is the "Lago-Mare"? This widely employed expression in the MSC literature encompasses a variety of meanings that make its application doubtful and misleading. The root of the wording "Lago-Mare" is to be found in the Russian scientific literature of the late 1800s. Nikolai Andrusov (1890) used the corresponding Russian term with a geographical and chronological connotation in reference to the series of central-eastern European basins that during the Miocene turned from marine settings to desalinized semi-isolated lakes with an endemic fresh-brackish water biota association (e.g. Popov et al., 2006 and references therein). The original monograph of

Andrusov (1890) was not widely available outside Russia, but his attendance of international conferences allowed his research to spread outside the Russian borders. From the publications of the French geologists Suzette Gillet (Gillet, 1932, 1933) and Maurice Gignoux (Gignoux, 1936) we can state with relative certainty that the original meaning of the word "Lago-Mare" (here reported with the French counterpart "Lac-Mer") had its provenance in the Russian literature:

"[…] *An isolation of the basin, that became a brackish, isolated basin. Then, a uniform fauna populated this immense lac-mer which was divided […] into Pannonian basin, […] Dacique Basin, and Euxin and Caspian basin* […]" (Gillet, 1932).
"[…] *During the Volhynien (Sarmatique inferior) there was a lac-mer of uniform fauna that extended through all the eastern Europe. […] and the fauna of the eastern regions of that huge lac-mer was completely differenciated [sic] from the one in the western regions.* […]" (Gillet, 1933).
"[…] *The Pontien fauna is not anymore a fauna characteristic of an internal saline sea, as in the Sarmantien, but is a fauna of a "desalinated lagoon", a lac-mer, as the Russian geologists named it*. […]" (Gignoux, 1936).

In the late 19th (Capellini, 1880) and 20th century (Ogniben, 1955; Ruggieri, 1962, 1967; Decima, 1964), late Messinian ostracod- and mollusk-bearing deposits in the Mediterranean were described at several Italian localities. Initially, the expressions "*Congeria* beds" (Capellini, 1880) and "*Melanopsis* beds" (Ruggieri, 1962) were used. Later on, Ruggieri (1967) pointed out the affinity of these faunal elements with those of the Pontian of the Paratethys. Consequently, he speculated on a feasible Paratethys-like paleoenvironmental configuration for the Mediterranean in the latest Messinian and he coined the Italian translation (i.e. "Lago-Mare") from the French "Lac-Mer" in reference to the shallow-water lakes claimed to be widely distributed across the Mediterranean. Progress in the 1970s in onshore and offshore exploration highlighted the temporally well-constrained distribution of the Paratethyan organisms in the Mediterranean (Carbonnel, 1978). On this premise, Hsü et al. (1978a) proposed to use "Lago-Mare" to "designate the latest Messinian oligohaline environment, postdating evaporite deposition and predating Pliocene marine sedimentation […] in order to distinguish it from "lac mer" which, strictly speaking, was a Paratethyan environment". Notwithstanding the new definition, in various parts of the text they used "Lago-Mare" to refer to the Paratethyan lakes (pp. 1071-1072: "[...] The upper Messinian Mediterranean was floored by a series of desert basins, some with salt lakes, prior to inundation by the Lago-Mare."), thus giving rise to the confusion on how to use the term properly.

In the most recent stratigraphic overview of the MSC (Fig. 1a; Roveri et al., 2014a), the terminal MSC stage is called Stage 3, which is in turn subdivided into substages 3.1 and 3.2 (also termed Lago-Mare). Beside such a chronostratigraphic definition, the term "Lago-Mare"

has also been used for a typical biofacies of the late Messinian Mediterranean (e.g. Fortuin et al., 1995; Gliozzi, 1999; Gliozzi and Grossi, 2008; Sciuto et al., 2018), for the pelitic beds encasing the Paratethyan-related fauna (i.e. a lithofacies; e.g. Fortuin and Krijgsman, 2003; Sciuto et al., 2018), as the name of an informal lithostratigraphic unit (usually distinguished by its fossil content) sandwiched between the Sicilian Upper Gypsum and the Arenazzolo Fm. (Fig. 1.4b; Clauzon et al., 2005; Londeix et al., 2007; Popescu et al., 2009; Bache et al., 2012) and to denote multiple (3 to 4) spilling events of the Paratethys into the Mediterranean (Clauzon et al., 2005, 2015; Popescu et al., 2007, 2009, 2015; Suc et al., 2011; Bache et al., 2012; Do Couto et al., 2014; Frigui et al., 2016; Mas and Fornós, 2020).

This being a review, we use the widely employed definition of the model of Roveri et al. (2014a; Fig. 1.1a) and regard the Lago-Mare as a "phase of massive biota migration from the Paratethys realm, cyclostratigraphically constrained between 5.42 Ma and 5.332 Ma (Roveri et al., 2008a; Grossi et al., 2011), during which the Mediterranean sedimentary environments underwent an impressive freshening". Nevertheless, we call for caution in the use of this definition of "Lago-Mare" in future studies, since 5.42 Ma as the (astronomical) age of the first entrance of Paratethyan organisms into the Mediterranean is likely to be incorrect (see section 1.5.1) and evidence of 'impressive freshening' are already present much earlier than 5.42 Ma (e.g. at Eraclea Minoa; Vasiliev et al., 2017; García-Veigas et al., 2018).

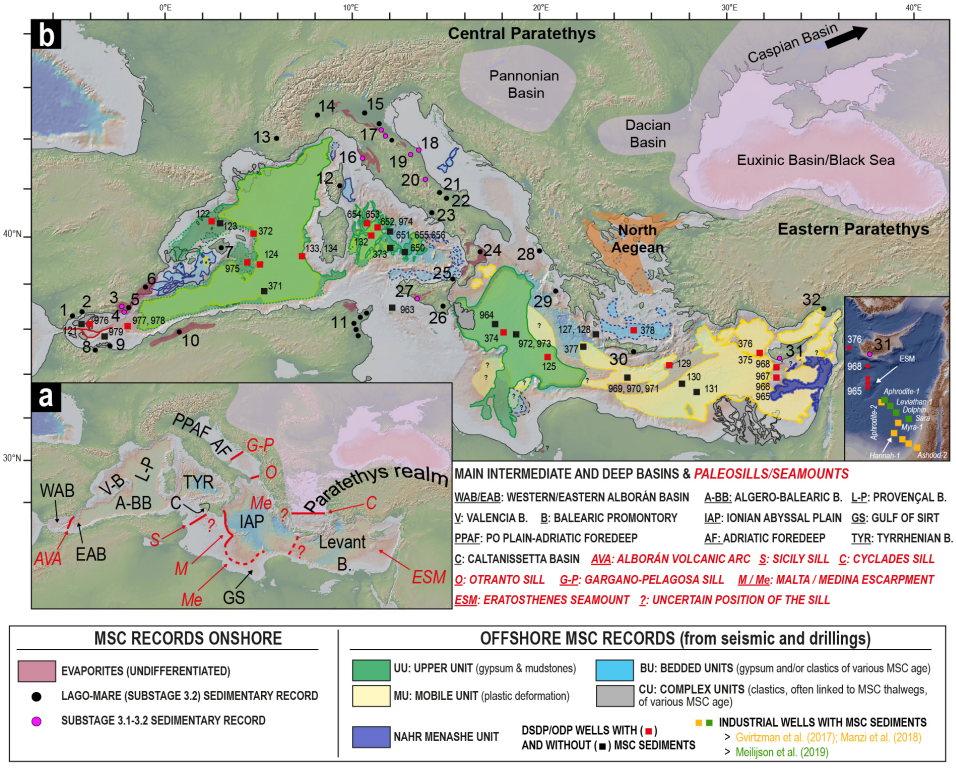

Fig. 1.2 (previous page). *Map of the Mediterranean Basin (modified from Lofi, 2018) showing:* **(a)** *the location of the key intermediate and deep basins as well as physical thresholds that influenced the connectivity history of the Mediterranean;* **(b)** *the onshore (i.e. basins and/or sections) and offshore (DSDP/ODP/Industrial drill sites) localities where deposits attributed to MSC Stage 3 have been studied. Mixed assemblages of Paratethyan-like ostracods and foraminifera are known from all mentioned onshore localities and some offshore locations (see text). The present-day spatial extent of the MSC seismic units, except for the Lower Unit, is also shown. The paleogeography of the (Eastern and Central) Paratethys and of the North Aegean domain is contoured after Van Baak et al. (2017) and Krijgsman et al. (2020a), respectively. W-E onshore localities: 1-6 Betic Cordillera (SE Spain): 1-Marbella and 2-Malaga basins (Guerra-Merchán et al., 2010); 3-Sorbas Basin (Roveri et al., 2009, 2019a); 4-Nijar Basin (Fortuin and Krijgsman, 2003); 5-Vera Basin (Fortuin et al., 1995); 6-Bajo Segura Basin (Soria et al., 2005, 2008a, b); 7-Mallorca (Mas and Fornós, 2020); 8-Melilla Basin (Rouchy et al., 2003); 9-Boudinar Basin (Merzeraud et al., 2019); 10-Chelif Basin (Rouchy et al., 2007); 11-Sahel area (Frigui et al., 2016); 12-Aléria Basin and 13-Rhône Valley (Carbonnel, 1978); 14-Piedmont Basin (Dela Pierre et al., 2011, 2016); 15-Po Plain (Ghielmi et al., 2010, 2013; Amadori et al., 2018); 16-Fine Basin (Cava Serredi section; Carnevale et al., 2006a, 2008). 17-21 Apennine system: Romagna sections (17, Roveri et al., 1998), Trave section (18, Iaccarino et al., 2008), Maccarone section (19, Bertini, 2006; Grossi et al., 2008; Sampalmieri et al., 2010; Pellen et al., 2017), Colle di Votta (20)-Fonte dei Pulcini (21)-Stingeti (22) sections (Cosentino et al., 2005, 2012, 2013, 2018), Mondragone 1 well (23, Cosentino et al., 2006), Crotone Basin (24, Roveri et al., 2008a); 25-27 Sicily: Villafranca Tirrena (25) and Licodia Eubea (26) sections (Sciuto et al., 2018), Caltanissetta Basin (27, Manzi et al., 2009); 28-Corfu (Pierre et al., 2006); 29-Zakinthos (Karakitsios et al., 2017b); 30-Crete (Cosentino et al., 2007); 31-Cyprus (Rouchy et al., 2001; Manzi et al., 2016a); 32-Adana Basin (Radeff et al., 2016).*

1.2.2 Development of a chronostratigraphic framework

Issues of the timing and duration of the MSC only began to be tackled in the 1990s, in parallel with discussion concerning the nature of its extreme paleoenvironments (Schmalz, 1969; Hsü et al., 1973a, b, c, 1978a, b; Nesteroff, 1973; De Benedetti, 1982). While published models (Butler et al., 1995; Clauzon et al., 1996; Krijgsman et al., 1999a; Rouchy and Caruso, 2006) mostly converged on the (astronomical) age of the marine replenishment at the beginning of the Pliocene (5.332 Ma; Van Couvering et al., 2000), there were disagreements about the age of the onset of the MSC (synchronous vs diachronous) and of specific events within it (see discussion in Roveri et al., 2014a). Among these, the work of Krijgsman et al. (1999a) has obtained wide consensus. Their cyclostratigraphic tuning and correlation of continuous and bio-magnetostratigraphically constrained pre-evaporitic sections in Spain (Sorbas), Sicily (Gibliscemi/Falconara) and Greece (Metochia) resulted in a synchronous age of 5.96±0.02 Ma for the MSC onset (later refined to 5.97 Ma by Manzi et al., 2013). The astronomical ages for the onset (Krijgsman et al., 1999a) and termination (Van Couvering et al., 2000) of the MSC are not

contentious since the characteristic sedimentary cyclicity and sediments' properties (e.g. color of the lithologies and biota content) of the pre- and post-MSC successions fit robustly with the insolation curve (see also Van der Laan et al., 2006 and Topper and Meijer, 2015). The cyclic arrangement of the MSC sediments (Fig. 1.3a) led scientists to interpret that the same cyclostratigraphic approach could be used to gain precise dates for events within the MSC (e.g. Hilgen et al., 1995; Vai, 1997; Krijgsman et al., 1999b, 2001), bypassing the challenge posed by the unsuitability of the classic biomagnetostratigraphic tools for the MSC successions. Characteristic interference patterns of eccentricity and precession have been tentatively recognized in the Sicilian Eraclea Minoa section (see subsection 3.8; Van der Laan et al., 2006). However, clear orbital signals are typically poorly expressed in MSC records and, when they are present, like in Sicily, they are not (vertically) repeated with sufficient frequency to establish clear phase relations with the astronomical cyclicity. For this reason, the simple counting of cycles with no analysis of cyclostratigraphic pattern in proxy records has mostly been employed as a correlation method (Roveri et al., 2008a; Manzi et al., 2009, 2016a; Cosentino et al., 2013).

The age of the base of Stage 3 is largely determined by correlating the sedimentary cycles of the Upper Gypsum unit (UG) at Eraclea Minoa (Sicily) with the astronomical curve La2004 (Laskar et al., 2004). The UG sedimentary cyclicity consists of alternating gypsum and mudstone beds of variable thickness (Figs. 1.5g-i; see section 1.3.8). Precessional variation of the Mediterranean freshwater budget tied tightly to the African monsoon and Atlantic storms are the drivers interpreted to lie behind the gypsum-mudstone cycles (e.g. Marzocchi et al., 2015, 2019; Simon et al., 2017). Variations of the freshwater discharge cause the pycnocline to shift vertically, resulting in brine concentration and gypsum precipitation during to the arid/dry phases of the precession cycles (precession maxima-insolation minima) and brine dilution and mudstone deposition during the humid/wet phases (precession minima-insolation maxima) (Van der Laan et al., 2006; Manzi et al., 2009). Two different tuning options exist in literature (Van der Laan et al., 2006 versus Manzi et al., 2009; Fig. 1.3a).

Van der Laan et al. (2006) tentatively recognized sedimentary patterns that they correlated with the astronomical curves by using the same phase relationships between the sedimentary cycles and the astronomical cycles as are seen in Plio-Pleistocene sapropel-bearing marine successions of the Mediterranean (Hilgen, 1991). The four closely spaced gypsum beds III to VI were regarded as a cluster, i.e. the sedimentary expression of a 100-kyr eccentricity maximum (Hilgen, 1991; Strasser et al., 2006), whereas the preceding and following evaporite-free marly interval were attributed to a phase of low-amplitude precession oscillations caused by a 100-kyr eccentricity minimum (Fig. 1.3a). Tuning downward from the conformable M/P boundary (Fig. 1.6d) and arguing that the precession peak at ~5.38 Ma, which has an extremely low amplitude, is not expressed in the sedimentary record, Van der Laan et al. (2006) correlated gypsums III to VI with the four successive precession/insolation peaks of the 100 kyr eccentricity maximum dated around 5.44 Ma and the overlying and underlying gypsum-free marly interval fell within

100 kyr eccentricity minimum cycles (Fig. 1.3a, right log). This tuning resulted in an astronomical age of ~5.51 Ma for the first gypsum bed in their log (i.e. gypsum II in the log of Manzi et al., 2009), and an approximate duration of 175 kyr for Stage 3 as whole.

An alternative tuning by Manzi et al. (2009; Fig. 1.3a, left log) argued that every precessional/insolation peak must have an expression in the rock record. Manzi et al. (2009) agreed with the solution of Van der Laan et al. (2006) on the sedimentary inexpressiveness of the (barely visible) insolation minima peak at ~5.38 Ma. However, these authors considered the insolation minima peaks immediately above and below of too low amplitude to promote the conditions required for gypsum precipitation, but also too high not to have some sedimentary expression. They therefore identified sandstone horizons VI' and VI" as the sedimentary response to these weak insolation/precession signals. The addition of two precessional cycles (i.e. a total of 9) resulted in an astronomical solution that was adjusted one precessional cycle lower than that of Van der Laan et al. (2006), translating into an age of 5.53 Ma for the base of the UG and a total duration of ~200 kyr for Stage 3. But the more conspicuous difference between the two astronomical solutions discussed lies in the timing at which gypsum precipitation occurred, restricted to the 100 kyr eccentricity maxima according to Van der Laan et al. (2006), extended to the 100 kyr eccentricity minima by Manzi et al. (2009).

An age of 5.53 Ma for the first gypsum bed was also obtained by the astronomical tuning of the Upper Gypsum in Cyprus (Manzi et al., 2016a), but there the tuning is performed just by following the recognition, from the base up, of 6 gypsum beds just like in Sicily and therefore arguing for a bed-to-bed correlation with the Sicilian gypsums I-VI. In the consensus model of Roveri et al. (2014a) the base of Stage 3 coincides with the base of the Sicilian UG, placed by Manzi et al. (2009) at 5.55 Ma (Fig. 1.1a). However, in the model of Manzi et al. (2009) this age is attributed to a cumulate gypsum horizon interpreted as laterally equivalent of the Halite (i.e. Stage 2), and therefore implying the kickoff of Stage 3 at 5.53 Ma (Fig. 1.3a).

The post-evaporitic successions of the Romagna (Cusercoli and Sapigno sections; Roveri et al., 1998) and Marche (e.g. Trave and Maccarone sections; Iaccarino et al., 2008; Cosentino et al., 2013) areas provided evidence that led to the splitting of Stage 3 into substage 3.1 and 3.2. In the resulting composite section (Roveri et al., 2008a), a shift in the sedimentary facies and stacking pattern is observed (see description in subsection 1.3.7). Correlation of the sedimentary cyclicity in Romagna was from the (conformable) base of the Pliocene downwards (or from an $^{206}U/^{238}Pb$-dated ash layer upward; Cosentino et a., 2013) and linked three fluvial conglomerates and two black mudstone layers of unknown sedimentological significance to the arid phases of the precession cycles (Fig. 1.3a; Roveri et al., 2008a). The greater thickness of the oldest conglomerate was possibly assumed to be evocative of an oscillation of the amplitude of the corresponding precession minima peak rather than the amplitude of the peaks responsible for the formation of the other facies. This approach resulted in an age of 5.42 Ma for the first conglomerate (i.e. the substage 3.1/3.2 transition; Fig. 1.5g) and an approximate duration of 90

kyr for substage 3.2 (the Lago-Mare phase). The same astronomical age is obtained by tuning the Upper Member of the Feos Formation in the Nijar Basin (Omodeo Salé et al., 2012), where four pelite-conglomerate cycles plus one sandstone capped by the Miocene/Pliocene boundary mark the interval attributed to Stage 3.2 (Fortuin and Krijgsman, 2003). Although the substage 3.1/3.2 transition is linked to a major Mediterranean-scale hydrological re-organization possibly coinciding with the migration of the Paratethyan biota (Roveri et al., 2008a; Grossi et al., 2011), the facies change used for its definition is hardly recognizable elsewhere (see chapter 5). As such, other tools have been used to equip fragmentary and/or lithological cyclicity-lacking sections with an age model: the (highly controversial) ostracod biozonation (see subsection 1.5.1; e.g. Stoica et al., 2016; Karakitsios et al., 2017a; Cosentino et al., 2018; Caruso et al., 2020) and the astronomical tuning of magnetic susceptibility records (e.g. Fonte dei Pulcini section, Central Apennines; Cosentino et al., 2012).

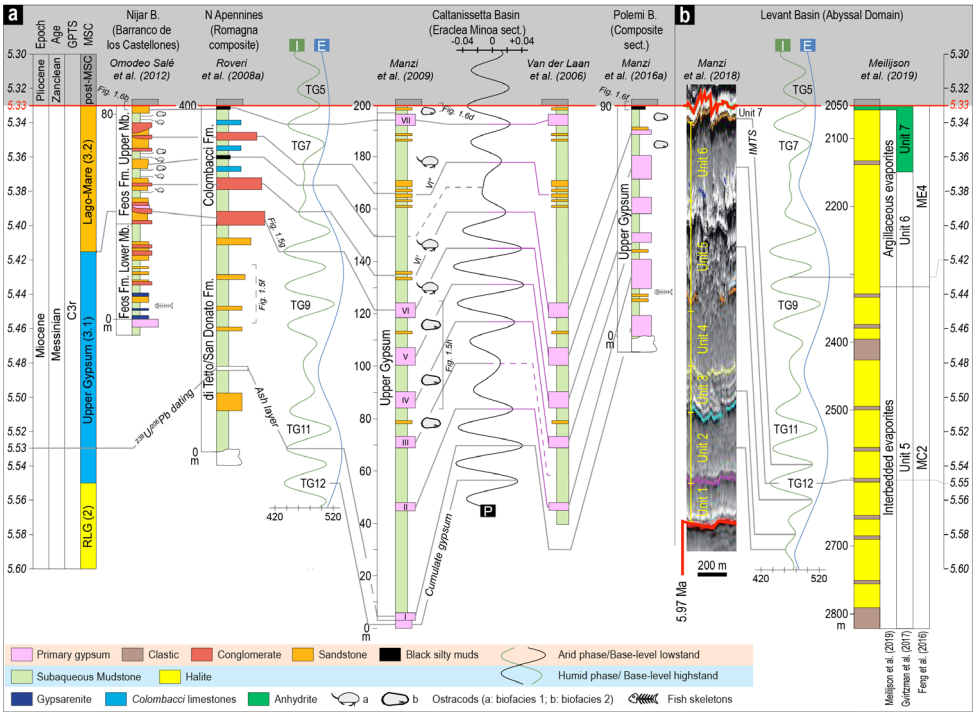

Fig. 1.3. (a), (b) *Available astronomical tunings to astronomic curves of climatic precession (P), 100 kyr eccentricity (E) and 65°N insolation curve (I) of Laskar et al. (2004) of the lithological cyclicity of onshore Stage 3sections (a) and of the seismic cycles and/or well logs (gamma ray and resistivity) of the MU in the Levant Basin (b). Tunings of onshore sections in (a) are carried out downward from the M/P boundary (conformable in all sections). Astronomically-tuned glacial (even numbers) and interglacial (odd numbers) stages (i.e. TG) as defined by Hodell et al. (1994) are also indicated.*

Comparison of Atlantic oxygen isotope records (Van der Laan et al., 2005, 2006) and the chronostratigraphy of Roveri et al. (2014a) revealed that Stage 3 sedimentation started during a prominent global eustatic lowstand associated with oxygen isotope (glacial) stage TG12, followed by a latest Messinian deglacial interval which comprised multiple obliquity- and possibly precession-forced global eustatic phases. As documented by Hodell et al. (2001) (later revised by Drury et al., 2018), Van der Laan et al. (2006) and Roveri et al. (2014a), the marine replenishment of the Mediterranean did not coincide with any major deglaciation, so non-eustatic causes of the Zanclean megaflood hypothesis are required.

1.3 Onshore domain: key sections, sedimentary expression and faunal content

1.3.1 The Alborán region

The westernmost outcrops of Stage 3 deposits in the Mediterranean are located in the Alborán region, close to the present-day Strait of Gibraltar (Fig. 1.2b). MSC deposits on the margins of this region are poorly developed, possibly because of a late Tortonian uplift that raised the margins above the Mediterranean water level (López-Garrido and Sanz de Galdeano, 1999). Near Malaga, however, two facies associations consisting of m-thick conglomerate-sandstone beds alternating with laminated pelites are documented in the Rio Mendelín section (informally referred to as "LM unit"; Guerra-Merchán et al., 2010) and attributed to (part of) the Lago-Mare phase (Fig. 1.4a) based on their paleontological content. These sediments are squeezed between the Paleozoic basement units, with an erosive contact and associated angular unconformity, and the Pliocene, from which they are separated by another erosional surface draped by conglomeratic accumulations (Fig. 1.6a). A well-preserved and diverse in situ Paratethyan-type ostracod and molluskan fauna (i.e. *Lymnocardiinae* and *Dreissenidae*) typical of shallow waterbodies (up to 100 m deep; Grossi et al., 2008; Gliozzi and Grossi, 2008) with low salinities (5-18‰) is reported from the pelitic units (Guerra-Merchán et al., 2010). The overlying Pliocene in the deeper depocenters starts with 30 m-thick littoral conglomerates with marine mollusks passing progressively upwards into deeper water facies, while fan deltas developed at the basin margins (López-Garrido and Sanz de Galdeano, 1999; Guerra-Merchán et al., 2010, 2014). Notably, the overall thickness of the Pliocene deposits reaches 600 m. The detailed regional studies by López-Garrido and Sanz de Galdeano (1999) and Guerra-Merchán et al. (2014) concluded that accommodation space was created during (Zanclean) sedimentation by local fault-driven subsidence, and that movement on these faults only reversed at the end of the Zanclean causing uplift. An alternative scenario, based on the finding of (a few) specimens of the nannofossil Ceratolithus acutus, ascribed the LM unit of Guerra-Merchán et al. (2010) to the earliest Zanclean (Fig. 1.4b; Do Couto et al., 2014).

On the southern Alborán margin in Morocco, latest Messinian deposits are reported from the Boudinar and Melilla basins (Fig. 1.2b). Up to 100 m-thick chaotic deposits containing selenite gypsum fragments, azoic conglomerates, sandstones yielding planktic foraminifera

and nannofossils and lacustrine limestones are capped by early Pliocene marine marls (Rouchy et al., 2003; Azdimousa et al., 2006; Cornée et al., 2016; Merzeraud et al., 2019). Due to their stratigraphic position, these continental to lacustrine deposits are interpreted as the local expression of the Lago-Mare phase (Cornée et al., 2016) or alternatively as Zanclean successions (Azdimousa et al., 2006).

1.3.2 Algeria

The Chelif Basin in Algeria (Fig. 1.2b) displays the typical marginal Messinian succession comprising Tortonian to lower Messinian blue marls, diatomite-rich sediments (Tripoli unit), cyclically-arranged primary evaporites (13 couplets), ostracod-rich post-evaporitic deposits and Zanclean foraminiferal marls (Rouchy et al., 2007). The post-evaporitic sediments show a great lateral variability in both thickness (from few meters up to 125 m) and facies. They are mainly dominated by terrigenous clastic lithologies, associated in the marginal areas with sandy carbonates and stromatolitic limestones. A mixed faunal assemblage of non-marine (Paratethyan-like ostracods) and marine (benthic and planktic foraminifera) organisms is present, showing an increase in ostracod species diversity from the bottom to the top (Rouchy et al., 2007).

1.3.3 Neogene basins of the Eastern Betics (Spain)

The external Neogene basins (Sorbas, Nijar, Vera and Bajo Segura) of the eastern Betic Cordillera (SE Spain; Fig. 1.2b) represent an important laboratory for understanding Messinian events. In particular, the Sorbas and Nijar basins preserve two allegedly continuous successions spanning the entire MSC (e.g. Roveri et al., 2009; Omodeo Salé et al., 2012). The two basins are similar in many respects. Their stratigraphic organization, for example, suggests they were connected for much of the late Miocene up until MSC Stage 1 (Fortuin and Krijgsman, 2003), which is represented by the gypsiferous Yesares Member (e.g. Lu, 2006). However, facies differences are prominent in the Stage 3 formations according to the chronostratigraphic frameworks of Roveri et al. (2009) for the Sorbas Basin and Omodeo Salé et al. (2012) for the Nijar Basin (Fig. 1.4a). Lithostratigraphically, two members are discerned between the Yesares Member and the basal Zanclean: the Sorbas and Zorreras members in the Sorbas Basin (Figs. 1.4a, 1.5a) and the lower and upper members of the Feos Fm. in Nijar (Figs. 1.3a, 1.4a; Roep et al., 1998; Krijgsman et al., 2001; Fortuin and Krijgsman, 2003; Braga et al., 2006; Roveri et al., 2009, 2019a; Omodeo Salé et al., 2012). The Sorbas Member (see Roep et al., 1998 and Aufgebauer and McCann, 2010 for a more detailed sedimentological description) consists of three overlapping coarsening-upward depositional sequences made of offshore clays and marls passing upward into shelf muds and coastal sandstone bodies. Still unclear is the chemistry of the subaqueous environment during the formation of the Sorbas Member and the provenance of the water fluxes. These shallow-water deposits are conformably replaced upward by the

Zorreras Member that comprises alternations of reddish siltstones and sandstones (Fig. 1.5a) organized in five (or eight) lithological cycles expressing continental environments (Martín-Suárez et al., 2000; Aufgebauer and McCann, 2010). Up to four lenticular white limestone beds bearing brackish Paratethyan-like ostracods (*Cyprideis*, *Loxocorniculina djafarovi* and freshwater species of the family *Limnocytheridae*), bivalves and *Chara* oogonia (Roep and Van Harten, 1979; Aufgebauer and McCann, 2010) are found interrupting the fluviatile sequence (Fig. 1.5a) and are linked to either episodic flooding by local rivers (Braga et al., 2006; Aufgebauer and McCann, 2010) or episodic Mediterranean ingressions (Fortuin and Krijgsman, 2003; Andreetto et al., 2021b). A correct interpretation of the paleodepositional environment of these limestone beds is crucial for the discussion concerning the Mediterranean base-level position during the Lago-Mare phase. In fact, if the Sorbas Basin was relatively shallow during Zorreras deposition (50-100 m; Roveri et al., 2019a, 2020), repeated and sudden Mediterranean incursions would indicate that the Mediterranean Basin was relatively full and that its base level was oscillating, possibly with precessional periodicity (Andreetto et al., 2021b). The contact between the Zorreras Mb. and the overlying nearshore Pliocene (<50 m depositional paleodepth; Roveri et al., 2019a) in the Sorbas Basin is conformable and expressed differently around the basin, ranging from a bivalves-rich bed overlain by a yellow, fossiliferous calcarenite floored by a gravelly lag deposit (Mather et al., 2001) to a grey marl horizon with marine foraminifera assemblages followed by a second shell-rich bed (Roveri et al., 2019a). Similar to the situation in Malaga, the rare identification of *Ceratolithus acutus* in sediments of the continental Zorreras Mb. led Clauzon et al. (2015) to put forward an alternative chronostratigraphic and paleoenvironmental interpretation for the Sorbas MSC succession, shifting the Zorreras Mb. into the Pliocene (Fig. 1.4b) and thus associating the presence of brackish Paratethyan-like ostracods with exchanges between the Mediterranean and Paratethys following the Mediterranean re-filling, at high sea level.

In the Nijar Basin (Fig. 1.2b), the latest Messinian Feos Formation is bracketed at the base and top by an erosional surface along the basin margins and its correlative conformity in the deeper parts (Fig. 1.3a; Fortuin and Krijgsman, 2003; Aguirre and Sánchez-Almazo, 2004; Omodeo Salé et al., 2012). The Lower Feos Member consists of azoic, graded and locally slumped siliciclastic-carbonate beds alternating with gypsarenites and gypsiltites and including a laterally continuous Mn-rich bed (Fortuin and Krijgsman, 2003; Omodeo Salé et al., 2012). In the basin center (e.g. Barranco de los Castellones section; Fig. 1.3a) the Upper Feos Member comprises four complete lithological cycles of m-thick conglomerate to sandstone beds alternating with laminated pelites (Fig. 1.5b) and one incomplete cycle, which only consists of a sandstone horizon conformably capped by the Pliocene Cuevas Fm. (Fig. 1.6b; Fortuin and Krijgsman, 2003). A rich fauna of mixed brackish ostracods and marine foraminifera is found in all four pelitic beds (Bassetti et al., 2006). Its origin is questionable. These ostracods were regarded as endemic to the Mediterranean and inhabiting endorheic lakes by Bassetti et al.

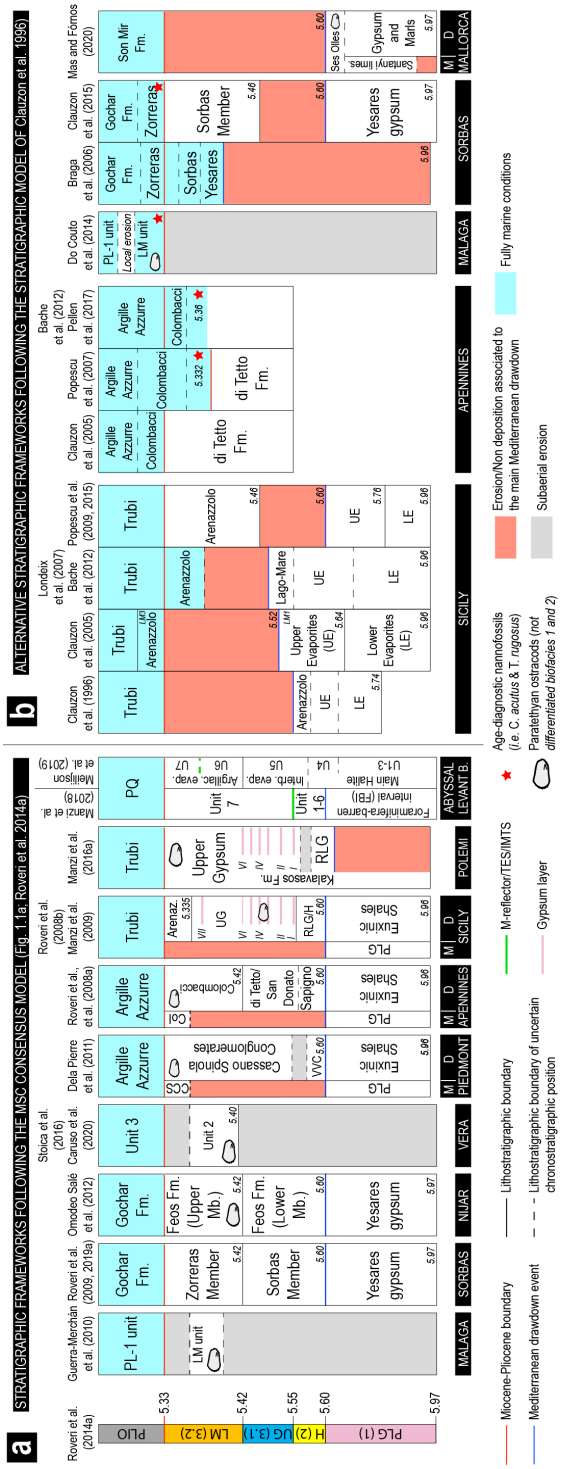

(2006). However, later they were shown to have been misidentified and were instead considered Paratethys-derived by Stoica et al. (2016; see section 1.5.1). Planktonic and deep-water benthic foraminifera are widely considered reworked by Fortuin and Krijgsman (2003), Bassetti et al. (2006) and Omodeo Salé et al. (2012), in place by Aguirre and Sánchez-Almazo (2004).

In the Vera Basin (Fig. 1.2b), in-situ gypsum deposits are missing because of widespread erosion or non-deposition and MSC deposits are only represented by ~12 m of laminated varicolored marly clays (Unit 2; Fig. 1.4a), which are best exposed in the Cuevas del Almanzora section (Fortuin et al., 1995; Fig. 1.5c). These clays contain a well-preserved and diversified in situ fauna of Paratethyan ostracod and shallow-water, benthic foraminifera mixed with physically reworked (mostly from the lower Messinian Abad marls) planktic and deep-water benthic foraminifera (Fortuin et al., 1995; Stoica et al., 2016; Caruso et al., 2020). The marly clays are assigned by Stoica et al. (2016) and Caruso et al. (2020) to (roughly) the whole late Messinian Lago-Mare phase (Fig. 4a) based on the ostracod biozonation of Grossi et al. (2011) and are considered to represent either sedimentation in an isolated lake subject to base-level

Fig. 1.4 (previous page). *Schematic overview of different chronostratigraphic models for some of the Messinian successions presented in Chapter 3. Note the large controversies in timing, duration and chronostratigraphic position of the main erosion phase between models in (a) and (b). Models in* **(a)** *follow the recently established MSC chronostratigraphic model of Roveri et al. (2014a), according to which the Mediterranean base-level dropped and halite deposited on sea floor during Stage 2 and the Upper Gypsum/ Upper Evaporites-Lago-Mare sequence followed. Models in* **(b)** *were proposed following the alternative scenario of Clauzon et al. (1996, 2005), which envisaged two Lago-Mare episodes (LM1 and LM3) that occurred before and after the main Mediterranean drawdown event, during which LM2 was deposited in the deep desiccated basins (Do Couto et al., 2014; Popescu et al., 2015; see Roveri et al., 2008c and Grothe et al., 2018 for further explanations). Note, in (b), the shifting of the position of the main erosional phase in Sicily through time as well as the time of the marine replenishment in the Apennines.)*

and salinity fluctuations (Caruso et al., 2020) or deposition in a coastal lagoon that was connected to the water mass filling the open Mediterranean (Stoica et al., 2016; Andreetto et al., 2021b). Similar to Malaga, these sediments are topped by an erosive surface draped by a conglomeratic accumulation which is overlain by the open marine fauna-rich sediments of the basal Zanclean (Fortuin et al., 1995; Caruso et al., 2020). This erosion feature likely indicates that the Miocene/Pliocene transition followed a base-level lowstand in the Vera Basin.

Stage 3 deposits (Garrucha Fm.) in the easternmost basin of the Betic Cordillera, the Bajo Segura Basin (Fig. 1.2b), are bounded below and above by two erosional surfaces related to lowered Mediterranean base-levels and discontinuously present due to the widespread fluvial erosion that occurred at the M/P boundary (Soria et al., 2005, 2008a, b). The Garrucha Fm. shows a maximum thickness of 100 m in its type section (Soria et al., 2007, 2008b). It consists of 20-50 cm thick sandstone bodies interrupting a dominantly marly succession deposited in a subaqueous environment inhabited by *Cyprideis* sp. and euryhaline, shallow-water benthic foraminifera (*Ammonia beccarii, Elphidium granosum, Elphidium macellum, Haynesina germanica* and *Quinqueloculina laevigata*). Planktic foraminifera are also observed and for a long time were considered to be physically reworked (Soria et al., 2005, 2008b). However, some stratigraphic levels contain dwarf tests of long-ranging taxa such as *Globoturborotalita decoraperta, Globigerina bulloides*, and *Neogloboquadrina* spp. which recently have been interpreted as being in-situ mostly due to the absence of notable signs of reworking (Corbí and Soria, 2016). Among these dwarf taxa is *Neogloboquadrina acostaensis* (dextral; Corbí and Soria, 2016). Since this group is mainly dextral in the latest Messinian Atlantic successions (e.g. Sierro et al. 1993; Bassetti et al., 2006), this may indicate that Atlantic inflow to the Mediterranean occurred during the late Messinian and the base level of the Mediterranean was high enough to reach the marginal Bajo Segura Basin. The M/P boundary is, once again, marked by an erosional surface which outlines up to 200 m deep paleovalleys engraved down into the pre-

MSC sediments and filled with conglomerates and sandstones of claimed coastal and shallow marine environments (Soria et al., 2005, 2008b; García-García et al., 2011; Corbí et al., 2016).

1.3.4 Mallorca

Mallorca, which constitutes an emerged segment of the Balearic Promontory (Fig. 1.2), does not expose the classical MSC evaporite sequence. Instead, two main MSC-related units are found above late Tortonian-Messinian reefal carbonates (Reef Complex Unit) and beneath the Pliocene: the Santanyí limestones and the Ses Olles Formation (Mas and Fornós, 2020 and references therein). The Santanyí limestones are microbialites and oolite-dominated sediments in which a baleen whale neurocranium has been found (Mas et al., 2018). This unit was interpreted either as a Terminal Carbonate Complex (TCC) laterally equivalent to the Primary Lower Gypsum (PLG) which has been drilled in the deeper parts of the bay of Palma (Mas and Fornós, 2020) or as time-equivalent to the Reef Complex Unit (e.g. Arenas and Pomar, 2010; Suárez-González et al., 2019). The Ses Olles Formation consists of marls, sandy-marls and marly-calcareous lacustrine deposits rich in in-situ freshwater *Chara* spp., brackish water Paratethyan-like mollusks and ostracods and littoral benthic foraminifera (*Elphidium* sp., *Ammonia* sp.). The upper contact of the Ses Olles Formation with the Pliocene corresponds to an erosional ravinement surface draped by a transgressive lag of coastal deposits usually containing coquinas and/or conglomerates (Mas, 2013, 2015; Mas and Fornós, 2020). The lower contact of the Ses Olles Formation with the Santanyí limestones is sporadically marked by a well-developed reddish paleosol (Mas, 2013, 2015; Mas and Fornós, 2020), which indicates that a (unquantified) period of subaerial exposure occurred before the emplacement of the Ses Olles Fm. However, in their more recent study, Mas and Fornós (2020) surprisingly conclude that the Ses Olles Formation has a conformable contact with the Santanyí limestones, ascribed to part of Stage 1. This led Mas and Fornós (2020) to conclude that the emplacement of the Ses Olles Fm. pre-dated the MSC peak and that the erosional surface marking the Miocene/Pliocene boundary is associated with a 270 kyr hiatus linked to the main MSC base-level drawdown (Fig. 1.4b). This conclusion is, however, in disagreement with the unconformity at the base of the Ses Olles Fm., which instead points to the deposition of the Ses Olles Fm. (and therefore to the arrival of the Paratethyan fauna in Mallorca) at some point during Stage 3 of Roveri et al. (2014a).

1.3.5 Piedmont Basin

The Piedmont Basin (NW Italy) contains the northernmost record of the MSC (Fig. 1.2b). The terminal MSC sediments (i.e. the Cassano Spinola Conglomerates Fm.) overlay pre-MSC units, the PLG deposits (Gessoso Solfifera Fm.) or reworked evaporites (Valle Versa chaotic complex, VVC) and underly the Zanclean marls of the Argille Azzurre Fm. (Dela Pierre et al., 2011). The Cassano Spinola Conglomerates is splitted in two sub-units by Dela Pierre et

al. (2016). Sub-unit a consists of azoic grey mudstones turning to yellowish silty mudstones (Fig. 1.5d) typified by in situ root traces, paleosols and mud cracks and including three/four intercalated lens-shaped, cross-bedded conglomeratic layers (Ghibaudo et al., 1985; Dela Pierre et al., 2011, 2016). Abundant land plant leaves and a diverse terrestrial vertebrate fauna are found in the yellowish siltstones, which have been interpreted as overbank deposits (Harzhauser et al., 2015; Colombero et al., 2017 and references therein). In this continental interval, a low-diversity fish fauna consisting of otoliths of marine and Paratethyan species is found (Grunert et al., 2016; Carnevale et al., 2018; Schwarzhans et al., 2020). These otoliths were Sr-dated to the early-middle Miocene (Grunert et al., 2016). Nevertheless, they were concluded not to be physically reworked, but rather to have been transported by large marine predators, therefore implying a Piedmont Basin-(marine) Mediterranean connection was in force (Grunert et al., 2016; see section 1.5.6). Sub-unit b (i.e. Strati a Congeria *sensu* Sturani, 1973) is made of grey mudstones bearing a mixture of in-situ brackish water mollusks (Sturani, 1973; Esu, 2007) and ostracods (Trenkwalder et al., 2008) of Paratethyan affinity along with physically reworked foraminifera and calcareous nannofossils (Trenkwalder et al., 2008; Violanti et al., 2009). The transition to the Pliocene Argille Azzurre Fm. is sharp above a characteristic black and azoic sandy layer (Fig. 1.6c) rich in terrigenous and intrabasinal (i.e. glaucony and phosphates) grains and disarticulated valves of both brackish-water and continental bivalves, but barren of in-situ fossils (Trenkwalder et al., 2008). The occurrence, at its top and directly below the Argille Azzurre Fm., of abundant *Thalassinoides* trace fossils filled with Pliocene sediments led Trenkwalder et al. (2008) and Dela Pierre et al. (2016) to interpret the top surface of this layer as an omission surface. This surface indicates a period of basin starvation (and therefore a hiatus) due to a sudden increase in water-depth, ascribed by Trenkwalder et al. (2008) to the Zanclean reflooding. This hiatus may have lasted for only part of the late Messinian (Violanti et al., 2009; Dela Pierre et al., 2016) or may have endured into the Pliocene (Trenkwalder et al., 2008).

1.3.6 Po Plain

To the east, the Messinian sediments in the Piedmont Basin disappear beneath the km-thick Plio-Quaternary succession of the Po Plain-Adriatic Foredeep (PPAF; Fig. 1.2a). By definition of Ghielmi et al. (2010) and Amadori et al. (2018), the PPAF includes two main elongated depocenters enclosed within the northern Apennines to the South and the Southern Alps to the North: the easternmost portion of the Po Plain and the whole present-day northern Adriatic Sea. Here, for simplicity, we include in the definition of PPAF also its westernmost depocenters of the Western Po Plain Foredeep. The Messinian-Pleistocene sedimentary sequence, studied through the integration of seismic and borehole observations, is mostly represented by thick sequences of turbidite deposits in the foreland depocenter passing, towards the margins, to fluvial and deltaic systems related to the proximity of the marginal thrust-fold-belts (Cipollari et al., 1999; Ghielmi et al., 2010, 2013; Rossi et al., 2015a; Rossi, 2017). During MSC Stage 1,

primary evaporites and dolomicrites were deposited in some shallow-water settings, while evaporitic deposition was inhibited in the deep-water settings, where it was replaced by deposition of anoxic mudstones (Ghielmi et al., 2010). Instead, the post-evaporitic deposits consist of large thicknesses (up to 1 km) and volumes of coarse-grained clastics (LM1 and LM2 of Rossi and Rogledi, 1988; ME3 or Fusignano Fm. of Ghielmi et al., 2010; ME4 of Ghielmi et al., 2013; ME3b and possibly ME3a of Rossi et al., 2015a). Several authors (Ghielmi et al., 2010, 2013; Rossi et al., 2015a; Amadori et al., 2018; Cazzini et al., 2020) showed that these post-evaporitic sediments are the infilling of ca. N-S and NW-SE trending, V-shaped valleys (Fig. 1.5e). These valleys were carved at least as far as 50 km into the Alps, to a depth up to 1 km into the pre- and syn-evaporitic Messinian deposits and nicely shape the present-day river network of the southern Alps (Amadori et al., 2018).

Different mechanisms for the incision have been proposed, with major implications for the desiccated vs full Mediterranean controversy (Figs. 1.1b-c). Ghielmi et al. (2010, 2013), Rossi et al. (2015a), Amadori et al. (2018) and Cazzini et al. (2020) ascribed the valley incision along the PPAF northern margin to fluvial erosion, whose basinward shifting was triggered by the Stage 2 Mediterranean drawdown, estimated to have been around 800-900 m (Ghielmi et al., 2013; Amadori et al., 2018). In this case, Stage 3 deposition in the PPAF occurred in endorheic lakes fed by the Alpine rivers and kept isolated until the Zanclean, when the sudden sea-level rise following the Zanclean reflooding was enough to bypass morphological highs (e.g. Gargano-Pelagosa and/or Otranto paleosills) located in the southern Adriatic foredeep (Fig. 1.2a; see Pellen et al., 2017; Amadori et al., 2018; Manzi et al., 2020). Conversely, Winterberg et al. (2020) suggested that the over-deepened valleys on the southern slope of the Alps are related to Pleistocene glacial erosion. Although Winterberg et al. (2020) do not address the paleoenvironment during the Messinian, this interpretation does not rule out the possibility that (at least part of) Stage 3 sedimentation occurred in a PPAF connected to the Mediterranean water mass and that no catastrophic reflooding occurred at the Miocene/Pliocene boundary. The conclusion of a non-catastrophic refilling was also drawn by Pellen et al. (2017) on the basis of the onshore Adriatic record (see subsection 1.3.7).

1.3.7 Apennine system

The Messinian deposits resurface to the south of the PPAF sector and extensive sections are found in several basins on both the foreland domain (Adriatic side of the partially uplifted Apennine chain), subjected to compressional tectonics during the late Messinian, and the back-arc domain (Tyrrhenian side), contemporaneously affected by extension (Fig. 1.2b; Cipollari et al., 1999; Schildgen et al., 2014; Cosentino et al., 2018). Overall, the MSC record of the Apennines is subdivided into an evaporitic and post-evaporitic interval squeezed in between two marine units (Messinian Euxinic Shales Fm. at the base and Zanclean Argille Azzurre Fm. atop; Fig. 1.4a). Different vertical motions related to ongoing Apenninic tectonics

resulted in the deposition of Stage 3 sediments with highly variable sedimentary expression and stratigraphic resolution from basin to basin. The post-evaporitic deposits are alternatively found resting unconformably, with an erosional contact associated to an angular unconformity, above the alternations of the Gessoso Solfifera Fm./PLG, or conformably above evaporitic-free cycles lateral equivalent of the marginal PLG (Fig. 1.4a; e.g. Roveri et al., 1998, 2008a). This led to the conclusion that both shallow and deep-water successions are present in the Apennine foredeep system (Roveri et al., 2001).

The physical-stratigraphic model developed for the post-evaporitic interval in the Romagna area (i.e. Northern Apennines) and applied to the whole Apennine domain was subdivided into two allounits (named p-ev1 and p-ev2) based on a basin-wide shift in facies, overall stacking patterns and depositional trends (i.e. progradational and retrogradational, respectively; Roveri et., 1998, 2001, 2005, 2008a; Manzi et al., 2005, 2007, 2020). Allounit p-ev1 only accumulated in deep-water settings (e.g. Cusercoli, Sapigno, Maccaroneand Trave sections; Roveri et al., 1998; Iaccarino et al., 2008; Cosentino et al., 2013) during the subaerial exposure of the basin margins (e.g. Vena del Gesso Basin, Monticino quarry, Pellen et al., 2017). It starts with resedimented clastic evaporites (i.e. Sapigno Fm.) followed by a coarsening- and shallowing-upward succession (i.e. di Tetto or San Donato Fm.) of mudstones with intercalated turbiditic sandstones (Fig. 1.5f) and a volcaniclastic marker bed dated initially by $^{40}Ar/^{39}Ar$ at ~5.50 Ma (Odin et al., 1997) and later by $^{238}U/^{206}Pb$ at 5.5320±0.0046/0.0074 Ma (Cosentino et al., 2013; Fig. 1.3a). Allounit p-ev2 (i.e. Colombacci Fm.) occurs in the deeper depocenters in 4/5 sedimentary cycles consisting of three >5 m-thick coarse-grained bodies (conglomerates and sandstones) and two black-colored mudstone beds alternating with fine-grained mudstones/clays with intercalated three micritic limestones (known in literature as Colombacci limestones; Figs. 1.3a, 1.5g; Bassetti et al., 2004). By contrast, an incomplete Colombacci Fm. deposited in the shallower thrust-top basins (e.g. Vena del Gesso Basin and Molise sections; Pellen et al., 2017; Cosentino et al., 2018). The p-ev2 cycles have been interpreted as reflecting the alternation of wet (mudstones and Colombacci limestones in Eastern Romagna) and dry (coarse-grained facies and Colombacci limestones in the Maccarone section) phases controlled by Milankovitch-driven climatic factors (Fig. 1.3a; Roveri et al., 2008a; Cosentino et al., 2013) and, as such, they have been used for the astronomical tuning of the Colombacci Fm. to the Lago-Mare phase (Figs. 1.3a, 1.4a; see section 1.2.2). By contrast, Clauzon et al. (2005) and Popescu et al. (2007) moved the Colombacci Fm. into the Pliocene (Fig. 1.4b). However, this conclusion has been proven to rely on wrong stratigraphic and paleontological arguments (see Roveri et al., 2008c, Grothe et al., 2018, section 1.5.5 and chapter 5). Substage 3.2 records in the Apennines do not always contain the three prominent conglomeratic facies as in Romagna, but only laminated to massive clays with sandy intercalations equivalent to the ones typifying substage 3.1 records (e.g. Maccarone section; Sampalmieri et al., 2010; Cosentino et al., 2013; Fig. 1.5f). The absence of a lithological cyclicity that clearly mimics an orbital signal largely hampered the

astronomical tuning of these clay-dominated sections, although an attempt has been made with the Maccarone section (Cosentino et al., 2013). The only exception is represented by the Fonte dei Pulcini section, which has been equipped with an age framework by astronomical tuning of the magnetic susceptibility (Cosentino et al., 2012). Despite the lack of outstanding lithological changes these sections are often provided with a lithostratigraphic subdivision using the same nomenclature as in the Romagna area. When applied, the di Tetto Fm./Colombacci Fm. boundary is placed high in the sections, i.e. few tens of meters underneath the M/P boundary, resulting in a much different thickness of the formations compared to the Romagna area.

Stage 3 sediments are poorly exposed on the Tyrrhenian Sea onshore side of Italy (Fig. 1.2b). The best known succession crops out in the Cava Serredi quarry in the Fine Basin (Tuscany; Bossio et al., 1978, 1993; Carnevale et al., 2006b, 2008). Here the MSC has a thickness of ~150 m, of which only the uppermost ~100 m are attributed, without clear arguments, to Stage 3 by Carnevale et al. (2006b). The lowermost ~40 m of the Stage 3 unit consist of mudstone with alternating sandstone bodies which have been attributed to Roveri et al. (1998)'s p-ev1 allounit, while the uppermost ~60 m form the p-ev2 allounit and include two prominent conglomerate bodies alternating with mudstones interbedded with sandstone horizons and black, organic-rich layers (Carnevale et al., 2006b). A few and more fragmented sections are also described on the Tyrrhenian Sea side of Italy by Cipollari et al. (1999).

The M/P boundary is variably expressed through the Apennine system: unconformable above the ostracod-bearing clays and highlighted by erosional surfaces draped by conglomeratic accumulations (e.g. Stingeti section in Molise; Cosentino et al., 2018), conformable above 0.5-1 m-thick black mudstones similar to how it is observed in Piedmont and of equally unknown paleoenvironmental significance (e.g. Romagna area and Maccarone section; Roveri et al., 1998; Gennari et al., 2008) or conformable above the ostracod-rich mudstones (e.g. Maccarone and Fonte dei Pulcini sections; Cosentino et al., 2005, 2012, 2013; Sampalmieri et al., 2010).

All p-ev1 deposits studied are almost devoid of in-situ biota, except for fish otoliths and three fish skeletons found in the upper substage 3.1 part of Cava Serredi (Carnevale et al., 2006b). The p-ev2/Colombacci deposits, instead, host typical Paratethyan assemblages of brackish-water mollusks, ostracods, dinocysts and fish (Bassetti et al., 2003; Bertini, 2006; Popescu et al., 2007; Grossi et al., 2008; Iaccarino et al., 2008; Cosentino et al., 2012, 2018; Schwarzhans et al., 2020). A diverse array of marine fossils (benthic and planktic foraminifera, calcareous nannofossils, dinocysts and fish otoliths and skeletons) has also been reported from the horizons containing these Paratethyan taxa (Bertini, 2006; Carnevale et al., 2006a; Popescu et al., 2007; Pellen et al., 2017). While the autochthony of ostracods, when considered, is unquestioned, the allochthonous vs autochthonous character of the other mentioned fossils is disputed and still unclear (see section 1.1.5).

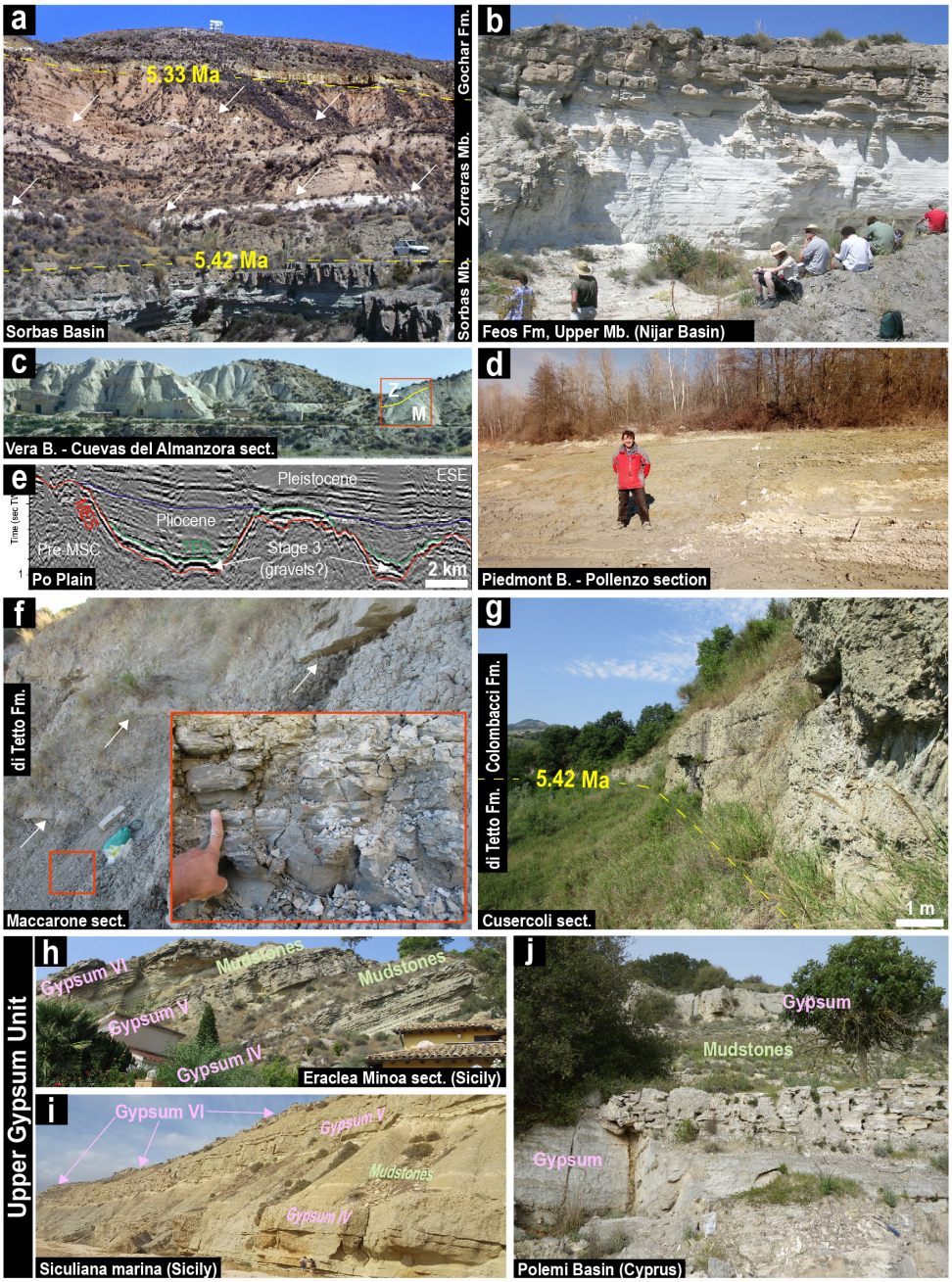

Fig. 1.5. *Sedimentary expression of Stage 3 from selected onshore Mediterranean localities.* **(a)** *Photograph from the Sorbas Basin showing the red continental sediments of the Zorreras member with intercalated white limestones (white arrows; from Andreetto et al., 2021b). The conformable resting of the Zorreras Mb. above the*

Sorbas Mb. and underneath the Gochar Fm. of Pliocene age is also appreciable. Car for scale. **(b)** *One typical lithological (and precessional) cycle of the Upper Mb. of the Feos Fm. in the Nijar Basin, here constituted by an ostracod-bearing, white and laminated mudstone bed overlain by an azoic fluvial sandstone (courtesy of Anne Fortuin).* **(c)** *Panoramic view of the Cuevas del Almanzora section (from Andreetto et al., 2021). Red rectangle indicates the position of the section straddling the Messinian (M)/Zanclean (Z) transition and studied by Fortuin et al. (1995), Stoica et al. (2016), Caruso et al. (2020) and Andreetto et al. (2021b). Buildings for scale.* **(d)** *The sub-unit a of the Piedmont Basin composed of azoic grey mudstones grading into yellowish, mammal-rich overbank deposits.* **(e)** *WNW-ESE seismic profile in the Po Plain showing incised valleys filled during Stage 3 by suggested clastic deposits and sealed by deep-water turbidites in the Zanclean (modified from Amadori et al., 2018).* **(f)** *Typical aspect of the di Tetto/San Donato Formation in the Northern Apennines composed by grey mudstones (detail in the inset) with interbedded sandstone bodies (white arrows). The picture is taken from the Maccarone section.* **(g)** *The di Tetto Fm.-Colombacci Fm. transition in the Cusercoli area (Eastern Romagna; Fig. 1.2b), defined by the facies change underlined by the appearance of a fluvial conglomerate. This lithostratigraphic boundary also corresponds to substage 3.1/3.2 boundary of Roveri et al. (2014a).* **(h)**, **(i)**, **(l)** *Lithological cycles of the Upper Gypsum Unit in Eraclea Minoa (h), Siculiana Marina (i) and Polemi (l) sections. Cycles are several m-thick and primarily composed by beds of primary gypsum alternating with mudstones bearing Paratethyan ostracods (at least in Eraclea Minoa).*

1.3.8 Sicily

The MSC record is widely exposed on Sicily, mainly in the Caltanissetta Basin and in scattered locations on the Hyblean Plateau (i.e. Ragusa-Siracusa area) and the Messina area (Fig. 1.2b; Butler et al., 1995; Manzi et al., 2009; Sciuto et al., 2018). Like the Northern Apennines, it shows a complex distribution and variable stratigraphy that mirrors the structuring of Sicily into basins with different characters, geometries and depocenters which subsided at different times and rates (Butler et al., 1995; Catalano et al., 2013). This structural setting permitted the simultaneous deposition of shallow- and intermediate-water sediments (Roveri et al., 2008b). Mostly found in the Caltanissetta Basin, these intermediate-water successions have for decades been considered the onshore counterpart of the offshore evaporitic trilogy seen in seismic data from the Western Mediterranean Basin (Decima and Wezel, 1973). More recently, Raad et al. (2021) attempted a similar onshore-offshore correlation but with the intermediate Central Mallorca Depression. The currently endorsed stratigraphic model (Fig. 1.4a), refined over the years by Decima and Wezel (1971, 1973), Decima et al. (1988), Butler et al. (1995), García-Veigas et al. (1995), Rouchy and Caruso (2006), Roveri et al. (2008b) and Manzi et al. (2009), envisages two 'evaporitic cycles'. The 'First cycle', overlying both alluvial and deep-water sediments (Tripoli Fm., Licata Fm. and Terravecchia Fm.; see Maniscalco et al., 2019 and references therein), comprises the disputed Calcare di Base (Manzi et al., 2011, 2016b vs Caruso et al., 2015), PLG or Gessi di Cattolica Fm. (Decima and Wezel, 1973; Lugli et al.,

2010) and the Halite Unit (Lugli et al., 1999). The 'Second cycle' comprises the Upper Gypsum (UG) or Gessi di Pasquasia Fm., which is only present in depocenters of the Caltanissetta Basin (see Manzi et al., 2009 for a detailed overview), sporadically overlain by the siliciclastic Arenazzolo Fm. (Decima and Wezel, 1973; Cita and Colombo, 1979). The whole succession is sealed by the Pliocene marine Trubi Fm. (Fig. 1.4a). The two evaporite cycles are separated by an erosional surface (MES) associated with an angular discordance broadly linked to the main Mediterranean drawdown event (e.g. Butler et al., 1995; Roveri et al., 2008b). Clauzon et al. (1996), however, placed the MES at the Arenazzolo Fm./Trubi Fm. transition, implying that the entire evaporitic deposition in the Caltanissetta Basin pre-dated the offshore one, but they do not provide evidence of erosion at that level. In more recent publications from the same research group, the MES is shifted towards the base of the Arenazzolo Fm. (e.g. Bache et al., 2012), again without evidence of major erosion, and different ages are assigned (see Fig. 1.4b and Grothe et al., 2018 for details).

The Upper Gypsum successions are commonly incomplete in many of the Caltanissetta Basin sections (Pasquasia-Capodarso, Casteltermini, Alimena, Nicosia, Siculiana-Marina; Decima and Sprovieri, 1973; Rouchy and Caruso, 2006; Manzi et al., 2009; Fig. 1.5i). In the most complete section, Eraclea Minoa (Fig. 1.3a), the Upper Gypsum Unit consists of 6 (Van der Laan et al., 2006) to 7 (Manzi et al., 2009) primary gypsum beds with a repetitive internal organization of facies (see Schreiber, 1997 and Manzi et al., 2009 for facies description) interbedded with marls and lenticular terrigenous sandstone bodies, gypsarenites and gypsrudites (Fig. 1.5h). Two of the terrigenous sandstone bodies are highlighted by Manzi et al. (2009) in the thick (~60 m), *Cyprideis agrigentina*-rich (Grossi et al., 2015), marly interval dividing gypsum VI and VII for its alleged astronomical significance (Fig. 1.3a; see section 1.2.2). A mixed (physically reworked) marine (foraminifera and dinocysts) and (in-situ) brackish biota (ostracods and dinocysts) of Paratethyan origin characterizes the marly interbeds from at least gypsum III upwards (following the investigations carried on the Eraclea Minoa section; Bonaduce and Sgarella, 1999; Rouchy and Caruso, 2006; Londeix et al., 2007; Grossi et al., 2015; Fig. 1.3a). Calcareous nannofossils have been found along with the above organisms in a more northerly location by Maniscalco et al. (2019) and considered reworked. Above the last gypsum, the ~6-7 m-thick Arenazzolo Fm. is found, represented by reddish arkosic cross-laminated and poorly consolidated sand (Bonaduce and Sgarella, 1999; Roveri et al., 2008b) and interpreted as the expression of a shallow-water delta, albeit without a sedimentological investigation (e.g. Decima and Wezel, 1973; Cita and Colombo, 1979). The whole Stage 3 sequence is conformably overlain by the Zanclean marine Trubi Fm. in the basin center (e.g. at Eraclea Minoa and Capo Rossello; Brolsma 1975; Cita and Colombo, 1979; Van Couvering et al., 2000; Rouchy and Caruso, 2006; Manzi et al., 2009; Fig. 1.6d) and unconformably in the shallower, marginal areas (Manzi et al., 2009; Roveri et al., 2019b). Only Decima and Wezel (1973) and Raad et al. (2021) report the M/P transition in the key, intermediate water-

representative section of Eraclea Minoa as erosive. However, they do not provide evidence (e.g. photographic documentation) for the presence of an erosional unconformity and, moreover, Raad et al. (2021) erroneously refer to Cita and Colombo (1979), where no erosion is mentioned at the M/P boundary in Eraclea Minoa.

The bathymetric jump between the <100 m of water depth during the late Messinian and the >200 m at the base of the Trubi Fm. is often regarded as a key onshore evidence of the sudden and catastrophic Mediterranean-Atlantic re-connection at the M/P boundary (e.g. Caruso et al., 2020). However, the real depth of the base of the Trubi is all but obvious. In fact, variable estimates have been proposed based on the observed benthic foraminifera and/or psychrospheric ostracods at Capo Rossello and Eraclea Minoa: 200-500 m (Decima and Wezel, 1973), 600-800 m (Sgarrella et al., 1997, 1999; Barra et al., 1998), 1400-2400 m (Cita and Colombo, 1979).

1.3.9 Greece

Several MSC localities are reported from the Greek Ionian Islands (Corfu, Cephalonia and Zakynthos) and from Crete (Fig. 1.2b).

On the NW coast of Corfu (Aghios Stefanos section), the PLG unit is missing and only a 32 m-thick cyclically-arranged terrigenous succession is present comprising three m-thick conglomerate beds alternating with fine-grained deposits rich in unspecified species of brackish water ostracods (Pierre et al., 2006).

In the southern part of Zakynthos, an evaporitic succession composed of eight gypsum cycles (Kalamaki section) occurs above marine marly deposits (Karakitsios et al., 2017b). These gypsum beds were initially ascribed to the UG unit (Pierre et al., 2006) and later to the PLG (Karakitsios et al., 2017b). The gypsum unit is overlain by approximately ~13 m of siltstones and marls with scattered, cm-thick beds of sandstones, conglomerates and carbonates with nodular texture (Pierre et al., 2006; Karakitsios et al., 2017b). Although no ostracods are reported from this interval, due to its stratigraphic position the post-evaporitic unit is correlated to the Lago-Mare phase (Karakitsios et al., 2017b). Except for the rare presence of marine nannofossils (*Ceratolithus acutus* together with *Reticulofenestra zancleana*) just below the Miocene/Pliocene boundary, only reworked marine fauna has been reported from the post-evaporitic package (Karakitsios et al., 2017b). This dominantly terrigenous succession is unconformably overlain by the Zanclean Trubi Formation (Fig. 1.6e; Karakitsios et al., 2017b).

MSC deposits on Crete (e.g. Meulenkamp et al., 1979; Delrieu et al., 1993; Cosentino et al., 2007; Roveri et al., 2008a; Zachariasse et al., 2008, 2011) were deposited in Miocene extensional, fault-bound basins driven by tectonic subsidence that ceased in the late Pliocene and Pleistocene (van Hinsbergen and Meulenkamp, 2006). Because of the strong tectonic and eustatic sea-level-related fragmentation of the stratigraphic record, reconstructing the late Miocene stratigraphy of Crete has not been straightforward (Zachariasse et al., 2008, 2011).

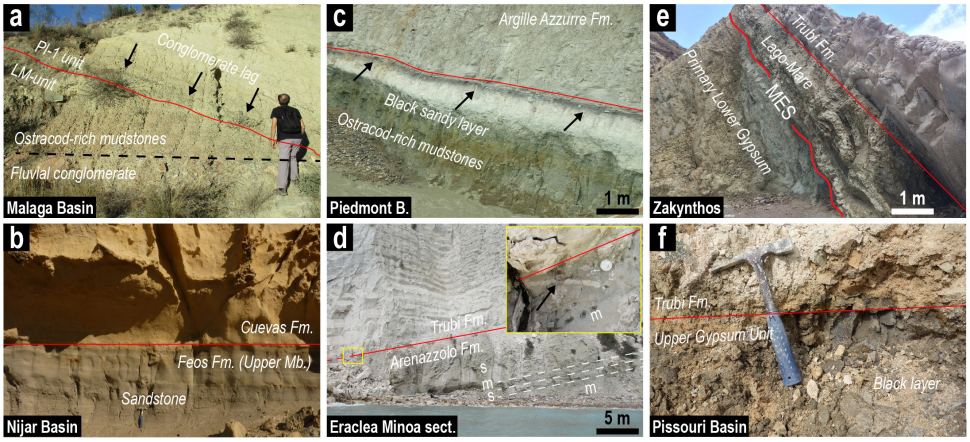

Fig. 1.6. *Photographs of the Miocene/Pliocene boundary (yellow lines) from selected onshore Mediterranean localities.* ***(a)*** *Erosive M/P transition in the Mendelín section (Malaga Basin). Note the conglomeratic lag draping the erosional surface and sharply overlain by foraminifera-rich marls.* ***(b)*** *Conformable stratigraphic contact between the uppermost Messinian sandstone of the Feos Fm. and the Zanclean biocalcarenites of the Cuevas Fm. in the Barranco de los Castellones section, Nijar Basin (hammer for scale; modified from Andreetto et al., 2021).* ***(c)*** *The Messinian/Zanclean boundary in the Pollenzo section (Piedmont Basin) marked by a characteristic black layer interbedded between Paratethyan ostracods-rich mudstones and marine foraminifera-rich marls (modified from Dela Pierre et al., 2016).* ***(d)*** *Uppermost segment of the Eraclea Minoa section (Caltanissetta Basin, Sicily) displaying the (non erosive) contact between the Pliocene Trubi Formation above and the sandy Arenazzolo Formation below. The inset is a close view of the transition, which occurs above a ~50 cm-thick burrowed mudstone horizon rich in Paratethyan ostracods and marine foraminifera.* ***(e)*** *Lago-Mare sediments in the Kalamaki section (Zakynthos) unconformable, through an erosional surface (i.e. the Messinian Erosional Surface, MES), over the PLG unit and also unconformable beneath the Trubi Fm. (modified from Karakitsios et al., 2017b).* ***(f)*** *Close view of the M/P boundary in the Pissouri Basin, where the foraminifera-rich Trubi marls lie above a black layer (paleosol according to Rouchy et al., 2001).*

Several primary and clastic gypsum facies are recognized, but their correlation with the MSC stratigraphy is disputed (see Cosentino et al., 2007; Roveri et al., 2008a, 2014a; Zachariasse et al., 2008). Coarse-grained, mammal-bearing terrigenous facies irregularly alternating with marls are in places found unconformably overlying the gypsum and separated from the Pliocene facies by an erosion surface (see Meulenkamp et al., 1979; Delrieu et al., 1993; Cosentino et al., 2007). In two localities on the Messarà Plain, Cosentino et al. (2007) described a highly diversified ostracod fauna with Paratethyan affinity in some marly intervals.

Messinian evaporites and/or Lago-Mare deposits are also reported from the North Aegean region onshore in the Strymon Basin (Snel et al., 2006; Suc et al., 2015; Karakitsios et al., 2017a) and Dardanelles region (Melinte-Dobrinescu et al., 2009) and offshore (Prinos-Nestos Basin;

Karakitsios et al., 2017a), but recent integrated studies suggested that the sections studied by the above listed authors are older than the MSC (see Krijgsman et al., 2020a, b). In particular, Krijgsman et al. (2020a) proposed that for most, if not all, of the MSC the North Aegean was a brackish water, mostly Paratethyan-fed basin restricted by the Cyclades sill to the south (Fig. 1.2a) and forming a passageway for Paratethyan overspill waters towards the Mediterranean.

1.3.10 Cyprus

MSC deposits on Cyprus outcrop in the Pissouri, Psematismenos, Mesaoria and Polemi basins on the southerly fringe of the Troodos massif (Fig. 1.2b; Rouchy et al., 2001; Manzi et al., 2016a). According to Rouchy et al. (2001) and Orszag-Sperber et al. (2009), sediments belonging to all MSC stages of Roveri et al. (2014a) are preserved in the Cypriot basins. By contrast, Robertson et al. (1995) and Manzi et al. (2016a) considered that PLG evaporites on Cyprus are only present as fragments reworked within a chaotic unit (the Lower Gypsum and Intermediate breccia units of Orszag-Sperber et al., 2009) and that the only in situ evaporites belong to the overlying Upper Gypsum Unit, which encompasses the whole of Stage 3 (Figs. 1.3a, 1.4a). A continuous, Eraclea Minoa-like section is not known in Cyprus (Manzi et al., 2016a). The best exposure of the lower 60 m of this unit is found in the Polemi Basin (Manzi et al., 2016a). It comprises up to six gypsum beds (the lower two and the fifth of which are mainly selenitic, while the third, fourth and sixth are predominantly laminated; Fig. 1.3a). Gypsum beds range in thickness from 1 to 6 m and are separated by laminated marls (Fig. 1.5j) occasionally interbedded with conglomerates and sandstones (e.g. between the 5th and 6th gypsum layers; Rouchy, 1982; Rouchy et al., 2001; Manzi et al., 2016a). The sixth gypsum bed is reported by Rouchy et al. (2001) to be hollowed in the upper part with the cavities filled with overlying sediments. The similarity of the cyclicity and facies association of this Cyprus succession with the substage 3.1 interval of the Sicilian UG led Manzi et al. (2016a) to propose a bed-to-bed correlation and to recognize the substage 3.1/3.2 boundary at the top of the last gypsum bed (Fig. 1.3a). According to Orszag-Sperber et al. (2000) and Rouchy et al. (2001), this chronostratigraphic boundary coincides with a Mediterranean-scale sea-level drop, a conclusion that arises from the interpretation of the cavities in the uppermost gypsum as the product of karstic dissolution following a prolonged period of subaerial exposure.

The sedimentary sequence overlying the last gypsum bed and assigned by Manzi et al. (2016a) to the Lago-Mare phase lacks a clear and rhythmic sedimentary cyclicity. In the Pissouri Basin this interval (up to 25-30 m-thick) mostly consists of conglomerates, sandstones, limestones, paleosols (which appear as dm to m-thick dark marly horizons, in one case with pulmonated gastropods) and subordinated clay-marly horizons (Rouchy et al., 2001). By contrast, in the Polemi sections the clay-marly facies dominates this interval (Rouchy et al., 2001). In situ fresh-brackish water species of articulated mollusks (*Limnocardiidae*, *Melanopsis*), Paratethyan (*Loxocorniculina djafarovi, Euxynocythere praebaquana*) and Mediterranean

(*Cyprideis agrigentina*) ostracods and foraminifera (*Ammonia beccarii*), Characeae, abundant fragments of the marine euryhaline fish Clupeidae and a fish skeleton of the euryhaline *Aphanius crassicaudus* are described from some of the substage 3.1 and 3.2 fine-grained facies and within the terrigenous laminae of some balatino gypsum (Orszag-Sperber et al., 2000; Rouchy et al., 2001; Orszag-Sperber, 2006; Manzi et al., 2016a). The upward change in diversity of the ostracod fauna seen elsewhere (e.g. Malaga, Nijar, Vera, Apennines and Eraclea Minoa) is not reported in Cyprus, but this may be because no detailed study of ostracod assemblages in Stage 3 sediments has been published. The M/P boundary near Polemi village is described by Manzi et al. (2016a) as a sharp contact above a dark, organic-rich layer (Fig. 1.6f). It appears to be similar to the boundary reported from Piedmont (Fig. 1.6c; Trenkwalder et al., 2008; Dela Pierre et al., 2016) and Northern Apennines (Gennari et al., 2008; Grossi et al., 2008), if not for the presence, in Cyprus, of (possibly) in-situ *Cyprideis agrigentina* (Manzi et al. 2016a). A layer with the same field appearance, thickness (~ 1 m) and stratigraphic position is reported in Pissouri by Rouchy et al. (2001), which they interpreted as a paleosol based on mottling, oxidized roots, carbonate concretions and plant fragments.

1.3.11 Southern Turkey

The tectonically active, during the Miocene, thrust-top basin of Adana in southern Turkey (Radeff et al., 2017) retains the most complete and better exposed easternmost successions of the MSC (Fig. 1.2b), whose deposits were attributed to the Handere Fm. (Cosentino et al., 2010a; Radeff et al., 2016).

MSC Stage 3 finds expression in a >1 km thick continental unit unconformable, through an erosional surface, above the pre-evaporitic, Stage 1 anhydrite-shale alternations (Radeff et al., 2016) and resedimented gypsum-bearing Stage 2 deposits (Cosentino et al., 2010a; Cipollari et al., 2013). This unit mainly consists of fluvial coarse- and fine-grained deposits representing channel fill and overbank deposits. Sporadically, some fine-grained intercalations are found containing a mixed brackish (ostracod) and marine (foraminifera and calcareous nannofossils) fauna. The ostracod fauna has affinity with the Paratethyan fauna but, unlike to many other Mediterranean onshore localities, is poorly diversified, with monospecific assemblages of *Cyprideis agrigentina* (Avadan section and T-191 borehole; Cipollari et al., 2013) or with *Cyprideis agrigentina* accompanied by rare to abundant specimens of *Loxoconcha muelleri, Euxinocyhere (Maeotocythere) praebaquana*, and *Loxoconcha* sp. (Adana section; Faranda et al., 2013). Ostracods are often associated with *Ammonia beccarii* and rare *Elphidium* and *Cribroelphidium*, which are the only foraminifera considered as autochthonous. Conversely, the entire nannoflora is interpreted as physically reworked (Cipollari et al., 2013; Faranda et al., 2013).

The Handere Fm. is followed by early Zanclean marine sediments (Avadan Fm.) deposited, according to the paleoecology of the benthic foraminifera species recognized, at bathymetries

ranging from 200 to 500 m (Cipollari et al., 2013). The lithological nature of the M/P boundary in the Adana Basin is not clear, but it occurs either above the continental or subaqueous, ostracod-bearing facies.

A similar stratigraphic sequence is present in the subsurface. Here, however, chaotic gypsum-bearing deposits are not found and two halite bodies ~20 and ~170 m-thick are present, separated and followed by fluvial gravels, sands and silts (Cipollari et al., 2013).

1.3.12 Summary of the onshore Stage 3 record

Most of the onshore Stage 3 records formed in shallow marginal Mediterranean basins, which underwent substantial uplift from the Messinian till nowadays and are assumed to have had their depocenter at ~200 to 50 m below the Atlantic level during the late Messinian (Roveri et al., 2014a, 2019a; Radeff et al., 2016, 2017). The Caltanissetta Basin (Sicily), some basins along the Apennines and (possibly) Cyprus represent, instead, possible onshore representative of intermediate basins. The nature and duration of these records is quite variable, and there are only six sections that may record an entire Stage 3 sequence (i.e. Sorbas, Nijar, Northern Apennines, Eraclea Minoa and Cyprus; Fig. 1.3a). Reasons for the fragmentary nature of the Stage 3 sedimentary record include different durations of subaerial exposure following the Stage 2 drawdown, local tectonics and associated syn-depositional erosion and deposition. One of the consequences of this is that any sedimentary cyclicity that resulted from orbital fluctuations is typically either less well developed or poorly preserved, making the chronology of Stage 3 rather uncertain or controversial in places.

Despite this variability, several fairly consistent characteristics are widely expressed. These are:

(1) Stage 3 sedimentation follows a period of intensive tectonic and/or eustatic-driven erosion of the margins, as demonstrated by the frequent presence of erosional unconformities and/or chaotic Stage 2 deposits (RLG unit);

(2) Stage 3 lithologies are mostly terrigenous (conglomerates, sandstones and mudstones) and deposited in a variety of continental (fan delta, fluvial channels and alluvial plains) and shallow water environments (endorheic lakes or water bodies connected with the Mediterranean water mass is the riddle). Carbonate intercalations are sometimes present (e.g. Sorbas Basin and Colombacci limestones in the Apennines). Stage 3 gypsum is only found in deeper-water intermediate basins of Caltanissetta in Sicily and Cyprus.

(3) A diversified fossil assemblage with Paratethyan affiliation (ostracods, dinocysts, mollusks) is commonly found in the shallow-water sediments of Lago-Mare successions. Only in the intermediate Caltanissetta Basin (Sicily) do these diversified Paratethyan forms (only ostracods) occur earlier, in the sediments from substage 3.1. Where these have been studied in detail, these assemblages typically show an increase in diversity with time (possibly every wet phase of the precession cycles). Some of these sediments also contain marine fossils and there is controversy over whether these are in situ and contemporaneous or reworked.

In outcrop, the M/P boundary has four main sedimentary expressions: erosive and followed by a conglomeratic lag (e.g. Malaga, Vera, Mallorca; Fig. 1.6a); conformable above continental facies (e.g. Nijar Basin; Fig. 1.6b); conformable above ostracod-rich mudstones (e.g. Eraclea Minoa; Fig. 1.6d); sharp contact above a black layer of still largely unknown paleoenvironmental significance (Piedmont, Apennines and Cyprus; Figs. 1.6c, f). For a better understanding of how Stage 3 developed across the Mediterranean these marginal records now need to be considered alongside the evidence from intermediate to deep offshore settings.

We note that alternative chronostratigraphic frameworks have been proposed for several onshore (Malaga, Sorbas, Mallorca, Apennines, Sicily) and offshore (Sites 134B, 976B, 978A) locations (see Fig. 1.4b for references), but we have omitted them as they are shown to rely on incorrect (bio)stratigraphic arguments (see Roveri et al., 2008c, Grothe et al., 2018 and section 1.5.5).

1.4. Offshore domain

The offshore Mediterranean is a complex array of variable-depth and morphologically complex subbasins framed by morphological highs or sills. Traditionally it is divided into two main domains (Fig. 1.2a), the Western and Eastern Mediterranean, with the intervening divide (or Sicily sill) situated in the Sicily channel at present with a maximum depth of 316 m. The Alborán Basin, the depressions on the Balearic Promontory, the Corsica, Valencia, Algero-Balearic, Liguro (or Sardo)-Provençal and Tyrrhenian basins belong to the "Western Mediterranean" (Fig. 1.2a). The Adriatic foredeep, the Ionian, Sirte, Aegean and Levant basins belong in the "Eastern Mediterranean" (Fig. 1.2a). Smaller-sized depressions, again surrounded by sills of variable depth, are identified and labelled within each of these subbasins.

Although the exact topography and hypsometry of the Messinian Mediterranean is difficult to reconstruct, this present-day geography is generally assumed to have been in place, with five main differences: (1) the Alborán Basin was split into a Western (WAB) and Eastern Alborán (EAB) by a volcanic arc (Booth-Rea et al., 2018); (2) the Tyrrhenian Basin was only partly opened (Lymer et al., 2018); (3) the precise depth and width of the ancient Sicily Sill are difficult to estimate, but may have been much deeper than today (~300 m; Meijer and Krijgsman, 2005 Jolivet et al., 2006). Paleodepth estimations for the Messinian configuration range from 380 m (Just et al., 2011) to 430 m (García-Castellanos et al., 2009); (4) one or two sills were present at the southern termination of the Adriatic foredeep (Pellen et al., 2017; Amadori et al., 2018; Manzi et al., 2020); (5) the North Aegean was partially isolated from the Mediterranean by the Cyclades Sill and with high Paratethys affinity (Krijgsman et al., 2020a). Following the schematic classification of the Messinian sub-basins by Roveri et al. (2014a), all these subbasins are regarded as either intermediate (i.e. relatively deep-water, 200–1000 m) or deep (water depth >1000 m). Compared with the onshore domain, the offshore basins hold a far greater percentage of the total volume of MSC sediments (Ryan, 1973; Haq et al., 2020). The

architecture, geometry and main lithologies of the MSC and younger deposits are well known thanks to the high density of seismic data and the fact that evaporites (halite particularly) are easily identified on seismic profiles due to their unusual seismic properties, especially compared to those of terrigenous and carbonate sediments (see Lofi et al., 2011a, b; Lofi, 2018 and Haq et al., 2020). However, the detailed lithological, sedimentological, paleontological and geochemical nature and their chronostratigraphy are still poorly constrained offshore because these cannot be univocally defined on the basis of seismic data alone (Roveri et al., 2019b) and direct information about these deep MSC successions is limited to a small number of cores (16) drilled during the DSDP (Ryan et al., 1973; Hsü et al., 1978b) and ODP (Kastens et al., 1987; Comas et al., 1996; Emeis et al., 1996) drilling campaigns that penetrated exclusively the uppermost tens of meters of the deep MSC suite in very scattered localities (Fig. 1.2b). Only recently, access to industrial boreholes crossing the base of the halite in the deep Levant Basin has been granted, providing a rare glimpse of the deep MSC deposits in the easternmost part of the Mediterranean

The MSC is commonly described as tripartite ('Messinian trilogy' after Montadert et al., 1978) in the Western Mediterranean (Lower-Mobile-Upper units: LU-MU-UU, respectively). However, in the Ionian Basin is described as bipartite (MU-UU) by Camerlenghi et al. (2019), whereas according to Lofi et al. (2011), Gvirtzman et al. (2013, 2017), Lofi (2018) and Camerlenghi et al. (2019), the Levant Basin consists of the MU and the UU is only present locally and possibly represented by evaporite-free terrigenous accumulations (Kartveit et al., 2019; Madof et al., 2019). The lack of many age constraints within the offshore MSC successions hampers unambiguous correlation with onshore sequences (Fig. 1.1a; Roveri et al., 2014a). Nevertheless, different authors have proposed onshore-offshore correlation of specific events (e.g. onset, Ochoa et al., 2015; and termination of the MSC, Biscaye et al., 1972, Iaccarino et al, 1999) and stratigraphic schemes (Decima and Wezel, 1971; Raad et al., 2021) based on and biostratigraphic evidence (Cosentino et al., 2006), $^{87}Sr/^{86}Sr$ isotope ratios (Roveri et al., 2014b; Gvirtzman et al., 2017; Manzi et al., 2018) and astronomical tuning of the deep seismic record (Ochoa et al., 2015, 2018; Manzi et al., 2018; Meilijson et al., 2018, 2019). Here we focus on the seismic and geological (core-derived) properties of the Upper Unit (and laterally grading/interfingering sediments when present), stratigraphically below the Plio-Quaternary deposits (PQ) suggesting that it belongs to (at least part of) Stage 3.

1.4.1 Western Alborán Basin and westernmost East Alborán Basin

The Alborán Basin has received particular attention because of its proximity to the Gibraltar Corridor (Estrada et al., 2011; Popescu et al., 2015 and references therein). Evaporites only occur on the eastern side of the EAB (which is treated in subsection 4.2; Fig. 1.2a). To the west of the volcanic archipelago (Booth-Rea et al., 2018, i.e. the WAB) and immediately to the east on the western side of the EAB, only terrigenous sediments occur in the MSC interval (Booth-

Rea et al., 2018; de la Peña et al., 2020). Sediments at the M/P boundary appear in the seismic reflection data as parallel reflectors with increasing reflectivity (Comas et al., 1996, 1999; Booth-Rea et al., 2018). Locally, just below the M discontinuity, some of the reflectors suggest a chaotic seismic facies (Fig. 1.7a; Booth-Rea et al., 2018; Bulian et al., 2021). Miocene sediments with a maximum thickness of 100 m have been recovered from two out of nine holes drilled in the region (ODP 976B, 978A; Comas et al., 1996, 1999). These sediments mostly consist of claystones, siltstones and sandstones with Chondrites and Zoophycos ichnofacies at site 976B and include a conglomerate close to the M/P boundary at Site 978A. The lack of age-diagnostic fossils hampers their correlation with the Geologic Time Scale (GTS). However, the presence, high in the Miocene section, of an oligotypic association of ostracods (*Candona* sp., *Loxoconcha muelleri*, and *Cyprideis* sp.) with different stages of growth (Site 978A; Iaccarino and Bossio, 1999) and Paratethyan dinocysts (including *Galeacysta etrusca*; see section 1.5.2; Popescu et al. 2015) indicates a latest Messinian (substage 3.2) age and brackish paleodepositional conditions. Foraminifera and nannofossils are also present, but all species recognized are of no help in narrowing down the paleoenvironmental interpretation because they are considered either definitely or likely to be reworked (Iaccarino and Bossio, 1999). By contrast, Popescu et al. (2015) interpreted some species of calcareous nannofossils (*Reticulofenestra pseudoumbilicus, Discoaster quinqueramus, Ceratolithus acutus, Triquetrorhabdulus rugosus, Amaurolithus primus*) and marine dinocysts as autochthonous.

The nature of the M/P boundary is also uncertain. According to some authors, the "M" discontinuity is a high-amplitude reflector with evidence of erosion attributed to subaerial processes (Estrada et al., 2011; Urgeles et al., 2011) and locally (e.g. close to Site 121; Ryan et al., 1973) associated with an angular unconformity that abruptly truncates the upper Miocene deposits and morphological highs (Comas et al., 1999; Estrada et al., 2011; GarcIa-Castellanos et al., 2020). Although the M-reflector was drilled at Sites 976B, 977A and 978A, a lithological contact was only recovered at Site 976B coinciding with a major erosional surface between the early Messinian and the base of the Pliocene (Bulian et al., 2021). Only at Site 978A (and possibly 977A) was a few meters of what may be the contact interval recovered (Comas et al., 1996). This comprises a 25 m-thick cemented succession containing pebbles of volcanic and sedimentary rocks likely to derive from the Alborán substrate (46R, 620.9-630.67 mbsf, between the Pliocene-bearing core 45R and the Messinian-bearing core 47R; Comas et al., 1996). In contrast, Booth-Rea et al. (2018) concluded that the M-reflector is an unconformity only close to the mud diapirs and owes its erosive shape and angular discordance to the activity of these structures (Fig. 1.7a). In more undisturbed sectors these authors argue that the boundary is a paraconformity with no evidence of erosion (Fig. 1.7a). The lack of Messinian erosion in the shallow regions of the WAB margins has prompted the hypothesis that this area did not desiccate during the MSC (Booth-Rea et al., 2018; de la Peña et al., 2020). This contradicts much of the interpretation made of the DSDP and ODP cores of this interval in the Alborán

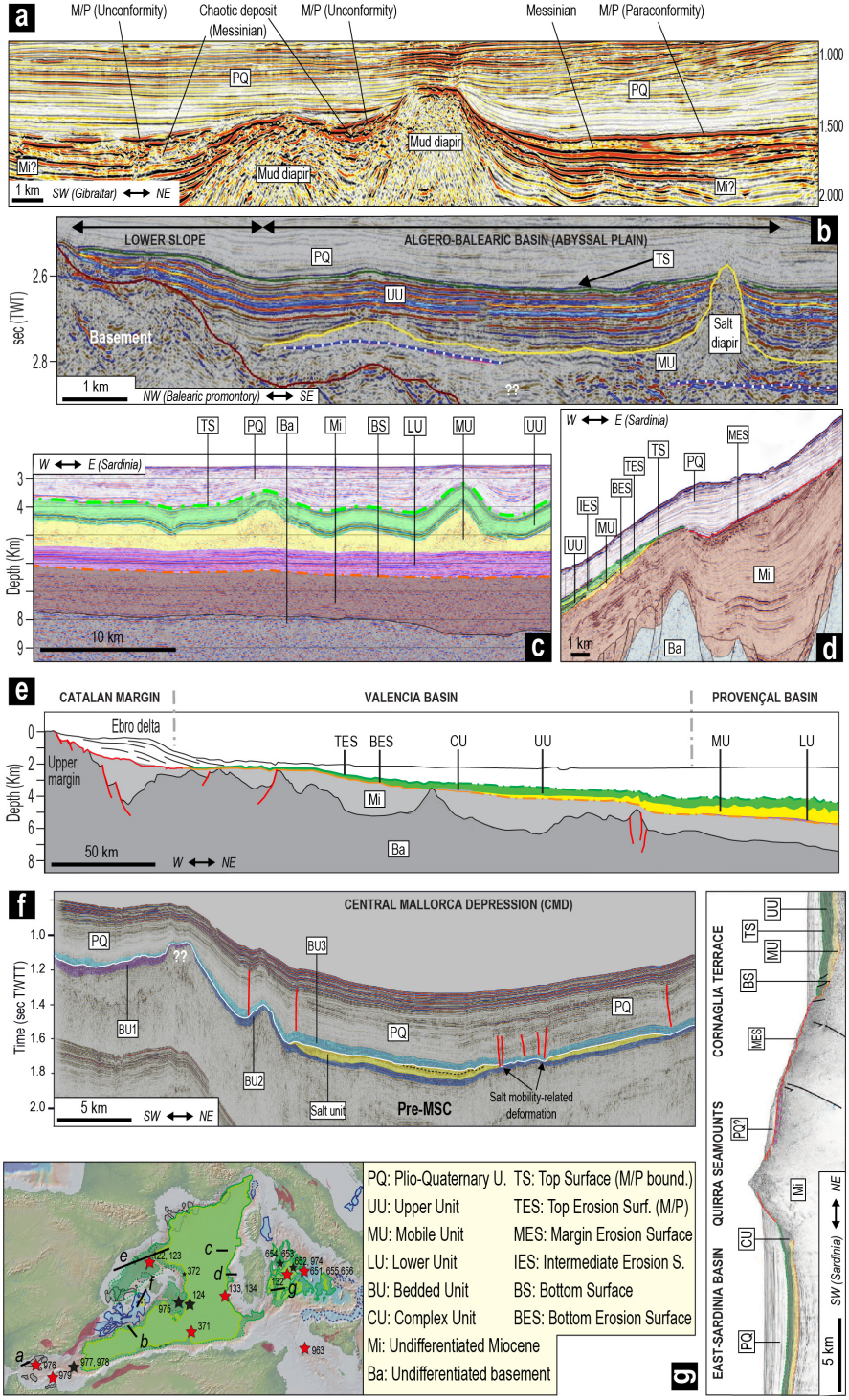
a
M/P (Unconformity)
Chaotic deposit (Messinian)
M/P (Unconformity)
Messinian
M/P (Paraconformity)
PQ
Mud diapir
Mi?
1 km
SW (Gibraltar) NE
1.000
1.500
2.000
b
LOWER SLOPE
ALGERO-BALEARIC BASIN (ABYSSAL PLAIN)
TS
UU
Salt diapir
MU
Basement
sec (TWT)
NW (Balearic promontory) SE
c
TS PQ Ba Mi BS LU MU UU
W E (Sardinia)
Depth (Km)
10 km
d
MES
TES
BES
IES
e
CATALAN MARGIN
VALENCIA BASIN
PROVENÇAL BASIN
Ebro delta
Upper margin
CU
50 km
f
CENTRAL MALLORCA DEPRESSION (CMD)
BU1
BU2
BU3
Salt unit
Pre-MSC
Salt mobility-related deformation
Time (sec TWTT)
5 km
SW NE
CORNAGLIA TERRACE
QUIRRA SEAMOUNTS
EAST-SARDINIA BASIN
SW (Sardinia) NE
PQ: Plio-Quaternary U.
UU: Upper Unit
MU: Mobile Unit
LU: Lower Unit
BU: Bedded Unit
CU: Complex Unit
Mi: Undifferentiated Miocene
Ba: Undifferentiated basement
TS: Top Surface (M/P bound.)
TES: Top Erosion Surf. (M/P)
MES: Margin Erosion Surface
IES: Intermediate Erosion S.
BS: Bottom Surface
BES: Bottom Erosion Surface

Fig. 1.7. *Seismic profiles from intermediate-deep Western Mediterranean containing MSC markers/units.* **(a)** *Seismic reflection line CAB01-104 from the WAB (modified from Booth-Rea et al., 2018). The line shows the variable geometry of the inferred M/P boundary, erosive in proximity of mud diapirs, (para)conformable in tectonically undisturbed sectors. Chaotic reflectors are occasionally imaged below the inferred M/P boundary.* **(b)** *Seismic profile SF12-09 imaging the lower slope of the south Algero-Balearic margin and part of the Algero-Balearic abyssal plain (modified from Mocnik et al., 2014). Here a high reflecting and horizontally stratified UU covers a thin layer of MU evidenced by salt diapirism. Note the concordant deformation of the UU and MU.* **(c)** *Line MS-39 from the abyssal plain of the Liguro-Provençal Basin showing the Messinian trilogy and non-erosive bottom and top surfaces (BS and TS; Dal Cin et al., 2016). Halokinesis of MU gives rise to domes that deform the UU and PQ units.* **(d)** *Interpreted seismic profile from the lower-middle slope of the west Sardinian margin (modified from Dal Cin et al., 2016). Thin MU and UU are present on the lower slope, while on the middle slope (and upper slope here not shown) they converge in the margin erosion surface MES.* **(e)** *Line drawing of seismic line imaging from the Catalan margin (or Ebro Basin) to the abyss of the Liguro-Provençal basin (modified from Maillard et al., 2011b). Note the pinch out of the MU in the Valencia Basin and of the UU in the Ebro Basin, which is MSC free.* **(f)** *Interpreted seismic profile Simbad 15 crossing the depocenter of the CMD showing all the MSC units and erosional surfaces (modified from Raad et al., 2021).* **(g)** *Interpreted seismic profile MYS40 illustrating the MU-UU-PQ units in the East-Sardinia Basin and Cornaglia Terrace, separated by the MSC deposits-free Quirra Seamounts (modified from Lymer et al., 2018).*

Sea. The succession recovered by drilling from beneath the Pliocene comprises gravels that contain a mixed Miocene fauna. These sediments and their faunal content are thought to have been reworked from older sediments exposed as Alborán substrate with no evidence of an extensive wet Lago Mare interval immediately before the Zanclean (Comas et al., 1996).

Two W-E-aligned erosional channels straddling the Strait of Gibraltar and stretching for 390 km from the easternmost Gulf of Cádiz (Atlantic Ocean) into the Alborán Basin are clearly observed in seismic profiles (GarcIa-Castellanos et al., 2009; Estrada et al., 2011). There is disagreement, however, concerning the timing and nature of their formation. These incisions are classically considered to occur at the very top of the MSC suite (when present) and to be the consequence of the Zanclean megaflood (García-Castellanos et al., 2009, 2020; Estrada et al., 2011 among others). More recently, Krijgsman et al. (2018) highlighted that an accurate age determination for these channel incisions is lacking and that they might have been formed earlier during the MSC as a result of the Mediterranean-Atlantic gateway currents. Interpretation of E-W seismic profiles across the Alborán Basin combined with mammal records in Africa and Iberia led Booth-Rea et al. (2018) suggest the existence of an emergent volcanic archipelago that temporarily connected southeastern Iberia with northern Africa, separating an open marine, Atlantic-influenced West Alborán Basin realm from a restricted, hydrologically complex Mediterranean realm to the east.

1.4.2 Eastern Alborán, Algero-Balearic and Liguro-Provençal basins

From the eastern margin of the EAB as far east as the Tyrrhenian coast of Italy, the Messinian (evaporites-bearing) trilogy LU-MU-UU is found and sealed by the PQ. The MU and UU are interpreted to fill the deepest depocenters (Algero-Balearic, Valencia and Liguro-Provençal basins; with minor interruptions due to seamounts) and the lower slope domain, where they comprise ~500 to ~800 m of UU and ~1000 m of MU/halite (Figs. 1.7b-d; Camerlenghi et al., 2009; Lofi et al., 2011a, b; Geletti et al., 2014; Mocnik et al., 2014; Dal Cin et al., 2016; Lofi, 2018). Upslope, a thinner, possibly incomplete UU is locally described on the middle-upper continental slopes of Western Corsica (Guennoc et al., 2011) and Sardinia (Mocnik et al., 2014; Dal Cin et al., 2016) and the northern (Maillard et al., 2006) and southern (Maillard and Mauffret, 2013; Mocnik et al., 2014; Dal Cin et al., 2016) flanks of the Balearic Promontory, even though the structural settings of these locations are mostly dominated by erosion (Fig. 1.7d). MSC evaporites are absent on the continental shelves bordering the deep Algero-Balearic and Liguro-Provençal basins, where the PQ directly overlies the MES, which, in turn, cuts through the middle Miocene deposits (Gorini et al., 2005; Lofi et al., 2005). The only late Messinian sediments are present as Complex Units (Gulf of Lion, Bessis, 1986; Gorini et al., 2005; Lofi et al., 2005; Algerian Basin, Medaouri et al., 2014; Arab et al., 2016; Fig. 1.7e). CUs can have various origin (Lofi et al., 2011a, b), but when identified at the outlet of drainage systems, they are commonly interpreted as Messinian clastics supplied by rivers (Lofi et al., 2005). In the Gulf of Lion, the MES is a high angle unconformity with substantial erosion along highly rugged relief thought to have been generated by fluvial incision (Lofi et al., 2005). In contrast, Roveri et al. (2014c) suggested that the drainage networks visible on the seismic could be of subaqueous origin.

When not involved in MU-related deformation processes, the UU appears as a highly reflective series of flat reflectors alternating with less reflective, but concordant, reflectors (Figs. 1.7b-c; Lofi et al., 2011a, b) aggrading in the basin center and onlapping the margins (Fig. 1.7b; Camerlenghi et al., 2009; Lofi et al., 2011a, b; Geletti et al., 2014; Mocnik et al., 2014; Dal Cin et al., 2016). The aggrading nature, shelf-ward thinning and the onlap terminations of the UU are interpreted as evidence of sedimentation in a lake with fluctuating base level (e.g. Lofi et al., 2005, 2011). In the abyssal plains (Figs. 1.2a, 1.7c), nine to ten cycles have been interpreted on high resolution seismic profiles as corresponding to gypsum-marl alternations (Geletti et al., 2014; Mocnik et al., 2014). At Sites 124 and 372, ~40-50 m of the UU have been drilled at the feet of the east Menorca continental rise and the northern Menorca slope, where 3-4 gypsum-marl cycles are recognized (Fig. 1.2b; Ryan et al. 1973; Hsü et al., 1978a). Primary gypsum facies are widely overprinted by post-depositional diagenetic processes, but the still recognizable laminated and clastic primary textures indicate precipitation at the water-air interface and emplacement by gravity flows, respectively (Lugli et al., 2015). The marl interbeds are made from stiff to firm dolomitic mud containing substantial quantities of detrital material

intercalated with current-bedded sandstones and, at Site 124, with diatomites (Ryan et al. 1973). *Cyprideis* sp. specimens are reported from some mudstone interbeds at Site 372, while dwarf planktonic foraminifera are present just below the M/P boundary at Site 124 (Ryan et al. 1973).

The M/P boundary coincides with the top of the UU where present (labelled TES when erosional and TS when conformable; Lofi et al., 2011a, b). In the abyssal plain-lower slope domain it appears to be undulating, although this geometry is related to the deformation of the underlying salt (Figs. 1.7b-c), and it actually corresponds to a sharp surface lacking signs of erosion (Lofi et al., 2011a, b; Geletti et al., 2014; Mocnik et al., 2014). By contrast, the UU-PQ boundary commonly appears strongly erosional in the middle-upper slope and shelf domain, where it coincides with the MES (Fig. 1.7d; Lofi et al., 2005; Maillard et al., 2006; Geletti et al., 2014; Mocnik et al., 2014). Among the six DSDP-ODP Sites drilled in this region (Fig. 1.2b), only Hole 975B recovered the M/P boundary (Iaccarino and Bossio, 1999; Marsaglia and Tribble, 1999). Here the Messinian is a few centimeters thick and consists of banded micritic silty clays with minor calcareous siltstones to sandstones typified by a diverse faunal assemblage consisting of dwarf planktonic foraminifera, *Ammonia tepida* tests and brackish Paratethyan ostracods (*Loxocorniculina djafarovi, Euxinocythere praebaquana, Amnicythere idonea, Leptocythere limbate, Candona* sp., and *Cyprideis* sp.; Iaccarino and Bossio, 1999).

Halite is present at the bottom of Hole 134 drilled within the UU (Ryan et al., 1973; Sage et al., 2005; Lugli et al., 2015). High-resolution seismic profiles from both the Algero-Balearic and Ligurian-Provençal basins confirm the presence of a halite layer high in the UU sequence (Geletti et al., 2014; Mocnik et al., 2014). This layer is up to 50 m thick (Dal Cin et al., 2016) and is correlated with an erosional surface (called IES: Intermediate Erosional Surface by Lofi et al., 2011a, b) associated with an angular unconformity which is better developed on the lower slope (Fig. 1.7d). Geletti et al. (2014) and Mocnik et al. (2014) interpreted this layer as autochtonous and indicative of at least one important sea level drop during UU deposition. However, this intra UU halite layer is always described from areas strongly affected by salt diapirism (just like in the Ionian Abyssal Plain; see section 1.4.6.1) and is never found in adjacent, undisturbed areas (see Camerlenghi et al., 2009; Geletti et al., 2014; Mocnik et al., 2014; Dal Cin et al., 2016), two features that may suggest it has an allochthonous origin. Site 134 shows evidence of a "desiccation crack" cutting through a sandy silt layer interbedded with unaffected laminated halite (Hsü et al., 1973c). Unfortunately, the core photograph of this crack has been published in two different orientations (Hsü et al., 1973a, b), leading both Hardie and Lowenstein (2004) and Lugli et al. (2015) to question the evidence for subaerial desiccation. Because of these ambiguities, we suggest to dismiss this example from the book of evidence.

1.4.3 Valencia Basin

The Valencia Basin (VB; Fig. 1.2a) is an aborted rift formed during the late Oligocene-early Miocene opening of the back-arc Liguro-Provençal Basin (e.g. Jolivet et al., 2006). It is located

between the Spanish Ebro Margin to the west and the Balearic Promontory to the east, while it grades into the Liguro-Provençal Basin to the E/NE (Fig. 1.7e; Maillard and Mauffret, 2006; Maillard et al., 2006).

Numerous exploratory boreholes exist on the western Ebro margin. These boreholes, tied to seismic data, confirm that MSC-related sediments on the northwestern shelf are missing (Fig. 1.7e; Urgeles et al., 2011; Pellen et al., 2019). The only MSC feature present is a prominent erosional surface (the MES) incising Serravallian-early Messinian sediments (Urgeles et al., 2011). By contrast, on the southwestern and southern part of the margin, well data show the presence of evaporitic sediments (e.g. Delta L and Golfo de Valencia D1 boreholes; Del Olmo, 2011; Del Olmo and Martín, 2016; Lozano, 2016). Del Olmo and Martín (2016) described these evaporites as primary selenites and ascribed them to MSC Stage 1 (their unit M7). Lozano (2016) described the same evaporitic deposits in the same boreholes as 'white anhydrites', leaving open the question as to whether the anhydrite is primary (sabhka's) or secondary at the expense of a primary gypsum facies. On the eastern margin of the VB boreholes and seismic studies suggest there are no MSC units with only a prominent MES cutting pre-MSC sediments (Driussi et al., 2015; Raad et al., 2021). All authors conclude that the shelves of VB were exposed to subaerial erosion during and following the main drawdown. MSC deposits are also absent along the slopes and, where present, consist of coarse- and fine-grained terrigenous facies filling valleys largely related to fluvial incision (Fig. 1.7e; Stampfli and Höcker, 1989).

A different situation features in the depocenter. Despite its present-day depth of > 2000 m, no MU is observed in the depocenter, as the salt pinches-out at the edge of the deeper Provençal Basin (Fig. 1.7e). Only the seismic properties of UU suggest that it is roughly continuous from the Provençal Basin into the VB (Fig. 1.7e; see section 1.4.2), although it thins from ~1000 m to <500 m. The UU is characterized by aggrading and onlapping geometries towards the slopes, where it also thins out until it disappears along the middle-upper slope (Fig. 1.7e; Maillard et al., 2006; Cameselle and Urgeles, 2017). Maillard et al. (2006), Urgeles et al. (2011), Cameselle et al. (2014) and Cameselle and Urgeles (2017) all stated that the UU formed during an important Mediterranean-level lowstand (~1000 m). Several Complex Units (CU), with different origin, have been observed and described as belonging to the MSC (Cameselle and Urgeles, 2017).

DSDP Site 122, drilled at the mouth of a valley incision, recovered a few meters of sand-gravels made of well-rounded basalt, marine limestones, nodules of crystalline gypsum and mollusk fragments in a clay-silty matrix rich in deep-water benthonic foraminifera and early Pliocene nannofossils, all interpreted as erosional products of the VB seabed (Ryan et al., 1973). The uppermost Messinian in two industrial wells (Ibiza Marino and Cabriel boreholes; see Lozano, 2016) is represented by intercalations of clastic gypsum/anhydrite and marls (unit M8-P1 of Del Olmo and Martín, 2016). These are interpreted as turbidites sourced from the shelf and/or slope during a lowstand phase of the Mediterranean base level (Del Olmo et al., 2011; Del Olmo and Martín, 2016; Cameselle and Urgeles, 2017).

In seismic profiles, the UU/PQ transition (M-reflector or TES) is locally both sharp and smooth (in more distal settings) and erosional (in more proximal settings; Fig. 1.7e). Maillard and Mauffret (2006) indicate that the smooth parts have been caused by increasing fresh water influx during the Lago-Mare phase, leading to dissolution of the evaporites, and the rough erosional segments are of subaerial origin. For Cameselle and Urgeles (2017), the top of the UU is a smooth and conformable downlap surface, representing the rapid inundation of the basin with only local minor erosional features.

1.4.4 Balearic Promontory

Sticking out from the surrounding deep-water locations, the Balearic Promontory (BP; Fig. 1.2a) is a continental high that has undergone tectonic extension since the late Serravallian (Roca and Guimera, 1992; Sabat et al., 2011). During the Messinian, it comprised in topographic lows/subbasins at different water depths and separated by structural highs/sills (Maillard et al., 2014; Driussi et al., 2015; Roveri et al., 2019b; Raad et al., 2021). The area has been the subject of multiple studies (Maillard et al., 2014; Driussi et al., 2015; Ochoa et al., 2015; Roveri et al., 2019b; Raad et al., 2021) and several controversies arose after the publication of Roveri et al. (2019b).

The first controversy concerns the Messinian paleodepth of the BP's subbasins. According to Roveri et al. (2019b) the subbasins were shallow during the Messinian and acquired today's paleodepths following a strong post-MSC subsidence; Maillard and Mauffret (2011), Maillard et al. (2014) and Raad et al. (2021), instead, consider the tectonic movements in the BP to have been minor since the late Miocene (Messinian) and the region to have been already structured as it is today during the MSC. Well-to-seismic ties in the shallower basins closer to the Spanish coast (i.e. Bajo Segura, San Pedro and Elche basins) comprise up to 14 Stage 1 primary gypsum-marl cycles similar to the onshore PLG unit (Lugli et al., 2010) truncated at the top by the MES (Soria et al., 2008a, b; Ochoa et al., 2015). At first, Ochoa et al. (2015) concluded that all sediments overlying the MES are Pliocene in age. A later re-appraisal of the same downhole logging data and cuttings led Ochoa et al. (2018) to attribute the first ~13 m-thick micritic and evaporite-free sediments to the late Messinian (stage 2 or 3 of the MSC according to the authors). The MSC stratigraphy of the shallowest offshore basins of the BP closely resembles that described from cores and outcrops onshore Mallorca (see subsection 1.3.4; Roveri et al. 2019b).

High resolution seismic reflection data in the Central Mallorca Depression (CMD) highlighted up to 500 m of MSC deposits made of a Bedded Unit (BU) and a thin salt layer (Maillard et al., 2014; Driussi et al., 2015). This BU has never been drilled and, therefore, lacks lithological and chronostratigraphic constraints. Two contrasting chronostratigraphic and lithological interpretations are proposed: Roveri et al. (2019b) ascribed these sediments to Stage 2 and 3 and suggested that only reworked evaporites and halite are present. By contrast,

following the seismostratigraphic description of Maillard et al. (2014), Ochoa et al. (2015) and Raad et al. (2021) inferred the presence of Stage 1 gypsum also in the CMD.

Raad et al. (2021) made a step forward by disclosing a possible tripartition of the BU unit (Fig. 1.7f). In their seismostratigraphic framework, Raad et al. (2021) noticed that the uppermost evaporite-bearing unit (called BU3), ~120 m-thick in the CMD, has geometric, stratigraphic and facies analogies with the astronomically-tuned UG unit of the Caltanissetta Basin (Fig. 1.3a) that endorse its attribution to Stage 3. Similar to the UU in the deepest basins (see section 1.4.2), BU3 consists of up to 9 low- and medium-amplitude reflectors that are interpreted as alternating terrigenous and gypsum beds (Maillard et al., 2014; Raad et al., 2021). Reflectors are parallel and continuous in the more distal areas, while they appear more chaotic in the more proximal sectors (Raad et al., 2021). The base of BU3 coincides with the erosional top of the salt, interpreted as created by salt exposure, dissolution and locally salt gliding towards the depocenter (Fig. 1.7f; Raad et al., 2021). By contrast, the top of BU3, which corresponds to the Miocene/Pliocene boundary, is largely flat without signs of erosion (Fig. 1.7f; Maillard et al., 2014; Raad et al., 2021). An irregular geometry is sometimes visible, but is likely to be related to deformation of the underlying salt (Fig. 1.7f; Raad et al., 2021).

1.4.5 Tyrrhenian Basin

The Tyrrhenian Basin to the east of Sardinia is a back-arc basin that opened by continental rifting and oceanic spreading related to the eastward migration of the Apennine subduction system from middle Miocene to Pliocene times (Gaullier et al., 2014, Lymer et al., 2018, Loreto et al., 2020 and references therein). Three main domains are traditionally identified (Lymer et al., 2018 and references therein): (1) the East Sardinia Basin, with present-day water depths between 200-2000 m consisting of a system of seamounts and depressions that do not contain MSC sediments (Lymer et al., 2018); (2) the Cornaglia Terrace (2000-3000 m deep), a wide, flat area with dispersed structural highs; (3) the Tyrrhenian Basin s.s., with water depths varying from 3000-3600 m. Whether the Tyrrhenian Basin acquired the present-day topography and hypsometry before the MSC (Lymer et al., 2018) or at least part of it (e.g. Eastern Sardinia margin, where Site 654 is located, and Northern Tyrrhenian) was much shallower (possibly comparable to the Caltanissetta Basin; Roveri et al., 2014b) and underwent extension and subsidence during the Messinian-Pliocene (e.g. Kastens and Mascle, 1990; Loreto et al., 2020) is still unresolved.

The MSC units in seismic profiles from the Tyrrhenian Basin (Fig. 1.7g) are very similar to the ones described in the Algero-Balearic and Liguro-Provençal basins (Figs. 1.7b-c; Gaullier et al., 2014; Lymer et al., 2018). ODP Sites 652, 653 and 654 confirmed the seismic-inferred lithological nature of UU as consisting, of gypsum-mudstone alternations (8 are counted at Site 654; Kastens et al., 1987; Borsetti et al., 1990; Roveri et al., 2014b). Intercalations of ripple–cross-laminated, fine-grained, azoic sandstones occur within the mudstone intervals in places (Cita

et al., 1990; Iaccarino and Bossio, 1999). In some mudstone samples, the ostracod *Cyprideis* sp. (Site 654) and *Candona* sp. (DSDP Hole 974B) and the foraminifera *Ammonia beccarii* and *Ammonia tepida* have been found, indicating a shallow-water (<50 m) brackish environment (see sections 1.5.1 and 1.5.4; Cita et al., 1990; Iaccarino and Bossio, 1999). $^{87}Sr/^{86}Sr$ isotope ratios of UU gypsum and planktic foraminifera of the overlying Pliocene (Unit 1 at Site 654) show values much lower (from 0.708627 to 0.708745) and roughly equivalent (from 0.708935 to 0.709112) to coeval ocean water (~0.709020-30; McArthur et al., 2012), respectively (Müller et al., 1990; Müller and Mueller, 1991). Similar $^{87}Sr/^{86}Sr$ values were obtained from the gypsum cored at Site 652 (0.708626-0.708773; Müller and Mueller, 1991).

The M/P boundary at DSDP Site 132 is placed above a cross-bedded sand rich in quartz, mica, pyrite, rounded fragments of gypsum and specimens of *Ammonia beccarii* and *Elphidium macellus* (Ryan et al., 1973). In the adjacent ODP Site 653 a similar sandstone is found slightly below the biostratigraphically-defined M/P boundary and ~70 cm of grey mudstones with foraminifera and nannofossils of undisclosed provenance are squeezed in between (Cita et al., 1990). These mudstones also contain rare dwarf planktic foraminifera (*Globorotalia acostaensis, Orbulina univers* and *Globigerina bulbosa*; Cita et al., 1990).

Overall, the uppermost Messinian sediments of the Tyrrhenian Basin are interpreted as having been deposited in lakes with periodic episodes of increased salinity and dilution under the strong influence of high energy rivers and, perhaps ocassionally, of the Atlantic (Cita et al., 1990; Müller et al., 1990; Müller and Mueller, 1991).

1.4.6 Ionian Basin

The deepest basin in the Mediterranean today is the Ionian Basin, with its lowest point at 5.267 meters. The so-called Ionian Abyssal Plain (IAP) is bounded on all sides by pre-MSC structural highs (Fig. 1.2a; Camerlenghi et al., 2019): the Malta Escarpment to the west; the Medina Escarpment to the south separating it from the Gulf of Sirt (Fig. 1.8a); the Gargano-Pelagosa and/or Otranto sill to the north dividing it from the Adriatic Foreland and, finally, an unnamed sill to the east, separating the IAP from the Levant Basin. Evidence from recent high-resolution seismic studies across the region have been used to support Stage 3 desiccation models (e.g. Hsü et al., 1978a, b; Bowman, 2012; Micallef et al., 2018, 2019; Camerlenghi et al., 2019; Spatola et al., 2020).

1.4.6.1 Ionian Abyssal Plain

The typical "trilogy" of seismic units representing the MSC deposition in the Western Mediterranean is recognized also in the IAP by Gallais et al. (2018) and Mocnik et al. (2018). However, Camerlenghi et al. (2019) states the MSC sequence in the IAP is ~1,300 m-thick and composed of only two units (Fig. 1.8a). The lowermost 150-700 m-thick Mobile Unit (MU) is seismically transparent without discernible bedding and with diapiric structures, all features

diagnostic of halite. By contrast, the 350-1.000 m-thick Upper Unit (UU) alternates highly reflective with acoustically transparent reflectors (Figs. 1.8a-b), similar to those described of the UU sequences of the Western Mediterranean (Figs. 1.7b-c). These are therefore assumed to represent gypsum-mudstone cycles (Camerlenghi et al., 2019). The uppermost 80 m of UU has been recovered from DSDP Site 374 (Hsü et al., 1978b), confirming the presence of gypsum (both primary cumulate and clastic; Lugli et al., 2015) alternating with mudstones (Unit III; Hsü et al., 1978b). These mudstones are largely barren of in situ fossils. However, the presence of some foraminifera and siliceous microfossils led Cita et al. (1978) and Hsü et al. (1978a) to suggest that sporadic marine incursions, possibly from the Indian Ocean, took place during Stage 3. Similar to Site 372, the basal part of Hole 374 intercepted one thin (~3.5 m) halite layer within the UU (Hsü et al., 1978b).

The UU and the overlying Zanclean (subunit PQc of Camerlenghi et al., 2019) reflectors are conformably folded throughout most of the abyssal plain, locally showing chaotic internal structure, irregular folding mimicking V-shaped incisions and truncations (Fig. 1.8b; Camerlenghi et al., 2019). These features are interpreted by Camerlenghi et al. (2019) as fluvial valleys carved in subaerially exposed evaporites by the Eso-Sahabi fluvial system, the closest fluvial drainage network to the area (see Micallef et al., 2018) that drained Libya in the late Miocene (Griffin, 2002) and has been traced across the Gulf of Sirt offshore (Sabato Ceraldi et al., 2010; Bowman, 2012). Several arguments counteract this interpretation: (1) the coherent, deformation, mostly of post-Messinian age, of both the UU and the lower Zanclean; (2) the absence of fluvial facies above the bottom of the "valleys", which instead correspond to a mudstone interval that underwent post-depositional dolomitization (Unit II; see below; Fig. 1.8b); (3) the unlikelihood that the Eso-Sahabi fluvial system managed to bypass the Medina Ridge divide (Fig. 1.8a). Alternatively, the apparent incisions at the M/P boundary in the IAP may represent post-sedimentary folds resulting from post-Messinian tectonic and/or salt movements-driven deformation (e.g. Mocnik et al., 2018). At Site 374 the M/P boundary has been recovered (Unit II), but its primary nature (likely a mudstone) is obscured by diagenesis (cementation by dolomite; Hsü et al., 1978b). A lithified dolostone at the (seismic) predicted depth of the M-Horizon is a characteristic of several sites. Sometimes this interval has been recovered (e.g. Sites 125 and 374; Ryan et al., 1973; Hsü et al., 1978b; Comas et al., 1996); at others the hard lithology is inferred by the torqueing of the drill string (resistance to turning) accompanied by bouncing of the drill bit at the (e.g. Sites 122, 124, 125, 132, 133 and 134; Ryan et al., 1973). Dolomitization was (Hsü et al., 1973a, b; Ryan et al., 1973) and still is (e.g. Ryan, 2009) largely considered a "diagnostic feature of tidal (sabkha) sediments" (Friedman, 1973, p. 705). Its occurrence at locations with present-day water depth exceeding 2000 m was therefore considered strong evidence that the Mediterranean floor was subaerially exposed prior to the Zanclean marine replenishment (e.g. Ryan et al., 1973). It is, however, now widely accepted that dolomite precipitation is not exclusive of sabkha environments, but rather is a common process

also in bottom sediments under a relatively deep water column (see Dela Pierre et al., 2012, 2014 and references therein). In the specific case of the offshore Mediterranean's M/P boundary on the Ionian Abyssal Plain, already in the '70s dolomitization was thought to have occurred after burial (Hsü et al., 1978b), a conclusion recently reinforced by McKenzie et al. (2017).

1.4.6.2 Malta Escarpment

At the foot of the Malta Escarpment, Micallef et al. (2018, 2019) and Spatola et al. (2020) amalgamated the MU and UU into one seismic unit, Unit 3, which is separated from the Plio-Quaternary marine sediments (Unit 1) by Unit 2, a chaotic transparent seismic package (Fig. 1.8c). Unit 2 has a maximum thickness of 760-860 m, a volume of 1430–1620 km^3 and a wedge-shaped geometry that thins eastwards, disappearing before reaching the IAP (Micallef et al., 2018). Micallef et al. (2018) and Spatola et al. (2020) proposed a lithological/sedimentological interpretation of this chaotic body, suggesting it is composed of well-sorted sediments of the Pelagian Platform to the west of the Malta Escarpment, with coarser material at the mouth grading into more distal finer sediments. This chaotic body has recently been attributed to the Zanclean megaflood during its passage from the western to the eastern Mediterranean via a gateway located in south-eastern Sicily (Micallef et al., 2018, 2019; Spatola et al., 2020). Given the rapidity of the reflooding (≤2 years, Garcia-Castellanos et al., 2009, 2020), this interpretation implies rapid mass deposition. Other interpretations of this Unit 2 include being the result of extensive marine mass movement (Polonia et al., 2011), being folded UU (Butler et al., 2015) or being a complex unit built during lower sea level phases (Lofi et al., 2011a, b).

1.4.6.3 Gulf of Sirt

The Gulf of Sirt (or Sirt embayment; Figs. 1.2a, 1.8a), the offshore extension of the Sirt Basin onshore Libya (Griffin, 2002 and references therein), is cross-cut by high-density seismic and well datasets as a result of oil potential of the region (Fiduk, 2009). However, only few studies have tackled the MSC (e.g. Hallett, 2002; Fiduk, 2009; Bowman, 2012). In the Sirt embayment the MSC unit(s) is unevenly distributed in sub-basins controlled by a pre-existing topography, there is little distinction between the MU and UU, the overall thickness of the MSC unit(s) is lower and the degree of deformation is higher than in the adjacent IAP (Fig. 1.8a; Camerlenghi et al., 2019). The presence of halite in the Sirt embayment is debated, but most authors think it is absent (see Fiduk, 2009; Sabato Ceraldi et al., 2010; Lofi, 2018; Jagger et al., 2020; Fig. 1.2b). Bowman (2012) distinguishes seven seismic units within the MSC-related sequence (Fig. 1.8d). On the basis of high-resolution 3D and 2D data, each seismic unit has been interpreted consisting of clastics filling erosional channels cutting up to 100 m deep and wide (Fig. 1.8d) and evaporites (gypsum and anhydrite) alternating with precessional cyclicity (Bowman, 2012). The presence of anhydrite in the topmost part of the sequence is confirmed by the B1 NC 35A well (Hallett, 2002). Sabato Ceraldi et al. (2010) and Bowman (2012) envisaged a three-

step evolution of each unit: (1) evaporitic deposition during precession maxima in a dried out Sirt embayment; (2) erosion of the valleys during the arid-wet transition fed by the Eso-Sahabi paleofluvial system; (3) filling of the valleys with the fluvial sediments during the wet phase. Based on this chronostratigraphic interpretation, the evaporite cycles should be time equivalent to most of Stage 3, with the upper four seismic units reflecting the Lago-Mare phase (Fig. 1.1a).

1.4.7 Levant Basin

1.4.7.1 Abyssal plain

Old seismic data in the Levant Basin show an up to 2 km-thick, high velocity, acoustically transparent sequence bounded by the N-reflector at the base and the M-reflector at the top (Figs. 1.8e-f; Ryan, 1978; Netzeband et al., 2006). This sequence thickens and extends for tens of kilometers towards WNW and thins eastward along the continental margin (Fig. 1.8e), where the N and M-reflectors converge forming the condensed MSC section of the Mavqiim and Afiq formations (described in subsection 1.4.7.2; Gvirtzman et al., 2017; Manzi et al., 2018). High resolution 2D and 3D industrial seismic and well data from the southern Levant Basin revealed that this transparent sequence is largely made of pure halite with internal stratification picked out by diatomite, clay- and clastic-rich layers that allowed the division of the sequence into six sub-units, basinward-tilted and truncated at the top by the flat TES (Fig. 1.8f; Gvirtzman et al., 2013, 2015, 2017; Feng et al., 2016, 2017; Manzi et al., 2018; Meilijson et al., 2018, 2019). Clastic beds ~3 to 20 m-thick are abundant in the highly reflective and chaotic Unit 5 (i.e. Interbedded evaporites of Meilijson et al., 2019; MC2 unit of Feng et al., 2016; Figs. 1.3b, 1.4a), where they are interbedded with evaporites (probably halite with minor occurrences of anhydrite) varying in thickness from ~6 to 30 m (Manzi et al., 2018; Meilijson et al., 2019). Paleontological analyses of cuttings probably belonging to one of the clastic beds revealed the presence of a few mollusk fragments, ostracods, echinoid spines and a relatively rich assemblage of benthic and planktic foraminifera which Meilijson et al. (2019) concluded to be reworked. Based on seismic and well-log data, clastic intercalations (probably of clays, silts and sands) within a halite-dominated sequence are thought to persist in the overlying Unit 6, although they diminish in thickness and frequency (Gvirtzman et al., 2013; Feng et al., 2016; Meilijson et al., 2019). The expression of the end of the MSC is highly controversial. Until recently, the M-reflector of Ryan (1978) (later renamed as the Top Erosion Surface, TES; Lofi et al., 2011a, b) bounding Unit 6 at the top was considered to be the Miocene/Pliocene boundary (Fig. 1.8f; Ryan, 1978; Gvirtzman et al., 2013; Feng et al., 2016). Instead, Gvirtzman et al. (2017) showed that in higher resolution seismic data the M-reflector/TES is a bundle of reflectors forming a distinct layer (Unit 7) overlying a truncation surface (i.e. Unit 6/7 boundary) that they re-labelled intra-Messinian truncation surface (IMTS; Fig. 1.8g) and ascribed to subaqueous dissolution rather than subaerial incision (e.g. Bertoni and Cartwright, 2007; Lofi et al., 2011a, b; Kartveit et al., 2019; Madof et al., 2019). This conclusion was recently corroborated by the independent study of Kirkham et

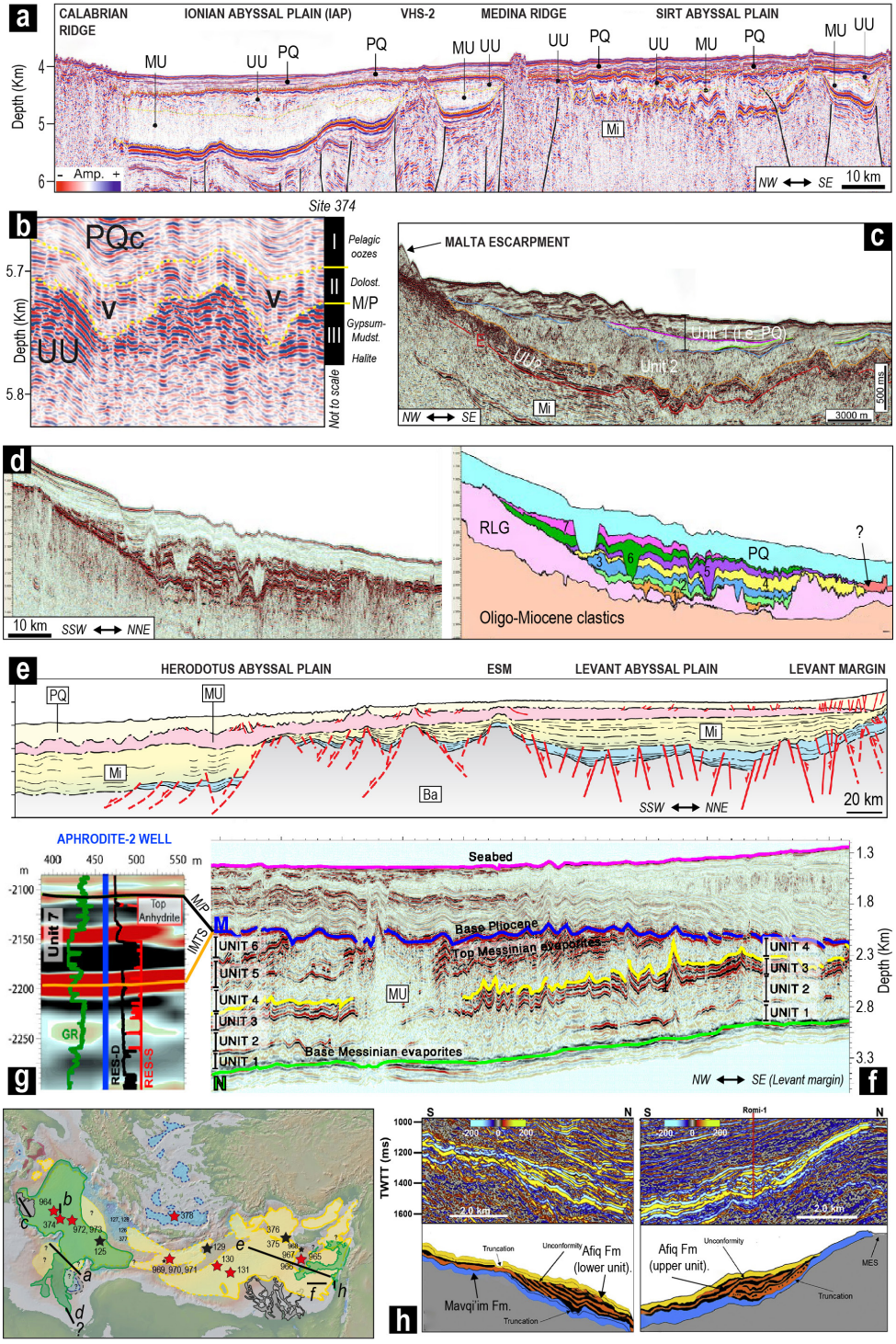
a
CALABRIAN RIDGE
IONIAN ABYSSAL PLAIN (IAP)
VHS-2
MEDINA RIDGE
SIRT ABYSSAL PLAIN
Depth (Km)
MU
UU
PQ
Mi
Amp.
NW SE
10 km
b
Site 374
PQc
V
UU
Depth (Km)
Pelagic oozes
Dolost.
M/P
Gypsum-Mudst.
Halite
Not to scale
c
MALTA ESCARPMENT
Unit 1 (i.e. PQ)
Unit 2
Mi
NW SE
3000 m
500 ms
d
10 km
SSW NNE
RLG
PQ
?
Oligo-Miocene clastics
e
HERODOTUS ABYSSAL PLAIN
ESM
LEVANT ABYSSAL PLAIN
LEVANT MARGIN
PQ
MU
Mi
Ba
SSW NNE
20 km
APHRODITE-2 WELL
Top Anhydrite
Unit 7
GR
RES-D
RES-S
MIP
IMTS
g
Seabed
Base Pliocene
Top Messinian evaporites
Base Messinian evaporites
UNIT 6
UNIT 5
UNIT 4
UNIT 3
UNIT 2
UNIT 1
MU
NW SE (Levant margin)
Depth (Km)
f
TWTT (ms)
Truncation
Unconformity
Afiq Fm (lower unit).
Mavqi'im Fm.
Afiq Fm (upper unit).
MES
Romi-1
h

Fig. 1.8 (previous page). *Seismic profiles from intermediate-deep Eastern Mediterranean basins containing MSC markers/units (see Fig. 1.7 for abbreviations).* **(a)** *High-resolution seismic line MS27 imaging the PQ and the uppermost MSC's UU and MU in the Ionian Abyssal Plain and Gulf of Sirt (modified from Camerlenghi et al., 2019). Note how the MSC units are thinner, more difficult to distinguish and more deformed in the Sirt Abyssal Plain than in the IAP. PQ, UU and MU all onlap the structural highs of the Medina Ridge and VHS-2 sill.* **(b)** *High-resolution imaging of the lower part of the Plio-Quaternary (PQc unit) and upper part of the Messinian (UU) in the IAP (Camerlenghi et al., 2019). The MSC-PQ boundary is a highly irregular surface, describing apparent V-shaped incisions (symbol V) of controversial origin (see subsection 1.4.6.1 for insights). Note the coherent deformation of PQc with the underlying MSC sequence and the absence of fluvial facies within the incisions (Unit II is made of lower Pliocene dolomitic marls recovered in Site 374 drilled nearby the seismic line; see text).* **(c)** *Multichannel seismic reflection profile MEM-07-203 running approximately parallel to the Malta Escarpment and showing the relationship between Unit 2 of Micallef et al. (2018) with the overlying and underlying Zanclean and Messinian sediments, respectively (modified from Spatola et al., 2020).* **(d)** *Uninterpreted (left) and interpreted (right) seismic profiles showing the cyclic and channelized nature of the uppermost Messinian observed in the offshore Sirt Basin (modified from Bowman, 2012).* **(e)** *Interpreted 2D regional WNW–ESE seismic profile crossing the continental shelf and offshore Levant Basin and the Herodotus Abyssal Plain (Jagger et al., 2020). Note the lateral continuity of the Messinian MU.* **(f)** *Seismic profile from the Levant Basin showing the 6 sub-units distinguished inside the MU as well as its lower (N-reflector) and upper (M-reflector) boundaries (modified from Gvirtzman et al., 2013).* **(g)** *High-resolution seismic reflection image with wireline logs from Aphrodite-2 well illustrating that M-reflector previously considered as top evaporitic sequence and M/P boundary here consists of a ~100-m-thick unit (i.e. Unit 7 of Gvirtzman et al., 2017) in which different layers are distinguished (modified from Gvirtzman et al., 2017).* **(h)** *Interpreted and uninterpreted seismic profiles imaging the Mavqi'im and Afiq formations described in the canyons on the Levant continental margin (modified from Ben Moshe et al., 2020).*

al. (2020). Analysis of gamma-ray and resistivity logs in three deep basin wells (Aphrodite-2, Myra-1, Sara-1; Fig. 1.2b) and correlation with the Or-South-1 well (located between the deep basin and the shelf) showed that Unit 7 maintains a constant thickness of ~100 m-thick and consists of clastic-rich anhydrite of undisclosed provenance. Meilijson et al. (2019)'s lithological interpretation of industrial boreholes slightly farther to the NE (Fig. 1.2b) give Unit 7 a significantly smaller thickness (5 m; Fig. 1.3b). Independent studies offshore Lebanon and Syria (Kartveit et al., 2019, Madof et al., 2019) describe a unit (Nahr Menashe complex) interpreted as a thicker (up to 300 m; Madof et al., 2019), but lateral equivalent of Gvirtzman et al. (2017)'s Unit 7. Based on its channelized morphology identified upslope near the Lebanese coast, Kartveit et al. (2019) and Madof et al. (2019) interpreted the Nahr Menashe Unit and the IMTS underneath as fluvial in origin, deposited/formed on a subaerially exposed floor of the Levant Basin. Six (Madof et al., 2019) to eight (Madof and Connell, 2018) lobes were identified and are

proposed to have stacked with precessional frequency. The Nahr Menashe sequence has been correlated by the same authors with the Abu Madi Fm. located within the Messinian canyons offshore Egypt (Abdel Aal et al., 2000; Loncke et al., 2006; Abdel-Fattah, 2014), the Handere Formation offshore Turkey (Radeff et al., 2017) and with the Eosahabi deposits offshore Libya (Bowman, 2012). This interpretation implies a low base-level during the final stage of the MSC. Manzi et al. (2018) and Meilijson et al. (2018, 2019) attempted astronomical dating of the abyssal MSC succession of the Levant Basin by integrating biostratigraphy on the pre-MU succession, reflector counting within the MU (only Meilijson et al., 2019) and well-log data (Fig. 1.3b). They achieved two contrasting results that gave rise to an outstanding controversy (Figs. 1.3b, 1.4a). Manzi et al. (2018) proposed that Stage 1 in the deep Levant is represented by a foraminifera-barren, evaporite-free shales interval labelled FBI (foraminifer barren interval) observed in the deep Aprodite-2 well and in the more proximal Myra-1 well. In this interpretation Unit 7 comprises the whole of Stage 3 (with the IMTS corresponding to the Stage 2/3 transition) and all halite deposition took place in ~50 kyr estimated during Stage 2 of the MSC (Fig. 1.1a; Roveri et al., 2014a). By contrast, the FBI is not present in the Dolphin well targeted by Meilijson et al. (2019), which is located in an intermediate position between the Aprodite-2 and Myra-1 wells studied by Manzi et al. (2018; Fig. 1.2b). Instead, in the Dolphin well a relatively open-marine, foraminifera-rich sequence extends below the (conformable) base of the MU, placed in correspondence to a ~2 to 5.5 m-thick anhydrite/shale (Unit 0; Manzi et al. 2018 and Meilijson et al., 2018, respectively). Astronomical tuning of the ~33 cycles counted in the MU in the Dolphin well, which are assumed to be precessional, results in the Main Halite body (i.e. Unit 0-4 of Gvirtzman et al., 2013 and Manzi et al., 2018) spanning MSC Stage 1 and 2, the Interbedded Evaporites/Unit 5 covering substage 3.1 and the Argillaceous Evaporites/Unit 6-7 to encompass the Lago-Mare phase (Figs. 1.3b, 1.4a). In this interpretation from Meilijson et al. (2019), halite deposition in the Levant Basin started in Stage 1 and persisted throughout the entire MSC, including Stage 3, during which more allochthonous material was delivered to the basin (Fig. 1.3b). Madof and Connell (2018) and Madof et al. (2019) also attempted an astronomical tuning of the Nahr Menashe Unit, concluding that it spans throughout substage 3.2 and part of substage 3.1. Feng et al. (2016) claim, however, that the impressive thickness of clastics found in the Levantine MU is more indicative of distinct short-term events (shorter than the precession cycle) associated with transport of extraordinary power and magnitude.

Late Messinian sediments have also been recovered at several DSDP (129, 375, 376; Ryan et al., 1973; Hsü et al., 1978b) and ODP Sites (965, 967, 968; Emeis et al., 1996), but the assignment of the retrieved sediments to seismostratigraphic units is problematic. Nevertheless, they provide several key nuggets of precious information about the Stage 3 paleoenvironment:

> Sites 965 and 966, located roughly on the crest of the Eratosthenes Seamount, just south of Cyprus (Fig. 1.2b), recovered soil structures above the evaporites indicating exposure above sea level (Robertson, 1998a, b; Maillard et al., 2011a; Reiche et al., 2016).

> ODP Sites 967 and 968, located at the base of the northern and southern slope of Eratosthenes Seamount (Fig. 1.2b), respectively, revealed the presence, within the MSC interval, of calcareous turbidites with Cyprus-derived clasts and clays containing *Ammonia tepida, Cyprideis pannonica* and pulmonate gastropods (Blanc-Valleron et al., 1998; Robertson, 1998a, b; Reiche et al., 2016).

> Abundant *Cyprideis pannonica* specimens were also recovered from DSDP Site 375 and 376 drilled on the crest of the Florence Rise, west of Cyprus (Fig. 1.2b; Hsü et al. 1978b).

> Abundant, well-preserved *Ammonia* tests and *Cyprideis* specimens are also known from Site 129A (Fig. 1.2b), occurring with dwarf planktonic foraminifera (Ryan et al., 1973).

All the evidence listed above suggest that a base-level fall leading to subaerial exposure occurred at some point(s) during Stage 3 in the Eastern Mediterranean (Ryan, 2009). However, it must be kept in mind that both the Florence Rise and Eratosthenes Seamount are likely to have been much more elevated during the Messinian than they are today because of Pliocene-Quaternary subsidence related to the Cyprus subduction zone (Robertson, 1998a, b; Maillard et al., 2011a; Reiche et al., 2016).

Sites 375 and 376 display several discrete layers of primary and clastic gypsum interbedded in the *Cyprideis*-rich mudstones (McCulloch and De Deckker, 1989; Lugli et al., 2015). This succession shares several similarities with sites drilled in the Western Mediterranean (e.g. ODP 654A) and Ionian Basin (DSDP 374), where they have been correlated with the seismic Upper Unit (see sections 1.4.5 and 1.4.6). This may suggest that a Western Mediterranean-like gypsum-bearing UU was also locally deposited in the easternmost abyss of the Mediterranean (see Güneş et al., 2018).

1.4.7.2 Levant continental margin

Evaporitic and non-evaporitic deposits are buried beneath PQ deposits (Yafo Formation) along the Levant continental margin, where they are mostly preserved within canyons carved underwater in pre-Messinian time (Druckman et al., 1995; Lugli et al., 2013). Within the Afiq canyon, Druckman et al. (1995) distinguished three formations in the Messinian sequence: the evaporitic Mavqi'im Formation, 115 m-thick and mostly composed of anhydrite in places interbedded with micritic limestones; the Be'eri Formation, cmprising gypsum; the Afiq Formation, varying in thickness from 30 to 90 m and consisting of conglomerates, sandstones and marls interpreted as representing fluvial and lacustrine-marsh environments (Druckman et al., 1995). The Afiq Fm. is only present in the deepest portions of the canyon where it overlies the Mavqi'im Fm. By contrast, the Be'eri gypsum is only found along the canyon shoulders covered by the Pliocene, at elevations > 600 m with respect to the Mavqi'im Fm. Based on Sr values, Druckman et al. (1995) attributed the Mavqi'im Fm. to MSC Stage 1, the Be'eri Fm. to substage 3.1 and the Afiq Fm. to the Lago-Mare phase. These authors also suggested that gypsum precipitation occurred under subaqueous conditions, with the water level ~600 m (i.e.

the difference in altitude between the Mavqi'im and Be'eri fms.) higher during the deposition of the Be'eri Fm. Two base-level falls of approximately the same magnitude are thought to have occurred between the evaporitic phases and after Mavqi'im deposition. A lowstand phase was therefore in force during Afiq deposition (Druckman et al., 1995).

However, combining stratigraphic, sedimentological and geochemical ($^{87}Sr/^{86}Sr$ isotopes) considerations, Lugli et al. (2013) revealed the clastic nature of both the Mavqi'im and Be'eri evaporites and suggested the persistent drowning of the canyon(s), filled with turbidites (Lugli et al., 2013). Due to the presence of clastic evaporites, Gvirtzman et al. (2017) suggested that the Mavqiim Formation is a condensed section encompassing MSC Stage 2 and early Stage 3, while the evaporite-free Afiq Formation represents the Lago-Mare phase.

Ben Moshe et al. (2020) ascribed (at least part of) the Afiq Fm. to the whole of Stage 3 as a wedge-shape clastic complex lying on top of the Mavqi'im Fm. and with the basal surface corresponding to the correlative conformity of the MES developed landward, at the expense of the Mavqi'im Fm (Fig. 1.8h). Ben Moshe et al. (2020) distinguished a lower sub-unit composed of clastic gypsum and with fore-stepping and down-stepping internal geometry typical of progradational wedges, and an upper sub-unit containing anhydrite fragments and marls with Lago-Mare fauna (e.g. *Cyprideis torosa*; Rosenfeld, 1977) and with seismic characteristics typical of a transgressive systems tract. Incisions are reported throughout the Afiq Fm. at different depths, while erosional surfaces bound both sub-units (Ben Moshe et al., 2020). In particular, the surface capping the upper subunit and correlated to the M horizon or TES basinward (see section 1.4.7.1) shows dendritic drainage patterns of gullies and channels (Ben Moshe et al., 2020). Ben Moshe et al. (2020) identify the variation of base level specifically during Stage 3 by analyzing the morphology of truncation surfaces bounding the Afiq Formation on the continental margin of the Levant Basin. This suggests high amplitude fluctuations of base-level in the order of one hundred meters, with development of subaerial erosion surfaces and the deposition of clastics and incision by fluvial drainage systems that occurred during the lowstand phases, while aggradational units (of unknown lithological nature) accumulated during the highstand phases. According to their analysis, base level dropped down to a maximum 535 m during Afiq deposition (i.e. below the maximum 430 m estimated paleodepth of the Sicily Sill; García-Castellanos et al., 2009), implying hydrological disconnection between the Eastern and Western basins at various times during Stage 3. A regression to 615-885 m is proposed to have occurred at the top of the Afiq Fm., pre-dating the abrupt refilling at the base of the Zanclean (e.g. Micallef et al., 2018, 2019; Garcia-Castellanos et al., 2020; Spatola et al., 2020).

1.4.8 Summary of the offshore Stage 3 record

Knowledge of the Stage 3 sequence offshore is mainly based on the integration of seismic interpretations and analysis of material recovered from fragmentary and unevenly distributed DSDP/ODP/industrial cores.

i. MSC sediments are absent on the eroded continental shelves bordering the deep basins, except in the Messinian thalwegs and at their mouth. Here the PQ lies directly above the MES which, in turn, cuts through the pre-MSC deposits (Fig. 1.7e). A similar stratigraphic arrangement is found along the middle-upper slopes (Fig. 1.7d), although the presence of a thin, possibly incomplete UU in morphological depressions is sometimes postulated. Seamounts also lack MSC Stage 3 sediments and are strongly incised by the MES (Fig. 1.7g).

ii. The thick UU is widespread and roughly present everywhere in the abyssal plains from west of the Alborán volcanic arc to the eastern edge of the Ionian Basin (Fig. 1.2b). In the abyssal plains its seismic facies appears homogeneous, comprising parallel and relatively continuous high amplitude reflections (Figs. 1.7b-c). The UU pinches out towards the foot of continental slopes and seamounts (Figs. 1.7b, d-g), where it can be irregularly bedded or relatively well bedded (Lofi et al., 2011a, b). The uppermost part of the BUs (defined in depressions physically disconnected from the abyssal plains and, therefore, from the UU; e.g. CMD and Corsica Basin; Maillard et al., 2014; Thinon et al., 2016; Raad et al., 2021) shows seismic features comparable to those of the UU.

iii. Drill Sites revealed that the reflections of relatively high amplitude in seismic profiles correspond to gypsum and mudstone alternations with sporadic intercalations of massive to cross-bedded sandstones. Some mudstone interbeds contain low-diversity assemblages of benthic organisms (ostracods, foraminifera and diatoms) indicative of shallow to neritic environments. Except for dwarfed forms of planktonic foraminifera and the monospecific nannofossil assemblages described by Castradori (1998), the rest of planktonic foraminifera and nannofossils are largely regarded as reworked.

iv. The deep Levant Basin contains a ~1.8-2.0 km-thick MU (Figs. 1.8e-f), consisting of 6 to 7 seismic units depending on the resolution of the seismic employed. In high resolution seismic data, the lateral equivalent of part of the UU is identified as a ~100-m-thick, clastic-rich, anhydrite layer (Unit 7 of Gvirtzman 1207) offshore Israel, thickening to 300 m offshore Lebanon (Nahr Menashe complex, Madof et al., 2019). The Levant Basin still has major controversies concerning the timing of halite deposition (~50 kyr vs ~550 kyr; Manzi et al., 2018 vs Meilijson et al., 2019), the origin of the clastic accumulations overlying the halite (fluvial vs subaqueous) and the presence or absence of gypsum-mudstone cycles.

v. Apart from the halite flow-related deformation, the Miocene/Pliocene boundary (i.e. UU/PQ transition) is conformable in intermediate (e.g. Balearic Promontory) and deep (WAB, EAB, Algero-Balearic, Liguro-Provençal, Tyrrhenian, Ionian and Levant) depocenters, while it shows signs of erosion on the shelf domain and along the upper-middle continental slopes and seamounts. Clear arguments of floor exposure at the M/P boundary are absent in all drill sites but 978A.

1.5 The paleontological perspective

Paleontological data have been used to define and identify Stage 3 sediments, but have also been a source of profound contention over the interpretation of its paleoenvironmental and paleohydrological nature. Biotic groups impacted by the evolution of the gateways linking the Mediterranean with the Atlantic, Indian Ocean and Paratethys include marine species (e.g. foraminifera, calcareous nannofossils, fish) and brackish water-species (ostracods, fish, mollusks and dinocysts endemic or with affinity to species of the Paratethys region) that were unable to migrate when these corridors were closed, and terrestrial species (e.g. mammals) that, conversely, got across the gateway during periods of exposure (see Colombero et al., 2017, Booth-Rea et al., 2018 and Mas et al., 2018b). Analysis of these faunal datasets provides key insights into likely gateway dimensions and the timing of their opening, restriction and closure (e.g. Palcu et al., 2017). Furthermore, they are a key constraint on the water sources likely to have been affecting the Mediterranean during MSC Stage 3.

1.5.1 Ostracods

Ostracods are by far the most prolific faunal group during Stage 3. Brackish species are known from both land sections and deep-sea cores across the whole Mediterranean (see Fig. 1.2b for sites and references; Fig. 1.9a). Two characteristic biofacies are commonly distinguished: Biofacies 1 (Bonaduce and Sgarrella, 1999) or *Cyprideis* assemblage (Iaccarino and Bossio, 1999) consists of an monospecific population of *Cyprideis* species or of an oligotypic population dominated by *Cyprideis* species alongside rare specimens of *Tyrrhenocythere ruggierii, Loxoconcha kochi, Loxoconcha muelleri* and *Caspiocypris alta*); Biofacies 2 (Bonaduce and Sgarrella, 1999) or *Loxocorniculina djafarovi* assemblage (Iaccarino and Bossio, 1999) has a higher species diversity characterized by the abundant occurrence of truly Paratethyan species belonging to the genera Amnicythere, Loxoconcha, Loxocauda, Cytheromorpha, Cyprinotus and Tyrrenhocythere (see species names in Fig. 1.9a). The number of species reported in the onshore sections is variable, ranging from a dozen (e.g. Caruso et al., 2020) to more than sixty (e.g. Gliozzi et al., 2007; Grossi et al., 2008). This variability is not explained, but it may result from the application of different taxonomic concepts that resulted in the recognition of more or fewer species (Stoica et al., 2016) or from local environmental conditions that differed from basin to basin and resulted in different patterns of colonization.

Compared to the onshore domain, the ostracod fauna offshore is impoverished. Monospecific assemblages of *Cyprideis* sp. (Sites 372, 129A, 376, 654A, 967, 968; Ryan et al., 1973; Cita et al., 1990) or oligospecific assemblages dominated by *Cyprideis* and rare specimens of *Candona* sp. (Hole 974B, Iaccarino and Bossio, 1999) and L. muelleri (Hole 978, Iaccarino and Bossio, 1999) are the more widely reported. Interestingly, these assemblages are always associated with *Ammonia* sp. tests and, in some cases, with other species of shallow-water, euryhaline benthic foraminifera (see subsection 1.5.4). Only in Hole 975, close to the M/P

boundary is a more heterotypic ostracod assemblage found (*Euxinocythere praebaquana, Amnicythere idonea, Leptocythere limbate, Loxocorniculina djafarovi, Candona* sp., and *Cyprideis* sp.; Iaccarino and Bossio, 1999) and lacking of euryhaline benthic foraminifera. The likely cause of the widespread barrenness of ostracods in most of the offshore samples is perhaps because environmental conditions in the deep basins (depth and/or salinity) where not suitable to permit population by this benthic fauna (see below for the ecological requirements; e.g. Hsü et al., 1978b in reference to Site 374). Finally, one must bear in mind that studying these organisms require much more material (some hundreds of grams) than the quantity of core sediments usually processed (i.e. ~10 cm^3; Iaccarino and Bossio, 1999).

The paleoecology (salinity and depth ranges) of Stage 3 ostracods has been based on both observations of few species that still live in the Caspian and Black seas today and have affinities with the Stage 3 species and on the interpretation of sedimentological, geochemical and mineralogical data of the surrounding sediments (see Gliozzi and Grossi, 2008 and Grossi et al., 2008 for insights). Biofacies 1 is thought to represent very shallow water environments (i.e. <15 m) with salinity fluctuating between mesohaline and hypersaline when the euryhaline Cyprideis is dominant. Instead, more stable oligo-mesohaline water is inferred when the other species are more abundant in Biofacies 1. The variegated Biofacies 2, on the other hand, is thought to represent somewhat deeper environments (up to 100 m) and less salty conditions (oligo-low mesohaline; Gliozzi and Grossi, 2008; Grossi et al., 2008; Caruso et al., 2020).

Some authors consider the time when the Paratethyan ostracods arrived in the Mediterranean to be well constrained (e.g. Roveri et al., 2008a; Grossi et al., 2011; Cosentino et al., 2018) by the scarce occurrence of the first Paratethyan immigrant *Loxoconcha muelleri* 20 cm below the ash layer in the Colla di Votta section, which has a $^{238}U/^{206}Pb$ age of 5.5320±0.0074 Ma (Cosentino et al., 2013), and in the chaotic deposits of the Adana Basin, ascribed to Stage 2 (Faranda et al., 2013). Instead, the first appearance of *Loxocorniculina djafarovi* has been considered to coincide with the biofacies 1-2 shift and to have occurred Mediterranean-wide synchronously at 5.40 Ma (Roveri et al., 2008a; Grossi et al., 2011; Cosentino et al., 2013). Roveri et al. (2008a) also showed Biofacies 2 diversity as increasing linearly through the Lago-Mare phase, reaching its maximum diversity just beneath the Miocene/Pliocene boundary and before disappearing in the Pliocene. Following the claimed synchronicity of the FO of both *Loxoconcha muelleri* and *Loxocorniculina djafarovi*, Roveri et al. (2008a) and Grossi et al. (2011) recognized one biozone in each biofacies: the *Loxoconcha muelleri* Biozone, spanning from 5.59 to 5.40 Ma, and the *Loxocorniculina djafarovi* Biozone, whose boundaries correspond respectively to the first (5.40 Ma) and last occurrence (5.33 Ma) of *L. djafarovi* in the Mediterranean. This biozonation, erected by Grossi et al. (2011), is often used for dating incomplete successions (e.g. Vera Basin; Stoica et al., 2016; Caruso et al., 2020). However, the first appearance of a diversified ostracod assemblage (including *L. djafarovi*) occurred in already cycle 3 of the Sicilian Upper Gypsum at Eraclea Minoa (Fig. 1.3a; Grossi et al., 2015), which has an astronomical age of

5.45 Ma (Van der Laan et al., 2006) or 5.47 Ma (Manzi et al., 2009). Furthermore, the sudden appearance of Biofacies 2 and its linear, upward increase in diversity have not been recognized in localities like Nijar and Malaga, where biofacies 1 and 2 are found stacked in more than one lithological (possibly precession-controlled) cycle in the Lago-Mare succession (Bassetti et al., 2006; Guerra-Merchán et al., 2010). These findings argue that the appearance of Paratethyan ostracods in the Mediterranean may not have been synchronous, therefore casting serious doubts upon the biostratigraphic relevance of the Mediterranean ostracods.

Except for *Cyprideis* specimens, where species attribution is debated (see discussion in Stoica et al., 2016), the affinity of all other ostracod species observed in Mediterranean Stage 3 sediments (Fig. 1.9a) with those of the Eastern Paratethys basins (i.e. Dacian, Euxinic and Caspian) has been demonstrated in several publications (e.g. Ruggieri, 1967; Gliozzi et al., 2007; Stoica et al., 2016; Sciuto et al., 2018). Only Bassetti et al. (2003, 2006) have questioned the Paratethyan affinity by suggesting that species from the Northern Apennines and Nijar Basin have ambiguous affinities with Paratethyan fauna as described in the mainly Russian literature from the '60-'70s. However, these differences between the late Messinian Mediterranean and Paratethyan ostracods resulted from misidentifications and/or a different use of species nomenclature (Stoica et al., 2016). Recently acquired knowledge of the Pontian assemblages of the Dacian, Euxinic and Caspian basins now permit to trace the provenance of Mediterranean Stage 3 ostracod species from the entire Black Sea region (Stoica et al., 2016) and, for a few species, from the Dacian (Stoica et al., 2013; Lazarev et al., 2020), Caspian (Van Baak et al., 2016) and North Aegean (see references in Krijgsman et al., 2020a) basins.

The means by which the ostracods travelled from the Paratethys to and across the Mediterranean during Stage 3 is as crucial for reconstructing the Stage 3 paleoenvironment as it is poorly addressed in onshore studies or overlooked in seismic and computational studies. Two migratory mechanisms have been suggested:

1) the aerial dispersion of ostracods through the migration of aquatic birds (Benson, 1978; Caruso et al., 2020); this hypothesis was proposed because, in a Mediterranean concluded to have been desiccated, it was the only possible migration mechanism.

2) direct aqueous migration by the ostracods themselves (which are planktonic in the larval stage) through the establishment of similar paleoenvironmental conditions; by this mechanism, the dispersion of Paratethyan ostracod fauna from right across the Mediterranean requires E-W intraconnection and a Mediterranean water-level high enough to reach the marginal basins (Gliozzi et al., 2007; Stoica et al., 2016; Sciuto et al., 2018; Sciuto and Baldanza 2020).

Finally, Carnevale et al. (2006a, b, 2008, 2018) recognized the Paratethyan affinity of the Mediterranean Stage 3 species but, in view of their occurrence with in-situ species of marine fish, they suggested that Stage 3 ostracods descended from a Paratethyan stock that migrated into the Mediterranean well before the MSC and survived the extreme salinity conditions of Stage 1 and 2 in marginal, fresher water refugia. In this scenario the brackish-water ostracod

assemblages found in Stage 3 have no paleoecological significance for Stage 3 paleoenvironment (Carnevale et al., 2006a, b; 2008, 2018). However, there are two, unflagged problems with this hypothesis: (1) the Mediterranean-Central Paratethys connection through the Trans-Tethyan gateway in Slovenia already closed in the early Tortonian (Kováč et al., 2007; Sant et al., 2017; Palcu et al., 2017); (2) No Paratethyan ostracod species have been found in the Mediterranean before the MSC (see Gliozzi et al., 2007).

1.5.2 Dinoflagellate cysts

Dinoflagellate cysts (dinocysts) are the fossil remains of unicellular protists that live in the upper water column of many water bodies (e.g. Zonneveld et al., 2013; Mudie et al., 2017). They can be used as paleoenvironmental indicators and for biostratigraphy, providing the ages of speciation and extinction events, as well as supplying evidence of age diagnostic dispersals of characteristic taxa/assemblages. Influxes of these microorganisms into a basin may occur as the result of interconnection with another basin and dinocysts can therefore be useful indicators of the open gateways between adjacent basins and the resultant changes in conditions (e.g. Grothe et al., 2018). In the case of the MSC, presence of in situ marine and/or Paratethys dinocyst assemblages in a marginal basin are likely to indicate the presence of Atlantic and/or Eastern Paratethys water (respectively) in the Mediterranean and (relatively) high water level conditions (e.g. Pellen et al., 2017).

Palynological studies on the late Messinian Mediterranean dinocysts record are rather scarce, confined to a limited number of outcrops (Malaga Basin, Do Couto et al., 2014; Northern Apennines, Bertini, 2006; Popescu et al., 2007; Iaccarino et al., 2008; Cosentino et al., 2012; Pellen et al., 2017; Caltanissetta Basin, Londeix et al., 2007) and deep wells (976B, 977A, 978A and 134B, Popescu et al., 2015). These studies describe substage 3.1 as being barren of dinocysts. By contrast, substage 3.2 dinocyst assemblages are diverse particularly a few meters/tens of meters below the Miocene/Pliocene boundary and show recurrent vertical variation in abundance between brackish, Paratethyan-type taxa and marine stenohaline and euryhaline species. Taxa with Paratethyan affinities are largely considered to be autochthonous by all aforementioned authors. The extent to which reworking may have affected the marine assemblages is more controversial and debated between none (in Malaga and in the Apennines; Popescu et al., 2007; Do Couto et al., 2014; Pellen et al., 2017), partial (in the uppermost part of the Sicilian Upper Gypsum; Londeix et al., 2007) and total (in the Apennines; e.g. Bertini, 2006; Iaccarino et al., 2008; Cosentino et al., 2012). Given the extent of the implications (i.e. re-establishment of a Mediterranean-Atlantic flow or connection earlier than the Zanclean; e.g. Pellen et al., 2017), this is an issue that will require further clarification.

A key dinocyst influencing our understanding of the late Miocene Lago-Mare phase is *Galeacysta etrusca* (Fig. 1.9b; see Bertini and Corradini, 1998; Popescu et al., 2009 and Grothe et al., 2018 for more insights). This species was originally described from sediments in the

Mediterranean (Corradini and Biffi, 1988), but has since been discovered in much older deposits in Paratethys (Magyar et al., 1999a, b). The earliest recorded occurrence of *Galeacysta etrusca* is in sediments from the Pannonian Basin dated at ~8 Ma (Magyar et al., 1999a, b). It subsequently dispersed throughout Paratethys at ~6 Ma and was present in the Black Sea throughout the MSC interval (Grothe et al., 2014, 2018). Despite a Mediterranean-Eastern Paratethys connection that is thought to have been established at ~6.1 Ma (Krijgsman et al., 2010; Van Baak et al., 2016; Grothe et al., 2020), *G. etrusca* is not found in the Mediterranean during MSC Stages 1, 2 and 3.1 (5.97-5.42 Ma; Bertini 2006, Londeix et al., 2007, Manzi et al., 2007, Iaccarino et al., 2008, Gennari et al., 2013) and is only reported in the uppermost part of the Lago-Mare phase, very close to the transition to the Pliocene (e.g. Bertini, 2006; Londeix et al., 2007; Popescu et al., 2007; Iaccarino et al., 2008; Cosentino et al., 2012; Pellen et al., 2017). This implies that *G. etrusca* may have migrated from Paratethys into the Mediterranean after 5.42 Ma or that environmental conditions in the Mediterranean and in its marginal basins were only suitable for this species (and more generally the whole dinocysts Paratethyan contingent) to proliferate in the uppermost Messinian. Several authors report multiple occurrences of *G. etrusca* within the Zanclean (e.g. Clauzon et al., 2005; Londeix et al., 2007; Popescu et al., 2007, 2015; Do Couto et al., 2014; Clauzon et al., 2015), but these interpretations are based on the use of an alternative stratigraphic model for the MSC sections (Fig. 1.4b; see Grothe et al., 2018 for details).

1.5.3 Diatoms

Among the fresh-brackish organisms found in Stage 3 sediments are also species of diatoms. To date (and to our knowledge), there are no onshore studies that have ever looked for these organisms. By contrast, two samples from DSDP Site 124 in the Algero-Balearic Basin (Fig. 1.2b) revealed the presence of littoral planktonic forms accompanied by brackish water, and even freshwater, euryhaline, benthonic, and epiphytic species in considerable numbers (Hajós, 1973). Diatoms of undisclosed paleoecological significance are also reported from the ~ 60 cm-thick mudstone bed between an anhydrite and halite bed found in the last core of Site 134 (Ryan et al., 1973). According to Hajós (1973) and Ryan (2009), the diatoms found in these drill cores attest to an extremely low salinity and a base level in the Balearic and Valencia basins below wave action. Further study of these indicative species and a wider distribution is required to apply this interpretation more generally.

1.5.4 Foraminifera

A reasonably diverse benthic and planktic foraminiferal assemblage containing no age-diagnostic taxa have been found co-occurring with the brackish Paratethyan fauna in both the onshore and offshore record throughout the Mediterranean (Fig. 1.2b for localities and references).

The benthic foraminifera assemblage is dominated by euryhaline representatives of the genus *Ammonia*, which today dwell in marginal marine (lagoons, estuaries, fjords and deltas) and lacustrine environments at depths <50 m and tolerate salinities of up to 50‰ (Milker and Schmiedl, 2012; Consorti et al., 2020). *Ammonia tepida* and *Ammonia beccari* (Fig. 1.9c) are by far the most abundant species in both onshore (see Fig. 1.2b for localities and references) and offshore (e.g. Site 968A, Blanc-Valleron et al., 1998; Sites 375, 376, 965-968, Orszag-Sperber, 2006) localities, where they co-occur with ostracods belonging to Biofacies 1. Other commonly occurring benthic euryhaline taxa are *Elphidium* sp., *Cribroelphidium excavatum, Haynesina* sp., *Nonion* sp., *Quinqueloculina* sp., *Discorbis* sp. and *Trichohyalus* sp., *Brizalina dentellata, Bulimina echinate* and *Bolivina* spp. (Ryan et al., 1973; Hsü et al., 1978a, b; Rouchy et al., 2001, 2003, 2007; Iaccarino et al., 2008; Caruso et al., 2020). These species are frequently mixed with poorly preserved and older in age bathyal species (e.g. Caruso et al., 2020).

Planktic foraminifera are represented both by species whose last occurrence pre-dates the MSC (e.g. Praeorbulina spp., Paragloborotalia partimlabiata, P. siakensis, Neogloquadrina atlantica praeatlantica, Globigerinoides subquadratus, Globorotalia saheliana, Globorotalia conomiozea, Acarinina sp., Hedbergella sp.) and by taxa with extended biostratigraphic ranges (e.g. *Sphaeroidinellopsis seminulina, Turborotalita quinqueloba, Globorotalia miotumida, Globoturborotalita decoraperta, Neogloboquadrina acostaensis, Neogloboquadrina spp., Orbulina universa, Globigerinoides trilobus, Globigerinoides obliquus, Globorotalia scitula, Globigerina bulloides, G. Mediterranea* and *G. humerosa*; see Fig. 1.2b for references).

The mixing of foraminifera species with different ecological and salinity requirements and the widespread agreement that the brackish Paratethyan fauna are autochthonous (see section 1.5.1) has always complicated the interpretation of the origin of the foraminiferal assemblages. Among the benthic species, *Ammonia* taxa and the other benthic euryhaline taxa are generally considered autochthonous because they are typically well-preserved and their ecological and salinity requirements could be compatible with those of the Paratethyan ostracods. The habitat of these benthic foraminifera today in environments both influenced by and disconnected from the open ocean indicates that the Stage 3 sediments in which they occur were deposited in a shallow-water environment subject to salinity fluctuations (Caruso et al., 2020 and references therein), but they do not provide insights into the water provenance. By contrast, the poor preservation, older age and low diversity of the bathyal taxa strongly suggest that these species are reworked (Bassetti et al., 2006; Iaccarino et al., 2008; Caruso et al., 2020). Their mode of life is also incompatible with the shallower water elements of the faunal assemblage. The planktic species which went extinct before the MSC are also undoubtedly reworked (Iaccarino et al., 2008; Caruso et al., 2020). It is more challenging to discriminate between in situ and reworked specimens of the long range Neogene taxa. Most of them are considered to be reworked because of their scarcity, their occurrence with in-situ brackish organisms and their poor preservation (e.g. Iaccarino et al., 2008; Caruso et al., 2020).

A more complex controversy surrounds the long-range dwarf specimens (Fig. 1.9c) occurring in onshore substage 3.1 (di Tetto Fm. in the Trave section; Iaccarino et al., 2008) and Lago-Mare sediments (Upper Mb. of the Nijar Feos Fm., Fortuin and Krijgsman, 2003; Aguirre and Sánchez-Almazo, 2004; Bassetti et al., 2006; Sorbas Basin, Roveri et al., 2019a; Bajo Segura Basin, Corbí and Soria, 2016; Colombacci Fm. in Northern Apennines localities, Casati et al., 1976; Colalongo et al., 1976; Rio and Negri, 1988; Popescu et al., 2007; Cyprus, Rouchy et al., 2001) and in some offshore localities (e.g. Sites 124, 125, 129A, 132, 134, 372, 376, 653, 974B, 975, 978; Cita, 1973; Cita et al., 1978; Kastens et al., 1987; Cita et al., 1990; Iaccarino and Bossio, 1999). This fauna is variably interpreted as:

1) reworked and size-sorted during transport, therefore lacking any paleoenvironmental significance (e.g. Kastens et al., 1987; Iaccarino and Bossio, 1999; Fortuin and Krijgsman, 2003; Bassetti et al., 2006);

2) in situ and indicating normal marine conditions (Aguirre and Sánchez-Almazo, 2004; Braga et al., 2006) or temporary Atlantic incursions (Rouchy et al., 2001);

3) in situ and indicative of high-stress environments (Keller and Abramovich, 2009), such as restricted and/or diluted marine environments (Corbí and Soria, 2016; Corbí et al., 2016, 2020). However, the paleoecological significance of dwarfism in foraminifer tests is not well understood and, given its potential implications for the Lago-Mare environment, it needs to be explored in greater detail.

1.5.5 Calcareous nannofossils and the *C. acutus* conundrum

Calcareous nannofossils are the fossil remains of coccolithophores, single-celled marine algae which dwell in the eutrophic and photic zone of the ocean (e.g. Ziveri et al., 2004). The potential recognition of marine calcareous nannofossils in marginal Stage 3 deposits would therefore have implications for the Mediterranean base-level and the hydrological riddle of MSC Stage 3. However, like foraminifera and dinocysts, the in situ versus reworking issue also impacts the nannoflora.

MSC Stage 3 is crossed by three important nannofossil bio-events astronomically calibrated in the ocean record: the top of *Discoaster quinqueramus* at 5.537 Ma, the base of *Ceratolithus acutus* at 5.36 Ma and the top of *Triquetrorhabdulus rugosus* at 5.231 Ma (Backman et al., 2012; Agnini et al., 2017). Most of the (few) studies that addressed the nannoflora component of Stage 3 deposits did not report taxa belonging to the biozones defined by these bio-events, but only taxa of Cenozoic and Cretaceous age, clearly physically reworked (e.g. Sites 132, 134, 653, 654A, 967A, 969B, Ryan et al., 1973; Hsü et al., 1978b; Müller et al., 1990; Castradori, 1998; Piedmont Basin, Trenkwalder et al., 2008; Violanti et al., 2009; Trave, Fonte dei Pulcini and Stingeti sections and Mondragone well in the Apennines, Cosentino et al., 2006, 2012, 2018; Iaccarino et al., 2008). An exception is the nannoflora observed in the uppermost Messinian sediments at Sites 978A, 975B and 967A (Levant Basin; Fig. 1.2b). Here, among the plethora of reworked

and long-ranging Neogene taxa, Castradori (1998) reported the anomalous abundance of *Sphenolithus* spp. (mostly *Sphenolithus* gr *abies*/*moriformis*). Although the assemblage points to the absence of a primary marine signature, the unlikely possibility that reworking and/or sorting lies behind the observed peak of *Sphenolithus* spp. led Castradori (1998) to conclude that at least one incursion of marine water occurred during the (uppermost) Lago-Mare.

By contrast, some authors (i.e. Popescu et al., 2007, 2015; Do Couto et al., 2014; Clauzon et al., 2015; Pellen et al., 2017) described the nannofossil assemblage of the LM Unit in Malaga, the Zorreras Member in Sorbas, the uppermost di Tetto/Colombacci Fm. in some Apenninic localities and offshore in the Alborán Basin as having good preservation and showing no erratic fluctuations, all characteristics that led to their interpretation as autochthonous and to the conclusion that these sediments were deposited in a Mediterranean already replenished of Atlantic water (Fig. 1.4b). In addition, these authors reported the low abundance, but continuous presence of the biostratigraphic markers for the Zanclean *Triquetrorhabdulus rugosus* and *Ceratolithus acutus* (Fig. 1.9d) below the formally defined M/P boundary (Van Couvering et al., 2000) in several onshore and offshore Mediterranean (as well as Paratethyan) localities (see Popescu et al., 2017 for details and a complete list of finding locations).

Such findings (especially that of *C. acutus*) are in sharp disagreement with most of the existing literature and have resulted in an important debate amongst the MSC community (e.g. Popescu et al., 2007, 2008 vs Roveri et al., 2008c and Stoica et al., 2016 vs Popescu et al., 2017), not only for their paleoenvironmental implications (i.e. presence of Atlantic water in the Mediterranean), but also for the chronostratigraphic repercussions (Fig. 1.4b). The chronostratigraphic value of *C. acutus* lies in its short temporal distribution straddling the M/P boundary (astrochronologically calibrated at 5.332 Ma; Van Couvering et al., 2000; Lourens et al., 2004). However, the corresponding biozone is established in oceanic areas (Zone CNPL1: 5.36-5.05 Ma; Backman et al., 2012; Agnini et al., 2017) and is considered not applicable to the Mediterranean region during the MSC due to the harsh physicochemical conditions that are unsuitable for marine biota (Di Stefano and Sturiale, 2010). The interpretation of these nannofossil assemblages in the westernmost areas of the Mediterranean has been countered with several observations: (1) the observation of these age-diagnostic taxa is often not replicated by other studies (e.g. Roveri et al., 2008a; Van Baak et al., 2015; Krijgsman et al., 2020b); (2) *C. acutus* is very rare also in fully marine open-ocean sediments (e.g. Di Stefano and Sturiale, 2010); (3) despite being rare in the late Messinian Mediterranean, this species has never been documented together with other long-range taxa, generally predominant in the assemblage, in Stage 3 deposits (see discussion in Krijgsman et al., 2020b). Recently, Golovina et al. (2019) showed that the morphology and size of *C. acutus* overlaps with the shape and dimensions of destroyed ascidian spicules (i.e. calcareous elements produced by benthic tunicates; Fig. 1.9d), providing an explanation for erroneous identification of *C. acutus* in the Black Sea Basin (Golovina et al., 2019) and perhaps in the western Mediterranean Lago-Mare sediments as well.

1.5.6 Fish

Fossil fish remains provide information about salinity and depth and have been used to contradict the brackish nature of the Lago-Mare deposits by Carnevale et al. (2006a, b, 2008, 2018) and Grunert et al. (2016). Euryhaline fish species inhabit marine to brackish environments and dominate settings with strong salinity variations while stenohaline fish have specific salinity requirements (marine, brackish, or freshwater) and cannot survive under different conditions. Demersal fish (i.e. those living in or immediately above the sea floor) have specific depth requirements, whereas pelagic fish occupy the water column within a wide range of depth variable from species to species. Fossil fish remains are found either as articulated or disarticulated skeletal parts, including teeth and otoliths, which are identified to the species level. Articulated fish skeletons typically indicate autochthonous deposition because of the difficulty in reworking and transporting intact skeletons. Otoliths and fish teeth are much more likely to be transported.

Otoliths and rare articulated skeletons (Fig. 1.9e) of marine and Paratethyan species have been reported from Stage 3 deposits, but commonly huge volumes of sediment are required to find even quite small numbers of these fossils (e.g. 20 tons from Moncucco, 6 tons from Cava Serredi, 700 kg from Capanne di Bronzo; Schwarzhans et al., 2020), much more than what is expected for normal marine deposits (i.e. <30 kg; Agiadi et al., 2017; Karakitsios et al., 2017b). Substage 3.1 sediments contain articulated skeletons (Fig. 1.9e) of the marine fish species *Lampanyctus licatae* and *Maurolicus muelleri*, and the shallow water, euryhaline species Aphanius crassicaudus in the Lower Feos Member in the Nijar Basin (de la Chapelle and Gaudant, 1987) and the marls of the first UG cycle in the Polemi Basin (Manzi et al., 2016a; Fig. 1.3a). Cava Serredi (Tuscany), Verduno and Moncucco (Piedmont) are the only other localities in which fish remains (only otoliths) in (claimed) substage 3.1 sediments are known (Carnevale et al., 2006a, 2008, 2018; Grunert et al., 2016).

The more diverse and abundant ichtyofaunal record occurs in substage 3.2 in a few marginal sections on the Italian peninsula (Ciabot Cagna in the Piedmont Basin; Cava Serredi and Podere Torricella in Tuscany; Capanne di Bronzo, La Vicenne and Ca' Ciuccio in thrust-top basins of the Northern and Central Apennines). The Lago-Mare fish remains mainly comprise otoliths of both euryhaline and stenohaline taxa indicative of marine, brackish, and freshwater habitats (Carnevale et al., 2018). Three articulated skeletons of the euryhaline marine taxa *Mugil* cf. *cephalus* (Fig. 1.9e), the marine Indo-Pacific species *Spratelloides gracilis* and of *Gobius* sp. have been identified at Cava Serredi in a horizon <1 m below the Miocene/Pliocene boundary (Carnevale et al., 2006b). The dominant stenohaline families in these assemblages are Gobiidae, a family of demersal fish occupying shallow-water marine, brackish and freshwater environments, and Myctophidae, which are marine mesopelagic fish that live below 200 m depth during the day, but feed at night in surface waters. A recent review of the Tortonian-Zanclean Gobiidae of the Mediterranean (Schwarzhans et al., 2020) showed that the otoliths

of this family, described by Carnevale et al., (2006a, 2008, 2018) and Grunert et al. (2016) as belonging to marine Atlantic species, instead belong to brackish and freshwater species of Paratethyan affinity inhabiting sheltered prodelta environments. In fact, no normal marine demersal taxa were recognized in these assemblages by Schwarzhans et al. (2020). As for the Myctophidae, the vast majority of the taxa belonging to this family were recovered in Moncucco and Verduno from alluvial plain silty mudstones along with terrestrial mammals (Dela Pierre et al., 2011; Colombero et al., 2017 and references therein), pointing to a physically reworked origin. When $^{87}Sr/^{86}Sr$ ratios are measured (Carnevale et al., 2008; Grunert et al., 2016), the resulting Sr-based age of the otoliths is >7 Ma, therefore further arguing against their in-situ origin. Since the good preservation of the otoliths suggests they did not suffer physical reworking (Carnevale et al., 2006a, b, 2008, 2018; Grunert et al., 2016), predators foraging in open marine settings and migrating to marginal environments are proposed as a way out of the enigma (Carnevale et al., 2008, 2018; Grunert et al., 2016; Colombero et al., 2017). However, Carnevale et al. (2006a) also rule out that so well preserved otoliths may have suffered post-mortem transport and action of the digestive acids in the stomach of predators. Rare findings of Myctophidae from Ciabot Cagna (3 species), Cava Serredi (1 species), Capanne di Bronzo (1 species) and Podere Torricella (6 species) (Carnevale et al., 2018) are all from sections where the host sediments have not been studied in sufficient detail to be clear about the in situ or reworked nature of the fossil assemblage. This lack of sedimentological uncertainty also extends to the stratigraphic position of many samples, because a stratigraphic log is provided for only a few sections (i.e. Ca' Ciuccio, Cava Serredi and Moncucco; Carnevale et al., 2006a, b). What this stratigraphic information suggests is that euryhaline fish taxa are widespread throughout substage 3.2, whereas strictly Myctophidae, which are an oceanic, marine stenohaline species, only occur very close to the base of the Pliocene, plausibly corresponding to the uppermost lithological cycle in substage 3.2 (~5.35-5.33 Ma; Carnevale et al., 2018).

1.5.7 Summary of the Stage 3 paleontological record

The aquatic fossil record of MSC Stage 3 indicates that substage 3.1 in onshore sections is mostly barren, while diverse assemblages characterize substage 3.2 deposits. By contrast, the deep record as a whole contains relatively few, low diversity assemblages. This might be as a consequence either of the limited sample locations recovered from the offshore areas (see Fig. 1.2b) or because the environmental conditions in the intermediate-deep basins were less favorable for sustaining the life forms typical of the onshore domain. Nevertheless, the assemblages that are found in both marginal and deep locations comprise mixed brackish and marine species.

Brackish species are mostly represented by ostracods and dinocysts (and mollusks here not addressed because poorly studied; see Esu, 2007 and Guerra-Merchán et al., 2010). Prominent is the affinity of these late Messinian Mediterranean brackish species with the same species that

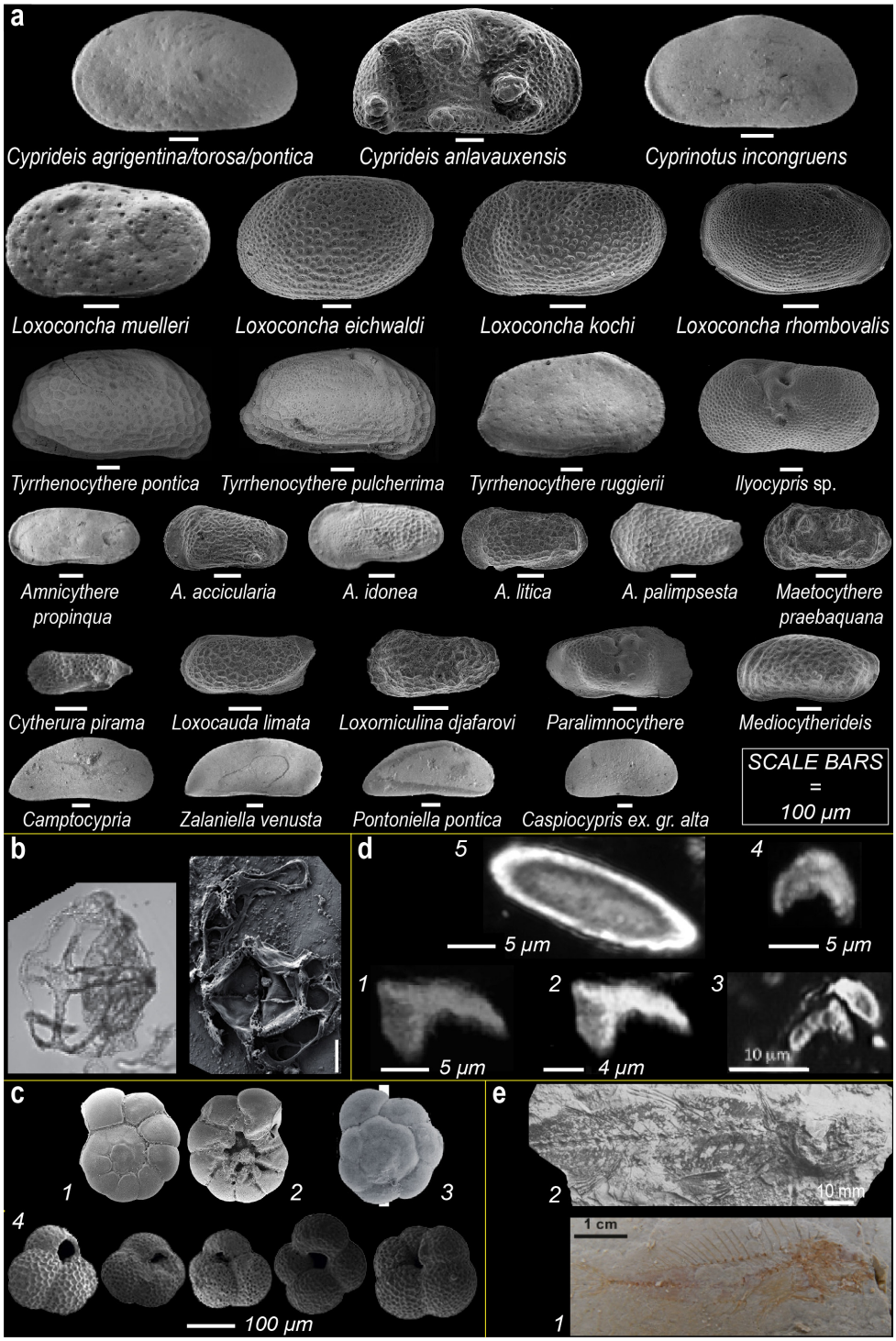
a
Cyprideis agrigentina/torosa/pontica
Cyprideis anlavauxensis
Cyprinotus incongruens
Loxoconcha muelleri
Loxoconcha eichwaldi
Loxoconcha kochi
Loxoconcha rhombovalis
Tyrrhenocythere pontica
Tyrrhenocythere pulcherrima
Tyrrhenocythere ruggierii
Ilyocypris sp.
Amnicythere propinqua
A. accicularia
A. idonea
A. litica
A. palimpsesta
Maetocythere praebaquana
Cytherura pirama
Loxocauda limata
Loxorniculina djafarovi
Paralimnocythere
Mediocytherideis
Camptocypria
Zalaniella venusta
Pontoniella pontica
Caspiocypris ex. gr. alta
SCALE BARS = 100 µm
b
d
5
5 µm
4
5 µm
1
5 µm
2
4 µm
3
10 µm
c
1
2
3
4
100 µm
e
2
10 mm
1 cm
1

Fig. 1.9 (previous page). *Photomicrographs of the key micro- and macrofossils featuring Stage 3 sediments.* **(a)** *Scanning electron microscope (SEM) photographs of the more common Paratethyan ostracod species in substage 3.1 and 3.2 sediments (compiled from Stoica et al., 2016, Cosentino et al., 2018 and Sciuto et al., 2018).* **(b)** *Photomicrographs of the Paratethyan dinoflagellate cyst Galeacysta etrusca under the optical microscope (left) and SEM (right) (modified from Do Couto et al., 2014 and Grothe et al., 2018). Scale=20 μm.* **(c)** *SEM microphotographs of the euryhaline, shallow-water benthic foraminifera Ammonia beccarii (1-spiral side, 2-umbilical side) and Ammonia tepida (3-spiral side; Carnevale et al., 2019) and of the dwarf fauna of planktonic foraminifera from the Bajo Segura Basin (4; Corbí and Soria, 2016).* **(d)** *Photographs in polarized light (crossed nicols) of some specimens of Ceratolithus acutus (1-3) described in the Lago-Mare unit of Malaga (1-Do Couto et al., 2014), the Zorreras Mb. of Sorbas (2-Clauzon et al., 2015) and the Colombacci Fm. of the Northern Apennines (3-Popescu et al., 2017) and of destroyed (4) and intact (5) ascidian spicules of Micrascidiscus sp. (Golovina et al., 2019). Note that C. acutus specimens closely resemble ascidian spicules of Micrascidiscus sp., which may lead to misinterpretation of the C. acutus (see Golovina et al., 2019), and that pictures 1 and 2 are identical, despite they are attributed to samples taken from two different localities.* **(e)** *Articulated skeletons of marine fish from substage 3.1 mudstone horizons in Cyprus (1-Aphanius crassicaudus; Manzi et al., 2016a) and substage 3.2 deposits in Cava Serredi (2-Mugil cf. cephalus; Carnevale et al., 2018).*

were simultaneously dwelling in the Eastern Paratethyan basins (Dacian, Euxinic and Caspian) and in the North Aegean. Since these organisms were not present in the Mediterranean at any time before the MSC, they are considered, with a broad consensus, as in situ. This conclusion is further corroborated by the mixing of adult and juvenile forms in the ostracod assemblages and by the good preservation of the specimens, which do not show typical evidence of physical reworking like abrasion, dissolution, or fragmentation. Still problematic is the time of their arrival in the Mediterranean and their likelihood as biostratigraphic tool. From our review it seems more likely that truly Paratethyan species of ostracods entered the Mediterranean already during substage 3.1, when they colonized intermediate-deep settings, while they entered the marginal basins at different times during substage 3.2. As for dinocysts, characteristic is their occurrence only in the uppermost Messinian. However, it must be noted that samples from the substage 3.1 interval are rarely processed for dinocysts, especially in age model-equipped sections (Fig. 1.3a). The route followed by the Paratethyan immigrants is equally contested and important for paleoenvironmental and paleohydrological interpretations. In view of a desiccated Mediterranean, their migration can only have taken place passively by means of aquatic migratory birds. Conversely, the homogeneity of the ostracod assemblages throughout the Mediterranean marginal basins is more indicative of the presence of a water body fed by Eastern Paratethys and connecting all Mediterranean subbasins, therefore implying relatively high water-level conditions (at least at times when ostracod-bearing sediments deposited; see Andreetto et al., 2021b).

Marine assemblages are composed by foraminifera, nannofossils, dinocysts and calcareous nannofossils. Their reworked or in situ nature is in many cases contested but critical for paleoenvironmental interpretation. The picture that emerges from our review is that an open marine signature is questionable in the foraminifera, nannofossils, dinocyst and fish records, as well as in other biotic groups (e.g. corals, echinoids and mammals) here not tackled (and for which we refer the reader to Dominici et al., 2018 and Carnevale et al., 2019). All marine representatives of the above mentioned categories were reintroduced into the Mediterranean only at the beginning of the Pliocene and at the expense of the Paratethys species that, instead, disappeared. Collectively, these observations lead us to conclude that the marine model as conceived by Carnevale et al. (2006a, b, 2008, 2018) and Grunert et al. (2016) has no foundation and therefore will not be further discussed.

1.6. The geochemical perspective

Variations in the water sources draining into the Mediterranean are expected to be reflected also in (geo)chemical properties of the paleodepositional environments. Important information about the nature of the connectivity framework of the Mediterranean can be gained by interpreting geochemical signals that respond to the presence or absence of an exchange with a chemically-unique water body. Four main geochemical proxies have been applied so far to MSC Stage 3 sedimentary and paleontological records. These includes both radiogenic ($^{87}Sr/^{86}Sr$ ratios) and stable isotopes (sulfate and oxygen) measured on fossils and minerals and hydrogen isotopes on molecular biomarkers. This section summarizes the dataset available for geochemical proxies (Fig. 1.10) and its interpretation(s) for MSC Stage 3.

1.6.1 Strontium isotope ratios ($^{87}Sr/^{86}Sr$)

The available strontium isotope data for Stage 3 (Fig. 1.10a) derive from measurements on both Ca^{2+}-bearing fossils (ostracod valves, mollusk shells, fish otoliths; Fig. 1.9a) and minerals (calcite and gypsum), where Sr^{2+} dissolved in an aqueous solution substitutes Ca atoms due to their similar ionic radius (e.g. Hajj et al., 2017). Here we screen the available dataset and discuss only results that (1) reflect the original primary isotopic signal, i.e. the isotopic signal of the fluid at time of shell calcification or mineral precipitation, and (2) for which timing of mineral precipitation can be constrained. This screening excludes bulk carbonate samples (e.g. Colombacci limestones; Bassetti et al., 2004), which contain carbonate compounds of various and/or unknown provenance, measurements from mollusk shells and otoliths (e.g. Carnevale et al., 2008; Grunert et al., 2016; Roveri et al., 2019a), because they are made of mineral phases easily altered during diagenesis (e.g. aragonite; Marcano et al., 2015), and data coming from reworked material (e.g. all reworked gypsum or transported foraminifera). $^{87}Sr/^{86}Sr$ isotope ratios have also been measured by Müller and Mueller (1991) and Roveri et al. (2014b) on the halite beds recovered at Sites 134, 374 and 376 (Ryan et al., 1973; Hsü et al., 1978b). Although

they provide interesting interpretative aspects, we do not consider these $^{87}Sr/^{86}Sr$ measurements because the position of Sr^{2+} in the crystal lattice of halite is unknown and the removal of all contaminants, that is not a straightforward procedure (see Meilijson et al., 2019), is not clear it was achieved by Müller and Mueller (1991) and Roveri et al. (2014b). As a matter of fact, there is no consistency between data generated from roughly the same interval in Core 134 by Müller and Mueller (1991) (0.708968) and Roveri et al. (2014b) (0.708800-0.708896). Added to this is the uncertainty over the provenance of halite in Sites 134 and 374 (see sections 1.4.2 and 1.4.6.1), which violates both criteria mentioned above.

The general trend of the Mediterranean $^{87}Sr/^{86}Sr$ isotope ratio during the MSC deviates from the ocean curve towards the less radiogenic values of the major peri-Mediterranean rivers and Paratethys and returns abruptly to oceanic values at the M/P boundary (Fig. 1.10a inset). This trend is regarded to reflect the progressive restriction of Mediterranean-Atlantic exchange and the relative increase in the proportion of non-marine source waters (Topper et al., 2011; Roveri et al., 2014a). At first glance it seems that each MSC Stage was characterized by a well-defined range of Sr ratios (Fig. 1.10a inset), an observation that led Roveri et al. (2014b) to attribute a chronostratigraphic value to MSC $^{87}Sr/^{86}Sr$ ratios. A closer look, however, shows that MSC substages are anything but homogeneous with respect to $^{87}Sr/^{86}Sr$ ratios. At least in the marginal basins, local lithological differences in the catchments (each lithology carries a unique $^{87}Sr/^{86}Sr$ fingerprint; see section 1.8.1) explain the different Sr isotopic compositions from basin to basin (see Schildgen et al., 2014; Modestou et al., 2017; Andreetto et al., 2021b), therefore arguing against the use of $^{87}Sr/^{86}Sr$ ratios for chronostratigraphic purposes in the MSC record.

Most of the data characterizing substage 3.1 (Fig. 1.10a) are from the Eraclea Minoa gypsum (Fig. 1.5h). These data define a narrow range of $^{87}Sr/^{86}Sr$ ratios between 0.708747 and 0.708793 (García-Veigas et al., 2018). Similar values were reported from both Eraclea Minoa and the nearby Siculiana Marina section (0.708710-0.708760; Keogh and Butler, 1999; Fig. 1.5i). The dominance of Sicily samples gives the appearance of a consistent Sr isotope signal for gypsum beds. However, data points from elsewhere (Cyprus, Manzi et al., 2016a; DSDPs 122, 371 and 372 in the Algero-Balearic Basin, ODPs 652, 653 and 654 in the Tyrrhenian Basin, DSDP 374 in the Ionian Basin; Müller et al., 1990; Müller and Mueller, 1991; Roveri et al., 2014b) display a wider range (from ~0.7087 to 0.708847; Fig. 1.10a) that may indicate a different hydrological regime for each basin (e.g. Müller et al., 1990; Müller and Mueller, 1991; Ryan, 2009). The one published $^{87}Sr/^{86}Sr$ value for ostracods found within one of the marl interbeds at Eraclea Minoa also has a lower value outside the typical Sicily gypsum range (Grossi et al., 2015). This suggests that a different hydrological regime may also have characterised precession minima stages of the precessional cycle.

The Sr isotope dataset for the Lago-Mare phase includes the lowest values measured on MSC sediments (~0.7085 from between gypsum VI and VII at Eraclea Minoa; Fig. 1.3a; Grossi et al., 2015) and the widest range of ratios spanning from 0.7085 to 0.7091, which is above

coeval oceanic values (Fig. 1.10a). Again, the conspicuously high Sr isotope values in substage 3.2 come from two areas, the marginal basins of southern Spain (Andreetto et al., 2021b and references therein; Figs. 1.5a-c) and the intermediate Polemi Basin on Cyprus (McCulloch and De Deckker, 1989). The lower values are drawn from right across the intermediate-deep Mediterranean (Algero-Balearic, Sicily, Levant; Fig. 1.2a) and are therefore more likely to represent a Mediterranean-wide Sr isotope signal.

New $^{87}Sr/^{86}Sr$ data from Eastern Paratethys (i.e. Dacian and Caspian basins; Fig. 1.2b) are now available for the interval corresponding to MSC Stage 3 (inset Fig. 1.10a). The $^{87}Sr/^{86}Sr$ ratios of the Dacian Basin (0.708865-0.708982; Vasiliev et al., 2010, 2021) are slightly lower than coeval ocean water (0.709020), but much higher than coeval Mediterranean values. However, the Dacian Basin is regarded as highly restricted from the Mediterranean throughout the MSC (Vasiliev et al., 2010). By contrast, the Caspian has very low values (0.708402 to 0.708473, Grothe et al., 2020) which are thought to reflect both the very low Sr isotope ratio of the Volga river (0.708020; Vasiliev et al., 2010 and references therein) and some input from the Mediterranean (Grothe et al., 2020).

1.6.2 Sulfate isotopes

Sulfur isotopic investigations have been carried out only on sulfate minerals (gypsum and more rarely anhydrite) of the MSC Stage 3 deposits with samples drawn from both onshore intermediate sequences (Caltanissetta Basin and Cypriot basins) and deep basinal records (Sites 122, 124, 125A, 132, 134, 372, 374, 375, 376, 652, 653, 654, 968, 969, 970; Fig. 1.10b; Fontes et al., 1973; Pierre, 1974, 1982; Pierre and Fontes, 1978; Ricchiuto and McKenzie, 1978; Pierre and Rouchy, 1990; Blanc-Valleron et al., 1998). Because the incorporation of dissolved sulfate into gypsum produces a nearly constant fractionation of $\delta^{18}O$ (+3.5‰) and $\delta^{34}S$ (+1.65‰) at earth surface temperatures (Thode and Monster, 1965; Lloyd, 1968; Warren, 2016), $\delta^{18}O$ and $\delta^{34}S$ isotopic values measured in gypsum should be corrected with the above mentioned fractionation factors in order to reconstruct the sulfate isotopic composition of the basin waters at the time of gypsum formation.

The deep Mediterranean samples exhibit a wide range of $\delta^{34}S_{SO4}$, but the majority of samples display $\delta^{34}S_{SO4}$ values between 18 and 22‰, strongly indicative of a marine origin of the sulfate forming the gypsum (Fig. 1.10b; Fontes et al., 1973; Pierre, 1974, 1982; Pierre and Fontes, 1978; Pierre and Rouchy, 1990; Blanc-Valleron et al., 1998). The $\delta^{34}S_{SO4}$ values lower than marine sulfate in the dataset are generally considered to represent a greater influence of continental sulfate input to the basin (Fig. 1.10b; Pierre, 1974; Pierre and Fontes, 1978; Pierre and Rouchy, 1990). By contrast, the data display $\delta^{18}O_{SO4}$ isotopic values that deviate substantially from marine $\delta^{18}O_{SO4}$ values towards higher values (Fig. 1.10). This is consistent with the influence of sulfate produced by reoxidation of reduced sulfur compounds generated by microbial sulfate reduction (MSR; Kaplan and Rittenberg, 1964; Brunner and Bernasconi, 2005; Sim et al., 2011;

Leavitt et al., 2013). The microbial use of SO_4^{2-} leads to an equilibration of $\delta^{18}O_{SO4}$ with ambient water oxygen, whereas the $\delta^{34}S_{SO4}$ returns towards its initial value as a higher fraction of sulfide produced by MSR is re-oxidated. This mechanism has been suggested for Sites in the Algero-Balearic, Tyrrhenian and Ionian basins and offshore Cyprus (Pierre, 1974; Pierre and Fontes, 1978; Pierre and Rouchy, 1990). Although some authors have suggested that partial equilibration of sulfate oxygen toward $\delta^{18}O_{H2O}$ values of the basin enriched in heavy oxygen isotopes by evaporation have led to an increase in $\delta^{18}O_{SO4}$ values without significant changes in $\delta^{34}S_{SO4}$ (Fontes et al., 1973; Pierre, 1974; Ricchiuto and McKenzie, 1978), this hypothesis seems highly unlikely as the abiotic equilibration between sulfate and water oxygen take about 20 Myr at normal marine pH (Lloyd, 1968; Longinelli and Craig, 1967; Turchyn et al., 2006). Moreover, the microbial sulfate reduction process is supported by the presence of pyrite at Sites 132, 654A and 968 (Pierre, 1982; Pierre and Rouchy.,1990; Blanc-Valleron et al., 1998) and the existence of filaments of possible microbial origin at Site 654A (Pierre and Rouchy,1990).

The sulfate isotopic values reported by Longinelli (1979) and Pierre (1982) from the Upper Gypsum of Eraclea Minoa (Caltanissetta Basin, Sicily) are considerably more scattered than those from a recent study by García-Veigas et al. (2018; Fig. 1.10b). Such discrepancies are probably a consequence of different sample selection: García-Veigas et al. (2018) analyzed only pristine whitish selenite and balatino samples, while Longinelli (1979) and Pierre (1982) analyzed all types of gypsum-bearing samples such as "gypsiferous marl" and gypsum laminae intercalated in carbonate or diatomaceous intervals. These less pristine samples probably contain high quantities of 34S-depleted solid sulfides or diagenetic gypsum formed by oxidation of sulfides (see Liu et al., 2017 for more details on this process) and are therefore unlikely to be representative of the primary gypsum facies. Once these data are excluded, the Eraclea Minoa sulfate values (δ18OSO4 from 12.4 to 14.6‰ and δ34SSO4 from 21.0 to 22.3‰) suggest a marine origin of the sulfate and stable redox conditions during gypsum deposition (Fig 9.b; García-Veigas et al., 2018). Interestingly, the Eraclea Minoa sulfate values are in compliance with the isotopic values (δ18OSO4=15.2 to 16.8‰; δ34SSO4= 20.4 to 21.9‰) measured by Pierre (1982) in the Polemi Basin (Cyprus).

1.6.3 Hydrogen isotopes on molecular biomarkers

From the point of view of the application of organic geochemistry proxies, the Miocene Mediterranean Basin received little attention so far, with biomarker-based proxies that have been mostly applied to (a limited number of) pre-MSC sequences (Tzanova et al., 2015; Herbert et al., 2016; Mayser et al. 2017; Natalicchio et al., 2017, 2019; Vasiliev et al. 2019) and pre-Stage 3 sedimentary records (Lower Evaporites on Sicily, Andersen et al., 2001; Vena del Gesso Basin, Sinninghe Damsté et al., 1995 and Vasiliev et al., 2017; Levant Basin, Meilijson et al., 2019). To date, only one study analyzed Stage 3 samples (Vasiliev et al., 2017). This study used compound specific hydrogen isotope (δD) analyses, measured on both terrestrial (long chain C_{29} and C_{31}

Fig. 1.10 (next page). *Isotopic record of MSC Stage 3 for the Mediterranean Basin.* **(a)** *Compilation of MSC Stage 3 $^{87}Sr/^{86}Sr$ isotope data sourced from ostracod valves and gypsum crystals (see Supplementary material 1 and subsection 6.1 for references). Data are plotted with the global $^{87}Sr/^{86}Sr$ seawater curve (McArthur et al., 2012). Error bars indicate analytical error, which is so small in some cases that no error bars are visible at this scale. To not complicate the figure, horizontal error bars have not been added for the sections/cores unprovided of a chronostratigraphic framework and for which age uncertainties are present (i.e. all but Nijar and Vera basins, Eraclea Minoa and onshore Cyprus; see Fig. 1.3). Note that none of the $^{87}Sr/^{86}Sr$ isotope ratios but one from Nijar plot on the ocean curve. In the inset is shown the Mediterranean Sr record for the entire MSC as well as the time-equivalent Eastern Paratethys record (modified after Andreetto et al., 2021).* **(b)** *Plot of $\delta^{34}S_{SO4}$ and $\delta^{18}O_{SO4}$ in Stage 3 gypsum and anhydrite beds from onshore and offshore localities (see Supplementary material 1 and section 1.6.2 for references). No measures are available from the marginal basins, where gypsum did not deposit during Stage 3. The dark blue and black rectangles represent the sulfate isotopic composition of the Global Messinian ocean and Stage 1 (PLG) evaporites, respectively. The light blue area represents the sulfate isotopic composition of mixtures of Messinian marine waters with non-marine sources. The red area represents the isotopic composition of the residual sulfate ion in a basin where marine Messinian sulfate is consumed by microbial sulfate reduction to produce H_2S. The arrow represents the isotope trajectory of dissolved sulfate resulting from the mixing of residual ^{34}S-enriched sulfate produced by MSR and ^{34}S-depleted sulfate produced by H_2S oxidation. All the published $\delta^{34}S_{SO4}$ and $\delta^{18}O_{SO4}$ values are provided corrected with the fractionation factors $\delta^{34}S$=+1.65‰ and $\delta^{18}O$=+3.5‰ to smooth the isotopic fractionation effects experienced by dissolved sulfate and to reason on values reproducing the isotopic composition at the time of gypsum precipitation.* **(c)** *δD isotopes of C_{29} and C_{31} n-alkanes and C_{37} and C_{38} long chain alkenones recorded in the Stage 3 gypsums and marls of the Eraclea Minoa section (modified from Vasiliev et al., 2017). Blue lines indicate the values recorded in the present day lacustrine settings for the n-alkanes (Sachse et al., 2006) and in the alkenones from the Mediterranean in the recent times (Van der Meer et al., 2007). Error bars indicate standard errors of the mean.*

n-alkanes; Sachse et al., 2006) and aquatic (alkenones; Englebrecht and Sachs, 2005) biomarkers from the gypsum beds of the Upper Gypsum at Eraclea Minoa to reconstruct the hydrological cycle during gypsum precipitation.

Both $\delta D_{C29n\text{-alkanes}}$ and $\delta D_{alkenones}$ results (Fig. 1.10c) suggested that conditions in Sicily were significantly dryer than today, with highly enriched values of $\delta D_{C29n\text{-alkanes}}$ (up to −125‰). The $\delta D_{alkenones}$ varied between values suggesting evaporative conditions (−125‰) and values typical for present-day $\delta D_{alkenones}$ in the Mediterranean (−203‰; Vasiliev et al., 2017).

No time-equivalent biomarker data from the open ocean settings are currently available. Instead, Vasiliev et al. (2017) compared their Mediterranean data with data from the Black Sea (DSDP 42B Hole 380 and Taman peninsula; Vasiliev et al., 2013, 2015). The UG $\delta D_{n\text{-alkanes}}$ were more enriched when compared to their time equivalent deposits of the DSDP 42B 380 borehole of the Black Sea (−180‰). This probably reflects the more intracontinental position of

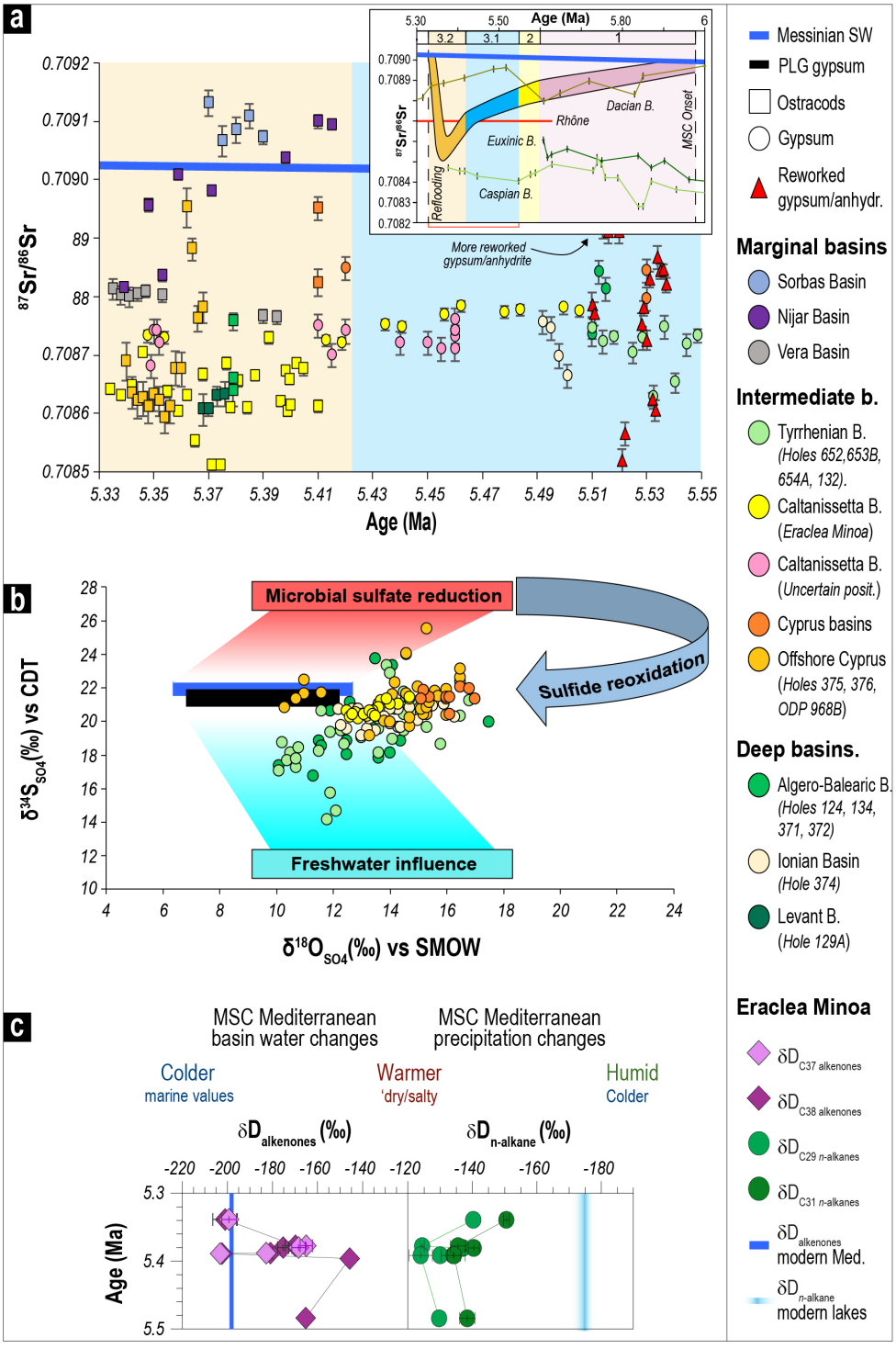
a
0.7092
0.7091
0.7090
89
88
0.7087
0.7086
0.7085
87Sr/86Sr
5.33 5.35 5.37 5.39 5.41 5.43 5.45 5.47 5.49 5.51 5.53 5.55
Age (Ma)
5.30 5.50 Age (Ma) 5.80 6
3.2 3.1 2 1
0.7090
0.7089
0.7084
0.7083
0.7082
87Sr/86Sr
Reflooding
Rhône
Euxinic B.
Caspian B.
Dacian B.
MSC Onset
More reworked gypsum/anhydrite
b
Microbial sulfate reduction
Sulfide reoxidation
Freshwater influence
28 26 24 22 20 18 16 14 12 10
δ34SSO4(‰) vs CDT
4 6 8 10 12 14 16 18 20 22 24
δ18OSO4(‰) vs SMOW
c
MSC Mediterranean basin water changes
MSC Mediterranean precipitation changes
Colder
marine values
Warmer
'dry/salty
Humid
Colder
δDalkenones (‰)
δDn-alkane (‰)
-220 -200 -180 -160 -140 -120 -140 -160 -180
5.3
5.4
5.5
Age (Ma)
Messinian SW
PLG gypsum
Ostracods
Gypsum
Reworked gypsum/anhydr.
Marginal basins
Sorbas Basin
Nijar Basin
Vera Basin
Intermediate b.
Tyrrhenian B. (Holes 652,653B, 654A, 132).
Caltanissetta B. (Eraclea Minoa)
Caltanissetta B. (Uncertain posit.)
Cyprus basins
Offshore Cyprus (Holes 375, 376, ODP 968B)
Deep basins.
Algero-Balearic B. (Holes 124, 134, 371, 372)
Ionian Basin (Hole 374)
Levant B. (Hole 129A)
Eraclea Minoa
δDC37 alkenones
δDC38 alkenones
δDC29 n-alkanes
δDC31 n-alkanes
δDalkenones modern Med.
δDn-alkane modern lakes

the Black Sea which commonly translates into more depleted values for $\delta D_{precipitation}$ used by the vegetation, resulting in more depleted $\delta D_{C29n\text{-}alkanes}$. However, there is a 30 to 40‰ enrichment relative to present in the $\delta D_{n\text{-}alkanes}$ (i.e. $\delta D_{precipitation}$) in both Mediterranean and Paratethys domains, indicating concurrent changes in both areas during the latest MSC phase. Both the Mediterranean and Paratethyan samples contain δDalkenones with low values (~-200‰) (Fig. 1.10c) leading Vasiliev et al. (2017) to suggest that either the surface water from the Upper Gypsum was derived from the Black Sea, or that the Mediterranean and Paratethys were exchanging surface water during gypsum precipitation. Similarity between the relative contribution of the C37, C38 and C39 alkenones at Eraclea Minoa and one of the Black Sea samples may suggest common alkenone producers for the two areas, again supporting the idea of a Mediterranean-Paratethys connection during Stage 3 (Vasiliev et al., 2017).

A final speculative insight from this biomarker dataset is that the relative contribution of alkenones found in the Upper Gypsum of Eraclea Minoa is strikingly similar to present-day open marine samples, even though *Emiliania huxleyi*, the principal ocean alkenone producer today, did not exist in the late Miocene. Vasiliev et al. (2017) suggested that this could imply the existence of a connection to the open ocean during Upper Gypsum deposition in Sicily (i.e. throughout Stage 3; Fig. 1.3a).

1.6.4 Oxygen isotopes

Oxygen stable isotope data ($\delta^{18}O$) are available from bulk samples (Rouchy et al., 2001, 2003, 2007; Pierre et al., 2006; Cosentino et al., 2012), gypsum (Pierre and Fontes, 1978; Ricchiuto and McKenzie, 1978; Lugli et al., 2007), mollusk shells (Carnevale et al., 2008; Grunert et al., 2016) and ostracod valves (Cosentino et al., 2012; Grossi et al., 2015).

For all the sub-basins for which there is latest Messinian data (e.g. Sites 974 and 975; Eraclea Minoa section, Sicily; Aghios Stefanos section, Corfu; Kalamaki section, Zakynthos; Pissouri Basin, Cyprus; Rouchy et al., 2001, Pierre et al., 2006), each has its own range of oxygen isotopic compositions and its own degree of variability. Values from above the Miocene/Pliocene boundary regain seawater values of 0.3 to 1‰ (e.g. Pierre et al., 2006).

In marginal marine settings and lakes, the controls over $\delta^{18}O$ are poorly constrained as oxygen does not respond simply to the freshwater flux, but to a combination of variables such as temperature, rainfall and evaporation (e.g. Placzek et al., 2011). Freshwater input may contribute to the signal, resulting in $\delta^{18}O$ more negative than seawater (0.3‰ to 0.8‰ SMOW; Dettman et al., 2004), but under prevailing evaporating conditions it is likely that the $\delta^{18}O$ will be primarily influenced by evaporation, leading to $\delta^{18}O$ more positive than seawater (e.g. Dettman et al., 2004), making any data very difficult to interpret. Furthermore, the lack of a unique $\delta^{18}O$ signature for each water source makes oxygen isotopes a difficult tracer proxy to use.

1.6.5 Summary of the Stage 3 geochemical dataset

The variety of paleoenvironmental and connectivity proxies applied to MSC Stage 3 record provide valuable insights into the hydrological conditions during Stage 3. The more outstanding results from all discussed proxies are that:

i. Paleodepositional subaqueous environments where gypsum was precipitating and ostracods and biomarker-producers were thriving were strongly dominated by non-oceanic inputs;
ii. The an indisputable marine signal is absent and only regained above the M/P boundary.

Sulfate and oxygen isotopes are currently difficult to use for water provenance reconstruction because the non-marine sources (local and major rivers and Eastern Paratethys) that are likely to be of influence lack distinctive isotopic signatures and, especially for oxygen, respond to a combination of controls (e.g. temperature, rainfall, evaporation) with local variability. $\delta^{34}S_{SO4}$ are claimed by several authors to be an evidence of the presence of an Atlantic inflow ($\delta^{34}S_{SO4}$=22‰; Turchyn and Schrag, 2004) in a Mediterranean strongly affected by non-marine waters (Manzi et al., 2009, 2016a and García-Veigas et al., 2018 among others). However, the same values can be obtained by means of the recycling of PLG deposits (~23‰; Lu et al., 2001; Lugli et al., 2010; García-Veigas et al., 2018). Similarities between the $\delta D_{alkenones}$ of the Upper Gypsum at Eraclea Minoa and coeval Black Sea sediments and $\delta D_{n\text{-alkanes}}$ similar to present-day marine settings, suggest that Eastern Paratethys and the Atlantic were simultaneously contributing to the Mediterranean hydrological budget. $^{87}Sr/^{86}Sr$ isotope ratios are a useful water-mass tracer because each water body carries a unique Sr isotope fingerprint (see section 1.8.1.1). Our plotting of Stage 3 $^{87}Sr/^{86}Sr$ isotope values (Fig. 1.10a) highlights the large geographical variability of the values and the sharp division between Sr isotope ratios measured in marginal basins versus those in intermediate-deep water locations. This is only noticeable in substage 3.2, since no (or not enough) material suitable for Sr analyses is present in substage 3.1 deposits from the marginal basins. Some authors see this variability as an indication of isolated subbasins with unique hydrological conditions driven by their catchment rivers (e.g. Müller et al., 1990; Müller and Mueller, 1991; Ryan, 2009). If some degree of connection was present, it involved only neighbouring basins (e.g. Tyrrhenian subbasins; Müller et al., 1990; Müller and Mueller, 1991). A recent comparison of the Sr isotope record of the Spanish marginal basins of Sorbas, Nijar and Vera with the Sr isotope ratios likely to have typified the local riverine sources demonstrated that a local sources-mixed signal expected from an endorheic lake in that location is absent. In this instance mixing of intrabasinal water sources with a non-marine Mediterranean water mass is used to explain the measured values (Andreetto et al., 2021b). If this explanation is more widely applicable, then it may result in a re-interpretation of the spread of Sr isotope data from the latest Messinian interval.

To conclude, geochemical proxies have great potential to test the different scenarios, but data are currently too numerically and geographically limited to be robust.

1.7 Paleoenvironmental scenarios for freshening the salt giant: desiccated versus full Mediterranean

The riddle of the Mediterranean environmental and hydrological conditions during Stage 3 is a highly debated topic and it is key to understanding the means by which open marine conditions were restored at the base of the Zanclean and on the potential impact that the Atlantic-Mediterranean re-connection had on the Atlantic and global climate (Flecker et al., 2015; Capella et al., 2019). In this chapter, the paleoenvironmental scenarios, in terms of base-level position (desiccated or full Mediterranean) and hydrological configuration (connections to the Atlantic and/or Paratethys), proposed for the Mediterranean during Stage 3 are described, as well as the different timings of the reflooding (instantaneous, gradual, step-like increments). The low-salinity Stage 3 followed the hypersaline Stage 2 and the transition between the two likely influences the plausibility of the various paleoenvironmental scenarios proposed for the terminal stage. We therefore first summarize the current understanding of the configuration of the Mediterranean during Stage 2 and the enduring controversies (see Roveri et al., 2014a for a more extensive review).

1.7.1 Stage 2 (5.59-5.55 Ma): Formation of the Mediterranean salt giant

Numerical modelling based on hydrological budget calculations shows that in order to reach salinity levels compatible with halite saturation and to accumulate the substantial thicknesses of halite observed in the seismic profiles (Ryan, 1973; Haq et al., 2020), the Atlantic-Mediterranean gateway needs to have permitted inflow from the Atlantic, but may have completely blocked outflow (Blanc, 2002; Krijgsman and Meijer, 2008). Numerical models also showed that without Atlantic inflow into the Mediterranean Sea its base level is forced to drop on time scales in the order of a few thousand years by virtue of the basin's negative hydrological budget, where more water is lost to the atmosphere by evaporation than is received from rainfall and river runoff (e.g. Meijer and Krijgsman, 2005; Krijgsman and Meijer, 2008; Simon et al., 2017). The idea of a drawdown is supported by several arguments: (1) the widespread presence, from the margins to the slopes, of the Messinian Erosional Surface cutting through Stage 1 and pre-MSC deposits and canyon incisions following today's drainage networks (e.g. Chumakov, 1973; Clauzon, 1982; Lofi et al., 2005, 2011a, b; Loget et al., 2006; Maillard et al., 2006, 2020; Estrada et al., 2011; Just et al., 2011; Urgeles et al., 2011; Amadori et al., 2018; Lymer et al., 2018; Cazzini et al., 2020; Figs. 5e, 7e); (2) their morphology interpreted as subaerial in origin; (3) the clastic fans at the outlet of the valleys onlapped by Stage 3 deposits and interpreted as fluvial accumulations (e.g. Lofi et al., 2005; Maillard et al., 2006; Pellen et al., 2019). A number of studies have tried to quantify the magnitude of the sea-level fall by compensating for the isostatic vertical motion since the Messinian to obtain the original depth of the erosional features and Messinian deposits. However, this depends on the assumptions about when the drawdown occurred relative to the halite precipitation: before (e.g. Cartwright and Jackson,

2008; Bache et al., 2009, 2012), during (e.g. Ryan, 2008, 2009) or after (e.g. Ryan, 1978; Bertoni and Cartwright, 2007; Lofi et al., 2011a, b). How shallow the Mediterranean became during Stage 2 is also a matter of disagreement. Estimates in the Western Mediterranean vary from a maximum drawdown of 2500 m (Ryan, 1976) to 1000-1500 m (Bache et al., 2012) in the Gulf of Lion, 800-1200 m in the Balearic promontory (Mas et al., 2018b) and 400 m in the Ebro delta region (Frey-Martinez et al., 2004). A later backstripping analysis of this delta yielded a drawdown of ~1300 m (Urgeles et al., 2011). East of the Sicily sill, backstripping studies estimated base-level drops of 1800-2000 m in the Ionian basin (Micallef et al., 2018, 2019; Camerlenghi et al., 2019; Spatola et al., 2020), 800-900 m in the Adriatic foredeep and Po plain (Ghielmi et al., 2013; Amadori et al., 2018), 800-1300 m (Ben-Gal et al., 2005), 600 m (Druckman et al., 1995) and 800 m (Cartwright and Jackson, 2008) in the Levant Basin.

None of these quantifications could unequivocally constrain the timing of the drawdown within the MSC sequence, but numerical modeling studies show that, if the blocking of the outflow was controlled by a tectonic uplift counteracted by inflow erosion across the Strait of Gibraltar, then the expected drawdown of the Mediterranean Sea should be moderate (<400 m; and possibly harmonic) due to an equilibrium between incision and uplift before the complete blocking of inflow and larger (up to complete desiccation) only after tectonic uplift overcame incision rates (Garcia-Castellanos and Villaseñor, 2011). The same model suggests that the initiation of halite precipitation might overlap in time with the late primary gypsum deposition, right before the full disconnection from the Atlantic Ocean.

The interpretation of the deep evaporites and their associated seismic markers (erosional surfaces and deep engravings along the shelf-slope systems) is not straightforward. Recently, it was suggested that the deep evaporitic facies and the seismic morphological features could have been produced without a significant drop of the Mediterranean base-level, therefore promoting the persistence of a relatively deep-water Mediterranean basin even during halite deposition (Lugli et al., 2013, 2015; Roveri et al., 2014b). For example, Roveri et al. (2014c) proposed that downslope flows of dense, hypersaline waters sourced from evaporation in shallower water areas could have generated both the observed shelf-slope erosion and have created one or multiple deep brine(s), supersaturated in the ions necessary for precipitating halite. The following areas are tentatively appointed as Messinian salt brine factories: the Gulf of Lion and north Africa shelf are held responsible for the formation of the salt giant of the Western Mediterranean (Roveri et al., 2014c); the Levant margin shelf is held accountable for the Mobile Unit in the deep Levant Basin (Roveri et al., 2014c); the Adriatic Basin is hypothesized to have sourced salt brines to the deepest basins to its south, namely the Crotone Basin and the IAP (Manzi et al., 2020). These subaqueous hyperpycnal flows are consistent with the observed clastic evaporites that filled the Levant margin canyons (Lugli et al., 2013) and, more generally, with the widespread presence of Complex Units at the outlet of the MES drainage systems (see Lofi et al., 2005, 2011a, b; Lofi, 2018). These sediments are dominated by reworked PLG that

would have been exposed by a sea-level fall as little as 200 m (Lugli et al., 2010). However, the hypersaline environment that is presumed to be established by these hyperpycnal flows during the deposition of the RLG is in contrast with the occurrence of the Paratethyan ostracod *L. muelleri* within the clastic evaporites (RLG) in several marginal sections (e.g. Adana Basin, Faranda et al. 2013; Radeff et al., 2016, 2017).

Whatever the state of Mediterranean base-level during Stage 2, the more commonly used chronostratigraphic model for the MSC (Fig. 1.1a; Roveri et al., 2014a) states that massive halite precipitation ceased at 5.55 Ma and was superseded by an environment that, with precession periodicity (Fig. 1.3a), cycled between gypsum precipitation and conditions that saw fresh-brackish organisms thriving. The question is whether these conditions cycled homogeneously in several isolated lakes or in basins largely connected to the same Atlantic and Eastern Paratethys-influenced water mass (Fig. 1.11).

1.7.2 Stage 3 (5.55-5.33 Ma): Resumption of (upper) gypsum precipitation and Paratethys fauna invasion

1.7.2.1 An isolated Mediterranean dotted by sabkhas and lakes

The first and long-lasting paleoenvironmental interpretation of the evaporite-bearing UG/UU units and (possibly) time-equivalent evaporite-free units (e.g. LM Unit in Malaga, Sorbas and Zorreras Mb. in Sorbas, Feos Fm. in Nijar, Cassano Spinola Conglomerates in Piedmont, San Donato/Colombacci fms. in the Apennines, Handere Fm. in Turkey) envisaged their sedimentation in a Mediterranean mostly isolated from the Paratethys (which may have added water only to some basins in the Eastern Mediterranean) and totally isolated from the Atlantic where, in each subbasin, continental settings (e.g. alluvial plains, river channels, alluvial fans, playa lakes, sabkhas) alternated/interfingered with shallow, endorheic lakes (Figs. 1.11a, c; e.g. Ruggieri, 1962, 1967; Decima and Sprovieri, 1973; Decima and Wezel, 1973; Friedman, 1973; Hsü et al., 1973a,b,c, 1978a, b; Ryan et al., 1973; Selli, 1973; Sturani, 1973; Sissingh, 1976; Benson, 1978; Bossio et al., 1978; Cita et al., 1978, 1990; Ricchiuto and McKenzie, 1978; Ryan, 1978, 2008, 2009; Cita and Colombo, 1979; Orszag-Sperber and Rouchy, 1979; Ghibaudo et al., 1985; Müller et al., 1990; Benson and Rakic-el-Bied, 1991; Benson et al., 1991; Müller and Mueller, 1991; Orszag-Sperber et al., 2000; Rouchy et al., 2001, 2003, 2007; Blanc, 2002; Lofi et al., 2005, 2011; Bassetti et al., 2006; Rouchy and Caruso, 2006; Bertoni and Cartwright, 2007; Cameselle and Urgeles, 2017; Amadori et al., 2018; Camerlenghi et al., 2019; Kartveit et al., 2019; Madof et al., 2019; Ben Moshe et al., 2020; Caruso et al., 2020; Cazzini et al., 2020; Raad et al., 2021). The full disconnection is also supported by observations that support an abrupt Zanclean reflooding (e.g. Blanc, 2002; Micallef et al., 2018, 2019; Garcia-Castellanos et al., 2020; Spatola et al., 2020), since a rapid outburst flood requires a large sea level difference prior to the flood that can only be developed in a scenario of a full Mediterranean-Atlantic disconnection (Garcia-Castellanos et al., 2009; Garcia-Castellanos and Villaseñor, 2011).

Although rarely explicitly stated, all these studies must assume that:

1. all Paratethyan biota (and possibly other organisms of undisclosed provenance like diatoms) migrated passively via aquatic migratory birds across the entire Mediterranean (Fig. 1.11a; Benson, 1978; Benson and Rakic-El Bied, 1991; Caruso et al., 2020);

2. chemical and physical conditions (brackish water and water depth not exceeding 100 m; e.g. Hajós, 1973; Gliozzi and Grossi, 2008) that allowed alternated conditions suitable for gypsum to precipitate and Paratethyan biota and euryhaline benthic foraminifera to thrive were related to changes in the local freshwater budget;

3. The marine isotopic signals in UU/UG gypsum (Fig. 1.10) are entirely the reflection of the lithologies that are leached by continental waters in surficial and/or underground drainage areas (e.g. Ryan, 2009; Raad et al., 2021);

4. Stage 3 gypsum precipitated in extremely shallow-water (playa lakes) to completely dried environments (sabkhas) and the excessive sulfate necessary is completely derived from "clastic reworking, dissolution, re-precipitation and diagenesis of materials belonging to the PLG and halite of the previous MSC Stage 2 (Ryan, 2009).

Observations endorsing a Mediterranean isolated throughout Stage 3 and only at the mercy of local freshwater inputs (Fig. 1.11a) are: (1) the lack of evidence for in situ marine fauna and flora in UU (e.g. Ryan et al., 1973; Hsü et al., 1978a; Cita et al., 1990; Ryan, 2009; Lofi et al., 2011a); (2) the shallow-water mode of life and highly likely in-situ nature of ostracods and euryhaline, shallow-water benthic foraminifera observed in DSDP/ODP wells from intermediate and deep basins (e.g. Cita et al., 1978; Iaccarino and Bossio, 1999); (3) the bathymetric contrast (up to several hundred meters) between the late Messinian paleoenvironments and the marine Zanclean on top (e.g. Cita and Colombo, 1979; Bonaduce and Sgarrella, 1999; Caruso et al., 2020); (4) the presence of paleosols in Cyprus (Orszag-Sperber et al., 2000; Rouchy et al., 2001) and on the crest of the Eratosthenes seamount (Robertson, 1998a, b); (5) the erosional features preserved on the continental shelves and lower-middle slopes and interpreted in most seismic stratigraphic studies as the result of subaerial exposure (e.g. Lofi et al., 2005, 2011; Lymer et al., 2018; Ben Moshe et al., 2020); (6) the pinching out of the UU/BU units towards evaporite-free pre-Messinian structural highs (Figs. 1.7b-g, 1.8a, e; Ryan, 2009; Lymer et al., 2018; Camerlenghi et al., 2019; Raad et al., 2021); (7) the more abundant terrigenous clasts and reworked calcareous fossils in Stage 3 samples compared to the overlying, deep-water Pliocene (Ryan et al., 1973; Hsü et al., 1978b; Ryan, 2009); (8) the erosional nature of the M-reflector/TES/IMTS in the Levant Basin (Figs. 1.8e-g), by some linked to subaerial exposure of the Levant seafloor (e.g. Bertoni and Cartwright, 2007; Lofi et al., 2011a, b; Maillard et al., 2011a) before the emplacement of deposits interpreted as fluvial from seismic observations (Bowman, 2012; Radeff et al., 2017; Leila et al., 2018; Kartveit et al., 2019; Madof et al., 2019). Furthermore, (9) isolated hydrological circuits with unique chemical composition are regarded by Camerlenghi et al. (2019) as the most plausible explanation for the

W-E change in the MSC sedimentary expression in the deep basins, represented by the trilogy LU-MU-UU in the Algero-Balearic-Liguro-Provençal basins, missing the LU in the Tyrrhenian and (possibly) Ionian basins, by terrigenous deposits with hiatuses in the WAB and Adriatic foredeep and by halite, anhydrite and clastics in the Levant Basin (Interbedded and Argillaceous evaporites of Meilijson et al., 2019; Fig. 1.3b). The main problems with the isolated scenario lasting throughout Stage 3 are: (1) it does not provide an explanation neither for the homogeneity of Paratethyan ostracod assemblages in the marginal basins (e.g. Gliozzi et al., 2007; Stoica et al., 2016), an aspect difficult to explain when fauna migration takes place passively via either birds or wind, nor for the biomarkers (Vasiliev et al., 2017), which cannot be transported effectively by aquatic birds; (2) it does not explain the mismatch between $^{87}Sr/^{86}Sr$ measured on marginal ostracods and $^{87}Sr/^{86}Sr$ expected from local freshwater-fed endorheic lakes (Andreetto et al., 2021); (3) it misses to substantiate, with geochemical arguments, the precipitation of gypsum in lakes, a process that is everything but straightforward (see Warren, 2016); (4) except for the salt-bearing basins, the source(s) of solutes which makes freshwater-fed endorheic lakes brackish and causes similar physico-chemical conditions to exist in each lake is also difficult to explain in the context of a Mediterranean only at the mercy of local rivers.

1.7.2.2 The half-full, density-stratified Mediterranean scenarios

An alternative concept to the isolated scenario envisages the Mediterranean connected with the Atlantic and/or the Eastern Paratethys and relatively full of water connecting the different subbasins (Fig. 1.11b). To our knowledge, this scenario was first developed by McCulloch and De Deckker (1989) on the basis of the similar $^{87}Sr/^{86}Sr$ ratios from marginal (Spain and Cyprus) and deep (Levantine and Algero-Balearic) basins. This intuition was a significant departure from the far more in vogue desiccated scenario (see conclusion of Hsü et al., 1973b), and for this was long overlooked. Sr isotope ratios lower than contemporary ocean water led McCulloch and De Deckker (1989) to conclude that a brackish water mass created by the mixing of water from the peri-Mediterranean rivers (e.g. Nile, Rhône and African rivers that no longer flow today, etc.; see Griffin, 2002 and Gladstone et al., 2007) with water of the Eastern Paratethys filled the Mediterranean, resembling the Caspian Sea today. This conclusion is consistent with the impoverished (or absent) marine fauna and flora of Stage 3 sediments and the enhanced assemblage of fresh-brackish water biota (see section 1.5.7; Figs. 1.9a-c), but is problematic as a viable origin for Stage 3 gypsum to precipitate at depth. Furthermore, climate models for the late Miocene fail to fill the Mediterranean Basin with fluvial and Paratethys waters alone (Gladstone et al., 2007; Marzocchi et al., 2016, 2019; Simon et al., 2017). A marine contribution is therefore required to fill the Mediterranean (Marzocchi et al., 2016). In the event, the contribution is most likely to have derived from the Atlantic via the Gibraltar Corridor (Flecker et al., 2015; Booth-Rea et al., 2018; Krijgsman et al., 2018) either through a karst system (Krijgsman et al., 2018) or an emerged volcanic archipelago in the Alborán Basin (Booth-Rea et

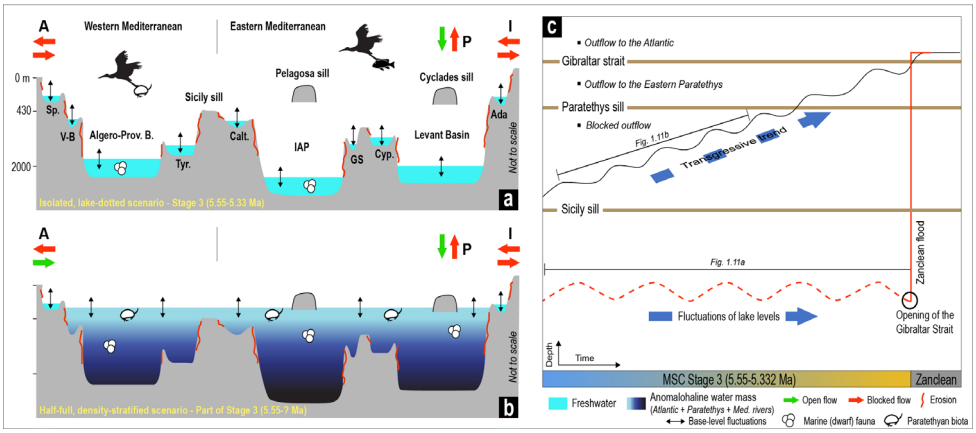

Fig. 1.11. (a), (b) *Schematic W-E profiles across the Mediterranean Basin showing the contrasting paleoenvironmental, paleohydrological and paleoconnectivity interpretations proposed for Stage 3. When a water flow is present (green arrow) from and/or to an extra-Mediterranean water mass (i.e., A: Atlantic Ocean; I: Indian Ocean; P: Eastern Paratethys), the direction of the arrow gives the direction of flow. For simplicity, water added by the major and local rivers is not shown, but it adds to the hydrological budget at any time in each scenario. Note the main difference between the isolated (a) and density-stratified (b) scenario lies in the connectivity framework (Atlantic connection closed and negligible influence from the Paratethys in the isolated scenario; influence from both Atlantic and Paratethys in the density-stratified scenario), which affects the position of the base level of the Mediterranean water mass and its hydrochemistry (see extensive discussion in subsection 7.2). Abbreviations: Sp.: SE Spain; V-B: Valencia Basin; Tyr: Tyrrhenian Basin; Calt: Caltanissetta Basin; IAP: Ionian Abyssal Plain; GS: Gulf of Sirt; Cyp: Cyprus; Ada: Adana Basin. See Fig. 2 for the geographic position of each basin.* **(c)** *Schematic plot showing the evolution of the Mediterranean base-level during Stage 3 according to both the isolated (red line) and half-full (black line) scenarios. The critical sills for controlling intra- and extra-Mediterranean connectivity are also shown.*

al., 2018). In fact, although an Indian Ocean contribution was proposed (Cita et al., 1978; Hsü et al., 1978a) and the possibility discussed (Ryan, 2009; Vai, 2016), palinspastic reconstructions concluded that the Neo-Tethys Mediterranean-Indian Ocean connection via southern Turkey and Iran already closed before the Tortonian (Rögl, 1998; Popov et al., 2004; Gargani et al., 2008; Bialik et al., 2019; Gülyüz et al., 2020), while a seaway via the Red Sea and Gulf of Aden, although not completely ruled out (e.g. Schütz, 1994; Bosworth et al., 2005; Gargani et al., 2008; Ryan, 2009), is highly contested (e.g. Meulenkamp and Sissingh, 2003; Segev et al., 2017).

In light of this, Roveri et al. (2014c), Gvirtzman et al. (2017), Vasiliev et al. (2017), García-Veigas et al. (2018) and Grothe et al. (2020) suggested that the Mediterranean was likely density-stratified during this interval as a result of the simultaneous influx of isotopically-different marine and non-marine (major Mediterranean rivers and Eastern Paratethys) water sources

(Fig. 1.11b). This connectivity framework resulted in a brackish layer carrying low-salinity (mostly Paratethyan) biota (Gliozzi et al., 2007; Stoica et al., 2016; Grothe et al., 2018, 2020; Figs. 1.9a-b) to lay on top of a more saline layer formed by Atlantic-derived seawater from which UU/UG gypsum (Figs. 1.5h-j, 1.7b-g, 1.8a-d), that facies analyses demonstrated to result from subaqueous deposition (Hardie and Lowenstein, 2004; Lugli et al., 2015), precipitated at intermediate and greater depths (e.g. García-Veigas et al., 2018). A dense, anoxic deep-water mass, possibly inherited from Stage 2, is envisaged at the bottom of the Mediterranean by Marzocchi et al. (2016) and García-Veigas et al. (2018), albeit without conclusive arguments, and by Gvirtzman et al. (2017) following the observation that the tilted halite body of the Levant Basin was simultaneously eroded landward and preserved basinward (Fig. 1.8f).

This scenario accounts for the erosive/non-depositional features (Figs. 1.5e, 1.6a, e) and continental/lacustrine facies (Figs. 1.5a-b, d-g) widespread around the margins and shelves and suggestive of a Mediterranean base-level somewhat lower than the Atlantic level suggesting a one-way inflow from both the Atlantic and the Eastern Paratethys after Stage 2 (e.g. Marzocchi et al., 2016; Figs. 1.11b-c), a connectivity configuration that effectively translates in a half-full Mediterranean (e.g. Krijgsman and Meijer, 2008). Refilling as a result of persistent Atlantic inflow, in part perhaps because of the latest Messinian deglaciation (see section 1.2.2; Van der Laan et al., 2006; Hilgen et al., 2007), would have resulted in the establishment of two-way exchange first with the Paratethys at some point during the Lago-Mare phase and later, i.e. slightly before or at the Messinian/Zanclean boundary, with the Atlantic Ocean (Fig. 1.11c; Marzocchi et al., 2016). The moment the Mediterranean base-level reached the sill with the adjacent water body (Paratethys and Atlantic) and a two-way exchange was initiated, the density contrast will have prompted an enhanced inflow into the Mediterranean (Marzocchi et al., 2016). The overall transgressive trend leading to the Zanclean marine replenishment was accompanied by base-level fluctuations in the order of 400±100 m every precessional cycle (Fig. 1.11c; Fortuin and Krijgsman, 2003; Ben Moshe et al., 2020; Andreetto et al., 2021b). These fluctuations are ascribed to switch in the Mediterranean freshwater budget driven by the African summer monsoon and Atlantic winter storms (e.g. Marzocchi et al., 2015, 2019; Simon et al., 2017). Since higher freshwater discharge rates occur at precession minima times and their Stage 3 sedimentary expression is considered to be the mudstone intervals (Fig. 1.3a; Manzi et al., 2009), mudstone interbeds (both onshore and offshore; e.g. Figs. 1.5h-j) represent the highstand episodes (e.g. Manzi et al., 2009; Roveri et al., 2008a; Omodeo Salé et al., 2012; Fig. 1.3), while continental facies onshore (e.g. conglomerates in the Apennines; Fig. 1.5g) and offshore (clastic beds in the Levant Basin) and gypsum beds (Algero-Balearic, Liguro-Provencal, CMD, Tyrrhenian, Caltanissetta, Ionian, Sirte and Polemi-Pissouri basins; Figs. 5h-j) represent the lowstand (e.g. Roveri et al., 2008a; Manzi et al., 2009; Meilijson et al., 2019; Fig. 1.3). If Atlantic was the major source of sulfate for Stage 3 gypsum (e.g. García-Veigas et al., 2018) and an intervening, relatively shallow (Sicily) sill was establishing Western and Eastern

Mediterranean remained connected also during the arid (lowstand) phases of the precession cycles.

A Mediterranean step-wise refilled and at times filled with water up to the marginal belt agrees with: (1) Paratethyan biota being present only in intermediate-deeper settings during substage 3.1, but more widespread including marginal settings during substage 3.2; (2) the E-W homogeneity of Paratethyan ostracod assemblages around the Mediterranean marginal belt (Gliozzi et al., 2007; Stoica et al., 2016; Sciuto et al., 2018; Sciuto and Baldanza, 2020; Fig. 1.9a); (3) the presence, in marginal basins, of Paratethyan fish (Bannikov et al., 2018; Schwarzhans et al., 2020), dinocysts (e.g. Pellen et al., 2017; Fig. 1.9b) and biomarkers (Vasiliev et al., 2017; Fig. 1.10c); (4) the occurrence of a monospecific assemblage of abundant *Sphenolithus* spp. just below the M/P boundary at ODP Sites 978, 975 and 967 (Castradori, 1998); (5) the requirement of water from the Mediterranean to explain the $^{87}Sr/^{86}Sr$ ratios of ostracods that inhabited marginal subaqueous environments (Andreetto et al., 2021b); (6) the Atlantic-like sulfate values (although variably diluted and affected by microbial processes; Fig. 1.10b) of the UU/UG gypsum beds (García-Veigas et al., 2018); (7) the presence of long chain alkenones in the Sicilian UG beds similar to those observed in present-day marine settings (Fig. 1.10c; Vasiliev et al., 2017).

Major problems also exist with the half-full stratified scenario: (1) it does not provide a proper mechanism for gypsum precipitation at several hundreds, or thousands, meters water depth; (2) it fails to explain how unquestionable shallow-water (<50 m) benthic organisms such as *Ammonia tepida* and *Cyprideis* sp. could survive at hundreds of meters of depth and beyond; (3) it does not provide an explanation for the high abundance of coarse-grained detritus at intermediate and deep-water locations, especially when compared to deep-water Pliocene samples, as well as for the broad absence of MSC deposits in the shelf domain; (4) a persistent Atlantic inflow without outflow seems to be a configuration that cannot be maintained stable for ~200 kyr. Indeed, models coupling the inflow of marine waters with the erosion of the gateway channel concluded that, if the Mediterranean level was lowered by at least several hundred meters below present sea level, any small overtopping of water from the Atlantic would inevitably trigger a fast refill of the basin that, if responsible for the erosion trough the Alborán Basin should have involved an unprecedented water discharge and be completed within a few years or less (Garcia-Castellanos et al., 2020 and references therein). The scenario arising from Meilijson et al. (2019; Figs. 1.3b, 1.4a) is also problematic for a high base-level Mediterranean. In order to simultaneously reach precipitation of gypsum and halite in different basins sharing the same water, the water has to be of high salinity and stratified. Simon and Meijer (2017) demonstrated that this can be achieved with slow overturning circulation, but it is currently unclear how realistic this process is.

1.7.3 Demise of the MSC (5.33 Ma): The Zanclean marine replenishment

The conspicuous and abrupt transition to normal marine sediments in the Mediterranean is globally and historically important because it is the origin of the stratigraphic position of the M/P boundary (Van Couvering et al., 2000). From an ocean perspective, it is not an ideal stratigraphic location being difficult to locate from biozone data even in the adjacent Atlantic (Hodell et al., 2001; Krijgsman et al., 2004; Van den Berg et al., 2015). However, from a Mediterranean perspective it provides a clear and unambiguous end to the MSC and the restoration of normal marine conditions. All evidence show that the onset of the Zanclean marine replenishment followed a period of relative lowstand that exposed all the Mediterranean margins (see section 1.3.12; Figs. 1.6a-b, f) and kept intermediate and deep basins underwater (see section 1.4.8). Yet again, the key dispute concerns the exact depth of the Mediterranean base level preceding the M/P transition.

Building on the isolated Mediterranean scenario, base level immediately before the early Zanclean was more than thousand kilometers below eustatic sea level (Fig. 1.10e; e.g. Hsü et al., 1973a; Blanc, 2002; Loget et al., 2006; Garcia-Castellanos et al., 2009; Pérez-Asensio et al., 2012; García-Alix et al., 2016; Amadori et al., 2018; Micallef et al., 2018, 2019; Camerlenghi et al., 2019; Kartveit et al., 2019; Madof et al., 2019; Ben Moshe et al., 2020; Caruso et al., 2020; Cazzini et al., 2020; Mas and Fornós, 2020; Spatola et al., 2020). Hydrodynamic erosional models allowed a reinterpretation of the erosional features across the strait of Gibraltar (Campillo et al., 1992; Blanc, 2002) suggesting that a sudden breach of the Mediterranean-Atlantic divide at Gibraltar resulted in a vast cascade of Atlantic water that refilled the entire Mediterranean in less than 2 years (i.e. rates of ten meters per day) spilling first into the Western Mediterranean (see the extensive review in Garcia-Castellanos et al., 2020) and then, after reaching the level of the Sicily sill, pouring into the Eastern Mediterranean (Micallef et al., 2018, 2019; Ben Moshe et al., 2020; Spatola et al., 2020). This concept of catastrophic refilling has led to terms such as "Zanclean flood" or "deluge". Evidence supporting the catastrophic flood mechanism mostly comes from the seismic reflection dataset and includes: (1) the presence of >250 m deep and 390-km-long incisions on both sides of the Gibraltar Strait (Garcia-Castellanos et al., 2020); (2) the detection of (allegedly) Pliocene-aged chaotic sedimentary bodies stretching for kilometers in the Alborán Basin (Garcia-Castellanos et al., 2020 and references therein) and Ionian Basin at the foot of the Malta Escarpment (Micallef et al., 2018, 2019; Spatola et al., 2020; Fig. 1.8c). A further argument is the bathymetric jump of several hundred meters between the late Messinian and the early Pliocene sediments (e.g. Caruso et al., 2020; Fig. 1.6d).

Instantaneous sea level rise is not the only possible refilling model. Bache et al. (2012) suggested the reflooding occurred in two steps at ~5.60 Ma, accompanied by a moderate (≤500 m) rise, followed by a rapid rise of 600-900 m at around 5.46 Ma tracking the deposition of the deep basin evaporites and resulting from the collapse of the Gibraltar divide. There is also the reconnection model that follows from a Stage 3 Mediterranean that is already relatively full and with the base level possibly oscillating of 400±100 m with precessional frequency (Fig. 1.10h;

Fortuin and Krijgsman, 2003; Ben Moshe et al., 2020; Andreetto et al., 2021b). In this case, only a sea level rise of a few hundred meters is required to restore the Mediterranean to the Atlantic level (Fig. 1.10h), which was hypothesized to have occurred in the last precessional cycle of the Messinian (Marzocchi et al., 2016; Fig. 1.3a). In detail, the re-establishment of a fully marine faunal diversity and oceanic geochemistry ($^{87}Sr/^{86}Sr$ ratios and $\delta^{18}O$) occurred more gradually over one or more precessional cycles in the earliest Zanclean (e.g. Iaccarino et al., 1999; Pierre et al., 1998, 2006; Cipollari et al., 2013; Roveri et al., 2019a; Bulian et al., 2021). This suggests that stressed ecological conditions at first only suitable for opportunistic organisms to survive (e.g. Bulian et al., 2021) developed (or persisted) in the Mediterranean as marine replenishment occurred (e.g. Rouchy et al., 2003). One possible mechanism for achieving this may be the physico-chemical turnover in the water column triggered by the re-established two-way exchange with the Atlantic which, for reasons that are largely unknown, took time (at least one precession cycle; Pierre et al., 2006) to displace surficial Paratethyan water and restore normal marine conditions (Marzocchi et al., 2016).

1.8 Methods and proxies to better reconstruct base level and connectivity changes

Chronological uncertainty and spatial variability limit the use of both sedimentological and paleontological information to achieve a comprehensive and coherent basin-wide interpretation of the conditions and drivers of Stage 3 environments and water levels. Alternative methods are therefore required to clarify connectivity relationships and constrain base-level conditions. This section explores the principles and potential of geochemical, backstripping and numerical modelling techniques that could be used to further test existing hypotheses and enhance understanding of the complex environmental conditions experienced by the Mediterranean during the latest Messinian.

1.8.1 Geochemical proxies

Radiogenic strontium isotopes. Radiogenic strontium isotope ratio ($^{87}Sr/^{86}Sr$) is a widely applied geochemical tool in provenance studies, including the reconstruction of the hydrological circuit and connectivity of basins with little or null oceanic entries. Its potential to detect the provenance of the hydrological fluxes derives from the unique $^{87}Sr/^{86}Sr$ ratio that typifies each water source and from the negligible effects of isotopic fractionation during the liquid-solid transition (see Hajj et al., 2017).

Mineral phases precipitating in endorheic lakes uptake Sr^{2+} with $^{87}Sr/^{86}Sr$ ratio that reflects the mixing of all feeding surficial and underground streams and whose $^{87}Sr/^{86}Sr$ fingerprint hinges on the composition and age of watershed bedrock (see Peucker-Ehrenbrink and Fiske, 2019, Andreetto et al., 2021b and references therein). When river water mixes with seawater such as in the oceans, semi-enclosed basins or estuaries, mineral phases uptake Sr^{2+} with oceanic $^{87}Sr/^{86}Sr$ ratios because the high oceanic Sr concentration (~7.8 mg/l today; Veizer,

1989) masks the impact of the ~100 times lower concentrated continental Sr-sources (~0.0780 mg/l; Palmer and Edmond, 1992). This is valid as long as a certain ratio of continental-marine water mixing is fulfilled, beyond which $^{87}Sr/^{86}Sr$ ratios deviate towards the $^{87}Sr/^{86}Sr$ ratios of the non-marine source(s) (Ingram and Sloan, 1992). For the Mediterranean to attain non-marine $^{87}Sr/^{86}Sr$ ratios (like during the MSC), Topper et al. (2014) calculated a mixing of at least 1:4 (Atlantic:freshwater) to be required.

If Mediterranean subbasins hosted endorheic lakes (Figs. 1.10c, e), the $^{87}Sr/^{86}Sr$ isotope ratios measured on ostracod valves or gypsum crystals of each lake are expected to generate a scattered distribution by virtue of the different geology in the hinterland of each basin. By contrast, some degree of connection between different basins and the Mediterranean water mass (Figs. 1.10d, f) is expected to result in more homogeneous $^{87}Sr/^{86}Sr$ ratios because, although isotopically-different, local rivers mix with a water mass that has the same $^{87}Sr/^{86}Sr$ value and (much higher) Sr concentration for each basin (Andreetto et al., 2021b). In this scenario, differences in the $^{87}Sr/^{86}Sr$ ratios between basins are likely the reflection of the different $^{87}Sr/^{86}Sr$ ratio of the local input in each basin (Andreetto et al., 2021b). The application of numerical models assists to identify and quantify the different water sources feeding the basin(s) in question and (e.g. Placzek et al., 2011; Topper et al., 2011, 2014; Doebbert et al., 2014; Rossi et al., 2015b; Modestou et al., 2017; Grothe et al., 2020; Andreetto et al., 2021).

Sulfate isotopes. When sulfate-bearing minerals precipitate in a basin they uptake dissolved S and O with $\delta^{34}S_{SO4}$ and $\delta^{18}O_{SO4}$ isotopic composition that, once corrected for the fractionation effects during liquid-solid transition (see section 1.6.2), can be assimilated to that of the mother brine. The higher concentrated source of sulfate is seawater (with present-day $\delta^{34}S_{SO4}$=21.15±0.15‰ and $\delta^{18}O_{SO4}$=8.67±0.21‰, Johnston et al., 2014; with Messinian values of ~22±0.2‰ for the $\delta^{34}S_{SO4}$ and ~9±2‰ for the $\delta^{18}O_{SO4}$; Turchyn and Schrag, 2004; Markovic et al., 2016; Masterson et al., 2016). Significantly higher inputs from the ~1000 times less concentrated riverine freshwater (both surficial and underground) with respect to the ocean water (more than 1:5 according to Lu et al., 2001) can modify the marine $\delta^{34}S_{SO4}$ and $\delta^{18}O_{SO4}$ isotopic composition of the mother brine (Utrilla et al., 1992; Lu et al., 2001) and have it deviated from that of the ocean (Lu et al., 2001). This deviation is normally towards lower values, because river-derived dissolved sulfate is generally depleted in heavy isotopes ^{34}S and ^{18}O compared to oceanic sulfate because these isotopes mainly come from the oxidation of ^{34}S-depleted pyrite (FeS_2) on the continents and to a lesser extent from the dissolution of older sulfate-bearing minerals (Claypool et al., 1980; Turchyn and Schrag, 2004; Burke et al., 2018). However, when marine sulfate is preferentially leached in the catchment, ^{34}S of the freshwater-dissolved sulfate and [SO_4^{2-}] likely increase, therefore reducing the continental-marine mixing ratio necessary to deviate the resulting sulfate isotopic signature away from marine values. Unfortunately, the sulfate isotopic composition is not provided for a number of major

Mediterranean rivers (Burke et al., 2018) nor for the Eastern Paratethys and it is hardly assessed with the catchment-forming lithologies (Liu et al., 2017; Burke et al., 2018), making sulfate isotopes still an unsuitable tracer of non-marine water provenance in Mediterranean subbasins.

Deviation of $\delta^{34}S_{SO4}$ and $\delta^{18}O_{SO4}$ from the marine average can also be the result of isotopic fractionation during microbial sulfate reduction (MSR; Fritz et al., 1989; Berner, 1999). MSR produces ^{34}S-depleted hydrogen sulfide (~0 to 70‰ lighter than initial sulfate; Brunner and Bernasconi, 2005; Sim et al., 2011; Leavitt et al., 2013) and induces the enrichment in ^{34}S and ^{18}O of the residual sulfate pool (Kaplan and Rittenberg, 1964; Thode and Monster, 1965; Turchyn et al., 2006; Wortmann et al., 2007). Therefore, if isotopically light H_2S produced by MSR leaves the system as a sulfide mineral (most likely pyrite), the resulting dissolved sulfate would have $\delta^{34}S_{SO4}$ and $\delta^{18}O_{SO4}$ isotopic signatures higher than the oceanic one (Brunner et al., 2005). However, if the MSR-produced H_2S is re-oxidized back to sulfate through abiotic or microbial sulfide oxidation, isotopically light sulfate will be brought back to the ^{34}S-enriched sulfate pool, producing little or no enrichment in ^{34}S observed in the resulting sulfate (Gomes and Johnston, 2017 and references therein; Pellerin et al., 2019). Slight deviations from marine $\delta^{18}O_{SO4}$ and $\delta^{34}S_{SO4}$ values of sulfate reflect both biological sulfur cycling and/or freshwater riverine inputs (e.g. Utrilla et al., 1992; Lu et al., 2001; Turchyn et al., 2009; Fig. 1.10b). Untangling the relative importance of these processes is key to understanding the Mediterranean sulfur isotope record and gleaning paleoenvironmental insights into Stage 3.

Hydrogen isotopes. Organic geochemistry biomarker-based tools can be used as independent proxies for reconstructing sea surface temperatures, relative changes in the basin hydrology and, indirectly, salinity. Basin water properties are reflected in a variety of life forms. Different types of organisms produce specific organic compounds that serve as molecular biomarkers. These large biomolecules record the changes in the hydrogen isotopic composition of the water used by different groups of biomarker producers (i.e. different organisms). The principle behind the method is to measure δD on biomarkers produced in Mediterranean Sea waters (e.g. alkenones, produced by a few species of haptophyte coccolithophores algae) during the MSC and compare the results with the δD signals retrieved from biomarkers produced in the open ocean ideally at the same time intervals. The influence of precipitation on the changes in hydrological budget can be monitored by measuring the δD of long chain n-alkanes (Sachse et al., 2006), biomarkers predominantly produced by higher terrestrial plants that rely on precipitation for plant growth, therefore reflecting the changes in the δD of the precipitation. The extreme base level drop(s) suggested for the Mediterranean during the MSC would, in principle, indicate a negative precipitation (P) + runoff (R) – evaporation (E) ratio. Such a negative water budget (E>P+R) results in waters increasingly enriched in δD whereas, a positive water balance (E<P+R) results instead in a negative shift of δD values. The analysis of compound specific δD of alkenones, long and short chain *n*-alkanes can be used to constrain E/(P+E) relationships.

1.8.2 Backstripping analyses

Backstripping uses paleobathymetry, sea level and sediment thickness to quantify the tectonic and isostatic components of subsidence. If tectonic subsidence or uplift history are known relative to the current position and depth of paleoshoreline markers, an inverse approach allows base level to be estimated. A number of approaches have been applied to the MSC, using erosional surfaces (e.g. Amadori et al., 2018), terraces (Micallef et al., 2018) or fluvial network characteristics (Urgeles et al., 2011) as paleoshoreline indicators. The relief on erosional features has also been used to estimate minimum base-level variation (Frey-Martinez et al., 2004). Apart from the quantitative constraints on base level that backstripping provides, consideration of the regional implications of isostatic subsidence and the gravitational impact of redistributing water masses (such as in the cascading model of Roveri et al., 2014c; Fig. 1.10b) and evaporite precipitation is important in gateway regions like Gibraltar, which due to their shallow and restricted nature are exceptionally sensitive to vertical motions. Here, both flexural effects and gravitational effects on local sea level on the Atlantic side of the strait has the potential to influence Mediterranean-Atlantic connectivity driving paleoenvironmental changes in the basin itself (Coulson et al., 2019).

1.8.3 Modelling

Numerical models can be used complementary to lab- and field-based studies, or to find answers to open questions by testing the physical plausibility of hypotheses and their compatibility with the available sedimentological/stratigraphic/paleontological/geochemical data, which have to constrain model results and not adjust to it. For example, whether gypsum beds in marginal/intermediate basins can precipitate at the same time as the halite in deep basins is an intriguing question that circulates in the MSC literature (e.g. Van Couvering et al., 1976), but whether this is physically and geochemically possible is yet to be answered. In a first model analysis, Simon and Meijer (2017) found that the required stratification can indeed be achieved for specific conditions including a slow overturning circulation. A different approach is needed to determine whether such slow circulation is to be expected or if other scenarios should be considered. A thermo-haline stratification that enables coeval precipitation of two evaporites for a considerable time span might also influence the degree of heterogeneity of other parameters, such as strontium concentration. Previous models showed the influence of the Atlantic Ocean and major rivers (Topper et al., 2014) and of evaporation (Flecker et al., 2002) on the Sr value of a basin with restricted oceanic inflow and assuming a homogeneous distribution of strontium throughout the water column (Flecker et al., 2002; Topper et al., 2011, 2014; Modestou et al., 2017), but it is uncertain if this holds true in conditions of water stratification. New insights into this behavior would have consequences for the way the strontium dataset (Fig. 1.10a) must be interpreted. Another loose end where the model approach can provide insight relates to the question whether a high water level could have been

reached without an inflow from the Atlantic. Climate simulations conducted by Gladstone et al. (2007), Simon et al. (2017) and Marzocchi et al. (2019) indicate that this is not possible with today's bathymetry. A quantitative analysis exploring the Mediterranean water level reached in different situations (i.e. with or without an Atlantic or Paratethys in and outflow) and with information on the Mediterranean hypsometry that may be provided by isostatic restoration of the seafloor topography (flexural backstripping) could help understanding how the Messinian Salinity Crisis ended.

1.9 Certainties, open problems and future directions

Our understanding of the nature of MSC Stage 3 has evolved considerably over the last fifty years. However, there are still such disparate models for the paleoenvironmental conditions and basin connectivity that led to Stage 3 deposition and that express the challenges that the study of this interval presents: it is a relatively short interval and its sedimentary expression varies spatially. It is no surprise that the main point of contention lies in reconciling the observations from seismic profiles and well data, which are largely interpreted as favoring the desiccated scenario, with the sedimentological, paleontological and geochemical data from the marginal basins record, largely discontinuous and unaddressed from seismic-based and computational-based studies and mainly supporting the full-Mediterranean hypothesis. To a large extent this mismatch is the result of the lack of intersection of the two datasets. Some Stage 3 onshore localities are meticulously studied from the stratigraphic, sedimentological, paleontological and geochemical point of view, showing remarkably consistent and homogenous trends and patterns (as previously highlighted by Roveri et al., 2008a). However, changes at precessional and subprecessional scale are difficult to trace from one exposure to another and are well below the level of seismic resolution, making onshore-offshore correlation at this scale impossible. Even correlation between onshore sections is problematic since most of the stratigraphic sections are incomplete, with erosion surfaces at the bottom and/or top (i.e. the M/P boundary), and this lack of stratigraphic continuity frustrates attempts to constrain ages by cyclostratigraphy. A future focus on strengthening the available chronostratigraphic framework (Fig. 1.3) and making it inclusive of the fragmented outcrops, is required to better understand the paleoenvironmental and paleohydrological changes suffered by the Mediterranean marginal belt through time. The successful drilling of the three IODP proposals currently in the scheduling pool (see Camerlenghi and Aloisi, 2020), all of which propose to recover Stage 3 sediments, will also provide transformative information enabling far better offshore-onshore correlation and interpretation of currently enigmatic seismic data. In the meantime, re-evaluation of existing DSDP and ODP material, particularly through the application of more novel geochemical techniques and, where possible, access to material collected during industrial drilling would be helpful for understanding the deep Mediterranean Basin during this interval. Extensive paleontological studies have established that Stage 3 contains in situ

biota assemblages of Paratethyan provenance implying brackish water conditions. More problematic is the differentiation of in situ and reworked marine microfauna and flora and the paleoecological significance of dwarfism in marine calcareous microfossils/algae. These have important repercussions for the Mediterranean connectivity and base-level reconstruction. The geochemical dataset for Stage 3, particularly strontium isotopes and hydrogen isotopes on biomarkers, is both demonstrably valuable in providing key constraints on connectivity and environmental conditions, and frustratingly inadequate in terms of data distribution. It has great potential as a constraint on quantitative sensitivity analysis of the different hydrochemistry scenarios that follow from the endmember Stage 3 hypotheses, but substantially more data is required. An approach which combines geological, geochemical, geophysical and paleontological data with numerical modelling (e.g. climate simulations, backstripping analyses and paleoceanographic models) will provide a more accurate reconstruction of Mediterranean paleogeography and the processes that occurred during the final phase of the Messinian Salinity Crisis.

Acknowledgments

We thank the entire SALTGIANT community for many profitable workshops that inspired the development of this manuscript. This research was supported by the project SALTGIANT-Understanding the Mediterranean Salt Giant, a European project which has received funding from the European Union's Horizon 2020 research and innovation program, under the Marie Sklodowska-Curie [grant agreement No 765256]. We greatly thank the two reviewers Domenico Cosentino and William Ryan and the editor Alessandra Negri for the fruitful comments provided that led to a substantial improvement of the manuscript.

Part of the Nijar village (Almeria province, Spain).

2

HIGH MEDITERRANEAN WATER-LEVEL DURING THE LAGO-MARE PHASE OF THE MESSINIAN SALINITY CRISIS: INSIGHTS FROM THE SR ISOTOPES RECORDS OF SPANISH MARGINAL BASINS (SE SPAIN)

Andreetto, F., Matsubara, K., Beets, C.J., Fortuin, A.R., Flecker, R., Krijgsman, W.

ABSTRACT

The Messinian Salinity Crisis (MSC) successions record extreme fluctuations in the Mediterranean's environmental conditions. However, some of the scenarios that are thought to have caused these extreme environments are contentious. One prominent example of this is the Mediterranean water level during the Lago-Mare stage of the MSC, which is interpreted either as being very low during a largely desiccated Mediterranean punctuated by endorheic lakes (lacustrine scenario) or sufficiently high to enable basin-wide connectivity across the Mediterranean and with the Atlantic and the Eastern Paratethys (lagoonal scenario). In SE Spain, adjoining marginal basins of Sorbas, Nijar and Vera exhibit sedimentary records of the Lago-Mare stage. Here we present 11 new $^{87}Sr/^{86}Sr$ ratios measured on ostracod (Cyprideis sp.) valves from these successions, which add to the 11 already published data from these basins and whose significance, in terms of water provenance, has not been fully explored. In parallel, we construct a mass balance model that provides quantitative insights into the $^{87}Sr/^{86}Sr$ composition of the water in which the ostracods dwelt. Overall, measured and published $^{87}Sr/^{86}Sr$ ratios from Sorbas (0.709066-0.709131), Nijar (0.708814-0.709099) and Vera (0.708764-0.708813) all show lower values than modelled ratios for endorheic lakes (>0.7100). These Spanish basins therefore require an additional source of water with a lower $^{87}Sr/^{86}Sr$ signature which is likely to have been derived from the main Mediterranean waterbody (0.7086-0.7087). This interpretation implies that at least the Western Mediterranean had a relatively high and fluctuating water level during the Lago-Mare stage of the MSC.

This chapter is peer-reviewed and published as:
Andreetto, F., Matsubara, K., Beets, C.J., Fortuin, A.R., Flecker, R., Krijgsman, W., 2021. High Mediterranean water-level during the Lago-Mare phase of the Messinian Salinity Crisis: insights from the Sr isotope records of Spanish marginal basins (SE Spain). Palaeogeography, Palaeoclimatology, Palaeoecology, 562.

2.1 Introduction

Late Messinian hydrological changes in the Mediterranean, instigated by reduced connectivity with the Atlantic Ocean (Flecker et al., 2015; Krijgsman et al., 2018) and increased sensitivity to the Eastern Paratethys (Flecker and Ellam, 2006; Krijgsman et al., 2010; Grothe et al., 2020) and circum-Mediterranean continental runoff (Topper et al., 2011; Marzocchi et al., 2015, 2019; Simon et al., 2017), are considered to have been the main cause of the ecological and environmental extremes experienced by the Mediterranean during the Messinian Salinity Crisis (MSC, Roveri et al., 2014a). Stage 1 (5.97-5.60 Ma) of the consensus chronostratigraphic model (Roveri et al., 2014a) is documented, mostly in onshore sedimentary records, by successions of alternating primary gypsum-shale and marl-shale couplets (Primary Lower Gypsum, PLG; e.g. Lu, 2006; Lugli et al., 2010; Dela Pierre et al., 2011). Following a period (MSC Stage 2; 5.60-5.55 Ma) of extensive subaerial erosion (Hsü et al., 1973; Lofi et al., 2005) and salt deposition (Lugli et al., 1999), a second unit (Upper Gypsum (UG) onshore or Upper Unit (UU) offshore) of alternating gypsums and marls was deposited in more central basins (e.g. Caltanissetta, Cyprus, Algero-Provencal and Ionian Manzi et al., 2009, 2016; Lofi, 2018) during MSC Stage 3 (5.55-5.332), which is splitted in substages 3.1 and 3.2 (or Lago-Mare phase) in the "consensus" chronostratigraphic model of Roveri et al. (2014a). Multi-disciplinary observations relating to Mediterranean-Atlantic connectivity suggest that a persistent Atlantic inflow to the Mediterranean with restricted outflow is likely to have existed during PLG deposition (Hardie and Lowenstein, 2004; Lu, 2006; Krijgsman and Meijer, 2008; Lugli et al., 2007, 2010, 2013, 2015; Dela Pierre et al., 2011; Roveri, et al., 2014a, b; Flecker et al., 2015; García-Veigas et al., 2018; Manzi et al., 2018; Reghizzi et al., 2018), whereas a one-way flow with blocked outflow prevailed during halite and UG/UU precipitation (Krijgsman and Meijer, 2008; Roveri et al., 2014c; Marzocchi et al., 2016; Krijgsman et al., 2018). This connectivity configuration translated into a Mediterranean base-level at Atlantic level during PLG deposition and below during halite precipitation (Krijgsman and Meijer, 2008; Roveri et al., 2014a), even though halite precipitation in a full Mediterranean cannot be rule out (Roveri et al., 2014c; Meilijson et al., 2019). However, the connectivity history and water level of the Mediterranean during the final Stage 3 remain highly contested (see Orszag-Sperber, 2006; Roveri et al., 2014a; Caruso et al., 2020).

Along the Mediterranean margins, rocks of this terminal MSC interval comprise mainly coarse- to fine-grained siliciclastic deposits (e.g. Roveri et al., 1998; Rouchy et al., 2001; Guerra-Merchán et al., 2010; Dela Pierre et al., 2011). The sedimentary successions are frequently organized in cycles interpreted to be precession driven (Fortuin and Krijgsman, 2003; Roveri et al., 2008a; Omodeo Salé et al., 2012). Some of the fine-grained interbeds contain faunal assemblages that include brackish mollusks, ostracods and dinoflagellate cysts typical of the Eastern Paratethys region (Gliozzi et al., 2007; Stoica et al., 2016; Grothe et al., 2018; Sciuto et al., 2018). Such anomalohaline faunal associations have been recognized throughout the Mediterranean in both marginal settings (Malaga, Sorbas, Nijar and Vera basins in SE Spain,

Piedmont Basin, Northern Apennines and Sicily in Italy, Crete, Cyprus and S Turkey) and in deep-sea records (DSDP 129A, 375, 376 and ODP 967, 968, 975, 978; Roep and Van Harten, 1979; Cita et al., 1978; McCulloch and De Deckker, 1989; Blanc-Valleron et al., 1998; Spezzaferri et al., 1998; Bonaduce and Sgarrella, 1999; Iaccarino and Bossio, 1999; Rouchy et al., 2001; Bassetti et al., 2006; Cosentino et al., 2007; Grossi et al., 2008, 2015; Guerra-Merchán et al., 2010; Dela Pierre et al., 2011; Stoica et al., 2016).

The traditional view of Mediterranean paleogeography during Stage 3 is an isolated and desiccated Mediterranean studded with low-salinity endorheic lakes supplied with sediments and dissolved elements by local rivers (e.g. Ruggieri, 1967; Hsü et al., 1973a; Cita et al., 1978; Orszag-Sperber et al., 2000; Ryan, 2009; Lymer et al., 2018; Camerlenghi et al., 2019; Kartveit et al., 2019; Madof et al., 2019; Caruso et al., 2020; Raad et al., 2021). In this scenario, the Black Sea ostracods, mollusks and dinoflagellates are considered to be transported by migratory aquatic birds (Benson et al., 1978; Benson and Rakic-El Bied, 1991; Caruso et al., 2020). Although it is not explicitly stated what paleoenvironment was in force in each Mediterranean subbasin and what the migration mechanism of the Paratethyan biota was, the same scenario is endorsed by all those that conclude the Mediterranean was an isolated basin (e.g. Orszag-Sperber et al., 2000; Lofi et al., 2005, 2011; Garcia-Castellanos et al., 2009, 2020; Cameselle and Urgeles, 2017; Amadori et al., 2018; Micallef et al., 2018, 2019; Ben Moshe et al., 2020; Spatola et al., 2020; Raad et al., 2021). In fact, it is physically impossible that Paratethyan water entering the eastern Mediterranean could have spread westward in an isolated and desiccated Mediterranean Basin. By contrast, a Mediterranean almost completely full and dominated by non-marine waters from the major drainage systems (Roveri et al., 2008a) and from Eastern Paratethys (Flecker and Ellam, 2006; Vasiliev et al., 2010, 2017; Marzocchi et al., 2016; Van Baak et al., 2016; Grothe et al., 2020) has been proposed in the light of the occurrence of the same species of ostracods everywhere in the Mediterranean (Gliozzi et al., 2007; Stoica et al., 2016; Sciuto et al., 2018). The discovery of dwarf specimens of long-ranging planktic foraminifera species in the Lago-Mare of the Bajo Segura record (Corbí and Soria, 2016), the anomalous peak in the abundance of the calcareous nannofossil *Sphenolithus abies* underneath the Miocene/Pliocene (M/P) boundary in ODP Site 968 (Castradori, 1998) and molecular biomarkers with hydrogen isotope compositions ($\delta D_{n\text{-alkanes}}$) similar to present-day marine settings (Vasiliev et al., 2017) point to some supply also from the Atlantic.

In a restricted Mediterranean Basin where several isotopically-distinct water sources are thought to have contributed to its hydrological configuration, $^{87}Sr/^{86}Sr$ ratios can be used to discriminate between the various sources of water (Flecker et al., 2002; Flecker and Ellam, 2006; Topper et al., 2011) and to infer phases of isolation or connectivity (e.g. McCulloch and De Deckker, 1989). In most Mediterranean marginal basins (e.g. Apenninic sub-basins; Schildgen et al., 2014), however, the predominance of Mesozoic carbonates in the catchments ($^{87}Sr/^{86}Sr$ ratios vary from ~0.7071 to ~0.7076; McArthur et al., 2012) means that local runoff

has a relatively low $^{87}Sr/^{86}Sr$ ratio, which could be similar to a mixture of the three potential sources of the Mediterranean Basin, i.e. Atlantic (~0.7090 during the late Messinian; McArthur et al., 2012), main Mediterranean rivers (e.g. Nile with 0.7060 and Rhône with 0.7087; Brass, 1976; Albarède and Michard, 1987) and Eastern Paratethys (0.7084-0.7085; Grothe et al., 2020), making local and Mediterranean inputs challenging to distinguish. By contrast, the adjoining Sorbas, Nijar and Vera basins in SE Spain all have present-day fluvial catchments dominated by (Sorbas and Nijar) or with abundant (Vera) Paleozoic mica schists and phyllites (Sanz de Galdeano and Santamaría-López, 2019) and Miocene volcanic rocks (e.g. Toscani et al., 1990; Zeck et al., 1998; Conticelli et al., 2009). Rivers draining these rocks have substantially higher $^{87}Sr/^{86}Sr$ ratios (>0.7100 on average; e.g. Zeck et al., 1998; Toscani et al., 1990; Conticelli et al., 2009). This contrast makes it possible to distinguish local fluvial supply to these Spanish marginal basins from the lower $^{87}Sr/^{86}Sr$ ratios of Mediterranean's water sources. We therefore investigated the hydrology of this cluster of marginal basins in SE Spain using new and published (McCulloch and De Deckker, 1989; Fortuin et al., 1995; Roveri et al., 2019a) $^{87}Sr/^{86}Sr$ data measured on well-preserved ostracod valves of *Cyprideis* sp. from the latest Messinian deposits of the Sorbas (Zorreras Mb.), Nijar (Upper Mb. of Feos Fm.) and Vera (Unit 2) basins. The measured $^{87}Sr/^{86}Sr$ ratios correspond to the $^{87}Sr/^{86}Sr$ composition of the water inhabited by the ostracods. The $^{87}Sr/^{86}Sr$ of each watersheds' lithology is used to estimate the local river water compositions, whereas a mass balance model is used to identify and quantify the different water sources feeding each marginal Spanish basins. Combining these geochemical data and model constraints with new paleontological findings and previous sedimentological data we provide insights into the Mediterranean water level during the latest Messinian.

2.2 Geological setting

2.2.1 Evolution of the Neogene basins of the Betic Cordillera

The Sorbas-Nijar-Vera basins are ENE-WSW elongated depressions belonging to the Betic Cordillera in southern Spain (Fig. 2.1a; Sanz de Galdeano and Vera, 1991, 1992; Vera, 2000). The post-orogenic evolution of the arc-shaped Betic-Rif mountain belt is dominated by both vertical (Martinez-Diaz and Hernandez-Enrile, 2004; Capella et al., 2017) and strike-slip motions (Montenat and Ott d'Estevou, 1999; Jonk and Biermann, 2002) that generated narrow subsiding depressions filled with the erosional products of adjacent basement highs (Krijgsman et al., 2000; Vera, 2000, 2001; Braga et al., 2006; Capella et al., 2018). The subsiding basins of SE Spain were part of the Betic Corridor, a set of four narrow marine gateways that during the late Miocene connected the Atlantic Ocean and the Mediterranean Sea via southern Spain (Martín et al., 2014; Flecker et al., 2015; Krijgsman et al., 2018). From the latest Tortonian onwards, continuous uplift of the Betic-Rif system progressively changed the dimensions of the marine corridors in both Spain and Morocco (Krijgsman et al., 2006, 2018; Martín et al., 2014), inducing severe restriction of Mediterranean-Atlantic exchange, substantial hydrological

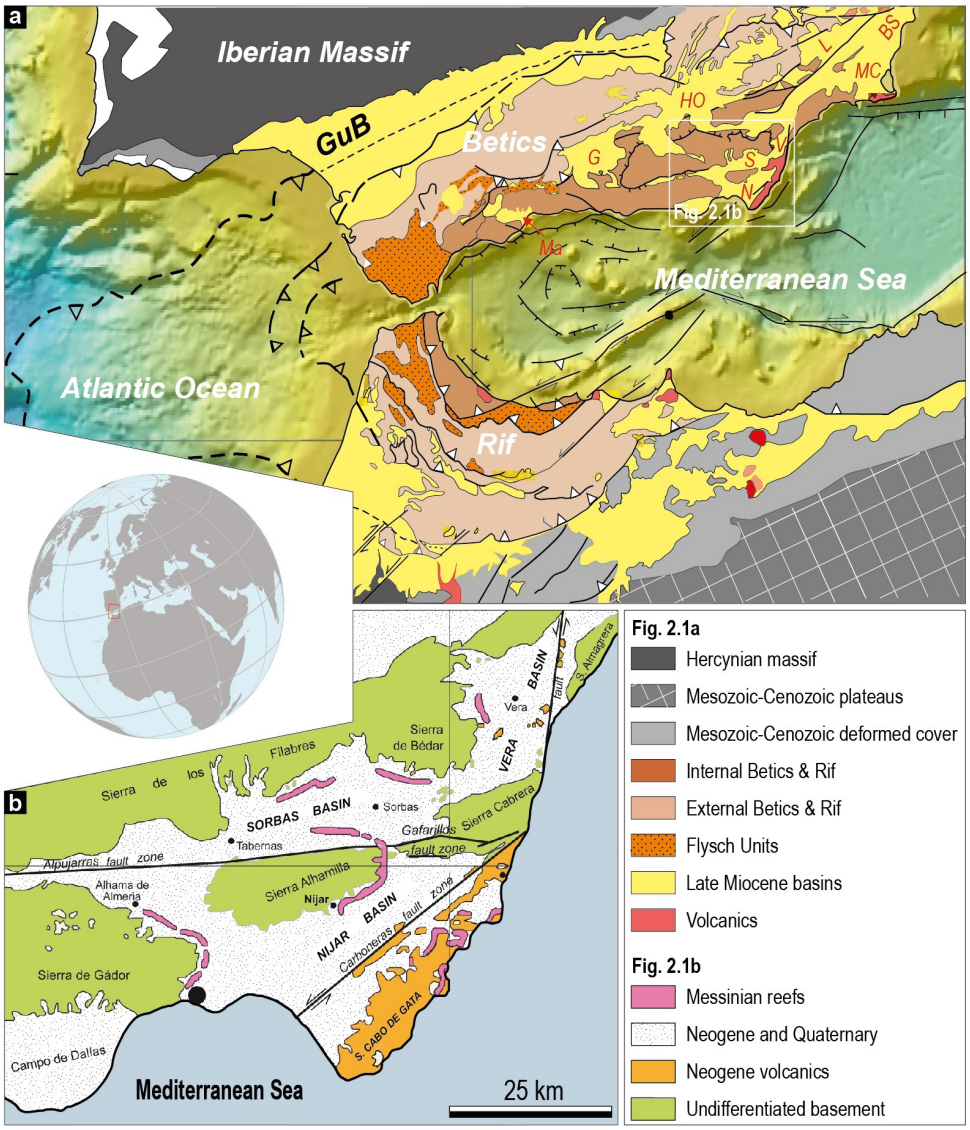

Fig. 2.1. (a) *Generalized tectonic and geological map of the Betic-Rif arc showing the location of the internal (G: Granada, HO: Huércal-Overa, L: Lorca, F: Fortuna) and external (Ma: Malaga, N: Nijar, S: Sorbas, V: Vera, MC: Murcia-Cartagena, BS: Bajo Segura) Neogene basins (modified from Capella et al., 2017).* **(b)** *Schematic geological map of the eastern end of the Betic Cordillera (modified after Fortuin and Dabrio, 2008). Blue squares indicate the location of the studied sections in the Nijar (BcD: Barranco de los Castellones; CdR: Cerro de los Ranchos) and Vera (CdA: Cuevas del Almanzora) sections. Samples' provenance from the Sorbas Basin is unknown.*

reorganization of Mediterranean circulation patterns (Flecker et al., 2015 and references therein) and ultimately the MSC (Roveri et al., 2014a). While the internal basins (Lorca, Fortuna, Granada, Huércal-Overa, Campo Coy) were isolated before the Messinian, preserving evaporitic successions referred to as the "Tortonian Salinity Crisis of the eastern Betics" (Krijgsman et al., 2000; Corbí et al., 2012), the external basins (Malaga, Nijar, Sorbas, Vera, Murcia-Cartagena, Bajo Segura) contain sedimentary records of the Messinian Salinity Crisis (Fig. 2.1a; Fortuin et al., 1995; Fortuin and Krijgsman, 2003; Braga et al., 2006; Guerra-Merchán et al., 2010).

2.2.2 Late Miocene connectivity evolution and stratigraphy of the Sorbas-Nijar basins

The Nijar and Sorbas basins are today separated from each other by the sierras de Gádor, Alhamilla and Cabrera (Fig. 2.1b). The Sierra de los Filabres and Sierra de Bédar border the Sorbas Basin to the north, whereas the Sierra de Gata (or Cabo de Gata, CdG) constitutes the SE edge of the Nijar Basin (Fig. 2.1b). Cabo de Gata is a volcanic complex belonging to the Alborán volcanic province, a 500-600 km long, SW-NE trending belt stretching from N Africa to SE Spain and characterized by magmatic activity of Neogene age (ca. 20 to 2 Ma; Zeck et al., 1998). During the Miocene, and until the end of MSC Stage 1, both basins were connected to the Atlantic Ocean via the Mediterranean, which made its entrance in the Nijar Basin from the south and in the Sorbas Basin through NW-SE trending corridors north to Nijar (Fortuin and Krijgsman, 2003; Fig. 2.1b). Despite the fact that sedimentation in both basins has been strongly affected by the activity of three major strike-slip fault zones, namely the NE-SW Serrata-Carboneras Fault, the E-W trending Gafarillos Fault Zone and the N-S Palomares Fault Zone (Montenat and Ott d'Estevou, 1999; Fig. 2.1b), the intimate communication between the Nijar and Sorbas basins is reflected in their similar pre-MSC Stage 2 successions.

The hundred meter thick pre-MSC infill of both basins unconformably overlies the metamorphic basement of the Betic Cordillera and, for the Nijar Basin only, the volcanic complex of Cabo de Gata (Fig. 2.1b). The oldest sediments are of Serravallian-early Tortonian age (Brachert et al., 2002). The late Tortonian-early Messinian period is preserved in the marginal areas of the basins as fossil-rich calc-lithic arenites (Azagador Member of Turre Formation, Völk and Rondeel, 1964) and reef carbonates (Cantera Reef Member of Turre Formation; Völk and Rondeel, 1964). In the basin center, the deepest water facies are represented by epibathyal marls (Abad Member of Turre Formation). This unit is characterized by a well-developed, precession-controlled lithological cyclicity exemplified in the lower part by homogenous marls and more indurated, opal-CT-rich layers that change up-section to sapropelitic laminites, marls and chalks (van de Poel, 1991; Sierro et al., 2001 and references therein). Particular attention has been paid to the sediments of the MSC, because both Sorbas and Nijar preserve two of the most complete records of this period in the Mediterranean. The

MSC starts here with the Yesares Fm. (Dronkert, 1976; van de Poel, 1991; Krijgsman et al., 2001; Fortuin and Krijgsman, 2003; Lu, 2006), equivalent to the PLG elsewhere in the Mediterranean (Lugli et al., 2010; Dela Pierre et al., 2011; Karakitsios et al., 2017b) and attributed to MSC Stage 1 (Omodeo Salé et al., 2012). Locally in the Nijar Basin, vuggy limestones, limestone breccias, calciturbidites and sandstones belonging to the Manco Limestone Member pass upward, with an erosional contact, into dominantly detrital gypsum beds.

Sorbas-Nijar-Mediterranean connectivity was severed in the late Messinian by differential uplift of the basement highs, which resulted in the erosion of Paleozoic crystalline rocks (mostly mica schists and phyllites; Sanz de Galdeano and Santamariá-López, 2019), Permo-Mesozoic sediments and early-middle Miocene volcanics of Cabo de Gata and their incorporation in Messinian strata (Roep et al., 1998; Fortuin and Krijgsman, 2003). The triple connection may have recurred during deposition of the shallow-water carbonates of the Sorbas Mb. in Sorbas, which are reported to contain marine fauna (echinoids, scleractinians and bivalves; Braga et al., 2006). The time-equivalent strata of the Sorbas Mb. in Nijar are thought to be the conglomerate-marl alternations of the Lower Mb. of the Feos Fm. (Omodeo Salé et al., 2012; Fig. 2.2), but these sediments are poorly studied for their fossiliferous content. The connection between Sorbas, Nijar and the Mediterranean is thought to have been absent during the upper part of Stage 3 (i.e. substage 3.2 of Roveri et al., 2014a), characterized in both the basins by fluvial sediments and fine-grained deposition (marls or white limestones) in a subaqueous environment interpreted as an endorheic lake (Zorreras Mb. of Sorbas and Upper Mb. of the Feos Fm. in Nijar; Bassetti et al., 2006; Aufgebauer and McCann, 2010). The Sorbas-Nijar-Mediterranean connection was undoubtedly restored at the base of the Zanclean with the deposition of foraminifer-rich biocalcarenites (Gochar Fm. in Sorbas and Cuevas Fm. in Nijar; Aguirre, 1998; Roep et al., 1998; Roveri et al., 2019a).

2.2.3 Late Miocene connectivity evolution and stratigraphy of the Vera Basin

The Vera Basin is located to the NE of the Sorbas and Nijar basins, enclosed by the Sierra de Bédar to the NNW, Sierra Cabrera to the S and Sierra Almagrera to the NE (Fig. 2.1b). The late Tortonian-Messinian (i.e. pre-MSC) sedimentation in Vera was similar to the adjacent Sorbas and Nijar basins, with pelagic marls passing upslope into reef carbonates (Fortuin et al., 1995). In Vera, turbidites, slumps and volcanites are frequently found in the "Abad" marls (Unit 1 or Santiago Beds; Fortuin et al., 1995) and related to the initiation of the activity of the Palomares fault (Fortuin et al., 1995). The younger deposits known to unconformably overlain the Santiago beds are shallow-water laminated mudstones (Unit 2 of Fortuin et al., 1995) containing Black Sea-type brackish-water ostracods which prompted their assignment to substage 3.2 (Stoica et al., 2016; Caruso et al., 2020). Unit 2 is in turn covered by marine marls of Pliocene age (Cuevas Fm. or Unit 3; Fortuin et al., 1995). Reworked gypsum occurs associated with olistostrome-like deposits in the area surrounding the village of Garrucha, suggesting that evaporites probably

were deposited in Vera as well, but subsequently removed by sin- to post-depositional erosion (Fortuin et al., 1995). In terms of connectivity, the stratigraphy of the Vera Basin indicates that it was part of the Sorbas-Nijar-Mediterranean system until the onset of the MSC and possibly during evaporite deposition, although Late Messinian primary evaporites are absent in Vera (Fortuin et al., 1995; Fortuin and Krijgsman, 2003). Splitting of the Sorbas-Nijar-Vera system is thought to have occurred in late Yesares times probably due to the uplift of the Sierra Cabrera (Fortuin et al., 1995) and persisted throughout the Lago-Mare stage, when an endorheic lake was filling the Vera Basin (Benson and Rakic-El Bied, 1991; Caruso et al., 2020). An opposite interpretation described a continuous Mediterranean connection during the Lago-Mare phase sensu Roveri et al. (2014a), with Vera depicted as an embayment of the Mediterranean, which was therefore topped up with water (Stoica et al., 2016).

2.3 The post-evaporitic records and the studied sections

2.3.1 Feos Formation (Nijar)

Following the lithostratigraphic scheme of Omodeo Salé et al. (2012), the Feos Formation has been subdivided into two members sandwiched between two major stratigraphic surfaces: (I) the Messinian erosional surface (MES) and its correlative conformity (MES c.c.) at the base; (II) the Zanclean flooding surface (ZFS) at the top (Fig. 2.2). The Lower Member is mainly a resedimented and gypsum-bearing chaotic unit overlain by alternating silt and reworked gypsum crystals with mudstones (Fig. 2.4a). Noticeable here is the presence of a brown-black Mn-hydroxide-enriched level ~10 m above the boundary with the Yesares Formation (Fig. 2.2). This bed is a useful marker that can be traced throughout the southeastern sector of the basin (Fortuin and Krijgsman, 2003). Approximately 20 m above this marker bed, the boundary with the more terrigenous and less carbonate-rich Upper Member is placed, denoting an important change in depositional environment (Fortuin and Krijgsman, 2003; Omodeo Salé et al., 2012). The Upper Member is characterized by red to grey coarse-grained continental lithofacies (conglomerates and sandstones) alternating with white to grey, laminated chalky-marls (Figs. 2.3a, 2.4b; Fortuin and Krijgsman, 2003; Omodeo Salé et al., 2012). In the of Barranco de los Castellones section (BdC; 37°00'51.1"N, 2°00'05.7"W), that among the many sections known in the Nijar Basin offers one of the best exposures of the Feos Fm. (Fortuin and Krijgsman, 2003; Fortuin and Dabrio, 2008), dark brown mudstones are recognized at the base and/or above the white marls (Figs. 2.4c). Four complete alternations and one incomplete cycle only consisting of continental lithofacies are observed in the those sections (e.g. BdC and Cerro de los Ranchos) that offer a complete exposure of the Feos Fm., sealed by the marine Pliocene strata of the overlying Cuevas Formation (Fig. 2.2). The sharp lithological transition to open marine deposits is slightly erosional at the basin margins, but appears to be conformable above a fluvial sandstone (BdC, Fig. 1.6b) or conglomerate (Cerro de los Ranchos) in the central parts of the basin (Fortuin and Krijgsman, 2003). Based on the assumption that these alternations are

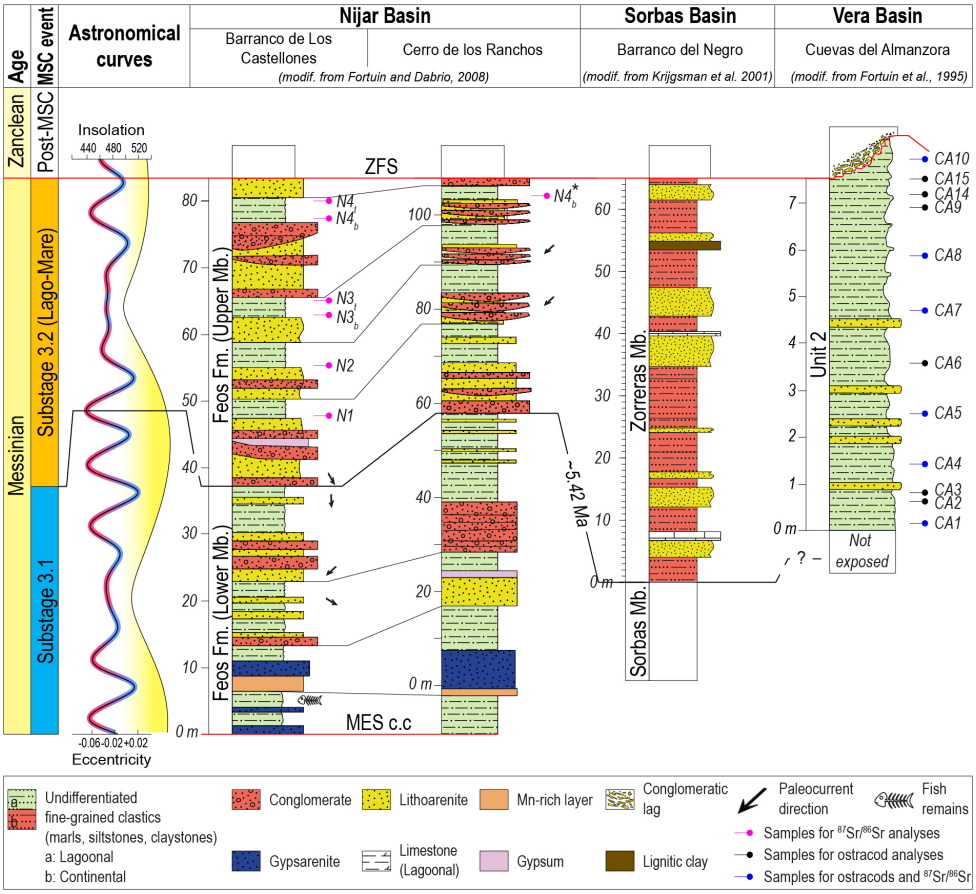

Fig. 2.2. *Stratigraphic logs of the studied sections. Correlations among the Nijar sections is based on Fortuin and Dabrio (2008). Astronomical tuning of the Nijar sections to climatic precession (P), 100 kyr eccentricity (E) and the 65°N insolation curve (I) of Laskar et al. (2004) is based on Hilgen et al. (2007). MES c.c.: Messinian Erosional Surface correlative conformity; ZFS: Zanclean Flooding Surface (see paragraph 2.3.1 for further insights).*

precessional cycles, the Lower Mb.-Upper Mb. transition has been cyclostratigraphically dated at ~5.44 Ma by Hilgen et al. (2007) and ~5.42 Ma by Omodeo Salé et al., 2012 (Fig. 2.2). This latter age corresponds to the substage 3.1/3.2 transition of the consensus model (Roveri et al., 2014a) as defined in the Northern Apennines (Roveri et al., 2008a and references therein).

The four fine-grained intervals of the Nijar's Upper Member host a microfaunal assemblage mainly composed of shallow-water, brackish ostracods mixed with marine foraminifera (Aguirre and Sánchez-Almazo, 2004; Bassetti et al., 2006). Bassetti et al. (2006) recognized significant variations in the diversity of the ostracod species within each marl bed. They

differentiated two main assemblages: the first occurs at the base of the fine-grained hemicycle and is characterized by low species diversity dominated by *Cyprideis agrigentina* with rare specimens of *Tyrrhenocythere* sp. The second assemblage, which occurs at the top of each marl bed, has a higher diversity of taxa belonging to different genera (e.g. *Candona, Loxorniculina, Amnicythere, Loxoconcha*). All those taxa recognized to the species level by Bassetti et al. (2006) are known from several other localities across the Mediterranean (Cosentino et al., 2007, 2018; Grossi et al., 2008, 2015), including the adjacent Vera (Stoica et al., 2016; Caruso et al., 2020) and Malaga (Guerra-Merchán et al., 2010) basins, and shown to be endemic of the Eastern Paratethys (Gliozzi et al., 2007; Stoica et al., 2016). It is noteworthy to point out that Bassetti et al. (2006) claimed that these ostracod species have little affinity with the coeval Paratethyan species. However, Stoica et al. (2016) showed that this conclusion arose from the employment of different taxonomic concept. Consequently, Paratethyan ostracods also inhabited the Nijar Basin. The foraminiferal assemblage found in the pelitic intervals is considered to be in situ by Aguirre and Sánchez-Almazo (2004), but physically reworked by all others (Fortuin and Krijgsman, 2003; Bassetti et al., 2006; Fortuin and Dabrio, 2008; Omodeo Salé et al., 2012).

2.3.2 Sorbas-Zorreras members (Sorbas Basin)

The package of sediments sandwiched between the Yesares Formation and the Pliocene in Sorbas are subdivided into two members: the Sorbas Member and the Zorreras Member (Fig. 2.3b). The Sorbas Member, studied in detail by Roep et al. (1998), is ~70 m thick and consists of marls, silts and sands arranged in three parasequences recording base-level fluctuations that pass marginally into the so-called Terminal Carbonate Complex (TCC), a carbonate platform system constituted by heterogeneous limestones and minor coarse siliciclastic sediments (Roveri et al., 2009; Bourillot et al., 2010). The Sorbas Member is interpreted as having been deposited in a shallowing-upward environment surrounded by shallower carbonate factories and emerged areas supplying the coarser siliciclastic fraction (Roep et al., 1998; Braga et al., 2006; Aufgebauer and McCann, 2010).

The Sorbas Member and TCC are conformably overlain by the up to 75 m thick Zorreras Member (Fig. 2.3b). This unit mainly consists of azoic paleosoils, reddish silt- and sandstones, grey-coloured sandstones and conglomerates with intercalated white limestone beds (Fig. 2.3b), whose exact number is debated from two to four (Roveri et al., 2009, 2019a; Aufgebauer and McCann, 2010). In the Cerro Zorreras section, which is the type section for the Zorreras Mb. (37°06'10.2"N, 2°06'45.2"W; Krijgsman et al., 2001) due to its complete exposure between the Sorbas Mb. and the Zanclean Gochar Fm. (Fig. 2.3e), these limestones range in thickness from ~95 cm (the uppermost one; Fig. 2.4d) to 130 cm (the lowermost one; Figs. 2.4e). They are whitish, massive and with little evidence of internal structures. Non-marine ostracods with Paratethyan affinity are known to be present in these limestones, but assemblages are reported to be poorly diversified, only consisting of the euryhaline *Cyprideis* sp., *Loxocorniculina*

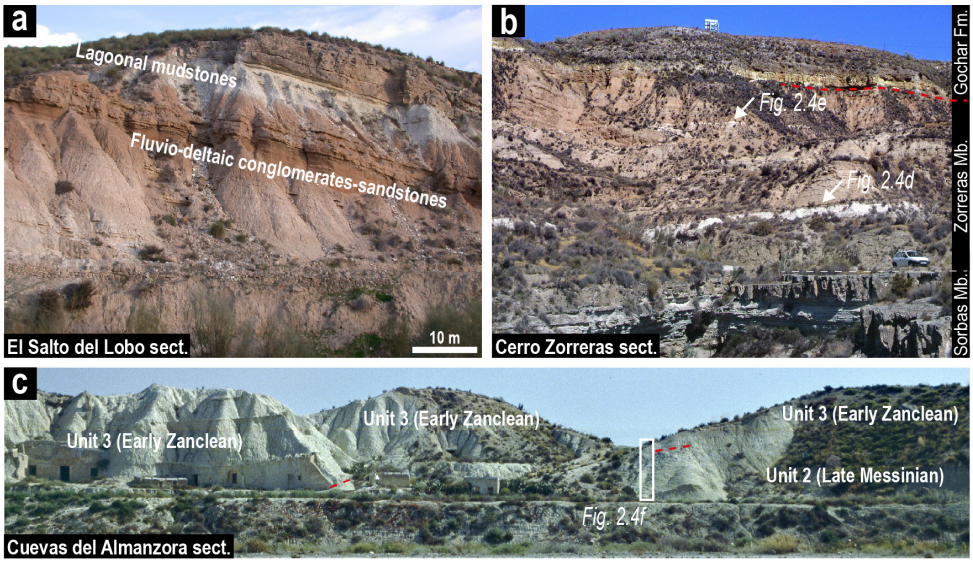

Fig. 2.3. (a) *Part of the type section of the Feos Fm. along the river Alias at Los Feos. The cliff section (herein named El Salto del Lobo) shows the superposition of a thick pink and reddish continental interval, followed by white ostracods-bearing laminated mudstones, passing upwards into a next coarse clastic, continental interval.* **(b)** *Photograph of the type-section for the Zorreras Mb., the Cerro Zorreras section, showing the largely red continental sediments locally interrupted by white limestones (white arrows). The gradual transition of the Zorreras Mb. from the Sorbas Mb. underneath and to the Gochar Fm. on top is also appreciable. Car for scale.* **(c)** *Panoramic view of the Cuevas del Almanzora section and detail of the sampling site logged in Fig. 2.2.*

djaffarovi and undisclosed freshwater taxa belonging to the family Limnocytheridae (Roep and Van Harten, 1979; Aufgebauer and McCann, 2010). In some outcrops, a thin bed (3-10 cm) of green-grey-coloured mudstone is present below the carbonate beds and this might contain thick laminae (0.6-1 cm) of bituminous material (Aufgebauer and McCann, 2010). At present, the Zorreras Mb. is interpreted as representative of the repetitive development of alluvial fan systems sporadically interrupted by the expansion of lacustrine conditions related to either intra-basinal flooding events (Aufgebauer and McCann, 2010; Roveri et al., 2019a) or water incursions from the Nijar Basin (Mather and Stokes, 2001; Fortuin and Krijgsman, 2003). Whatever the provenance of the water was, the position and thickness of the carbonate layers indicates that subaqueous conditions established suddenly and lasted ephemerally (Aufgebauer and McCann, 2010). The attribution of the Sorbas and Zorreras mbs. to the MSC stages is controversial (see summary in Krijgsman et al., 2001 and Roveri et al., 2019a). In this paper we adopt the chronostratigraphic framework of Roveri et al. (2019a), which attributed the Sorbas Mb. to Stage 2 and substage 3.1 and the Zorreras mb. to the Lago-Mare phase (Fig. 2.2).

2.3.3 Unit 2 (Vera Basin)

Unlike in Nijar and Sorbas, the Lago-Mare phase in Vera is only expressed by ~12 m of varicoloured laminated mudstones (Unit 2 of Fortuin et al., 1995; Fig. 2.2), whose best exposure is found in the Cuevas del Almanzora section (CdA; 37°17'00"N, 1°50'33"W; Figs. 2.3c, 2.4f; Montenat and Bizon, 1976; Benson and Rakic-El Bied, 1991; Fortuin et al., 1995; Stoica et al., 2016; Caruso et al., 2020). An ostracod fauna with Paratethyan affinity typifies the mudstones (Stoica et al., 2016; Caruso et al., 2020). The ostracod fauna changes in diversity from the base of the section, where it is dominated by *Cyprideis* sp., to the top, which is rich in species typical of the Pontian of the Euxinic and Caspian basins (Stoica et al., 2016), similarly to the mudstone horizons of the Upper Mb. of the Feos Fm. in Nijar. The lower contact of these sediments with older lithologies is not exposed, whereas on top they are capped by an erosional surface draped by conglomeratic accumulations (Fortuin et al., 1995; Stoica et al., 2016; Caruso et al., 2020; Fig. 2.2).

2.4 Material and methods

2.4.1 Evaluation of ostracods $^{87}Sr/^{86}Sr$ ratios

2.4.1.1 Sample selection

Strontium ($^{87}Sr/^{86}Sr$) isotope compositions were measured on the low-Mg calcitic valves of the ostracod *Cyprideis* sp. Ostracods are an archive of the water Sr chemistry, because during valves secretion they extract Sr^{2+} from the water in which they dwelt (Fig. 2.7) with isotopic fractionation effects that may occur during the liquid-solid transition, but that are removed during data reduction (Hajj et al., 2017 and references therein). All the other lithologies present in the stratigraphic intervals studied (conglomerates, sands and reddish pelites; Fig. 2.2) were deposited in a continental environment and lack abiotic and/or biotic phases suitable for $^{87}Sr/^{86}Sr$ analyses. The *Cyprideis* valves were picked from the uppermost four marl beds of the Upper Member of the Feos Formation in the BdC section in Nijar (Fig. 2.2), the lowermost limestone horizon of Sorbas (unknown locality) and the marly mudstones of Vera in an outcrop next to the CdA section. In the Nijar Basin, two additional samples, one from the Cerro de los Ranchos section (Fig. 2.2) and one from an outcrop (named El Salto del Lobo; Fig. 2.3a) along the river Alias, were studied. The samples selected and analyzed for their $^{87}Sr/^{86}Sr$ signature from the BdC, CdA, Cerro de los Ranchos and El Salto del Lobo sections come from a sample set collected and measured in the '90s/early 2000s and provided to us by Anne Fortuin. The new data from Sorbas, Nijar and Vera are intended to update and widen the Lago-Mare dataset already built in the past by McCulloch and De Deckker (1989) for the Sorbas Basin, Roveri et al. (2019a) for the Nijar Basin and Fortuin et al. (1995) for the Vera Basin. Roveri et al. (2019a) measured one sample from the uppermost mudstone horizon of the Feos Upper Mb. in the BdC section. Fortuin et al. (1995) run seven measurements of samples from the CdA section (one of these data has not been considered due to a large analytical error). McCulloch and De

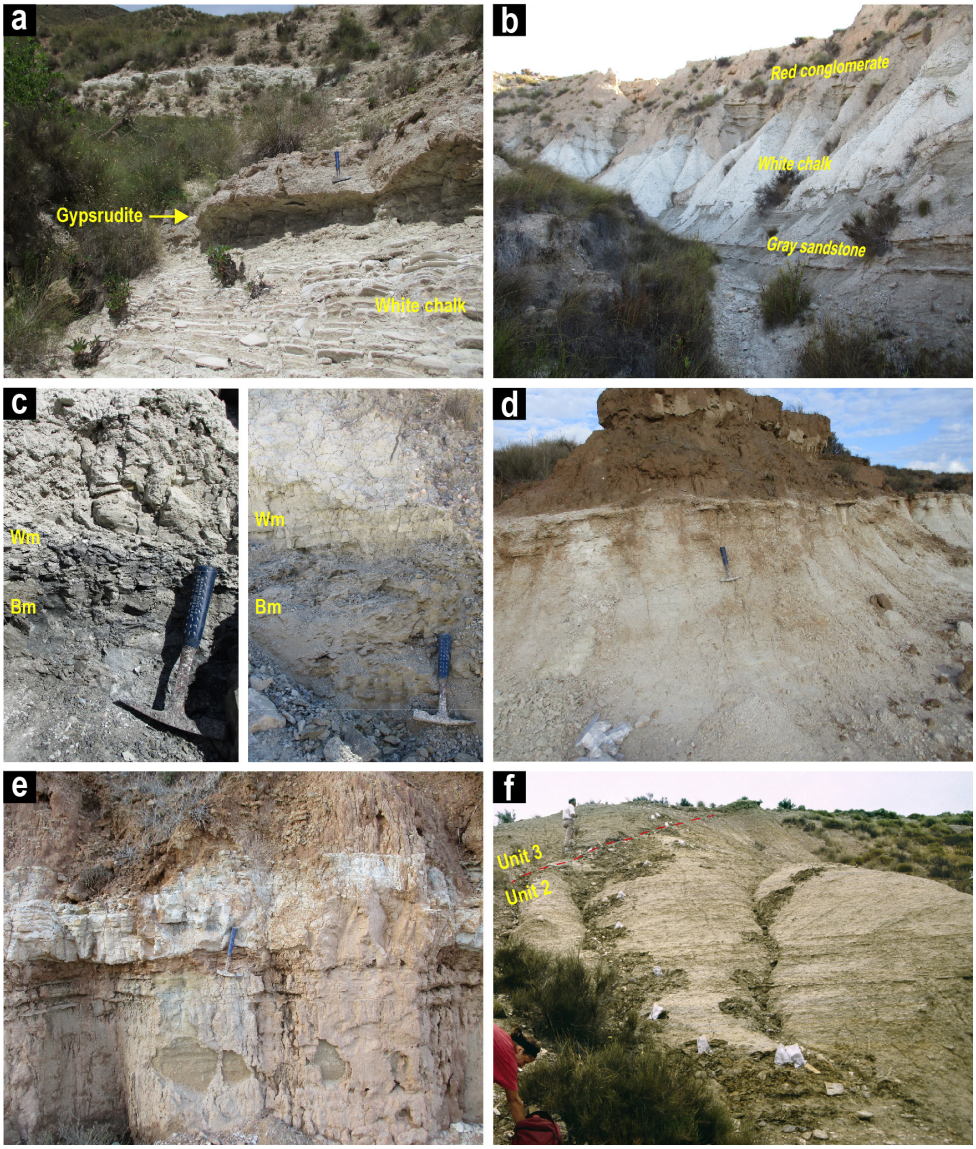

Fig. 2.4. (a), (b) *Field view of the coarser bed-white chalk alternations characteristic of the lower member* **(a)** *and upper member* **(b)** *of the Feos Formation. Pictures are taken near El Argamason (a) and along the Barranco de los Castellones river bed (b), respectively.* **(c)** *Close view of the brown mudstones (Bm) at the base of the uppermost two chalk intervals (Wm) in the Barranco de los Castellones section.* **(d), (e)** *Detail of the lowermost* **(d)** *and uppermost* **(e)** *white limestones interbedded with the red continental lithofacies of the Zorreras Mb.* **(f)** *Detail of the sampling site of the Cuevas del Almanzora section logged in Fig. 2.2.*

Deckker (1989) did not specify from which of the two (or four) lacustrine levels their Sorbas measurements came from (Fig. 2.2).

2.4.1.2 Sample preparation and measurement

For each sample, single *Cyprideis* sp. valves (~10) were first repeatedly cleaned in Milli-Q water by mild ultrasonification lasting 30 seconds, after which the liquid and any contamination was pipetted off. Visual inspection using binocular microscope and SEM indicates that all adherent clays had been removed by this process. The valves were then placed in acid-cleaned 1 ml centrifuge tubes and dissolved in ~0.5 ml 5N acetic acid for ~2.5 hours. After centrifuging at 12.000 rpm for 8 minutes, 400 µl of the fluid was taken out and dried overnight in open, acid-cleaned, savillex PFA 24mm rocket beakers at ~110˚C. Two drops of concentrated HNO_3 were added to all dried samples, which were then taken up in 3N HNO_3. The elemental composition (Ca, Sr, Mg and Mn) was determined on a weighted aliquot of this solution using a Liberty II Varian ICP-AES, in order to assess the total amount of strontium. Subsequently, based on the ICP-AES analyses ~1 microgram of strontium was purified using column separation with ion-specific Sr-spec resin. The $^{87}Sr/^{86}Sr$ ratio was analyzed by thermal ionisation mass spectrometry using a Finnigan MAT 262, mostly following the method as described in Beets (1991) and Fortuin et al. (1995). Briefly, aliquots of ~500 ng of the selected samples were loaded on single, zone-refined rhenium filaments with a mixture of $TaCl_5$ and H_3PO_4 emitter-fluid. During the measurements of the Lago-Mare ostracods, three NBS 987 standards were added to the sample turret to monitor the reproducibility of the measurements. Also a procedural blank, including separation chemistry and loading, was measured. Average NBS 987 $^{87}Sr/^{86}Sr$ is 0.710247±0.000011 (1sd; n = 3), whereas the in-run precision of individual measurements was better than 0.000010 (1sd). The blank was determined at 0.124 ng Sr, which is less than 0.025% of the average amount of loaded Sr and therefore negligible. All isotope analyses were carried out in a clean-lab environment at the Vrije Universiteit Amsterdam.

2.4.2 Mass-balance calculations

The $^{87}Sr/^{86}Sr$ isotopic composition of Sr^{2+} dissolved in a subaqueous sedimentary environment is dependent upon the $^{87}Sr/^{86}Sr$ isotopic composition and Sr concentration of all the reservoirs that contribute to shape the water body (e.g. Doebbert et al., 2014; Zielinski et al., 2017). Knowing the strontium parameters (i.e. $^{87}Sr/^{86}Sr$ ratios and strontium concentration) and the relative contribution of each water source, the $^{87}Sr/^{86}Sr$ isotopic composition ($^{87/86}Sr_{mixture}$) of a mixture of multiple (1, 2, … n) water sources can be calculated by means of a chemical mass balance approach (e.g. Placzek et al., 2011; Doebbert et al., 2014; Grothe et al., 2020):

$$^{87/86}Sr_{mixture} = F_{R1} \ ^{87}Sr/^{86}Sr_{R1} + F_{R2} \ ^{87}Sr/^{86}Sr_{R2} + \ldots + F_{Rn} \ ^{87}Sr/^{86}Sr_{Rn} \quad (1)$$

where $F_{R1,2,...}$ is the fraction of Sr that each source contributes and $^{87}Sr/^{86}Sr_{R1,2,...}$ is the $^{87}Sr/^{86}Sr$ ratio (dimensionless) specific to each reservoir. In turn, the Sr fractional contribution (F) of individual sources is:

$$F_{R1}=[Sr]_{R1}*d_1/[Sr]_{R1}*d_1+[Sr]_{R2}*d_2+...+[Sr]_{Rn}*d_n \quad (2)$$

where $[Sr]R_n$ (mg/l) is the strontium concentration and dn (dimensionless) is the fraction of discharge of each water source. Using these equations, we developed a strontium mass-balance model to help constrain the evolution of the $^{87}Sr/^{86}Sr$ composition of the Sorbas, Nijar and Vera water bodies inhabited by the ostracods, varying the mixing proportion between the different water sources. We explored the mutually exclusive possibilities of a system of isolated endorheic lakes supplied only by intrabasinal inputs (surface runoff and groundwater; Fig. 2.7a) and of a system of basins that received additional extrabasinal water (and therefore Sr^{2+}) from the Mediterranean Basin (Fig. 2.7b). The model requires knowledge of the Sr flux into the basins from every major source (Table 2.1). As for the runoff terms, given the lack of direct measurements on present-day analogs we considered each of the main catchment-forming lithologies (Fig. 2.6a; see section 2.5.2) to have been a source of Sr^{2+} with the same $^{87}Sr/^{86}Sr$ ratio as the one measured on the bulk rock, while the values of strontium concentration for source (herein mentioned as local rivers) are based on [Sr] observed in modern rivers draining carbonate and silicate rocks (e.g. Brenot, 2006; Doebbert et al., 2014; Zielinski et al., 2017). The Sr concentration of the carbonate end member has been adjusted to a higher value than the average (e.g. Brenot, 2006) to account for the higher solubility relative to igneous or metamorphic basement rocks. The assumption of using $^{87}Sr/^{86}Sr$ ratios of bedrocks as analogue of the $^{87}Sr/^{86}Sr$ ratios of rivers derives from the fact that Sr^{2+} dissolved in rivers inherits the isotope signature of the rocks weathered in the catchment (Brenot, 2006; Doebbert et al., 2014; Hajj et al., 2017; Zielinski et al., 2017). $^{87}Sr/^{86}Sr$ value of 0.7086 for the Mediterranean water is (roughly) the midpoint value of the range of Sr values (0.7085-0.7087; Fig. 2.5a) measured on ostracods recovered from the intermediate basin of Caltanissetta in Sicily (Grossi et al., 2015) and from DSDP sites drilled in the central Mediterranean basins (McCulloch and De Deckker, 1989) and, as of now, thought to represent the highstand phases of the Mediterranean base-level (Manzi et al., 2009). Three values of Sr concentration have been employed: an extremely high value of 8 mg/l, which corresponds to the value of the present-day seawater (Veizer, 1989), an extremely low value of 0.5 mg/l, which is a more fluvial-like value, and an intermediate (and more likely) value of 1 mg/l. The input of Sr from groundwater is the major unknown as it cannot be realistically reconstructed and sampled and present-day estimates are absent. For this reason, the groundwater component is not incorporated in the model.

Mass balance calculations can be applied to n-component systems (Eq. 1), but the results are difficult to represent graphically. Accordingly, here we apply the procedure considering each

basin as a three-component system (only local rivers in the lacustrine scenario, local rivers and Mediterranean water in the lagoonal scenario; Fig. 2.7) and we plot the isotopic signature of each mixture on a ternary diagram (Fig. 2.8). When the Mediterranean is not part of the system (i.e. lacustrine scenario; Fig. 2.7a), three continental fluvial sources are considered in the model (Figs. 2.8a-b). When the Mediterranean is considered (i.e. lagoonal scenario; Fig. 2.7b), only two riverine sources are taken into account (Figs. 2.8c-e) by combining those with the same Sr concentration (see Table 2.1) and calculating the arithmetic mean of the $^{87}Sr/^{86}Sr$ ratios of the individual sources. A detailed explanation of the approach pursued to constrain model results is provided in section 2.5.3.

2.5 Results

2.5.1 $^{87}Sr/^{86}Sr$ ratios of Spanish (Lago-Mare) ostracods

The new $^{87}Sr/^{86}Sr$ values from the Sorbas, Nijar and Vera basins are comparable with the values obtained by McCulloch and De Deckker (1989), Fortuin et al. (1995) and Roveri et al. (2019a) from the same source material (Fig. 2.5b; Table 2.2). Overall, the $^{87}Sr/^{86}Sr$ ratios from these three Spanish basins encompass a wide range of values (from 0.708764 to 0.709131) straddling the ocean water ratio during the Lago-Mare phase (~0.709024; McArthur et al., 2012; Fig. 2.5b). Other than one sample ($N1_b$) from Nijar Basin's $^{87}Sr/^{86}Sr$ record (0.708814-0.709099), none of the data are within error of coeval ocean water (~0.709024; McArthur et al., 2012), but the Nijar record links the higher values recorded in Sorbas (0.709066-0.709131), with much lower ones from Vera, that are close to published ratios (<0.7088) typical of Lago-Mare sediments (substage 3.2) elsewhere in the Mediterranean (Fig. 2.5a). The $^{87}Sr/^{86}Sr$ record of the astronomically tuned BdC section in Nijar, despite the low resolution of the data, is more variable (Fig. 2.5b) and provides us with some hints as to the variation in isotopic composition of the water mass at subprecessional scale (see section 2.6.4). The measured $^{87}Sr/^{86}Sr$ for cycle I plots within error of coeval global seawater $^{87}Sr/^{86}Sr$ ratios, whereas the other values from the base of the pelitic beds are all less radiogenic than ocean water (Fig. 2.5b). The samples from the upper parts of cycles III and IV are substantially lower than the rest of the Nijar data (0.708835-0.708814, respectively) and they are similar to values measured from substage 3.2 ostracods that inhabited the neighbouring Vera Basin.

Table 2.1. *Summary of the $^{87}Sr/^{86}Sr$ and Sr concentration of each water source considered in the mass-balance calculation. $^{87}Sr/^{86}Sr$ ratio of river 5 and 6 are the arithmetic average of the mixed sources.*

Water source	$^{87}Sr/^{86}Sr$	[Sr]	References
Late Messinian Medit. water	0.708600	0.5, 1, 8	Section 2.4.2
River 1 (Sch)	0.726545	0.035	Sec. 2.4.2/2.5.2
River 2 (Dol)	0.708612	0.260	Sec. 2.4.2/2.5.2
River 3 (Orth)	0.713684	0.035	Sec. 2.4.2/2.5.2
River 4 (Vol)	0.712496	0.035	Sec. 2.4.2/2.5.2
River 5 (Sch+Orth)	0.720115	0.035	Sec. 2.4.2/2.5.2
R6 (Sch+ Orth +Vol)	0.712668	0.035	Sec. 2.4.2/2.5.2

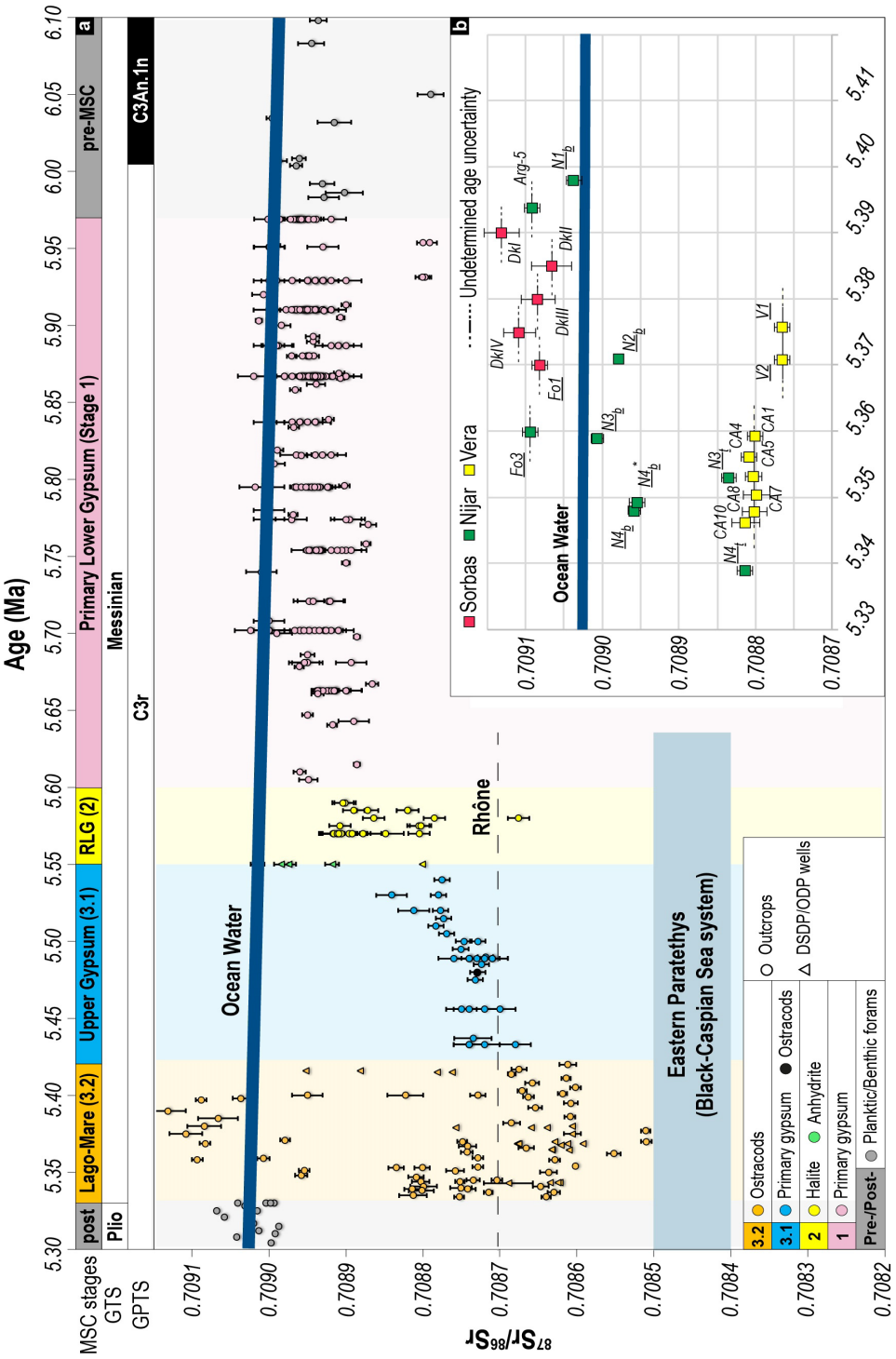
Age (Ma)
MSC stages
GTS
GPTS
87Sr/86Sr
a
b
post
Lago-Mare (3.2)
Upper Gypsum (3.1)
RLG (2)
Primary Lower Gypsum (Stage 1)
pre-MSC
Plio
Messinian
C3r
C3An.1n
Ocean Water
Rhône
Eastern Paratethys
(Black-Caspian Sea system)
Sorbas
Nijar
Vera
Undetermined age uncertainty
Ostracods
Primary gypsum
Halite
Primary gypsum
Pre-/Post-
Outcrops
Ostracods
Anhydrite
DSDP/ODP wells
Planktic/Benthic forams

Fig. 2.5 (previous page). (a) *Compilation of $^{87}Sr/^{86}Sr$ data for the Mediterranean during the Messinian Salinity Crisis. A cyclostratigraphic age has been assigned to each sample according to the chronostratigraphic framework of Roveri et al. (2014a) for outcropping sections and Roveri et al. (2014b) for DSDP and ODP cores. Error bars indicate analytical error which is so small in some cases that no error bars are visible at this scale. Mediterranean $^{87}Sr/^{86}Sr$ data are derived from: McKenzie et al. (1988); McCulloch and De Deckker (1989); Müller and Mueller (1991); Fortuin et al. (1995); Flecker and Ellam (1999, 2006); Keogh and Butler (1999); Lugli et al. (2007, 2010); Roveri et al. (2014b, 2019a); Schildgen et al. (2014); Evans et al. (2015); Grossi et al. (2015); Karakitsios et al. (2017); Reghizzi et al. (2017, 2018); García-Veigas et al. (2018). This data set has been compiled and evaluated and is available in the supplementary information. Ocean water ratios are from McArthur et al. (2012); Black-Caspian Sea data are from Grothe et al. (2020); Rhône value is from Albarède and Michard (1987).* **(b)** *Detailed $^{87}Sr/^{86}Sr$ record for Lago-Mare data from the Sorbas, Nijar and Vera basins and the coeval ocean ratio. New Nijar values generated during this project from the Barranco de Los Castellones and Cerro de los Ranchos sections are plotted using the chronostratigraphic framework of Hilgen et al. (2007). For the remaining values, age uncertainties are present. Underlined sample labels refer to the new measurements generated in this work.*

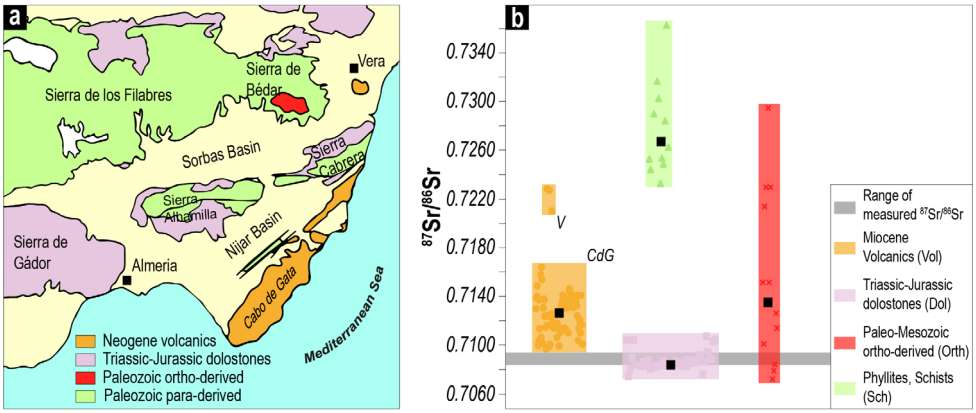

Fig. 2.6. (a) *Simplified geological map of the sierras surrounding the Sorbas, Nijar and Vera basins (modified from Murillo-Barroso et al., 2019 and Sanz de Galdeano and Santamaría-López, 2019).* **(b)** *Delimitation of isotopic fields of the main catchments-forming lithologies in the $^{87}Sr/^{86}Sr$ ratios. Analytical errors are smaller than the symbols. Black squares indicate the average $^{87}Sr/^{86}Sr$ ratio of each isotopic field, which has been employed in the mass-balance calculation (values are listed in table 2.1).*

2.5.2 Bedrock $^{87}Sr/^{86}Sr$ ratios

Measurements of present-day $^{87}Sr/^{86}Sr$ ratios are available for all the main lithologies forming the crystalline basement and the overlying sedimentary covers in the watershed of the three marginal Spanish basins (Fig. 2.6a). We group these rock-types into four categories:

para-derived rocks (i.e. phyllites and mica schists), ortho-derived rocks, volcanic rocks and dolostones (Fig. 2.6b). The sierras de los Filabres and de Bédar to the north of the Sorbas and Vera basins consist of tectonic units belonging to the Nevado-Filabride complex (Sanz de Galdeano and Santamaría-López, 2019). Here, both para- and ortho-derived metamorphic rocks are found (Fig. 2.6a). The recent cartography of the western side of the Sierra de los Filabres by Sanz de Galdeano and Santamaría-López (2019) revealed that para-derived rocks are by far the more widespread. Among them, high-grade Paleozoic (±Mesozoic) phyllites and mica schists are the major constituent, with subordinate quartzites and sandstones (Fig. 2.6a; Sanz de Galdeano and Santamaría-López, 2019). These meta-sediments have highly radiogenic $^{87}Sr/^{86}Sr$ ratios ratios (0.713310-0.731679; Arribas et al., 1995; Nieto et al., 2000; Kirchner et al., 2016; Fig. 2.6b), compatible with $^{87}Sr/^{86}Sr$ ratios values carried by the same rocks of the same age forming the metamorphic basement of the Mesozoic covers in Tuscany, Italy (0.713310-0.724882-0.738229; Conticelli et al., 2009). Ortho-derived rocks (e.g. metabasites, ophiolites, gneiss) of ages ranging from the Carboniferous to the Paleocene are found as isolated intrusions. These rocks are characterized by highly variable $^{87}Sr/^{86}Sr$ values (Puga et al., 2002), ranging from very low (0.703243) to very high (0.729459) ratios. Rare occurrence of Triassic marbles are also observed (Sanz de Galdeano and Santamaría-López, 2019), but no measurements of their $^{87}Sr/^{86}Sr$ ratios ratios are available. In general, the abundance of carbonates, especially Triassic (possibly also Jurassic) dolomites, is relatively higher in the Sierra Alhamilla and Sierra Cabrera bordering the Nijar and Vera basins than in the sierras de los Filabres and de Bédar (Fig. 2.6a). The $^{87}Sr/^{86}Sr$ ratios values of these carbonate bedrock lithologies range between a minimum of 0.707606 to a maximum of 0.710737 (Arribas et al., 1995; Conticelli et al., 2009; Mueller et al., 2020), averaging 0.708612 (Fig. 2.6b). These values are higher than the range predicted for the catchment limestones of both Triassic (from 0.707663 at 251.9 Ma to 0.707335 at 201.3 Ma, average of 0.707761; McArthur et al., 2012) and Jurassic age (from 0. 0.707335 at 201.3 Ma to 0.707189 at 145 Ma, average of 0.707182; McArthur et al., 2012). This aspect is common in metamorphic settings where carbonates are surrounded by silicate-rich rocks with high $^{87}Sr/^{86}Sr$ ratios and is generally related to post-depositional processes that cause phyllosilicate mineral phases with radiogenic $^{87}Sr/^{86}Sr$ ratios ratios to disseminate in limestones, making the $^{87}Sr/^{86}Sr$ ratioscomposition of these carbonates more radiogenic (e.g. Bickle et al., 2001). An important source of allochthonous material supplied to the Nijar Basin is derived from the Sierra de Gata to the SE (Figs. 2.1b, 2.6a). The Cabo de Gata volcanic complex is mainly made up of Burdigalian-Pliocene volcanic rocks and minor leucogranitic intrusions intercalated within the Miocene and older sedimentary fill and resting discordantly over the basement rocks (Zeck et al., 1998). The younger (i.e. Messinian-Pliocene) lithologies are ultrapotassic rocks (lamproites: fortunites, jumillites, verites) and alkali-basalts that form only small and widely scattered bodies at the two southern and northern extremes of the Sierra de Gata (Zeck et al., 1998). The core of the complex is concentrated in its central parts and is made up of calc-alkaline volcanics (e.g.

andesite; Zeck et al., 1998). Several (i.e. >80 to our knowledge) $^{87}Sr/^{86}Sr$ ratios of the calc-alkaline rocks are available from localities spanning the entire extent of the Sierra (Toscani et al., 1990; Arribas et al., 1995; Zeck et al., 1998; Conticelli et al., 2009). Cabo de Gata volcanics are grouped in a relatively well-defined cluster of very radiogenic isotopic values between 0.709691 and 0.716403 (Toscani et al., 1990; Arribas et al., 1995; Zeck et al., 1998; Conticelli et al., 2009; Fig. 2.6b). Neogene magmatic rocks of the Alborán volcanic province also occur in the Vera Basin (Figs. 2.1b, 2.6a). These rocks are dated to the early Messinian (Conticelli et al., 2009 and references therein) and are also characterized by high $^{87}Sr/^{86}Sr$ ratios, ranging from 0.721029 to 0.722831 (Conticelli et al., 2009).

2.5.3 Model results

Mass balance modeling of the $^{87}Sr/^{86}Sr$ signal of the Spanish marginal basins produces a wide range of $^{87}Sr/^{86}Sr$ ratios (Fig. 2.8). Ideally, the Sr fluxes for each of the water sources would constrain the mixing proportion required to reproduce each measured Messinian $^{87}Sr/^{86}Sr$ ratio. Unfortunately, reliable values for Messinian fluvial Sr fluxes cannot be obtained directly, but instead are deduced from the catchment's geology (Fig. 2.6b). To do this, we use the standard assumption that catchment area is proportional to discharge (e.g. Placzek et al., 2011). This means that the larger the volume of a specific lithology in the catchment, the more influence it has over the Sr flux of the river draining the catchment. The mountains surrounding the Sorbas, Nijar and Vera basins today were already partially uplifted during Lago-Mare times (e.g. Benson and Rakic-El Bied, 1991; Roep et al., 1998; Fortuin and Krijgsman, 2003). They are dominated by mica schists and phyllites with more minor carbonates (Fig. 2.6a). To constrain the $^{87}Sr/^{86}Sr$ ratios of a hypothetical lake filling the Sorbas Basin, which has a drainage basin with >50% mica schists and phyllites (labelled Sch; Fig. 2.6b), we assumed that these lithologies accounted for more than 50% of the dissolved Sr^{2+} (Fig. 2.8a). The same threshold value is employed for all model outputs in the lagoonal scenario (Figs. 2.8c-e), where schists and phyllites are merged together with other similar lithologies carrying similar Sr concentration (Table 2.1; see paragraph 2.4.2 for insights). The Sr flux from mica schists and phyllites is decreased to 40% for the Nijar Basin and to 30% for the Vera Basin (Fig. 2.8b) to account for the higher volume of carbonates in the catchments of these two basins (Fig. 2.6a).

Using this approach the Sr dissolved in a hypothetical Messinian lake in the Sorbas Basin would have $^{87}Sr/^{86}Sr>0.7100$. Lower ratios are predicted for lakes in the Nijar (down to 0.7096) and Vera (down to 0.7092) basins. When Mediterranean water is added to the system of local rivers, the range of possible $^{87}Sr/^{86}Sr$ ratios in all basins is substantially lower, from 0.7088 to >0.7092 (Figs. 2.8c-e). Plotting the range of $^{87}Sr/^{86}Sr$ ratios measured on ostracods on top of the model results demonstrates that none of the predicted $^{87}Sr/^{86}Sr$ ratios for three endorheic lakes, one in each basin, overlaps with the measured values (Figs. 2.8a-b). Instead, measured and modeled $^{87}Sr/^{86}Sr$ ratios are in better agreement when Mediterranean Sr^{2+} is mixed with the

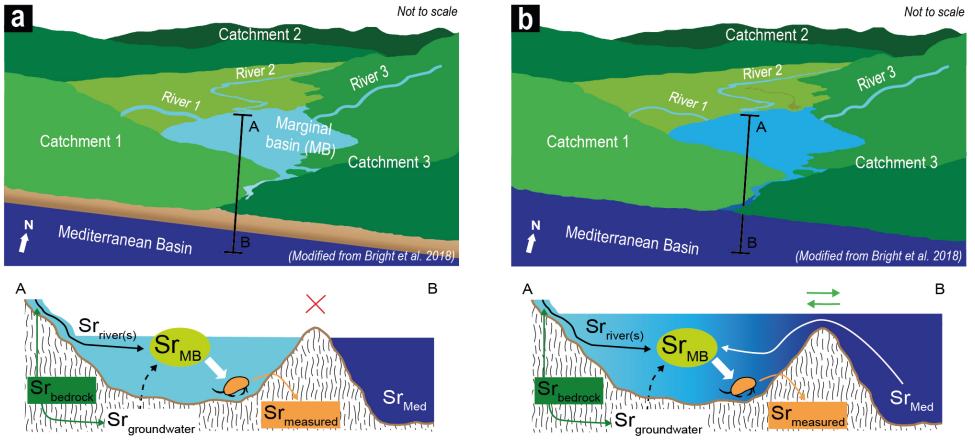

Fig. 2.7. *Schematic presentation of the Sr cycle in a Mediterranean marginal basin (MB) disconnected from* **(a)** *and connected to* **(b)** *the Mediterranean water mass (modified from Bright et al., 2018).*

local riverine Sr^{2+} (Figs. 2.8c-e).

2.6 Discussion

2.6.1 Is "desiccation" the only answer to the non-marine $^{87}Sr/^{86}Sr$ ratios of Stage 3?

The Stage 3 scenario of non-marine sedimentation in a deep desiccated Mediterranean (here labelled to as "lacustrine scenario"; e.g. Ruggieri, 1967; Hsü et al., 1973; Cita et al., 1978; Benson and Rakic-El Bied, 1991; Orszag-Sperber et al., 2000; Ryan, 2009; Maillard et al., 2014; Camerlenghi et al., 2019; Kartveit et al., 2019; Madof et al., 2019; Caruso et al., 2020; Raad et al., 2021) implies that each disconnected sub-basin had a unique base-level history and water chemistry. By contrast, the alternative scenario (i.e. "lagoonal scenario") envisages connection between sub-basins raised at elevations close to normal sea level by the same water mass filling the Mediterranean Basin (e.g. McCulloch and De Deckker, 1989; Roveri et al., 2014b, c; Marzocchi et al., 2016; Vasiliev et al., 2017; García-Veigas et al., 2018; Grothe et al., 2020), which is expected to result in a more chemically-homogeneous water mass. Radiogenic strontium isotope ratios ($^{87}Sr/^{86}Sr$) reflect the source water inputs and can be used to discriminate between scenarios where the water sources have different $^{87}Sr/^{86}Sr$ ratios (e.g. Ingram and Sloan, 1992; Vonhof et al., 1998; Flecker et al., 2002; Doebbert et al., 2014). Strontium influx in the lacustrine scenario is derived from drainage within each catchment (Fig. 2.7a). The $^{87}Sr/^{86}Sr$ ratio of each water source is dependent upon the lithologies weathered in the watersheds and the $^{87}Sr/^{86}Sr$ratio of the resulting endorheic lake reflects all these inputs (Fig. 2.7a; Brenot, 2006; Bataille et al., 2012; Doebbert et al., 2014; Baddouh et al., 2016). In the lagoonal scenario, each marginal basin receives additional water from the Mediterranean (Fig. 2.7b), which in turn was supplied from the major peri-Mediterranean drainage systems, both still existing (e.g. Nile and

Table 2.2. *$^{87}Sr/^{86}Sr$ composition and details of the analyzed samples. References: 1: McCulloch and De Deckker, 1989; 2: this work; 3: Roveri et al. (2019a); 4: Fortuin et al. (1995).*

Basin	Section	Sample	Unit	Material	$^{87}Sr/^{86}Sr$	2σ (*10^{-6})	Ref.
Sorbas	Not applicable*	Dk75059 I	Zorreras Mb.	Limestone	0.709131	0.000023	1
Sorbas	Not applicable*	Dk75059 II	Zorreras Mb.	Limestone	0.709066	0.000026	1
Sorbas	Not applicable*	Dk75059 III	Zorreras Mb.	Limestone	0.709084	0.000022	1
Sorbas	Not applicable*	Dk75059 IV	Zorreras Mb.	Limestone	0.709108	0.000021	1
Sorbas	Not applicable*	Fo1	Zorreras Mb.	Limestone	0.709072	0.000011	2
Nijar	CdIR	$N4_b^*$	Feos Fm.	*Cyprideis sp.*	0.708954	0.000008	2
Nijar	BdC	$N4_t$	Feos Fm.	*Cyprideis sp.*	0.708814	0.000010	2
Nijar	BdC	$N4_b$	Feos Fm.	*Cyprideis sp.*	0.708958	0.000008	2
Nijar	BdC	$N3_t$	Feos Fm.	*Cyprideis sp.*	0.708835	0.000010	2
Nijar	BdC	$N3_b$	Feos Fm.	*Cyprideis sp.*	0.709007	0.000008	2
Nijar	BdC	N2	Feos Fm.	*Cyprideis sp.*	0.708979	0.000006	2
Nijar	BdC	N1	Feos Fm.	*Cyprideis sp.*	0.709037	0.000010	2
Nijar	El Salto del Lobo	Fo3	Feos Fm.	*Cyprideis sp.*	0.709099	0.000012	2
Nijar	El Argamason	Arg-5	Feos Fm.	Ostr. valves	0.709099	0.000012	3
Vera	Not applicable**	V2	Unit 2	*Cyprideis sp.*	0.708764	0.000012	2
Vera	Not applicable**	V1	Unit 2	*Cyprideis sp.*	0.708766	0.000011	2
Vera	CdA	CA10	Unit 2	*Cyprideis sp.*	0.708813	0.000018	4
Vera	CdA	CA8	Unit 2	*Cyprideis sp.*	0.708802	0.000016	4
Vera	CdA	CA7	Unit 2	*Cyprideis sp.*	0.708799	0.000017	4
Vera	CdA	CA5	Unit 2	*Cyprideis sp.*	0.708802	0.000011	4
Vera	CdA	CA4	Unit 2	*Cyprideis sp.*	0.708809	0.000010	4
Vera	CdA	CA1	Unit 2	*Cyprideis sp.*	0.708801	0.000010	4

* *The measurements are performed on the white limestones of the Zorreras Mb. However, the provenance of the samples (section and which of the two imestones) is unknown. As a consequence, the age and cycle also cannot be determined.*

** *The amalyzed samples come from an outcrop an outcrop next to the Cuevas del Almanzora section. However, the stratigraphic log is not available.*

Rhône) and now dried (e.g. the Eosahabi River that flowed from Lake Chad; Griffin, 2002, 2006; Topper et al., 2011; Simon et al., 2017), plus the Eastern Paratethys (Flecker and Ellam, 2006; Krijgsman et al., 2010; Stoica et al., 2016; Grothe et al., 2020) and, possibly, the Atlantic (Manzi et al., 2009; Marzocchi et al., 2016; Vasiliev et al., 2017; García-Veigas et al., 2018; Grothe et al., 2020). Today, water masses strongly influenced by continental water but fully connected to ocean water (e.g. the Mediterranean and its coastal lagoons and estuaries) typically have an oceanic $^{87}Sr/^{86}Sr$ signature (Veizer, 1989; Flecker et al., 2002), because ocean water has a much higher (~100 times) Sr concentration (7.8 mg/l; Palmer and Edmond, 1992) than average river water (0.0780 mg/l; Palmer and Edmond, 1992). Because of the considerable difference in Sr concentration between marine and non-marine-derived Sr^{2+}, a measurable deviation from global ocean $^{87}Sr/^{86}Sr$ ratios will only be achieved by a substantial increase in the source of non-marine Sr^{2+} with respect to the marine-derived Sr^{2+}, similarly to what is observed in the more inland portions of estuaries (e.g. Ingram and Sloan, 1992). Numerical models applied to the Mediterranean Basin suggest that >25% of total water input needs to be fluvial discharge for the water mass to become more sensitive to the non-marine fluxes and evolve an $^{87}Sr/^{86}Sr$ away from the ocean $^{87}Sr/^{86}Sr$ signature towards that of its contributing rivers (Topper et al., 2014).

Late Miocene $^{87}Sr/^{86}Sr$ data show that Mediterranean $^{87}Sr/^{86}Sr$ ratios progressively diverged

from global ocean values during the MSC, before going back to follow the oceanic trend in the Pliocene (Fig. 2.5a). This trend has been interpreted as geochemical evidence for the restriction of Mediterranean-Atlantic connectivity accompanied by a proportional increase in low-salinity water supplied from Eastern Paratethys and/or major peri-Mediterranean rivers (Flecker et al., 2002; Flecker and Ellam, 2006; Vasiliev et al., 2010, 2017; Reghizzi et al., 2018; Grothe et al., 2020). Stage 3 yields the largest range of $^{87}Sr/^{86}Sr$ ratios during the MSC, from values higher than coeval ocean water (0.709027-0.709021; McArthur et al., 2012) to much lower ratios (down to ~0.7085; Fig. 2.5a). Most of the relatively high values (>0.708750) come from marginal areas across the Mediterranean, whereas lower values are from the intermediate basin of Caltanissetta in Sicily (Grossi et al., 2015) and basinal locations accessed through DSDP drilling (Fig. 2.5a; McCulloch and De Deckker, 1989). Combined with the low salinity levels inferred from the Paratethyan ostracods, the Lago-Mare $^{87}Sr/^{86}Sr$ dataset is consistent with negligible ocean water input and multiple isolated lakes fed by local streams.

Stage 3 is not the only time during the late Miocene when $^{87}Sr/^{86}Sr$ ratios drifted away from ratios within error of oceanic values (Fig. 2.5a). Some excursions have also been observed in pre-MSC marginal marine successions (Southern Turkey, Adriatic, Tyrrhenian Sea, Sorbas Basin; Flecker and Ellam, 1999, 2006; Flecker et al., 2002; Schildgen et al., 2014; Modestou et al., 2017; Reghizzi et al., 2017) and in equally marginal PLG sequences (Lugli et al., 2010; Schildgen et al., 2014; Reghizzi et al., 2018; Fig. 2.5a). However, despite the non-oceanic $^{87}Sr/^{86}Sr$ ratio of some pre-MSC and PLG samples, the hypothesis of foraminifera dwelling and gypsum precipitating in endorheic lakes has never been contemplated because several lines of evidence indicated that a Mediterranean-Atlantic connection was present at that time (e.g. calcareous microplankton, marine sulfate of the gypsum, requirement of Atlantic salt for evaporite precipitation to take place; Krijgsman and Meijer, 2008; Lugli et al., 2010; Roveri et al., 2014a; García-Veigas et al., 2018). Although marine indicators in the Lago-Mare sediments (i.e. presence of gypsum with marine-like sulfate isotopic composition in the Balearic, Caltanissetta, Ionian, Levant and Polemi basins, Ricchiuto and McKenzie, 1978; Pierre, 1982; Pierre and Rouchy, 1990; Manzi et al., 2009; García-Veigas et al., 2018; dwarf fauna of in situ-claimed planktonic foraminifera, Corbí and Soria, 2016; $\delta D_{n\text{-alkanes}}$ values in the range of normal marine isotopic values, Vasiliev et al., 2017) are scarcer than in pre-MSC and PLG successions and they are mixed with brackish water indicators (e.g. the same species of Black Sea ostracods everywhere in the Mediterranean; Gliozzi et al., 2007; Grossi et al., 2008; Stoica et al., 2016), these sedimentological, paleontological and geochemical indicators are also regarded as evidence of a Mediterranean water mass that was standing high and was periodically flooding the marginal basins during the Lago-Mare phase (sensu Roveri et al., 2014a). As such, an influence of the Mediterranean water (and strontium) on marginal basins' sedimentary paleoenvironments, which would imply high sea level conditions, cannot be discarded a priori.

In a Mediterranean almost completely filled with oceanic water these deviations,

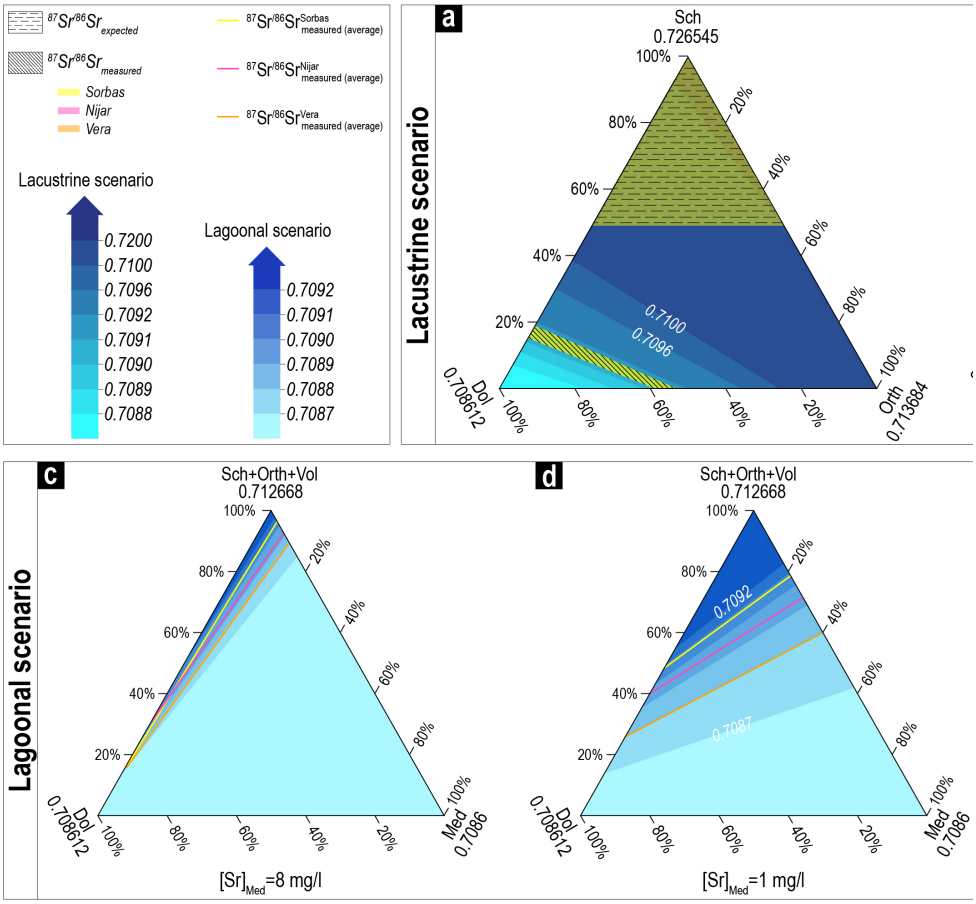

Fig. 2.8 (left and right). *Ternary diagrams of the $^{87}Sr/^{86}Sr$ ratios modelled for both the lacustrine* **(a, b)** *and lagoonal* **(c, d, e)** *scenarios. End member compositions and Sr concentrations are average values for the specific rock types in the catchment as shown in Fig. 2.6b and Table 2.1. These are schist and phyllites (Sch), ortho-derived metamorphic rocks (Orth), volcanic rocks (Vol) and dolostones (Dol). The Mediterranean $^{87}Sr/^{86}Sr$ ratio employed (i.e. 0.7086) corresponds to the midpoint value of the range of values for Lago-Mare $^{87}Sr/^{86}Sr$ ratios derived from intermediate and deep Mediterranean basins (Fig. 2.5a). The Sr concentration of Mediterranean water used to calculate the $^{87}Sr/^{86}Sr$ isofields is 8 mg/l (c), 1 mg/l (d) and 0.5 mg/l (e). The dashed areas of the ternary diagrams highlight the range of $^{87}Sr/^{86}Sr$ ratios anticipated from the outcropping geology shown in Fig. 2.6a for the lacustrine and lagoonal scenarios. The range of $^{87}Sr/^{86}Sr$ ratios measured for each basin (see Fig. 2.5b) is also plotted to facilitate the comparison with the model outputs.*

typically towards lower ratios, require an increase in the proportion of non-marine $^{87}Sr/^{86}Sr$ contributing to the Mediterranean (achieved either by increasing freshwater input or declining

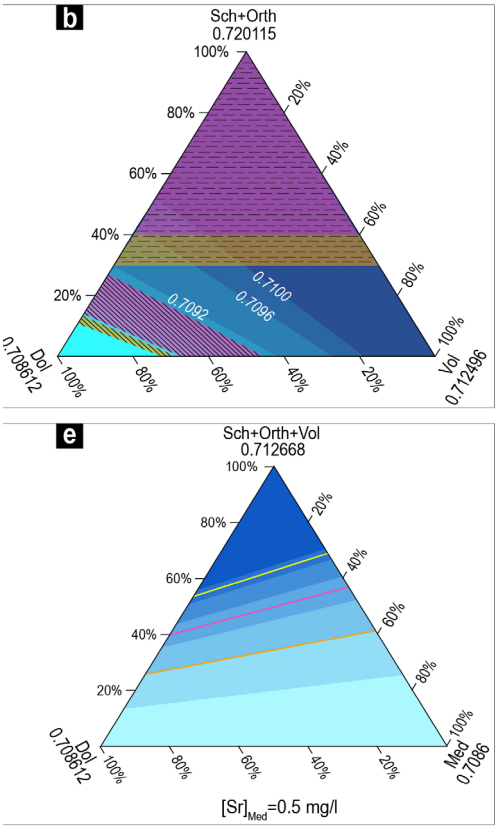

oceanic input) at a time when the oceanic input must have been close to the threshold at which non-marine $^{87}Sr/^{86}Sr$ ratios become analytically distinct from ocean water values. There are three controls on the proportion of fluvial and marine water sources in marginal marine settings:

(i) The freshwater flux which, in the Mediterranean, is modulated on astronomical timescales by the African summer monsoon (Marzocchi et al., 2015) and Atlantic winter storms (Marzocchi et al., 2019).

(ii) The size of the gateway between the marginal basin and the main Mediterranean basin (Topper et al., 2011, 2014);

(iii) The density contrast between the marginal basin and the Mediterranean which drives exchange through the gateway (Topper et al., 2011). In the Mediterranean, density is mainly a function of salinity and reflects the interplay of the fresh and ocean water fluxes and net evaporation (Flecker et al., 2002). Modestou et al., (2017)'s study of the pre-MSC Sorbas Basin demonstrates that even without a reduction in gateway dimension, exchange is inhibited during periods of minimal density contrast, increasing the dominance of the fluvial contribution to the marginal basin sufficiently for the Sr isotope ratio to become analytically distinct from the coeval ocean value.

Correct interpretation of the Lago-Mare Sr isotope dataset as a whole therefore needs to take into account the distribution of the sites, climate variability, catchment changes and the gateways that link the marginal basins with the main Mediterranean as well as the Mediterranean- Atlantic gateway(s). In the case of SE Spain, the gateways that are known to have linked Sorbas, Nijar and Vera basins with each other and the Mediterranean up until the end of PLG deposition may also have had the potential to influence the Sr isotope ratios during the Lago-Mare phase.

2.6.2 Hydrological setting of SE Spain

In the Spanish basins, all the Lago-Mare $^{87}Sr/^{86}Sr$ data but one in Nijar plot outside the error interval of coeval ocean water values (Fig. 2.5b). This pattern of essentially non-oceanic $^{87}Sr/^{86}Sr$

ratios could, in principle, be consistent with the presence of three endorheic lakes, one in each sedimentary basin, with their $^{87}Sr/^{86}Sr$ signature mostly driven by the geochemistry of their catchment-forming lithologies. This conclusion has already been suggested by some authors for the Sorbas (e.g. Aufgebauer and McCann, 2010) and Vera (Benson and Rakic-El Bied, 1991; Caruso et al., 2020) basins based on sedimentological and paleontological observations. Since calcium carbonate incorporates the Sr^{2+} in the water from which it precipitates, if the Sorbas, Nijar and Vera basins were completely isolated lacustrine systems during the Lago-Mare phase, the $^{87}Sr/^{86}Sr$ ratios of the hosted ostracods are expected to fall within the range of $^{87}Sr/^{86}Sr$values resulting from the mixing of only intrabasinal sources (i.e. rivers and groundwaters; Fig. 2.7a).

In the absence of knowledge about the chemistry of ancient river water, $^{87}Sr/^{86}Sr$ ratios of present-day rivers are typically used to reconstruct the paleohydrological regime of a water body at any specific time (e.g. Placzek et al., 2011; Doebbert et al., 2014). Measurements of the strontium concentration and isotope ratios of the rivers feeding the Sorbas, Nijar and Vera basins during the Late Miocene are unknown and no measurements on modern rivers are available. However, because the isotopic composition of river water is a function of the isotopic composition of the lithologies in the watershed (Fig. 2.7; e.g. Brenot, 2006; Peucker-Ehrenbrink et al., 2010; Doebbert et al., 2014; Peucker-Ehrenbrink and Fiske, 2019), some indicators of the paleofluvial geochemistry can be gleaned by analyzing the $^{87}Sr/^{86}Sr$ ratios of the rocks forming the sierras surrounding the basins (Figs. 2.1b, 2.8). Such an approach is justified for the Nijar, Vera and Sorbas basins by the widespread availability of Sr data and by the lithological composition of both the coarse and fine-grained lithofacies and some paleocurrent measurements (Fig. 2.2; Benson and Rakic-El Bied, 1991; Roep et al., 1998; Fortuin and Krijgsman, 2003), which suggest that all the main lithologies forming the sierras today supplied clastics from areas partially emerged during the Lago-Mare phase. All these lithologies differ from each other in their isotopic compositions (Fig. 2.6b). Paleozoic para- and ortho-derived metamorphic rocks and Miocene volcanics are more radiogenic, with $^{87}Sr/^{86}Sr$ from 0.709691 up to 0.722831. In contrast, Triassic-Jurassic dolostones carry less radiogenic $^{87}Sr/^{86}Sr$ (average of 0.708612).

A closer look to the $^{87}Sr/^{86}Sr$ values measured on the Sorbas-Nijar-Vera Lago-Mare ostracods reveals a trend of diminishing values from Sorbas (0.709066-0.709131) to Nijar (0.708835-0.709099) to Vera (0.708764-0.708813; Fig. 2.5b). This trend indicates that from Sorbas to Vera, the water body filling each basin integrated more Sr^{2+} from a lower radiogenic source. In the lacustrine scenario, rivers draining the Triassic-Jurassic carbonates could have provided dissolved Sr^{2+} with a low radiogenic $^{87}Sr/^{86}Sr$ signature. Given that these carbonates are more widespread in the catchment of Vera than in Nijar and they are very rare in Sorbas (Fig. 2.6a), the range of $^{87}Sr/^{86}Sr$ values measured on the Sorbas-Nijar-Vera ostracods might be the result of mixing of higher and lower intrabasinal water sources. However, modelling the $^{87}Sr/^{86}Sr$ resulting from the mixing of only intrabasinal rivers indicates that Sr^{2+} provided by

the Triassic-Jurassic carbonates would need to contribute >50% of the total Sr^{2+} released into each basin in order to reproduce the $^{87}Sr/^{86}Sr$ ratios measured on the ostracods (Figs. 2.10a-b). Although the exact fraction of Sr^{2+} provided by each of the rivers is unknown, such a high contribution from carbonates is at odds with the outcropping geology in the catchments which are dominated by the other rock types (Fig. 2.6a), even adjusting for the higher solubility of carbonates as we have done here. Groundwater, which has been shown to make significant contributions to Sr budgets (e.g. Hart et al., 2004; Schildgen et al., 2014), is an alternative water source. The role of past groundwaters is difficult to assess (e.g. Placzek et al., 2011; Doebbert et al., 2014) and present-day measurements of the groundwater system of the region (e.g. Doebbert et al., 2014) are also lacking. However, geological cross-sections of the area (see Sanz de Galdeano and Santamaría-López, 2019 and references therein) reveal a subsurface geology similar to the one exposed to subaerial weathering. This means that if a substantial groundwater network was present in the region during the Lago-Mare time, it is likely that it was adding to the hydrologic system isotopic compositions and concentrations similar to the one provided by surface water.

The results of modelling the lacustrine $^{87}Sr/^{86}Sr$ ratios of the three Spanish basins based on their catchment geology suggest that these would have been as low as 0.7092 in Vera, 0.7096 in Nijar (Fig. 2.8b) and 0.7100 in Sorbas (Fig. 2.8a), all values substantially higher than those measured on the ostracods (Fig. 2.5b; Figs. 2.8a-b). This mismatch between the $^{87}Sr/^{86}Sr$ values measured on ostracods and $^{87}Sr/^{86}Sr$ ratios expected from the lake water implies that, to satisfy the mixing relationships, there was an additional contribution of less radiogenic water during deposition of the Lago-Mare carbonates in Sorbas and mudstones in Nijar and Vera. One possibility is that the source of less radiogenic Sr^{2+} was the dissolution of pre-existing evaporites in the basins, which is a process observed to have played a major role in the formation of the late Tortonian gypsum deposits of the internal Betic basins (Fig. 2.1a; e.g. Campo Coy, Lorca and Fortuna; Ortí et al., 2014; García-Veigas et al., 2019; Artiaga et al., 2020), and/or Stage 1 brines remained in the basins after their disconnection from the Mediterranean during Stage 2. However, Stage 1 gypsum has $^{87}Sr/^{86}Sr$ ratios similar to coeval sea water (Reghizzi et al., 2018) and this is too high to depress the fluvial signal to the $^{87}Sr/^{86}Sr$ ratios measured on Lago-Mare ostracods. Stage 2 halite, which potentially have sufficiently low $^{87}Sr/^{86}Sr$ to draw modelled values down to the ostracod values (Fig. 2.5a), has not been found in these basins and so cannot be a dissolved source of low $^{87}Sr/^{86}Sr$ water during Stage 3. If local streams, groundwater and Stage 1 evaporites/water cannot account for the $^{87}Sr/^{86}Sr$ ratios measured on Lago-Mare ostracods, the only left source of low radiogenic Sr is the Mediterranean water mass during Stage 3. For the Mediterranean to have contributed to these marginal basins, its base level must have been fairly high during the Lago-Mare.

2.6.3 Sr isotope consequences of the lagoonal scenario for the Lago-Mare story

The main challenge to modelling the input of Mediterranean water into the Spanish marginal basins is its compositional uncertainty during the Lago-Mare. The literature contains interpretations of Mediterranean water in the Lago-Mare as being totally marine (e.g. Carnevale et al., 2018) or brackish (McCulloch and De Deckker, 1989; Roveri et al., 2008a) or density-stratified (Roveri et al., 2014c; Marzocchi et al., 2016; Vasiliev et al., 2017; García-Veigas et al., 2018) with a hypersaline brine of unknown composition possibly resting at the bottom (Marzocchi et al., 2016; Gvirtzman et al., 2017; García-Veigas et al., 2018). Each compositional interpretation involves different contributing water sources (fluvial, epi-continental and oceanic), and each therefore suggests a different Mediterranean $^{87}Sr/^{86}Sr$ and [Sr]. Fortunately, well-preserved in situ Lago Mare ostracods (e.g. Iaccarino and Bossio, 1999; Grossi et al., 2015) are present in more central Mediterranean basins like the intermediate basin of Caltanissetta (Grossi et al., 2015) and the deeper Balearic and Levantine basins (e.g. McCulloch and De Deckker, 1989; Iaccarino and Bossio, 1999). Regardless of the salinity of the Mediterranean water mass at the time, the $^{87}Sr/^{86}Sr$ of these central basin ostracods, which are considered to represent phases of highstands of the Mediterranean base-level (Manzi et al., 2009), provides us with an indication of its $^{87}Sr/^{86}Sr$ fingerprint. During the Lago-Mare, the $^{87}Sr/^{86}Sr$ ratio of the central Mediterranean basins was ~0.7085-0.7087 (Fig. 2.5a; McCulloch and De Deckker, 1989; Grossi et al., 2015), low relative to the measured values in the Spanish marginal basins.

More challenging is obtaining a reliable value for strontium concentration, which under normal circumstances varies with salinity such that [Sr] equal to the modern seawater (i.e. 8 mg/l; Veizer, 1989) is around two orders of magnitude greater than that of global river water (0.0780 mg/l; Palmer and Edmond, 1992). However, given that the latest Miocene Mediterranean record contains fossils that indicate it was not entirely marine and gypsum intervals indicating higher salt concentrations than purely fresh water, it is likely that Sr concentration during the Lago-Mare lays somewhere between these two end-member values.

To evaluate the impact of this uncertainty, we modelled the Mediterranean input with a range of different Sr concentrations (Figs. 2.10c-e). These results indicate that the combination of Spanish catchment rocks and Mediterranean-derived water can reproduce the $^{87}Sr/^{86}Sr$ratios of the Spanish ostracods in both the extreme (and unlikely) scenarios of a Mediterranean water mass carrying a present-day like Sr concentration (Fig. 2.8c) or an extremely low, fluvial-like Sr concentration (Fig. 2.8e). The difference among the scenarios resides in the quantity of Mediterranean water required to explain a fixed $^{87}Sr/^{86}Sr$ value, which varies from <20% for all four basins assuming a sea water [Sr] (Fig. 2.8c) up to ~60-70% for the Vera results where the [Sr] approaches freshwater concentrations (Fig. 2.8e). These modelling results are therefore compatible with a scenario in which the main Mediterranean Basin (or at least its western domain) was sufficiently full to allow it to contribute with water to these marginal Spanish basins during the Lago-Mare subaqueous sedimentation. This is consistent with published stratigraphic and sedimentological arguments concerning the Sorbas and Nijar basins (Fortuin

and Krijgsman, 2003; Omodeo Salé et al., 2012). It is also compatible with the homogeneity of the ostracod assemblages, not only among Spanish basins (including Malaga; Guerra-Merchán et al., 2010), but throughout the Mediterranean and the Eastern Paratethys, which points to a water body stretching from the Alborán margins as far as Eastern Europe (Stoica et al., 2016; Van Baak et al., 2016). Considerations over the $^{87}Sr/^{86}Sr$ ratios measured on the Paratethyan ostracods in SE Spain also counter the hypothesis that these Spanish basins persisted as isolated lakes throughout the Lago-Mare phase until the transition to the Zanclean (Aufgebauer and McCann, 2010; Caruso et al., 2020).

One further consideration is whether this scenario is compatible with seismic-based studies of the western Mediterranean's offshore record. Gypsum-bearing seismic units with different seismic facies and erosional base and top surfaces have been recognized in different intermediate and deep subbasins. The facies variability has been interpreted as being indicative of unique hydrological settings for each isolated subbasin, with the erosional surfaces ascribed to subaerial erosion during exposure periods (e.g. Maillard and Mauffret, 2006; Maillard et al., 2014; Thinon et al., 2016; Lymer et al., 2018; Raad et al., 2021). These conclusions are clearly at odds with a Stage 3 scenario of a near full Mediterranean, but alternatives to these interpretations are not provided. However, recent research suggests that these seismic features may be open to alternative explanations. Deep erosional surfaces, for example, are not only formed as a consequence of subaerial exposure, but can also form in deep-water well-stratified settings (Gvirtzman et al., 2017; Kirkham et al., 2020). Lateral facies changes, which are common in marginal, gypsum-precipitating settings (Piedmont Basin, Dela Pierre et al., 201l; Po Plain-Adriatic Foredeep, Ghielmi et al., 2013; Northern Apennines, Roveri et al., 2001; Caltanissetta Basin, Roveri et al., 2008b), may result from precession-controlled vertical oscillations of the chemocline in a deeper, stratified water column (e.g. Sabino et al., 2020). In addition, gypsum precipitating in endorheic, freshwater-fed basins is inconsistent with the marine isotopic signature of sulfate recovered from deep-water sites (e.g. Pierre and Fontes, 1978; Ricchiuto and McKenzie, 1978; Pierre, 1982; Pierre and Rouchy, 1990; García-Veigas et al., 2018).

It therefore seems possible to reconcile offshore with high Mediterranean water level conditions during the final stage of the MSC. In view of the foregoing, we stress that alternatives should be considered in future studies targeting/modeling the deep record and discussed in light of the observations/conclusions provided from the outcrops.

2.6.4 Was the Mediterranean base-level fluctuating with precessional periodicity?

This compilation of Sr isotope measurements on ostracods shows that a trend exists in the $^{87}Sr/^{86}Sr$ data of the Spanish basins (i.e. Sorbas shows more radiogenic values than Vera and with Nijar in between; Fig. 2.5b). Mass-balance calculations show that for a constant value of Mediterranean Sr concentration the percentage of Mediterranean water required to explain

the measured Sr isotope ratios increases from Sorbas to Nijar and to Vera (Figs. 2.8c-e). This is broadly compatible with their spatial relationship to the Mediterranean, with the Sorbas Basin located more landward relative to the Nijar and Vera basins. However, both the sedimentary successions and the Sr data (Fig. 2.5b) suggest that the amount of Mediterranean water entering the basins also varied through time (Fig. 2.9).

The alternation of continental conglomerate-sandstone and lagoonal mudstones of the Upper Mb. of the Feos Fm. in the Nijar Basin indicates that base-level changes were controlling the sedimentation during the Lago-Mare phase, possibly with precessional periodicity (Fortuin and Krijgsman, 2003; Omodeo Salé et al., 2012). Since Mediterranean water contributed to the hydrology of the lagoonal environment (Figs. 2.9c-e), it follows that Mediterranean fluctuations in water level are likely to have mirrored and driven the base-level changes seen in the Nijar Basin. During the arid phase of the cycle (i.e. precession maxima-insolation minima) fluvial conglomerates were being deposited by the intrabasinal rivers (Fig. 2.2). This means that the Nijar Basin could not have been receiving Mediterranean water during this phase (Fig. 2.9a) at least in the northern area of the basin, where the studied sections are located (Fig. 2.1b). Lagoonal deposition in Nijar occurred in the humid phase of the precessional cycle (Fig. 2.2), therefore indicating that a base-level rise occurred at the conglomerate-mudstone transition. The uppermost two mudstone horizons in the astronomically-tuned Barranco de los Castellones section show that mudstone deposition may have been accompanied by a systematic change in the $^{87}Sr/^{86}Sr$ values where the higher ratios, indicative of a more fluvially-dominated signal, come from immediately above the transition from fluvial conglomerates to lacustrine pelitic sedimentation. This sedimentary transition is interpreted as the onset of a transgression in each cycle (Fortuin and Krijgsman, 2003; Omodeo Salé et al., 2012) and it is therefore a moment at which only a limited amount of Mediterranean water was entering the basin (Fig. 2.9b). The less radiogenic values, suggesting a larger contribution from the Mediterranean, occur just below the transition to the overlying continental facies of the next precession cycle (Fig. 2.9c), when the basin, before emptying again (Fig. 2.9d), was more replenished. A dynamic contribution of Mediterranean water also seems the most logical way to explain the episodic appearance of lagoonal carbonates in the otherwise continental Sorbas Basin. Our observation that Sr values in Sorbas cannot be explained by simple mixing of local source water suggests that a short-lived Sorbas-Mediterranean connection was episodically established via one, if not both, of the two neighbouring basins during highest water level intervals (Fig. 2.9c).

A fluctuating Mediterranean base-level may also be mirrored in the ostracod record which, like strontium, correlates closely with the sedimentary facies. In the Vera and Nijar basins, a low-diversity assemblage mainly dominated by the euryhaline and shallow water *Cyprideis* sp. and indicative of more fluctuating environmental conditions characterizes the basal mudstones (Figs. 2.9a-b), while at the top a plethora of more stenohaline and deeper water species with Paratethyan affinity and indicative of a more stable environment occurs (Figs. 2.9b-c; Bassetti

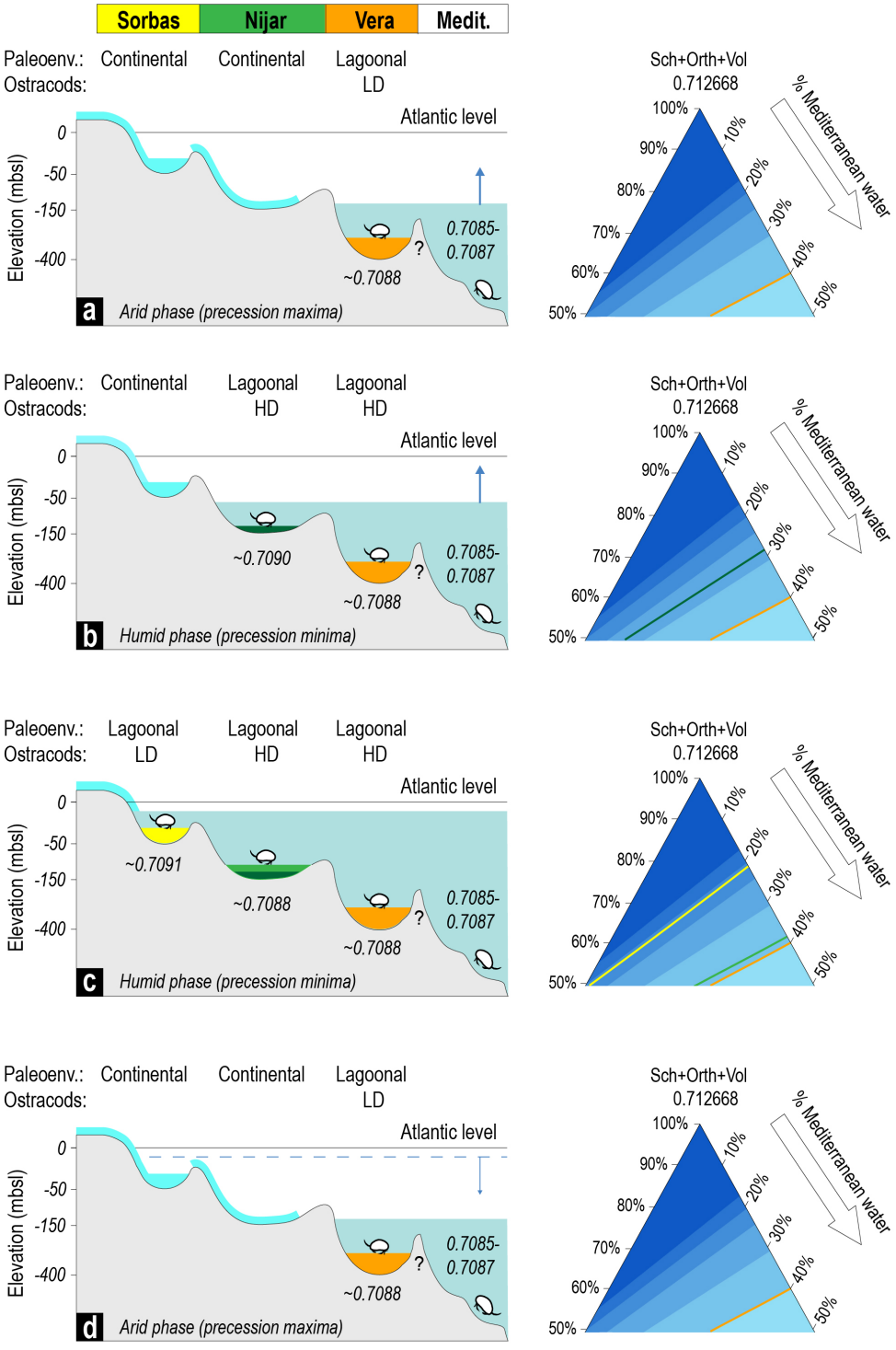
Sorbas
Nijar
Vera
Medit.
Paleoenv.: Continental Continental Lagoonal
Ostracods: LD
Atlantic level
Elevation (mbsl)
0
-50
-150
-400
0.7085-
0.7087
?
~0.7088
a
Arid phase (precession maxima)
Sch+Orth+Vol
0.712668
% Mediterranean water
100%
90%
80%
70%
60%
50%
10%
20%
30%
40%
50%
Paleoenv.: Continental Lagoonal Lagoonal
Ostracods: HD HD
~0.7090
b
Humid phase (precession minima)
Paleoenv.: Lagoonal Lagoonal Lagoonal
Ostracods: LD HD HD
~0.7091
~0.7088
c
Humid phase (precession minima)
Paleoenv.: Continental Continental Lagoonal
Ostracods: LD
d
Arid phase (precession maxima)

Fig. 2.9 (previous page). *Schematic illustration of the paleohydrological evolution of the Sorbas (yellow), Nijar (light and dark green) and Vera (orange) basins during a precessional cycle of the Lago-Mare phase.* **(a)** *Fluviatile accumulation occur in Nijar and Sorbas during arid phases at precession maxima (insolation minima), while the Mediterranean base-level is at its minimum and only enters the deeper Vera Basin.* **(b)** *Orbitally-driven fluctuations of the Mediterranean base-level cause the transition, in Nijar, from continental to lagoonal conditions during humid phases at precession minima (insolation maxima). Water depth and ostracod species diversity increase in Vera. Continental conditions persist in Sorbas.* **(c)** *Before entering the arid conditions again,* **(d)** *the Mediterranean base-level reach the climax. Ostracods diversity further increase in Vera and Nijar and $^{87}Sr/^{86}Sr$ ratios among the two basins are leveled. Mediterranean waters penetrate in the Sorbas Basin, interrupting the fluviatile sedimentation and bringing few species of ostracods. The triangular plot on the right side (portion of Fig. 2.8d) aims to visualize the different amount of water necessary to explain the $^{87}Sr/^{86}Sr$ data of each basin. The dark green line corresponds to the $^{87}Sr/^{86}Sr$ data from the base of the mudstone horizons in the Barranco de los Castellones section (see Fig. 2.2). Light green like corresponds to the $^{87}Sr/^{86}Sr$ data from the top of the mudstone horizons in the Barranco de los Castellones section (see Fig. 2.2). Ostracods data are from Roep and Van Harten (1979) for Sorbas, Bassetti et al. (2006) for Nijar and Stoica et al. (2016) for Vera. LD: Low diversity; HD=High diversity. The depth scale is from the depth data from the base of the Pliocene (see paragraph 2.6.4 for explanation and references).*

et al., 2006; Stoica et al., 2016; Caruso et al., 2020). This trend suggests that during the lowstand phases in each of the two basins (Figs. 2.9a-b) physical and chemical conditions were only suitable for species more tolerant to harsh and fluctuating environmental conditions, while only during the highstands (Figs. 2.9b-c) more favorable and stable environmental conditions required by the Paratethyan species were created. The full Paratethyan contingent apparently never reached the Sorbas Basin, where only few opportunistic species are found (Roep and Van Harten, 1979; Aufgebauer and McCann, 2010). The lower diversity with respect to the adjacent basins suggests that environmental parameters in Sorbas did not evolve sufficiently favorable conditions for the Black Sea ostracods to flourish, possibly because Mediterranean incursions and retreats happened only over a relatively short period of time (not quantifiable with our dataset). This is in agreement with the ephemeral character of the lagoonal environment suggested by the intercalation of thin and spatially-confined limestones in a dominantly continental succession (Fig. 2.3b; Aufgebauer and McCann, 2010).

The entrance of Mediterranean water in the few tens of meters deep Sorbas Basin (Roveri et al., 2019a) means that Mediterranean base-level was standing slightly beneath if not at the level of the Atlantic during the highstand phases (Fig. 2.9c). Conversely, the deepest Vera Basin provides us with an idea of the lower limit of the fluctuations of the base level. The persistence of fine sedimentation in Vera through the Lago-Mare phase (Fig. 2.2) and rather constant

vertical trend of the Sr isotope ratio (Fig. 2.5b) indicate that even though the base level of the Mediterranean has changed over time, the amount of water delivered to the basin during the lowstand (Fig. 2.9a) and highstand (Fig. 2.9c) phases did not change enough to expose the basin subaerially, to trigger a facies change or to shift the Sr signature of the lagoon towards more local sources' values as is seen in Nijar. This means that the Mediterranean base-level did not drop beneath the bottom of the Vera Basin, estimated to stand at 400-500 m at the base of the Pliocene (Ott d'Estevou et al., 1990), or beneath its sill height if there was one. Putting together all these sedimentological and geochemical constrains, we suggest that (western) Mediterranean base-level during the Lago-Mare was high, probably close to the Atlantic level and that it fluctuated by a maximum of ~400±100 m per precession cycle. The inferred precessional character of the lithological cyclicity (Krijgsman et al., 2001; Fortuin and Krijgsman, 2003; Roveri et al., 2009; Omodeo Salé et al., 2012) suggests that an orbitally-forced climatic driver lies behind such variations.

2.6.5 Future direction: merging together marginal and deep basins observations

Considering that the Mediterranean Basin was subdivided in a complex system of variably deep sub-basins separated by physical thresholds of largely unknown depths (Amadori et al., 2018; Camerlenghi et al., 2019), a high and fluctuating Mediterranean base-level cannot be straightforwardly extrapolated to the whole Mediterranean on the basis of data exclusively from the far western end. A high Mediterranean base-level during the Lago-Mare has always been regarded at odds with Mediterranean-wide seismic (e.g. Maillard and Mauffret, 2006; Maillard et al., 2014; Thinon et al., 2016; Lymer et al., 2018; Amadori et al., 2018; Micallef et al., 2018, 2019; Camerlenghi et al., 2019; Kartveit et al., 2019; Madof et al., 2019; Raad et al., 2021; Spatola et al., 2020) and modelling (Garcia-Castellanos et al., 2020 and references therein) interpretations, which mostly point to a low Mediterranean water level in the latest Messinian and, as a consequence, to a sudden and catastrophic restoration of high sea-level conditions at the Miocene/Pliocene boundary. However, we showed that some data, mostly from the margins ($^{87}Sr/^{86}Sr$ ratios and W-E homogeneity of Paratethyan ostracod assemblages), but also from deeper, offshore settings (sulfate isotopes of the Upper Evaporites units) are not explainable in the lacustrine scenario, whereas arguments apparently in favor of it may have alternative explanations that, however, are rarely addressed and discussed. Furthermore, a base-level fluctuating hundreds of meters in a Mediterranean compartmentalized into sub-basins of variable depth and area do not necessarily imply that marginal and basinal observations are mutually exclusive, with the erosional features and fluvial deposits imaged by the seismic that may have been formed during lowstand phases. Waiting for the success of the on-going Mediterranean drilling proposals (DEMISE, DREAM and IMMAGE; Camerlenghi and Aloisi, 2020) that would provide the Messinian community with cores potentially suitable to solve the onshore-offshore correlation riddle, we suggest that future studies targeting the deep basinal

successions should examine whether base-level fluctuations of hundreds of meters in a relatively full Mediterranean could reproduce the sedimentological, paleontological and geochemical features observed in existing seismic profiles and wells.

2.7 Conclusions

Compiled $^{87}Sr/^{86}Sr$ data from the ostracods that inhabited the adjoining Sorbas, Nijar and Vera basins during the Lago-Mare along with strontium mass-balancing modeling and existing sedimentological and paleontological data shed new light on the terminal Lago-Mare phase of the MSC. The $^{87}Sr/^{86}Sr$ ratios from these three Spanish basins cannot be explained by an environment shaped only by local river and groundwater inputs, or with Mediterranean Stage 1 Sr retained in the system after the isolation of the basins during Stage 2 or in solution into groundwaters draining buried PLG deposits, but require an additional external water source with a low radiogenic Sr isotope ratio. Instead, the measured isotopic data are reproduced when the Mediterranean is added to the hydrologic system. This is compatible with a near full Mediterranean during the Lago-Mare rather than the hypothesis that these Spanish basins were isolated lakes perched above a deeply desiccated Mediterranean. Combined analysis of sedimentological, paleontological and geochemical data suggest that Mediterranean base-level during the Lago-Mare fluctuated by several hundred meters with precessional periodicity, with the lowstand reached during the arid phase of the cycle (precession maxima-insolation minima) and the highstand reached during the humid phase (precession minima-insolation maxima). Consequently, we conclude that sedimentation in the marginal Spanish basins (and in other marginal Mediterranean systems) during the wet precessional phases of the Lago-Mare stage occurred in a relatively full Mediterranean.

Acknowledgments

This research was supported by the project SALTGIANT-Understanding the Mediterranean Salt Giant, a European project which has received funding from the European Union's Horizon 2020 research and innovation program, under the Marie Sklodowska-Curie [grant agreement No 765256]. This work was further partly supported by NWO 813.02.007 to C.J. Beets. We are very grateful to the three anonymous reviewers and the journal editor, with their valuable feedback contributed to the success of the manuscript.

Looking towards the Monviso from the left bank of the Tanaro river.

3

MULTI-PROXY INVESTIGATION OF THE POST-EVAPORITIC SUCCESSION OF THE PIEDMONT BASIN (POLLENZO SECTION, NW ITALY): A NEW PIECE IN THE STAGE 3 PUZZLE OF THE MESSINIAN SALINITY CRISIS

Andreetto, F., Mancini, A.M., Flecker, R., Gennari, R., Lewis, J., Lozar, F., Natalicchio, M., Sangiorgi, F., Stoica, M., Dela Pierre, F., Krijgsman, W.

ABSTRACT

Paleoenvironmental reconstruction of the Mediterranean Basin at the end of the Messinian Salinity Crisis (MSC) is contentious. One section that records this final Stage 3 is the Pollenzo Section in the Piedmont Basin (NW Italy). Here, we present new stratigraphic, sedimentological, petrographic, micropaleontological (ostracods, calcareous nannofossils, foraminifera, dinoflagellates) and geochemical ($^{87}Sr/^{86}Sr$ ratios) data from the Cassano Spinola Conglomerates (CSC) and interpret the paleoenvironment of this northernmost tip of the Mediterranean Basin. The CSC comprise three depositional units: members A and C, which were deposited subaqueously, and the intervening member B, which is continental. The CSC is topped by a ~50 cm-thick black layer, which is directly overlain by the open marine Argille Azzurre Fm. of early Zanclean age. Our investigation reveals that member A is largely barren of autochtonous microfossils, except for an almost monospecific ostracod assemblage of Cyprideis torosa at the top, which indicates shallow-water (<30 m) conditions. Paratethyan ostracods and, possibly, taxa of calcareous nannofossils adapted to low-salinity water first occur in member C. $^{87}Sr/^{86}Sr$ ratios measured on ostracod valves from the member A/B transition (0.708871-0.708870) and member C (0.708834-0.708746) are lower than the coeval Messinian seawater values (~0.709024) and the $^{87}Sr/^{86}Sr$ ratios of a hypothetical lake filling Piedmont (>0.7090) estimated by means of the present-day $^{87}Sr/^{86}Sr$ signature of the Po river, the main drainage system of Northern Italy that receives the weathering products (including ions) of the Alps and Apennines. These values are likely to reflect the mixing of local high $^{87}Sr/^{86}Sr$ river water with low $^{87}Sr/^{86}Sr$ from the Mediterranean, which at the time was dominated by inputs from Eastern Paratethys, circum-Mediterranean rivers and Atlantic Ocean. Our results suggest that, at times during the final stage of the MSC, the Piedmont Basin was hydrologically connected with the main Mediterranean Basin. At regional scale, this implies that the water level in the Mediterranean Basin was relatively high.

This chapter is peer-reviewed and published as:
Andreetto, F., Mancini, A.M., Flecker, R, Gennari, R., Lewis, [...], Krijgsman, W., 2022. Multi-Proxy investigation of the post-evaporitic succession of the Piedmont Basin (Pollenzo section, NW Italy): a new piece in the Stage 3 puzzle of the Messinian Salinity Crisis. Palaeogeography, Palaeoclimatology, Palaeoecology, 594.

3.1 Introduction

The terminal Stage 3 (5.55-5.332 Ma) of the Messinian Salinity Crisis (MSC) in the Mediterranean (5.97-5.332 Ma; Roveri et al., 2014a) has attracted attention over the last two decades as attempts are made to integrate a variety of different data of this interval (Roveri et al., 2008a; Andreetto et al., 2021a). The nub of the controversy concerns the isolation or connectivity between the Stage 3 depocentres. One end-member hypothesis argues that Stage 3 sedimentation happened in endorheic lakes (e.g. Hsü et al., 1973a, 1978a; Cita et al., 1978, 1990; Orszag-Sperber et al., 2000; Ryan, 2009; Madof et al., 2019, 2022; Caruso et al., 2020; Heida et al., 2021; Raad et al., 2021). The other suggests that water sources such as Atlantic and/or Eastern Paratethys and large Mediterranean rivers (e.g. Nile and Rhône) filled the Mediterranean sufficiently to link more marginal and deeper subbasins together (McCulloch and De Deckker, 1989; Roveri et al., 2008a, 2014b, c; Manzi et al., 2009, 2016a; Marzocchi et al., 2016; Stoica et al., 2016; Gvirtzman et al., 2017; Pellen et al., 2017; Vasiliev et al., 2017; García-Veigas et al., 2018), at least episodically (Andreetto et al., 2021b). Much of this controversy originates from the interpretation of the Stage 3 fossil records, which yield both marine and brackish, Paratethys-derived fossils (Benson, 1978; Cita et al., 1978; Iaccarino and Bossio, 1999; Roveri et al., 2008a; Guerra-Merchán et al., 2010; Cosentino et al., 2012; Popescu et al., 2015, 2021; Pellen et al., 2017; Andreetto et al., 2021a for further references). Associations mixing fossils with different ecological requirements always pose a challenge to the reconstruction of the paleodepositional environment(s), because it is often unclear which are reworked and which coeval with sedimentation (e.g. Bright et al., 2018).

The sub-basins at the periphery of the Mediterranean system are a good location for testing the isolated/connected hypothesis, since evidence of connectivity with the Atlantic and/or Eastern Paratethys requires the Mediterranean Basin to have been relatively full. The Piedmont Basin at the northernmost tip of the Mediterranean system, which was, during the late Messinian, enclosed on three sides by the Alps and the Apennines and open to the Mediterranean to the east via the Po Plain foredeep and Adriatic Basin (Fig. 3.1a; Boccaletti et al., 1990; Foeken et al., 2003; Beltrando et al., 2010; Cosentino et al., 2018), meets these geographical criterion. The Cassano Spinola Conglomerates (CSC) assigned in the Piedmont Basin to Stage 3 (Dela Pierre et al., 2011) have, however, received far less attention than both pre-Stage 3 deposits in the same region (Irace et al., 2005; Dela Pierre et al., 2002, 2007, 2011, 2012; 2014, 2015; Lozar et al., 2010, 2018; Violanti et al., 2013; Natalicchio et al., 2014, 2017, 2019, 2021; Gennari et al., 2020; Sabino et al., 2020, 2021; García-Veigas et al., 2021; Pellegrino et al., 2021) and time-equivalent deposits exposed onland elsewhere in the Mediterranean (see Andreetto et al., 2021a). Existing studies of the CSC have largely focused on the paleontological study of the macrofossiliferous content (Sardella, 2008; Angelone et al., 2011; Colombero et al., 2013, 2014, 2017; Harzhauser et al., 2015; Grunert et al., 2016; Carnevale et al., 2018), whereas few papers have explored the micropaleontological content and geochemical signatures of its

fine-grained subaqueous portions (Sturani, 1973; Trenkwalder et al., 2008; Esu and Popov, 2012), which might contain the evidence of the hydrological input from the Mediterranean Basin.

In this paper we present results from a continuous exposure of the CSC preserved in the Pollenzo section. These include lithological, sedimentological, micropaleontological (ostracods, foraminifera, calcareous nannofossils, dinoflagellates) and geochemical ($^{87}Sr/^{86}Sr$ ratios) analyzes. The results will be discussed in the context of evolving base level and hydrological changes simultaneously affecting the Mediterranean and impacting its connectivity with its northernmost branch.

3.2 Geological setting

The Piedmont Basin (NW Italy, Fig. 3.1a) is a wedge-top basin that developed on a tectonic wedge of Alpine, Ligurian and Adria basement units juxtaposed during the mesoalpine collisional event between the Adriatic promontory and the European plate (e.g. Schmid and Kissling, 2000; Carrapa and García-Castellanos, 2005; Beltrando et al., 2010). Since the late Oligocene, the basin was involved in N-verging Apennine tectonics that finally resulted in overthrusting on the Padane foredeep along the Pliocene-Pleistocene Padane Thrust Front (e.g. Mosca et al., 2009; Rossi, 2017; Ghielmi et al., 2019). The Piedmont Basin comprises 4000-5000 m of upper Eocene-Holocene sediments. The upper Eocene-lower Oligocene units consist of continental and shallow marine sediments grading up into upper Oligocene-upper Miocene deeper water hemipelagites with interbedded turbiditic sandstones recording the main accretionary phases of the Apennine fold and thrust belt (Rossi, 2017). Gypsum bodies and hyposaline sediments bearing Paratethyan fossils were deposited during the MSC (Sturani, 1973; Dela Pierre et al., 2011; Ghielmi et al., 2019). MSC deposits reach a maximum thickness in the Savigliano (~500 m; Irace et al., 2009) and Alessandria sub-basins (~800 m; Irace et al., 2009), where they are buried underneath km-thick Plio-Quaternary deposits (Figs. 3.1a-b). Zanclean marine deposits seal the MSC succession (Trenkwalder et al., 2008; Violanti et al., 2009, 2011).

3.3 The Messinian of Piedmont

3.3.1 General stratigraphy and architecture

Following the stratigraphic scheme developed by Dela Pierre et al. (2011) along the south-western margin of the Piedmont Basin (Langhe in Fig. 3.1a), the Messinian succession comprises, from bottom to top, the following lithostratigraphic units (Fig. 3.1b): the Sant'Agata Fossili Marls (SAF) representing the pre-MSC interval and, in the deeper part of the Piedmont Basin, part of MSC Stage 1; the Primary Lower Gypsum Unit (PLG), Vena del Gesso Fm. or Gessoso Solfifera Fm., entirely deposited during MSC Stage 1; the Valle Versa Chaotic Complex (VVC), equivalent of the Resedimented Lower Gypsum Unit (RLG) of Roveri et al. (2014a) and

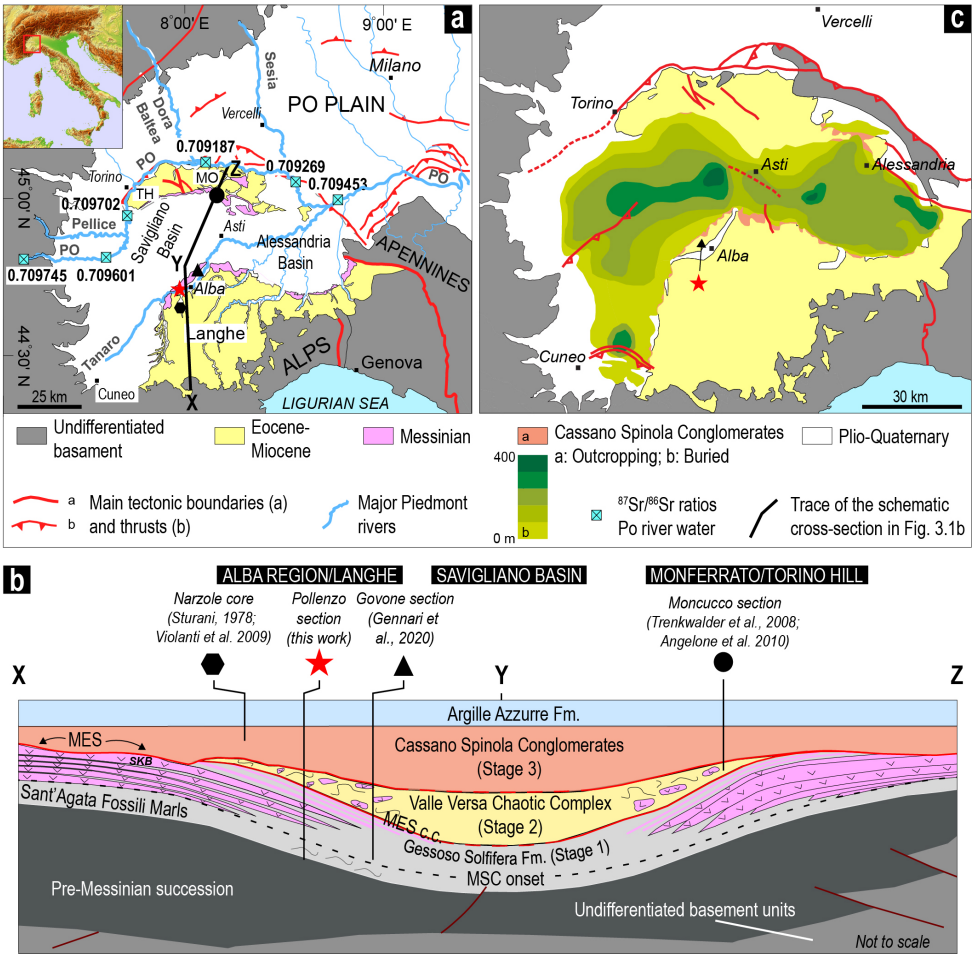

Fig. 3.1. (a) *Structural sketch map of the Piedmont Basin showing the location of the studied Pollenzo section (red star) and of other sites studied for their Stage 3 sedimentary record (black hexagon: Narzole core; black triangle: Moncucco section) or mentioned in the text (Govone section; black circle). The* $^{87}Sr/^{86}Sr$ *ratios for the Po river water (from Marchina et al., 2018) employed to constrain the* $^{87}Sr/^{86}Sr$ *signature of a hypothetical Piedmont lake (see paragraph 3.6.2 for insights) is also shown. TH: Torino Hill; MO: Monferrato.* **(b)** *Schematic cross-section through the Piedmont Basin emphasizing the latero-vertical relationships between the MSC and pre-MSC lithostratigraphic units (modified from Dela Pierre et al., 2011). The trace of the cross section is reported in Fig. 3.1a. SKB: Sturani key-bed; MES: Messinian erosional surface; MES c.c.: correlative conformity of the Messinian erosional surface.* **(c)** *Surface and subsurface distribution of the CSC in the Savigliano and Alessandria Basins (modified from Irace et al., 2009).*

deposited during MSC Stage 2; the Cassano Spinola Conglomerates (CSC) representing (at least part of) MSC Stage 3.

The Sant'Agata Fossili Marls (Tortonian-Messinian) consist of shelf to slope calcareous microfossil-bearing marls and organic-rich laminated shales arranged in 2-3 m-thick sedimentary cycles related to precession (Lozar et al., 2010, 2018; Dela Pierre et al., 2011; Violanti et al., 2013). At 5.97 Ma gypsum precipitation started at the basin margins, synchronously to other potentially silled basins around the Mediterranean margins (Krijgsman et al., 1999; Lugli et al., 2010; Manzi et al., 2013). The onset of gypsum deposition is progressively younger towards the depocenter of the Piedmont Basin, where gypsum layers are replaced by marls (Dela Pierre et al., 2011; Ghielmi et al., 2019; Gennari et al., 2020; Fig. 3.1b). Barren shales are interbedded with both the gypsum and the marl layers (Dela Pierre et al., 2011). The PLG unit in the Piedmont Basin has similar lithofacies and stratigraphic stacking pattern of coeval gypsum deposits described in other Mediterranean marginal localities (e.g. Sorbas and Nijar basins in SE Spain, Vena del Gesso Basin in the Northern Apennines and Zakynthos; Krijgsman et al., 1999a, b; Lugli et al., 2010; Manzi et al., 2013; Karakitsios et al., 2017b). In these settings, the lithologic cyclicity was ascribed to precession-driven climate changes and the sedimentary cycles tuned to the precession curve, with gypsum and marls reflecting drier climate at precession maxima (insolation minima) and the intervening shales recording more humid conditions at precession minima (insolation maxima; Krijgsman et al., 1999a, b; Lugli et al., 2010; Roveri et al., 2014a). Given the aforementioned similarities, Dela Pierre et al. (2011) provided a similar interpretation of the PLG of the Piedmont Basin. More recently, fluctuations in major and trace elements, total organic carbon (TOC) and molecular fossils content in the marl-shale alternations of the Pollenzo (Natalicchio et al., 2019) and Govone (Sabino et al., 2020) sections revealed for the first time independent evidence that the lithological cyclicity of the Piedmont PLG was precession-driven, with the phase relations between the lithofacies and the orbital parameters hypothesized by Krijgsman et al. (1999a, b).

The PLG is truncated at the top by an erosional surface progressively cutting into older beds towards the basin margins (Fig. 3.1b; Dela Pierre et al., 2011). This erosional surface is associated with an angular unconformity, particularly noticeable in seismic profiles (Ghielmi et al., 2019), suggesting uplift and deformation of the basin margin during the intra-Messinian tectonic phase (Dela Pierre et al., 2007). Dela Pierre et al. (2011) attributed this surface to the Messinian Erosional Surface (MES), traditionally ascribed to either a modest (<200 m; Roveri et al., 2014c) or extreme (several hundreds to thousands of meters; e.g. Clauzon, 1982; Loget et al., 2006; Amadori et al., 2018) base-level fall concomitant with the intra-Messinian tectonic phase (see Roveri et al., 2014a). Towards the basin depocenter, the MES passes into a correlative conformity flooring m-thick chaotic bodies emplaced by various types of gravity flows and including blocks of carbonates and MSC evaporites ranging in size from few meters to hundreds of meters (Dela Pierre et al., 2002, 2007, 2011). These sediments, both outcropping

(VVC, Dela Pierre et al., 2002, 2007; Irace et al., 2005) and buried (Castellania Chaotic Complex of Ghielmi et al., 2019), are equivalent to the RLG unit that is found in several Mediterranean localities (e.g. Northern Apennines, Sicily, Cyprus; Roveri et al., 2001; Manzi et al., 2016a, 2021). The VVC accumulated in various depocenters in the Piedmont Basin with variable thickness ranging from few meters up to 200 m (Ghielmi et al., 2019).

The VVC is capped by another erosional unconformity which merges with the MES at the basin margins (Fig. 3.1b; Dela Pierre et al., 2011). This surface is overlain by fine-grained deposits interbedded with sandstones and conglomerates. These sediments are currently grouped in the CSC, which reaches a maximum thickness of 100 m (Ghielmi et al., 2019). Lateral equivalent deposits of the CSC, now buried at depth in the Savigliano and Alessandria basins, have been observed in ENI seismic profiles and boreholes (https://www.videpi.com/videpi/pozzi/consultabili.asp). In the Savigliano Basin they are grouped in a single seismic sequence (ME3b) with maximum estimated thickness of ~370 m (Fig. 3.1c; Ghielmi et al., 2019). The stratigraphic architecture of the CSC and equivalent seismic unit(s) is, however, poorly known, as a consequence of the scarcity of outcrops (Fig. 3.1c) and the absence of marker beds suitable for basin-wide physical stratigraphic correlations.

The Pollenzo section is the only locality in the Piedmont Basin where a continuous section from the Stage 2 VVC to the basal Zanclean open marine deposits (Argille Azzurre Formation, AAF) is exposed. The base of the AAF marks the end of the MSC and is dated at 5.332 Ma (Trenkwalder et al., 2008; Violanti et al., 2011) as elsewhere in the Mediterranean (Roveri et al., 2014a).

3.3.2 The Pollenzo section

The Pollenzo section (44°41'08"N, 7°55'33"E), located in the southern part of the Piedmont Basin in an intermediate position between the basin margin and the depocenter, records the entire Messinian succession (Figs. 3.1b, 3.2a). The section begins with the Sant'Agata Fossili Marls, which show a precession-driven cyclic stacking pattern given by couplets of laminated shales and marls (Lozar et al., 2010; Dela Pierre et al., 2011; Natalicchio et al., 2017). Indurated carbonate-rich beds are found intercalated with the marls in the upper part of the unit (Dela Pierre et al., 2012). In detail, seven lithological, precession-driven cycles were recognized in the topmost portion of this unit above a slump (Dela Pierre et al., 2011). The overlying PLG unit comprises 9 lithological cycles composed of shales and different types of gypsum lithofacies (massive selenite in the lower two cycles; laminar gypsum and branching selenite in the remaining cycles; Dela Pierre et al., 2011; Natalicchio et al., 2021). Physical stratigraphic, biostratigraphic and cyclostratigraphic data allowed the onset of the MSC to be identified three cycles below the base of the PLG (Lozar et al., 2010, 2018; Dela Pierre et al., 2011). The PLG is overlain by ~5 m of slumped mudstones enclosing up to meter-sized blocks of PLG gypsums and carbonates attributed to the VVC, the basal surface of which corresponds to the MES.

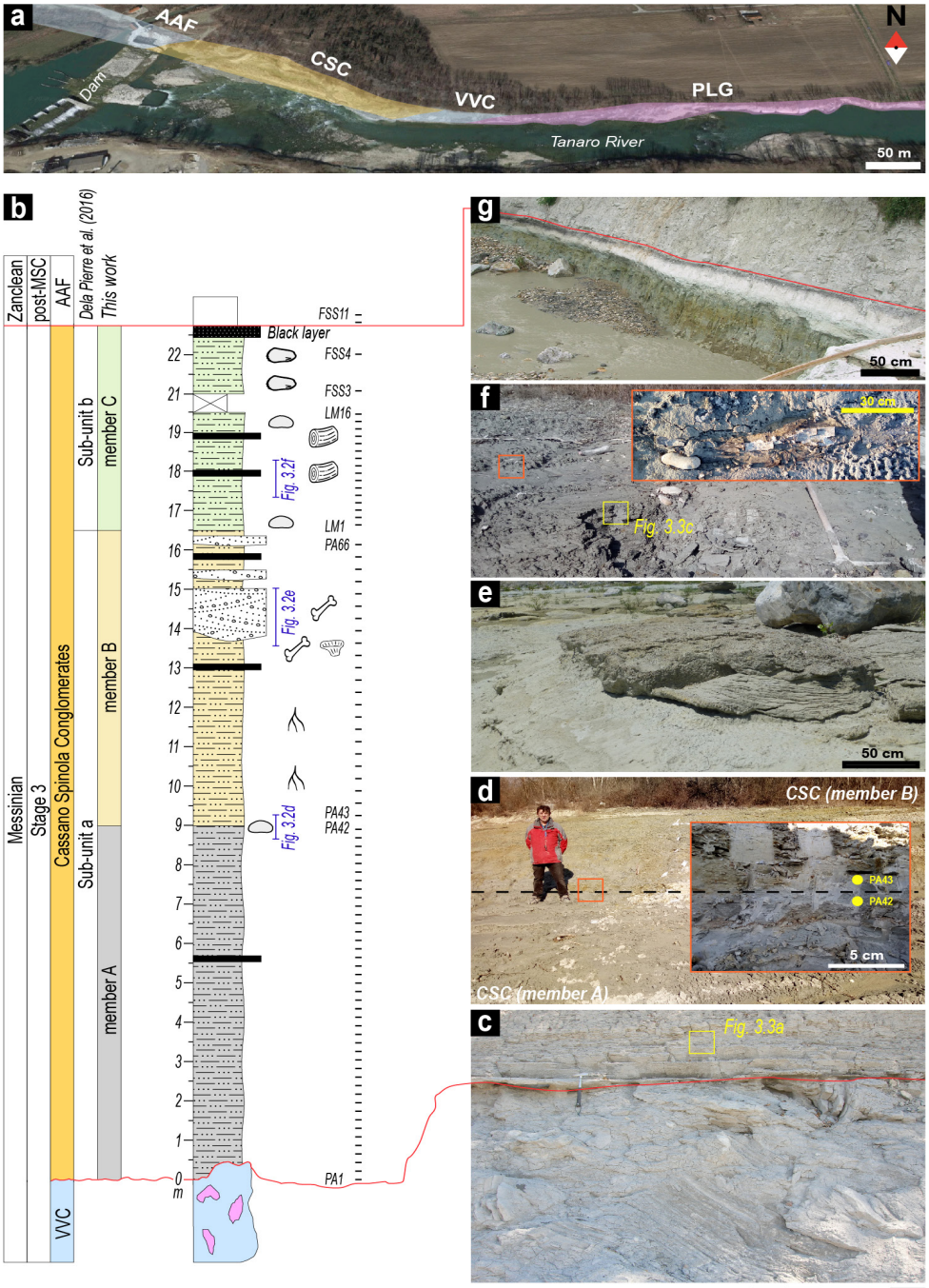
a
AAF
CSC
VVC
PLG
Dam
Tanaro River
N
50 m
b
Zanclean
post-MSC
AAF
Dela Pierre et al. (2016)
This work
Messinian
Stage 3
Cassano Spinola Conglomerates
Sub-unit b
member C
Sub-unit a
member B
member A
VVC
FSS11
Black layer
FSS4
FSS3
LM16
LM1
PA66
PA43
PA42
PA1
Fig. 3.2f
Fig. 3.2e
Fig. 3.2d
m
g
50 cm
f
20 cm
Fig. 3.3c
e
50 cm
d
CSC (member B)
PA43
PA42
5 cm
CSC (member A)
c
Fig. 3.3a
Black mudstone
Black sandstone
Mudstone
Conglomerate
Chaotic deposits
Not exposed
Logs
Vertebrates
Biofacies 1
Biofacies 2
Otoliths
Roots

Fig. 3.2 (previous page). (a) *Aerial view of the Pollenzo section (image credit: Google Earth) showing the distribution of the Messinian lithostratigraphic units. PLG: Primary Lower Gypsum; VVC: Valle Versa Chaotic Complex; CSC: Cassano Spinola Conglomerates; AAF: Argille Azzurre Fm.* **(b)** *Detailed sedimentary log of the Cassano Spinola Conglomerates in the Pollenzo section. The exposure gap in member C is due to the recent construction of a dam (see Fig. 3.2a). (c-g). Outcrop view of the Cassano Spinola Conglomerates.* **(c)** *Close up of the boundary between the VVC and the CSC.* **(d)** *Member A/B boundary (dotted line). The inset shows a close up of the boundary, which corresponds to a marked change in color of the sediments from greyish (member A) to yellowish (member B).* **(e)** *Outcrop view of the lowermost conglomerate layer.* **(f)** *Member C, mostly composed of grey laminated mudstones. The inset shows a close view of a land plant remain, which corresponds to the bark of a tree trunk.* **(g)** *The M/P boundary at the top of a prominent and laterally continuous black layer, which divides Paratethyan ostracod-rich mudstones of the CSC from open marine fauna-rich marls of the AAF. The different color of the member C mudstones is due to weathering. This picture is taken from Dela Pierre et al. (2016) and predates the building of the dam.*

The section continues with the CSC (Fig. 3.2b). It was subdivided into two sub-units by Dela Pierre et al. (2016): sub-unit a, that comprises gray to yellowish mudstones, sandstones and conglomeratic lenses with terrestrial mammal and fish fossils (Colombero et al., 2013; Carnevale et al., 2018); sub-unit b, which largely consists of grey-green mudstones with a distinct mollusk assemblage comprising both species endemic to the Mediterranean and indigenous of the Eastern Paratethys (see Sturani, 1973, 1976 and Esu and Popov, 2012 for details on the mollusks). The top of the CSC and the boundary with the overlying AAF was submerged in 2014 by the building of a dam on the Tanaro River (Fig. 3.2a). Earlier studies of this interval describe the boundary as a dm-thick, black layer burrowed at the top (Sturani, 1973; Dela Pierre et al., 2016; Fig. 3.2b).

3.4 Material and methods

3.4.1 Field studies

Field studies of the lithological and sedimentological characteristics of the CSC have been carried out at Pollenzo in February 2019 and a detailed stratigraphic section was logged (Fig. 3.2b). A total of 82 samples of mudstones were collected: 42 from member A (samples PA1-42), 24 from member B (samples PA43-66) and 16 from member C (samples LM1-16; see section 3.5.1 for the definition of the members). Four additional samples from the stratigraphic interval now under water and collected previously by some of the authors (FD, FL, MN) have also been analyzed: two (FSS3-4) from the top of the CSC and two (FSS10-11) from the base of the Zanclean AAF, 30 and 35 cm above the Miocene/Pliocene (M/P) boundary. Samples were processed for sedimentological, petrographic (composition and mineralogy), paleontological (ostracods, foraminifera, nannofossils and dinoflagellate cysts) and $^{87}Sr/^{86}Sr$ isotope analyzes.

3.4.2 Petrography

Eight petrographic thin sections were obtained from representative samples of the CSC (after epoxy impregnation) and studied using conventional transmitted, reflected and ultraviolet (UV) light microscopy. Scanning electron microscopy (SEM) analyzes were performed on 10 samples mounted on aluminum stubs, using a JEOL JSM IT300LV scanning electron microscope (JEOL Limited, Tokyo, Japan) at the Department of Earth Sciences, University of Torino. Carbon-coated thin sections were used for backscattered electron imagery. Qualitative energy dispersive spectroscopy (EDS) was performed on both thin sections and stubs.

3.4.3 Paleontology

3.4.3.1 Foraminifera and ostracods

36 out of 82 samples from the CSC and the two samples from the Argille Azzurre Fm. were processed for ostracod and foraminifera analyzes at the Department of Paleontology of the University of Bucharest. Micropaleontological samples were prepared by soaking previously air-dried sediments in chemical-free tap water and then washing the disaggregated material through a 63 μm sieve. Each sample's fraction was oven-dried at 50°C and observed under an optical microscope, where individual specimens of ostracods and foraminifera were hand-picked and identified from the >63 μm fraction. Pictures were taken with a NIKON digital camera. For ostracods, the total number of species was too low for quantitative analyzes. We performed a semi-quantitative analyzes where the terms rare (=<5 valves), medium (5-15 valves) and abundant (>15 valves) have been employed. Ostracod taxonomy applies the taxonomic concepts of Stoica et al. (2013, 2016) to Stage 3 sediments in the Paratethys and Mediterranean. Foraminifera are observed discontinuously and commonly dispersed in an abundant terrigenous fraction. Their presence was used qualitatively to highlight the presence of biostratigraphic or environmental markers. We applied the foraminiferal taxonomy according to Kenneth and Srinivasan (1983), Milker and Schmidl (2012) and www.mikrotax.org.

3.4.3.2 Calcareous nannofossils

The analysis of calcareous nannofossil relative abundance was performed on 9 samples of member A, 16 of member B, 18 of member C and two from the AAF. Standard smear slides were prepared at the Department of Earth Sciences, University of Torino and observed at 1250X under polarized light microscopy. In each slide, 400 species were identified and counted; clearly reworked calcareous nannofossil (i.e. of stratigraphic range older than the age of the CSC) were counted separately.

3.4.3.3 Dinoflagellates

A total of twenty samples (18 from member C and 2 from the AAF), about 10-12 grams each, were qualitatively screened for their palynological content. Carbonates were removed

using hydrochloric acid (HCl, 30%) and the samples were then allowed to settle overnight and rinsed with demineralized water until pH was neutral. Samples were then processed with 38% cold hydrofluoric acid (HF). Fluorosilicates were removed with HCl. The residues were sieved over a 10-µm nylon mesh screen and mounted on a microscopic slide in a drop of liquid glycerol gelatin. The slides were coated with a cover slip and sealed with nail polish. Slides are stored in the collection of the Marine Palynology and Paleoceanography group at the Department of Earth Sciences (Utrecht University). Two slides per sample were screened for the presence of dinoflagellate cysts and other aquatic and terrestrial palynomorphs and organic matter using a binocular transmitted light microscope at 40x magnification. Dinocyst taxonomy follows Williams et al. (2017).

3.4.4 Radiogenic strontium isotopes

$^{87}Sr/^{86}Sr$ ratios in the MSC context were analyzed to evaluate the relative contribution of local and external (i.e. Atlantic Ocean, Eastern Paratethys and large Mediterranean rivers) sources of water to the basin (e.g. Reghizzi et al., 2018; Andreetto et al., 2021b). Ca^{2+}-bearing minerals, which incorporate dissolved Sr^{2+} ions during precipitation, must satisfy three requirements to be selected for analysis: (1) they must not be reworked; (2) they must not have undergone significant diagenetic alteration with the introduction of exogenous Sr after formation; (3) in case fossil shells are selected: (3.1) they must be cleaned of the surrounding matrix, which is a contaminant; (3.2) they should be preferentially composed of low-Mg calcite, which is more resistant (i.e. less soluble) to post-depositional alteration than high-Mg calcite and aragonite skeletal grains (Bennett et al., 2011; Marcano et al., 2015).

$^{87}Sr/^{86}Sr$ analysis was carried out on six samples, every sample for which sufficient ostracod material was available. These samples derive from the member A/B transition (samples PA42-43; Fig. 3.2b) and from the topmost part of member C. Planktonic foraminifera in sample FSS11 from the base of the AAF were also analyzed. The $^{87}Sr/^{86}Sr$ composition of Ca^{2+}-bearing minerals is influenced by fractionation effects involving physico-chemical or biological processes, but any effect is cancelled out during measurement (see Hajj et al., 2017). Nevertheless, efforts have been made to minimize the number of species analyzed (Table 3.1). To this end, six of the (visually) cleanest valves of adult *Cyprideis torosa* were chosen from the lowermost 4 (out 6) samples analyzed (PO42-43, LM14 and 16). However, *Cyprideis torosa* is too rare in the uppermost two CSC samples (FSS3-4) to be selected for analyzes. Instead, 6 valves of *Tyrrhenocythere ruggierii* were picked. Disarticulated valves were preferentially analyzed rather than entire carapaces to facilitate the cleaning of the inner side. For the AAF samples, 15 *Orbulina universa* tests were picked and mechanically cracked open for the same reason.

$^{87}Sr/^{86}Sr$ values were measured at the Bristol isotope group Laboratory at Bristol University. Sample preparation and measurement followed the procedure outlined by Lewis et al. (2017). All work was carried out in a class 1000 clean room with chemistry in class 100 laminar flow

hoods. Samples were first cleaned three times in an ultrasonic bath with ultra-pure water (18.2 MΩ) to mechanically remove contaminating clay particles that adhere to the valves/tests. Samples were then washed twice with methanol then three more times with ultra-pure water to remove contamination and leaching reagents. After a visual inspection under a binocular microscope, cleaned valves were then dissolved in 0.5N HNO_3 in a centrifuge tube at room temperature. Samples were then centrifuged to separate any undissolved residue and the supernatant was then transferred to a PFA beaker, evaporated to dryness and fluxed in 300 µl of 15.4N HNO_3 to dissolve any possible organic material still present before being evaporated to dryness and taken back up in 500 µl of 3N HNO_3. Sr separation was carried out using pipette tip columns with ~100 µl of cleaned Sr Spec. resin (Eichrom, Horwitz et al. 1992). Appropriate standards (NIST SRM 987 and SRM 1400) are processed alongside the samples to calibrate the chemistry. Samples are loaded in 0.5 ml 3N HNO_3, the matrix eluted in 2 ml of 3N HNO_3 and Sr fractions collected in 1.5 ml of ultra-pure water. Samples were then evaporated to dryness, refluxed in 300 µl 15.4N HNO_3 and 30 µl of 0.3N H_3PO_4 and evaporated to dryness again for mass spectrometry. Samples are taken up in 1 µl 1.5N HNO_3 and loaded onto degassed rhenium filaments with 1 µl of $TaCL_5$ activator solution (Birck, 1986). $^{87}Sr/^{86}Sr$ measurements were made on Thermo-Finnigan Triton thermal ionisation mass spectrometer. Samples were manually heated for full control of Sr emission with measurements started when ^{88}Sr beams were roughly 40 pA. $^{87}Sr/^{86}Sr$ was measured using a multi-dynamic 'triple jump' method (Thirlwall, 1991; Avanzinelli et al., 2004) with a 4.194 second integration time per cycle and 200 cycles per measurement. Instrumental mass bias was corrected using an exponential mass bias law and an $^{86}Sr/^{88}Sr$ of 0.1194 (Nier, 1938; Russell et al., 1978), ^{87}Rb is corrected by monitoring ^{85}Rb and using an $^{85}Rb/^{87}Rb$ of 2.59265 (Steiger and Jäger, 1977). The mean of NIST SRM 987 analyzed during this session was 0.710249 ± 0.000008 (2 SD) and does not differ from that of NIST SRM 987 which has undergone chemical purification (mean 0.710248 ± 0.000001, 2 SD) and is in good agreement with the accepted values of SRM 987 of 0.710250 (Thirlwall, 1991). The mean $^{87}Sr/^{86}Sr$ of NIST SRM 1400 (Bone ash) is 0.713118 ± 0.000002 (2 SD) is in agreement with published values for this standard. Procedural blanks processed with samples and blanks are quantified using a small amount of ^{87}Sr-^{84}Sr double spike added to the blank at the filament loading stage. The procedural Sr blank for this session was 8 pg.

3.5 Results

3.5.1 Field and petrographic observations

In the Pollenzo section, three members of the ~20 m-thick CSC can be recognized on the basis of lithological features.

Member A is a ~9 m-thick monotonous muddy succession resting on the erosional surface above the VVC (Fig. 3.2c). It is mainly composed of dark grey laminated silty mudstones with dm-thick intercalations of dark grey sandstones.

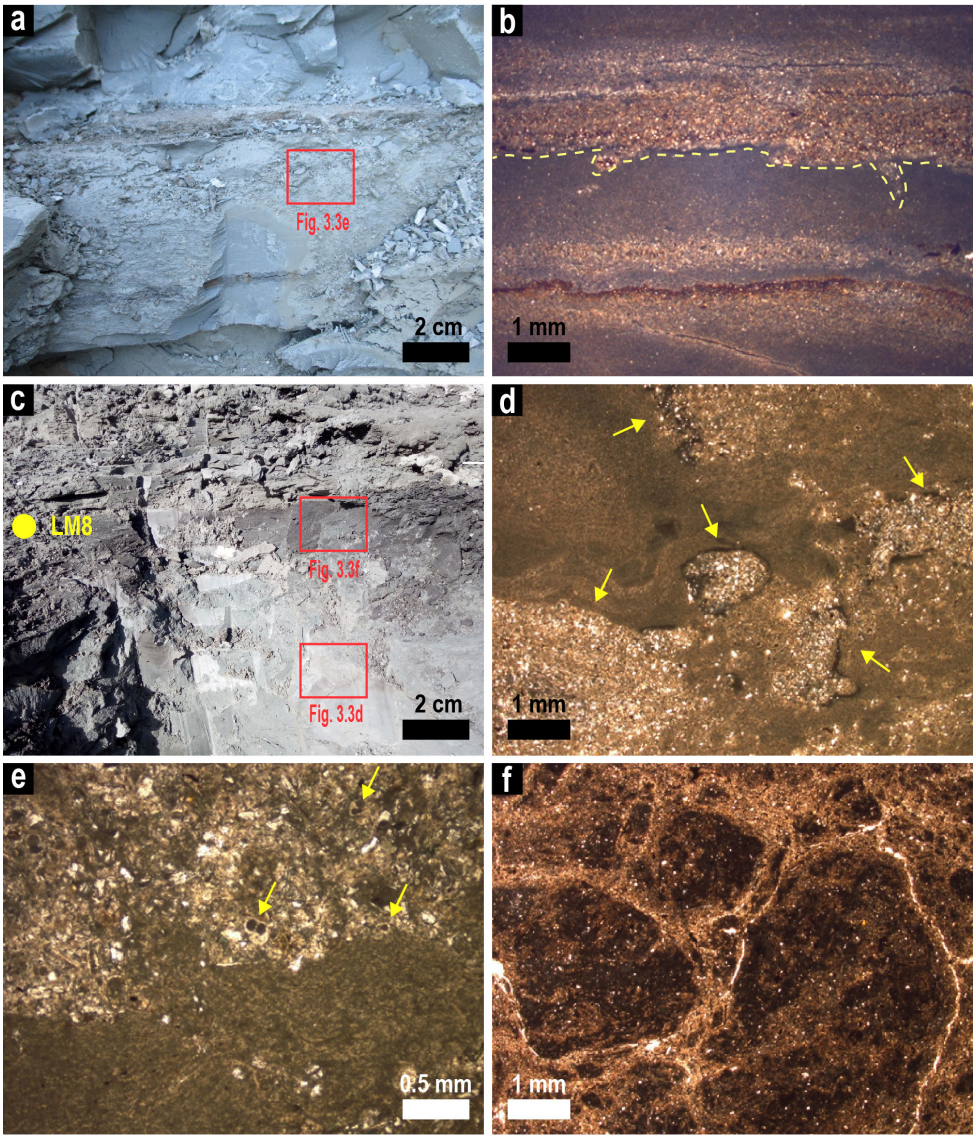

Fig. 3.3. *Field images (a, c) and corresponding transmitted light optical photomicrographs (b, d-f) of the fine-grained sediments of the CSC.* **(a)** *Bedded greyish mudstones of member A;* **(b)** *Graded sandy layers interbedded to homogeneous mudstones. Note the erosional basal contact of the sandy layer (yellow dotted line; sample PA56);* **(c)** *greyish mudstone of member C with, on top, a cm-thick black horizon interpreted as a paleosol;* **(d)** *Member C mudstone with burrows (yellow arrows) filled with fine-grained sand;* **(e)** *Closer view of the fine-grained sand filling the burrows showed in Fig. 3.3d. Note the abundance of skeletal remains (mostly foraminifera; yellow arrows). Foraminifera tests are possibly filled with pyrite.* **(f)** *Rounded pedogenetic nodules with circumgranular cracks (sample LM8). The cracks are partially filled with calcite.*

Member B is composed of mottled yellowish silty mudstones (Fig. 3.2d) with abundant land plant debris, leaves and root casts. Two brown to blackish indurated beds are present (Fig. 3.2b), corresponding to homogeneous mudstones alternating with cm-thick graded sandstones with an erosional basal contact. Three lenticular conglomeratic layers are interbedded with the yellowish mudstones (Figs. 3.2b, e). They are composed of rounded and smoothed pebbles of selenitic gypsum and Alpine metamorphic rocks and are interpreted as fluvial deposits (Colombero et al., 2013). A diverse terrestrial vertebrate fauna is found in the lowermost conglomeratic layer including disarticulated remains of amphibians, reptiles, birds, large herbivores and carnivores (Sardella, 2008; Colombero et al., 2013). In addition, in situ articulated skeletal remains of a single individual of a gomphotheriid, a large elephant-like proboscidean, were found in the yellowish mudstones below the lowermost conglomeratic layer (Colombero et al., 2013). Disarticulated bones and otoliths of coastal marine benthic fish have also been reported occurring with the terrestrial vertebrate fauna: one attributed to the benthopelagic, euryhaline *Aphanius crassicaudus* and one of an undetermined species of Lophiiformes (Carnevale et al., 2018).

Member C is composed of grey laminated mudstones with intercalated lenticular dark grey layers (Fig. 3.2f). In thin section, member C mudstones appear strongly bioturbated (Fig. 3.3d). Burrows are filled with sand typified by high contents of benthic and planktic foraminifers (Fig. 3.3e). Three dark grey layers (Figs. 3.2b, 3.3c) contain plant remains (leaves, wood fragments), which are particularly abundant and well exposed in the uppermost of the three dark layers (sample LM13; Fig. 3.2f). Cm-sized rounded nodules surrounded by circumgranular cracks are observed under the microscope (Fig. 3.3f). Member C is overlain by the lower Zanclean open marine deposits of the AAF (Fig. 3.2b). The contact is marked by a dm-thick dark-grey arenitic layer (Fig. 3.2g), reported from other sites of the Piedmont Basin as well (Moncucco; Trenkwalder et al., 2008; Violanti et al., 2011; Narzole borehole; Sturani 1978; Violanti et al., 2009). In the Pollenzo section, burrows of *Thalassinoides* were recognized at the contact between the dark arenitic layer and the AAF (Dela Pierre et al., 2016).

3.5.2 Paleontological content

3.5.2.1 Ostracods

Ostracods (Fig. 3.5) are first observed at the member A/B transition, they disappear in member B and re-appear in member C (Figs. 3.2b, 3.4). Here they occur discontinuously in the first ~3.50 m (samples LM1-13), whereas they are ubiquitous in the remaining ~2-3 m below the base of the topmost black layer (Fig. 3.4). In the lowermost ~3.50 m of member C ostracods mostly consist of fragments of disarticulated valves of *Cyprideis* sp. Fragments could not be selected for $^{87}Sr/^{86}Sr$ analyzes because they are commonly too small to subject them to the cleaning procedure. Similarly, the absence of intact valves hinders the taxonomic classification at the species level. By contrast, in the uppermost ~2-3 m they are well preserved (Fig. 3.5)

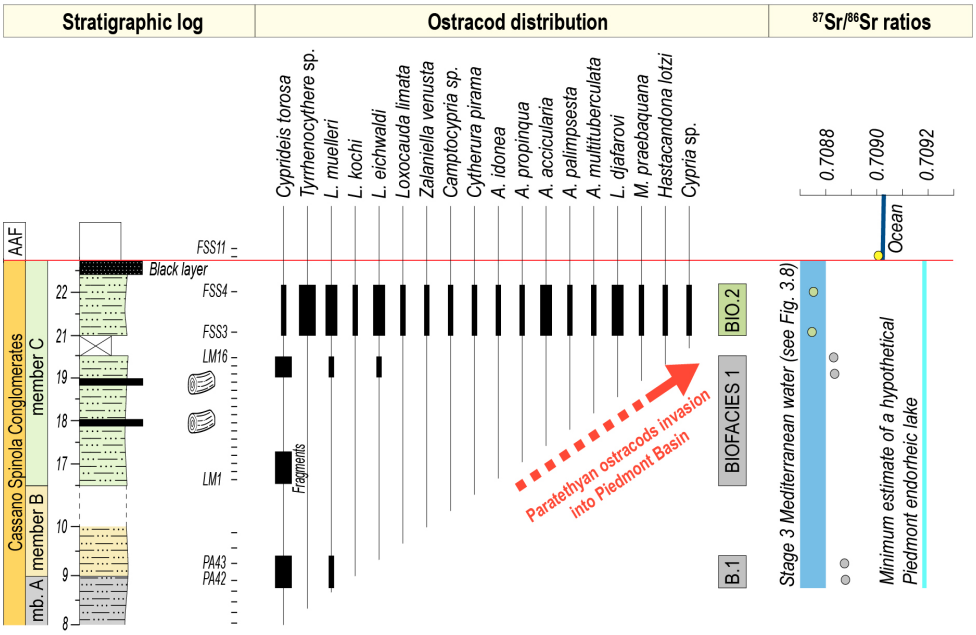

Fig. 3.4. *Ostracod distribution chart along with variations in the* $^{87}Sr/^{86}Sr$ *ratios measured on ostracod valves. Analytical errors are so small that no error bars are visible at this scale. Note the abrupt increase in ostracod species diversity that typifies the uppermost part of member C. Samples with diversified ostracod assemblages (Biofacies 2) have significantly lower* $^{87}Sr/^{86}Sr$ *ratios than samples with poorly diversified, Cyprideis torosa-dominated assemblages (Biofacies 1). Tyrrhenocythere ruggierii and Tyrrhenocythere pontica are grouped together in the informal group Tyrrhenocythere sp.* $^{87}Sr/^{86}Sr$ *ratios are plotted against three water sources: (1) average signature of the coeval ocean water (the thickness of the line includes the analytical error; McArthur et al., 2012); (2) minimum estimated signature of a hypothetical lake occupying the Piedmont Basin corresponding to the* $^{87}Sr/^{86}Sr$ *ratios of the Po River at its confluence with the Tanaro River (Fig. 3.1a; see paragraph 3.6.2 for insights); (3) inferred signature of the water mass filling the Mediterranean Basin during Stage 3 (see paragraph 3.6.2 for insights).*

and consist of multiple moult stages of both articulated and disarticulated valves, which are diagnostic features of in-situ preservation (e.g. Gliozzi et al., 2007; Cosentino et al., 2012; Stoica et al., 2016; Sciuto et al., 2018).

Overall, two assemblages can be distinguished based on different diversity patterns (Fig. 3.4). We interpret these assemblages as the Biofacies 1 (low diversity) and Biofacies 2 (high diversity) of Bonaduce and Sgarrella (1999), which are recognized in many other Stage 3 Mediterranean sections (Malaga, Nijar and Vera basins in SE Spain, Bassetti et al., 2006; Guerra-Merchán et al., 2010; Stoica et al., 2016; Apennine basins, Grossi et al., 2008; Cosentino et al., 2012, 2018; Caltanissetta Basin, Grossi et al., 2015; Crete, Cosentino et al., 2007).

Biofacies 1 in the Pollenzo section comprises an almost monospecific assemblage of the euryhaline and shallow-water *Cyprideis torosa* with very rare individuals of *Loxoconcha muelleri* (Fig. 3.4). Well preserved gyrogonites of Chara sp. are also observed. Biofacies 1 is found at the member A/B transition and in the lower part of member C (Fig. 3.4). In the Pollenzo section Biofacies 2 includes the following species (other than *C. torosa* and *L. muelleri*): *Loxorniculina djafarovi*, *Amnicythere multituberculata*, *Amnicythere propinqua*, *Amnicythere palimpsesta*, *Amnicythere idonea*, *Amnicythere accicularia*, *Cypria* sp., *Tyrrhenocythere ruggierii*, *Tyrrhenocythere pontica*, *Cytherura pirama*, *Camptocypria* sp., *Loxoconcha eichwaldi*, *Loxoconcha kochi*, *Loxocauda limata*, *Zalaniella venusta*, *Euxinocythere* (*Maeotocythere*) *praebaquana* and *Hastacandona lotzi* (Fig. 3.5). Biofacies 2 is recognized only in the two samples taken from the uppermost meter below the black layer at the AAF transition (Fig. 3.4). The described ostracod species are only known from the Pontian of the Eastern Paratethys (i.e. Euxinic, Caspian and Dacian basins; Stoica et al., 2013, 2016; Van Baak et al., 2016; Grothe et al., 2018; Lazarev et al., 2020) and the Northern Aegean (Krijgsman et al., 2020a and references therein), where they migrated at ~6.1 Ma from the endorheic Pannonian Basin (Popov et al., 2006; Krijgsman et al., 2010; Grothe et al., 2018). This observation further corroborates the in-situ character of the Biofacies 2 ostracods.

3.5.2.2 Foraminifera

Most of the samples collected in the basal member A are barren of foraminifera. Only two samples (PA28 and 42) yield rare small-sized (<125 μm) planktic foraminifera (*Turborotalita quinqueloba*, *T. multiloba*, *globigeriniids* and few left coiled *Neogloboquadrina acostaensis*). The residues are mostly composed of terrigenous material, typically mica flakes and lithic fragments.

The lowermost sample of member B (PA43; Fig. 3.2d) is characterized by a reduced content of terrigenous grains and by the presence of mainly planktic foraminifera. Among them, *T. quinqueloba* is most frequent, followed by *T. multiloba*, *Globigerinoides* spp., *Globorotalia scitula* and both left and right coiled *N. acostaensis*. Among the benthic foraminifera, species belonging to the *Bolivina, Anomalinoides, Oridorsalis, Cibicides* and *Uvigerina* genera were observed. The rest of member B is barren of foraminifera or only yields scattered benthic foraminifera in sample PA64. Samples of the lower part of member C (LM1-3) yield quite diversified foraminifer assemblages, with the planktic component being once again more abundant than the benthic. Among the planktic foraminifera *T. quinqueloba, T. multiloba, Globigerina bulloides, Orbulina universa*, *G. scitula*, *Globorotalia miotumida* and *Globigerinita glutinata* were recognized. *Elphidium, Bolivina, Bulimina, Cibicides, Cancris, Valvulineria* and *Rectuvigerina* are among the most common benthic taxa. From LM4 upwards foraminifera are generally scattered, except in samples LM10 and LM11, where *T. quinqueloba* is again common and occurs together with rare *T. multiloba* and *G. bulloides*. The associations that are observed here closely resemble those of the older Sant'Agata Fossili Marls (see Lozar et al., 2010).

Fig. 3.5. *Messinian (Lago-Mare) ostracods from member C of the Cassano Spinola Conglomerates of the Pollenzo section. All pictures are taken on external lateral views. RV: right valve; LV: left valve.*

Some of the common forms found in these assemblages such as *T. multiloba* and *G. miotumida* are thought to have become extinct before Stage 3 (see Lirer et al., 2019). Consequently, it is likely that the foraminifera are reworked. This is supported by the observation that several of the benthic and planktic species are deep-dwelling forms, which is a paleoecological requirement that clearly contrasts with the presence of sedimentological and other micropaleontological features pointing to a shallow and brackish water body during deposition of the CSC (see discussion in section 3.6.1). *Elphidium* sp. may represent the only exception, being this genus a typical inhabitant of shallow and euryhaline environments that matches with our paleoenvironmental and paleohydrological reconstruction of member C (see discussion in section 3.6.1). However, since it also frequently found in the SAF (Violanti et al., 2013), reworking cannot be excluded.

3.5.2.3 Calcareous nannofossils

In all three members, calcareous nannofossil assemblages are made up of both forms clearly reworked because of their biostratigraphic range (Cretaceous, Oligocene and lower-middle Miocene) incompatible with the age of the CSC and taxa which are potentially stratigraphically consistent with the time interval spanned from the CSC and consequently cannot be a priori considered as reworked (Fig. 3.6). Regrettably, the age-diagnostic taxa *Ceratolithus acutus* (first appearance at 5.36 Ma; Agnini et al., 2017) and *Triquetrorhabdulus rugosus* (last appearance datum at 5.23 Ma; Backman et al., 2012), often reported in late Messinian sediments of both the Mediterranean and Paratethys (Popescu et al., 2017 and references therein) and, therefore, of significant chronostratigraphic and paleoenvironmental implications (see discussion in Andreetto et al., 2021a), have not been found in the CSC of Pollenzo. Quantitative analysis reveals that calcareous nannofossils reworked from older than late Miocene stratigraphic levels constitute a small percentage (lower than 6%) compared to taxa that are consistent with the age of the CSC. Among these taxa whose stratigraphic distribution is compatible with the age of CSC, the following are observed: *Reticulofenestra antarctica, Reticulofenestra haqii, Reticulofenestra minuta, Reticulofenestra procera, Reticulofenestra pseudoumbilicus, Sphenolitus abies, Sphenolitus moriformis, Helicosphera carteri, Umbilicosphaera jafari, Umbilicosphaera rotula, Calcidiscus leptoporus, Discoaster variabilis, Discoaster brouweri, Coccolithus pelagicus, Toracosphaera, Pontosphaera discopora, Pontosphaera japonica, Pontosphaera multipora, Calcidiscus macintyrei* and *Syracosphaera pulchra*. Besides *D. variabilis* and *D. brouweri*, other species belonging to the genus *Discoaster* are present. However, they show high degree of fragmentation and recrystallization, hampering their identification at the species level. More in detail, *Reticulofenestra* is by far the most abundant genus, ranging from ~73 to 86% of the total. *R. minuta* makes up more than 38% of the *Reticulofenestra* taxa, followed by *R. haqii* (7-33%, average of 16%), *R. antarctica* (0.5-27%, average of 6%) and *R. procera* (<1%). *H. carteri, R. pseudoumbilicus, C. pelagicus, U. jafari and Sphenolithus gr.* (herein consisting of *S. abies* and *S. moriformis*; Fig. 3.6) constitute a minor component (i.e. average abundance between 1 and 5%) of the assemblages. All remaining "age-compatible" taxa occur at abundances <1%.

Calcareous nannofossils assemblages are similar in terms of abundance, (good state of) preservation and taxonomy between the three members and to the older assemblages commonly found in the pre-MSC SAF (Lozar et al., 2010). In member C alone, however, abundant, intact coccospheres were observed. This observation is generally related to conditions of exceptional preservation (e.g. Bown et al., 2014) which, as such, could be indicative of the pristine nature of the member C assemblage (see section 3.6.1 for a more thorough discussion of the nature of the long-ranging taxa in member C).

The nannofossil associations in the AAF contain the same taxa as in the CSC, with the addition of *Reticulofenestra zancleana*, marker species of the lower Zanclean (Di Stefano and Sturiale, 2010).

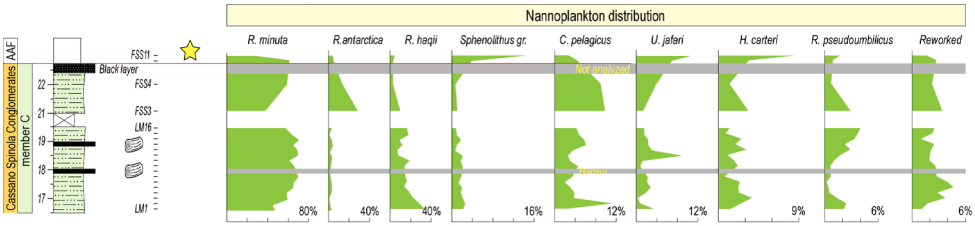

Fig. 3.6. *Relative abundance of dominant calcareous nannofossils taxa in member C of the CSC and at the base of the AAF. Sphenolithus abies and Sphenolithus moriformis were grouped together in the informal group Sphenolithus gr. The yellow star indicates the presence of the age-diagnostic taxon Reticulofenestra zancleana. Note changes in scale.*

3.5.2.4 Dinoflagellate cysts

The 18 samples from member C are very rich in pollen grains and organic terrestrial material such as leaf, cuticles, tetrads, fungal spores and woody fragments indicating relatively large amount of terrestrial input. Dinoflagellate cyst (dinocysts) occurrence and diversity vary significantly. Some samples are virtually barren of dinocysts (LM1-9, LM11-13) others show very low abundance and diversity (LM10, LM14-16, FSS3-4). Marine taxa such as *Achomosphera*/*Spiniferites* spp., *Spiniferites bentori, Homotryblium, Operculodinium israelianum, Operculodinium janduchenei* and *Polysphaeridium zoharyi* have been identified. One specimen of Mendicodinium robustum has been observed in samples FSS4. This species was informally described from restricted marine and brackish Mediterranean latest middle Miocene-early late Miocene sediments (Zevenboom, 1995). Only one specimen of the Paratethyan species *Caspidinium rugosum* and three specimens of *Spiniferites cruciformis* were identified in sample LM15.

Early Zanclean samples FSS10-11 from the AAF are marked by a large increase in dinocyst abundance and species richness and by remarkable improvement in the dinocyst preservation. The most abundant taxa in sample FSS10 are *Impagidinium patulum, Operculodinium* spp., *Lingulodinium machaerophorum* (some specimens with reduced processes), *Spiniferites* spp., *Brigantedinium* spp., *Nematosphaeropsis labyrinthus* and *Reticulatosphaera actinocoronata*, which are known from coastal to (outer) neritic environments. In sample FSS11 *Impagidinium patulum* is dominant and *Nematosphaeropsis labyrinthus, Reticulatosphaera actinocoronata, Operculodinium janduchenei* and *Lingulodinium macherophorum* (with fully developed processes) are present. This association reflects an outer neritic/oceanic environment.

In the lower Zanclean samples, marine dinocysts are well preserved, diverse and abundant, all features that corroborate their in-situ character. By contrast, the taxa recognized in member C are often poorly preserved. This makes the identification at the species level and the discrimination of possible in-situ components, for instance, by means of fluorescence microscopy (Pellen et al., 2017; Hoyle et al., 2018), really challenging. The different preservation

and abundance of the dinocysts between the lower ~3.5 m of member C (i.e. samples LM1-13) and the base of the AAF allows us to hypothesize that the few dinocysts recovered in the lower part of member C are reworked. By contrast, the subtle increase in the dinocyst preservation and abundance in the uppermost ~3 m (i.e. samples LM14-16, FSS3-4) may point to in-situ deposition.

3.5.3 $^{87}Sr/^{86}Sr$ ratios

$^{87}Sr/^{86}Sr$ ratios from the CSC range from 0.708871 to 0.708746 (Fig. 3.4, Table 3.1). The higher values of 0.708870-0.708871 (PA42-43) and 0.708831-0.708834 (LM 14-15) come from *C. torosa* specimens forming the oligotypic Biofacies 1 (Fig. 3.4). Instead, the lower values of 0.708746 (FSS3) and 0.708752 (FSS4) come from *T. ruggierii* specimens forming the more diversified Biofacies 2 (Fig. 3.4). In contrast with the CSC data where the $^{87}Sr/^{86}Sr$ ratios are substantially lower than Messinian ocean water, $^{87}Sr/^{86}Sr$ at the base of the AAF (0.709006) are close to the global ocean Sr curve for the lowermost Pliocene (McArthur et al., 2012), but still outside its error range (Fig. 3.4).

Table 3.1. *$^{87}Sr/^{86}Sr$ composition and details of the analyzed samples.*

Sample	Unit	Age	Material	$^{87}Sr/^{86}Sr$	2σ (*10^{-6})
FSS11	AAF	early Zanclean	*T. ruggierii*	0.708746	0.000005
FSS4	CSC (Mb. C)	late Messinian	*T. ruggierii*	0.708752	0.000005
FSS3	CSC (Mb. C)	late Messinian	*T. ruggierii*	0.708746	0.000005
LM15	CSC (Mb. C)	late Messinian	*C. torosa*	0.708831	0.000006
LM14	CSC (Mb. C)	late Messinian	*C. torosa*	0.708834	0.000005
PA43	CSC (Mb. A)	late Messinian	*C. torosa*	0.708871	0.000004
PA42	CSC (Mb. A)	late Messinian	*C. torosa*	0.708870	0.000004

3.6 Discussion

3.6.1 Paleoenvironmental evolution of the Piedmont Basin during Stage 3

Our newly acquired sedimentological and paleontological data, together with previously published results from both Pollenzo and other localities in the Piedmont Basin, say little about the duration of Stage 3 in Pollenzo because of the lack of chronological controls, but they reveal that at least three distinct environmental conditions occurred during the here recorded time slice of Stage 3.

Member A: The fine-grained and thinly laminated deposits of member A (Fig. 3.2c) reflect deposition in a low-energy subaqueous environment after a period of tectonic-driven basin instability resulting in the deposition of the VVC (Fig. 3.7a). The absence of in-situ fauna and bioturbation throughout most of member A may suggest that the oxygen content was low. Only in the uppermost part of member A, the presence of abundant *Cyprideis torosa*, which is known today to be a shallow-water dweller (up to 30-50 m of depth, optimum around 7 m; Neale, 1988; Meisch, 2000; Meyer et al., 2016), indicates a shallow-water paleoenvironment at Pollenzo (i.e. <10-30 m deep). Instead, little can be said about the paleosalinity: both *Cyprideis torosa* and charophytes can withstand and thrive in a very wide range of aquatic environments and

salinity (Pełechaty et al., 2013; Grossi et al., 2015; De Deckker and Lord, 2017 and references therein). The Moncucco section (Fig. 3.1b) located in the northern side of the Piedmont Basin (Torino Hill; Figs. 3.1a-b) may provide an estimation of paleosalinity during deposition of the topmost part of member A. At Moncucco, a poorly diversified ostracod assemblage is found in mudstones resting just below mammal-rich sediments (Angelone et al., 2011) likely referable to member B (see below). Besides *Cyprideis*, identified at the species level as *Cyprideis agrigentina* by Angelone et al., (2011), and *L. kochi*, some specimens of *A. propinqua* are also found (Angelone et al., 2011). This species is reported to have depth ranges compatible with those of *C. agrigentina* and *L. kochi*, but stricter salinity requirements, which has to stay within the oligo-mesohaline field (3-14‰; Gliozzi and Grossi, 2008). These findings therefore suggest that the shallow-water paleoenvironment depositing member A was typified by brackish conditions. Fine-grained deposits similar to those of member A of Pollenzo are also reported on top of the VVC in cores that penetrated the CSC in the Alessandria and Savigliano depocenters (Fig. 3.1a; Ghielmi et al., 2019). In contrast, member A mudstones are absent in localities further away from the deepest sectors both to the S and to the N, where the erosional surface capping the VVC is directly overlain by the AAF (e.g. Monregalese area; Ghielmi et al., 2019).

Member B: The transition from the grey shales of member A to yellowish mudstones of member B (Fig. 3.3c) with rhizoliths, terrestrial mammals (Colombero et al., 2013) and three conglomerate beds (Figs. 3.2b, 3.2e) with typical features of fluvial transport demonstrates the basinward shift of the coastline and the establishment, at Pollenzo, of a recurrently dried alluvial plain crossed by a fluvial network and surrounded by a variety of continental environments (grasslands, woody areas, rocky habitats; Fig. 3.7b). These continental environments provided a corridor for migrating mammals from mainland Europe into the Italian peninsula (Sardella, 2008; Angelone et al., 2011). The occurrence of Alpine metamorphic pebbles in the conglomerates indicate that the Alpine chain was already partially emerged during deposition of the member B and it was undergoing intense erosion. Scattered brownish to black shaley lenses intercalated with the yellowish pelites (Fig. 3.2b) are possibly indicative of ephemeral, marshes that punctuated the alluvial plain. Sediments similar to the ones attributed, in Pollenzo, to member B, and rich in terrestrial mammal fossils, freshwater and continental gastropods (Angelone et al., 2011; Colombero et al., 2014, 2017; Harzhauser et al., 2015; Grunert et al., 2016) are also found in the Moncucco section. This suggests that continental conditions involved a larger sector of the Piedmont Basin than only the Alba region (Fig. 3.7b). A very low density of very well preserved fish otoliths mixing a diverse array of stenohaline open marine taxa (mostly Myctophidae with subordinated Trachichthyidae, Gadidae and Moridae) alongside marginal marine/estuarine (Bythitidae, Sciaenidae; and Paratethyan taxa (Gobiidae) adapted to brackish environments is also found together with the terrestrial mammal fossils in Moncucco and Pollenzo (Grunert et al., 2016; Colombero et al., 2017; Carnevale et al., 2018; Schwarzhans et al., 2020). According to Grunert et al. (2016), the co-occurrence of taxa with

such different ecological requirements evidence the presence of large marine predators that were foraging in the open, fully marine Mediterranean, where they gobbled the otoliths, and that were periodically migrating to marginal/estuarine brackish environments in the Piedmont Basin. In light of this, Grunert et al. (2016) and Carnevale et al. (2018) suggested that the Piedmont Basin was connected to a fully marine Mediterranean during Stage 3. However, according to Carnevale et al. (2006a) otoliths are unlikely to be found excellently preserved after a post-mortem transport due to the action of the digestive acids in the stomach of predators. This aspect argues against the in-situ nature of the otoliths of stenohaline oceanic fish. This is consistent with their occurrence in mudstones rich in terrestrial mammals, with the absence of other open marine paleontological and geochemical signatures (both in Piedmont and across the Mediterranean; Andreetto et al., 2021a) and with their $^{87}Sr/^{86}Sr$ ratios (0.708896-0.708947), which point to a late Tortonian age.

Member C: The transition from the continental deposits of member B to the grey laminated mudstones of member C indicates the renewal of a subaqueous environment. Additionally, they are interbedded with dark silty layers (Figs. 3.2c-d) with cm-sized rounded nodules surrounded by circumgranular cracks (Fig. 3.3h), which we interpret to possibly represent immature paleosols. Overall, these features indicate that member C is the sedimentary expression of a shallow water body with a fluctuating base-level responsible for periodic subaerial exposure. The amplitude of the fluctuations was probably rather small (<30 m), based on the shallow-water mode of life of the ostracod *C. torosa* which, albeit discontinuously, dominates the benthic assemblages for most of member C (Fig. 3.4). In the uppermost 1-2 meters before the topmost black layer, the ostracod assemblages are highly diverse, dominated by Paratethyan species (Fig. 3.5) and relatively impoverished in *C. torosa* (Fig. 3.4). This assemblage is similar to that of the Moncucco section (Fig. 3.1a; Trenkwalder et al., 2008) and other Messinian Mediterranean successions (e.g. Cosentino et al., 2007, 2012, 2018; Grossi et al., 2008; Guerra-Merchán et al., 2010; Stoica et al., 2016; see Andreetto et al., 2021a for further references). According to the paleoecological analyzes carried out by Gliozzi and Grossi (2008) on the Paratethyan ostracods, the stacking of Biofacies 2 over Biofacies 1 in the uppermost ~2 m (Fig. 3.4) indicates a deepening- and freshening-upward trend. Paratethyan ostracods, however, occur with the diverse calcareous nannofossil assemblages (which include intact coccospheres) dominated by *Reticulofenestra* and subordinate specimens of *Helicosphaera carteri, Coccolithus pelagicus, Sphenolithus abies* and *Umbilicosphaera jafari* (Fig. 3.6). The co-occurrence of calcareous nannofossils with Paratethyan organisms in the same sediments raises a concern, which is not new in Stage 3 studies (e.g. Cita et al., 1978; Bertini, 2006; Popescu et al., 2007; Roveri et al., 2008a; Cosentino et al., 2012; Pellen et al., 2017; Caruso et al., 2020). Marine microfossils have paleoecological requirements apparently incompatible with those of the Paratethyan ostracods: following the paleoenvironmental significance of the MSC ostracod assemblages proposed by Gliozzi and Grossi (2008), Biofacies 2 is indicative of an oligo-

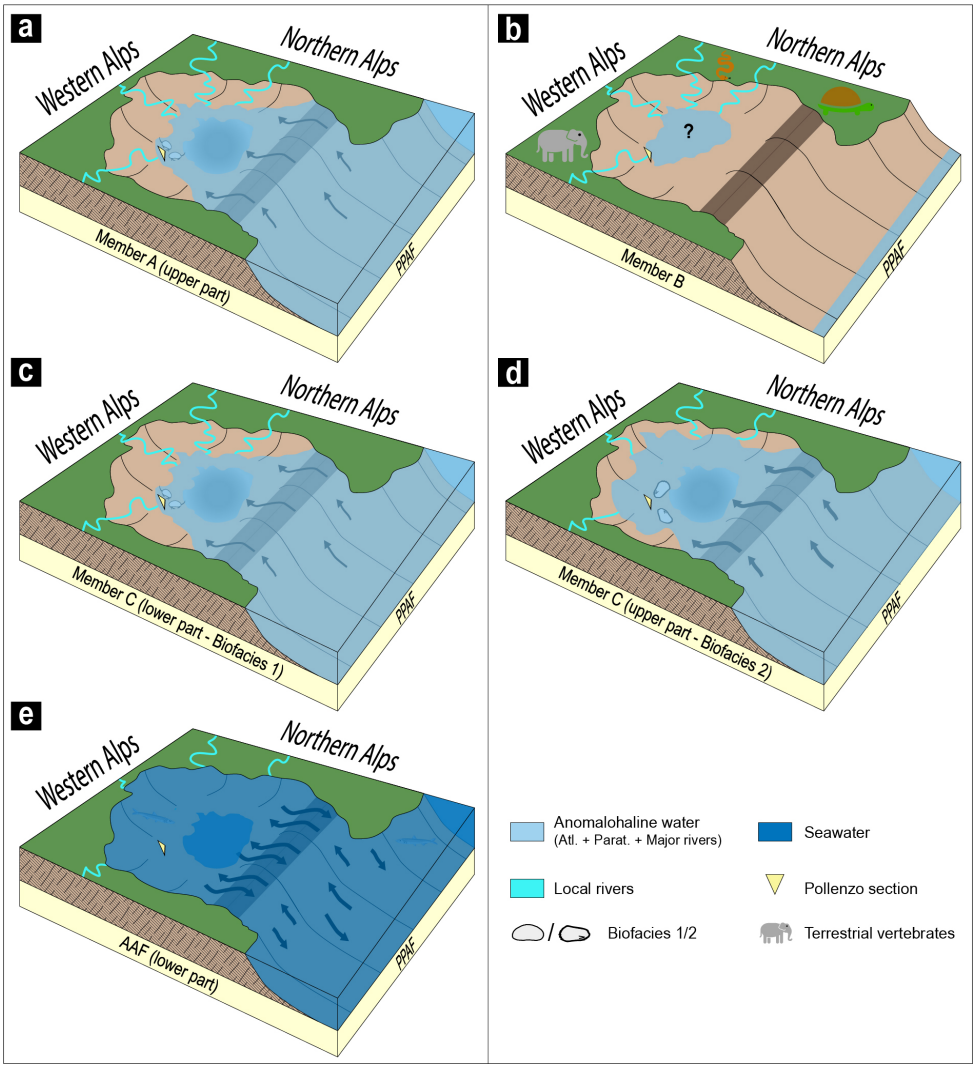

Fig. 3.7. *Evolution through part of MSC Stage 3 of the Piedmont Basin related to base-level variations in the open Mediterranean Basin.* **(a)** *A shallow-water subaqueous environment establishes in the Alba region after the emplacement of the VVC.* **(b)** *Falling stage of the Mediterranean base level, witnessed by the spreading of continental conditions.* **(c)** *The rising Mediterranean base-level establishes, in Pollenzo, a shallow-water environment inhabited by C. torosa with higher, more local river-like $^{87}Sr/^{86}Sr$.* **(d)** *The ongoing transgression causes a deepening and freshening of the Piedmont lagoon, setting up the environmental conditions for the truly Paratethyan ostracods to thrive. The increased contribution of Mediterranean waters with $^{87}Sr/^{86}Sr$ lower than the local rivers' causes a lowering of the $^{87}Sr/^{86}Sr$ of the water mass.* **(e)** *Changes in the Mediterranean-Atlantic gateway configuration re-establish a normal marine environment at the base of the Zanclean.*

mesohaline environment (0.5-18 g/l; The Venice System for the Classification of Marine Waters According to Salinity, 1958); instead, calcareous nannofossils are generally adapted to higher, oceanic salinities typically ranging between 33-37 g/l. On this basis, and considering that Paratethyan ostracods are certainly in-situ (e.g. Gliozzi et al., 2007; Stoica et al., 2016; Sciuto et al., 2018; Caruso et al., 2020; Andreetto et al., 2021a), the marine microfossils in Stage 3 sediments are generally considered to be reworked. However, some calcareous nannoplankton today bloom sufficiently intensively to dominate the phytoplankton assemblage in basins where oligo-mesohaline conditions are seasonally or permanently established. Examples include the Black Sea (Giunta et al., 2006), Baltic Sea (Hällfors, 2004; Thomsen, 2016), Adriatic Sea (Skejić et al., 2021) and Thessaloniki Bay (Dimiza et al., 2020). These studies of calcareous nannoplankton in modern, low salinity marine environments therefore do not preclude the coexistence of brackish Paratethyan ostracods and marine calcareous nannofossils in member C. Those species that have been identified here as potentially in-situ (see Fig. 3.6) are largely accepted to be adaptable to lower than normal marine salinity and to thrive during times of strongly fluctuating environmental conditions (Wade and Bown, 2006; Auer et al., 2014). In particular, *R. minuta*, which accounts for up to 70% of the assemblages of member C (Fig. 3.6), is considered a hardy, opportunistic and euryhaline taxon capable of withstanding highly stressed environments (Wade and Bown, 2006 and references therein). If Wade and Bown (2006) and Auer et al. (2014), among others, are correct in their hypothesis that *R. minuta* and the other nannotaxa listed in Fig. 3.6 can occur in low-salinity environments, then member C of the Pollenzo section documents that the Piedmont Basin was, during its deposition, exchanging water with the rest of the Mediterranean Basin via the Po Plain-Adriatic Foredeep (PPAF; Figs. 3.7c-d), which in turn was being simultaneously supplied by the Atlantic seawater other than Eastern Paratethys brackish water. In-situ assemblages of calcareous nannofossils including the most abundant taxa recognized in the CSC have already been reported by Popescu et al. (2007) and Pellen et al. (2017) in Stage 3 sediments from more southerly localities in the Adriatic region (i.e. Monticino, Maccarone, Civitella del Tronto, Fonte dei Pulcini and Fonte della Casa). The evidence used to argue that the nannofossils were in situ was the presence of rare *C. acutus* and *T. rugosus*. These are biostratigraphic markers of the uppermost Messinian/early Zanclean (Di Stefano and Sturiale, 2010; Agnini et al., 2017) and, therefore, cannot be reworked from older sediments. However, neither Roveri et al. (2008c) nor Cosentino et al. (2012) identified these age-diagnostic taxa in the same sections and they have also not been found by us in the CSC of the Piedmont Basin. We therefore suggest that taphonomic and paleoecological evidence, rather than biostratigraphic criteria, should be used in the interpretation of calcareous nannoplankton assemblages in Stage 3 sediments.

Occurring with the Biofacies 1-2 ostracods in the upper part of member C are also low diversity marine dinocyst assemblages, which include *Achomosphera/Spiniferites* spp., *Spiniferites bentori, Homotryblium, Operculodinium israelianum, Operculodinium janduchenei,*

Polysphaeridium zoharyi and one specimen of *Mendicodinium robustum*. Although these assemblages are of difficult interpretation due to their extremely poor preservation, their sudden appearance in concomitance with the ostracods may suggest that they were transported into the Piedmont Basin from the same water mass. In agreement with the environment indicated by the taxa of potentially in situ calcareous nannofossils, the occurrence of these dinocyst taxa known to inhabit restricted shallow marine, lagoonal settings (Pross and Brinkhuis, 2005; Zonneveld et al. 2013) is reconcilable with the presence of the ostracods.

The black layer capping member C (Fig. 3.2g) and marking the paleohydrological change from brackish to normal marine salinity conditions shares a very similar sandy texture and black color with other dark beds found in the CSC (Figs. 3.2c-d). Similar black layers found just below the lowermost Zanclean sediments in a number of localities of the Northern-Central Apennines (Gennari et al., 2008) and in the Cypriot Pissouri Basin (Rouchy et al., 2001) have also been interpreted as paleosols. However, the presence of *Thalassinoides*, which are marine firm ground burrows today constructed by a variety of marine organisms (Myrow, 1995), at the top of the topmost black layer of the Piedmont Basin (Dela Pierre et al., 2016) may be indicative that at least part of it was deposited under marine conditions. However, more detailed sedimentological, geochemical and paleontological investigations are required to fully confirm its paleoenvironmental significance.

3.6.2 Episodic establishment of water exchange between the Piedmont Basin and the Mediterranean during Stage 3

Sr^{2+} cations in solution and absorbed by Ca^{2+}-bearing minerals during precipitation have an $^{87}Sr/^{86}Sr$ ratio that results from the integration of Sr^{2+} from isotopically-different and variably-concentrated water sources flowing into the basin. As long as the $^{87}Sr/^{86}Sr$ fingerprint of these sources is known, then the hydrologic fluxes to the basin can be reconstructed (e.g. Doebbert et al., 2014; Reghizzi et al., 2018; Andreetto et al., 2021b). This methodology is only applicable to continental environments (lakes and rivers) or sedimentary basins which have a restricted connection with the global ocean (like the Mediterranean Basin during the MSC; Roveri et al., 2014a). Continental inputs are, in fact, not distinguishable in normal oceanic settings (e.g. Kuznetsov et al., 2012; Benito et al., 2021) due to the far higher Sr concentration in seawater (7.8 mg/l; Palmer and Edmond, 1992) than in river water (<<1 mg/l; Palmer and Edmond, 1992; Gaillardet et al., 1999; Marchina et al., 2018). $^{87}Sr/^{86}Sr$ ratios from the CSC (0.708834-0.708746) are significantly lower than those of the coeval seawater (~0.709024; McArthur et al., 2012). These data strongly indicate that sedimentation of member A and C mudstones took place in a subaqueous environment exclusively (endorheic lake) or mainly (lagoon connected to the external sources via the Mediterranean) formed by non-marine inputs. If this water body was an endorheic lake, like suggested by Amadori et al. (2018), then the $^{87}Sr/^{86}Sr$ value of the Paratethyan ostracod valves must be representative of the $^{87}Sr/^{86}Sr$ ratio of the lake water, which

is the product of all the river(s) flowing into the lake (e.g. Joordens et al., 2011; Baddouh et al., 2016) after the weathering and erosion of the isotopically-different, catchment-forming lithologies (e.g. Palmer and Edmond, 1992; Brenot et al., 2008; Hajj et al., 2017; Marchina et al., 2018; Peucker-Ehrenbrink and Fiske, 2019). The presence, in member B, of pebbles of metamorphic rocks exposed in the Alpine chain today indicates that the bedrocks forming the proto-Alps were a source of Sr^{2+} ions into the Piedmont Basin. Measurements of the Sr signatures of the rivers that flowed into the Piedmont Basin during MSC Stage 3 are obviously not available, but can be reliably approximated assuming that the paleorivers had similar $^{87}Sr/^{86}Sr$ ratios to those of the present-day rivers (e.g. Vasiliev et al., 2010, 2021; Placzek et al., 2011; Doebbert et al., 2014; Grothe et al., 2020) because the catchments of modern rivers of the Mediterranean area, including the Piedmont region, did not change significantly since the latest Messinian (e.g. Brass, 1976; Goudie, 2005; Schildgen et al., 2014; Cosentino et al., 2018). $^{87}Sr/^{86}Sr$ data are available for all major rivers draining Northern Italy today (Marchina et al., 2018). Among them, only the $^{87}Sr/^{86}Sr$ data of the longest river in Northern Italy, the Po River, are chosen as the local reference $^{87}Sr/^{86}Sr$ signal because the Po River integrates at its mouth and, along its course, via its tributaries, the dissolved solutes provided by the lithologies forming the Alps and Apennines, were the catchments are located (Marchina et al., 2018). The $^{87}Sr/^{86}Sr$ composition at any given point of the Po River course is therefore representative of the mixing of isotopically-different Sr^{2+} coming from all the lithologies outcropping in the catchments upstream of that point. We consider the lowest $^{87}Sr/^{86}Sr$ ratio of the Po River before its confluence with the Tanaro River, which occurs approximately at the far eastern border of the Piedmont Basin (Fig. 3.1a), as the minimum estimate of the $^{87}Sr/^{86}Sr$ composition of a lake that could have hypothetically existed in the late Messinian Piedmont Basin. The $^{87}Sr/^{86}Sr$ values measured for the Po water at six locations before confluence with the Tanaro River range between 0.709187 and 0.709745 (Fig. 3.8). These values are compatible with the mixing of high radiogenic Sr^{2+} provided by the igneous and metamorphic rocks forming the great majority of the Alpine sector with less radiogenic Sr^{2+} released by Jurassic ophiolites and Mesozoic carbonates locally outcropping along the course of the tributaries Dora Baltea and Tanaro (Fig. 3.1a; see Dal Piaz, 2010 for insights into the geology of Northern Italy). This range of values, however, is substantially higher than the $^{87}Sr/^{86}Sr$ values measured on ostracods valves from both the member A/B transition (0.708870-0.708871) and from member C (0.708746-0.708834; Fig. 3.8). Another possibility, if the Piedmont Basin had in the latest Messinian an areal extent and/or an arrangement of the fluvial network different than today, would be that tributaries of the Po River further east of the Tanaro River also supplied Sr^{2+}. Even if so, at no point beyond the present-day eastern margin of the Piedmont Basin the Po River attains $^{87}Sr/^{86}Sr$ values low enough that overlap with the ostracod data (Fig. 3.8). This includes its lower reaches where, compared to the upper reaches, there is a higher contribution of water that drains carbonates and that gives some of the northeastern Po tributaries lower $^{87}Sr/^{86}Sr$ ratios (Marchina et al.,

2018). Consequently, the $^{87}Sr/^{86}Sr$ ratios from today rivers of Northern Italy do not support the notion that the biota of the CSC inhabited an endorheic lake fed by northern Italian rivers (e.g. Amadori et al., 2018). Instead, $^{87}Sr/^{86}Sr$ ratios measured on Stage 3 Piedmont ostracods must be accounted for by mixing of local freshwaters with their relatively high $^{87}Sr/^{86}Sr$ signatures with water derived from an external source and carrying Sr^{2+} cations with a lower $^{87}Sr/^{86}Sr$ ratio.

A similar disparity between high $^{87}Sr/^{86}Sr$ ratio river water and low $^{87}Sr/^{86}Sr$ ratios measured on Stage 3 ostracods was found to occur also in the Sorbas-Nijar-Vera basins in SE Spain (Fig. 3.8; Andreetto et al., 2021b). These Spanish data were interpreted to reflect a combination of (local) fluvial and Mediterranean input, which is thought to have had, at times during MSC Stage 3, a $^{87}Sr/^{86}Sr$ signature sufficiently low to draw the higher ratios of the Spanish rivers down to the values acquired by the ostracods (Andreetto et al., 2021b). $^{87}Sr/^{86}Sr$ values measured on gypsum and ostracod valves from more central Mediterranean basins, far from the influence of the local fluvial input during the highstand phases and where waters from the lower radiogenic large rivers (e.g. Nile: 0.7060, Brass, 1976; Rhône: ~0.7087, Albarède and Michard, 1987 and Gaillardet et al., 1999) and Eastern Paratethys (0.70840.7085, Grothe et al., 2020) and the higher radiogenic Atlantic Ocean (~0.709024; McArthur et al., 2012), were coming together (e.g. Manzi et al., 2009; Roveri et al., 2014c; Marzocchi et al., 2016; Vasiliev et al., 2017; García-Veigas et al., 2018), are consistently lower than 0.708850 (Andreetto et al., 2021a). We therefore suggest that the $^{87}Sr/^{86}Sr$ Piedmont CSC data are also the consequence of mixed fluvial and

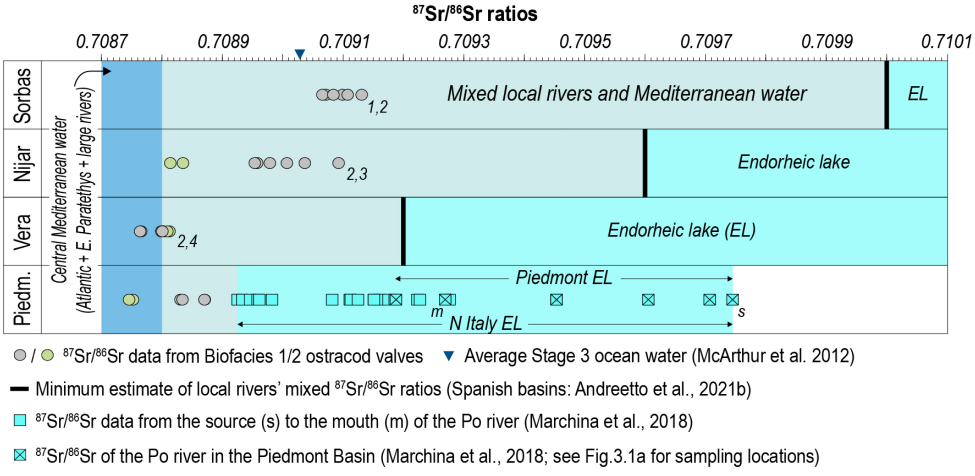

Fig. 3.8. *Comparison between the Stage 3* $^{87}Sr/^{86}Sr$ *record of the Piedmont Basin and of the marginal basins of SE Spain (1-McCulloch and De Deckker, 1989; 2-Andreetto et al., 2021b; 3-Roveri et al., 2019; 4-Fortuin et al., 1995).* $^{87}Sr/^{86}Sr$ *ratios are plotted against the* $^{87}Sr/^{86}Sr$ *fingerprint of the coeval water mass filling the Mediterranean (Andreetto et al., 2021b), the coeval seawater signature (McArthur et al., 2012) and the estimated* $^{87}Sr/^{86}Sr$ *for isolated lakes. Note that none of the* $^{87}Sr/^{86}Sr$ *ratios measured on Biofacies 1-2 ostracods from four separated marginal basins overlap with the* $^{87}Sr/^{86}Sr$ *ratio expected from endorheic lakes.*

Mediterranean input (Fig. 3.8). For this to be the case, the Mediterranean water level must have been full enough to reach the Piedmont Basin and have been dominated by non-marine water (e.g. Manzi et al., 2009, 2016; Roveri et al., 2014b, 2014c; Marzocchi et al., 2016; Stoica et al., 2016; Pellen et al., 2017; Vasiliev et al., 2017; García-Veigas et al., 2018), at least during times when Paratethyan ostracods were colonizing the marginal basins (e.g. Andreetto et al., 2021b).

3.6.3 Towards the marine replenishment of the Piedmont Basin

The upper part of member C comprises a stratigraphic increase in ostracod diversity. The poorly diversified, shallower Biofacies 1 is associated with higher river-like ratios, whereas the deeper water, more diverse Biofacies 2 has lower ratios, similar to those that characterize the Stage 3 Mediterranean water (Fig. 3.4). This decrease in $^{87}Sr/^{86}Sr$ in the upper part of member C is likely to reflect an enhanced contribution of Mediterranean water to the Piedmont Basin in parallel with increased water depth. The ambiguous nature of the topmost black layer at the M/P boundary (Fig. 3.2g) hampers the interpretation of this transition both at Piedmont and Mediterranean-wide. For the Zanclean transgression to have been catastrophic (e.g. Micallef et al., 2018; Caruso et al., 2020; Garcia-Castellanos et al., 2020; Spatola et al., 2020), the black layer would need to have been deposited during a regression following the rising Mediterranean base-level documented in the upper part of member C. The alternative, non-catastrophic M/P transition would instead require rising Mediterranean base-level to have continued into the Pliocene uninterrupted. Notwithstanding the nature of the transition, the Pliocene AAF sediments only contain stenohaline marine taxa, including some biostratigraphic markers of the early Zanclean such as the nannofossil *Reticulofenestra zancleana* (Di Stefano and Sturiale, 2010). This indicates that early Pliocene sedimentation in Piedmont took place under open marine conditions (Fig. 3.7e). The dinocyst association in AAF samples FSS10 and FSS11, 30 and 35 cm above the M/P boundary, reflects a deepening-upward trend from coastal/(outer) neritic to outer neritic/oceanic environments. The proportion of deep bathyal foraminifera and ostracod taxa in Lower Zanclean samples from the Narzole core (Figs. 3.1a-b) suggests that the Early Zanclean bathymetry was ~500-700 m in the Pollenzo area (Violanti et al., 2009). Similar Early Zanclean faunal associations have previously been described from the AAF exposed in the Piedmont Basin (Sturani, 1973; Trenkwalder et al., 2008; Violanti et al., 2011) and basal Pliocene sediments elsewhere in the Mediterranean (e.g. Castradori, 1998; Iaccarino et al., 1999; Rouchy et al., 2003, 2007; Gennari et al., 2008; Guerra-Merchán et al., 2014; Corbí and Soria, 2016; Corbí et al., 2016; Frigui et al., 2016; Roveri et al., 2019; Caruso et al., 2020). These have also been interpreted as indicating that Atlantic waters had fully replenished the Mediterranean by 5.332 Ma. The $^{87}Sr/^{86}Sr$ of Early Zanclean microfossils should therefore be within error of ocean ratios. The $^{87}Sr/^{86}Sr$ is homogeneous in the global ocean (McArthur et al., 2012) and in semi-closed basins with an unrestricted oceanic gateway (e.g. Kuznetsov et al., 2012). The $^{87}Sr/^{86}Sr$ ratio measured on *Globigerina* tests (0.709006±0.00000702) 35 cm above the base of the

AAF (sample FSS11) is significantly higher than the CSC samples below it and is close to, but analytically lower than the coeval ocean value (~0.709024±0.000004; McArthur et al., 2012; Fig. 3.4). Model calculations from Topper et al. (2014) show that $^{87}Sr/^{86}Sr$ values measurably deviate from oceanic values towards riverine values if the river-derived Sr flux constitutes at least 25% of the total water flux. These conditions are more likely to be achieved when the connection between the ocean and the marginal basin is restricted (Topper et al., 2014). We suggest that this discrepancy reflects the delayed response of the system to the hydrological change occurring at the M/P boundary, with substantial amounts of non-marine Sr^{2+} still circulating in the Mediterranean. This geochemical evidence that fully marine conditions were not restored in Piedmont immediately after the Zanclean replenishment is mirrored by a higher resolution Zanclean $^{87}Sr/^{86}Sr$ dataset from the Adana Basin (S Turkey; Cipollari et al., 2013). Elsewhere in the Mediterranean (e.g. Chelif Basin in Algeria and the deep Alborán Basin; Rouchy et al., 2007; Bulian et al., 2021), some authors have reported low diversity foraminiferal assemblages that are consistent with a delay to the establishment of fully marine conditions in the lowermost Pliocene. The distribution of these data across both East and Western Mediterranean basins indicates that the delay in establishing fully marine conditions was at a Mediterranean scale, rather than a local phenomenon. It was estimated that such conditions possibly lasted for at least half of a precession cycle after the M/P transition (e.g. Pierre et al., 2006; Rouchy et al., 2007), but accurate chronological data showing the exact time at which normal marine fossil assemblages and geochemical signals returned in the Mediterranean are still lacking.

3.7 Conclusions

Our cross-disciplinary study of the Cassano Spinola Conglomerates in the marginal Piedmont Basin provides new multifaceted insights on Stage 3 of the Messinian Salinity Crisis. The Piedmont Basin remained underwater possibly for most of Stage 3, hosting an inhospitable subaqueous environment (member A) that only before being superseded by continental conditions (member B) gets populated mostly by the ostracod genus *Cyprideis* and shows evidence in the $^{87}Sr/^{86}Sr$ ratios that was exchanging water with the Mediterranean. At some point this environment shrinks from the more marginal areas of the basin, exposing terrestrial pathways for trans-European mammal migrations. The abrupt replacement of continental deposits by subaqueous mudstones (member C) provides evidence for a transgression. This event is accompanied by the appearance of progressively more diverse assemblages of Paratethyan ostracods possibly together with taxa of calcareous nannofossil and dinocysts adaptable to environments with lower than seawater salinity and fluctuating environmental conditions. $^{87}Sr/^{86}Sr$ ratios of the latest Messinian ostracods infer a mixture of local river and central Mediterranean waters, which demonstrate that the Piedmont Basin was already connected with the central Mediterranean water mass before the M/P boundary. The ostracods' diversity change observed at the top of the CSC matches with the decrease in $^{87}Sr/^{86}Sr$ ratios

from higher to lower values and together they reflect a progressive upward increase of the depth and freshening of the environment that we relate to the enhanced entrance of Mediterranean water in a general framework of Mediterranean base-level rise. When placed in a more regional context, our results indicate that the Mediterranean Basin was relatively full of water derived from Atlantic, Eastern Paratethys and the ever-flowing large rivers at times corresponding to Paratethyan ostracod colonization of the rims.

Acknowledgments

This research was supported by the project SALTGIANT-Understanding the Mediterranean Salt Giant, a European project which has received funding from the European Union's Horizon 2020 research and innovation program, under the Marie Sklodowska-Curie [grant agreement No 765256]. This manuscript benefited from the comments of two anonymous reviewers, who contributed to its improvement.

Sunset on Capo Bianco and the beach of Eraclea Minoa (Credit: Jasper Maars).

4

HIGH-AMPLITUDE WATER LEVEL FLUCTUATIONS AT THE END OF THE MESSINIAN SALINITY CRISIS: IMPLICATIONS FOR GYPSUM FORMATION, CONNECTIVITY AND GLOBAL CLIMATE

Andreetto, F., Flecker, R., Aloisi, G., Mancini, A.M., Guibourdenche, L., de Villiers, S., Krijgsman, W.

ABSTRACT

The formation and dissolution of salt giants impacts ocean chemistry on thousand-million year timescales. Gypsum precipitation and weathering changes the oceanic calcium concentration with implications for the carbon cycle and global temperatures. However, the connectivity of salt giants with the global ocean is necessarily restricted, making the timing of Ca^{2+} extraction and return more uncertain. Here we reconstruct the final phase of gypsum precipitation of the Late Miocene Mediterranean Salt Giant using micropaleontology, sedimentology and $^{87}Sr/^{86}Sr$ analyses on the most complete record preserved at Eraclea Minoa on Sicily and explore its implications for global climate. Precessional gypsum-marl couplets (Upper Gypsum) characterize the last 200 kyrs (Stage 3) of the Messinian Salinity Crisis (MSC; 5.97-5.332 Ma) in both intermediate (500-1000 m) and deep (>1000 m) Mediterranean basins. The interbedded selenitic gypsum layers contain well-preserved calcareous nannofossil assemblages dominated by Reticulofenestra minuta, a marine species which tolerates stressful conditions. Marine water is also required to explain the gypsum $^{87}Sr/^{86}Sr$ data, which describe a small range of ratios (0.708704-0.708813) lower than coeval ocean water. Mass-balance calculations indicate that during gypsum precipitation, the Atlantic made up ≤20% of a Mediterranean ("Lago-Mare") water mass dominated by low salinity discharge from large river systems and Eastern Paratethys. This suggests episodic extraction of calcium and sulfate ions from the ocean throughout MSC Stage 3. The marls commonly contain shallow (30-100 m) brackish-water ostracods of Paratethyan (Black Sea) origin. Marls with Paratethyan ostracods are also found in both marginal (<500 m) and deep Mediterranean settings. This indicates that marl deposition was not synchronous across the basin, but that it occurred in intermediate and deep basins during base-level lowstands at insolation minima and on the shallow Mediterranean margins during insolation maxima-driven highstands. These high-amplitude base-level fluctuations exposed the evaporites to weathering, but ponded the products in the Mediterranean basin until reconnection occurred at the beginning of the Pliocene.

This chapter is peer-reviewed and published as:
Andreetto, F., Flecker, R., Aloisi, G., Mancini, A.M., Guibourdenche, L., de Villiers, S., Krijgsman, W., 2022. High-amplitude water-level fluctuations at the end of the Mediterranean Messinian Salinity Crisis: implications for gypsum formation, connectivity and global climate. Earth and Planetary Science Letters, 595, 117767.

4.1 Introduction

Recent modeling of evaporite weathering and deposition suggests that, alongside the well-established silicate weathering and carbonate sedimentation feedback mechanisms, the formation and dissolution of giant calcium sulfate deposits may be an episodic driver of thousand-million year timescale changes in the carbon cycle (Shields and Mills, 2020). Salt giants have formed only episodically in Earth history, typically as a consequence of the tectonic restriction (opening or closing) of the connection between the global ocean and a mid-latitude marginal marine basin (Warren, 2016). Model experiments simulate the atmospheric CO_2 and temperature consequences of evaporite deposition and weathering events assuming a constant oceanic supply of Ca^{2+} and SO_4^{2-} ions to the marginal basins, or a constant riverine Ca^{2+} and SO_4^{2-} flux from continental weathering, both lasting an estimated 1 million years (Shields and Mills, 2020). The heterogenous geological record of these salt giants, however, suggests that the ocean-marginal basin connectivity must have varied considerably (Warren, 2016), impacting the duration and intensity of ion fluxes in relation to evaporite precipitation and weathering during the formation of a salt giant. Reconstructing, the nature and timing of that variable connectivity, its relationship with gypsum precipitation and base-level changes is a critical step in quantifying the importance of this mechanism in driving carbon cycle change.

The most recent of the Earth's salt giants accumulated in the Mediterranean during the Messinian Salinity Crisis (MSC; 5.97-5.332 Ma). This formed as a consequence of Late Miocene tectonic uplift of the Gibraltar region which restricted marine exchange between the Mediterranean Basin and the Atlantic Ocean (e.g. Krijgsman et al., 2018). The Mediterranean's environmental response was dramatic, resulting in the precipitation of >1 million km^3 of evaporites (e.g. Roveri et al., 2014a). Three evaporitic episodes with different connectivity configurations have been distinguished (Roveri et al., 2014a): Stage 1, dominated by gypsum-marl couplets which are thought to have been deposited during restricted two-way Atlantic-Mediterranean exchange (e.g. Reghizzi et al., 2018); Stage 2 comprises an up to 2 km-thick halite layer resulting from Atlantic inflow but no Mediterranean outflow (e.g. Krijgsman et al., 2018); and Stage 3 in which gypsum alternates with brackish-water, ostracod-bearing marls where the connectivity scenario is controversial (Andreetto et al., 2021a). It has proved difficult to explain both the outcrop data, which mostly suggest a relatively full Mediterranean, and evidence from deep-sea cores and seismics, which suggest low water conditions (see Andreetto et al., 2021a for summary). These different base level reconstructions have implications for Atlantic-Mediterranean connectivity at the end of the MSC and its impact on ocean chemistry.

Previous attempts to reconstruct Mediterranean hydrology, paleoenvironments and connectivity during Stage 3 have involved $^{87}Sr/^{86}Sr$ (Müller et al., 1990; Roveri et al., 2014b; García-Veigas et al., 2018) because water sources of different origin (i.e. ocean, lakes, rivers, groundwater) have distinct $^{87}Sr/^{86}Sr$ ratios (e.g. Reghizzi et al., 2018; Andreetto et al., 2021b, 2022; Bista et al., 2021). A solely geochemical approach to Stage 3 has proved inconclusive

however, because more than one combination of potential source waters can result in the same geochemical signal. In this multi-proxy study, we combine new and existing sedimentological and paleontological observations with $^{87}Sr/^{86}Sr$ analyses on selenite gypsum crystals and ostracod valves from the Eraclea Minoa section (Caltanissetta Basin, Sicily; Fig. 4.1). Eraclea Minoa is the most complete sedimentary record of Stage 3 exposed on land and previous works have described evidence of both Atlantic and Eastern Paratethys influence (Grossi et al., 2015; Vasiliev et al., 2017; García-Veigas et al., 2018). The succession shows strong precessional cyclicity from which an astronomical age model has been derived (van der Laan et al., 2006; Manzi et al., 2009). Unlike age-equivalent marginal exposures, which are dominated by continental clastics, the Caltanissetta Basin was, during Stage 3, at intermediate depths (500-1500 mbsl) and accumulated both gypsum and ostracod-bearing marls, allowing the Sr isotopic characterization of both lithological elements. This dataset allows us to reconstruct Stage 3 connectivity and consider its impact on Late Miocene ocean biogeochemistry and climate.

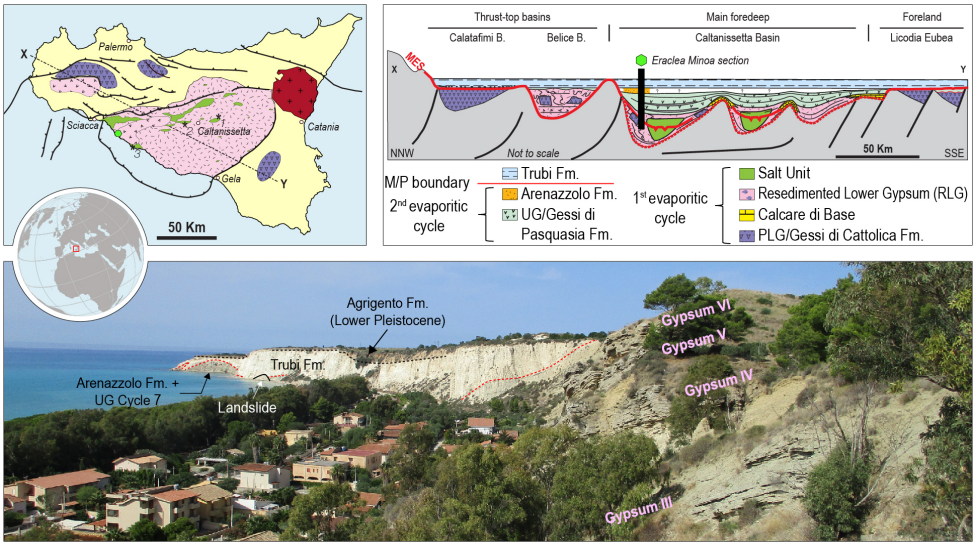

Fig. 4.1. *Simplified geological map of Sicily (upper left; modified from Manzi et al., 2021) and NW-SE-oriented geological cross section (upper right; modified from Manzi et al., 2021) showing the geographical and stratigraphic position of the Eraclea Minoa section, respectively. Asterisks indicate the position of other sections mentioned in the text (1: Balza Soletta, Maniscalco et al., 2019; 2: Montedoro, Rouchy and Caruso, 2006; 3: Siculiana Marina, Caruso and Rouchy, 2006). Below is a panoramic view of (part of) the Eraclea Minoa section. Four gypsum beds (III, IV, V and VI) overlooking the Eraclea Minoa village stand out in the foreground. The cliff of Cattolica Eraclea/Capo Bianco in the background is mainly composed of the white marly deposits of the Pliocene Trubi Fm. unconformably overlain by the Agrigento Fm. of Lower Pleistocene age. Locally, the topmost part of the UG and/or the Arenazzolo Fm. crop out at the cliff foot.*

4.2 Materials and methods

The Eraclea Minoa section (37°23'36"N, 13°17'10.38"E) is ~223 m-thick and comprises seven gypsum-marl alternations (Fig. 4.2). This Upper Gypsum succession is overlain sequentially by the Arenazzolo Fm., a ~6-7 m-thick fine to medium-grained sandstone, and the Pliocene Trubi marls (Fig. 4.2). Field work to log and sample the Eraclea Minoa section was undertaken in Spring 2001 and September 2020 and 2021.

Selenitic gypsum can preserve biomineralized structures (Pellegrino et al., 2021), so twenty selenite crystals were selected from gypsums II to VII for micropaleontological screening. Crystals were cleaned of surface dirt using a brush and MilliQ purified water, sliced with a cleaned box cutter into 1-2 mm-thick splits and qualitatively analyzed, prior to carbon-coating the slices. Samples were then analyzed at the Electron Microscopy Centre at Utrecht University using a JEOL Neoscope II JCM-6000 table-top SEM equipped with an energy-dispersive X-ray spectroscopy (EDS) and Electron Probe Microanalyser JEOL JXA 8530F.

We expanded the available ostracod and gypsum $^{87}Sr/^{86}Sr$ dataset at Eraclea Minoa (Grossi et al., 2015; García-Veigas et al., 2018) with 43 additional isotopic ratios on gypsums (39) and *Cyprideis agrigentina* valves from cycle 3 (4). Sample preparation and data acquisition followed standard procedures for gypsum (Reghizzi et al., 2018) and ostracods (Bista et al., 2021; Andreetto et al., 2022). The more vitreous selenites and balatino gypsum chips were mechanically isolated, washed with MilliQ-water and micromilled with a hand drill avoiding impurities trapped within crystals. 10 mg of gypsum powder was digested in 1M ammonium acetate, centrifuged with MilliQ-water, dried overnight at 120˚C on a hot plate, redissolved in 3M HNO_3, centrifuged and refluxed on the hot plate. 6-7 adult valves of *C. agrigentina* were hand-picked under an optical microscope, repeatedly rinsed with MilliQ-water and methanol to remove potential contaminants (clay particles and organic material), dissolved in 300 µl of 0.1M of HNO_3 and dried at 120˚C. Strontium of all samples was isolated using 100 µl of pre-cleaned Sr-Spec resin and loaded onto rhenium filaments with a $TaCl_5$ activator solution. $^{87}Sr/^{86}Sr$ ratios from gypsums V and VI were measured in SUERC (University of Glasgow) on a VG Sector 54-30 mass spectrometer in dynamic multi-collection mode. Instrumental mass fractionation was corrected using an exponential law and $^{86}Sr/^{88}Sr=0.1194$. NIST SRM987 values over the period the measurements were carried out were: $^{87}Sr/^{86}Sr$ =0.710251T20 (2cS.D.), n=95. $^{87}Sr/^{86}Sr$ ratios from the ostracods and gypsums I-IV and VII were measured at the Bristol Isotope Group Facilities (University of Bristol) on a Thermo-Finnigan Triton thermal ionization mass spectrometer using a multi-dynamic 'triple jump' method. The average $^{87}Sr/^{86}Sr$ is based on 200 ratios. The mean $^{87}Sr/^{86}Sr$ values of nine NIST SRM 987 analyzed during this session was 0.710245±0.000006267 and that of four NIST SRM 987 which have undergone chemical purification (mean 0.710268±0.0000236925) are in good agreement with the accepted values of SRM 987 of 0.710250.

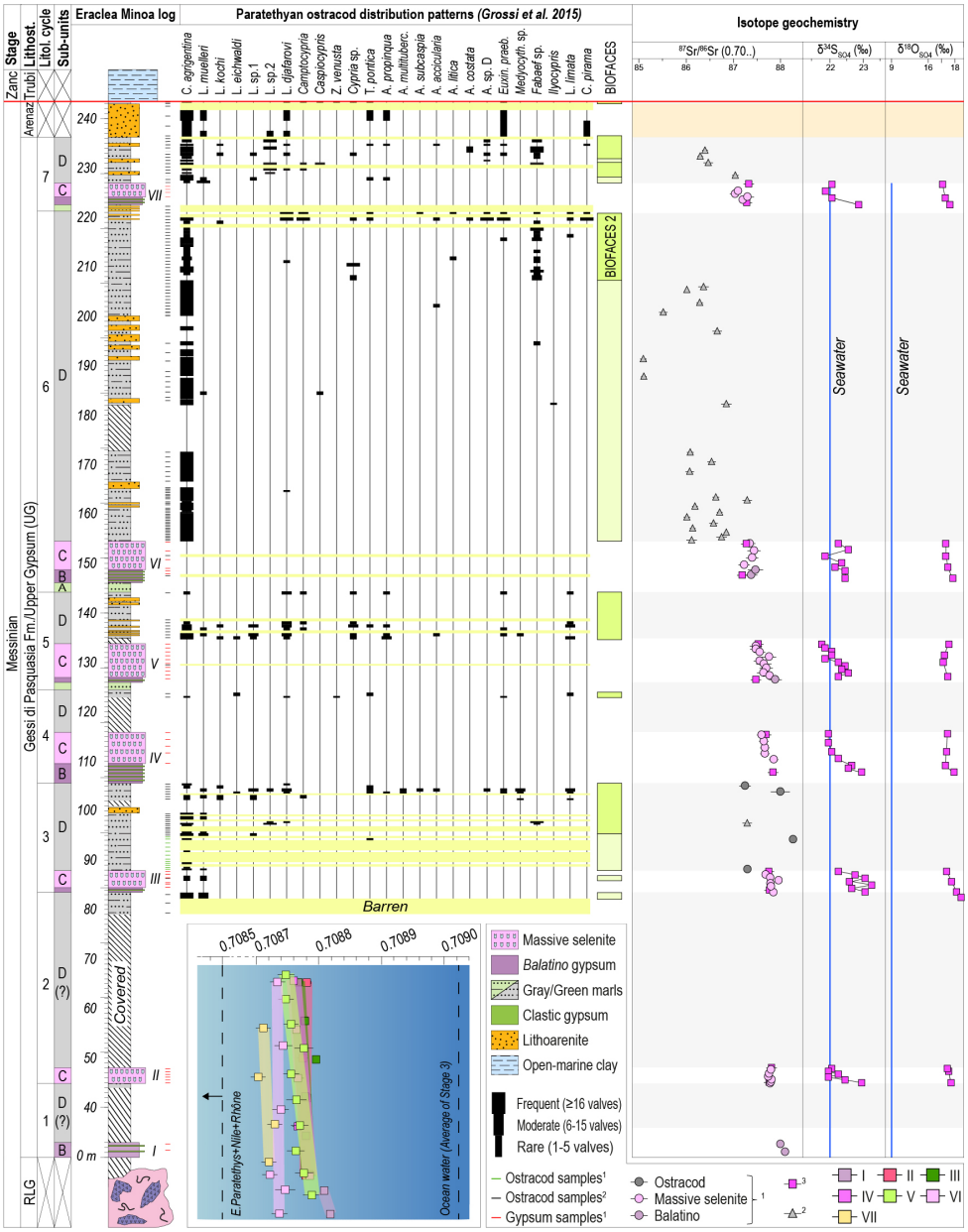

Fig. 4.2. *Lithological log of the Eraclea Minoa section (modified from Manzi et al., 2009). An ostracod stratigraphic distribution chart was constructed integrating the results of Grossi et al. (2015) with seventeen marl samples from the base of cycle 3 provided by Elsa Gliozzi and Domenico Cosentino and prepared at the Earth Science Department of the Universitá degli Studi Roma Tre with standard micropaleontological methods of washing, sieving and drying. New and published (Grossi et al., 2015; García-Veigas et al., 2018) $^{87}Sr/^{86}Sr$*

ratios measured on gypsum crystals and ostracod valves and sulfur and oxygen (in sulfate) isotope profiles from García-Veigas et al. (2018) are also plotted. The bottom diagram is a close view of the $^{87}Sr/^{86}Sr$ isotopic composition of the gypsum beds I-VII. Data are plotted against the coeval oceanic ratio (after McArthur et al., 2012) and the composition of a system mixing river water from Nile and Rhône (0.707427; Topper et al., 2011) and the Eastern Paratethys (0.7084-0.7085 during the latest Messinian; Grothe et al., 2020). The lack of overlap between gypsum and water data are evidence that the gypsum-precipitating water was a combination of all three sources mentioned above. (1): This study; (2): Grossi et al. (2015); (3): García-Veigas et al. (2018).

4.3 Results

4.3.1 Sedimentological description of a typical UG cycle

Manzi et al. (2009) described three repeated facies associations of the Upper Gypsum at Eraclea Minoa: two distinct gypsum-dominated facies associations (B and C) and a single gypsum-free facies association (A). On the basis of more detailed lithological and faunal analysis, we divide their facies association A into two sub-units A and D.

Our sub-unit A, arbitrarily chosen as the base of the lithological cycle, comprises cm- to dm-thick beds of greenish, homogeneous marls interbedded with white laminated diatomites (Figs. 4.3c-d). This sub-unit, typically 1-2 meters thick, occurs immediately beneath the gypsum-bearing sequence (Figs. 4.2, 4.3b-c). Sub-unit D, at the top of the cycle, is found directly above the gypsum and consists of gray marls intercalated with cm- to dm-thick siltstones and litharenites (Figs. 4.2, 4.3h). The gypsum layers at Eraclea Minoa typically start with cm- to dm-thick beds of laminar (or balatino) and clastic gypsum (gypsarenites) alternating with greenish homogeneous marls (sub-unit B; Figs. 4.3c, e) and show a sharp change to rhythmic alternations of dm-thick layers of massive selenite and mm- to cm-thick greenish marls (sub-unit C; Fig. 4.3f). The balatino gypsum comprises alternating mm-thick gypsum cumulate layers with clay-rich horizons only a few hundreds of microns thick (Fig. 4.3e). The gypsarenites are commonly massive (Fig. 4.3e) with occasional sedimentary structures such as normal grading and horizontal lamination (Manzi et al., 2009). The selenite beds comprise bottom-grown, swallow-tail gypsum crystals (or selenites) oriented with the re-entrant angle of the twins upward (Fig. 4.3f). Crystal size is relatively uniform in individual beds, but increases vertically through sub-unit C, from cm-scale crystals at the base to several dm in length at the top. The geometry of the gypsum beds also changes upwards, from tabular (Fig. 4.3f) to domal or cauliflower-shaped (Fig. 4.3b). The resulting irregular upper surface (Fig. 4.3b) led some authors to interpret an episode of subaerial erosion (e.g. Rouchy and Caruso, 2006; Raad et al., 2021). However, no karstic features are observed in the Eraclea Minoa gypsums (see also Manzi et al., 2009). At Eraclea Minoa, cycles 5, 6 and 7 all show a consistent facies sequence from the diatomite-bearing sub-unit A, through the cumulate and clastic gypsum sub-unit B, selenite-dominated sub-unit C, to the ostracod-bearing marls of sub-unit D (Fig. 4.2). Cycles 3

and 4 comprise sub-units B-D without the diatomaceous sub-unit A. Cycles 1 and 2 are poorly exposed with only sub-unit B visible in cycle 1 and C and D in cycle 2 and 3 (Fig. 4.2).

4.3.2 Micropaleontology

4.3.2.1 Ostracods in sub-unit D marls

Sub-unit D marls contain 25 ostracod species (Grossi et al., 2015). One of these, *C. agrigentina*, is of Mediterranean origin (Grossi et al., 2015). All the others are endemic to Paratethys (Fig. 4.2; Stoica et al., 2016). The absence of Paratethyan ostracods in Mediterranean sediments prior to MSC Stage 3 and the occurrence here of well-preserved valves of different moult stages indicate that these ostracods are in situ (Grossi et al., 2015). In cycles 3, 6 and 7 there is a clear increase in ostracod diversity through sub-unit D from almost (cycle 7) or completely (cycle 3 and 6) monospecific assemblages of *C. agrigentina* (Biofacies 1) at the base to diverse communities of Paratethyan taxa (Biofacies 2) at the top (Fig. 4.2; Grossi et al., 2015). Planktic and benthic foraminifera have also been reported from sub-unit D's marls (Caruso and Rouchy, 2006). However, only *Ammonia tepida*, which like *C. agrigentina* dwells in euryhaline and shallow-water, is considered to be in-situ (Grossi et al., 2015). One of the three samples from a marl layer interbedded with selenites (sub-unit C) also contained valves of *C. agrigentina* and *Loxoconcha muelleri* (Fig. 4.2; Grossi et al., 2015). Analysis of a small number of marl samples from sub-unit A suggests that these sediments contain no ostracods (Fig. 4.2).

4.3.2.2 Calcareous nannofossils in selenitic gypsum

The Eraclea Minoa selenites display alternating turbid/dark and transparent laminae (Fig. 4.4a). SEM inspection of samples from layers II-VII reveals that the dark color is associated with abundant, closely packed calcareous nannofossils associated with a small detrital component, mostly clay and rare silt- and clay-sized euhedral halite crystals (Fig. 4.4b), which might result from drying out of fluid inclusions. Since the analyzed samples are slices of selenite crystals, we can confirm that these are microfossils embedded within the gypsum (Figs. 4.4b-d). Well preserved calcareous nannofossils comprising pristine platelets and intact coccospheres (Fig. 4.4e) are observed both in cavities (Figs. 4.4b-c, e-f) and within the undamaged parts of the crystals (Fig. 4.4d). Poorly preserved specimens including fragments and intact platelets with the central area missing are preferentially found in the cavities (Figs. 4.4b-c, f). However, the preservation of fine details on the platelets allows species-level identification. *Reticulofenestra minuta* is by far the most abundant taxon forming dominant or monospecific assemblages (Figs. 4.4b-d). Rare specimens of *Reticulofenestra haqii, Reticulofenestra antarctica, Calcidiscus leptoporus, Coccolithus pelagicus, Helicosphaera carteri, Sphenolithus abies, Umbilicosphaera jafari* and *Chiasmolithus* sp. are also observed (Fig. 4.4f). All taxa with the exception of *Chiasmolithus* sp., which went extinct in the Chattian, have chronostratigraphic ranges that overlap with Stage 3.

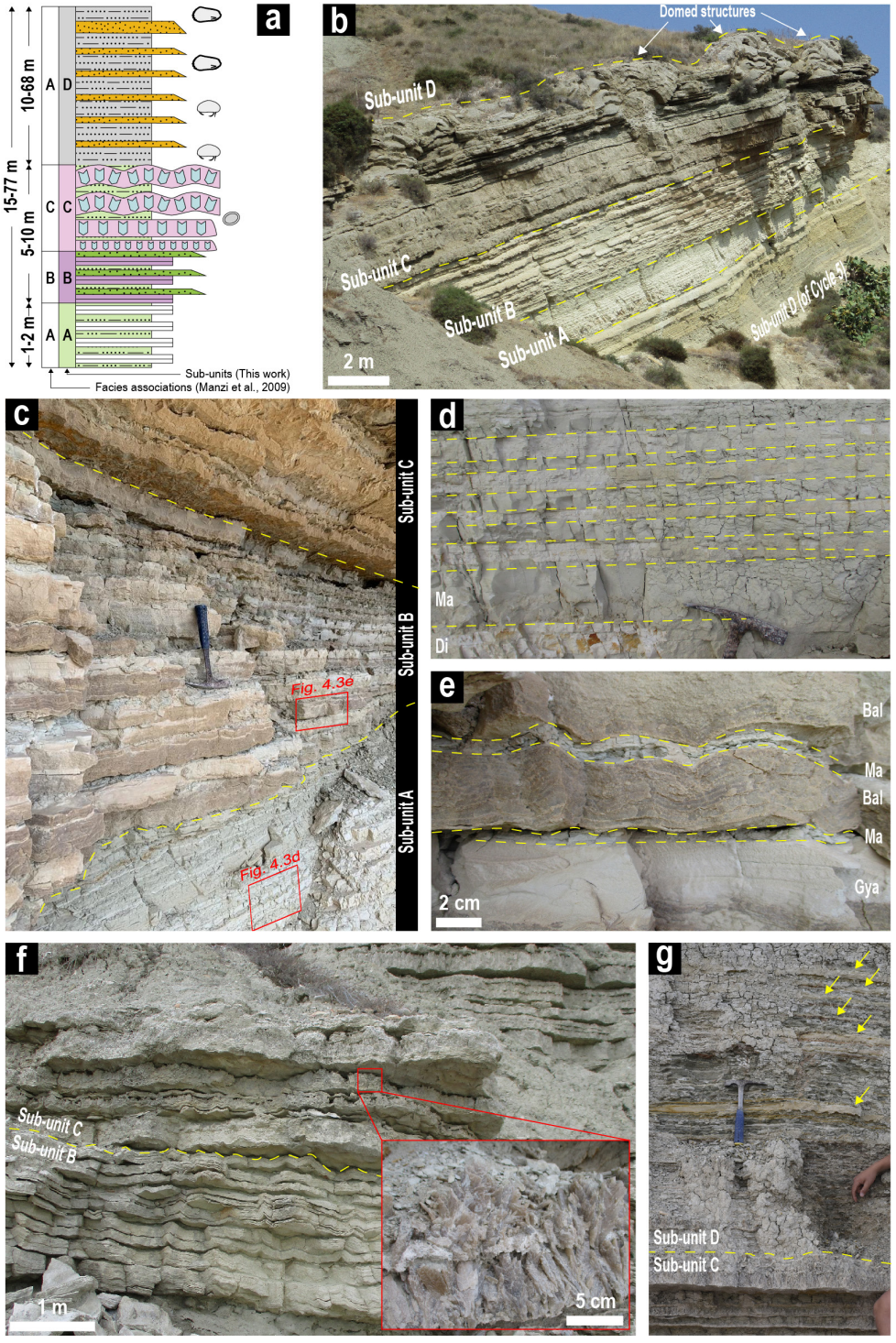
a
15-77 m
10-68 m
5-10 m
1-2 m
A D
C C
B B
A A
Sub-units (This work)
Facies associations (Manzi et al., 2009)
b
Domed structures
Sub-unit D
Sub-unit C
Sub-unit B
Sub-unit A
Sub-unit D (of Cycle 5)
2 m
c
Sub-unit C
Sub-unit B
Sub-unit A
Fig. 4.3e
Fig. 4.3d
d
Ma
Di
e
Bal
Ma
Bal
Ma
Gya
2 cm
f
Sub-unit C
Sub-unit B
1 m
5 cm
g
Sub-unit D
Sub-unit C

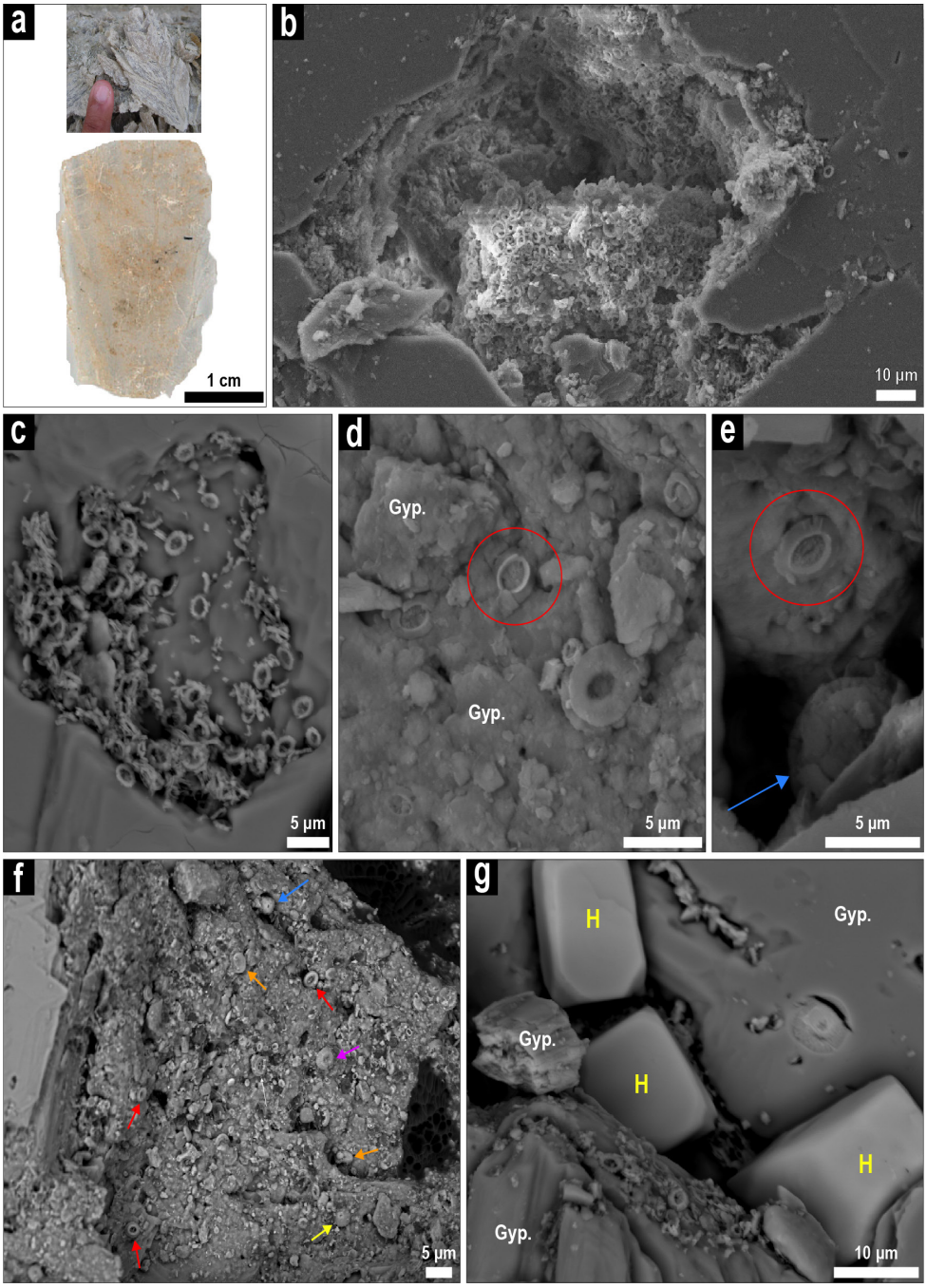

Fig. 4.3 (previous page). (a) *Schematic representation of a complete UG depositional cycle. Four sub-units (A to D) are distinguished alongside the three facies associations of Manzi et al (2009). See legend in Fig. 4.7a.*

(b) *Outcrop view of cycle 6 which contains all four sub-units. Note the sharp boundaries (red dashed lines) between the sub-units.* **(c)** *Close up of sub-units A to C of cycle 5. Yellow dashed lines indicate the sub-unit boundaries.* **(d)** *Alternations of white diatomites (Di) and greenish marls (Ma) in sub-unit A of cycle 5.* **(e)** *Close-up of sub-unit B in cycle 5 showing planar-laminated gypsarenite (Gya), greenish marls (Ma) and balatino gypsum beds (Bal). The laminae of the balatino gypsum locally show small scale folding.* **(f-g)**: *Transition from sub-unit B to C* **(f)** *and sub-unit C to D* **(g)** *from cycle 7 as exposed along the beach at the foot of the cliff Cattolica Eraclea/Capo Bianco cliff. Yellow arrows in Fig. 4.3g point to brownish litharenites interbedded with gray marls of sub-unit D.*

Fig. 4.4 (previous page). *SEM photomicrographs of calcareous nannofossils from Upper Gypsum selenitic crystals* (a) *of Eraclea Minoa. Platelets and coccospheres are better observable in cavities (b-c, e-g) and, to a lesser degree, where the crystal surface is pristine (d). The specimens can be regarded as embedded in the gypsum (gyp) since the analyzed surfaces are obtained after the removal of a portion of the crystal (see the materials and methods section for insights).* **(a)** *Swallow-tail selenite crystal from the second Upper Gypsum bed (fingertip for scale) and an example of a sliced selenite crystal (from gypsum VII) prepared for SEM. This thin gypsum slice shows the alternation of clear and turbid (brownish) laminae which are rich in calcareous nannofossils.* **(b-c)** *Monospecific accumulation of R. minuta with relatively well-preserved platelets.* **(d-e)** *Oligospecific assemblages of R. minuta and R. haqii (red circle). The blue arrow in Fig. 4.4e points to an intact coccosphere of R. minuta.* **(f)** *Oligospecific calcareous nannofossil assemblage including R. haqii (red arrows), Calcidiscus leptoporus (yellow arrow), Helicosphaera carteri (orange arrows), Coccolithus pelagicus (violet arrow) and Chiasmolitus sp. (white arrow). The remaining unmarked plates all belong to R. minuta. A coccosphere of R. minuta is also visible in the top of the picture (blue arrow).* **(g)** *Euhedral crystals of halite (H) in a gypsum crack. The plates of calcareous nannofossils belong to the genus R. minuta.*

4.3.3 $^{87}Sr/^{86}Sr$ results

Gypsum samples are characterized by a narrow range of $^{87}Sr/^{86}Sr$ (0.708704-0.708813; Table 4.1, Fig. 4.2). These data are substantially lower than $^{87}Sr/^{86}Sr$ ratios of coeval seawater (~0.709022; McArthur et al., 2012) and consistent with published $^{87}Sr/^{86}Sr$ ratios from Eraclea Minoa (García-Veigas et al., 2018) and from selenites of the Siculiana Marina section (0.708700-0.708760; Keogh and Butler, 1999), ~20 km to the SE (Fig. 4.1). Gypsum data from individual gypsum beds are either constant (II) or they show small-scale variability, commonly a decline from bottom to top (I, III-VII). There is also a small, but analytically resolvable decrease in $^{87}Sr/^{86}Sr$ ratios from the bottom of the section (Gypsum I) to the top (Gypsum VII).

The $^{87}Sr/^{86}Sr$ range of sub-unit D's ostracods is substantially larger than the gypsum (0.708510-0.708827; Fig. 4.2). Four of these samples (three in cycle 3 and one in cycle 7) have $^{87}Sr/^{86}Sr$ ratios higher or equivalent to the range of the gypsums; the remaining 25 have ratios lower than the gypsums. In the lowermost 52 m of sub-unit D of Cycle 6, which has the highest sampling resolution, fluctuations in $^{87}Sr/^{86}Sr$ are both high frequency and high-amplitude.

Table 4.1. *Compilation of the $^{87}Sr/^{86}Sr$ from the Eraclea Minoa section plotted in Fig. 4.2. Asterisks indicate that the analyzed samples are not assigned by the original authors to one of the sub-units distinguished in this work..1: This work (Bristol); 2: This work (Glasgow); 3: García-Veigas et al. (2018); 4: Grossi et al. (2015). Ages are in Ma (according to Fig. 4.8a). Stratigraphic heights are in meters.*

Sample	Age (cycle)	Strat. height	Sub-unit	Sample type	$^{87}Sr/^{86}Sr$	2σ (*10^{-6})	Ref
EM8-11	5.3380 (7)	233.5	D	*C. agrigentina*	0.708640	0.000006	4
EM8-9	5.3390 (7)	232	D	*C. agrigentina*	0.708630	0.000008	4
EM8-7	5.3405 (7)	231	D	*C. agrigentina*	0.708647	0.000010	4
EM8-3	5.3420 (7)	228.5	D	*C. agrigentina*	0.708704	0.000007	4
EM-44	5.3425 (7)	227	C	Selenitic gypsum	0.708732	0.000010	3
G7-8	5.3430 (7)	226.2	C	Selenitic gypsum	0.708710	0.000008	1
G7-6	5.3437(7)	225.7	C	Selenitic gypsum	0.708704	0.000011	1
G7-4	5.3440 (7)	225	C	Selenitic gypsum	0.708730	0.000014	1
G7-1	5.3450 (7)	224.2	C	Selenitic gypsum	0.708720	0.000007	1
EM-41	5.3500 (7)	223	B*	Balatino gypsum	0.708629	0.000010	3
EM7-10	5.3700 (6)	206	D	*C. agrigentina*	0.708637	0.000011	4
EM7-9	5.3710 (6)	205	D	*C. agrigentina*	0.708602	0.000002	4
EM7-5	5.3720 (6)	202.8	D	*C. agrigentina*	0.708629	0.000007	4
EM7-2	5.3730 (6)	201	D	*C. agrigentina*	0.708552	0.000009	4
EM6″-20	5.3740 (6)	197	D	*C. agrigentina*	0.708666	0.000010	4
EM6″-17	5.3750 (6)	191	D	*C. agrigentina*	0.708510	0.000007	4
EM6″-14a	5.3760 (6)	188	D	*C. agrigentina*	0.708511	0.000005	4
EM6″-8	5.3770 (6)	182.3	D	*C. agrigentina*	0.708685	0.000011	4
EM6″-7	5.3780 (6)	172.3	D	*C. agrigentina*	0.708609	0.000007	4
EM6″-5	5.3790 (6)	170.3	D	*C. agrigentina*	0.708654	0.000009	4
EM6″-3	5.3800 (6)	168.3	D	*C. agrigentina*	0.708608	0.000009	4
EM6′-27	5.3810 (6)	163.3	D	*C. agrigentina*	0.708663	0.000007	4
EM6′-25	5.3820 (6)	162.8	D	*C. agrigentina*	0.708729	0.000010	4
EM6′-22b	5.3830 (6)	161.3	D	*C. agrigentina*	0.708619	0.000005	4
EM6′-19	5.3840 (6)	160.3	D	*C. agrigentina*	0.708671	0.000005	4
EM6′-16	5.3850 (6)	159.3	D	*C. agrigentina*	0.708602	0.000007	4
EM6′-12	5.3860 (6)	158.3	D	*C. agrigentina*	0.708658	0.000009	4
EM6′-9	5.3870 (6)	157.3	D	*C. agrigentina*	0.708614	0.000005	4
EM6′-6	5.3880 (6)	156.3	D	*C. agrigentina*	0.708685	0.000005	4
EM6′-3	5.3890 (6)	155.3	D	*C. agrigentina*	0.708675	0.000010	4
EM6′-1	5.3900 (6)	154.8	D	*C. agrigentina*	0.708612	0.000011	4
EM-39	5.3906 (6)	154.2	C*	Selenitic gypsum	0.708724	0.000010	3
EM-84	5.3906 (6)	154.2	C	Selenitic gypsum	0.708735	0.000012	2
EM-78	5.3908 (6)	152.5	C	Selenitic gypsum	0.708744	0.000012	2
EM-76	5.3910 (6)	151	C	Selenitic gypsum	0.708740	0.000014	2
EM-69	5.3912 (6)	149	C	Selenitic gypsum	0.708723	0.000013	2
EM-64	5.3914 (6)	148.5	B	Balatino gypsum	0.708747	0.000012	2
EM-63	5.3916 (6)	148	B	Balatino gypsum	0.708738	0.000013	2
EM-33	5.3916 (6)	148	B*	Balatino gypsum	0.708719	0.000010	3
EM-31	5.4192 (5)	133.8	C*	Selenitic gypsum	0.708741	0.000010	3
EM-58	5.4192 (5)	133.8	C	Selenitic gypsum	0.708748	0.000013	2

EM-56	5.4198 (5)	132.8	C	Selenitic gypsum	0.708748	0.000012	2
EM-54	5.4202 (5)	132.2	C	Selenitic gypsum	0.708756	0.000012	2
EM-52	5.4206 (5)	131.3	C	Selenitic gypsum	0.708776	0.000014	2
EM-38	5.4210 (5)	130.6	C	Selenitic gypsum	0.708756	0.000013	2
EM-36	5.4214 (5)	129.8	C	Selenitic gypsum	0.708765	0.000016	2
EM-34	5.4218 (5)	129	C	Selenitic gypsum	0.708770	0.000014	2
EM-33	5.4222 (5)	128.2	C	Selenitic gypsum	0.708764	0.000014	2
EM-31	5.4226 (5)	127.5	C	Selenitic gypsum	0.708777	0.000014	2
EM-25	5.4230 (5)	126.6	B	Balatino gypsum	0.708789	0.000014	2
EM-22	5.4230 (5)	126.6	B*	Balatino gypsum	0.708747	0.000010	3
EM-20	5.4416 (4)	115.8	C*	Selenitic gypsum	0.708769	0.000010	3
G4-10	5.4416 (4)	115.8	C	Selenitic gypsum	0.708760	0.000006	3
G4-8	5.4422 (4)	114.5	C	Selenitic gypsum	0.708765	0.000005	1
G4-6	5.4428 (4)	113	C	Selenitic gypsum	0.708767	0.000009	1
G4-4	5.4434 (4)	111.5	C	Selenitic gypsum	0.708767	0.000008	1
G4-1	5.4440 (4)	109.5	C	Selenitic gypsum	0.708786	0.000004	1
EM-13	5.4442 (4)	108	B*	Balatino gypsum	0.708783	0.000010	3
EM4-19	5.4544 (3)	105	D	*C. agrigentina*	0.708725	0.000012	1
EM4-17	5.4558 (3)	104	D	*C. agrigentina*	0.708800	0.000030	1
EM4-7	5.4572 (3)	97	D	*C. agrigentina*	0.708729	0.000010	4
EM4-0K	5.4586 (3)	94	D	*C. agrigentina*	0.708827	0.000006	1
EM4-00a	5.4600 (3)	88	D	*C. agrigentina*	0.708730	0.000012	1
EM-12	5.4643 (3)	88	C*	Selenitic gypsum	0.708773	0.000010	3
G3-11	5.4645 (3)	87.70	C	Selenitic gypsum	0.708769	0.000006	1
G3-9	5.4650 (3)	87.05	C	Selenitic gypsum	0.708778	0.000006	1
G3-7	5.4655 (3)	86.4	C	Selenitic gypsum	0.708796	0.000007	1
G3-4	5.4660 (3)	85.5	C	Selenitic gypsum	0.708779	0.000006	1
G3-3	5.4665 (3)	85.15	C	Selenitic gypsum	0.708780	0.000006	1
G3-1	5.4670 (3)	84.5	C	Selenitic gypsum	0.708785	0.000006	1
EM-7	5.4672 (3)	84	B*	Balatino gypsum	0.708777	0.000010	3
EM-6	5.4912 (2)	48	C*	Selenitic gypsum	0.708780	0.000010	3
G2-11	5.4915 (2)	47.75	C	Selenitic gypsum	0.708780	0.000006	1
G2-9	5.4920 (2)	47.2	C	Selenitic gypsum	0.708776	0.000007	1
G2-7	5.4925 (2)	46.65	C	Selenitic gypsum	0.708774	0.000008	1
G2-5	5.4930 (2)	46.1	C	Selenitic gypsum	0.708781	0.000005	1
G2-3	5.4935 (2)	45.55	C	Selenitic gypsum	0.708780	0.000008	1
G2-1	5.494 (2)	45	C	Selenitic gypsum	0.708778	0.000006	1
EM-2(a)	5.494 (2)	45	C*	Selenitic gypsum	0.708775	0.000010	3
Cum-5	5.5100 (1)	2.7	B	Balatino gypsum	0.708800	0.000006	1
Cum-3	5.5155 (1)	1.5	B	Balatino gypsum	0.708810	0.000006	1

4.4 Discussion

4.4.1 Coccoliths in gypsums

The presence of marine calcareous nannofossils within the Eraclea Minoa UG selenites indicates that they were settling out from suspension while gypsum was growing on the basin floor. Fragmented, poorly preserved platelets with an empty central area are present, indicating

that some degree of physical reworking took place. The single occurrence of *Chiasmolithus* sp. corroborates this. However, fragmented platelets are preferentially found in large, irregularly-shaped cavities (Figs. 4.4b-c). When pristine areas of the gypsum slices (Fig. 4.4d) or small cracks (Fig. 4.4e) are inspected, preservation is better and complete coccospheres are observed. These delicate structures do not typically withstand erosion and transport intact. Other observations that are difficult to reconcile with an entirely reworked origin include the scarcity of terrigenous particles, the absence of bioclasts other than coccoliths and the limited diversity of these assemblages, which are solely or heavily dominated by *R. minuta* (Figs. 4.4b-d). The absence of other marine organisms is indicative of a stressed environment in which only a few species could thrive. Interestingly, the dominant species, *R. minuta*, is regarded as an opportunistic taxon capable of inhabiting a wide range of salinity conditions, from brackish to hypersaline (Auer et al., 2014). Taken together, these data suggest that while minor reworking occurred, at least *R. minuta*, which is abundant, thrived in the Caltanissetta Basin during selenite precipitation. Being that *R. minuta* is of marine origin, its finding in the Stage 3 selenites of Eraclea Minoa indicates that the Caltanissetta Basin was, at least during the evaporitic phases, supplied with Atlantic seawater. The seawater-like $\delta^{34}S_{SO4}$ signature of the gypsums is consistent with the nannofossil-based conclusion (Fig. 4.2; Manzi et al., 2009; García-Veigas et al., 2018).

Monospecific assemblages of dwarfed nannofossils, identified as likely belonging to the genus *Reticulofenestra*, have also been described from the thin calcareous laminae of the balatino lithofacies in ODP Site 653B (Tyrrhenian Basin; Pierre and Rouchy, 1990) and in the Montedoro section (Rouchy and Caruso, 2006), located some 50 km to the NE of Eraclea Minoa, and from the balatino lithofacies in ODP Site 968A (Eratosthenes Seamount; Blanc-Valleron et al., 1998), where again they are embedded within the gypsum crystals themselves. These findings in gypsums from intermediate-deep settings to the east and west of the Caltanissetta Basin suggest that the Stage 3 gypsum subbasins of the Mediterranean may have been, at least during the evaporitic phases, part of a single, Atlantic-fed water body (which we refer to as "Lago-Mare"; see next section) typified by stressful environmental conditions (Fig. 4.6). The Western Alborán, Adriatic and North Aegean basins, which are Stage 3 gypsum-free, are likely to have been sealed off from the gypsum-forming Lago-Mare water mass due to the presence of dividing sills and to have maintained, for at least part of Stage 3, different water masses subject to independent base-level and hydrologic evolution (Fig. 4.6). Studies of the sedimentary and paleontological records of these basins support this conclusion (Pellen et al., 2017; Booth-Rea et al., 2018; Krijgsman et al., 2020a).

4.4.2 $^{87}Sr/^{86}Sr$ characterization of the "Lago-Mare" water mass

The gypsum $^{87}Sr/^{86}Sr$ data at Eraclea Minoa (0.708704-0.708813; Fig. 4.2), like the Stage 3 gypsums elsewhere in the Mediterranean (<0.708850; Roveri et al., 2014b), have substantially lower ratios than coeval ocean water (~0.709022; McArthur et al., 2012). Modeled $^{87}Sr/^{86}Sr$ of

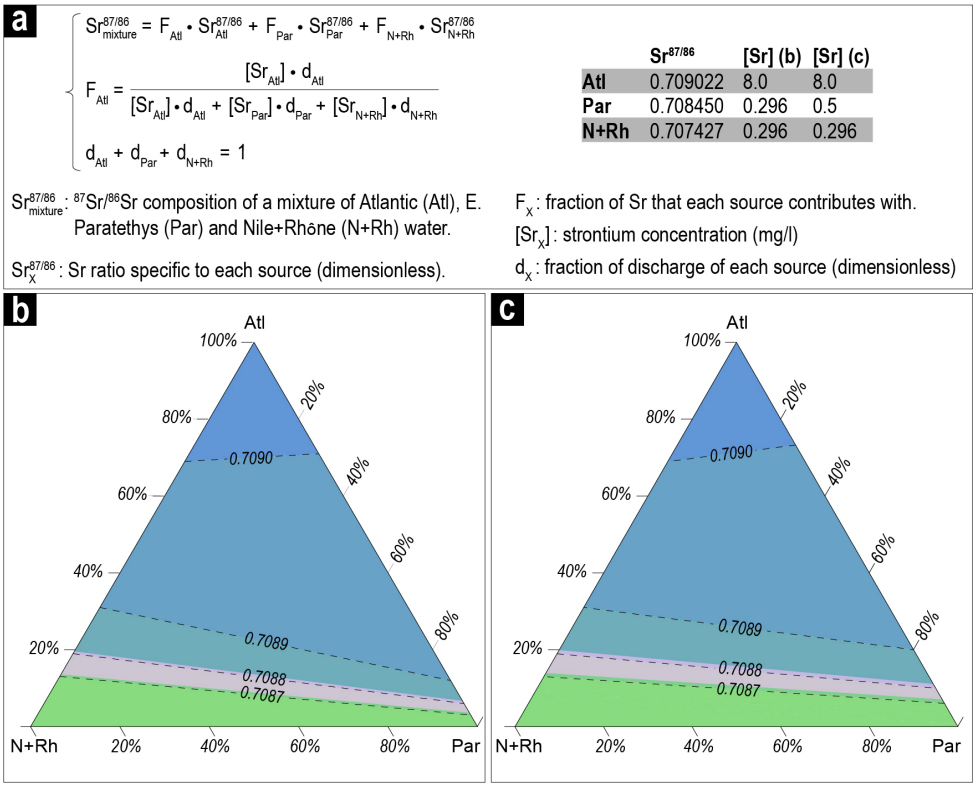

Fig. 4.5. (a) *Mass balance equations and strontium parameters employed to model the $^{87}Sr/^{86}Sr$ ratio of a water mass mixing Atlantic, Eastern Paratethys and large circum-Mediterranean rivers (Nile and Rhône) waters in various proportions. $^{87}Sr/^{86}Sr_{Atlantic}$ refers to the average value of the range of $^{87}Sr/^{86}Sr$ ratios (0.709017-0.709027) measured on calcareous material assigned to the time interval 5.55-5.30 Ma (McArthur et al., 2012). $^{87}Sr/^{86}Sr_{Nile+Rhône}$, $[Sr]_{Atlantic}$ and $[Sr]_{Nile+Rhône}$ are from present-day measurements (e.g. Topper et al., 2011). $^{87}Sr/^{86}Sr_{Paratethys}$ corresponds to the midpoint value of the range of $^{87}Sr/^{86}Sr$ ratios (0.7084-0.7085) derived from ostracods recovered from Stage 3-equivalent sediments in the Caspian Basin (Grothe et al., 2020).* **(b-c)** *Ternary plots of the modeled $^{87}Sr/^{86}Sr$ ratios. Two values of $[Sr]_{Paratethys}$, which is the major unknown in the model, are employed. In (b), $[Sr]_{Paratethys}$ is 0.296 mg/l, similar to the combination Nile+Rhône, whereas in c the $[Sr]_{Paratethys}$ is slightly higher (0.5 mg/l). The range of $^{87}Sr/^{86}Sr$ ratios measured for the Eraclea Minoa Upper Gypsum layers (pink area) is also plotted to facilitate the comparison with the model outputs. The ternary diagram is generated using the free and open-source software https://www.ternaryplot.com/.*

mixtures of Atlantic seawater and circum-Mediterranean freshwater show that measurable deviations from the oceanic $^{87}Sr/^{86}Sr$ signature are achieved when river discharge constitutes at least 25% of the total water fluxes (Topper et al., 2014). The Upper Gypsum $^{87}Sr/^{86}Sr$ data therefore indicate that the Lago-Mare water mass was a marine water body strongly influenced

Fig. 4.6. *Snapshot of the Atlantic-Mediterranean-Eastern Paratethys region during times of Stage 3 gypsum precipitation in Eraclea Minoa. The gypsum-precipitating Lago-Mare water mass is drawn following the present-day spatial distribution of the Upper Gypsum (UG) in the intermediate Sicily and Cyprus and Upper Unit (UU) in the deep basins (taken from Lofi, 2018). A different water mass was occupying the Stage 3 gypsum-free Northern Aegean, Adriatic and Alborán Basin, likely due to the presence of structural sills.*

by continental-derived sources with lower than marine $^{87}Sr/^{86}Sr$.

If Mediterranean base-level at times of gypsum precipitation was low enough to expose basin margin sediments, rivers draining these sediments may have influenced the Caltanissetta's composition. Primary Lower Gypsum, both in situ (Stage 1) and reworked (Stage 2; Manzi et al., 2021), is abundant in the Caltanissetta Basin. Local rivers draining the margins may therefore have provided additional Ca^{2+} and SO_4^{2-}, but would have had relatively high $^{87}Sr/^{86}Sr$ (~0.7090; Lugli et al., 2010). However, the catchments of these rivers today are dominated by Meso-Cenozoic limestones, which would have produced lower $^{87}Sr/^{86}Sr$ (<0.7080). On a more regional scale, the presence of ostracods derived from Eastern Paratethys suggests that this water body was a contributor of low $^{87}Sr/^{86}Sr$ non-marine water (0.7084-0.7085; Grothe et al., 2020) to the Mediterranean during Stage 3 (e.g. Andreetto et al., 2021a). The Mediterranean's major rivers, including the Nile and Rhône (0.7060 and 0.7087 respectively; e.g. Topper et al., 2011), which today make up >80% of the total Mediterranean river discharge, are also likely to have contributed low $^{87}Sr/^{86}Sr$ water, along with North African fluvial systems that are currently dry (e.g. the Eosahabi River that flowed from Messinian Lake Chad), but for which there is evidence of late Miocene flow (Griffin, 2006).

Mass-balance calculations were used to explore the relative proportions of Sr^{2+} derived from the possible sources that explain the $^{87}Sr/^{86}Sr$ data at Eraclea Minoa (Fig. 4.5a). If we assume that water from Eastern Paratethys was characterized by river-like Sr concentrations (Figs. 4.5b-c), our model suggests that a maximum of ~20% Atlantic seawater is required to reproduce the gypsum $^{87}Sr/^{86}Sr$ data (Fig. 4.5b). This result is in agreement with the box model calculations of Topper et al. (2014) and points to the presence of a strongly diluted marine water mass with a restricted Atlantic-Mediterranean connection during Stage 3 gypsum formation.

Restricted ocean inflow can be provided by an Atlantic-Mediterranean gateway either as a one-way flow or with a parallel outflow. The two-way flow configuration facilitates the formation of gypsum because it entails a larger inflow of water (and ions) and keeps the salinity below halite saturation (Krijgsman and Meijer, 2008). The presence of gypsum and absence of large volumes of demonstrably in-situ halite in Stage 1 and 3 units (Roveri et al., 2014a; Andreetto et al 2021a) is consistent with this scenario. However, two-way exchange requires Mediterranean base-level to be equal with the Atlantic sea-level (Krijgsman and Meijer, 2008), which means the marginal Mediterranean subbasins remain permanently submerged. This is the case in Stage 1. However, the evidence of substantial base-level change (section 4.4.5) and the frequent switching from subaqueous to continental sedimentation on the margins (Andreetto et al., 2021a, 2022) make persistent two-way exchange during the UG highly unlikely and support a small, unidirectional Atlantic input to the Mediterranean (Fig. 4.6). Existing box models simulations of the blocked outflow scenario result in rapid and voluminous halite precipitation (Krijgsman and Meijer, 2008). However, these simulations do not include the inflow of low-salinity water from Eastern Paratethys. One possibility is that inflow from

Paratethys, with a small Atlantic contribution, may have kept the Lago-Mare water mass below halite saturation, but allowed it, episodically, to achieve gypsum saturation. Some numerical models suggest that a unidirectional flow over a Gibraltar sill cannot be maintained throughout Stage 3, because headward erosion would breach the Atlantic-Mediterranean sill, raising the Mediterranean base-level and reestablishing two-way exchange within a few thousand years (Garcia-Castellanos and Villaseñor, 2011). If the mentioned calculations and our hypothesis that the outflow was blocked during Stage 3 are correct, then a mechanism for switching the Atlantic inflow on and off must have occurred. One possibility is that lithospheric loading and unloading by water during Mediterranean base-level change caused the isostatic adjustment of the Atlantic-Mediterranean sill. Alternatively (or complementary), the small-scale unidirectional seawater flow into the Mediterranean was constant from seepage through the sill (today, more than 25% of all the water draining into the Mediterranean has subterranean parts of its pathway; Aureli et al., 2008). Detailed assessment of these hypothesis are beyond the scope (and the data) of this study and are simply meant to set the framework for future studies.

4.4.3 Implications of UG cycles for base-level and insolation

Evaporite-marl alternations denote cycles of concentration and dilution of the water mass with respect to evaporitic ions and are commonly associated with water level changes (Lowenstein, 1988; Lugli et al., 2010). Reconstructing base-level changes in ancient evaporitic settings with confidence is difficult because reliable paleobathymetric indicators such as fossils and ichnofossils are commonly absent from high-salinity environments and evaporitic lithofacies are rarely diagnostic of any particular water depth. The UG cycles at Eraclea Minoa are unusual because sub-unit D contains in-situ ostracods which do have paleobathymetric requirements. Living relatives of *C. agrigentina* (e.g. *C. torosa*), which dominates Biofacies 1 (Fig. 4.2), tolerate only a few tens of meters of water depth (Grossi et al., 2015; Meyer et al., 2016). The more diverse Biofacies 2 at the top of sub-unit D, by contrast, is considered to indicate water depths up to 100 m (Stoica et al., 2016). The ostracod assemblages therefore suggest that the water depth increased during the deposition of sub-unit D (Fig. 4.7a).

The presence, in one marl layer interbedded with massive selenite beds (sub-unit C) in cycle 3, of both *C. agrigentina* and *L. muelleri*, which is extinct but also thought to have inhabited shallow water (Grossi et al., 2015), suggests that the selenites precipitated in shallow water. However, there is no physical and paleobiological evidence of very shallow water conditions in the cumulate gypsum of sub-unit B. In other ancient evaporitic settings, the transition from cumulates to bottom-grown selenites is commonly interpreted to indicate a shallowing-upward trend (Ortí et al., 2014b; Warren, 2016) and sequences of cumulate and bottom-grown halite layers characterize lake level falls in the Dead Sea today (Sirota et al., 2021). It is possible therefore that the transition from sub-unit B to C equates to a shallowing-upward trend through gypsum deposition (Fig. 4.7a).

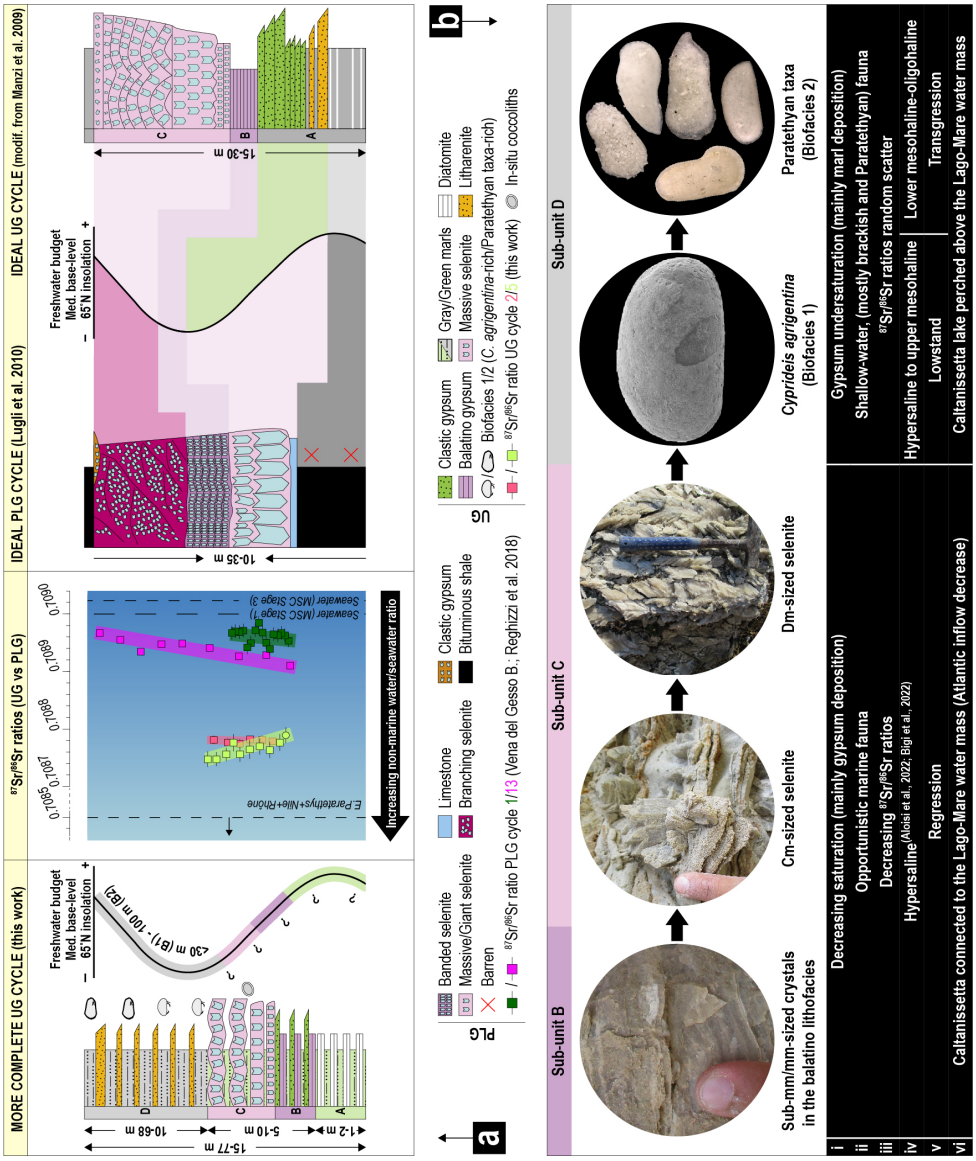

Fig. 4.7. (a) *Lithofacies of a complete UG cycle as a function of precession cycle and Mediterranean base-level according to Manzi et al. (2009) and this study. A comparison with the PLG interpretation is also shown (re-drawn after Roveri et al., 2008d). The question marks in the figure to the left refer to the uncertainty over the paleodepth during deposition of sub-units A, B and C. Note that our new interpretation of the UG challenges the long-lasting idea that PLG and UG reflect similar depositional mechanisms and paleoenvironmental conditions (Manzi et al., 2009; Roveri et al., 2014a). This is consistent in a number of ways: (1) UG and PLG sequences comprise different facies (UG contains more abundant balatino gypsum and*

is missing the banded and branching selenite lithofacies of the PLG). (2) Euxinic shales interbedded with the PLG contain possibly in-situ marine fossils (e.g. Corbí and Soria, 2016), whereas the marls interbedded with the UG contain brackish and shallow water ostracods and brackish water foraminifera such as A. tepida (Fig. 4.2; Grossi et al., 2015). This is likely to reflect a greater proportion of marine water in the Mediterranean during Stage 1. (3) $^{87}Sr/^{86}Sr$ isotopes are consistent with the above interpretation, being, on average, close to, or within error of coeval ocean values on stage 1 gypsums (average of 0.708941; Lugli et al., 2010; Reghizzi et al., 2018) and substantially higher than those measured on Stage 3 gypsum samples (average of 0.708752; Fig. 4.7a). (4) The Stage 3 gypsum $^{87}Sr/^{86}Sr$ data are either constant within the layer or show a subtle decline from base to top (Figs. 4.5a, 4.7). This is in contrast with a larger base to top increase in $^{87}Sr/^{86}Sr$ ratio in Stage 1 gypsum layers from the Vena del Gesso Basin (Northern Apennines; Reghizzi et al., 2018; Fig. 4.7a). (5) The PLG is largely restricted to marginal basins (e.g. Lugli et al., 2010; García-Veigas et al., 2018), whereas the UG is only found in intermediate-deep basins (Fig. 4.6). **(b)** *Summary outline of the main sedimentological (i), paleontological (ii) and geochemical (iii) data for each sub-units, their interpretation in terms of salinity (iv) and relationship with the base-level curve (v) and their paleoenvironmental and paleohydrological interpretation proposed in this work (vi).*

The distribution of gypsum and marl across the Caltanissetta Basin may also provide insights into the relative water depth of the two lithologies. Gypsum occurs throughout the basin with a fairly constant thickness, whereas the evaporite-free marl intervals thin eastward towards the foreland area and above intrabasinal structural highs (Manzi et al., 2009), where they are barren or only contain Biofacies 1 ostracods (e.g. Balza Soletta section; Maniscalco et al., 2019). Manzi et al. (2009) interpreted this distribution as the consequence of continuous subaqueous deposition with eastward thinning of the marls related to increased distance from the terrigenous source. An alternative interpretation is that the base-level was high enough to precipitate gypsum across the whole Caltanissetta Basin, but dropped during marl deposition, exposing more marginal areas to erosion and/or non-deposition and leaving only the deeper depocenters (e.g. Eraclea Minoa) underwater. During the subsequent base-level rise, recorded in Eraclea Minoa by the appearance of Biofacies 2 ostracods, these marginal areas were drowned again and accumulated thin, Biofacies 1-bearing marls. If correct, this interpretation suggests that there was a higher water level at the beginning of gypsum precipitation than at the beginning of sub-unit D marls (Fig. 4.7a).

If the Caltanissetta Basin is part of a larger Lago-Mare water mass, cyclical base-level changes seen there are likely to be the consequence of fluctuations in the discharge of one, or more, of the Mediterranean's water sources. The Mediterranean's freshwater budget is highly variable on precession timescales. It is enhanced during the insolation maxima, when more rainwater from North African monsoon and Atlantic storms is delivered to the Mediterranean (e.g. Marzocchi et al., 2016), and it reaches the lowest values during the insolation minima, when less freshwater is supplied and more water is lost by evaporation. It is therefore likely

that base-level variations were in phase with the insolation forcing: the highstands coincided with insolation maxima and the lowstands with insolation minima (e.g. Simon et al., 2017). Previously, the gypsums at Eraclea Minoa have been correlated with increasing insolation following the insolation minima and the diatomites and ostracod-bearing marls tied to the transition from insolation maxima to minima (Fig. 4.7a; van der Laan et al. 2006; Manzi et al. 2009). This is challenged by the relative base-level changes observed here, which instead suggest that the base of the ostracod-bearing marls at Eraclea Minoa represents lowstand phases, corresponding to insolation minima (Fig. 4.7a), while the shallowing through gypsum sub-units B and C, corresponds to part of the transition from insolation maxima to minima (Fig. 4.7a). This revised astronomical tuning dates the base of the Upper Gypsum at Eraclea Minoa to ~5.515 Ma and the first indication of Paratethyan ostracods to ~5.47 Ma. This is the oldest age known in the Mediterranean and contradicts the hypothesis that the migration of Paratethyan ostracods occurred as a single Mediterranean-wide event at 5.42 Ma (substages 3.1 and 3.2 (or Lago-Mare phase) of Roveri et al., 2014a; see also Roveri et al., 2008d and Grossi et al., 2011), possibly prompted by a sudden increase of the Paratethys outflow (Marzocchi et al., 2016).

4.4.4 Connectivity changes terminated gypsum precipitation

The UG sediments at Eraclea Minoa also contain evidence of changing palaeoenvironmental conditions. The vertical transition from sub-mm/mm-sized gypsum crystals in the balatino lithofacies (sub-unit B), which require supersaturated conditions favoring the formation of new nuclei over crystal growth (Lugli et al., 2010), to increasingly larger selenites (sub-unit C), which require gradually lower degree of brine supersaturation to grow larger (Lugli et al., 2010), is indicative of a progressive reduction of the brine concentration approaching the transition with sub-unit D. Then, the sub-unit C/D transition marks a major paleoenvironmental and paleohydrological event, testified by the abrupt cessation of gypsum precipitation and the appearance of shallow-water fauna. Microthermometry studies on fluid inclusions in gypsum lithofacies (Bigi et al., 2022) and thermodynamic calculations (Aloisi et al., 2022) show that the Eraclea gypsums precipitated from the evaporation of seawater at a salinity of ~115 g kg^{-1}. The ostracods in the overlying marls show a gradual transition from dominantly *C. agrigentina* (Biofacies 1), which tolerates a wide range of salinities (Grossi et al., 2015), to the more diverse Biofacies 2, which indicate fresher (oligohaline) conditions (Fig. 4.7b; Stoica et al., 2016).

One possibility is that the gradual drop in concentration with respect to gypsum and the salinity decrease across the sub-unit C/D transition and through sub-unit D were prompted by increased continental runoff (Manzi et al., 2009). In this case, however, a base-level rise should have accompanied the precipitation of the gypsums, reaching the highstand during deposition of Biofacies 2 (Fig. 4.7a; Manzi et al., 2009). This scenario is in contradiction with our water level reconstruction, that indicate a shallowing through the gypsum and a deepening through the sub-unit D marls (Fig. 4.7a). The lessening of Atlantic inflow, which achieves both the base-

level fall through sub-units B-C and the associated subtle declining trend in the $^{87}Sr/^{86}Sr$ ratios within individual gypsums (Figs. 4.2, 4.7a), seems to be a more plausible mechanism. In the context of deposition during a Mediterranean base-level fall, it is possible, therefore, that the abrupt transition from gypsum to ostracod-bearing marls was the consequence of the base level falling below the Caltanissetta Basin, leaving it as a perched lacustrine system above the deeper areas covered by the "Lago-Mare" water mass. The large $^{87}Sr/^{86}Sr$ variations in the Eraclea Minoa marls suggest that the Caltanissetta Basin formed a perched lake during these lowstands. Compared to seawater-influenced basins, lacustrine settings are, indeed, much more sensitive to subtle changes in fluvial discharge (e.g. Bista et al., 2021), resulting in rapid changes in the $^{87}Sr/^{86}Sr$ ratio measured on the ostracods.

4.4.5 High amplitude fluctuations of the Mediterranean base-level

The same ostracods biofacies as those in sub-unit D are found both in marginal Mediterranean marls, where they typically alternate with continental facies, and in the deep basins (e.g. Sites 975B, 372, 129A; see Andreetto et al., 2021a), where the marls alternate with laminated and clastic gypsum (Andreetto et al., 2021a). For the deep basins to develop the shallow-water conditions required by the ostracods, the Mediterranean water level had to fall below the intermediate position of the Caltanissetta Basin. This means that Caltanissetta and deeper basins accumulated the shallow-water ostracod-bearing marls during lowstand phases of the Lago-Mare water, exposing the marginal basins to continental deposition and/or erosion (Fig. 4.8e). By contrast, high Mediterranean water levels are required to populate the shallow marginal basins with these same Paratethyan ostracods (Stoica et al., 2016). This is supported by the $^{87}Sr/^{86}Sr$ ratios measured on some of these marginal basin ostracods, which point to mixing between high-$^{87}Sr/^{86}Sr$ local fluvial waters with the Lago-Mare water mass (Andreetto et al., 2021b, 2022). During these highstand phases of marginal basin ostracod-rich marl deposition, the Caltanissetta and deep basins were experiencing much deeper water conditions (i.e. several hundreds of meters; Fig. 4.8b).

The depth constraints provided by the shallow-water ostracod assemblages indicate that marl deposition was not synchronous across the Mediterranean during base-level highstands at insolation maxima (Roveri et al., 2008d, 2014a), but sequential, tracking Mediterranean-wide, high-amplitude (several hundred to thousands of meters) base-level fluctuations (Figs. 4.8b-e). This model of high-amplitude base level changes, earlier hypothesized by Hardie and Lowenstein (2004) and Rouchy and Caruso (2006) is now supported by integrated sedimentological, paleontological and geochemical observations that show that the Mediterranean was at times both relatively full (Fig. 4.8b) and empty (Fig. 4.8e) during each Stage 3 precession cycle. This model helps reconcile observations that support the full versus desiccated debate that has afflicted the MSC Stage 3 successions for decades (Andreetto et al., 2021a).

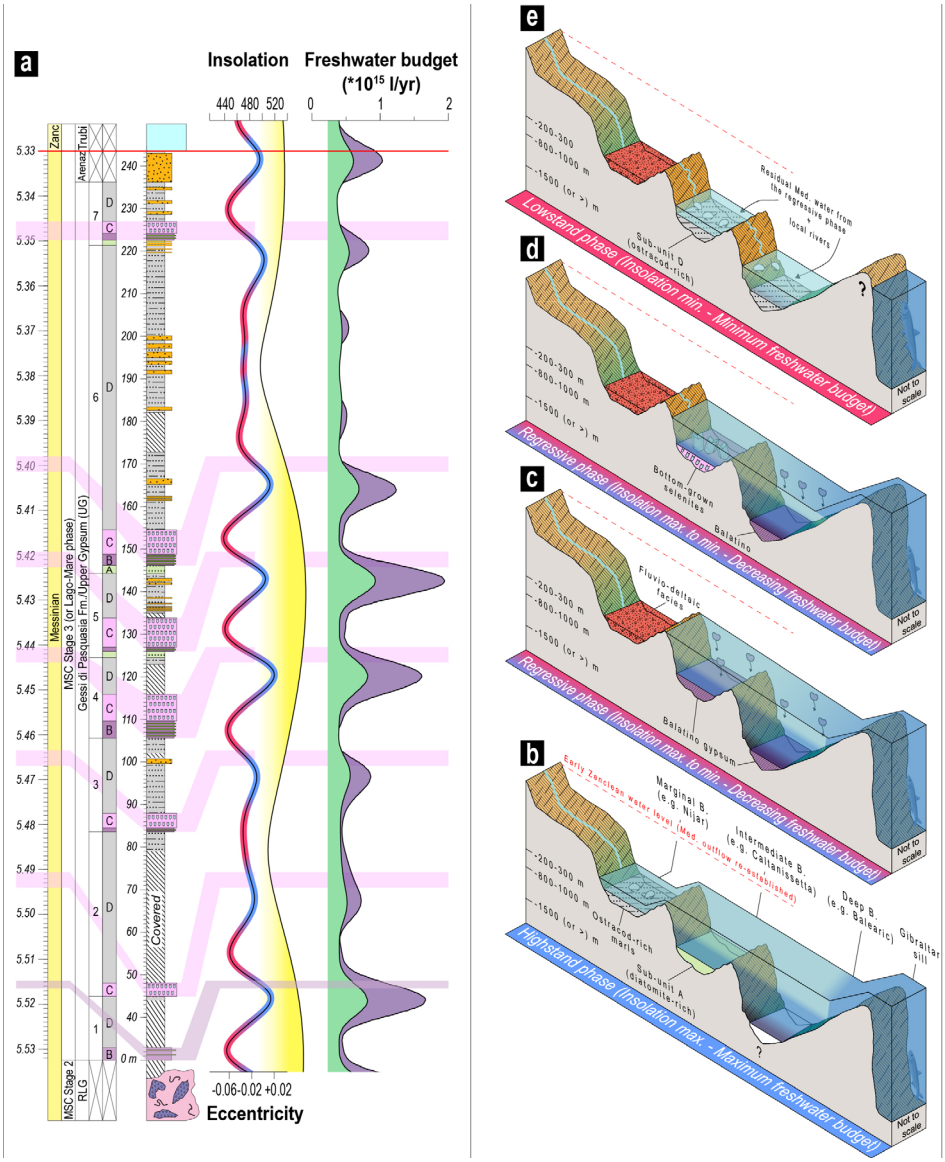

Fig. 4.8. (a) *Revised astronomical tuning of the Upper Gypsum Unit at Eraclea Minoa according to the newly proposed phase relationships between the UG lithofacies and the astronomical forcing (namely 65°N summer insolation and 100 kyr eccentricity curves). Starting from the conformable M/P boundary, we correlate the seven gypsum beds to successive transitions from insolation maxima to minima avoiding the insolation peaks associated with the 100-kyr eccentricity minima at ~5.38 Ma and ~5.50 Ma. Due to the low amplitude of insolation in these eccentricity low, these minor peaks are not expected to correspond to a gypsum bed in the sedimentary record (van der Laan et al., 2006). It is more likely that these low eccentricities corresponded to*

prolonged phases of very low base level in the Mediterranean. Pursuing this approach, all gypsum beds follow well pronounced insolation maxima and the thicker, gypsum-free, Cyprideis-rich sub-units D between gypsums II-III and VI-VII correlate with an eccentricity minimum. The overall Mediterranean run-off budget from Simon et al. (2017), with included (violet curve) and excluded (green curve) supply from the Chad lake, is also shown. **(b-e)** *Cartoons showing the proposed evolution of the Mediterranean environments and hydrology during one precession cycle of MSC Stage 3. The cartoons are inspired from Palcu et al. (2021).*

4.4.6 Implications of Atlantic-Mediterranean connectivity for ocean chemistry

On long timescales (>100 kyr), marine alkalinity and $CaCO_3$ burial are balanced by the response of silicate weathering to changes in atmospheric CO_2 and associated temperature (e.g. Berner, 2012). Many biogeochemical models (e.g. Berner, 1991; Lenton et al., 2018) assume that on these long timescales perturbations to seawater chemistry caused by evaporite precipitation are balanced by evaporite dissolution during weathering. However, evaporites form and dissolve three orders of magnitude more quickly than other sediments (Nichols et al., 2009) and this approach fails to consider whether abrupt and short-term evaporite-driven chemical perturbations can propagate into aspects of the carbonate cycle that have longer-term climate implications. The box model study by Shields and Mills (2020) explores the impact of gypsum on ocean chemistry and its knock-on consequences for $CaCO_3$ burial, atmospheric CO_2 and global temperature by allowing the non-steady-state ocean calcium inventory to be driven by $CaSO_4$ precipitation and the return flux to the ocean from weathering. Their results demonstrate that a decrease in ocean [Ca] as a consequence of gypsum deposition, because it is not associated with an alkalinity change, leads to decreasing $CaCO_3$ burial and higher oceanic pH, resulting in decreasing atmospheric CO_2 and global cooling (Shields and Mills, 2020). However, their sensitivity experiments impose a constant gypsum precipitation and weathering forcing for 1 million years which is not a realistic reflection of the pattern of ocean [Ca] extraction as a consequence of the MSC. Here we explore what a realistic evaporite precipitation and weathering flux would look like over the duration of the MSC and consider its possible implications.

In contrast with the constant precipitation driver modeled by Shields and Mills (2020), the precessional gypsum-marl cyclicity that characterizes both MSC Stage 1 and 3 suggests that extraction of Ca^{2+} and SO_4^{2-} ions from the global ocean was episodic and probably endured for only a few thousand years in each precession cycle. Further modelling experiments are required to evaluate the degree to which the regular switching on and off of gypsum precipitation modifies the modelled consequences for carbonate burial, atmospheric CO_2 and global temperatures (Shields and Mills, 2020) as a result of (partial) recovery of the system between evaporite pulses. However, without near synchronous return of Ca^{2+} ions to the ocean as a result of evaporite weathering, the reduction in oceanic [Ca] is unlikely to have bounced back completely, leading to a progressive decline in seawater [Ca] from one precessional evaporite

event to the next. Stage 2 evaporites are heavily dominated by halite, not gypsum. However, it is possible that constant extraction of these Ca^{2+} ions did characterize the ~50 kyr duration of this phase of the MSC, since the volumetrics of the halite succession preserved, requires constant input of ocean water (Krijgsman and Meijer, 2008) which must also have contained Ca^{2+} and SO_4^{2-}. Taken together then, the rate of Ca^{2+} ion extraction over the course of the entire MSC is likely to have varied and to have been most substantial during Stage 2. Recent evaporite volume estimates for the MSC (Haq et al., 2020) are broadly similar to those used by Shields and Mills (2020) to estimate the scale of the Ca^{2+} extraction during salt giant formation. Both are based on the volumes of evaporites that are still preserved in the Mediterranean today, and therefore represent a minimum. That being the case, whether pulsed or continuous, this Late Miocene episode of $CaSO_4$ extraction may have contributed to the cooling seen in time-equivalent SST records (Herbert et al., 2016).

Although the net effect of the MSC was to extract Ca^{2+} and SO_4^{2-} from the global ocean, the episodic nature of gypsum accumulation and Mediterranean-Atlantic connectivity also implies that the Mediterranean was, intermittently and at time-scales shorter than the MSC, a net source of Ca^{2+} and SO_4^{2-} to the Atlantic. Evaluating episodic net Ca^{2+} and SO_4^{2-} fluxes to the ocean during the MSC is particularly challenging since it depends not on the gypsum preserved today in the Mediterranean, but rather on what was originally precipitated and has been already dissolved (Wortmann and Payton, 2012). However, what we can evaluate from the Mediterranean's geological record is the nature of its connectivity with the Atlantic and from this it is possible to deduce the timing and likely duration of episodic net exchange of Ca^{2+} and SO_4^{2-} between the Mediterranean to the global ocean. Evidence from both $^{87}Sr/^{86}Sr$ data and box-modeling indicate that Stage 1 gypsum was precipitated while the Mediterranean experienced restricted, but two-way exchange with the Atlantic under conditions which broadly maintained eustatic sea level in the Mediterranean (e.g. Flecker et al., 2015 and references therein). This configuration will have resulted in net extraction of Ca^{2+} and SO_4^{2-} ions from the ocean, at least during gypsum precipitation. Maximum dissolution of gypsum occurs during subaerial exposure with the formation of aquifers associated with active hydrology (Gustavson et al., 1982). Since there is no evidence of substantial base-level fall during the marl intervals in Stage 1, it is probable that there was relatively little weathering of the gypsum and therefore a limited return flux of these ions to the ocean. The connectivity and base-level configuration during stages 2 and 3 is substantially different. Outflow to the Atlantic ceased, base-level fell and then, as shown in this study, fluctuated substantially during Stage 3. This exposed Stage 1 gypsum precipitated on the margins and stage 2 and 3 gypsum reworked or precipitated in deeper settings of the Mediterranean to dissolution. However, without Mediterranean outflow, these weathered evaporitic ions were trapped in the Mediterranean and had no influence on global ocean chemistry. Outflow to the Atlantic started abruptly at the beginning of the Pliocene with the termination of the MSC, triggering the return of two-way exchange and the

reestablishment of open marine conditions in the Mediterranean.

In summary, the MSC evaporite weathering flux to the ocean was episodic and largely out of phase with gypsum precipitation-driven extraction, potentially resulting in dynamic changes to ocean chemistry on the timescale of the MSC. Interestingly, the main impact Shields and Mills (2020) found of modeling a 1 million year $CaSO_4$ weathering event was a rapid rise in $CaCO_3$ burial and a transient peak in atmospheric CO_2 concentration and associated warming, that occurred only 150 kyrs after initiation. With this in mind, it is tempting to attribute at least part of the abrupt warming in early Pliocene sea surface temperature records (Herbert et al., 2016) to a Mediterranean-derived pulse of Ca^{2+} ions. Testing this hypothesis will require more sophisticated biogeochemical modeling and better quantitative constraints on the chemistry of Mediterranean outflow. If true however, it would suggest that the most important impact of the Zanclean deluge was not the sudden inundation of a Mediterranean empty of water for hundreds of thousands of years, but the abrupt flushing into the Atlantic of the ponded weathering products of a salt giant.

4.5. Conclusions

The UG selenites at Eraclea Minoa contain in-situ marine calcareous nannofossils and display $^{87}Sr/^{86}Sr$ which indicate that a small Atlantic flux (≤20%) supplied the Mediterranean with Ca^{2+} and SO_4^{2-} ions during gypsum precipitation. Mass-balance calculations suggest that the remaining ≥80% of the Lago-Mare water mass was supplied by Eastern Paratethys and large Mediterranean rivers. Gypsum precipitation, first from settling crystals nucleated in the water column (balatino, sub-unit B) and then from bottom-grown selenites (sub-unit C), occurred during a phase of base-level fall coincident with the transition from insolation maxima to minima. During insolation minima, low diversity ostracod-bearing marls (Biofacies 1 of sub-unit D), that constrain the water depth to a few tens of meters, were deposited in an isolated, lacustrine Caltanissetta Basin perched above the Lago-Mare water mass, which persisted in the deep subbasins. The transition from Biofacies 1 to 2 indicates rising water levels in the lake. Similar ostracod-bearing marls are found in both shallower and deeper settings across the Mediterranean, indicating that marl deposition was asynchronous during Stage 3, tracking high-amplitude, Mediterranean-wide base level changes (Fig. 4.8a). Sedimentological, geochemical and biological data from Eraclea Minoa suggest that the Mediterranean experienced (at least) 7 substantial, cyclic base-level changes during Stage 3. A revised astronomical tuning indicates that MSC Stage 3 started at 5.515 Ma, with the first occurrence of Paratethyan ostracods on Sicily at 5.47 Ma. This model for (upper) gypsum formation, which envisages periods during which the Mediterranean was both relatively full and empty, helps to reconcile many of the discrepancies between offshore- and onshore-based interpretations of the final phase of the Messinian Salinity Crisis. It also suggests that any impact of evaporite weathering on ocean biogeochemistry occurred in the Pliocene once Mediterranean outflow was re-established.

Acknowledgments

A special thanks goes to Jamie Lewis and Carolyn Taylor from the Bristol Isotope Group Facilities, who ran the Sr isotope analyses during the Covid pandemic, therefore giving continuity to the work. We thank Elsa Gliozzi and Domenico Cosentino for providing unwashed marl samples and the washed residues of Grossi et al. (2015), which helped to expand the ostracods' Sr dataset, Tilly Bouten for assistance with SEM analyses and Frits Hilgen, Paul Meijer, Rob Govers, Mhina de Vos for the numerous and fruitful discussions which this manuscript greatly benefited from. Antonio Caruso and Isabel Sanchez-Almazo are thanked for joining the field campaign in the early noughties. We thank the Editor and two anonymous reviewers for their thorough comments and suggestions, that greatly improved the original version of the manuscript. This research was supported by the project SALTGIANT-Understanding the Mediterranean Salt Giant, a European project which has received funding from the European Union's Horizon 2020 research and innovation program, under the Marie Sklodowska-Curie [grant agreement No 765256]. The Royal Society provided funding for the analytical and fieldwork that took place in the early noughties through a Wolfson Dorothy Hodgkin Fellowship to RF.

Adriatic Sea on May 18, 2002 (Credit: NASA). About 5.5 million years ago this sea was, instead, a large lake that stretched from north-western Italy, in Piedmont, to the Gargano promontory, in Puglia.

5

STEPWISE FLOODING OF THE LATE MESSINIAN ADRIATIC MEGALAKE

Andreetto, F., Negri, A., Stoica, M., Lourens, L.J., Hilgen, F.J., Flecker, R., Krijgsman, W.

ABSTRACT

In the late Messinian, between 5.59 and 5.55 Ma, the Mediterranean Basin experienced at least one major (>1 km) water level drop in response to reduced connectivity with the Atlantic Ocean. The consequences of this drawdown were the fluvial incision of the Mediterranean's shelf and slope systems, the deposition of 800-900 thousand km^3 (1.5-2 km in thickness) of halite on the abyssal plains and the formation of endorheic lakes in silled basins. A perched lake >100 times bigger than the largest lake in the region today, Lake Garda (~370 km^2) encompassed northern and eastern Italy. This "Adriatic megalake" was fenced by the proto-reliefs of the Alps, Apennines and Dinarides and by a southern sill in the offshore area of the present-day Gargano Peninsula. The timing and nature of the paleoenvironmental and paleohydrological changes in the late Messinian Adriatic megalake are still debated due to the scarcity of biota, reliable dating tools and employment of different proxies. Here we carried out an integrated stratigraphic study (sedimentology, paleontology, $^{87}Sr/^{86}Sr$ isotopes, XRF, grain-size distributions, magnetic susceptibility) on key sections of this megalake and propose a new, age-framed, evolutionary model for the Adriatic Basin that provides a unifying explanation for its connectivity phases and water level changes. We show that since its initiation between 5.59 and 5.55 Ma, the Adriatic megalake was for ~240 kyr almost devoid of fauna, probably hosting a largely SO_4^{2-}- and NaCl-enriched residual brine from a previous evaporitic stage when gypsum formed in shallower areas. The associated water level drop is estimated at 800-900 meters, paving the way to vigorous fluvial erosion of the Southern Alpine margin and the Po Plain. At ~5.36 Ma, an anomalohaline water mass passed over the Gargano sill and spread Black Sea type biota (ostracods, dinoflagellates, mollusks) and possibly some euryhaline marine species into the megalake. A second transgression took place straddling the Miocene/Pliocene boundary at 5.332 Ma and restored the open marine environment that persists to date. Our results from the Adriatic Basin confirm that MSC Stage 3 was a highly dynamic period and that the Mediterranean was a diluted marine basin at the mercy of non-marine inputs from the Eastern Paratethys and large drainage systems.

5.1 Introduction

The Miocene northward motion of the Nubian plate with respect to Europe progressively restricted the Tethys Ocean in the Africa-Eurasia collision zone. This vast ocean finally fragmented in two smaller seas, the Paratethys and the Mediterranean (Popov et al., 2004; van Hinsbergen et al., 2020). During the Late Miocene, the interplay between tectonics and climate gave rise to the formation of the anomalohaline Paratethys megalake, the largest Cenozoic lake on Earth (2.8 million km^2; Palcu et al., 2021). The Mediterranean Basin persisted as a fully marine epicontinental sea until the late Messinian, but ultimately also gave rise to megalakes in response to the restriction of its marine gateways. As the collisional process continued, first the Indian Gateway closed at the end of the Early Miocene (Rogl, 1999; Popov et al., 2004) followed by the gateways in southern Spain and northern Morocco during the Late Miocene (Flecker et al., 2015; Krijgsman et al., 2018). A restricted connection at Gibraltar transformed the Mediterranean into an inhospitable, gypsum-saturated sea, in an event known as the Messinian Salinity Crisis (MSC, 5.96-5.332 Ma; Roveri et al., 2014a). This environmental and hydrological crisis peaked between 5.60-5.55 Ma (MSC Stage 2), when at least one major sea-level drop, triggered by further restriction of the Atlantic-Mediterranean connection, led to the precipitation of 1.5-2 km of halite on the Mediterranean sea floor (Hsü et al., 1973a). A km-scale drawdown in the Mediterranean probably created several endorheic lakes in silled marginal subbasins. The largest endorheic water body that allegedly formed during MSC times filled the Adriatic Basin, the Po Plain and the Piedmont Basin (Fig. 5.1a), enclosed by the Alps to the north, the Apennines to the W, the Dinarides to the E (Boccaletti et al., 1990; Cosentino et al., 2018) and separated from the Mediterranean either by a structural sill located offshore the present-day Gargano peninsula (Bache et al., 2012; Pellen et al., 2017; Amadori et al., 2018; Manzi et al., 2020) or by two submarine ridges near the city of Otranto further south (Clauzon et al., 2005). The Messinian paleodepth of these submarine ridges is unknown, but several lines of evidence suggest that at least one of the two temporarily existed as a land bridge during times of low Mediterranean base-level in the late Miocene (Pellen et al., 2017 and references therein). The evolution of the Adriatic region during the transitional interval from the giant MSC salina to the marine Zanclean Mediterranean, also known as Lago-Mare phase (5.55-5.332 Ma; see Andreetto et al., 2021a), is still unclear and several different scenarios have been envisaged. Controversies regarding the timing and nature of the hydrological and paleoenvironmental changes persist (Popescu et al., 2007, 2009; Roveri et al., 2008a; Bache et al., 2012; Pellen et al., 2017; Amadori et al., 2018; Carnevale et al., 2018: Manzi et al., 2020). Here, we first provide a revised chronologic framework for the uppermost Messinian sedimentary succession of the Adriatic megalake. This allows us to constrain the timing of successive biotic incursions and integrate new and published information on ostracods and calcareous nannofossils with strontium isotope data, which is a geochemical tracer of water provenance. This approach permits the reconstruction of water level changes and source water fluxes to

the Adriatic domain and has implications for climatic and hydrologic changes in the adjacent Mediterranean.

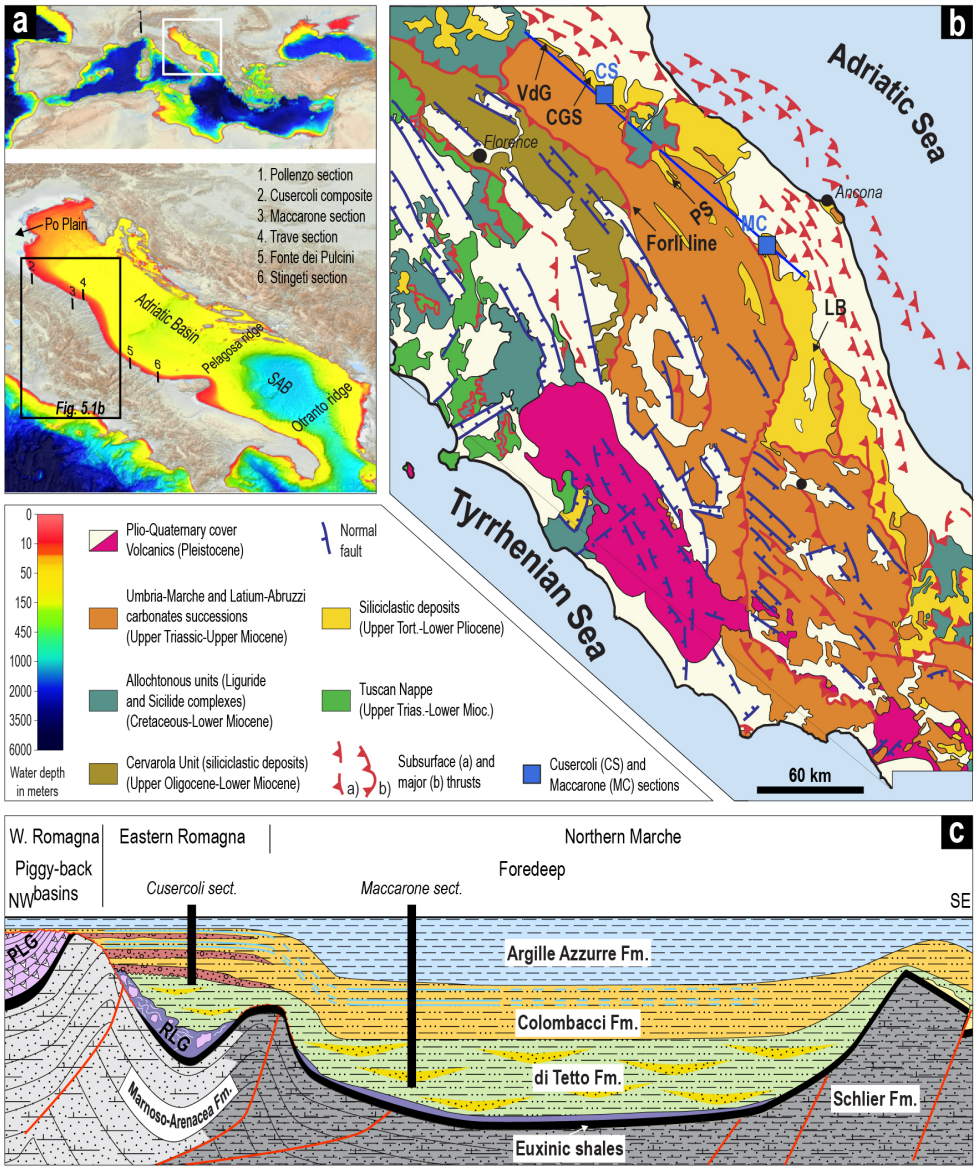

Fig. 5.1. (a) *Bathymetric map of the present-day Mediterranean Basin, with a close up of the Adriatic Basin, and location of the analysed sections (Cusercoli and Maccarone) and of other sections mentioned in the text. Source of the bathymetric map: www.emodnet-bathymetry.eu/.* **(b)** *Geological scheme of the northern and central Apennines showing the location of the Cusercoli (CS) and Maccarone (MC) sections (Sampalmieri et*

al., 2010). The blue line that cuts through the location of the Cusercoli and Maccarone sections corresponds to the trace of the cross section in Fig. 5.1c. Acronyms: PLG: Primary Lower Gypsum; RLG: Resedimented Lower Gypsum; VdG: Vena del Gesso Basin; CGS: Cella-Giaggiolo syncline; PS: Pietrarubbia syncline; LB: Laga Basin. **(c)** *Schematic stratigraphic model of the Apennine foredeep system (modified from Roveri et al., 2008e). The trace of the cross section is reported in Fig. 5.1b.*

5.2 The sedimentary record of the Adriatic megalake

The sedimentary succession of the Adriatic region that pertains to the Messinian Salinity Crisis starts with the Primary Lower Gypsum Unit (PLG; after Lugli et al., 2010; Fig. 5.1c), also known as Gessoso-Solfifera Fm. This unit comprises a gypsum member precipitated in shallow piggy-back basins, and a gypsum-free, euxinic shales member deposited in deeper, suboxic to anoxic settings (Lugli et al., 2010; Dela Pierre et al., 2011; Guibourdenche et al., 2022). The sediments of the Gessoso-Solfifera Fm. were deposited when the Mediterranean and Adriatic were still at their maximum water capacity, receiving constant, albeit reduced, supply of Atlantic seawater (Reghizzi et al., 2018), and therefore predate the establishment of the megalake. The first sediments potentially deposited in the Adriatic megalake are diverse gravity-driven deposits (ranging from debris flows to low-density turbidites) that include giant blocks of PLG gypsum (Sapigno Fm. or Resedimented Lower Gypsum (RLG); Fig. 5.1c). This chaotic unit was triggered by the Mediterranean base-level drop that subaerially exposed the PLG and led to the formation of the main phase of halite precipitation in the deep Mediterranean basins (Manzi et al., 2005). The RLG is overlain by a thick (up to 600 m) siliciclastic succession (the San Donato (or di Tetto) and Colombacci (or Cusercoli) formations), mainly comprising marls intercalated with turbiditic sandstones and only in the Colombacci Fm., with white laminated mudstones (known as 'colombacci'). Fluvio-deltaic conglomerates are also found interbedded with the Colombacci marls, but only in those basins of Eastern Romagna that are located in close proximity to the Forlì line (Molenaar and De Feyter, 1984, 1985; Roveri et al., 1998). This structural element consists in a NNW-SSE-oriented reverse fault with dominant vertical component that played a major role in the sedimentary evolution of the northern Apennines since Late Tortonian times (Ricci Lucchi, 1986; Roveri et al., 2002, 2003; Manzi et al., 2005). These late Messinian sediments are capped by the Argille Azzurre Fm., which consists of massive mudstones rich in marine biota (Gennari et al., 2008) that record the marine replenishment of the Mediterranean at the Miocene/Pliocene (M/P) boundary (Roveri et al., 2014a).

These MSC successions are now incorporated into the Apennine fold-and-thrust belt and they are now exposed in several locations along the Apennine arc, although the stratigraphic sections are commonly incomplete (Roveri et al., 2008a). Maccarone (43°24'22.9"N, 13°06'15.0"E), in the Laga Basin (Fig. 5.1b), is the only place known to expose a continuous succession of the di Tetto-Colombacci formations between a volcanic ash layer, which is dated

at ~5.532 Ma using high-precision chemical abrasion-thermal ionization mass spectrometry (CA-TIMS) U-Pb geochronology on single zircon grains (Cosentino et al., 2013), and the M/P boundary (5.332 Ma; Van Couvering et al., 2000), corresponding to the transition to the Argille Azzurre Fm. in the top part of the section (Gennari et al., 2008; Fig. 5.2a). The section is ~200 m-thick and consists of gray marls intercalated with turbiditic sandstones (Chapter 1, Fig. 1.5f) and up to four, dm- to m-thick black, laminated shales (Fig. 5.2). These indicate the persistence of a water mass that sporadically experienced dysaerobic or anoxic conditions (Sampalmieri et al., 2010). This section has been subject to extensive lithological and paleontological investigations (e.g. Bassetti et al., 1994; Odin et al., 1997; Bertini, 2006; Popescu et al., 2007; Grossi et al., 2008; Roveri et al., 2008a, d; Sampalmieri et al., 2010; Bache et al., 2012; Cosentino et al., 2013; Pellen et al., 2017). A fairly complete section can also be reconstructed by means of physical correlation of distinctive beds, mainly the three m-scale conglomerates recognizable throughout the landscape, between several shorter sections in the wedge-top basin of Cella-Giaggiolo, which occupies an asymmetric syncline bounded to the west by the Forlì line (Roveri et al., 1998; Fig. 5.1b). The resulting Cusercoli composite section consists of grey mudstones with intercalated turbiditic sandstones, three m-scale conglomerates (labelled I-III in Figs. 5.2b, 5.3; see Chapter 1, Fig. 1.5g for a close-up of conglomerate I) of fluvial origin and one colombaccio limestone (Roveri et al., 1998).

We sampled both the Maccarone and Cusercoli composite sections for sedimentology and microfossils (mainly ostracods), in order to elucidate the environmental and hydrological developments in the Adriatic Basin during the Lago-Mare phase. We analyzed the $^{87}Sr/^{86}Sr$ ratios (see the method in the Supplementary material 1) on the most pristine ostracod valves of the genus *Cyprideis* sp. to determine the provenance of the water they dwelt in. In addition, the paleontological and geochemical data available from three other fairly complete and multi-disciplinary studied north Italian sections (Pollenzo, Andreetto et al., 2021b; Trave, Iaccarino et al., 2008; Fonte dei Pulcini, Cosentino et al., 2012; Fig. 5.1b) have been incorporated to form a more comprehensive picture of the evolution of the Adriatic during the latest phase of the MSC.

5.3 Chronologic evolution of the Adriatic megalake

Our ostracod biostratigraphy of the Cusercoli composite section mainly shows intervals largely barren of in-situ biota and only sporadically containing some specimens of the cosmopolitan ostracod *Cyprideis* sp. (Fig. 5.3). Only in the Buttafuoco section, which is stratigraphically above conglomerate III as evidenced by the presence of the M/P boundary, abundant ostracods appear with highly diversified assemblages of Paratethyan taxa (Fig. 5.3). The lower 170 m of the Maccarone section is largely barren in ostracods with only sporadic samples containing *Cyprideis* sp. and *Loxoconcha muelleri* (Grossi et al., 2008; Fig. 5.4). In the uppermost ~25 m of the section, ostracod diversity and abundance increases sharply and is dominated by Paratethyan taxa (Fig. 5.4). The same transition from assemblages dominated

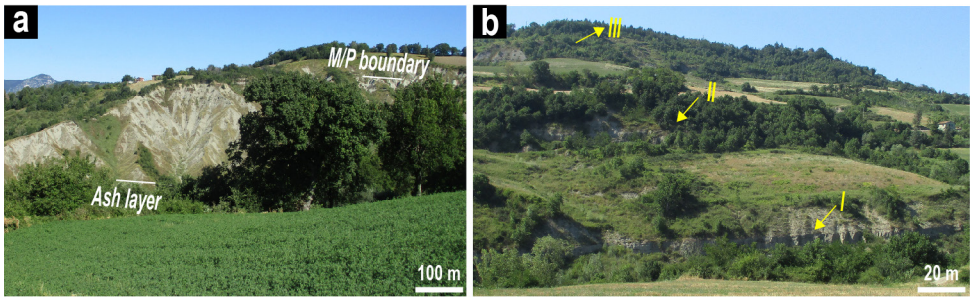

Fig. 5.2. (a) *Panoramic view of the Maccarone section.* **(b)** *Panoramic view of the right bank of the Voltre valley, where the (composite) stratigraphic interval corresponding to the Voltre section (see Fig. 5.3) was logged. Yellow arrows indicate the location of the three conglomerate-sandstone layers (labelled I-III).*

by *Cyprideis* sp. to assemblages diversified of Paratethyan taxa is observed in the successions immediately beneath the M/P boundary in the Pollenzo section (Piedmont Basin; Fig. 5.1a) at the northernmost end of the Adriatic Basin (Andreetto et al., 2022b), and in other Adriatic sections, such as the Trave section near Ancona (Iaccarino et al., 2008) and the Fonte dei Pulcini (Abruzzo) and Stingeti (Molise) sections, to the south (Cosentino et al., 2012, 2018; see location in Fig. 5.1a). The ostracod biostratigraphy of these NW-SE sections suggests that the diversification of the ostracod assemblages in the Adriatic megalake occurred roughly synchronously.

The generally accepted chronological framework for the uppermost Messinian in the Apennines that frames the arrival of the Paratethyan contingent and the associated paleoenvironmental change in time is based on the correlation of two different types of sedimentary cycles (conglomerate-marl couplets and black paleosol-marl pairs) recognized in the Cusercoli section to the 65°N summer insolation curve (Roveri et al., 2008a). Following the chronology of Roveri et al. (2008a), which is based on these cycles (Fig. SI5.1), and our ostracod data from the Cusercoli composite section, the initial influx of Paratethyan ostracods occurred at ~5.35 Ma. This age is substantially younger than the ~5.40 Ma of Roveri et al. (2008a), which is based on the assumption that the first record of Paratethyan ostracods in Cusercoli is from just above conglomerate I (Fig. SI5.1). However, we refrain from using the correlation lines of Roveri et al. (2008a) because syn-depositional tectonics could also have generated the conglomerates (Molenaar and De Feyter, 1984, 1985; Ghibaudo et al., 1985; Roveri et al., 1998), producing an apparent sedimentary cyclicity unrelated to precession, and a continuous climate proxy record that might detect cyclic signals with Milankovitch significance and that is commonly used to tune successions that do not have an obvious precession-related lithological cyclicity (e.g. Natalicchio et al., 2019; Kochann et al., 2021) is not provided (in addition it is difficult to sample a continuous section at Cusercoli; Fig. 5.3; see Supplementary material 2 for insights).

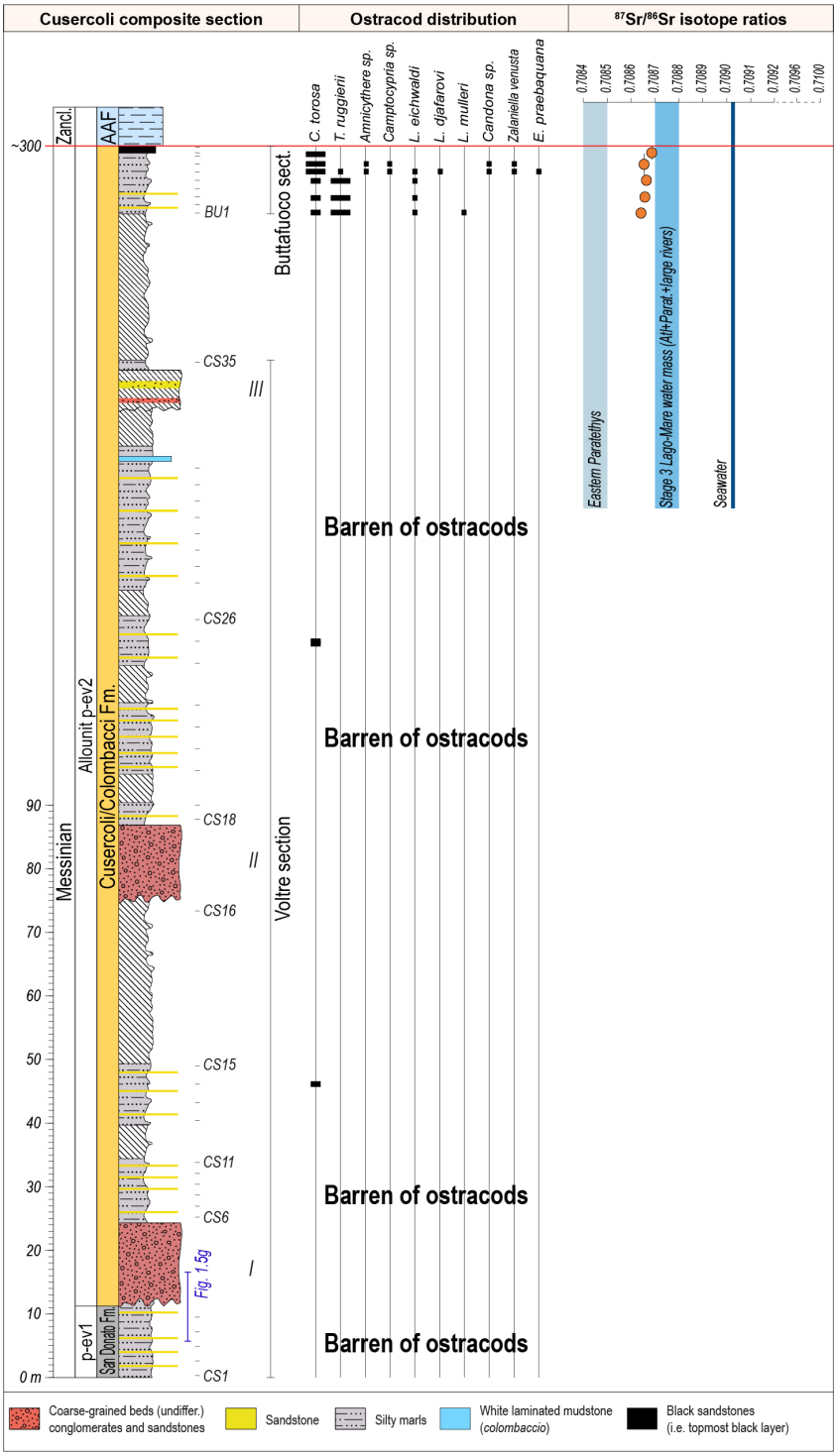
Cusercoli composite section
Ostracod distribution
87Sr/86Sr isotope ratios
C. torosa
T. ruggieriri
Amnicythere sp.
Camptocypria sp.
L. eichwaldi
L. djafarovi
L. mulleri
Candona sp.
Zalaniella venusta
E. praebaquana
0.7084
0.7085
0.7086
0.7087
0.7088
0.7089
0.7090
0.7091
0.7092
0.7096
0.7100
Eastern Paratethys
Stage 3 Lago-Mare water mass (Alt+Paratet.+large rivers)
Seawater
Zancl.
AAF
Messinian
Allounit p-ev2
Cusercoli/Colombacci Fm.
p-ev1
San Donato Fm.
~300
90
80
70
60
50
40
30
20
10
0 m
BU1
CS35
CS26
CS18
CS16
CS15
CS11
CS6
CS1
Fig. 1.5g
Buttafuoco sect.
Voltre section
III
II
I
Barren of ostracods
Barren of ostracods
Barren of ostracods
Barren of ostracods
Coarse-grained beds (undiffer.) conglomerates and sandstones
Sandstone
Silty marls
White laminated mudstone (colombaccio)
Black sandstones (i.e. topmost black layer)

Fig. 5.3. (previous page). *Stratigraphic log of the Cusercoli composite section. The ostracod distribution chart along with variations in the $^{87}Sr/^{86}Sr$ ratios measured on ostracod valves is also shown.*

Fig. 5.4. (next page). *Compilation of ostracods, $^{87}Sr/^{86}Sr$ ratios, magnetic susceptibility (and its wavelet power spectra) and element ratios for the Maccarone section. The dashed orange line corresponds to the Gaussian bandpass filter (Paillard et al., 1996), centered at f=0.028 or p=35.71m with a bandwidth of 0.02, applied to test the robustness of the magnetic susceptibility signal.*

To establish the exact timing of successive biotic incursions and comprehend the underlying mechanism(s), we have revised the chronological framework for the latest Messinian sedimentary succession of the Adriatic megalake based on the Maccarone section. We generated three proxy records, bulk magnetic susceptibility (MS), bulk XRF and grain-size, all of which have previously been used to detect orbitally-controlled paleoclimatic changes in anomalohaline lake settings (e.g. Chang et al., 2014; Natalicchio et al., 2019). These proxy records do not show any sign of precessional forcing on the lithological record. Only the magnetic susceptibility record revealed a prominent signal of 30-40 meters throughout the record (Fig. 5.4). The $^{206}U/^{238}Pb$-dated ash at the base of the section of ~5.532 Ma (Cosentino et al., 2013) and the base of the Pliocene (5.332 Ma) at the top (Fig. 5.2a) suggest that these ~35 m cycles have a duration of ~36 kyr. This signal might therefore reflect the climatological imprint of the obliquity cycle, which at this time seem to have controlled the waxing and waning of Antarctic ice sheets and deep ocean temperatures (Hodell et al., 2001). However, we refrain from attempting an astronomical tuning of the MS record with the obliquity curve because the filtered signal appears quite weak to make the obliquity tuning robust and it is likely that are record is not continuously sampled, since at ~170 m we made a jump from one gully, where we sampled the lowermost 170 m, to another gully, which is not based on the lateral correlation of a marker bed. Unlike the magnetic susceptibility, the grain-size and selected elemental ratios of the marls are fairly stable for the lower 170 m of the section, which mostly consist of a monotonous marl-turbidite succession, and only change significantly in the upper ~25 m, which is 8 m higher than the di Tetto/Colombacci boundary and the incursion of Paratethyan ostracods (and dinoflagellates; Bertini, 2006; Fig. 5.4). This general sedimentary and chemical homogeneity suggests that sedimentation rates and distribution patterns/source areas did not undergo striking modifications during sedimentation. Interpolating a constant sedimentation rate (~1 m/kyr), an age of ~5.36 Ma is obtained for the stratigraphic level at which Paratethyan ostracods appear in the Maccarone section and, more generally, in the Adriatic Basin. Our revised age for the influx of Paratethyan ostracods in the Adriatic region is further in agreement with the results of the Fonte dei Pulcini section (Fig. 5.6), where the abrupt increase in the diversity of the ostracod assemblages is dated at 5.354 Ma by astronomical tuning of the magnetic susceptibility record to the insolation curve (Cosentino et al., 2012).

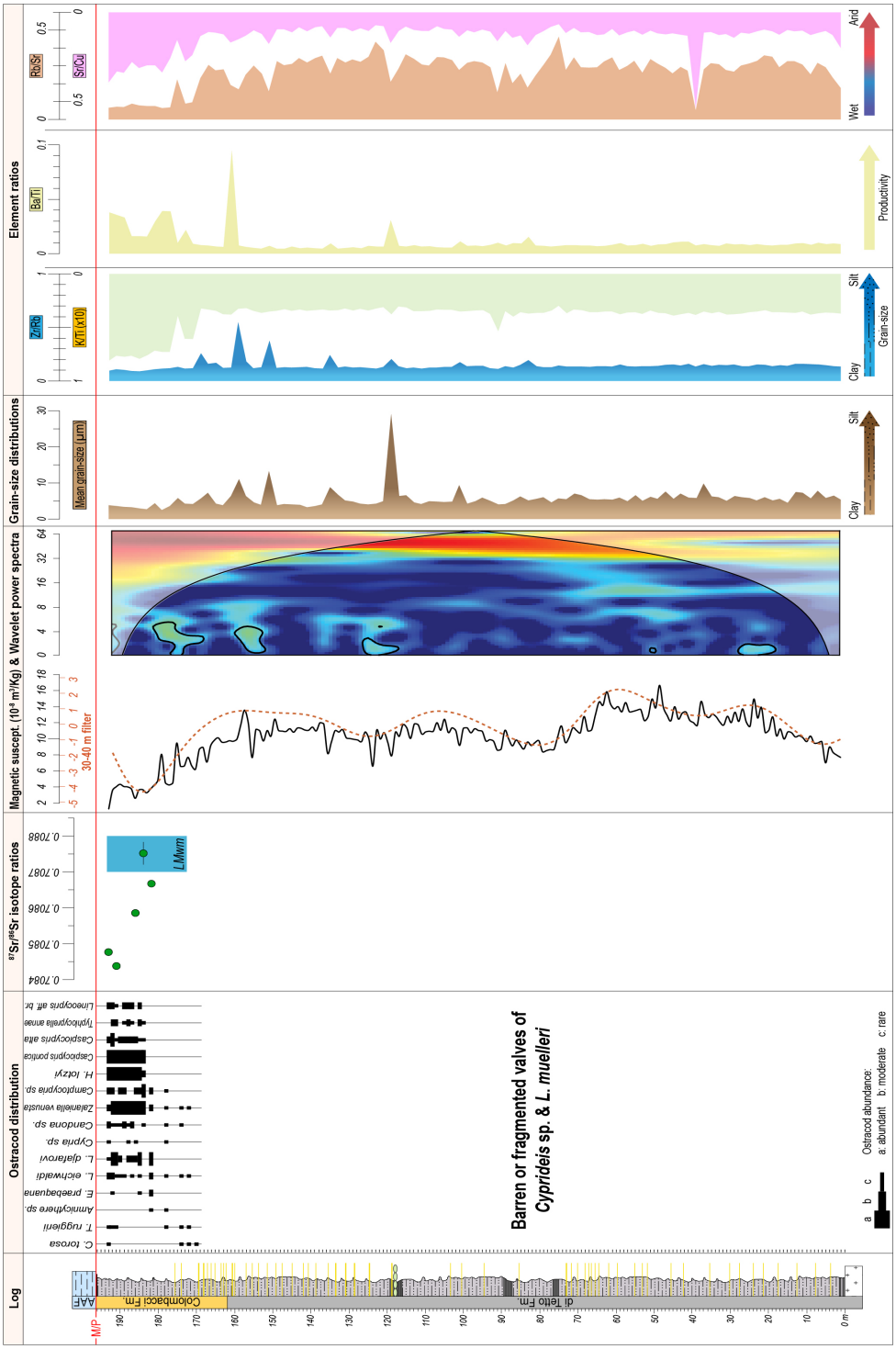
Log
Ostracod distribution
C. torosa
T. ruggieri
Ammicythere sp.
E. praebaquana
L. aichwaldi
L. djafarovi
Cytpria sp.
Candona sp.
Zalanella venusta
Camptocypria sp.
H. lotzyi
Caspiocypris pontica
Caspiocypris alta
Typhlocypretta annae
Limnocypris aff. bk
87Sr/86Sr isotope ratios
LMwm
Magnetic suscept. (10-3 m3/kg) & Wavelet power spectra
30-40 m filter
Grain-size distributions
Mean grain-size [µm]
Silt
Clay
Element ratios
Zr/Rb
K/Ti (x10)
Grain-size
Ba/Ti
Productivity
Rb/Sr
Sr/Cu
Arid
Wet
Barren or fragmented valves of
Cyprideis sp. & L. muelleri
Ostracod abundance:
a. abundant b. moderate c. rare
Colombacci Fm.
di Tetto Fm.
AAFS
M/P

In summary, considering the Maccarone section as archetype for the environmental change in the Adriatic region in the latest Messinian, we identify three intervals with different faunal and flora composition: (I) the first and longest interval between 5.59 and 5.36 Ma does not contain many traces of life. From the lithostratigraphic point of view, it corresponds to the entire Sapigno and di Tetto fms. and part of the Colombacci Fm. (II) the second interval between 5.36 and 5.332 Ma contains more or less abundant and diverse assemblages of ostracods, dinoflagellates and mollusks that are indicative of brackish and relatively shallow (up to 100 m) conditions (Gliozzi and Grossi, 2008; Grossi et al., 2008). This interval coincides with the uppermost part of the Colombacci Fm., just beneath the M/P boundary; (III) the third interval corresponds to the Zanclean Argille Azzurre Fm. and contains exclusively marine biota. In the paragraphs that follow, we explore the paleoenvironmental and paleohydrological significance of each of these intervals.

5.4 Birth of the Adriatic megalake

The Adriatic megalake formed between 5.59 and 5.55 Ma in response to the Mediterranean base-level drop(s) that deposited 821-927±50 thousand km^3 of halite on the Mediterranean sea floor (Haq et al., 2020) and incised canyons on the Mediterranean shelf and slopes (Hsü et al., 1973; Ryan, 2009). The more marginal zones emerged during this drawdown and underwent subaerial erosion (Amadori et al., 2018; Ghielmi et al., 2010, 2013; Cazzini et al., 2020), while the deeper depocenters probably remained full of residual brine diluted by the input of continental freshwater from local highs (Roveri et al., 2008a). Despite the fact that some reject the possibility that the Adriatic Basin ever lost its connection with the Mediterranean (Manzi et al., 2020) and even with the open ocean (Carnevale et al., 2018), several lines of evidence suggest that the water level in the Adriatic lowered by 800-900 m, leaving it as a perched lake (e.g. Bache et al., 2012; Pellen et al., 2017; Amadori et al., 2018): the substantial erosion of the PLG, witnessed by its erosional top (Roveri et al., 2003; Dela Pierre et al., 2011; Ghielmi et al., 2019) and downslope resedimentation to form the RLG (Manzi et al., 2005); the presence of only few meters of Colombacci Fm. on top of the erosional surface cutting through the PLG (e.g. the Vena del Gesso Basin, Roveri et al., 2003); the V-shaped paleocanyons along the Southern Alpine margin and in the Po Plain, which match the present-day southern Alpine valleys and are filled with Messinian post-evaporitic and Pliocene deposits (Amadori et al., 2018; Ghielmi et al., 2010, 2013; Cazzini et al., 2020).

Independent paleontological and geochemical evidence for a late Messinian Adriatic megalake are so far lacking, but our new chronology allows a direct correlation with other tuned successions in the open Mediterranean. Time equivalent sections in central Mediterranean basins comprise up to 7 gypsum-marl couplets of the Upper Gypsum unit, best exposed in the Caltanissetta Basin on Sicily (Manzi et al., 2009). The UG marls on Sicily record high diversity Paratethyan ostracod assemblages (Biofacies 2) from 5.47 Ma (Andreetto et al.,

2022a). Along the margins, where fluvial conglomerates-sandstones alternate with marls, the first known occurrence of Paratethyan ostracods is in the Nijar Basin (unpublished data; see Appendix I, p. 290), where it is dated at ~5.43 Ma (Hilgen et al., 2007) or ~5.41 Ma (Omodeo Salé et al., 2012). The occurrence of Paratethyan ostracods in the same precession cycle in the Nijar Basin, which had an estimated (maximum) paleodepth of ~250 m during the Early Zanclean (and therefore, possibly, during the latest Messinian), and in the >600 m deep (Sgarrella et al., 1997, 1999; Barra et al., 1998) Caltanissetta Basin (and even deeper localities such as the Balearic slope; Iaccarino et al., 1999) provides us with an ecological marker for precession-paced, high magnitude fluctuations of the Lago-Mare water level. As a matter of fact, the Paratethyan fauna entered the marginal basins of the Mediterranean during highstands, whereas it colonized deeper settings during lowstands (Andreetto et al., 2022a). The absence of both gypsum and ostracods in the Adriatic region, despite the fact that its subbasins are thought to have had similar paleodepths (600-1000 m; Gennari et al., 2008; Violanti et al., 2009) to those of the Caltanissetta Basin, suggests that prior to the first occurrence of ostracods at Maccarone at ~5.36 Ma, the water level in the Mediterranean was never high enough to spill over the Otranto and/or Gargano sill into the Adriatic Basin. This explains why the Adriatic Basin existed as an endorheic megalake impoverished of life for most of the latest Messinian and without sufficiently concentrated Ca^{2+} and SO_4^{2-} to precipitate gypsum (Fig. 5.7).

5.5 The Caspian-style brackish water phase

The appearance of the highly diversified Paratethyan ostracod fauna in the top part of the Adriatic sections indicates that the Adriatic megalake experienced a major influx of Lago-Mare waters at ~5.36 Ma, spreading the fauna that was already established in the Mediterranean Basin (Fig. 5.7). This transgression is also identified in dinoflagellate (Bertini, 2006) and mollusk (Esu, 2007) assemblages, where endemic Paratethyan species are only found towards the top of the Colombacci Fm.

The ostracods, dinoflagellates and mollusk species recognized in the Adriatic sections migrated from the Pannonian Basin (present-day Hungary) to the Black and Caspian seas at ~6.10 Ma (Krijgsman et al., 2010; Stoica et al., 2013, 2016; van Baak et al., 2016, 2017; Grothe et al., 2018; Lazarev et al., 2020). Therefore, at ~5.36 Ma, the Adriatic megalake was also connected, via the Mediterranean, to the Black and Caspian seas. The age of ~5.36 Ma roughly corresponds with the 65°N summer insolation maximum peak that in the Central Mediterranean coincides with the highstand phase that pre-dates the deposition of the last gypsum bed of the MSC (i.e. #7 in the Eraclea Minoa section; Fig. 4.8; Andreetto et al., 2022a). $^{87}Sr/^{86}Sr$ ratios from Member C of the Pollenzo section (0.708746-0.708834) were successfully demonstrated to have not been acquired by the ostracod valves in an endorheic lake, because these values are substantially different from the $^{87}Sr/^{86}Sr$ signature of the Po River, which integrates the dissolved solutes provided by the lithologies forming the Alps and Northern

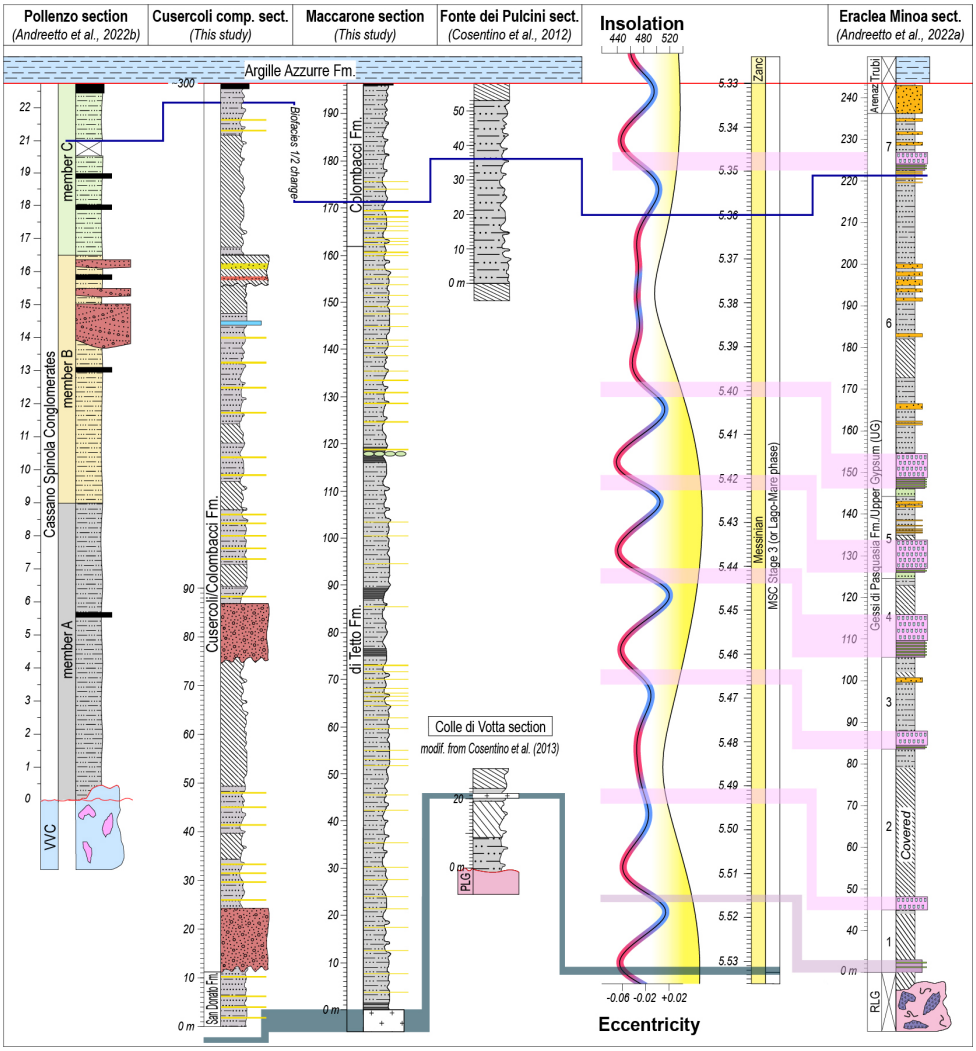

Fig. 5.5 (this page). *Tentative correlation between four sections across the Adriatic region and the astronomically-tuned Upper Gypsum unit in the Eraclea Minoa section, which is representative of the paleoenvironmental conditions in force Stage 3 in the open Mediterranean. Legend for the Adriatic sections: see figs. 5.3 and 5.4. Legend for the Eraclea Minoa section: see Fig. 4.2 (chapter 4, p. 203).*

Fig. 5.6 (next page). (a) *New (Buttafuoco and Maccarone sections) and published (Pollenzo section)* $^{87}Sr/^{86}Sr$ *data plotted against the coeval signature of the Atlantic Ocean and the Lago-Mare water mass filling the open Mediterranean and using the age constraints provided by the correlations in Fig. 5.5.* **(b)** *Simplified geological map of Italy showing the main rock-forming catchments surrounding the Piedmont, Cella-Giaggiolo and Laga basins (Cicchella et al., 2010).*

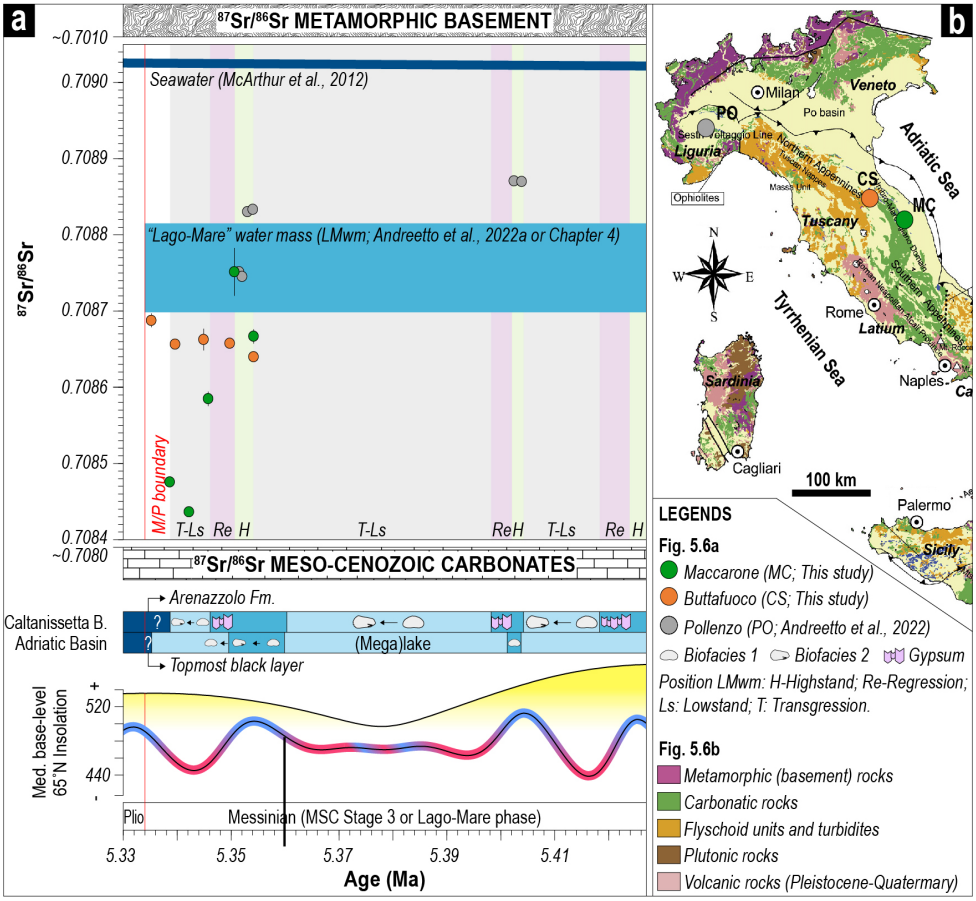

Table 5.1. *$^{87}Sr/^{86}Sr$ composition and details of the analyzed samples.*

Sample	Unit	Age	Material	$^{87}Sr/^{86}Sr$	2σ (*10^{-6})
BU9	Colombacci Fm.	late Messinian	*C. torosa*	0.708688	0.000009
BU7	Colombacci Fm.	late Messinian	*C. torosa*	0.708657	0.000004
BU5	Colombacci Fm.	late Messinian	*C. torosa*	0.708663	0.000014
BU3	Colombacci Fm.	late Messinian	*C. torosa*	0.708658	0.000008
BU1	Colombacci Fm.	late Messinian	*C. torosa*	0.708641	0.000006
MC193	Colombacci Fm.	late Messinian	*C. torosa*	0.708477	0.000005
MC191	Colombacci Fm.	late Messinian	*C. torosa*	0.708438	0.000002
MC186	Colombacci Fm.	late Messinian	*C. torosa*	0.708586	0.000009
MC184	Colombacci Fm.	late Messinian	*C. torosa*	0.708752	0.000031
MC182	Colombacci Fm.	late Messinian	*C. torosa*	0.708667	0.000009

Apennines, were the catchments are located (Marchina et al., 2018), at any point of its course (Andreetto et al., 2022b). These $^{87}Sr/^{86}Sr$ ratios imply mixing between local, continental runoff and Lago-Mare waters from the open Mediterranean (Andreetto et al., 2022b), that had a less radiogenic $^{87}Sr/^{86}Sr$ signature than the global ocean (0.7087-0.7088) due to the mixing of a substantial amount of low radiogenic

non-marine water from the Paratethys and the large rivers with little, higher radiogenic Atlantic seawater (Andreetto et al., 2022a). The $^{87}Sr/^{86}Sr$ ratios measured on ostracod valves from the Pollenzo section therefore suggest the establishment of an at least unidirectional Mediterranean-Adriatic connection and the at least temporary cessation of the isolation of the Adriatic megalake from the Mediterranean at ~5.36 Ma.

It is harder to reconstruct the probable $^{87}Sr/^{86}Sr$ signature of Messinian rivers draining into the Cella-Giaggiolo and Laga basins (Fig. 5.1b) than the Piedmont Basin because measurements on present-day rivers are scarce and the geology of the hinterland is more complicated. This means there are no fluvial $^{87}Sr/^{86}Sr$ to compare with those measured on the Cusercoli and Maccarone ostracods (Table 5.1; Fig. 5.6). Nevertheless, a closer look to the range of $^{87}Sr/^{86}Sr$ ratios measured on the NW-SE transect Pollenzo-Cusercoli-Maccarone reveals a trend of diminishing values from Piedmont (0.708746-0.708834, average of 0.708790) to Cusercoli (0.708641-0.708688, average of 0.708662) to Maccarone (0.708477-0.708752, average of 0.708626). This trend, which indicates that from Piedmont to Maccarone, the Lago-Mare water in the Adriatic was integrating more Sr^{2+} from lower radiogenic sources in each of the considered basins, seems to be consistent with the distribution of the isotopically-different lithologies across the Italian peninsula: the western Alps, which surround the Piedmont Basin, are dominated by rocks of the crystalline basement, which mainly provide Sr^{2+} with high radiogenic composition (Marchina et al., 2018); the Central Apennines, which enclose the Laga Basin, are dominated by Meso-Cenozoic carbonates, which provide Sr^{2+} with lower radiogenic composition (Cosentino et al., 2010); the Northern Apennines, where the Cusercoli composite section is located, supply both higher radiogenic Sr^{2+} from Tertiary flysch (alternation of sandstone, marls and pelite rocks) and lower radiogenic Sr^{2+} from the Jurassic ophiolites and Meso-Cenozoic carbonates (Marchina et al., 2018).

Marine foraminifera, dinoflagellates, calcareous nannofossils and fish consisting of both stenohaline and euryhaline taxa co-exist with Paratethyan organisms in the same uppermost Messinian sediments. The marine biota is largely considered to be reworked because it is generally badly preserved and consists of a mixture of forms from different stratigraphic intervals (e.g. Bertini, 2006; Iaccarino et al., 2008; Cosentino et al., 2012; Andreetto et al., 2021a), but since some Atlantic water was present in the Mediterranean, it is possible that some of the euryhaline taxa are in-situ (Andreetto et al., 2022a, b). As for the stenohaline fish, considered by Carnevale et al. (2018) as unquestionable proof of the existence of a fully marine environment, they are either reworked, as suggested by four $^{87}Sr/^{86}Sr$ ratios measured by Grunert et al. (2016) on otoliths of stenohaline Myctophidae from the Moncucco section in the Piedmont Basin (see Andreetto et al., 2021a), or also adapted to non-marine and fluctuating conditions in the water column.

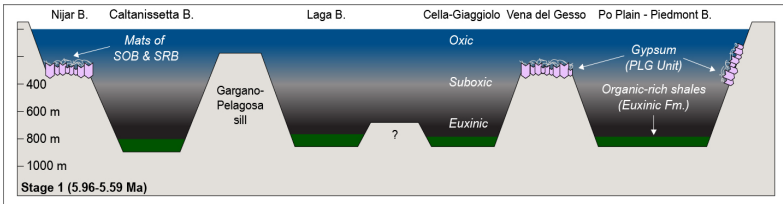

EVAPORITIC ADRIATIC

Bacteria-induced precipitation of gypsum[1, 2, 3, 4] in shallower basins during arid phases (marls during humid phases, not shown here[5]). Deposition of shales in deeper settings[5]). Stratified water column[6, 7] with (lower than) seawater salinity[8].Two-way (restricted) Atl.-Med. connection[9].

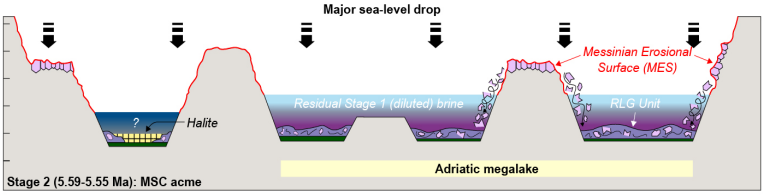

ADRIATIC MEGALAKE

The further restriction of the Atl.-Med. connection (loss of Med. outflow[9]) triggers a major sea-level drop & halite precipitation in the Med[8]. Birth of the **Adriatic megalake** (800-900 m of drop)[11], which likely consists of a residual Stage 1 brine diluted by the local runoff[12]. Deep erosion of its margins[11, 13].

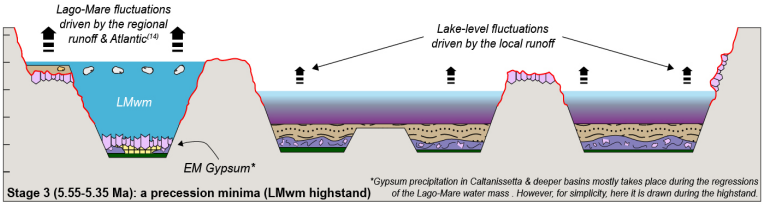

During Stage 3, the Mediterranean is filled with a "Lago-Mare water mass (LMwm) consisting of non-marine water from Paratethys and large rivers and minor (<20%) Atlantic seawater[14]. The LM water level have fluctuated several hundreds of meters with precession periodicity[14]. Paratethyan ostracod-rich marls deposit in the deeper basins during the lowstands and in marginal basins during the highstands; gypsum precipitates during the regressions[14]. Until ~5.36 Ma, none of the highstands reach the Adriatic, which persists as a mud-depositing, life-deprived endorheic lake.

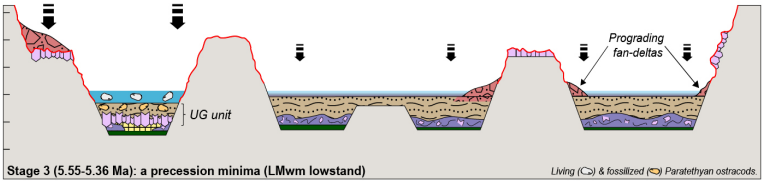

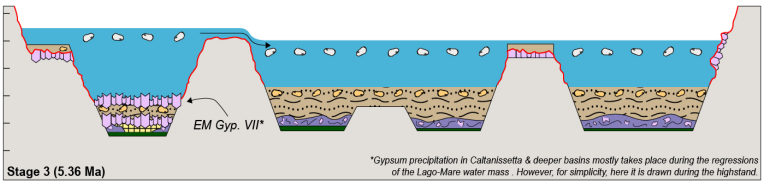

LAGO-MARE ADRIATIC

At ~5.36 Ma, the Adriatic megalake experienced a major influx of Lago-Mare waters, spreading the Paratethyan fauna that was already established in the Mediterranean Basin. This transgression is linked to highstand that leads, during the subsequent regression, to the precipitation of the last Messinian gypsum.

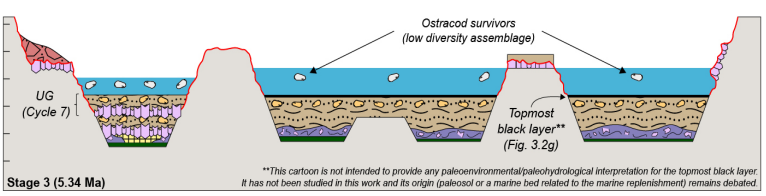

ADRIATIC MEGALAKE

After this transgressive event, lacustrine conditions were briefly re-established, but were terminated, at, or slightly before 5.332 Ma, by the Zanclean (or Terminal Messinian) Flood which re-established open marine conditions throughout the Mediterranean[15, 16].

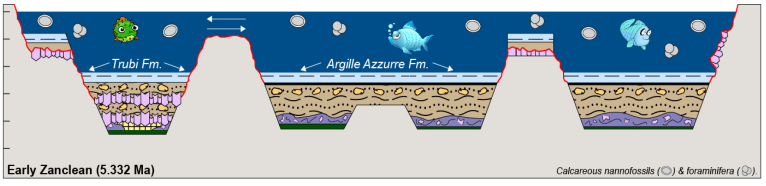

ADRIATIC SEA

Fig. 5.7 (previous page). *Cartoons showing the proposed evolution of the Adriatic Basin (and the Mediterranean) during the MSC. References: (1) Dela Pierre et al. (2015); (2, 3) Natalicchio et al. (2020, 2021); (4) Guibourdenche et al., 2022; (5) Lugli et al., 2010; (6) Natalicchio et al. (2019); (7) Sabino et al. (2021); (8) Aloisi et al. (2022); (9) Krijgsman et al. (2018); (10) Roveri et al. (2014a); (11) Amadori et al. (2018); (12) Roveri et al. (2008a); (13) Cazzini et al. (2020); (14) Andreetto et al. (2022a); (15) Micallef et al. (2018); (16) Garcia-Castellanos et al. (2020).*

5.6 Restoration of the Adriatic Sea

A second marked paleoenvironmental and paleohydrological change occurs in all sections at the Colombacci Fm./Argille Azzurre Fm boundary, which is dated at 5.332 Ma from integrate¬d microfossils and paleomagnetic data (Gennari et al., 2008). At this transition, all Paratethyan ostracods disappear and are replaced by exclusively marine foraminifera, calcareous nannofossils, dinoflagellates and fish (Fig. 5.7). The subtle (in Cusercoli) to more pronounced (in Maccarone) decrease in $^{87}Sr/^{86}Sr$ in the upper part of the Colombacci Fm. (Fig. 5.6) is likely to reflect an enhanced contribution of local waters draining low radiogenic limestones. For a seawater-fed Adriatic Basin to become more sensitive to local inputs, which are several order of magnitude less concentrated, means that the contribution of Mediterranean Lago-Mare water to the Adriatic Basin decreased over time. We therefore conclude that following the Lago-Mare transgression at ~5.36 Ma, a new water level fall took place in the Mediterranean, restoring a megalake in the Adriatic region. This means that the marine replenishment occurred rather catastrophically in the Adriatic Basin, following a Mediterranean water level rise of several hundreds of meters. The occurrence of shallow-water, Biofacies 2 ostracods just below the M/P boundary at Eraclea Minoa (Andreetto et al., 2022a) and in ODP Site 975B, which was at >2000 mbsl during the MSC (Heida et al., 2022), are an indication that the water level in the Mediterranean was extremely low when the marine replenishment took place, therefore supporting its catastrophic nature following the sudden breaching of the Gibraltar Strait (see Micallef et al., 2018 and Garcia-Castellanos et al., 2020).

5.7 Conclusions

Using an existing radiometric date and a new magnetic susceptibility record, we have constructed a new high-resolution age model for the Maccarone section, which samples a continuous succession of the uppermost 200 kyr of the Messinian stage. The orbitally tuned age model dates the influx of the first Paratethyan ostracods in the Maccarone section, and more generally in the Adriatic at ~5.36 Ma. We use this age model to integrate new and published and strontium isotope data to reconstruct the paleoenvironmental and paleohydrological evolution of the Adriatic during the final phase of the MSC. We conclude that somewhere between 5.59 and 5.55 Ma, which corresponds to the nadir of the MSC when the Mediterranean water level was probably at its lowest and halite precipitated in its deepest basins, the Adriatic

transitioned from an Atlantic-fed, gypsum-precipitating basin to an isolated megalake. In the first ~200-240 kyr that followed its initiation and the widespread precipitation of gypsum in its shallower subbasins, the lake comprised very harsh (possibly hypersaline and/or hyperalkaline) environmental conditions and not many traces of life are present. At ~5.36 Ma, a major hydrological change provoked by a Mediterranean highstand established a brackish water environment in the Adriatic supporting a thriving Paratethyan biota. After this transgressive event, lacustrine conditions were briefly re-established, but were terminated, at, or slightly before 5.332 Ma, by the Zanclean (or Terminal Messinian) Flood which re-established open marine conditions throughout the Mediterranean.

Supplementary information 5.1 - Material and methods

S5.1.1 Studied sections

The Cusercoli composite section is located in the wedge-top Cella-Giaggiolo Basin, which occupies an asymmetric, NE-vergent syncline (Fig. 5.1b) bounded to the west by the Forlì thrust (Roveri et al., 1998). Overall, it corresponds to the Cusercoli section of Roveri et al. (1998), except nowhere in the Cella-Giaggiolo Basin we have observed a continuous section from the Euxinic Shales Fm. to the Argille Azzurre Fm. Our section is a composite obtained through physical correlation of five subsections of river and road outcrops. Stratigraphic correlations between physically disjointed subsections were achieved by means of lateral tracing of three conglomeratic-sandy layers, which stand out in the landscape due to their greater cementation compared to mudstones they are intercalated with. Four of the five partial outcrops are exposed along the valley of the Voltre stream. Here we studied from the uppermost ~10 m of the San Donato Fm. (44°02'18.2"N, 12°02'31.3"E) until the uppermost conglomerate of the Colombacci Fm. (which we refer to as "Voltre section"). The presence of numerous stratigraphic gaps precludes the thickness of the investigated stratigraphic interval to be estimated with accuracy, but we estimated to be ~250-280 m by merging field and Google Earth measurements (Fig. 5.3). The Colombacci/AAF boundary (which coincides with the M/P boundary) is not exposed in the Voltre valley, but it is recognized in the Buttafuoco section (44°05'00.5"N 12°01'51.9"E), located on the left side of the valley of the Bidente river, some 9 km to the north of the Voltre village. This section is 10-15 m-thick and has already been investigated in detailed by Grossi et al. (2008) and Gennari et al. (2008) for its Messinian and Pliocene part, respectively.

The Maccarone section (43°24'22.9"N, 13°06'15.0"E) is a fairly steep cliff (Fig. 5.2a) located some 200 km to the south of Cusercoli within the Laga Basin (Marche region; Fig. 5.1b). We studied the ~196 m-thick stratigraphic interval that starts from right above the white volcaniclastic layer at the base of the cliff and terminates at the M/P boundary recognized in the topmost part of the cliff by means of planktonic foraminifera biostratigraphy (Gennari et al., 2008). Despite the continuous exposure of the entire di Tetto and Colombacci fms. (Fig. 5.2a),

we logged and sampled the section in two nearby gullies: one were we sampled up to ~170 m and the second one were we sampled the uppermost ~30 m. the correlation between the two gullies was performed by sight due to the absence of marker beds.

The Maccarone and Voltre sections were logged at m-scale and analyzed to record facies variations and sedimentological features indicative of the paleoenvironmental conditions at times of deposition. The mudstones of the Maccarone section were sampled at regular spacing of 1 m, therefore resulting in the collection of 196 samples (samples MC0-195; Fig. 5.4). The same evenly-spaced sampling could not be conducted in the Voltre composite section due to the poorer outcropping conditions. As a consequence, only 45 mudstone samples were collected (35 from the Voltre section, CS1-35; 10 from the Buttafuoco section, BU1-10).

S5.1.2 Paleontological analyses

All 45 samples from the Voltre composite section and 50 samples from Maccarone (mostly concentrated in the Colombacci Fm., since Grossi et al. 2008 already shown that the San Donato Fm. is largely barren) were processed in the laboratory of Utrecht University for ostracod investigations by standard micropaleontological methods of air drying, disintegrating and sieving under tap water through 125 and 63 μm sieves. The residues were dried overnight, transferred in cleaned, pre-labelled vials and subjected to a qualitative and semi-quantitative analysis of the foraminifer and ostracod fauna, respectively. Thirteen samples (MC145, 149, 153, 157, 161, 165, 169, 173, 177, 181, 185, 189, 193) were selected for calcareous nannofossil analyses from the stratigraphic interval were Popescu et al. (2007), Bache et al. (2012) and Pellen et al. (2017) report the presence of the age-diagnostic and marine stenohaline taxon Ceratolithus acutus. Sample preparation followed the standard smear slide technique, to retain the original sediment composition and nannofossil assemblages. Semiquantitative analyses to search *C. acutus* specimens were performed with a polarizing light microscope at a magnification of 500X, in order to obtain a wide coverage of the sample area with the spirit of avoiding time consuming. Frequencies were estimated by counting the number of specimens encountered in 3000 fields of view at 500× magnification (33.91 square millimeters). Qualitative analyses of the total assemblage composition were performed at magnification of 1250X.

S5.1.3 $^{87}Sr/^{86}Sr$ isotope analyses

Six-ten ostracod valves from 7 Maccarone samples and 6 Voltre samples were selected for $^{87}Sr/^{86}Sr$ analyses. Sample preparation and analyses were conducted at the Bristol isotope group Laboratory at the Bristol University following the three-step procedure thoroughly detailed by Andreetto et al. (2022b or chapter 3 of this work) of cleaning with milliQ water and methanol, dissolution with HNO_3 and Sr extraction by means of a Sr Spec resin. Purified Sr was loaded onto rhenium filaments with a $TaCl_5$ activator and the $^{87}Sr/^{86}Sr$ ratio of each sample was measured on a Thermo-Finnigan Triton thermal ionisation mass spectrometer in dynamic

multi-collection mode. Results are normalized using the value of 0.1194 for the $^{88}Sr/^{86}Sr$ ratio. Repeated analyses of NIST SRM 987 gave $^{87}Sr/^{86}Sr = 0.71021 \pm 0.00002$ (2s; n=6).

S5.1.4 Bulk magnetic susceptibility (MS)

Bulk magnetic susceptibility (MS), expressed on a mass-specific basis per sample, was measured on the all 194, oven-dried samples (MC0-MC193) with an Agico MFK1 Kappabridge at field strength of 200 A/m and a frequency of 900 Hz.

S5.1.5 Grain size analysis (GSA)

For GSDs, samples were treated in cleaned centrifuge tubes first with 20 ml of 10% H_2O_2 to remove all organic material, subsequently boiled with 4 ml of 10N HCl to remove all carbonate. The insoluble residues was topped up with milli-Q water up to the volume of 45 mL, centrifuged for 10 minutes at 3300 rpm and emptied of the supernatant. These steps were repeated four times. Prior to the analyses, to facilitate dispersion samples were ultrasonicated and poured in the sample dispersion unit Hydro 2000G along with 25 mL of a dispersing solution (44.6 g $Na_4P_2O_7x10H_2O$ and 4.24 g Na_2CO_3 in 1 L deionized H_2O). GSDs were measured using a Malvern Mastersizer 2000 laser grain-size analyzer with a measurement range of 0.02-2000 μm. Each measurement run was set to run for 30 seconds or 30,000 snaps. After every run the machine was rinsed and cleaned. Values of 1.544 and 0.9 were used for the refractive and absorption indices of the samples, respectively. The residual was always less than 1.6%.

S5.1.6 X-ray fluorescence (XRF) analysis

~30 g of the same odd-numbered samples measured for MS were grounded to powder in a pre-cleaned agate mortar and measured for bulk X-ray fluorescence (XRF), whereas ~1 g was treated for analyses of the grain-size distributions (GSDs) of the insoluble (i.e. non-biogenic) fraction. Concentration (in ppm) of a number of elements (P, S, Cl, K, Ca, Ti, Cr, Mn, Fe, Co, Ni, Cu, Zn, As, Se, Rb, Sr, Zr, Mo, Ag, Cd, Sn, Sb, Ba, Hg and Pb) was determined using a handheld XRF machine (Olympus Delta Premium with 50 kV screen, SN 550311, SIT 3064). Each sample was measured for 180 s at intervals of 60 s during which tube voltage increased from 15 kV to 40 kV and 50 kV because different elements react to different wavelengths. Each sample was analyzed three times and the average value was used as the abundance of each element. Relative precision and accuracy were established through duplicate analyses and standards and were better than 5% relatively for all elements except Zr (better than 7%). XRF data are presented as elemental ratios in Figure 5.4. We calculated some elemental ratios that are indicators of past climatic and environmental changes and that are typically found to record orbital oscillations. Zr/Rb and K/Ti ratios are related to bulk grain-size variations, because these elements are concentrated in different grain-size fractions: Zr and Ti are predominantly associated with heavy minerals such as zircon and titanite and normally enriched in medium to

coarse silts, whereas Rb and K are often associated with clay mineral assemblages (e.g. Dypvik and Harris, 2001; Heymann et al., 2009; Li et al., 2020; Izumi et al., 2021). Rydberg et al. (2016) use the Zr/Rb ratio to evaluate variations in eolian activity and transport. They found out that sediments that accumulated during periods with high eolian activity were enriched in Zr and depleted in Rb. Rb/Sr and Sr/Cu are considered a reliable proxy for chemical weathering intensity and paleoenvironmental change when measured in fine-grained sediments, because Rb and Cu mostly occur in K-bearing minerals, which are relatively resistant to weathering, whereas Sr is abundant in Ca-bearing minerals, which are more sensitive to weathering (e.g. Chen et al. 1999; Heymann et al., 2009; Chang et al., 2014; Fritz et al., 2018; Han et al., 2020; Yang et al., 2020). Several studies have demonstrated the utility of Ba/element ratios as proxies for paleoproductivity in some settings (e.g. Paytan et al., 1996; Van Santvoort et al., 1996; Hull and Norris, 2011) because Ba concentration is positively associated with organic material accumulations (Calvert and Pedersen, 2007; Schoepfer et al., 2015; Natalicchio et al., 2019). Therefore, a rise in Ba concentrations relative to a terrestrially sourced tracer such as Ti indicates enhanced productivity (Calvert and Pedersen, 2007; Hull and Norris, 2011; Schoepfer et al., 2015; Natalicchio et al., 2019).

S5.1.7 Spectral analysis

Time series analysis was performed on the MS data of the Maccarone section and the $\delta^{18}O$ record of ODP Site 982 (Hodell et al., 2011; Drury et al., 2018) using Wavelet analysis (Grinsted et al., 2004) and AnalySeries (Paillard et a., 1996). The wavelet analysis calculates both the evolutive spectral characteristics and significance levels of the signal through time (or depth) and the spectral characteristics of the total data series (global wavelet spectrum). A Gaussian filter (Paillard et al., 1996) was used to extract the main cyclic signals from both records. Note that only the MS record of the Maccarone section was subject to time series analysis, since the trends of both XRF and grainsize analysis were thought to be too constant to pick up any significant cyclicity. Prior to the analysis, all data series were linearly interpolated.

Supplementary information 5.2 - Pitfalls of the published chronostratigraphic frameworks of Stage 3 sedi-

Several chronostratigraphic frameworks of the post-evaporitic terrigenous successions of the Adriatic foredeep have been proposed over the years by using both Cusercoli (Roveri et al., 1998, 2008a) and Maccarone (Bache et al., 2012; Cosentino et al., 2013, supplementary material) as reference sections and different methods, including biostratigraphy and astronomical tuning of sedimentary cycles and climate proxy records. These frameworks are, however, substantially different from each other and present several incongruences and oddities. Below, we provide a description of the different models and the major points of disagreement.

S5.2.1 The "high-resolution stratigraphic framework" by Roveri et al. (2008a)

Model's description. The physical-chronostratigraphic framework for the late Messinian deposits in the Adriatic region by Roveri et al. (2008a) is built upon the assumption that the conglomerates of the Colombacci Fm. in the Cusercoli/Voltre section or, in their absence, two black layers interpreted as paleosols by Roveri et al. (1998), are "clearly controlled by arid to wet climatic oscillations […] and as for the cyclicity recognized in evaporitic and pre-evaporitic units, a precessional periodicity is suggested" (Roveri et al., 2008a). These coarser clastics (and paleosols) are made to correspond to precession maxima (insolation minima) and relatively dry climate, whereas the colombacci limestones interbedded with the mudstones to precession minima (insolation maxima) and relatively wet climate (Roveri et al., 1998, 2008a, e). Possibly proceeding downwards from the M/P boundary, Roveri et al. (2008a) tuned the two black layers and the three conglomerates to each precession maximum peak encountered, resulting in age of ~5.416 Ma (approximated to 5.42 Ma) for the p-ev1/p-ev2 boundary (Fig. SI5.2.1). This age model is extended across the Apennine foredeep by means of lateral correlation of the Cusercoli conglomerates and black layers with other coarser clastic bodies (mostly sandstones; Fig. SI5.2.1). According to Roveri et al. (2008a), the Biofacies 1/2 change, which they made to coincide with the first appearance of *L. djafarovi*, is roughly coincident with the p-ev1/p-ev2 boundary and therefore synchronous across the Adriatic region (pp. 335, their Fig. 9; Fig. SI5.2.1).

Pitfalls. (I) The alluvial-fan deposits and the black layers of the Cusercoli section have never been demonstrated to owe their development to orbitally-driven climate changes by means of a thorough cyclostratigraphic analysis considering time series analysis of climate proxy record. Furthermore, the development of fluvio-deltaic systems exclusively in basins adjacent to active tectonic structures, namely the Piedmont (Ghibaudo et al., 1985), Cella-Giaggiolo (Roveri et al., 1998) and Pietrarubbia (De Feyter and Molenaar, 1984; Molenaar and De Feyter, 1985) basins, strongly suggests that tectonics played an important, if not dominant, role in their genesis. In this sense, Ghibaudo et al. (1985) proposed that the progradation of the fan delta could testify the creation of new relief by tectonic uplift followed by subaerial (fluvial) erosion of the source areas, whereas the interbedded marls express phases of tectonic quiescence during which the source areas retreated landward and the mud-depositing water body filling the basin depocenter expanded. The angular discordance recognized by Roveri et al. (1998) at the base of the lowermost conglomerate body on the southwestern flank of the Cella-Giaggiolo syncline corroborates the notion that the tectonic played a major role in the genesis of these fluvio-deltaic conglomerates, therefore casting doubts on their employment for cyclostratigraphic correlations. (II) The physical-stratigraphic correlation between individual conglomerates and sandstone layers across the Apennines seems rather arbitrary because the correlated coarser beds are picked among many other clastics and lack readily distinguishable physical

characteristics that justify their elevation to "marker beds" and, therefore, their tracing over large horizontal distances.

S5.2.2 Dating of the reference section of Maccarone by Bache et al. (2012)

Model's description. Bache et al (2012) proposed a cyclostratigraphy of the Maccarone section based on the pollen record studied by Bertini (1992, 2006). They calculated the pollen ratio Subtropical Elements/Altitudinal Elements (SE/AE; i.e. amount of pollen grains of low-altitude thermophilous forests (i.e. SE) relative to those of coniferous forests growing in significantly cooler conditions at higher altitude) and determined the phase relations highs and lows in the SE/AE and individual astronomical parameters using the observation of Li et al. (1998) that in the Pliocene and Early Pleistocene cooling phases occurred during times of high eccentricity and vice versa for the warmer phases. Using these phase relations and an absolute age of 5.55±0.06 Ma for the ash layer, they tuned three minima in the SE/AE ratio, which are indicative of warmer climate, to the three eccentricity minima at 5.592, 5.486 and 5.378 Ma and three maxima in the SE/AE ratio, which are indicative of cooler climate, to the three eccentricity maxima at 5.533, 5.428 and 5.336 Ma (Fig. SI5.2.2). This chronological calibration of the section would also be consistent with the first occurrence (FO) of the age-diagnostic nannofossil *Ceratolithus acutus* (FO in the open ocean at 5.36 Ma; Agnini et al., 2017) ~30-35 m above the stratigraphic level tuned to the eccentricity minimum at 5.378 Ma (Popescu et al., 2007; Pellen et al., 2017; Fig. SI5.2.2).

Pitfalls. (I) The adopted radiometric age of the ash layer (5.55±0.06 Ma) is wrongly attributed to Cosentino et al. (2009), who clearly report another $^{40}Ar/^{39}Ar$ age (i.e. 5.49±0.06 Ma), and nowhere exists in the literature. If either this age, the older $^{40}Ar/^{39}Ar$ age of 5.51±0.04 Ma by Odin et al. (1997) (recalculated to 5.50±0.04 Ma by Cosentino et al., 2013) or the more recent and precise $^{206}U/^{238}Pb$ age of 5.532 Ma by Cosentino et al. (2013) are used, then the cyclostratigraphic correlation of the SE/AE as conceived by Bache et al. (2012) does not hold. The stratigraphic level that they correlate to the eccentricity maximum at 5.533 Ma would be older than the ash layer that occurs ~20 m below (Fig. SI5.2.2). (II) The claimed presence of the age-diagnostic *C. acutus* is not replicated neither by us nor by Roveri et al. (2008d). (III) Even if the model was correctly established, the ~8 times increase in sedimentation rate just before the M/P boundary in a basin that, according to the authors (as well as Popescu et al., 2007 and Pellen et al., 2017) was already full marine, is not justified nor finds expression in the sedimentary and (our) proxy record (Fig. 5.4).

S5.2.3 Dating of the reference section of Maccarone by Cosentino et al. (2013, supplementary material)

Model's description. In the supplementary material, Cosentino et al. (2013) draw correlation lines between insolation minima peaks and some intercalations to the Maccarone marls, namely the Fe-rich carbonates interbedded with the four black shales in the di Tetto Fm. and the four colombacci limestones in the Colombacci Fm. Possibly (because an explanation for the tuning is not provided) relying on the conclusion of Sampalmieri et al. (2010) that the Fe-rich carbonates deposited under arid and evaporative conditions, they tuned these carbonatic facies to successive insolation minima peaks, when evaporation exceeds precipitation. The Biofacies 1/2 change, which Grossi et al. (2008) identifies in proximity of the first colombaccio (Fig. SI5.2.1), is concluded to have occurred at ~5.40 Ma.

Pitfalls. (I) The interpretation of the colombacci limestones as representatives of arid conditions is possibly based on the earlier investigations of these limestones, who suggested that they are the product of calcite primary precipitation formed in the initial stages of evaporation-driven brine concentration in semi-isolated basins (shallow water ponds; Selli, 1954; Rabbi e Ricci Lucchi, 1968; Borsetti et al., 1975; Colalongo et al., 1978, 1979). However, more recent geochemical approaches to the study of the colombacci concluded that they precipitated during periods of highstands featured by low to negligible amount of terrigenous input and high meteoric water inflow (Molenaar and De Feyter, 1985; Bassetti et al., 2004). This latter interpretation implies that an opposite phase relationship with the astronomical forcing than the one used by Cosentino et al. (2013, tuning to the insolation minima) must be adopted (i.e. tuning to the insolation maxima; e.g. Roveri et al., 2008a). However, no explanation for this opposite view is provided by Cosentino et al. (2013). (II) The stratigraphic distribution of the carbonatic lithofacies do not evidence any regular sedimentary pattern that can be confidently linked to astronomical cycles (see Hilgen, 1991, Strasser et al., 2006 and van der Laan et al., 2006 for the definition of sedimentary patterns); furthermore, if the precessional signal would be clearly recorded in the sedimentary record, then we would expect it to display also in climate proxy records. A classic example is the Pliocene Trubi Fm. beautifully exposed along the southern coast of Sicily, which consists of metrescale quadruplets of grey marl–limestone to beige marl–limestone and in every alternate precessional quadruplet a consistent, cyclical variation in $CaCO_3$ content and $\delta^{18}O$ is observed (Hilgen, 1991). Other examples include the Paleogene rhythmic alternations of calcareous marl (low in $CaCO_3$ and high MS) and marly limestones (high in $CaCO_3$ and low MS) exposed in the Monte Cagnero section (Central Italy; Kochhann et al., 2021) and the shale-marl couplets of the Messinian PLG unit, with the marls enriched of Ti, Zr and Si and impoverished of K, Mg, TOC and *n*-alkanes and the shales impoverishment of Ti, Zr and Si and enrichment of K, Mg, TOC and *n*-alkanes (Natalicchio et al., 2019). Nevertheless, the Fe-rich carbonates and colombacci limestones do not seem to be expressed in the MS record and selected element ratios, therefore suggesting that an orbital signal is not present in the Maccarone sedimentary record. (III) The age model by Cosentino et

al. (2013) implies dramatic changes in sedimentation rates (from <0.01 m/kyr up to >3 m/kyr; Fig. SI5.2.2), which we find no evidence of in the field nor in the chemical composition of the mudstones, which is fairly constant, particularly during deposition of the di Tetto Fm. (Fig. 5.4).

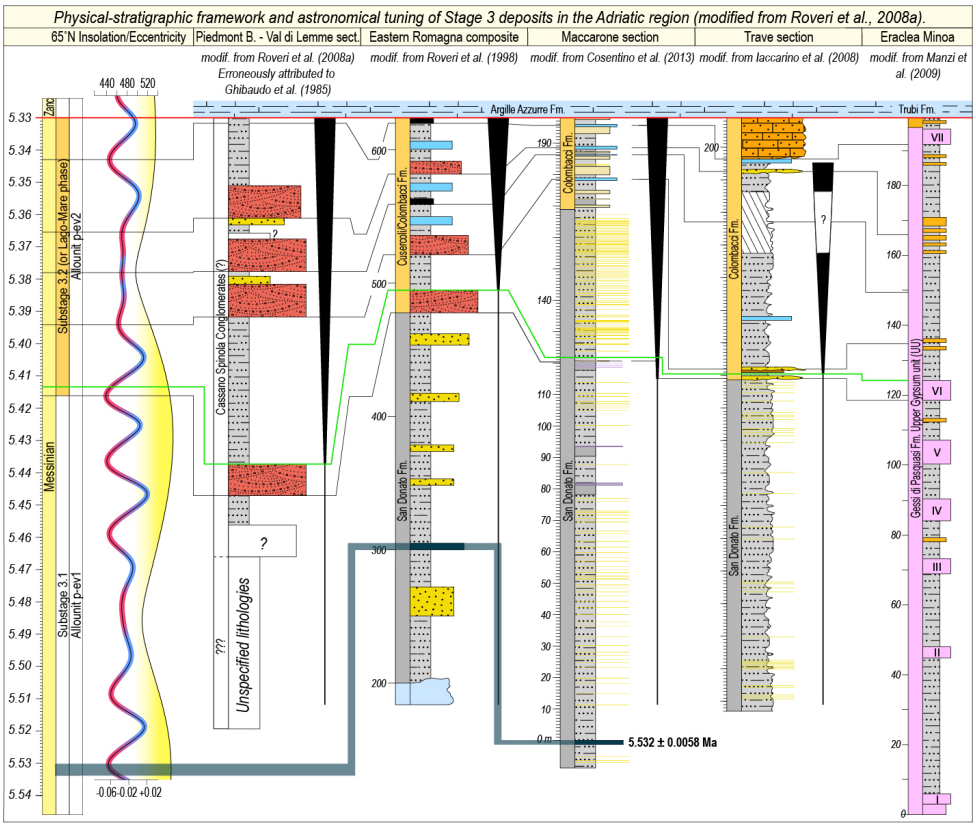

Fig. SI5.2.1 (this page). *Physical-stratigraphic correlation of uppermost Messinian successions across the Mediterranean basin (modified from Roveri et al, 2008a). The green line corresponds to the first occurrence of Paratethyan ostracods according to Roveri et al. (2008a). Legend of the Adriatic sections: see figs. 5.3 and 5.4. Legend of the Eraclea Minoa section: see Fig. 4.2 (chapter 4, p. 203).*

Fig. SI5.2.2 (next page). *Age-depth and age-sedimentation rate plots for the Maccarone section according to different chronostratigraphic models.*

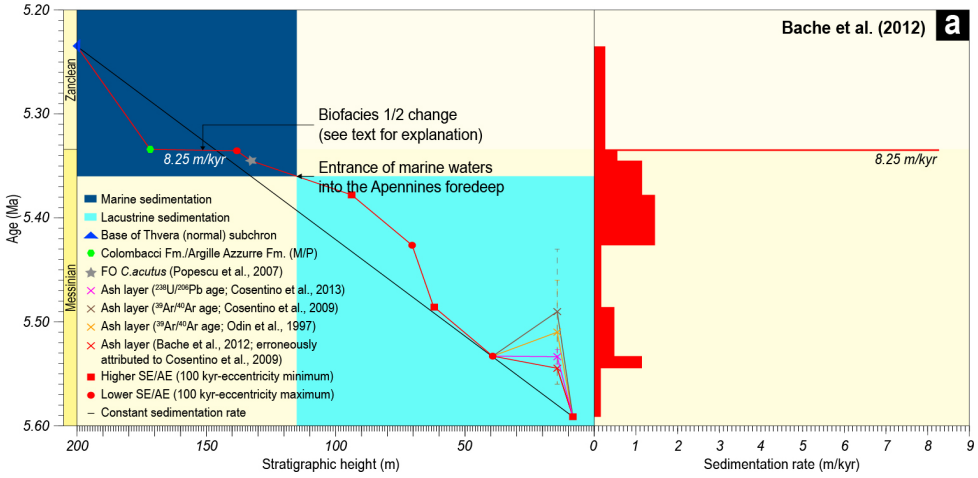
Bache et al. (2012)
a
Biofacies 1/2 change
(see text for explanation)
Entrance of marine waters
into the Apennines foredeep
8.25 m/kyr
8.25 m/kyr
Zanclean
Messinian
Age (Ma)
Marine sedimentation
Lacustrine sedimentation
Base of Thvera (normal) subchron
Colombacci Fm./Argille Azzurre Fm. (M/P)
FO C.acutus (Popescu et al., 2007)
Ash layer (238U/206Pb age; Cosentino et al., 2013)
Ash layer (39Ar/40Ar age; Cosentino et al., 2009)
Ash layer (39Ar/40Ar age; Odin et al., 1997)
Ash layer (Bache et al., 2012; erroneously attributed to Cosentino et al., 2009)
Higher SE/AE (100 kyr-eccentricity minimum)
Lower SE/AE (100 kyr-eccentricity maximum)
Constant sedimentation rate
Stratigraphic height (m)
Sedimentation rate (m/kyr)

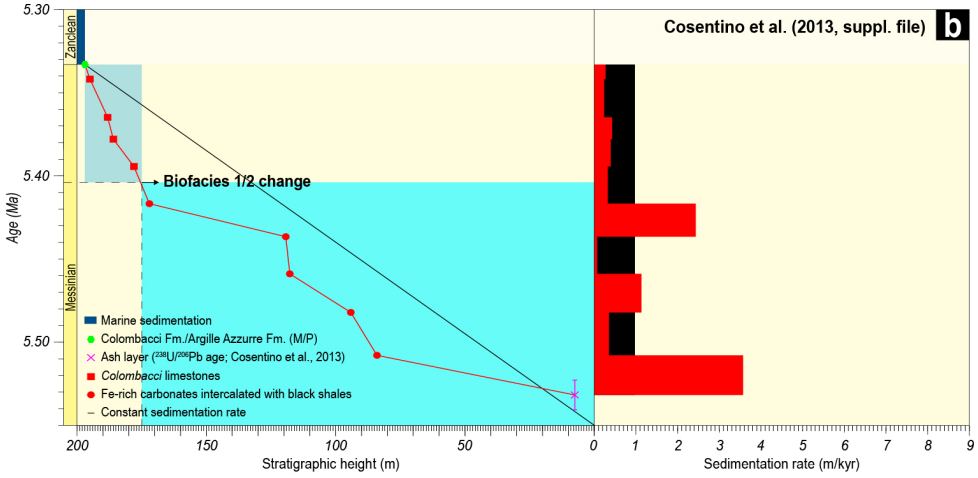
Cosentino et al. (2013, suppl. file)
b
Biofacies 1/2 change
Zanclean
Messinian
Age (Ma)
Marine sedimentation
Colombacci Fm./Argille Azzurre Fm. (M/P)
Ash layer (238U/206Pb age; Cosentino et al., 2013)
Colombacci limestones
Fe-rich carbonates intercalated with black shales
Constant sedimentation rate
Stratigraphic height (m)
Sedimentation rate (m/kyr)

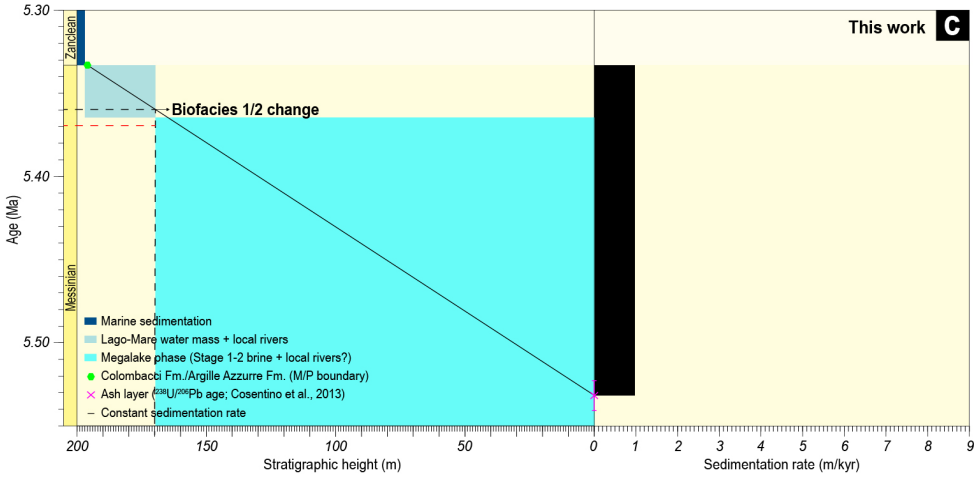
This work
c
Biofacies 1/2 change
Zanclean
Messinian
Age (Ma)
Marine sedimentation
Lago-Mare water mass + local rivers
Megalake phase (Stage 1-2 brine + local rivers?)
Colombacci Fm./Argille Azzurre Fm. (M/P boundary)
Ash layer (238U/206Pb age; Cosentino et al., 2013)
Constant sedimentation rate
Stratigraphic height (m)
Sedimentation rate (m/kyr)

A typical picturesque look of the countryside of Cyprus.

6

DIACHRONOUS PRECIPITATION OF LATE MESSINIAN GYPSUM TRACKING MEDITERRANEAN REGRESSIONS

Andreetto, F., Flecker, R., Krijgsman, W.

ABSTRACT

Both in the western and eastern Mediterranean, the 1.5-2 km-thick salt giant is sharply overlain by ostracod-rich marl-gypsum couplets. Onland, these alternations (Upper Gypsum, UG) are exposed in numerous localities in the Caltanissetta Basin (Sicily) and the Polemi Basin (Cyprus). Offshore, they are recovered in a number of wells (Upper Unit, UU). Previous strontium isotope data suggested that the intermediate and deep basins, which were positioned at >500 mbsl, were intraconnected during Mediterranean high-stands and gypsum precipitation and hosting endorheic lakes and marls during Mediterranean low-stands. In this work, we aim to demonstrate, by means of radiogenic strontium isotope analyses on pristine gypsum crystals, that gypsum beds across the Mediterranean precipitated from the same water mass. We selected samples from Hole 975B (Balearic Slope), Hole 654A (Tyrrhenian Basin) and the Polemi Basin (Cyprus). These sites, together with the recently investigated Eraclea Minoa section (Sicily, Caltanissetta Basin), make a W-E transect across the Mediterranean Basin and cover a wide range of bathymetric positions, from >2000 mbsl (Balearic Basin) to 800-1000 mbsl (Caltanissetta and Tyrrhenian basins) to 300-500 mbsl (Cyprus). We show that the gypsum beds of the UG and UU all precipitated from a single Atlantic seawater-fed water body dominated by low-salinity inputs from large peri-Mediterranean rivers and the Eastern Paratethys. The beginning of gypsum precipitation and the transition to isolated lakes are, however, slightly diachronous between the differently elevated basins. In this scenario, evaporite precipitation started and ended earlier in the shallow basins of Cyprus and migrated progressively into the deeper basins with increasing base level fall.

6.1 Introduction

During the final Stage 3 or Lago-Mare phase of the Messinian Salinity Crisis, which precedes the marine replenishment straddling the Miocene/Pliocene boundary, a large part of the Mediterranean Basin was covered by an hydrologically and chemically complex water mass (Vasiliev et al., 2017; García-Veigas et al., 2018). The water contribution to this Lago-Mare water body was mainly (>80%) low-salinity water from the Eastern Paratethys and the large peri-Mediterranean drainage systems (Rhône, Po, Nile and Esohabi which flowed from mega-lake Chad in the Late Miocene; Griffin 2002), with the Atlantic Ocean supplying the remaining <20% (Andreetto et al., 2022a). The restricted seawater input made the Mediterranean sensitive to the oscillations in the freshwater budget, which are controlled by precession (Marzocchi et al., 2015, 2019; Rohling et al., 2015; Simon et al., 2017). The variability in the freshwater budget and seawater flow caused high-magnitude oscillations of the Lago-Mare water level always below the Atlantic level, which was only reached at the base of the Zanclean stage (Ben Moshe et al., 2020; Andreetto et al., 2022a). These fluctuations induced connectivity changes between the Mediterranean subbasins (Andreetto et al., 2022a). The marginal (<500 mbsl), intermediate (500-1000 mbsl) and deep (>1000 mbsl) subbasins are thought to have been interconnected by the Lago-Mare water mass only during the highstands prompted by high Atlantic and freshwater discharges at insolation maxima. Ostracod-bearing marls are thought to have accumulated during these times of high water level along the margins (Stoica et al., 2016; Andreetto et al., 2021b, 2022b), whereas alternations of diatomites and barren marls possibly accumulated in deeper basins. The marginal basins were exposed during the regressions of the Lago-Mare water level triggered by the lessening of the freshwater budget and of the Atlantic inflow, undergoing erosion and/or non-deposition (e.g. Gulf of Lion; Lofi et al., 2005) or accumulation in prograding fluvio-deltaic settings (Fortuin and Krijgsman, 2003; Omodo Salé et al., 2012); the intermediate and deep subbasins remained interconnected in this phase, accumulating gypsum (Upper Gypsum and Bedded Units in the intermediate basins; Upper Unit in the deep basins; e.g. Lofi et al., 2005; Manzi et al., 2009, 2016; Thinon et al., 2016; Raad et al., 2021). Intermediate and deep basins disconnected at insolation minima in concomitance with the lowest freshwater discharge rates and deposited ostracod-bearing marls in endorheic lakes (Andreetto et al., 2022a).

Our hypothesis that the intermediate and deep subbasins formed a large interconnected system during gypsum precipitation is primarily based upon the Eraclea Minoa section in the Caltanissetta Basin, which is representative of an intermediate depth location (800-1000 mbsl), and needs to be substantiated by observations from more localities. Stage 3 gypsum-marl cycles are also exposed in Cyprus (Manzi et al., 2016a) and were recovered in 16 holes (122, 124, 125A, 132, 134, 371, 372, 374, 375, 376, 378A, 652, 653A, 654A, 975B, 975C; see Fig. 1.2b and references therein) during the DSDP and ODP scientific ocean drilling programs (Ryan et al., 1973; Hsü et al., 1978b; Kastens et al., 1987; Comas et al., 1996; Emeis et al., 1996). Here,

we selected one onland section (Polemi composite) in the Cypriot Polemi Basin and two OPD wells 975B and 654A drilled on the South Balearic and upper Sardinia margins, respectively. These sites were chosen for numerous reasons: (1) together with the Eraclea Minoa section in the Sicilian Caltanissetta Basin, they make a W-E transect across the entire Mediterranean Basin (Fig. 6.1a); (2) they are representative of both intermediate (Polemi and Site 654A) and deep water conditions (Site 975B; Roveri et al., 2014a, b); (3) Cyprus is the only other Mediterranean locality, besides the Caltanissetta Basin, where the gypsum-marl alternations of the Upper Gypsum are exposed onland (Fig. 6.1b); the Polemi Basin, in particular, preserves the most complete UG sedimentary sequence; (4) Site 654A represents the only offshore drilling site where a sedimentary succession spanning from the Upper Tortonian to the Pleistocene, including the entire Upper Unit, has been fully cored (Borsetti et al., 1990; Roveri et al., 2014b; Fig. 6.1c); (5) at Site 975B, only the top gypsum-marl couplet, out of seven or more that appear to be present on the seismic profiles, was recovered (Comas et al., 1996; Fig. 6.1d). Despite the low recovery of the UU, this hole is important because the coring and recovery were continuous through the Miocene/Pliocene (M/P) boundary, the sharp nature of the boundary hints at the absence of erosion and the Acme Base of Sphaeroidinellopsis (Zone MPl1), which marks the base of the Zanclean Stage (Lirer et al., 2019), was detected (Iaccarino et al., 1999). This means that the recovered gypsum-marl couplet is highly likely to represent the very end of Stage 3.

Our approach to test the hypothesis that Stage 3 gypsums across the Mediterranean precipitated synchronously and from the same water mass is to use radiogenic Sr isotope ratios. Today's seawater's $^{87}Sr/^{86}Sr$ composition is horizontally and vertically homogenous at any given time (Kuznetsov et al., 2012), even in basins, like the Black Sea, dominated by excess continent-derived freshwater (Bista et al., 2021). Relying on this observation, if our hypothesis is correct, then we expect that physically-distant, time-equivalent gypsums yield $^{87}Sr/^{86}Sr$ ratios within analytical error of each other if they are part of the same water mass. If the $^{87}Sr/^{86}Sr$ ratios measured are the same age, but dissimilar, then the synchronous nature of the precipitation of gypsum must be called into question and we have to seek for alternative explanations, such as gypsum precipitation in endorheic lakes subject to an independent hydrological balance (Ryan, 2009) or at different times between some of the basins.

6.2 Geological setting

6.2.1 Stratigraphic overview of the studied locations

Cyprus lies in a complex tectonic zone in the Eastern Mediterranean, where the African, Arabia and Eurasian plates collide. In the early Miocene, N-S compressional tectonics gave rise to a series of sub-basins (Polemi, Pissouri and Maroni/Psematismenos) in the south of the island (Fig. 6.1b). Of these three basins, the Polemi Basin has the best preserved UG in terms of outcropping conditions and stratigraphic resolution (Orszag-Sperber et al., 1980; Rouchy et al., 2001; Manzi et al., 2016a).

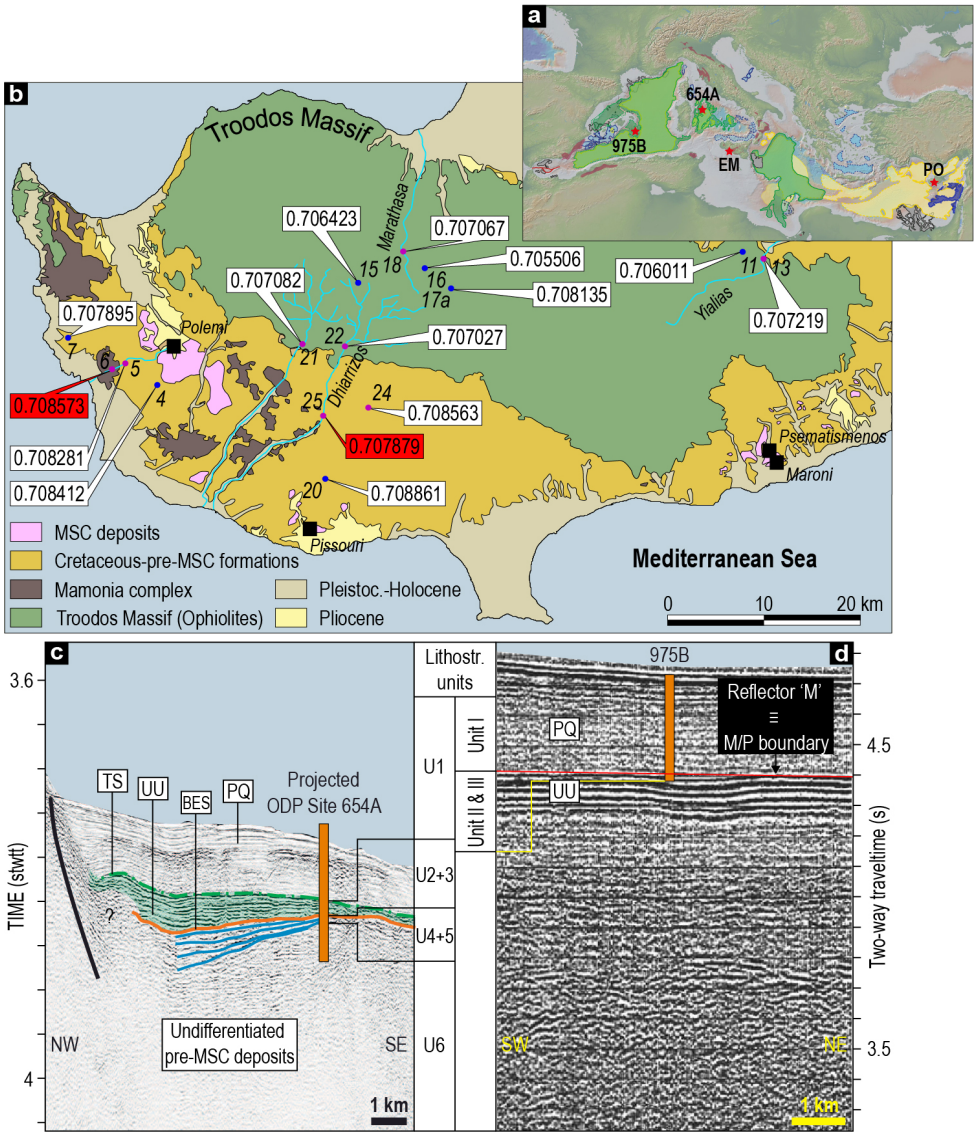

Fig. 6.1. **(a)** *Map of the Mediterranean Basin (modified from Lofi, 2018) showing the location of the Stage 3 sequences studied in this work (i.e. ODPs 975B and 654A and Polemi composite section (PO)). The locations of the Eraclea Minoa section (EM) used in Andreetto et al. (2022a) and here addressed is also shown.* **(b)** *Simplified geological map of Cyprus (Source: Geological Survey Department, Scale 1:250.000, digital version, modified) showing the $^{87}Sr/^{86}Sr$ ratios of surficial (violet circles) and underground (blue circles) water (from Ladegaard-Pedersen et al., 2020) employed to constrain the $^{87}Sr/^{86}Sr$ signature of a hypothetical Cyprus lake (paragraph 6.5.2).* **(c)** *MYS12 seismic line across the study area from ODP Site 654A (modified from Lymer et al., 2018).* **(d)** *Seismic profile across the study area from ODP Site 975B (modified from Comas et al., 1996).*

Hole 975B (38°53.786'N, 4°30.596'E; Fig. 6.1a) was drilled at 2415 m water depth at the edge of a small basin perched on the South Balearic Margin, which is the continental slope between the Balearic Promontory to the north and the South Balearic-Algerian Basin to the south (Comas et al., 1996; Fig. 1.2). The cored stratigraphic sequence in Hole 975B is 317.1 m and ranges from the Pleistocene to the uppermost Miocene (Fig. 6.1d). ODP hole 975B penetrates this unit at the bottom of the core (Unit III; 307.0-317.1 mbsf; Fig. 6.2).

ODP Site 654A is located on a normal fault-bounded, basinward-tilted block of continental crust of the upper Sardinia margin at a water depth of 2218 mbsl (Fig. 6.1a). The sedimentary succession of Site 654A, 478.3 m thick, is typically divided into six sedimentary units (Borsetti et al., 1990; Fig. 6.1c). Unit 1 (242.7 m thick) is a nannofossil ooze of Pleistocene and Pliocene age (post-MSC). Unit 2 (69.9 m thick) mainly consists of alternating gypsum and marl beds. According to well-to-seismic ties, it corresponds to the Upper Unit (Roveri et al., 2014b; Loreto et al., 2020). Unit 3 (36.3 m thick) is a dark, laminated, organic-rich, barren pelite, also thought to be part of the UU. Unit 4 (55 m thick) consists of another marine biota-rich ooze dated as lowermost Messinian-uppermost Tortonian (Borsetti et al., 1990). A bioturbated glauconitic sandstone (Unit 5; 11.8 m thick) and a conglomerate layer with basement clasts (see Sartori et al., 1990) and red beds (Unit 6; minimum 62.6 m thick) of undetermined ages (possibly upper Tortonian) comprise the oldest units recovered. Roveri et al. (2014b) correlated these six lithostratigraphic units with the chronostratigraphic consensus model of the MSC (Roveri et al., 2014a) based on the assumption that MSC Stages can be distinguished from one another based on $^{87}Sr/^{86}Sr$ values (Stage 2 is thought to have higher values than Stage 3). This correlation results in Unit 2 spanning both Stage 2 (Cores 35R and 36R) and 3 (Cores X-34R). The boundary between MSC stages 2 and 3 is placed at the top of Core 35R, below which $^{87}Sr/^{86}Sr$ ratios measured on two layers of clastic gypsum are slightly higher (0.708843-0.708866; Müller et al., 1990) than in cumulate and clastic gypsum layers from Cores 27R-34R (0.708605-0.708829; Müller et al., 1990). However, studies elsewhere on Stage 3 successions demonstrate that $^{87}Sr/^{86}Sr$ ratios cannot always be used as a chronostratigraphic tool in settings dominated by non-marine inputs (Schildgen et al., 2014; Andreetto et al., 2021a).

6.2.2 Late Messinian paleobathymetries

When the Messinian Salinity Crisis took place, the Mediterranean Basin was already segmented into a mosaic of subbasins of various depths and sizes, often separated from each other by sills (Hsü et al., 1973a, b; Rouchy and Caruso, 2006; Roveri et al., 2014a; Vai, 2016). However, the paleobathymetry of each of these subbasins during the MSC remains unconstrained or extremely uncertain. This uncertainty hampers understanding of the MSC. The most recent schematic classification of the Messinian Mediterranean sub-basins (Roveri et al., 2014a) differentiates between shallow (0–200 m water depth), intermediate (i.e. relatively deep-water, 200–1000 m) and deep basins (water depth >1000 m). In this classification, water

depth ranges refer to the vertical position relative to the oceanic sea level and indicate the maximum water depth attained when two-way Atlantic-Mediterranean exchange ensured a full Mediterranean.

The analyses of the foraminifera assemblages (see Van der Zwaan et al., 1999; Kouwenhoven et al., 2003; Van Hinsbergen et al., 2005 for insights on this method) along with the application of regression functions or other equations (e.g. Hohenegger, 2005; Hohenegger et al., 2008; Avnaim-Katav et al., 2016; Milker et al., 2017) is often used to reconstruct paleowater depths. Although the accuracy of this method is controversial (see Kouwenhoven et al., 2006 and Gennari et al., 2008 for insights), this is currently the best approach for reconstructing late Messinian Mediterranean bathymetries. Foraminifera-based paleobathymetric reconstructions cannot be performed for the MSC due to scarcity of the fauna in the sediments. Consequently, reconstructions of Stage 3 commonly assume that the basins' paleobathymetries were not dissimilar from those estimated for the lower Zanclean sediments, where foraminifera are abundant (e.g. Rouchy and Caruso, 2006; Andreetto et al., 2021a). In the absence of data from the Pliocene sediments, pre-MSC successions are sometimes used in the same way. These constraints are probably good enough to ensure that each basin is correctly attributed to the shallow, intermediate and deep categories.

Analyses of the pre-Messinian foraminiferal assemblage in DSDP Site 372 in the Balearic Basin and also on the Menorca Rise in Site 975B (Fig. 1.2) indicate a water depth in excess of 1200 meters during the late Burdigalian and an overall increase through time (Hsü et al., 1978). The "deep" status of the Balearic Basin during the Messinian is also supported by flexural-paleobathymetric reconstructions using 2D (planform, pseudo-3D) flexural backstripping technique on an extensive set of seismic data (Heida et al., 2022).

During the late Tortonian and early Messinian, the depth of the Caltanissetta Basin is estimated to have been around 800-1000 m or more (Kouwenhoven et al., 2003). This estimate derives from the analyses of the benthic foraminifera of the Tripoli Formation in its type-section of Monte Gibliscemi (see Kouwenhoven et al., 2003 for details). A range of different estimates have been proposed for the early Zanclean based on benthic foraminifera and/or psychrospheric ostracods at Capo Rossello and Eraclea Minoa: 200-500 m (Decima and Wezel, 1973), 600-800 m (Sgarrella et al., 1997, 1999; Barra et al., 1998), 1400-2400 m (Cita and Colombo, 1979). The major phase of uplift that ultimately exposed the Sicilian MSC successions above sea level is thought to have occurred in Pliocene-Quaternary time (Butler et al., 1995). On this basis, and in the absence of further constraints, we assume that the Caltanissetta Basin has remained somewhat deep throughout the MSC, around 800-1000 m.

Estimates of the pre- and/or post-MSC paleodepth of the Polemi Basin are not available to our knowledge. Only the pre-MSC paleodepth of the neighbouring Pissouri Basin was evaluated and has been estimated to have been around 300-500 m (Kouwenhoven et al., 2006).

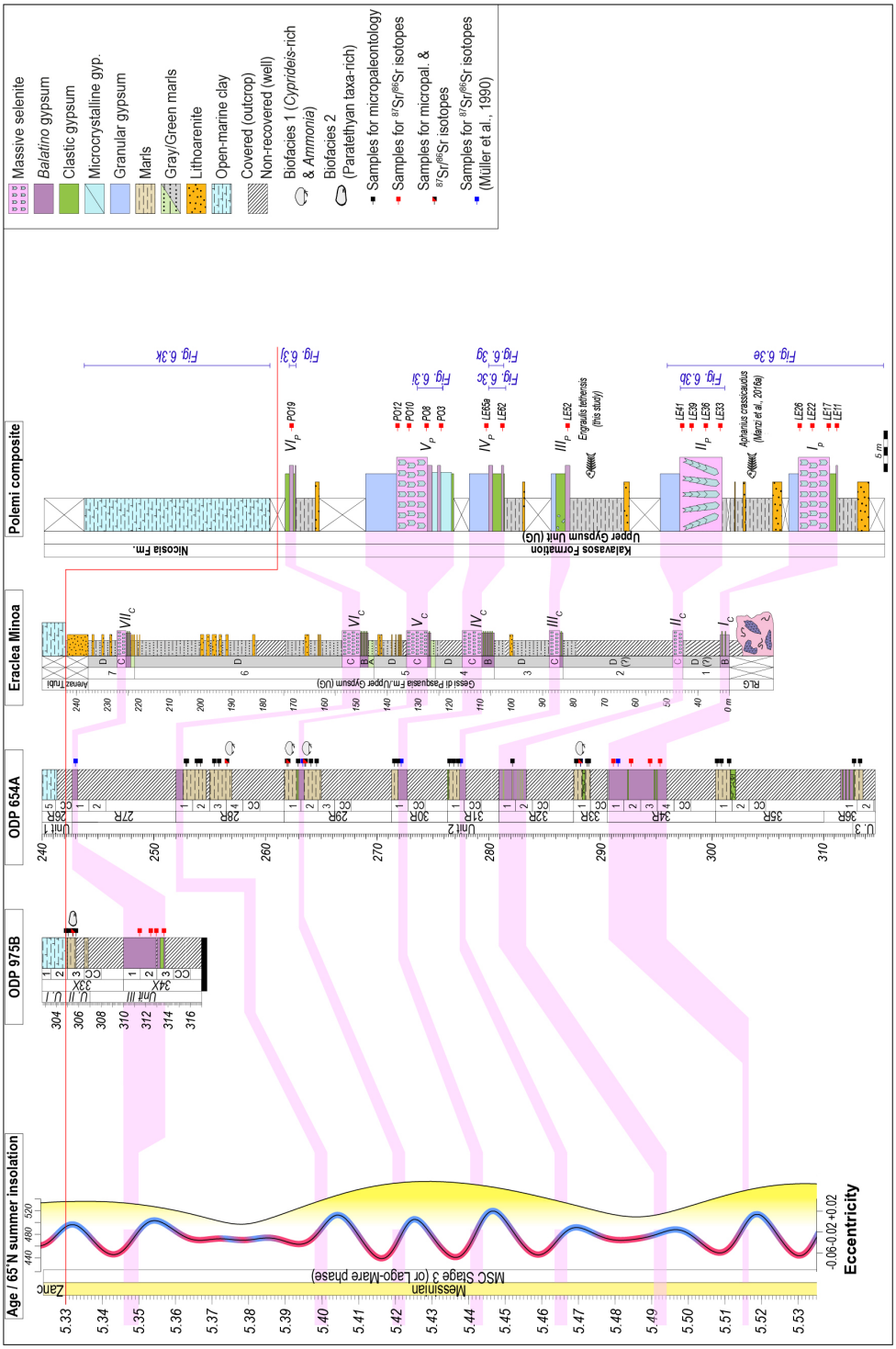
Massive selenite
Balatino gypsum
Clastic gypsum
Microcrystalline gyp.
Granular gypsum
Marls
Gray/Green marls
Lithoarenite
Open-marine clay
Covered (outcrop)
Non-recovered (well)
Biofacies 1 (Cyprideis-rich & Ammonia)
Biofacies 2 (Paratethyan taxa-rich)
Samples for micropaleontology
Samples for 87Sr/86Sr isotopes
Samples for micropal. & 87Sr/86Sr isotopes
Samples for 87Sr/86Sr isotopes (Müller et al., 1990)
Age / 65°N summer insolation
ODP 975B
ODP 654A
Eraclea Minoa
Polemi composite
Eccentricity
-0.06 -0.02 +0.02
MSC Stage 3 (or Lago-Mare phase)
Messinian
Zanc
Nicosia Fm.
Kalavasos Formation
Upper Gypsum Unit (UG)
Fig. 6.3k
Fig. 6.3j
Fig. 6.3i
Fig. 6.3h
Fig. 6.3g
Fig. 6.3f
Fig. 6.3e
Engraulis tetherosa (this study)
Atherinus craxicaudus (Marco et al., 2016a)
5 m

Fig. 6.2 (previous page). *Tentative correlation scheme between ODPs 975B and 654A and the two most complete exposures of the Upper Gypsum unit in Eraclea Minoa and Polemi. The astronomical correlation with the 65°N summer insolation and 100 kyr eccentricity curves of Laskar et al. (2004) is based upon Andreetto et al. (2022a).*

Fig. 6.3 (next page). *Collection of panoramic and close-up pictures from the main subsections investigated in the Polemi Basin. Sel: Massive selenites; Bal: Laminar (or balatino) gypsum; Micr: Massive, microcrystalline gypsum; Gya: Gypsarenite; Gr. gyp: Granular gypsum.* **(a)** *Panoramic view of the area corresponding to the Panagias section (i.e. the hillside behind the church Eksoklisi Panagias; 34°51'41"N, 32°30'28"E) and Lethymbou section (i.e. the hillside behind the village of Lethymbou; 34°51'43"N, 32°30'34"E).* **(b, c, d)** *Close view of gypsum beds* II_p *(34°51'41"N, 32°30'28"E),* IV_p *(34°51'45.4"N, 32°30'26.6"E) and* V_p *(34°51'44.9"N, 32°30'28.9"E) in the Panagias section.* **(e)** *Base of the Lethymbou section, where the lowermost two gypsum beds are nicely exposed (34°51'43"N, 32°30'34"E).* **(f, g)** *Close view of gypsum beds* III_p *(34°51'47.1"N, 32°30'30.5"E) and* IV_p *(34°51'36"N, 32°30'50"E) in the Lethymbou section.* **(h)** *Panoramic view of the Polemi 1 section.* **(i, j)** *Close view of gypsum beds* V_p *(34°52'17"N, 32°31'02"E) and* VI_p *(coordinates not available) in the Polemi 1 section.* **(k)** *The Polemi 2 section (34°52'29.8"N, 32°30'56.6"E), which might correspond to the early Zanclean.*

6.3 Material and methods

Field work to reconstruct the stratigraphy and sample the Polemi UG succession was undertaken in November 2021. A continuous exposure of the UG is not available in Polemi (see also Rouchy, 1982; Pierre, 1974; Orszag-Sperber et al., 1980; Manzi et al., 2016a). Five partial sections (Fig. 6.2) were therefore measured, logged and physically correlated using the gypsum beds as stratigraphic markers. These beds stand out in the landscape and have distinct petrological characteristics and thicknesses (see Fig. 6.3 and lithofacies description in section 6.4.1). The resulting composite section is illustrated in Figure 6.2. Sedimentary logs of ODP sites 654A and 975B (Fig. 6.2) were re-drawn after the post-cruise technical reports downloadable from the website https://www.marum.de/en/Research/Cores-at-BCR.html and samples were requested from the University of Bremen (see Fig. 6.2 for the stratigraphic position of the samples). The illustration and description of the gypsum lithofacies in these holes is based on the study of Lugli et al. (2015). Twenty-four gypsum samples (16 from Polemi, 4 from Hole 975B and 4 from Hole 654A) were selected for strontium isotopic analyses. Sample preparation followed the methodology described in Andreetto et al. (2022a; chapter 4 of this work). The isotopic measurements were performed with a Thermo Scientific™ Triton™ thermal ionization mass spectrometer at the University of Bristol. A total of 15 replicate analyses of the NBS 987 standard yielded a $^{87}Sr/^{86}Sr$ ratio of 0.710629 ± 0.000006 (2σ), which is in agreement with the accepted values of SRM 987 of 0.710250 (Thirlwall, 1991).

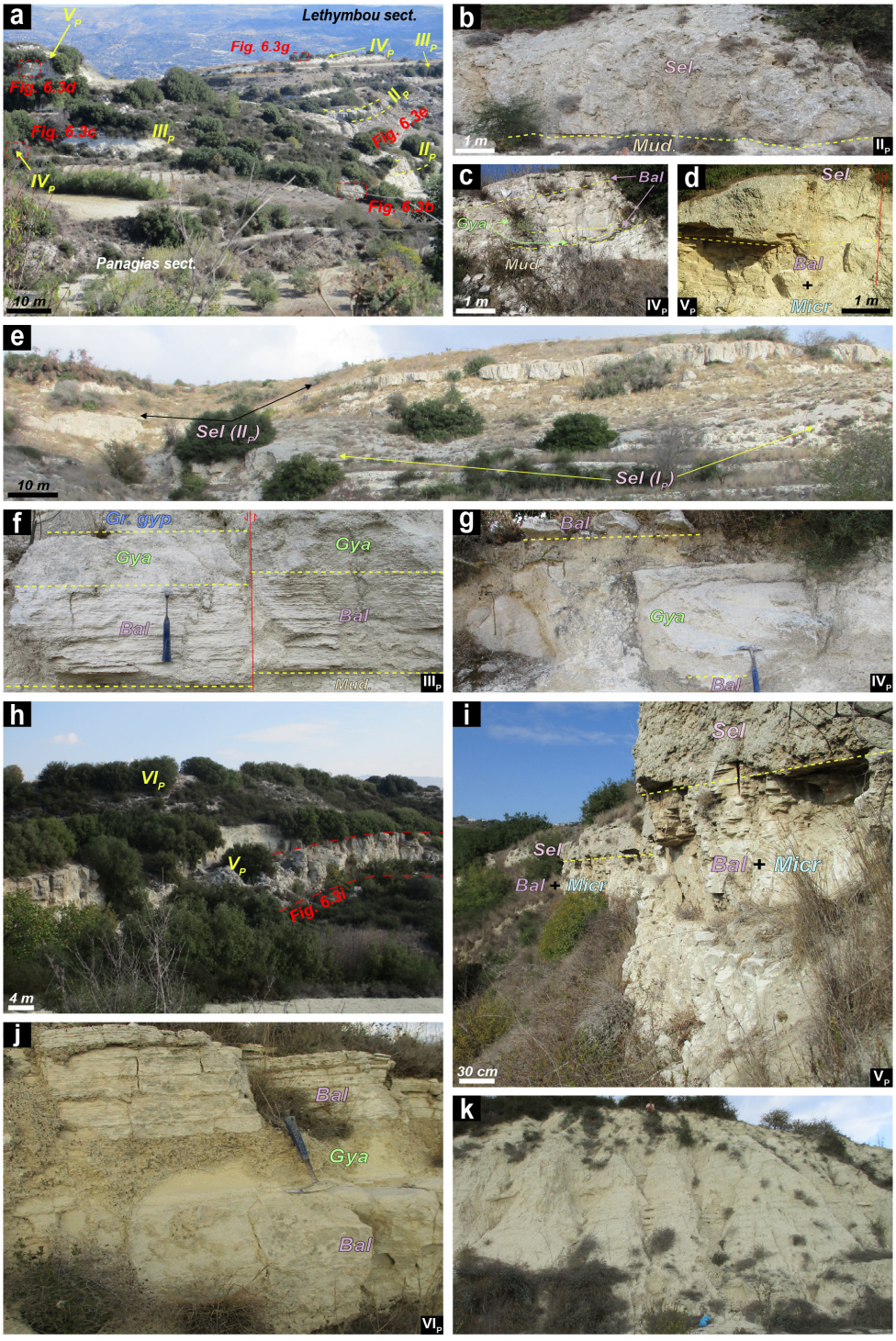
a
Lethymbou sect.
Fig. 6.3g
Fig. 6.3d
Fig. 6.3c
Fig. 6.3e
Fig. 6.3b
Panagias sect.
10 m
b
Sel
1 m
Mud.
c
Bal
Gya
Mud.
1 m
d
Sel
Bal
+
Micr
1 m
e
Sel (II$_P$)
Sel (I$_P$)
10 m
f
Gr. gyp.
Gya
Gya
Bal
Bal
Mud.
g
Bal
Gya
Bal
h
VI$_P$
V$_P$
Fig. 6.3i
4 m
i
Sel
Sel
Bal + Micr
Bal + Micr
30 cm
j
Bal
Gya
Bal
k

Thirty-four marls from holes 975B (n=5) and 654A (n=29) were prepared for micropaleontological analysis using the standard method of drying and soaking in tap water and washing through a 125-μm mesh sieve to recover carbonate microfossils that could be used for strontium isotope analysis. Only five of these samples contained ostracods (Tables 6.1, 6.2 and Fig. 6.2). Strontium isotopes ratios were measured on these samples (Table 6.3) in the same analytical session in which the ostracods of the Piedmont Basin (Andreetto et al., 2022b or chapter 3) and of Eraclea Minoa (Andreetto et al., 2022a or chapter 4) were also measured (see these chapter for details on the sample preparation and measurement).

6.4 Section/core description, paleontological content and stratigraphic correlation

6.4.1 Polemi composite section

The Upper Gypsum Unit of the Polemi Basin consists, in broad terms, of six, m-thick gypsum beds intercalated with white chalks or marly limestones, forming gypsum/marl couplets which are assumed to correspond to precessional cycles (Manzi et al., 2016). The overall thickness of the Polemi UG is estimated by means of field and Google Earth measurements not to exceed the 60-70 m, in agreement with previous estimations of 50-60 m by Rouchy (1982), Orszag-Sperber et al. (1980) and Manzi et al. (2016a). Five gypsum lithofacies were distinguished.

1. **Massive selenite**. This facies consists of twinned gypsum crystals (arrow-head or swallow-tail crystals or selenites) tightly packed together and vertically oriented with the re-entrant angle of the twins upward (Fig. 6.4a). Crystals size range from several centimeters to few decimeters in gypsum bed IP and VP to several decimeters in gypsum IIP. The massive selenite facies is thought to represent a bottom-grown precipitate from a brine with a relatively low degree of supersaturation, which allows the crystals to grow larger (Babel et al., 2007; Lugli et al., 2010; Ortí et al., 2014b; Warren, 2016; Natalicchio et al., 2021).

2. **Laminar (or balatino) gypsum**. This comprises finely-laminated beds of alternating white/crystalline and brownish laminae (typically mm- or sub-mm thick, more rarely cm-thick; Fig. 6.4b). The lighter laminae are mainly composed of gypsum, which is likely to be primary in the crystalline laminae and secondary in the white ones. The brownish laminae are composed of

Fig. 6.4 (next pages). *Close-up pictures of the main lithofacies and macrofossils recognized in the Polemi composite section.* **(a)** *Massive selenite (gypsum bed II_p, Lethymbou section).* **(b)** *Balatino gypsum (gypsum bed III_p, Lethymbou section).* **(c)** *Pristine mollusks embedded in the balatino gypsum of bed VI_p (Polemi 1 section).* **(d)** *Massive, microcrystalline gypsum (gypsum bed V_p, Polemi 1 section).* **(e)** *Sharp contact between a gypsarenite bed and a balatino gypsum (gypsum bed I_p, Lethymbou section).* **(f)** *Sharp contact between the massive selenite and the granular gypsum facies (gypsum bed I_p, Lethymbou section).* **(g, h)** *Close up of the granular facies.* **(i)** *Mudstones.* **(j)** *Specimen of the fish skeleton of Engraulis tethensis recovered in the marl interval below the gypsum bed III_p (Lethymbou section).*

Table 6.1. *Samples of Hole 975B investigated for ostracod (O) and/or $^{87}Sr/^{86}Sr$ (Sr) analyses.*

Core	Section	Interval (cm)	Depth (mbsl)	Lab code	Analysis
33X	2	135-137	305.25	58	O
33X	3	0-4	305.40	59	O
33X	3	41-44	305.81	1	O
33X	3	49-51	305.89	60	O+Sr
33X	3	77-79	306.17	2	O
34X	1	87-89	306.27	3	O+Sr
34X	1	142-145	311.45	975-2	Sr
34X	2	90-93	312.40	975-3	Sr
34X	2	144-147	312.90	975-4	Sr
34X	3	71-74	313.60	975-5	Sr

Table 6.2. *Samples of Hole 654A investigated for ostracod (O) and/or $^{87}Sr/^{86}Sr$ (Sr) analyses.*

Core	Section	Interval (cm)	Depth (mbsl)	Lab code	Analysis
28R	1	85-87	252.85	33	O
28R	1	94-98	252.94	34	O
28R	2	38-40	253.88	35	O
28R	2	65-67	254.2	36	O
28R	3	41-43	255.41	37	O
28R	3	85-87	255.85	38	O
28R	4	12-14	256.62	39	O+Sr
29R	1	20-22	261.90	29	O
29R	1	30-32	262	30	O+Sr
29R	1	122-126	262.92	40	O
29R	2	32-34	263.52	31	O+Sr
29R	2	40-42	263.60	32	O+Sr
29R	2	86-90	264.06	41	O
29R	2	137-139	264.57	42	O
30R	1	25-27	271.55	43	O
30R	1	53-55	271.83	44	O
31R	1	16-20	276.5	45	O
31R	1	56-60	276.85	46	O
31R	1	98-100	277.25	47	O
32R	1	118-120	282.1	48	O
33R	1	23-25	287.85	49	O
33R	1	60-62	288.22	50	O+Sr
33R	1	121-123	288.83	51	O
33R	1	135-137	288.97	52	O
34R	1	56-58	291.18	654-6	Sr
34R	2	63-65	293.78	654-7	Sr
34R	3	82-84	294.42	654-8	Sr
34R	4	26-27	295.38	654-9	Sr
35R	1	12-14	300.42	53	O
35R	1	56-60	300.86	54	O
35R	1	126-130	301.56	55	O
36R	1	134-136	312.84	56	O
36R	2	24-26	313.24	57	O

fine-grained terrigenous and/or carbonate material. This facies is typically considered to reflect pelagic accumulation on the basin floor of tiny gypsum crystals that crystallized at the air-water interface. The small size of the crystals indicates a higher degree of supersaturation of the brine compared to the massive selenite facies, favoring the formation of a lot of new nuclei, which inhibits them from growing larger (see Babel et al., 2007; Lugli et al., 2010; Ortí et al., 2014b; Warren et al., 2016; Natalicchio et al., 2021). The occurrence of thin laminae of clayey material is typically suggested to indicate unstable conditions, dominated by continuous fluctuations of the gypsum saturation surface (i.e. the pycnocline, Bąbel, 2007) that repeatedly stopped the growth of gypsum crystals (Dela Pierre et al., 2011). In the laminar gypsum of bed VI_p abundant, well preserved mollusks, possibly belonging to the genus *Limnocardiinae* spp. and *Dreissena* (Manzi et al., 2016a), have been documented (Fig. 6.4c).

3. **Massive, microcrystalline gypsum**. This facies consists of a homogeneous, massive paste of clay- to silt-sized gypsum crystals (Fig. 6.4d). The small size of the crystals suggests that the massive, microcrystalline facies is also a pelagic deposit. The absence of thin clay laminae. suggests that the brine was stable and permanently supersaturated with respect to gypsum.

4. **Clastic gypsum**. This facies consists of sand-sized gypsum crystals (Fig. 6.4e) with minor carbonate and mud. Parallel and cross laminations are sometimes visible. These beds of clastic gypsum usually alternate with the laminated gypsum beds. This facies results from the erosion of pre-existing gypsum beds and downslope transport and re-sedimentation of the clasts by gravity fluxes.

5. **Granular gypsum**. The beds representing this facies are generally several meters thick and are always found at the top of the gypsum layers, forming a transitional interval to marls (Fig. 6.4f). They are made of angular gypsum crystals the size of a coarse sand (0.5-2 mm) or granules (2-4 mm; Fig. 6.4g). The crystals are organized to form normally graded beds. Different beds typically form bands of different colors (Fig. 6.4h). This banded granular gypsum facies probably corresponds to the banded selenite facies of Manzi et al. (2016a). However, the banded selenite facies, as originally described by Lugli et al. (2010) in the Northern Apennines and later by other authors (e.g. Natalicchio et al., 2021 in the Piedmont Basin), consists of gypsum beds formed by small, vertically-oriented selenites separated by thin carbonate laminae, which is not what it is observed here. Due to the presence of angular crystals, this facies could be incorporated in the clastic gypsum facies. The reason behind our decision to make it a separate lithofacies is because, in the present case, the clastic appearance seems to be unrelated to processes of erosion, transport and resedimentation responsible for the

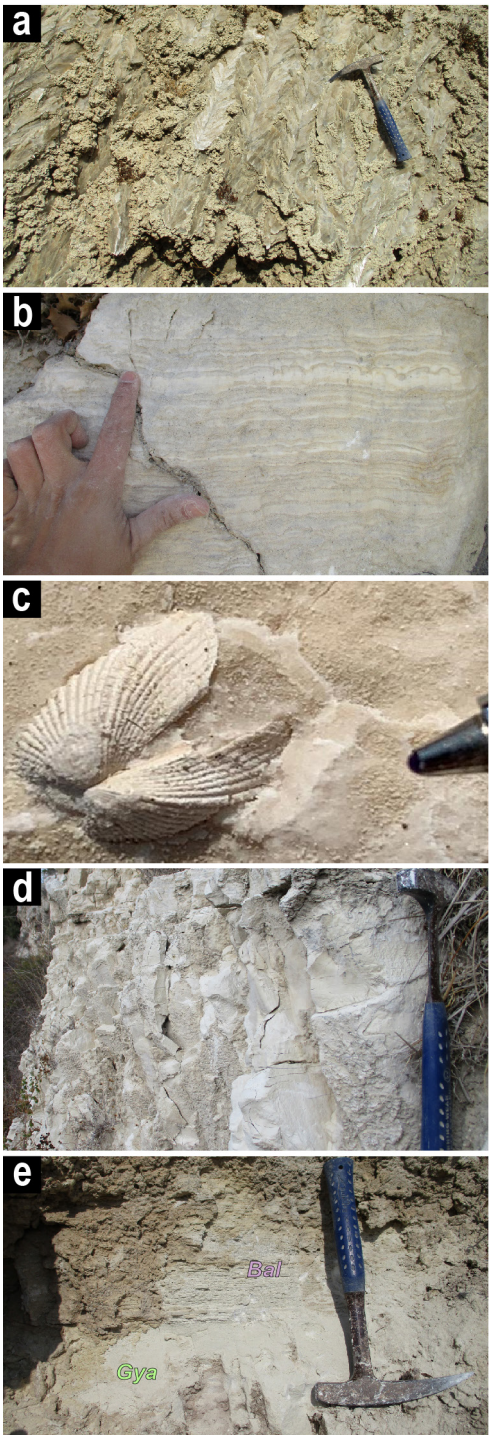

emplacement of gypsarenites/gypsrudites. The granular lithofacies has some resemblance with the rounded halite grains (halolites) found along the shoreline of the Dead Sea and that form when the lake level declines (Sirota et al., 2020). Based on this analogy with present-day settings, we hypothesize that this lithofacies is the product of in-situ gypsum precipitation from a very shallow supersaturated, residual brine before its disappearance and replacement with an undersaturated water mass from which mud deposited from suspension. However, more detailed sedimentological and petrographic studies are required to fully understand and interpret this gypsum facies.

Only gypsum bed V_p comprises the full facies sequence from the gypsarenites to alternating laminar and massive, microcrystalline gypsum into the massive selenites and, finally, the granular gypsum. All other gypsum beds lack one or more of the lithofacies (see Fig. 6.2).

The evaporite-free intervals dividing the gypsum beds consist of beige, marly limestones intercalated with litharenites (Fig. 6.4i). A well preserved fish skeleton has been recognized in one marl sample from the interval between gypsum IIP and IIIP (Fig. 6.4j). This skeleton possibly belonging to *Engraulis tethensis*, has already been recognized in Upper Miocene sediments on Cyprus by Grande and Nelson (1985). The closest living relative of this taxon is considered to be *Engraulis encrasicolus* (Grande and Nelson, 1985), a coastal pelagic foraging fish related to the herring that usually lives in water <50 m deep (although it may go

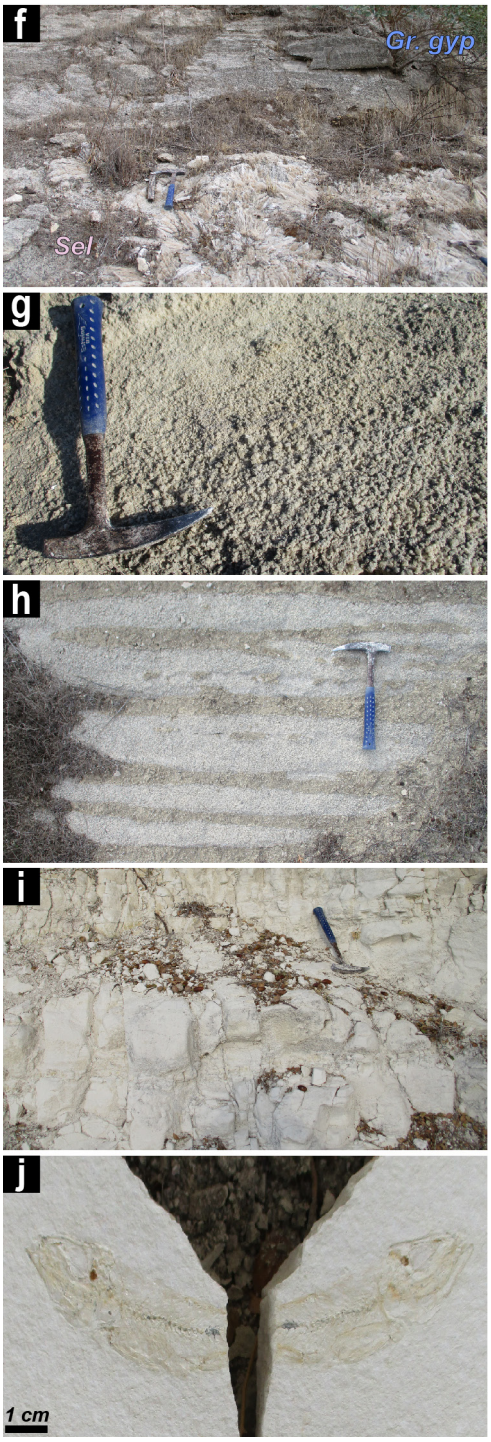

as deep as 400 m) and in a range of salinities (open marine to brackish coastal lagoons, estuaries and lakes). Another fish skeleton has been recognized by Manzi et al. (2016a) from the marl layer just below gypsum II. The taxonomy of this fish skeleton is uncertain. Manzi et al. (2016a; G. Carnevale, pers. comm.) identify it as the cyprinodontid *Aphanius crassicaudus*, which is an euryhaline taxon largely found in pre-MSC, MSC and post-MSC units (Carnevale et al., 2018; Carnevale and Schwarzhans, 2022). Carnevale and Schwarzhans (2022) suggest it is a species of the blennioid family Clinidae, which are exclusively marine benthic fish. Manzi et al. (2016a) also report the occurrence of a few Paratethyan (*Loxocorniculina djafarovi, Euxynocythere praebaquana*) and Mediterranean (*C. agrigentina*) ostracods in the grey clays located a few meters below the M/P boundary. However, a thorough investigation of the late Messinian marls of the Polemi Basin for their paleontological content is still lacking.

6.4.2 ODP Site 975B

The gypsum bed recovered in Hole 975B largely consists of the laminated gypsum facies (Lugli et al., 2015). A 30 cm-thick gypsarenite is recognized intercalated with the laminated gypsum in Core 34X, Sections 2 and 3 (Lugli et al., 2015). The marl interval in Core 33X consists of laminated micrites and micritic silty clays (Iaccarino and Bossio, 1999). These sediments commonly yield planktonic foraminiferal assemblages and rare benthic foraminifera and ostracods (Iaccarino and Bossio, 1999). Most of the foraminiferal tests are broken and show traces of dissolution and recrystallization. This has been interpreted as indicators of reworking from older, early Messinian and pre-Messinian sediments (Iaccarino and Bossio, 1999). The ostracods are typical brackish water, Paratethyan taxa and include *Loxochonca djaffarovi, Candona* sp., *Cyprideis* sp., In one sample (33X-3, 49-51 cm) from roughly the same stratigraphic interval (33X-3, 50-85 cm) studied by Iaccarino and Bossio (1999) we also recognized well-preserved specimens of *Cyhterura pirama, Euxinocythere (Maetocythere) praebaquana, Camptocypria* sp. and *Amnicythere* sp. Some of these species were also recognized by Iaccarino and Bossio (1999) in the equivalent interval of Hole 975C (Core 33X-4 to 33X-CC). In agreement with Iaccarino and Bossio (1999), we consider the ostracods and possibly the benthic foraminifer *A. tepida*, which is also typically a shallow-water species adapted to low salinity conditions, the only in-situ specimens here.

6.4.3 ODP Site 654A

At Site 654A, eight discrete gypsum layers of slightly less than a meter in thickness (Cores 27R to 31R) or more (cores 32R, 34R, 36R), were penetrated. The gypsum is mostly of the laminar gypsum facies with subordinate clastic gypsum (Lugli et al., 2015). The gypsum layers are interbedded with calcareous clay (marls/mudstones) with minor sandstones and breccias. Assemblages rich in well-preserved specimens of *A. beccarii* and/or *A. tepida* and *Cyprideis* sp., which indicate the existence of shallow-water conditions, were found by the Shipboard

Scientific Party in the marls of both Cores 654A-28R and 654A-29R. We also found these species in the marls of Core 33R.

6.4.4 Bed-to-bed onshore-offshore stratigraphic correlations

The deposits of the Polemi composite section and ODP sites 654A and 975B are vertically arranged to form gypsum-marl cycles. These lithological cycles are similar to the seven gypsum-marl cycles of the Eraclea Minoa Upper Gypsum, which is the reference section for the Upper Gypsum (or MSC Stage 3) due to its continuous exposure up to and through the M/P boundary (Roveri et al., 2014a; Andreetto et al., 2022a). Thus, a tentative bed-to-bed correlation of the Polemi section and ODP sites to the Eraclea Minoa section is here proposed (Fig. 2). Both in Eraclea Minoa and Hole 975B, the conformable contact between the Miocene and the Pliocene sediments and the occurrence of the *Sphaeroidinellopsis* Acme Zone (or Zone MP11) in the early Zanclean deposits are indication that the two sedimentary sequences are complete across the M/P boundary (Hilgen and Langereis, 1993; Sgarrella et al., 1997; Iaccarino et al., 1999). The one gypsum layer in Core 975B-34X that occurs ~5 m below the M/P boundary is therefore likely to correspond to the uppermost gypsum bed (VIIEM) at Eraclea Minoa (Fig. 6.2).

The correlations of the Polemi composite section and Site 654A are more uncertain and questionable because these two sedimentary sequences are not complete. In a previous attempt of correlation, Manzi et al. (2016a) linked the six gypsum beds of Polemi (I_p-VI_p) with the lowermost six gypsum beds of Eraclea Minoa (I_{EM}-VI_{EM}), suggesting that the seventh and uppermost Eraclea gypsum did not precipitate in Polemi due to local paleoenvironmental obstacles (e.g. too high local runoff). However, in the absence of reliable stratigraphic markers, a correlation of the six Polemi gypsums with the uppermost six Eraclea gypsum (II_{EM}-VII_{EM}) is equally valid. Here we adopt the Cyprus-Sicily correlation suggested by Manzi et al. (2016a) because we do not have new and/or robust arguments to disprove it and improve it.

The correlation of Core 654A is complicated by the numerous stratigraphic gaps in the sedimentary sequences, which hampers defining the exact number of lithological cycles. For example, the incomplete recovery in Core 31R prevents determining whether the two successive gypsum layers in Core 31R-Sections 1-CC and Core 32R-Sections 1-2 are part of the same gypsum beds or are two different gypsum layers separated by an unrecovered interval. The drill rate gives an indication of the presence of harder (gypsum, longer drilling time) and softer (marl, shorter drilling time) layers. This data from Site 654A suggests that intercalations of softer sediment are present between the gypsums in Core 31R and 32R (Kastens et al., 1987). We therefore consider these two gypsum beds as separate lithological cycles. The M/P boundary was not recovered at Site 654A, but it is confidently placed between Cores 26R and 27R due to presence of early Zanclean sediments in Core 26R, Section 5 (see Kastens et al., 1987). Therefore, starting from the M/P boundary, each of the gypsum beds encountered was correlated to one gypsum layer in Eraclea Minoa (Fig. 6.2).

6.5 Results and discussion of $^{87}Sr/^{86}Sr$ data

6.5.1 Stage 3 gypsums precipitated from the same water across the Mediterranean

The $^{87}Sr/^{86}Sr$ ratios from the gypsums in cores 654A-34R (0.708789-0.708814) and 975B-34X (0.708697-0.708725) are substantially lower than the average value of coeval seawater (~0.709022; McArthur et al., 2012) and are essentially the same as the range of $^{87}Sr/^{86}Sr$ ratios of the correlative gypsums in Eraclea Minoa, namely beds I_{EM} (0.708799-0.708807) and VII_{EM} (0.708704-0.708730; Fig. 6.5). This spatial distribution suggests that deposition of these gypsum beds have occurred in basins connected to each other from the same water mass rather than in isolated basins each fed by its own, isotopically-different watershed (Fig. 6.7; e.g. Ryan, 2009; Camerlenghi et al., 2019; Madof et al., 2019, 2022; Raad et al., 2021). Box model calculations show that $^{87}Sr/^{86}Sr$ values deviate measurably from relatively high oceanic values toward riverine values when the river discharge constitutes at least 25% of the water fluxes into a basin (Topper et al., 2014). Simple mass-balance calculations using the Stage 3 seawater signature, the $^{87}Sr/^{86}Sr$ fingerprint of the Nile and Rhône today (Topper et al., 2011) and the $^{87}Sr/^{86}Sr$ ratios measured on late Messinian ostracods from Black and Caspian seas successions (Grothe et al., 2020) show that the gypsum-saturated Lago-Mare water mass was mainly (≥80%) consisting of low-salinity water from the major circum-Mediterranean drainage systems (e.g. Nile and Rhône) and the Eastern Paratethys and only little (≤20%) influenced by the Atlantic seawater (Andreetto et al., 2022a; Fig. 4.5). The reconstructed paleobathymetric profile, based on the analyses of in-situ pre-MSC foraminifera assemblages, between the Caltanissetta Basin and the Balearic Basin (see section 6.2.2 for details) further suggests that the gypsum of the Upper Unit precipitated in the deep basins at depths of hundreds, if not thousands, of meters. This conclusion challenges the long-lasting idea that the pinch-out of the entire Upper Unit in the deep basins and the Bedded Units in intermediate basins (e.g. the Central Mallorca Depression and the Corsica Basin) mark the location of Stage 3 lake shorelines in each subbasin (e.g. Ryan, 2009; Lofi et al., 2011; Thinon et al., 2016; Cameselle and Urgeles, 2017; Camerlenghi et al., 2019; Raad et al., 2021; Heida et al., 2022). At least for the gypsum beds, an alternative explanation has to be found. A valid explanation for the onlap of the UU and BUs' gypsum beds in a deep-water context can be derived if the available sedimentological description of the UU gypsum lithofacies (the gypsums of the BUs have not been perforated by scientific drillings yet) and their meaning in terms of depositional processes are considered. The reexamination of the evaporite facies present in all the DSDP and ODP cores that cut through the UU by Lugli et al. (2015) show that the only primary gypsum lithofacies present is the laminar or cumulate gypsum. Gypsum crystals forming the cumulate beds typically grow at the air-brine interface if the water mass is entirely supersaturated (Warren, 2016) or at the pycnocline of a stratified basin (Natalicchio et al., 2021) and then sink to ultimately collect as pelagic accumulations. This process is dependent from the position of the pycnocline and can therefore occur at any water depth, making the cumulate lithofacies non-diagnostic of a specific sedimentary environment. Based on the above,

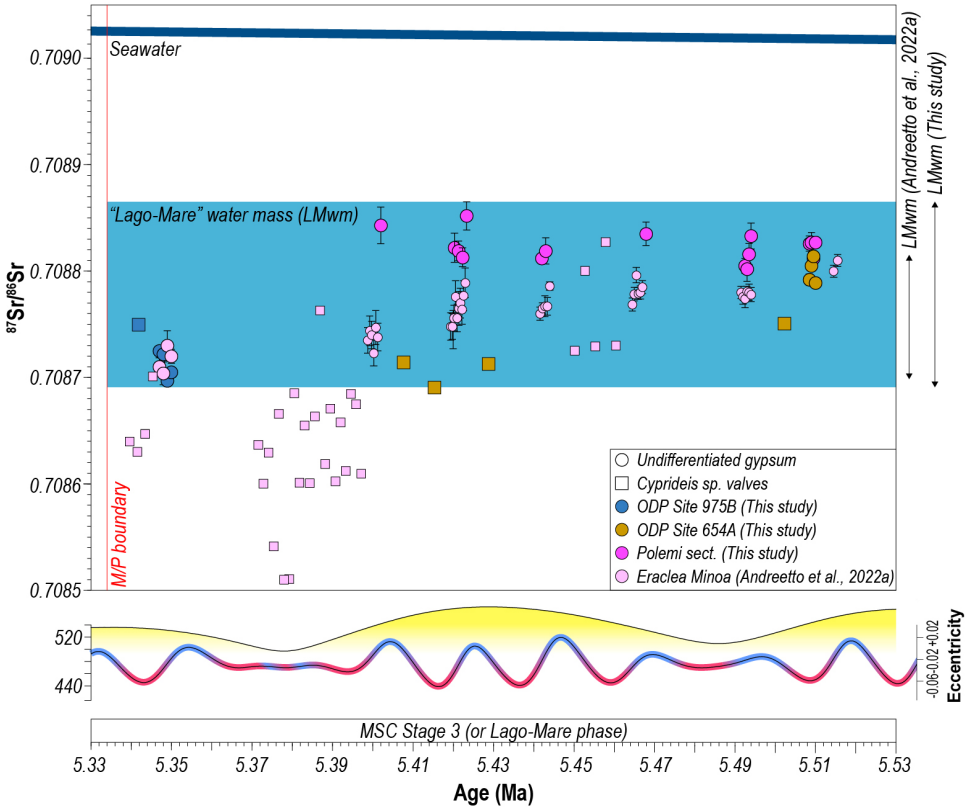

Fig. 6.5. *$^{87}Sr/^{86}Sr$ record for Lago-Mare data from the Polemi composite section and from ODPs 975B and 654A. The $^{87}Sr/^{86}Sr$ record of the Eraclea Minoa section (EM), which is the type section for the UG, is also shown for comparison. Data are plotted against the coeval ocean ratio (McArthur et al., 2012) and the ratio of the Lago-Mare water mass (LMwm), which was filling the Mediterranean during the last ~200 kyr of the Messinian stage (Andreetto et al., 2022a). The $^{87}Sr/^{86}Sr$ values are plotted using the correlation scheme proposed in this study (Fig. 6.2) and the chronostratigraphic framework of Andreetto et al. (2022a) for the EM.*

we suggest that the onlap of the UU gypsum beds is the result of the pelagic accumulation against pre-existing structural highs of floating gypsum crystals formed at the top or within a substantially deep water mass (Figs. 6.7b-c).

The Stage 3 gypsum layers alternate with marl horizons (Fig. 6.2). From the study of the Eraclea Minoa section, it was suggested that the marls of the local UG deposited when the base level of the Lago-Mare water mass was at its lowest point and the Caltanissetta Basin was isolated (Andreetto et al., 2022a). Three observations were brought forward to sustain this hypothesis (see Andreetto et al., 2022a for details): (i) the $^{87}Sr/^{86}Sr$ ratios measured on ostracod valves show high-frequency variations, which are characteristic of lacustrine systems; (ii) the

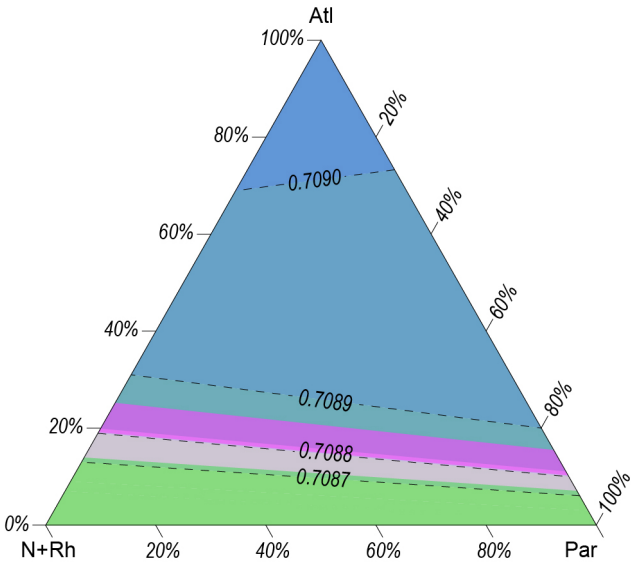

Fig. 6.6. *Range of $^{87}Sr/^{86}Sr$ ratios measured for the Polemi Upper Gypsum layers (violet area) plotted on the ternary plot that models the $^{87}Sr/^{86}Sr$ ratios of a water system (i.e. the Lago-Mare water mass) consisting of Atlantic seawater, brackish Eastern Paratethys water and freshwater from the large circum-Mediterranean rivers (see Andreetto et al., 2022a and/or Chapter 4 of this work for insights). The range of $^{87}Sr/^{86}Sr$ ratios measured for the Eraclea Minoa Upper Gypsum layers (pink area) is also plotted to facilitate the comparison with the Cyprus data. The ternary diagram is generated using the free and open-source software https://www.ternaryplot.com/.*

marl horizons, unlike the gypsum beds, are non-ubiquitous in Caltanissetta or they thin out considerably towards the basin margins, therefore pointing to periods of subaerial exposure or lower base-level; (iii) the presence of shallow-water fauna is incompatible with marl deposition during Mediterranean highstands (e.g. Manzi et al., 2009). $^{87}Sr/^{86}Sr$ ratios have been measured on ostracods from ODPs 975B (0.708750; n=1) and 654A (0.708690-0.708753; n=4), but the stratigraphic resolution is too low to pick up temporal trends with paleoenvironmental significance and taken individually these $^{87}Sr/^{86}Sr$ values are not diagnostic of a specific paleoenvironments. The isolated status of the deep basin is, however, consistent with the faunal content of the marls (*Cyprideis* sp., Paratethyan ostracods in Hole 975B and *A. tepida/beccarii*), which indicates shallow-water conditions (as deep as 100 m; Gliozzi and Grossi, 2008). These conditions could not, in fact, develop if the deep basins persisted connected to the intermediate basins through the gypsum/marl transition. In this sense, the pinch out of the seismic reflectors corresponding to the UU marl horizons might coincide, or at least approximate, a paleo-shoreline of the deep basins.

6.5.2 On the origin of the high $^{87}Sr/^{86}Sr$ ratios of the Polemi gypsums: basin isolation or earlier precipitation?

The $^{87}Sr/^{86}Sr$ ratios of the six Polemi gypsums define a narrow range of values, from 0.708802 to 0.708852 (Fig. 6.5). In general, values are within the standard error range of each other and therefore do not draw a trend from the bottom of the section (gypsum I_p) to

the top (VI_p). Only gypsums II_p and VI_p, for which four samples were analysed, show a subtle tendency to lower values toward the top of each bed. The Polemi $^{87}Sr/^{86}Sr$ ratios are higher than any $^{87}Sr/^{86}Sr$ ratios measured on time-equivalent Stage 3 gypsum beds in Eraclea Minoa and in DSDP-ODP holes (Fig. 6.5). The mismatch is independent of the adopted correlation scheme for the Polemi gypsums and the rest of the Mediterranean and indicates that the Polemi gypsum-precipitating water mass was featured by a different chemistry than anywhere else. If time-equivalent Stage 3 gypsum beds that have precipitated from the same water mass should yield similar $^{87}Sr/^{86}Sr$ ratios, then the most straightforward conclusion to this mismatch would be that the Polemi Basin was isolated during the Stage 3 evaporitic phases and the gypsums precipitated in an endorheic lake perched above the Lago-Mare water mass. This hypothesis is not so implausible given that Stage 3 evaporitic phases occurred during the regressive phases of the Lago-Mare water mass, triggered by the concomitant lessening of the freshwater and Atlantic supply (Andreetto et al., 2022a), and that Polemi was likely to be the most elevated basin among the four considered here. In this sense, either the Lago-Mare water mass has never gone, during each UG lithological cycle, high enough to connect also the Polemi Basin or it temporarily connected with Polemi during the highstands and achieved the saturation with respect to gypsum when its base level has already fallen below the depth of Polemi. Measurements of the Sr signatures of possible Messinian Cypriot rivers, which would have thereby been the source of solutes for the gypsum-precipitating Polemi lake, are obviously not available, but can be reliably approximated using the standard assumption (e.g. Vasiliev et al., 2010, 2021; Placzek et al., 2011; Doebbert et al., 2014; Grothe et al., 2020; Andreetto et al., 2022b) that the paleorivers had similar $^{87}Sr/^{86}Sr$ ratios to those of the present-day rivers. The $^{87}Sr/^{86}Sr$ ratio of present-day surficial and underground water was measured at several locations (Ladegaard-Pedersen et al., 2020; Fig. 6.1b). The local reference $^{87}Sr/^{86}Sr$ signal is made to coincide with the $^{87}Sr/^{86}Sr$ ratios measured at sampling locations #6 and #25, because here the river water incorporates Sr^{2+} ions from at least two out of the three main lithologies present in the Cypriot watersheds, namely the Troodos ophiolites, a wide array of Upper Cretaceous-Upper Miocene carbonate and terrigenous rocks (Mamonia complex and pre-MSC formations in Fig. 6.1b) and the Messinian evaporites. The selection of these two measuring points defines a wide range of $^{87}Sr/^{86}Sr$ values for the local signal (0.707879-0.708573), because the river measured at location #6, in contrast to the one measured at location #25, does not drain the Troodos ophiolites, which are characterized by extremely low Sr signatures, in its more upstream section. Irrespective of the exact value for the local $^{87}Sr/^{86}Sr$ signal, this range of values does not overlap with the $^{87}Sr/^{86}Sr$ values measured on the UG gypsum beds (i.e. >0.7088).

Using the $^{87}Sr/^{86}Sr$ ratios of the current fluvial discharge as a meter of comparison, we therefore rule out the hypothesis that the Polemi Basin was isolated from the Lago-Mare water mass during the Stage 3 evaporitic phases. However, one could argue that the geology of today's watersheds is not thoroughly representative of the Messinian time and that, back

then, there was a lot more PLG gypsum available for erosion. If that was the case, the measured Polemi $^{87}Sr/^{86}Sr$ ratios could very likely be explained in the isolated scenario, because the Cyprus PLG, like the PLG elsewhere in the Mediterranean, is characterized by $^{87}Sr/^{86}Sr$ ratios (~0.7089; Manzi et al., 2016a; Artiaga et al., 2021) higher than both the Stage 3 gypsum and the Troodos ophiolites, i.e. the main rock-forming catchment, and upon dissolution it releases Sr in far higher concentrations than ophiolites, terrigenous and carbonate rocks (Warren, 2016), therefore buffering the $^{87}Sr/^{86}Sr$ signal of the mixture towards PLG-like values. In principle, the amount of PLG-derived Sr^{2+} ions required to reproduce the measured Stage 3 $^{87}Sr/^{86}Sr$ ratios can be quantitatively assessed by applying mass-balance equations (e.g. Andreetto et al., 2021b). In practice, however, we think there is not much point to model this scenario. This approach would require a precise knowledge of the amount of PLG gypsum that was being effectively eroded and dissolved to constrain the model results, but a realistic value can be hardly obtained because substantial (but of unknown magnitude) erosion already occurred before MSC Stage 3, as witnessed by the presence of abundant PLG blocks in the Resedimented Lower Gypsum unit found below the UG (Manzi et al., 2016a). The riddle cannot be solved by means of $^{87}Sr/^{86}Sr$ ratios, but since the Stage 3 evaporitic phases occurred during the regressions of the Lago-Mare water level and a gradient of depth existed between the Polemi, Caltanissetta and Balearic basins, it has to be expected that the onset and/or end of gypsum precipitation started in the shallowest basins and migrated progressively into the deeper basins with increasing base level fall.

The vertical variation of $^{87}Sr/^{86}Sr$ ratios within individual gypsum beds of Eraclea Minoa indicates that the regressions were also accompanied by a change in the $^{87}Sr/^{86}Sr$ ratios of the Lago-Mare water mass. More specifically, the tendency from the bottom to the top of the gypsum beds is towards less radiogenic strontium to indicate a progressive lessening of the Atlantic flow, which is in agreement with the base-level lowering (the enhance of the freshwater budget provides an equally valid explanation for the decrease of $^{87}Sr/^{86}Sr$ ratios within individual gypsum beds, but it would result in a base-level rise; Andreetto et al., 2022a). The lack of overlap between the $^{87}Sr/^{86}Sr$ ratios measured on the Polemi's and the Caltanissetta's (and other basins's) gypsum can therefore signify that that these gypsums capture different time frames of the regressions. If we calculate the proportions of Atlantic seawater, brackish Paratethyan water and riverine freshwater required to reproduce the $^{87}Sr/^{86}Sr$ ratios measured on the Polemi gypsums, then it becomes evident that it precipitated when the Lago-Mare water mass was including ~6% more of Atlantic water than when the gypsum precipitated in the Caltanissetta Basin (Fig. 6.6). The higher, more Atlantic-influenced $^{87}Sr/^{86}Sr$ ratios of the Polemi gypsum therefore indicate that its precipitation began earlier than in Caltanissetta and deeper basins and at a time of the regression closer to the highstand phases, which are likely to coincide with insolation maxima times (Andreetto et al., 2022a). The total lack of overlap between the Polemi's $^{87}Sr/^{86}Sr$ ratios and the $^{87}Sr/^{86}Sr$ ratios of gypsum from deeper basins would indicate that the evaporitic phases

Table 6.3. *Compilation of the $^{87}Sr/^{86}Sr$ from the Polemi composite section and ODPs 975B and 654A.*

Location	Sample	Sample type	$^{87}Sr/^{86}Sr$	2σ (*10^{-6})
Polemi	PO19	Balatino gypsum	0.708843	0.000017
Polemi	PO12	Selenitic gypsum	0.708822	0.000014
Polemi	PO10	Selenitic gypsum	0.708819	0.000009
Polemi	PO9	Selenitic gypsum	0.708813	0.000009
Polemi	PO3	Microcrystal. gyp	0.708852	0.000013
Polemi	LE65a	Granular gyp.	0.708824	0.000016
Polemi	LE62	Balatino gypsum	0.708819	0.000012
Polemi	LE52	Balatino gypsum	0.708835	0.000011
Polemi	LE41	Selenitic gypsum	0.708805	0.000007
Polemi	LE39	Selenitic gypsum	0.708802	0.000012
Polemi	LE36	Selenitic gypsum	0.708816	0.000010
Polemi	LE33	Selenitic gypsum	0.708833	0.000012
Polemi	LE26	Selenitic gypsum	0.708926	0.000007
Polemi	LE22	Selenitic gypsum	0.708827	0.000009
Polemi	LE17	Selenitic gypsum	0.708817	0.000008
Polemi	LE11	Balatino gypsum	0.708827	0.000005
975B	33X-3, 49-51	Mixed. Parat. ostr.	0.708753	0.000007
975B	34X-1, 142-145	Balatino gypsum	0.708725	0.000002
975B	34X-2, 90-93	Balatino gypsum	0.708722	0.000004
975B	34X-2, 144-147	Balatino gypsum	0.708697	0.000005
975B	34R-3, 82-84	Balatino gypsum	0.708705	0.000005
654A	28R-4, 12-14	*Cyprideis sp.*	0.708718	0.000008
654A	29R-1, 30-32	*Cyprideis sp.*	0.708690	0.000007
654A	29R-2, 32-34	*Cyprideis sp.*	0.708713	0.000006
654A	33R-1, 60-62	*Cyprideis sp.*	0.708753	0.000007
654A	34R-1, 56-58	*Balatino gypsum*	0.708792	0.000005
654A	34R-2, 63-65	*Balatino gypsum*	0.708805	0.000007
654A	34R-3, 82-84	*Balatino gypsum*	0.708814	0.000009
654A	34R-4, 26-27	*Balatino gypsum*	0.708789	0.000004

in Polemi and Caltanissetta-deep basins are diachronous. In this scenario, the Polemi gypsum beds would be roughly time-equivalent with the diatomite-marl alternations (sub-unit A) that in Eraclea Minoa express the highstand phases of the Lago-Mare water mass, but in which material suitable for $^{87}Sr/^{86}Sr$ analyses was not found (Andreetto et al., 2022a). However, it must be taken into account that, unlike three out of six of the Polemi gypsums, none of the seven gypsum beds of Eraclea Minoa have been analyzed for their $^{87}Sr/^{86}Sr$ ratios from base to top. The vast majority of the data come from the massive selenites (sub-unit C), whereas only five data derive from the balatino layers of the underlying sub-unit B. It cannot therefore be excluded that the entire duration of the evaporitic phase in Polemi corresponds in Eraclea Minoa to at least part of the "balatino" phase and that gypsum precipitation continued in Caltanissetta with the bottom-grown selenites when the Polemi Basin was already isolated and depositing mud from suspension (Fig. 6.7). The finding, in Eraclea Minoa, of the shallow-water ostracods *C. agrigentina* and *L. muelleri* in some mud beds intercalated with the massive selenites supports this scenario. However, more $^{87}Sr/^{86}Sr$ data from the Sicilian balatino gypsums and from gypsums recovered by scientific drillings need to be generated to strengthen it.

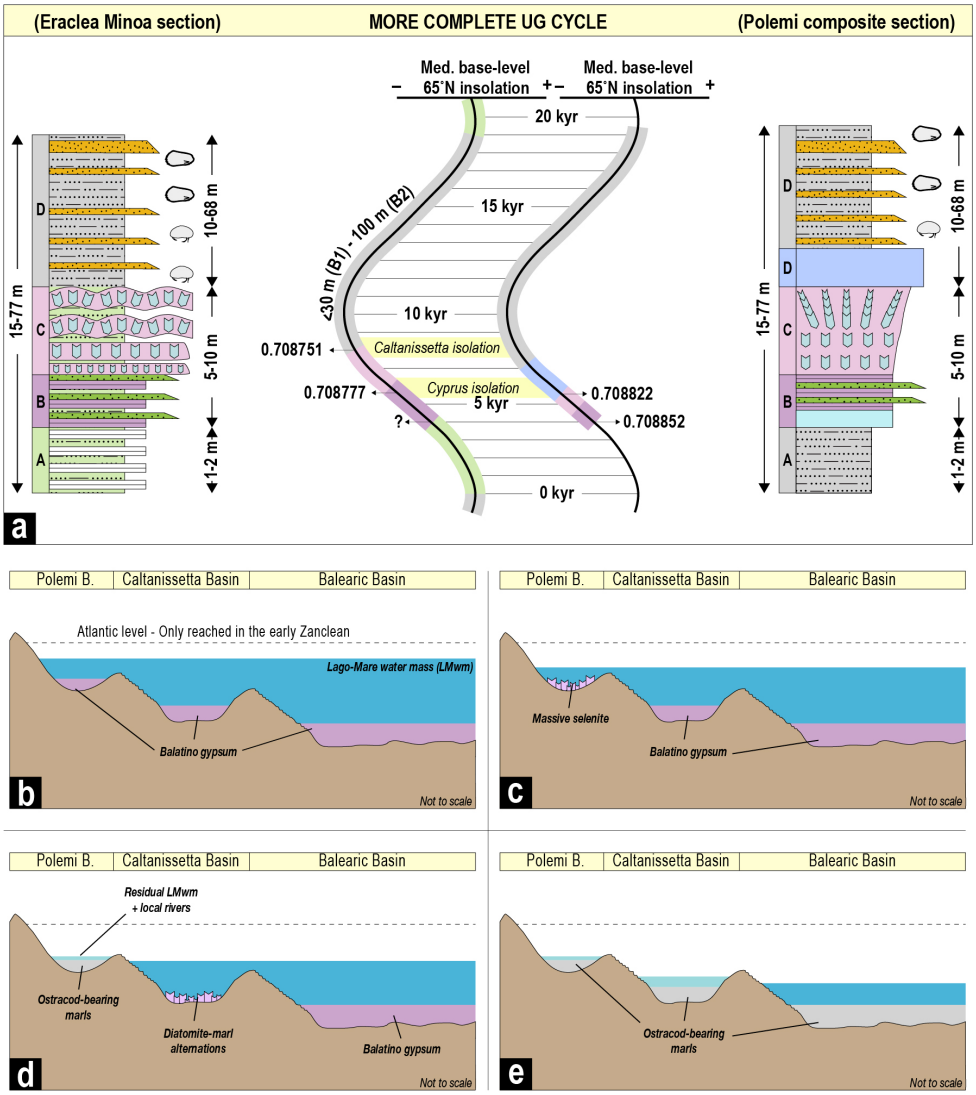

Fig. 6.7. (a) *Lithofacies of a complete Polemi UG cycle as a function of precession cycle and Mediterranean base-level. A comparison with the Sicilian UG interpretation (Andreetto et al., 2022a) is also shown.* **(b-e)** *Cartoons showing the proposed evolution of the Mediterranean intermediate-deep water environments and hydrology during one regression of the Lago-Mare water mass.*

The Saltgiant crew (kick-off meeting, Palermo 2018, Italy).

E

Epilogue

1.1 Main thesis outcomes

Stage 3 is the most ambiguous of all the phases of the Messinian Salinity Crisis in terms of Mediterranean's paleoenvironment, paleohydrology and connectivity. Two fundamental peculiarities make Stage 3 a highly puzzling period of time:

(i) the presence, all around the Mediterranean margins and in deeper settings, of marl beds which include microfossils (ostracods, mollusks and dinoflagellates) endemic to the Paratethys realm and indicative of brackish (~5-17 g/l) and shallow-water conditions (Gliozzi and Grossi, 2008; Stoica et al., 2016);

(ii) the alternation, in the intermediate and deeper basins, of these Paratethyan ostracod-bearing marls with gypsum beds. Microthermometry studies on fluid inclusions in gypsum lithofacies from Eraclea Minoa (Bigi et al., 2022) and thermodynamic calculations (Aloisi et al., 2022) suggest this gypsum precipitated from the evaporation of seawater at a salinity of about 115 g/L.

The repetitive transition from hypersaline evaporitic facies to fresh-brackish terrigenous facies implies huge hydrological changes in the region. At the dawn of the project, it was unclear and/or heavily debated how the migration of brackish biota from Eastern Paratethys took place and when, in which sedimentary environment, and triggered by which mechanism the gypsum-marl transition took place (chapter 1). To tackle these questions, we combined integrated biocyclostratigraphic analyses with high-resolution Sr-isotope records on key sections on-land and recovered from deep sea cores along an E-W and depth transect across the Mediterranean (chapters 2-6). The resulting data compilation and interpretation contribute to a better understanding of the paleoenvironmental history of the Mediterranean Basin during the final phase of the Messinian Salinity Crisis. The picture that has emerged is somewhat more complicated than when this project started, but now fits with most of the existing and newly obtained data.

The most important result from this thesis is the development of a paleoenvironmental model (chapter 4) that reconciles observations that support both the full and the desiccated scenarios that characterized an enduring controversy for MSC Stage 3 (chapter 1). The stratigraphic section used to evaluate and refine existing models is the Eraclea Minoa section

of Stage 3 gypsum-marl couplets. Its precessional cyclicity underpins an astronomical age model (van der Laan et al., 2006; Manzi et al., 2009; Andreetto et al., 2022a) and it represents an intermediate depth setting (500-1500 mbsl) during Stage 3 (Roveri et al., 2014a). The sedimentological, palaeontological and Sr isotopic examination of Eraclea Minoa's sedimentary record reinforced and refined several existing conclusions, such as that:

(i) during Stage 3, the Mediterranean base-level fluctuated repeatedly with precessional periodicity (e.g. Fortuin and Krijgsman, 2003; Roveri et al., 2008a; Manzi et al., 2009; Ben Moshe et al., 2020);

(ii) the Mediterranean was a basin strongly influenced by non-marine waters chiefly derived from the Eastern Paratethys and the large circum-Mediterranean rivers and including a small Atlantic component (e.g. Roveri et al., 2008a, 2014a, b, c; Vasiliev et al., 2017; García-Veigas et al., 2018; Grothe et al., 2020).

Several innovative ideas are also put forward. Among them are the following:

(i) With the aid of mass-balance calculations, we showed that this Atlantic contribution made up a maximum of ~20% of the Lago-Mare water mass (Fig. 4.5).

(ii) Gypsum precipitation in Stage 3 occurred during a phase of base-level fall coincident with the transition from insolation maxima (peak in freshwater discharge to the Mediterranean) to insolation minima (minimum in the Mediterranean freshwater budget). In chapter 6, by analyzing $^{87}Sr/^{86}Sr$ ratios from differently elevated basins, we show that the beginning and end of gypsum precipitation is likely to have been slightly diachronous, starting and ending earlier in shallower basins (e.g. Polemi in Cyprus) than in deeper basins (e.g. Balearic and Ionian basins).

(iii) Eraclea Minoa includes diverse assemblages of Paratethyan ostracods at ~5.47 Ma. This observation disproves the hypothesis that the deposition of marls and the migration of these organisms across the Mediterranean occurred as a synchronous event at 5.42 Ma (substages 3.1 and 3.2 of Roveri et al., 2014a; see also Roveri et al., 2008and Grossi et al., 2011), possibly prompted by a sudden increase of the Paratethys outflow (Marzocchi et al., 2016). Instead, it tracked Mediterranean-wide, base-level fluctuations, which were of high-amplitude (several hundred to thousands of meters; Figs. 4.8b-e), resulting in sequential marl sedimentation from deep-shallow-deep Mediterranean settings.

High water levels in the Mediterranean during the wettest period of each precessional cycle (i.e. straddling the insolation maxima-precession minima) occasionally resulted in the establishment of a connection between the shallower basins at the periphery of the Mediterranean and the main Lago-Mare water mass. During these highstands, the Paratethyan biota succeeded to colonize the shallower and most remote regions of the Mediterranean. The high percentage of Paratethyan (Pontian) ostracods in the ostracod assemblages of many Spanish (Sorbas, Vera, Nijar, Malaga; see appendix I) and Italian basins, as well as in Crete

(Cosentino et al., 2007), Algeria (Rouchy et al., 2007), Tunisia (Temani et al., 2020) and Cyprus (Manzi et al., 2016a; appendix I) and the strong similarity in the assemblages of these different basins (Fig. A(I).6) support the conclusion that the Mediterranean was relatively full during the highstands and that the main mechanism of migration was the active transport of these organisms by water (e.g. Gliozzi et al., 2007; Stoica et al., 2016). Therefore, the presence of Paratethyan biota in marginal basins could serve as ecological markers for the presence of a relatively full Mediterranean Basin.

This conclusion is reinforced by the $^{87}Sr/^{86}Sr$ analyses on ostracod valves, which provide insights into the region-of-origin of the water in specific basins. The newly obtained isotopic dataset for the Spanish basins of Malaga (appendix II), Sorbas, Vera, Nijar (chapter 2), the Piedmont, Cella-Giaggiolo and Laga basins along the Adriatic side of the Apennine chain (chapters 3 and 5) and the Cypriot Pissouri Basin at the far eastern end of the Mediterranean (appendix II) show that the measured values are all incompatible with the values expected for local river-fed endorheic lakes and that an additional source of water with a lower than marine $^{87}Sr/^{86}Sr$ signature was present. This source is demonstrated to have been the Lago-Mare water mass filling the main Mediterranean waterbody.

Marl deposition in the deep basins occurred during the lowstands of the Lago-Mare water mass. Endorheic lakes formed in perched silled basins during these lowstands, the largest of which encompassed northern and eastern Italy (chapter 5). This "Adriatic megalake" was fenced by the proto-reliefs of the Alps, Apennines and Dinarides and by a southern sill in the offshore area of the present-day Gargano Peninsula (Fig. 5.1). By integrating sedimentology, paleontology, $^{87}Sr/^{86}Sr$ isotopes, XRF, grain-size distribution and magnetic susceptibility data on key sections from this megalake, we showed that this region underwent three main hydrological changes:

(i) formation of the megalake occurred between 5.59 and 5.55 Ma, when Mediterranean water level was at its lowest and halite precipitated in its deepest basins;

(ii) at ~5.36 Ma, a major hydrological change provoked by the Mediterranean highstand that led to the precipitation of the last gypsum bed of the Messinian Salinity Crisis established a brackish water environment in the Adriatic supporting a thriving Paratethyan biota;

(iii) lacustrine (likely brackish) conditions were briefly re-established slightly before 5.332 Ma, but were terminated soon after (at, or slightly before 5.332 Ma), by the Zanclean (or Terminal Messinian) Flood which resulted in the abrupt transition to open marine conditions throughout the Mediterranean.

The results of this thesis also highlight the potential impact of large-scale gypsum precipitation and weathering in the Mediterranean and connectivity changes with the ocean on perturbations to the global carbon cycle (chapter 4). The connectivity history reconstructed from the Eraclea Minoa data describes an asymmetry between the extraction of Ca^{2+} from the ocean during gypsum formation in the Mediterranean and the return flux generated

by weathering of these evaporites during the high-amplitude base level changes, but returned to the open ocean in the Pliocene once the Mediterranean outflow was re-established. This aspect of our work challenges recent box-modelling experiments that explore the role of gypsum precipitation and weathering on ocean biogeochemistry, atmospheric CO_2 and global temperature (Shields and Mills, 2020). These models assume that the perturbations to seawater chemistry caused by evaporite precipitation, dissolution and weathering happen on long timescales (>100 kyr), whereas we show that evaporites form and dissolve three orders of magnitude more quickly than other sediments (Nichols et al., 2009), probably in a few thousand years in each precession cycle.

1.2 Open questions

Although the conclusion that the Mediterranean was both relatively full and empty during each Stage 3 precession cycle (Fig. 4.8) is a step towards a better understanding of the complex history of the Mediterranean during the Messinian Salinity Crisis, some key questions remain unresolved. Two important ones are:

(1) During which of the seven Mediterranean highstands that occurred during Stage 3 did the ostracod-bearing marls in the marginal and Adriatic subbasins deposit?

(2) What was (were) the forcing mechanism(s) behind such extreme sea level fluctuations?

Below, we reflect on both these questions and consider possible future studies that might help to answer them.

1.2.1 Suggestion for an updated chronostratigraphic framework for MSC Stage 3

The hypothesis that the Mediterranean underwent at least seven high amplitude fluctuations in base level on a precessional time-scale (Andreetto et al., 2022a; Figs. 4.8b-e) has several stratigraphic implications. These include:

> Mediterranean highstands at insolation maxima correspond to deposition of ostracod-bearing marls in the marginal basins and in the basins of the silled Adriatic region;

> Regressions in the Lago Mare water mass (transitions from insolation maxima to insolation minima) correspond to gypsum precipitation in intermediate and deep basins;

> lowstands (insolation minima) and transgressions (transitions from insolation minima to insolation maxima) coincide with continental sedimentation in the marginal basins and deposition of ostracod-bearing marls in endorheic lakes filling the same gypsum-bearing intermediate and deep basins.

The duration of each of these phases remains unknown and assumptions have to be made. Relying on sedimentological observations (Manzi et al., 2009, 2012; Reghizzi et al., 2018) and model results (Topper and Meijer, 2015) and assuming that everything preserved is representative of everything that was precipitated, it was concluded that a few meters of gypsum takes less than ¼ of the precession cycle to precipitate. Pending the discovery of a method

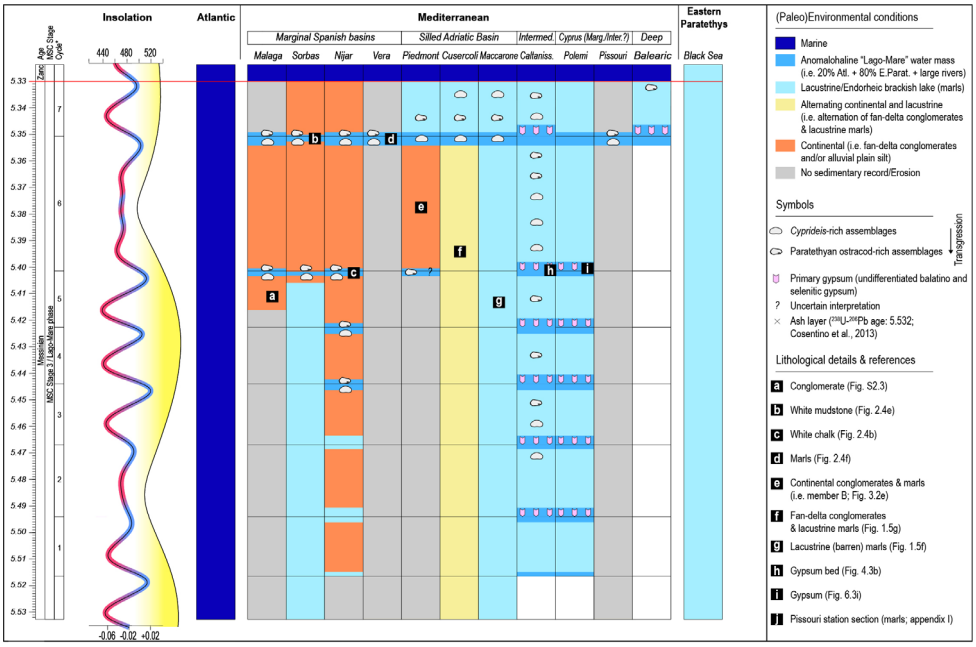

Fig. E.1. *Tentative chronostratigraphic correlations of Stage 3 successions across the Mediterranean Basin. See text for description of the basis on which it was constructed.*

that more accurately determines the exact duration of each evaporitic phase, we consider the regressive phases to have lasted ~4000 yr. The lowstands and the transgressions in the endorheic lakes are considered to last until about the next insolation maximum, when high freshwater discharges and, possibly, the reconnection with the Atlantic (see the next section for insights) prompted a fast, Mediterranean-wide transgression that re-established the highstand. This implies that the highstands lasted ~2000 yr, while the lowstands and the transgressions covered >10.000 yr. Based on the stratigraphic relationships and the timing implications, a high-resolution stratigraphic model for the Stage 3 deposits has been constructed (Fig. E.1) with the following constraints:

> the gypsum-beds of Eraclea Minoa are correlated on the basis of the astronomical tuning presented in Fig. 4.8a;

> the gypsum beds in Polemi and in ODP Site 975B are correlated based on the correlation scheme presented in Fig. 6.2;

> the Piedmont, Cusercoli and Maccarone sections in the Adriatic Basin are correlated following the conclusion of chapter 5 that ostracods appeared in this (silled) region of the Mediterranean at ~5.36 ± 0.01 Ma.

This model illustrates the conclusion that high biodiversity Paratethyan ostracod assemblages in the Mediterranean did not appear synchronously. The oldest recorded presence

is in the intermediate Caltanissetta Basin at ~5.47 Ma (see also chapter 4 for insights), whereas the first appearance in the shallow Mediterranean marginal sub-basins is at ~5.443 Ma in the Nijar Basin. Following high-amplitude water level fluctuations, these ostracods alternated several times between the shallower and the deeper basins (this is particularly evident when comparing the Eraclea Minoa and Nijar records) during highstands and lowstands of the Lago-Mare water mass, respectively. At the insolation maximum centered at ~5.35 Ma, which in our model corresponds to the last highstand of the Lago-Mare water mass and pre-dates the deposition of the last gypsum bed of the Messinian Salinity Crisis (i.e. gypsum VII at Eraclea Minoa), the base-level in the Mediterranean was apparently so high that it reached all the marginal (SE Spain, Pissouri) and silled (Adriatic region) basins, which all seem to have the highest ostracod biodiversity just below the M/P boundary. After this insolation maximum, the Mediterranean water level decreased again, as testified by the occurrence of erosion surfaces (Vera, Malaga), continental deposits (Sorbas, Nijar) and *Cyprideis*-rich marls (e.g. Buttafuoco and Pissouri) in marginal and intermediate areas (e.g. Adriatic region and Pissouri) before being superseded by the first Zanclean marine deposits. It is possible this pre-Zanclean drop in base-level was greater than 2 km, since shallow-water Paratethyan ostracods are present a few tens of centimeters below the M/P boundary at ODP Site 975B (Fig. 6.2), which lies today (and possibly also during the Messinian; Heida et al., 2022) at >2000 mbsl. This model is in agreement with the idea that just before the M/P boundary the level was probably low enough to isolate many Mediterranean subbasins (Amarathunga et al., 2022) and is therefore consistent with the Zanclean flood model (Garcia-Castellanos et al., 2020).

However, this model also presents significant difference with the existing chronostratigraphic models and oddities that future studies need to:

> In our model, the two white limestones intercalated with the continental sediments of the Zorreras Mb. in the Sorbas Basin (Spain) correspond to the last two Mediterranean highstands (~5.35 and 5.40 Ma) leading to gypsum VI and VII in the Eraclea Minoa section. This correlation is in disagreement with the astronomical tuning by Krijgsman et al. (2001), which dates these limestones at ~5.42 and ~5.51 Ma, and by Roveri et al. (2009), who places them between 5.42 and 5.332 Ma. Our interpretation also has significant paleoenvironmental implications for the underlying Sorbas Mb (see chapter 1). Implicit in our model is the assumption that every marginal basin-Mediterranean connection event is recorded by the presence of Paratethyan ostracods. The Sorbas Mb. is devoid of these organisms, and is therefore interpreted as being deposited in a perched Sorbas lake, rather than in a coastal to shelfal environment (Roep et al., 1998).

> The Nijar Basin (Spain) contains four incursions of the Lago-Mare water mass, which in our model corresponds to the uppermost four cycles of Stage 3, spanning ~5.445 to 5.332 Ma. This is different than the cyclostratigraphic correlation of Omodeo Salé et al. (2012), who correlate these cycles to the four (two minor) insolation maxima between 5.42 and 5.332 Ma.

> The Cuevas del Almanzora section (Vera Basin) in our interpretation spans a far shorter time window (~2000 years) than previously proposed (i.e. 5.40-5.332 Ma; Stoica et al., 2016; Caruso et al., 2020). The original dating was based on the hypothesis that the arrival of Paratethyan ostracods in the Mediterranean was synchronous event at 5.40 Ma (Roveri et al., 2008a; 2014a; Grossi et al., 2011), which we demonstrated was not the case (chapters 4 and 5).

> Member A of the Pollenzo section (Piedmont Basin, Italy), which contains evidence of a Mediterranean contribution during Stage 3 (see Chapter 3 for details), is inferred to have an age of ~5.40 Ma. However, the same Mediterranean inflow is not recorded in more southerly sections of the Adriatic domain such as Cusercoli and Maccarone.

> The highest Lago-Mare water level is implied to have been reached in cycle 7. However, this is not the cycle that in Simon et al. (2017)'s reconstruction of the late Miocene Mediterranean freshwater budget, has the highest freshwater budget of this period; cycles 1, 4, 5 and 6 in Stage 3 all have a higher freshwater budget than cycle 7; see Fig. 4.8a). In addition, the $^{87}Sr/^{86}Sr$ ratios of gypsum VII and VI at Eraclea Minoa are some of the lowest measured (Fig. 4.2). This suggests that the Atlantic contribution is proportionately less than in the earlier gypsum cycles. If both freshwater and Atlantic contributions to the Mediterranean during cycle VII were lower than in the previous cycles, how can the base-level be at its highest level? One option could be an increased inflow from Paratethys. We therefore suggest that future studies should examine the late Messinian record of the Black and Caspian seas to evaluate whether major paleoenvironmental changes there may have had an impact on the hydrological balance of the Mediterranean.

1.2.2 Configuration and duration of Atlantic input

A key conclusion of chapter 4 is that Atlantic seawater made up only ≤20% of the Lago-Mare water mass that precipitated gypsum in the intermediate and deep Mediterranean subbasins. A question that remains unsolved in this thesis is the nature of the Atlantic gateway and the route by which this seawater supplied the Mediterranean.

Stage 3 data suggest that the small ocean inflow to the Mediterranean was not compensated by a parallel outflow to the Atlantic (see discussion in section 4.4.2). This therefore requires either constant small-scale inflow perhaps resulting from seepage through the sill (Warren, 2016) or a mechanism for switching the Atlantic inflow on and off again before headward erosion catastrophically breaches the Atlantic-Mediterranean sill, raising the Mediterranean base-level above the Atlantic sill and reestablishing two-way exchange at the M/P boundary (Garcia-Castellanos and Villaseñor, 2011). Today, more than 25% of all the water draining into the Mediterranean has subterranean parts of its pathway (Aureli et al., 2008). Seepage is therefore highly likely to have contributed to the transfer of Atlantic water to the Mediterranean in the late Miocene, possibly utilizing some karst systems. Quantifying seepage flux is really difficult even at the present-day and is largely ignored in geochemically-

based paleoreconstructions (e.g. Andreetto et al., 2021b and references therein). In addition to seepage, a mechanism involving loading changes within the Mediterranean causing the isostatic adjustment of the Atlantic-Mediterranean sill is also a possibility. Govers (2009) modelled 30 m of uplift of the Mediterranean-Atlantic gateway region in response to the formation of hypersaline brine and precipitation of halite in the Mediterranean during MSC Stage 2. This is considered to be enough to shoal and ultimately choke seawater inflow (Govers, 2009). A similar flexural response in Stage 3 might result from lithospheric loading and unloading during Mediterranean base-level change. Detailed assessment of these hypotheses is beyond the scope of this study, but should be explored in the future.

1.3 Future directions

Although this thesis offers several innovative ideas, we are still far from having a complete understanding of MSC Stage 3. Here I list the major issues that currently detract from a full understanding:

(i) Higher-resolution, multidisciplinary analysis of the offshore sedimentary records and the expansion of the geochemical dataset with proxies that are less "material-dependent" are certainly two key aspects that future researchers should consider. Most of the results and conclusions derived from the study of onland sections represent shallow-water settings and only in the case of the Eraclea Minoa section (Sicily) and, possibly, Polemi (Cyprus), have deeper-water settings have been sampled. Future studies on MSC Stage 3 should therefore focus on the offshore domain, which hosts a far greater volume of sediments than the Mediterranean periphery and, in many cases, consists of basins that underwent only minor post-depositional deformation. Several cores from the DSDP and ODP drilling campaigns performed in the '70s-'90s are available and many more will, we hope, be provided by future scientific drilling projects DEMISE, DREAM and IMMAGE (Camerlenghi and Aloisi, 2020).

(ii) This thesis, besides showing the potential of radiogenic Sr isotope ratios to resolve the connectivity history between restricted basins, also showcases its limits: the dependence, for its application, on the presence, in the sedimentary record, of pristine chemical precipitates and appropriate biogenic material. Both materials are not ubiquitously present and therefore represent an obstacle to acquiring high-resolution isotopic datasets in space and time. Gypsum easily undergoes alteration and/or recrystallization by meteoric water; halite is hard to isolate reliably from contaminant phases coating the crystals (e.g. Meilijson et al., 2019) and carbonate-shelled organisms are not ubiquitous or, in some cases (e.g. the Adriatic megalake; see chapter 5), totally absent, because environmental conditions are often too harsh for life to develop.

(iii) Additional studies are also needed to improve Mediterranean hypsometry and bathymetry during the late Messinian, which is essential for a precise understanding of the environmental and hydrological changes in the different subbasins.

(iv) For sections that lack conspicuous sedimentary cyclicity, future research should

focus on generating high-resolution climate proxy records that may reveal the presence of Milankovitch cycles because this is such a key tool in inter-basin correlation.

My final take home message is that a comprehensive multidisciplinary research strategy that involves the entire Mediterranean is a precondition for achieving a complete and less controversial understanding of the Messinian Salinity Crisis of the Mediterranean Basin.

APPENDIX I - ADDITIONAL OSTRACOD DATA

A(I).1 Materials and methods

Here, additional ostracod results are presented from four locations in Spain (3) and Cyprus (1):

> Malaga Basin (Rio Mendelín section; 36°45'01.0"N 4°25'58.3"W);

> Sorbas Basin (Cerro Zorreras section; 37°06'10.2"N, 2°06'45.2"W; Fig. 2.3e);

> Nijar Basin (Barranco de los Castellones section, 37°00'51.1"N, 2°00'05.7"W; El Argamason section, 37°0'35.02"N, 1°58'23.02"W);

> Pissouri Basin (Pissouri "gas station" section, 34°40'54.9"N, 32°42'06.3"E).

Hundred-twenty samples were analyzed for ostracods:

> 51 marls from the Rio Mendelín section, which consists of conglomerates and ostracod-bearing marls organized in two fining-upward sequences and unconformably overlain by Zanclean marine sediments;

> 13 samples from the white limestone beds interrupting the continental sedimentation of the Zorreras member in the Cerro Zorreras section;

> 42 samples from the uppermost four marl intervals of the Upper Mb. of the Feos Fm. in the Barranco de los Castellones section and 4 from the topmost marl interval in the El Argamason section;

> 10 marls from the uppermost Messinian in the Pissouri "gas station" section.

Samples from Malaga were processed at the University of Salamanca, whereas samples from Sorbas, Nijar and Pissouri were processed at the University of Bucharest. All samples have been processed using standard micropalaeontological methods of air-drying to facilitate the disintegration in tap water followed by washing and sieving over a battery of two sieves (125-63 μm). The dried residue was handpicked using a light microscope and ostracods identified using the taxonomic criteria applied by Stoica et al. (2013, 2016).

Fig. A(I).1 (next page). (a) *Simplified geological map of the westernmost Betic (modified after Varas-Reus et al., 2017).* **(b)** *Panoramic view of the Rio Mendelín section. Vehicles for scale.* **(c)** *Close-up of the lowermost conglomerate.* **(d)** *Ostracod distribution patterns of the Rio Mendelín section. The $^{87}Sr/^{86}Sr$ ratios measured on ostracod valves are plotted against the $^{87}Sr/^{86}Sr$ signature of coeval water in the oceans (McArthur et al., 2012), Eastern Paratethys (Grothe et al., 2020) and Mediterranean (i.e. the Lago-Mare water mass, for which definition we refer the reader to Andreetto et al., 2022a or chapter 4 of this work). For the interpretation of the stratigraphic log and of the paleoenvironment column, refers to the legend of figure S2.2.*

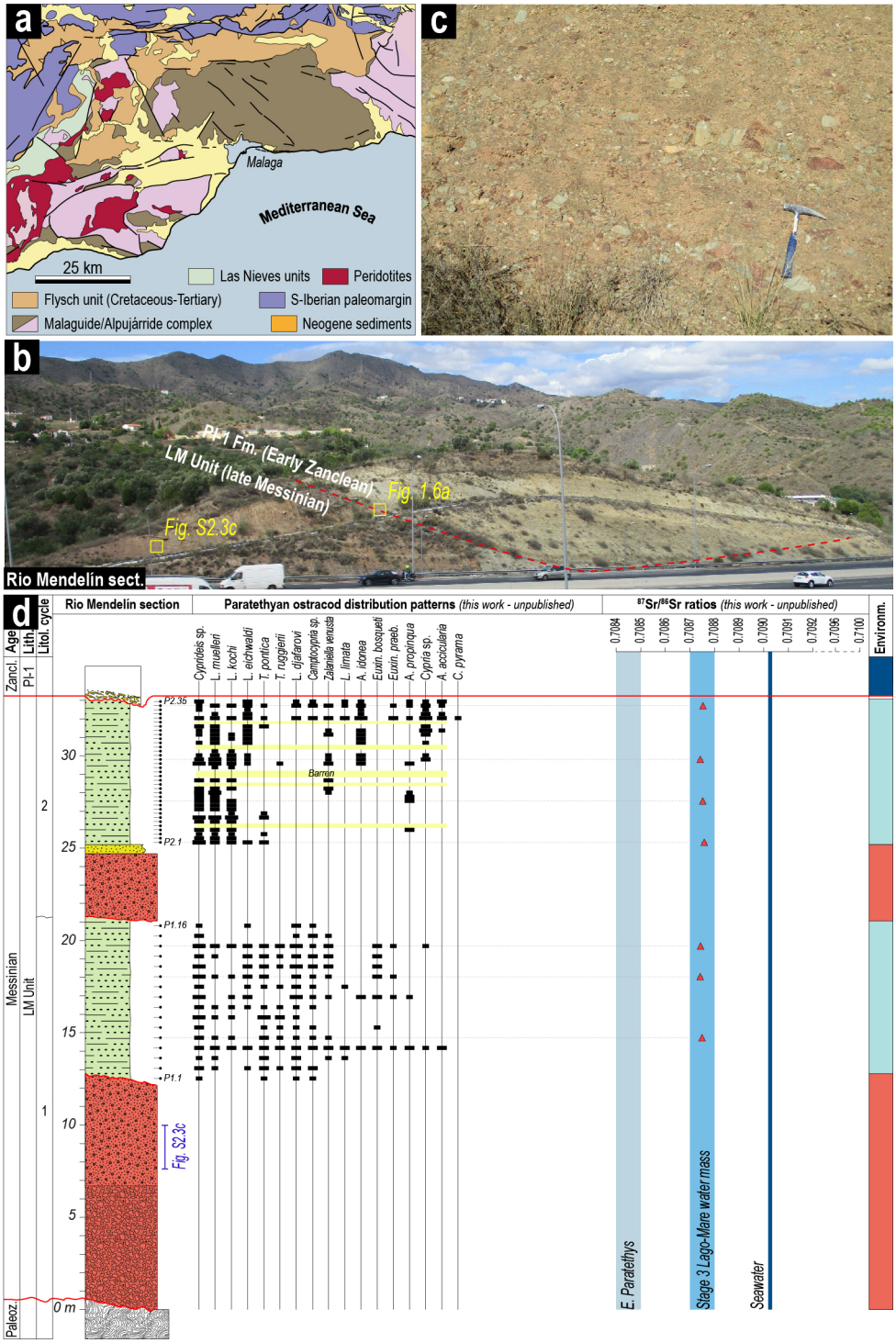
a
Malaga
Mediterranean Sea
25 km
Las Nieves units
Peridotites
Flysch unit (Cretaceous-Tertiary)
S-Iberian paleomargin
Malaguide/Alpujárride complex
Neogene sediments
c
b
PL-1 Fm. (Early Zanclean)
LM Unit (late Messinian)
Fig. 1.6a
Fig. S2.3c
Rio Mendelín sect.
d
Rio Mendelín section
Paratethyan ostracod distribution patterns (this work - unpublished)
87Sr/86Sr ratios (this work - unpublished)
Environm.
Age
Lith.
Litol. cycle
Zancl.
Pl-1
Messinian
LM Unit
Paleoz.
Cyprideis sp.
L. muelleri
L. kochi
L. eichwaldi
T. pontica
T. ruggieri
L. dilatarovi
Camptocypria sp.
Zalaniella venusta
L. limata
A. idonea
Euxin. bosqueti
Euxin. praeb.
A. propingua
Cyprina sp.
A. acicularia
C. pyrama
P2.35
P2.1
P1.16
P1.1
Barren
Fig. S2.3c
0.7084
0.7085
0.7086
0.7087
0.7088
0.7089
0.7090
0.7091
0.7092
0.7096
0.7100
E. Paratethys
Stage 3 Lago-Mare water mass
Seawater

A(I).2 Results

Malaga. Only six (P2.5, P2.15, P2.17, P2.18, P2.24, P2.30) out of the fifty-one samples analysed in the Rio Mendelín section were barren (Fig. A(I).1); the remaining 45 all have provided a well-preserved and overall abundant ostracod fauna mixing adults and different juvenile stages, which feature autochtonous assemblages. 16 species were recognized. In the lowermost marly interval, the first appearance of ostracods at ~13 m includes only four species, including *Cyprideis* sp., *Tyrrhenocythere pontica, Camptocypria* sp. and *Loxoconcha djafarovi*. Assemblages diversify upwards, reaching the higher diversity (15 taxa) at ~14.20 m (sample P1.4), where the ostracod community includes, besides the four taxa mentioned above, *Zalaniella venusta, Loxoconcha mülleri, Loxoconcha eichwaldi, Loxoconcha kochi, Euxinocythere (Maeotocythere) praebaquana, Euxinocythere (Maeotocythere) praebosqueti, Amnicythere idonea, Amnicythere propinqua, Amnicythere accicularia, Loxocauda limata, Tyrrhenocythere pontica, Tyrrhenocythere ruggierii, Cypria* sp. and *Camptocypria* sp. The diversity drops again in the

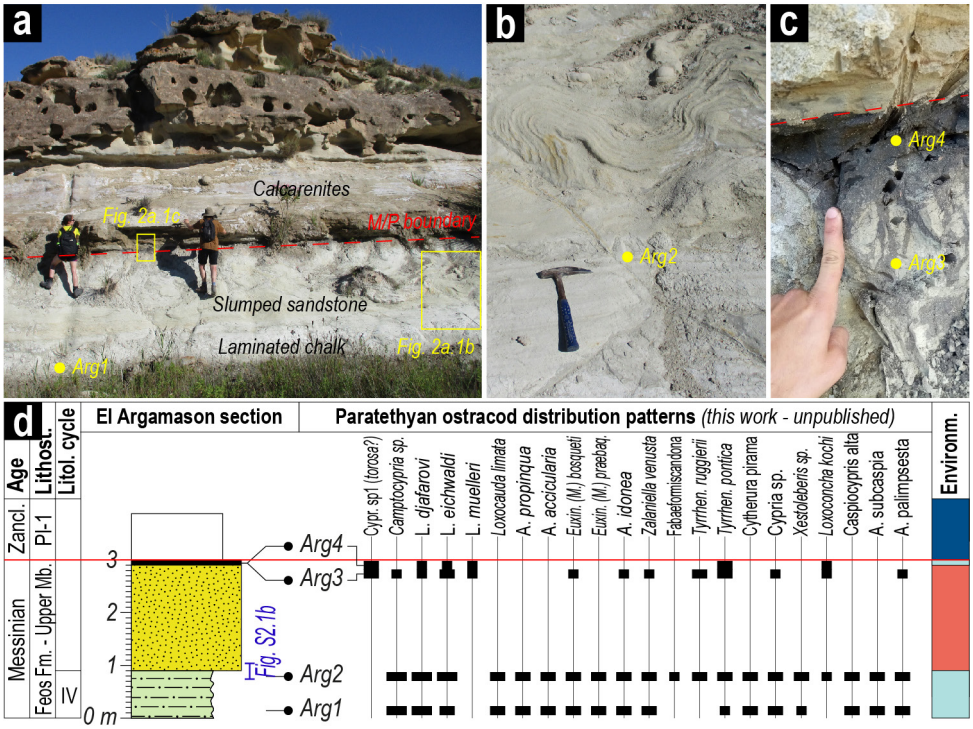

Fig. A(I).2. *El Argamason section: panoramic view* **(a)**, *close-ups of the laminated chalk-slumped sandstone* ***(b)*** *and Miocene/Pliocene* **(c)** *transitions and ostracod distribution patterns* **(d)**. *For the interpretation of the stratigraphic log and of the paleoenvironment column, refers to the legend of figure S2.2.*

uppermost ~1 m of the section (samples P1.15-1.16), which only consist of four taxa: *Cyprideis* sp., *Camptocypria* sp., *L. djafarovi* and either *Z. venusta* (P1.15) or *L. eichwaldi* (P1.16).

The uppermost marly interval contains the same species as the lower one, except for the addition of Cytherura pirama in sample P2.31. There is, however, a difference between the two marly intervals in respect of the species number and diversity pattern of the ostracod community, which are respectively higher and more clearly defined in the younger marl horizon. The lower ~4.5 m are dominated by *Cyprideis* sp., *L. muelleri* and *L. kochi* with the occasional presence of *L. eichwaldi, T. pontica, Z. venusta* and *A. propinqua*. The dominance of *Cyprideis* sp., *L. muelleri* and *L. kochi* continues in the uppermost 4-4.5 m, but assemblages are overall more diversified.

Our ostracod results are largely consistent with the results from Guerra-Merchán et al. (2010).

Sorbas. A total of 17 species are recognized between the two white limestones intercalated with the continental deposits of the Zorreras Mb. (Fig. A(I).3). These include: *Cyprideis* sp., *Zalaniella venusta, Loxocorniculina djafarovi, Loxoconcha muelleri, Loxoconcha eichwaldi, Euxinocythere (Maeotocythere) praebaquana, Euxinocythere (Maeotocythere) bosqueti, Amnicythere idonea, Amnicythere propinqua, Amnicythere accicularia, Loxocauda limata, Tyrrhenocythere pontica, Tyrrhenocythere ruggierii, Camptocypria* sp., *Cytherois* sp. *Fabaeformiscandona* and *Cytherura pirama*. Ostracods are well preserved, overall abundant and present in both adults and different juvenile stages. All together, these features show the in situ character of the fauna.

The first occurrence of ostracods is from a 3-5 cm-thick gray marl just below limestone I (sample Zor.1.0). This layer is composed of a monospecific assemblage of abundant *Cyprideis* sp., which are even visible to the naked eye. The assemblage diversifies in the lowermost ~60 cm of the limestone, corresponding to samples Zor1.1-1.3, where *Cyprideis* sp. is accompanied by *Camptocypria* sp., *L. muelleri* and either *A. propinqua* (Zor.1.1-1.2) or *E. (M.) praebaquana* (Zor.1.3). The uppermost ~50 cm of limestone I are characterized by the highest species diversity with the occurrence, along with the aforementioned taxa, of *L. djafarovi, L. eichwaldi, Loxocauda limata, A. accicularia, E. (M.) bosqueti* and *Cytherois* sp. A monospecific assemblage of abundant *Cyprideis* sp. occurs also at the base of the red siltstone/fine-grained sandstone overlying limestone I and underlying limestone II. To date, the origin of these monospecific assemblages remains unresolved: the occurrence in a fluvial sandstone with abundant clasts of the white limestone (this only applies to the sandstone overlying limestone I) points to a reworked origin; by contrast, the monospecific nature of the assemblage, the well preservation of the valves and, only for limestone II, its presence underneath the limestone argues for an autochtonous nature of the fauna. Compared to limestone I, ostracods in limestones II are more abundant in species numbers, assemblages are fairly diversified since the base and four more species are present, namely *A. idonea, Z. venusta, Fabaeformiscandona, Tyrrhenocythere pontica*,

Tyrrhenocythere ruggierii and *Cytherura pirama*. Our taxonomic investigation of the Zorreras limestones differs substantially from the previous studies, which only reported *Cyprideis* sp., *Loxorniculina djaffarovi, Maeotocythere (Euxinocythere) preabaquana* and *Tyrrhenocythere pontica* (Roep and Van Harten, 1979; Ott d'Estevou, 1980; Aufgebauer and McCann, 2010).

Nijar. In the Barranco de los Castellones section, all four marl beds of the Upper Mb. of the Feos Fm. contain ostracods (Fig. A(I).3) with morphological and compositional features indicative of their autochtonous origin, confirming the previous investigation from Bassetti et al. (2006). The lowermost marl horizon is the least diversified and where the less abundant species number is found. The taxonomic investigation revealed the presence of 17 species, including *Cyprideis* sp., *Camptocypria* sp., *L. djafarovi, Loxoconcha mülleri, Loxoconcha eichwaldi, Euxinocythere (Maeotocythere) praebaquana, Euxinocythere (Maeotocythere) bosqueti, Amnicythere idonea, Amnicythere propinqua, Amnicythere accicularia, Loxocauda limata, Tyrrhenocythere pontica, Tyrrhenocythere ruggierii, Cytherura pirama, Cypria* sp., *Fabaeformiscandona* and *Cytherois* sp. Both the number of species and of specimens increase in the uppermost three marl horizons. In cycle II, *Zalaniella venusta, C. incongruens, Xestoleberis* sp. and, although only in one sample, *Loxoconcha kochi* appear. *A. multituberculata, Caspiocypris alta* and *A. subcaspia* only appear in rare to moderate abundance at the top of cycle III. In terms of species diversity, cycle IV differs from cycle III only because of the presence of *A. palimpsesta*. The difference between the two cycle is, however, sharper, because all the species are more abundant and more consistently present within the entire marl bed. Besides the first marl horizon, which we missed to recognize the contact with the underlying coarser-grained lithofacies, in the other three beds assemblages start poorly diversified with abundant *Cyprideis* sp. and diversify upwards.

The lowermost two samples of the Barranco del Negro section are highly diversified (Fig. A(I).2) and contain all the species recognized at the top of cycle IV in the Barranco de los Castellones section. In the Barranco del Negro section, ostracods are also found in the topmost black layer.

Cyprus. Up to 17 species of ostracods have been recognized in the few meters of marls underlying the M/P boundary in the Pissouri "gas station" section (Fig. A(I).4). These include:

Fig. A(I).3 (next page). *Ostracod distribution patterns of the Cerro Zorreras (Sorbas Basin) and Barranco de los Castellones (Nijar Basin) sections. The $^{87}Sr/^{86}Sr$ ratios measured on ostracod valves are also plotted against the reconstructed $^{87}Sr/^{86}Sr$ signature of an endorheic lake (Andreetto et al., 2021b) and the $^{87}Sr/^{86}Sr$ signature of coeval water in the oceans (McArthur et al., 2012), Eastern Paratethys (Grothe et al., 2020) and Mediterranean (i.e. the Lago-Mare water mass, for which definition we refer the reader to Andreetto et al., 2022a or chapter 4 of this work).*

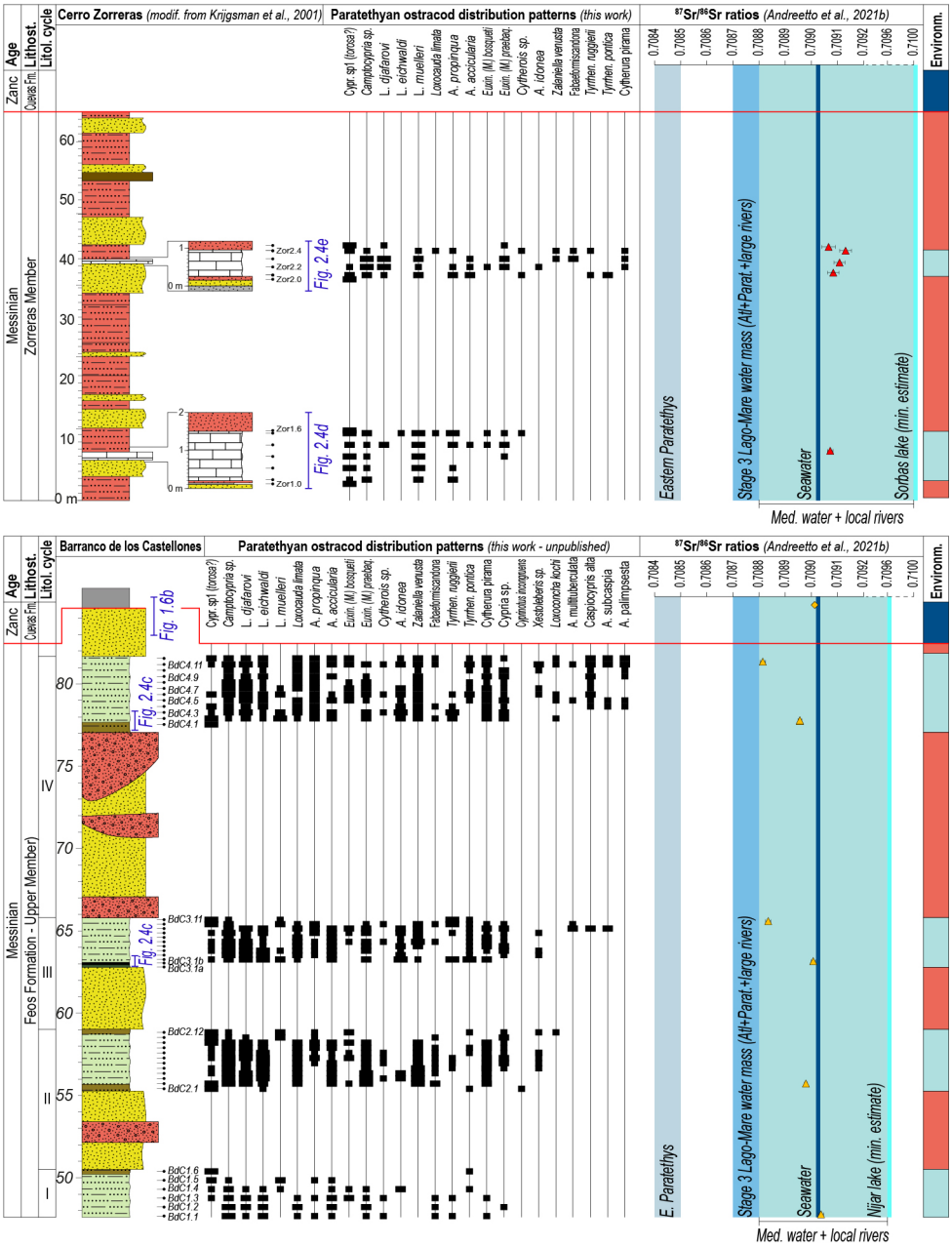
Cerro Zorreras (modif. from Krijgsman et al., 2001)
Paratethyan ostracod distribution patterns (this work)
87Sr/86Sr ratios (Andreetto et al., 2021b)
Age
Lithost.
Litol. cycle
Environm.
Messinian
Zorreras Member
Cyprideis Fm.
Zanc
Fig. 2.4e
Fig. 2.4d
Zor2.4
Zor2.2
Zor2.0
Zor1.6
Zor1.0
Cypr. sp1 (ironsa?)
Camptocypria sp.
L. djafarovi
L. eichwaldi
L. muelleri
Loxocauda limata
A. propinqua
A. acciculata
Euxin. (M.) bosquetti
Euxin. (M.) praebaq.
Cytheroïs sp.
A. idonea
Zalaniella venusta
Fabaeformiscandona
Tyrrhen. ruggieri
Tyrrhen. pontica
Cytherura pirama
0.7084
0.7085
0.7086
0.7087
0.7088
0.7089
0.7090
0.7091
0.7092
0.7096
0.7100
Eastern Paratethys
Stage 3 Lago-Mare water mass (Alt+Parat.+large rivers)
Seawater
Sorbas lake (min. estimate)
Med. water + local rivers
Barranco de los Castellones
Paratethyan ostracod distribution patterns (this work - unpublished)
Messinian
Feos Formation - Upper Member)
Fig. 1.6b
Fig. 2.4c
Fig. 2.4c
BdC4.11
BdC4.9
BdC4.7
BdC4.5
BdC4.3
BdC4.1
BdC3.11
BdC3.1b
BdC3.1a
BdC2.12
BdC2.1
BdC1.6
BdC1.5
BdC1.4
BdC1.3
BdC1.2
BdC1.1
Cypria sp.
Cyamotas iconigenis
Xestoleberis sp.
Loxoconcha kochi
A. multituberculata
Caspiocypris alta
A. subcaspia
A. palimpsesta
E. Paratethys
Stage 3 Lago-Mare water mass (Alt+Parat.+large rivers)
Seawater
Nijar lake (min. estimate)
Med. water + local rivers
Lithologies
Undifferentiated
fine-grained lithologies
a: White chalk (lagoonal); b: Red clay-/siltstones (continental)
c: Brown clays (lagoonal); d: White Zorreras limestones (lagoonal)
Conglomerate
Lithoarenite
Basement
Conglomeratic lag
Paleoenvironment
Marine
Lagoonal (i.e. connected to the LM water mass)
Continental

Fig. A(I).4. *Panoramic view of the Pissouri "gas station" section.*

Cyprideis torosa, Tyrrhenocythere pontica, Loxoconcha mulleri, L. kochi, L. eichwaldi, Loxorniculina djafarovi, Camptocypria sp., *Amnicythere idonea, A. propinqua, A. accicularia, Zalaniella venusta, Cypria* sp., *Euxinocythere praebaquana, Euxinocythere bosqueti, Loxocauda limata, Cytherura pirama, Xestoleberis* sp. (Fig. A(I).5).

A(I).3 Final considerations

The main conclusions that we can draw from these new data are the following:

> The ostracods assemblages identified in Malaga, Nijar, Sorbas and Pissouri are, taxonomically speaking, similar (they share more than 80% of the recognized species) and also with those found in roughly coeval sediments across the Mediterranean (chapter 1, see Fig. 1.2b for references) and the Black Sea (Stoica et al., 2016; Fig. A(I).6). Based on this taxonomic similarity, we consider that ostracods migrated from the Eastern Paratethys to the Mediterranean and from the Mediterranean into these marginal basins following the establishment of a water connection between the three settings.

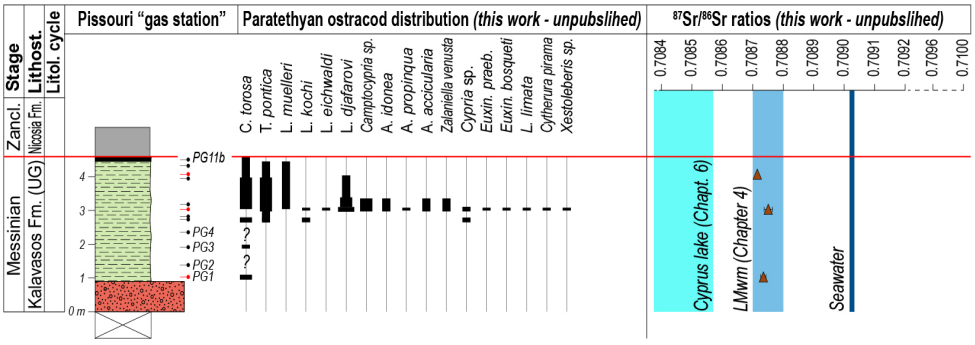

Fig. A(I).5. *Ostracod distribution patterns of the Pissouri "gas station" section, Cyprus. The $^{87}Sr/^{86}Sr$ratios measured on ostracod valves are also plotted against the reconstructed $^{87}Sr/^{86}Sr$ signature of an endorheic lake (Chapter 6) and the $^{87}Sr/^{86}Sr$ signature of coeval water in the oceans (McArthur et al., 2012) and in the Mediterranean (i.e. the Lago-Mare water mass, for which definition we refe the reader to Andreetto et al., 2022a or chapter 4 of this work).*

Region	SE Spain				Adriatic region						Sic	Crete	Cypr	
Basin/Section	Ma	V	So	Ni	Pd	Bu	Mc	Tr	Fp	Mo	Em	He	Pi	BS
References	1, 2	3	2	2	4	5, 6	5, 6	6	7	8	9	10	2	3
Cyprideis sp.	✖	✖	✖	✖	✖	✖	✖	✖	✖	✖	✖	✖	✖	✖
L. muelleri	✖	✖	✖	✖	✖	✖	✖	✖		✖	✖		✖	
L. kochi	✖	✖		✖	✖	✖		✖		✖	✖		✖	✖
L. eichwaldi	✖	✖		✖	✖	✖	✖	✖	✖	✖		✖	✖	✖
L. rhombovalis	✖					✖		✖		✖		✖		
L. djafarovi	✖	✖	✖	✖	✖	✖	✖	✖	✖	✖	✖	✖	✖	✖
Camptocypria sp.	✖	✖	✖	✖	✖	✖	✖	✖	✖	✖	✖	✖	✖	✖
Caspiocypris alta		✖		✖		✖	✖	✖	✖	✖	✖	✖		✖
Z. venusta	✖	✖	✖	✖	✖	✖	✖	✖	✖	✖		✖	✖	✖
Cypria sp.	✖			✖	✖	✖	✖	✖	✖	✖	✖		✖	
T. pontica	✖		✖	✖		✖	✖	✖	✖	✖	✖		✖	
T. ruggierii	✖	✖	✖	✖		✖	✖	✖	✖					✖
L. limata	✖	✖	✖	✖	✖		✖	✖	✖	✖		✖	✖	✖
C. pirama	✖	✖	✖	✖	✖		✖	✖	✖	✖	✖	✖	✖	✖
A. propinqua	✖	✖	✖	✖	✖	✖	✖	✖	✖	✖	✖	✖	✖	✖
A. multituberc.				✖	✖			✖				✖		✖
A. subcaspia				✖		✖		✖	✖	✖				✖
A. palimpsesta		✖		✖	✖	✖	✖	✖	✖	✖		✖		✖
A. accicularia	✖	✖	✖	✖	✖			✖	✖	✖	✖	✖	✖	✖
A. litica		✖							✖	✖				✖
A. idonea	✖	✖	✖	✖	✖								✖	
A. costata						✖			✖	✖	✖	✖		
Euxin. praebaquana		✖		✖	✖	✖	✖	✖	✖	✖	✖	✖	✖	✖
Euxin. praebosqueti	✖		✖	✖				✖	✖				✖	
Mediocytherideis sp.				✖				✖		✖				
Fabaef sp.							✖				✖			
Ilyocypris										✖				
Cypr. incongruens		✖												
Pontoniella pontica		✖				✖	✖	✖	✖			✖		✖
Cypria tocorjescui		✖												✖
Hastacandona lotzi					✖		✖							✖
Cytherois			✖	✖										
Typhlocypris sp.									✖					✖
Candona sp.				✖			✖							
Typhlocyprella annae							✖							
Lineocypris aff. br.							✖		✖					
Euxinocyth. bosqueti			✖	✖										
Xestoleberis sp.				✖									✖	

Fig. A(I).6. *Overview of the Black Sea (BS) ostracod distribution across the Mediterranean during cycle 7, which has the highest ostracod biodiversity. Acronyms: Ma: Malaga; V: Vera; So: Sorbas; Ni: Nijar; Pd: Piedmont; Bu: Buttafuoco; Mc: Maccarone; Tr: Trave; Fp: Fonte dei Pulcini; Mo: Molise; Em: Eraclea Minoa; He: Heraklion; Pi: Pissouri). References: 1: Guerra-Merchán et al. (2010); 2: Appendix I; 3: Stoica et al. (2016); 4: Chapter 3; 5: Chapter 5; 6: Grossi et al. (2008); 7: Cosentino et al. (2012); 8: Cosentino et al. (2018); 9: Grossi et al. (2015); 10: Cosentino et al. (2007). The blue color highlights those species that are reported from the late Miocene of the Black Sea region.*

> The Spanish basins and the Pissouri Basin were elevated thousands of meters above the Mediterranean floor and confirm our previous conclusion that occurrence of Paratethyan ostracods in these marginal basins serves as an ecological marker for the presence of a relatively full Mediterranean.

> An increase in ostracod species diversity typifies the ostracod-bearing sediments in the three Spanish basins considered here and in Pissouri. According to the paleoecological analyzes carried out by Gliozzi and Grossi (2008) on the Paratethyan ostracods, this increase in diversity indicates a deepening- and freshening-upward trend (see chapters 1, 2, 3, 4 for further insights).

> At least seven major highstands occurred during MSC Stage 3 prior to the initiation of gypsum precipitation in intermediate and deep basins. A problem that is not yet solved concerns the correlation of each ostracod-bearing lithology in these marginal basins with the Mediterranean highstands (see the Epilogue for insights).

APPENDIX II - ADDITIONAL STRONTIUM DATA & SUMMARY

A(II).1 Materials and methods

Additional strontium isotope ratios have been measured on samples from the Rio Mendelín section in the Malaga Basin, Spain (Fig. A(I).1) and in the Pissouri Basin, Cyprus (Fig. A(I).5).

Eleven (single) valves of *Cyprideis* sp. were hand-picked from ten ostracod-rich samples from the Rio Mendelín (7) and Pissouri "gas station" (3) section and prepared for strontium isotope analyses following the procedure detailed in Chapter 3. Isotopic measurements were carried out using a Thermo Scientific™ Triton™ thermal ionization mass spectrometer (TIMS) following the procedure of Lewis et al. (2017; see also Chapter 3 for details). Instrument performance was monitored using the NBS987 Sr standard, which gave an average of 0.710248 ± 0.00001 (2 SD, n=6). Procedural Sr blank is negligible based on replicate measurement of NBS987 Sr with the batch of column chromatography (0.710247±0.00001, n=2).

A(II).2 Results

The $^{87}Sr/^{86}Sr$ ratios measured on ostracod samples collected from the Rio Mendelín and Pissouri sections are lower than the range of coeval oceanic values (~0.709024; McArthur et al., 2012, Figs. A(I).1 and A(I).5). The $^{87}Sr/^{86}Sr$ isotope record is characterized by relatively stable $^{87}Sr/^{86}Sr$ ratios, ranging between 0.708742 and 0.708758 in Malaga (Fig. A(I).1) and 0.708715 to 0.708745 in Cyprus (Fig. A(I).5).

A(II).3 Preliminary interpretations and conclusions

The $^{87}Sr/^{86}Sr$ ratios from Malaga and Cyprus indicate that deposition of the marls took place in an environment strongly influenced by non-marine inputs. If this water body was an endorheic lake, then the $^{87}Sr/^{86}Sr$ value of the Paratethyan ostracod should reflect the $^{87}Sr/^{86}Sr$ ratio of all the river(s) flowing into the lake after the weathering and erosion of the isotopically-different, catchment-forming lithologies. $^{87}Sr/^{86}Sr$ data are available for present-day surficial and underground water at several locations in Cyprus (Ladegaard-Pedersen et al., 2020; Fig. 6.1b) and can be used to approximate the $^{87}Sr/^{86}Sr$ ratio of the paleorivers (e.g. Vasiliev et al., 2010, 2022; Andreetto et al., 2022b). As we explain in Chapter 6, the local reference $^{87}Sr/^{86}Sr$ signal ranges between 0.707879 and 0.708573. These two extremes corresponds to the $^{87}Sr/^{86}Sr$ ratios measured at sampling locations #6 and #25 (Ladegaard-Pedersen et al., 2020), where river water incorporates Sr^{2+} ions from at least two out of the three main lithologies present in the Cypriot watersheds, namely the Troodos ophiolites, a wide array of Upper Cretaceous-Upper Miocene carbonate and terrigenous rocks (Mamonia complex and pre-MSC formations in Fig. 6.1b) and the Messinian evaporites. $^{87}Sr/^{86}Sr$ ratios measured on the late Messinian ostracods in Pissouri

have acquired. This support the notion that the biota of the Pissouri "gas station" section thrived in an environment that was connected to the Lago-Mare water mass, which was carrying Sr^{2+} cations with a $^{87}Sr/^{86}Sr$ ratio (0.7087-0.7088; Andreetto et al., 2022a) compatible with the $^{87}Sr/^{86}Sr$ ratios of the ostracods.

$^{87}Sr/^{86}Sr$ data were recently made available also for the entire course of the Guadalhorce River, which is the main drainage system of the Malaga region today flowing through all the units forming the hinterland of the Malaga Basin (Glok-Galli et al., 2022). However, we believe that the $^{87}Sr/^{86}Sr$ data of the modern Guadalhorce River cannot be used as an analogue of the Messinian Malaga paleorivers. These $^{87}Sr/^{86}Sr$ data are concluded to be strongly affected by anthropogenic sources (Glok-Galli et al., 2022). Another possibility to gain insights into the $^{87}Sr/^{86}Sr$ signature of the Messinian Malaga paleorivers would be to use the $^{87}Sr/^{86}Sr$ ratios of the potential source rocks in the local hinterlands and to run a three-component mass-balance model to obtain the array of values of mixture of the selected end-members in different proportions (see chapter 2). However, we believe than an approximation of the $^{87}Sr/^{86}Sr$ signature of the Malaga paleorivers by means of this approach is difficult to accomplish for a twofold reason: (i) $^{87}Sr/^{86}Sr$ data from bulk rocks from the three most abundant catchment-forming units are scarce (Alpujárride; Varas-Reus et al., 2017) or absent (Malaguide and Flysch) in the literature; (ii) these units cover a fairly equal area (Fig. A(I).1), making it difficult to constrain the model results by means of the assumption adopted for the Sorbas, Nijar and Vera basins in chapter 2 that the catchment area is proportional to discharge (e.g. Placzek et al., 2011; see section 2.5.4 for insights). Nevertheless we cannot infer the $^{87}Sr/^{86}Sr$ ratios of an hypothetical endorheic lake filling the Malaga Basin, the presence of Paratethyan ostracods supports the notion that also the Malaga $^{87}Sr/^{86}Sr$ ratios reflect the mixing between local river water and Atlantic-Paratethys-large river waters from the open Mediterranean Basin.

A(II).4 Final considerations

The deposits belonging to the three stages of the Messinian Salinity Crisis have been traditionally regarded as being characterized by well-defined ranges of $^{87}Sr/^{86}Sr$ isotopic ratios (Topper et al., 2011; Roveri et al., 2014a, b): Stage 1 (mostly gypsum) samples show values between ~0.7090 and 0.7089, that are in the range or slightly detached from the coeval global ocean signature; Stage 2 halite samples are as low as 0.7088, therefore suggesting the presence of a more diluted water mass than during Stage 1; Stage 3 yields the lowest and most depleted values (as low as 0.7086; Fig. 2.4a). This trend has been interpreted as geochemical evidence for the restriction of Mediterranean-Atlantic connectivity accompanied by a proportional increase in low-salinity water supplied from Eastern Paratethys and/or major peri-Mediterranean rivers (Flecker et al., 2002; Flecker and Ellam, 2006; Vasiliev et al., 2010, 2017; Reghizzi et al., 2018; Grothe et al., 2020). This statement proves true only if only the measurements on samples of evaporites are considered. As we show in chapter 4, the more depleted values of the Stage 3

gypsums (0.7087-0.7088 in Eraclea Minoa; average of 0.708752) compared to the Stage 1 gypsums (0.7090-0.7089; average of 0.708941) reflect a decrease in the seawater/non-seawater ratio in the Mediterranean, which during Stage 3 was, at most, 1:5 (Fig. 4.5).

However, in this doctoral dissertation the $^{87}Sr/^{86}Sr$ database relative to Stage 3 of the Messinian Salinity Crisis has been significantly expanded. The addition of several new $^{87}Sr/^{86}Sr$ data (listed in table A1 and shown in Fig. A(III).1) from ostracods that inhabited marginal basins (Malaga, Sorbas, Nijar, Vera, Pissouri) or basins (Piedmont, Cella-Giaggiolo, Laga) belonging to a silled (Adriatic) region show that Stage 3 is not characterized by well-defined ranges of $^{87}Sr/^{86}Sr$ ratios, which span through a wide array of values from >0.7091 to ~0.7084. In Fig. A(II).1 are illustrated two of the key results of this thesis:

(i) $^{87}Sr/^{86}Sr$ ratios measured on Stage 3 material have no simple chronostratigraphic value;

(ii) At least in the marginal basins, local lithological differences in the catchments explain the different Sr isotopic compositions from basin to basin.

More broadly, our results show that a thorough analysis of the geology of the catchments of individual basins is prerequisite to a correct interpretation, in terms of water provenance and basin connectivity, of $^{87}Sr/^{86}Sr$ isotopes on material that precipitated/deposited in restricted basins.

Fig. A(II).1 (next page). *Schematic compilation of all $^{87}Sr/^{86}Sr$ isotope ratios measured in this thesis and compiled in Table A(III). The ratios measured by Grossi et al. (2015) on Eraclea Minoa ostracods, Fortuin et al. (1995) on Vera ostracods and McCulloch and De Deckker (1989) on Sorbas ostracods have been added for completeness. The height of each rectangle is determined by the largest and smallest value of each data cluster, including their analytical errors. The breadth of each rectangle is plotted using the chronostratigraphic framework proposed in Fig. E.1 to the resolution of the precessional cycle (see the epilogue for insights into how this chronostratigraphic framework was built and what the age uncertainties are). In cycle 7, all data from the marginal basins are entirely included in the highstand phase due to the lack of tools to determine their exact duration. According to the results of chapter 6, the data from the Polemi gypsums should pre-date the data from the coeval gypsums of Eraclea Minoa. However, for graphic reasons (the rectangle corresponding to the Polemi data would result too small to be appreciated), these data span the same time in this figure.*

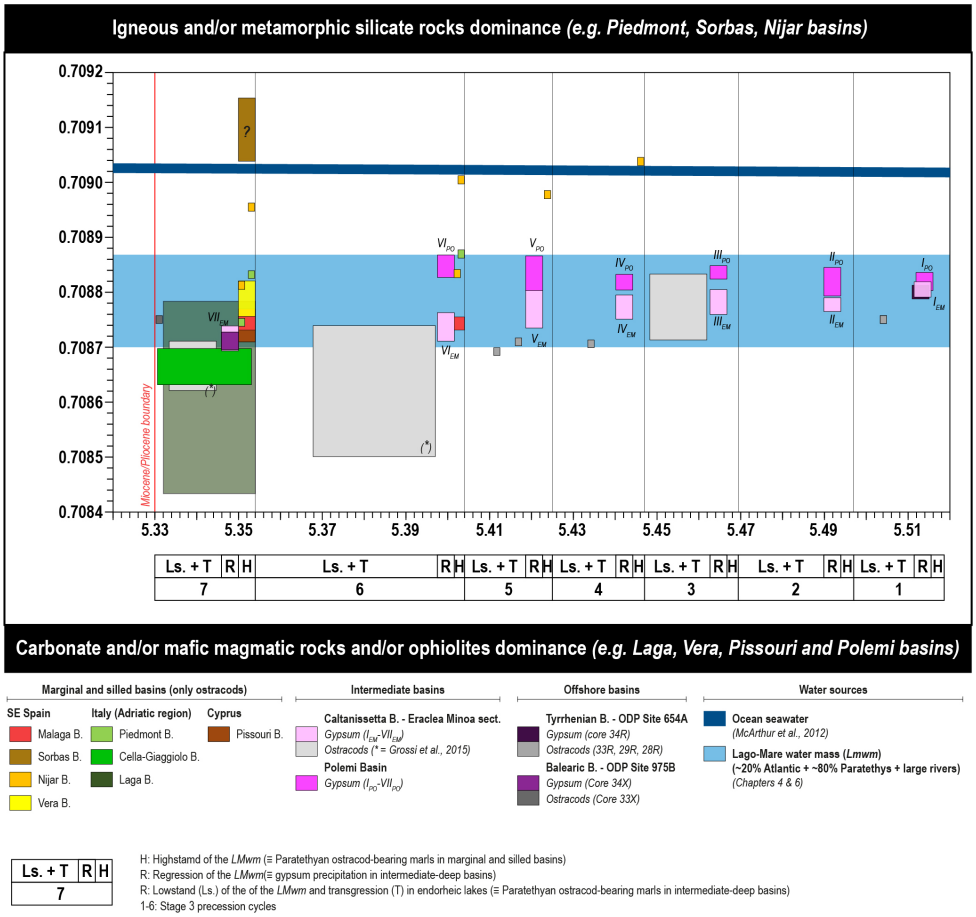

Table A1. Compilation of the $^{87}Sr/^{86}Sr$ ratios measured in this work for Stage 3 deposits onshore. The age and cycle number are assigned based on the chronostratigraphic scheme in the Epilogue (Fig. E.1; see for explanations).

Spain

Locality: Malaga
Basin - Section: Malaga - Rio Mendelín
Coordinates: 36°45'01.0"N, 4°25'58.3"W
Data source: Appendix II, unpublished data

Strat. height (m)	Sample	Unit	Age (Ma)-Cycle	Material	$^{87}Sr/^{86}Sr$	2σ (*10^{-6})
32.7	P2.34	LM Unit	5.3500 - 7	*Cyprideis sp.*	0.708753	0.000006
29.8	P2.21	LM Unit	5.3515 - 7	*Cyprideis sp.*	0.708742	0.000011
27.5	P2.11	LM Unit	5.3530 - 7	*Cyprideis sp.*	0.708752	0.000006
25.3	P2.1	LM Unit	5.3540 - 7	*Cyprideis sp.*	0.708758	0.000012
19.8	P1.14	LM Unit	5.4010 - 6	*Cyprideis sp.*	0.708743	0.000008
18	P1.11	LM Unit	5.4015 - 6	*Cyprideis sp.*	0.708742	0.000011
14.7	P1.5	LM Unit	5.4020 - 6	*Cyprideis sp.*	0.708749	0.000006

Locality: Sorbas
Basin - Section: Sorbas - unknown*
Coordinates: Not applicable*
Data source: Chapter 2, Andreetto et al. (2021b)

Strat. height (m)	Sample	Unit	Age (Ma)-Cycle	Material	$^{87}Sr/^{86}Sr$	2σ (*10^{-6})
Not applicable*	Fo1	Zorreras Mb.	Not applicable*	Limestone	0.709072	0.000011

* *The measurement is performed on one white limestones of the Zorreras Mb. However, the provenance of the sample (section and which of the two imestones) is unknown. As a consequence, the age and cycle also cannot be determined.*

Locality: Nijar
Basin - Sections: Nijar - Section: (1) Barranco de los Castellones (samples N1, N2, $N3_b$, $N3_t$, $N4_b$, $N4_T$), (2) Cerro de los Ranchos (sample $N4_b^*$), (3) El Salto del Lobo (sample: Fo3)
Coordinates: (1) 37°00'51.1"N, 2°00'05.7"W, (2) Unknown, (3) Unknown
Data source: Chapter 2, Andreetto et al. (2021b)

Strat. height (m)	Sample	Unit	Age (Ma)-Cycle	Material	$^{87}Sr/^{86}Sr$	2σ (*10^{-6})
105	$N4_b^*$	Feos Fm.	5.3540 - 7	*Cyprideis sp.*	0.708954	0.000008
80	$N4_t$	Feos Fm.	5.3500 - 7	*Cyprideis sp.*	0.708814	0.000010
77	$N4_b$	Feos Fm.	5.3540 - 7	*Cyprideis sp.*	0.708958	0.000008
65	$N3_t$	Feos Fm.	5.4010 - 6	*Cyprideis sp.*	0.708835	0.000010
63	$N3_b$	Feos Fm.	5.4020 - 6	*Cyprideis sp.*	0.709007	0.000008
55	N2	Feos Fm.	5.4240 - 5	*Cyprideis sp.*	0.708979	0.000006
48	N1	Feos Fm.	5.4460 - 4	*Cyprideis sp.*	0.709037	0.000010
Not applicable*	Fo3	Feos Fm.	Not applicable*	*Cyprideis sp.*	0.709099	0.000012

* *The stratigraphic log of the El Salto del Lobo section is not provided. As a consequence, the age and cycle also cannot be determined.*

Locality: Vera
Basin - Section: Vera - unknown section (V1-V2)
Coordinates: 37°17'00"N, 1°50'33"W
Data source: Chapter 2, Andreetto et al. (2021b)

Strat. height (m)	Sample	Unit	Age (Ma)-Cycle	Material	$^{87}Sr/^{86}Sr$	2σ (*10^{-6})
Not applicable*	V2	Unit 2	Not. applic.* - 7	*Cyprideis sp.*	0.708764	0.000012
Not applicable*	V1	Unit 2	Not. applic.* - 7	*Cyprideis sp.*	0.708766	0.000011

* *The analyzed samples come from an outcrop an outcrop next to the Cuevas del Almanzora section. However, the stratigraphic log is not available.*

Italy

Locality: Piedmont
Basin - Section: Piedmont - Pollenzo
Coordinates: 44°41'08"N, 7°55'33"E
Data source: Chapter 3, Andreetto et al. (2022b)

Strat. height (m)	Sample	Unit	Age (Ma)-Cycle	Material	$^{87}Sr/^{86}Sr$	2σ (*10^{-6})
23	FSS11	AAF	5.331	*T. ruggierii*	0.708746	0.000005
22	FSS4	CSC (Mb. C)	5.3500 - 7	*T. ruggierii*	0.708752	0.000005
21.1	FSS3	CSC (Mb. C)	5.3513 - 7	*T. ruggierii*	0.708746	0.000005
19.5	LM15	CSC (Mb. C)	5.3533 - 7	*C. torosa*	0.708831	0.000006
19.2	LM14	CSC (Mb. C)	5.3540 - 7	*C. torosa*	0.708834	0.000005
9.3	PA43	CSC (Mb. A)	5.4015 - 6	*C. torosa*	0.708871	0.000004
8.9	PA42	CSC (Mb. A)	5.4020 - 6	*C. torosa*	0.708870	0.000004

CSC: Cassano Spinola Conglomerates; Mb.: Member.

Locality: Romagna
Basin - Section: Cella-Giaggiolo - Buttafuoco
Coordinates: 44°05'00.5"N 12°01'51.9"E
Data source: Chapter 5, unpublished data

Strat. height (m)	Sample	Unit	Age (Ma)-Cycle	Material	$^{87}Sr/^{86}Sr$	2σ (*10^{-6})
0.50	BU9	Colombacci Fm.	5.3310 - 7	*C. torosa*	0.708688	0.000009
1.50	BU7	Colombacci Fm.	5.3400 - 7	*C. torosa*	0.708657	0.000004
3.50	BU5	Colombacci Fm.	5.3450 - 7	*C. torosa*	0.708663	0.000014
5.50	BU3	Colombacci Fm.	5.3500 - 7	*C. torosa*	0.708658	0.000008
7.50	BU1	Colombacci Fm.	5.3540 - 7	*C. torosa*	0.708641	0.000006

* *The stratigraphic height is here expressed in meters down from the Miocene/Pliocene boundary.*

Locality: Apiro
Basin - Section: Laga - Maccarone
Coordinates: 43°24'22.9"N, 13°06'15.0"E
Data source: Chapter 5, unpublished data

Strat. height (m)	Sample	Unit	Age (Ma)-Cycle	Material	$^{87}Sr/^{86}Sr$	2σ (*10^{-6})
193	MC193	Colombacci Fm.	5.3320 - 7	*C. torosa*	0.708477	0.000005
191	MC191	Colombacci Fm.	5.3390 - 7	*C. torosa*	0.708438	0.000002
186	MC186	Colombacci Fm.	5.3450 - 7	*C. torosa*	0.708586	0.000009
184	MC184	Colombacci Fm.	5.3500 - 7	*C. torosa*	0.708752	0.000031
182	MC182	Colombacci Fm.	5.3540 - 7	*C. torosa*	0.708667	0.000009

Locality: Eraclea Minoa (Sicily)
Basin - Section: Caltanissetta - Eraclea Minoa
Coordinates: 43°24'22.9"N, 13°06'15.0"E
Data source: Chapter 4, Andreetto et al. (2022a)

Strat. height (m)	Sample	Unit	Age (Ma)-Cycle	Material	$^{87}Sr/^{86}Sr$	2σ (*10^{-6})
233.5	EM8-11	Upper Gypsum	5.3380 - 7	*C. agrigentina*	0.708640	0.000006
232	EM8-9	Upper Gypsum	5.3390 - 7	*C. agrigentina*	0.708630	0.000008
231	EM8-7	Upper Gypsum	5.3405 - 7	*C. agrigentina*	0.708647	0.000010
228.5	EM8-3	Upper Gypsum	5.3420 - 7	*C. agrigentina*	0.708704	0.000007
226.2	G7-8	Upper Gypsum	5.3430 - 7	Selenitic gypsum	0.708710	0.000008
225.7	G7-6	Upper Gypsum	5.3437 - 7	Selenitic gypsum	0.708704	0.000011
225	G7-4	Upper Gypsum	5.3440 - 7	Selenitic gypsum	0.708730	0.000014
224.2	G7-1	Upper Gypsum	5.3450 - 7	Selenitic gypsum	0.708720	0.000007
154.2	EM-84	Upper Gypsum	5.3906 - 6	Selenitic gypsum	0.708735	0.000012
152.5	EM-78	Upper Gypsum	5.3908 - 6	Selenitic gypsum	0.708744	0.000012
151	EM-76	Upper Gypsum	5.3910 - 6	Selenitic gypsum	0.708740	0.000014
149	EM-69	Upper Gypsum	5.3912 - 6	Selenitic gypsum	0.708723	0.000013
148.5	EM-64	Upper Gypsum	5.3914 - 6	Balatino gypsum	0.708747	0.000012
148	EM-63	Upper Gypsum	5.3916 - 6	Balatino gypsum	0.708738	0.000013
133.8	EM-58	Upper Gypsum	5.4192 - 5	Selenitic gypsum	0.708748	0.000013
132.8	EM-56	Upper Gypsum	5.4198 - 5	Selenitic gypsum	0.708748	0.000012
132.2	EM-54	Upper Gypsum	5.4202 - 5	Selenitic gypsum	0.708756	0.000012
131.3	EM-52	Upper Gypsum	5.4206 - 5	Selenitic gypsum	0.708776	0.000014
130.6	EM-38	Upper Gypsum	5.4210 - 5	Selenitic gypsum	0.708756	0.000013
129.8	EM-36	Upper Gypsum	5.4214 - 5	Selenitic gypsum	0.708765	0.000016
129	EM-34	Upper Gypsum	5.4218 - 5	Selenitic gypsum	0.708770	0.000014
128.2	EM-33	Upper Gypsum	5.4222 - 5	Selenitic gypsum	0.708764	0.000014
127.5	EM-31	Upper Gypsum	5.4226 - 5	Selenitic gypsum	0.708777	0.000014
126.6	EM-25	Upper Gypsum	5.4230 - 5	Balatino gypsum	0.708789	0.000014
115.8	G4-10	Upper Gypsum	5.4416 - 4	Selenitic gypsum	0.708760	0.000006
114.5	G4-8	Upper Gypsum	5.4422 - 4	Selenitic gypsum	0.708765	0.000005
113	G4-6	Upper Gypsum	5.4428 - 4	Selenitic gypsum	0.708767	0.000009
111.5	G4-4	Upper Gypsum	5.4434 - 4	Selenitic gypsum	0.708767	0.000008
109.5	G4-1	Upper Gypsum	5.4440 - 4	Selenitic gypsum	0.708786	0.000004

105	EM4-19	Upper Gypsum	5.4544 - 3	*C. agrigentina*	0.708725	0.000012
104	EM4-17	Upper Gypsum	5.4558 - 3	*C. agrigentina*	0.708800	0.000030
94	EM4-0K	Upper Gypsum	5.4586 - 3	*C. agrigentina*	0.708827	0.000006
88	EM4-00a	Upper Gypsum	5.4600 - 3	*C. agrigentina*	0.708730	0.000012
87.70	G3-11	Upper Gypsum	5.4645 - 3	Selenitic gypsum	0.708769	0.000006
87.05	G3-9	Upper Gypsum	5.4650 - 3	Selenitic gypsum	0.708778	0.000006
86.4	G3-7	Upper Gypsum	5.4655 - 3	Selenitic gypsum	0.708796	0.000007
85.5	G3-4	Upper Gypsum	5.4660 - 3	Selenitic gypsum	0.708779	0.000006
85.15	G3-3	Upper Gypsum	5.4665 - 3	Selenitic gypsum	0.708780	0.000006
84.5	G3-1	Upper Gypsum	5.4670 - 3	Selenitic gypsum	0.708785	0.000006
47.75	G2-11	Upper Gypsum	5.4915 - 2	Selenitic gypsum	0.708780	0.000006
47.2	G2-9	Upper Gypsum	5.4920 - 2	Selenitic gypsum	0.708776	0.000007
46.65	G2-7	Upper Gypsum	5.4925 - 2	Selenitic gypsum	0.708774	0.000008
46.1	G2-5	Upper Gypsum	5.4930 - 2	Selenitic gypsum	0.708781	0.000005
45.55	G2-3	Upper Gypsum	5.4935 - 2	Selenitic gypsum	0.708780	0.000008
45	G2-1	Upper Gypsum	5.4940 - 2	Selenitic gypsum	0.708778	0.000006
2.7	Cum-5	Upper Gypsum	5.5100 - 1	Balatino gypsum	0.708800	0.000006
1.5	Cum-3	Upper Gypsum	5.5155 - 1	Balatino gypsum	0.708810	0.000006

Cyprus

Locality: Polemi
Basin - Section: Polemi - Polemi composite
Coordinates: 34°51′43″N, 32°30′34″E (LE11-LE26); 34°51′45″N, 32°30′33″E (LE33-LE41); 34°51′47.1″N, 32°30′30.5″E (LE52); 34°51′36″N, 32°30′50″E (LE62-LE65a); 34°52′17″N, 32°31′02″E (PO3-PO19).
Data source: Chapter 6, unpublished data

Strat. height (m)	Sample	Unit	Age (Ma) - Cycle	Material	$^{87}Sr/^{86}Sr$	2σ (*10^{-6})
Not applicable*	PO19	Upper Gypsum	5.3930 - 6	Balatino gypsum	0.708843	0.000017
Not applicable	PO12	Upper Gypsum	5.4240 - 5	Selenitic gypsum	0.708822	0.000014
Not applicable	PO10	Upper Gypsum	5.4244 - 5	Selenitic gypsum	0.708819	0.000009
Not applicable	PO9	Upper Gypsum	5.4248 - 5	Selenitic gypsum	0.708813	0.000009
Not applicable	PO3	Upper Gypsum	5.4252 - 5	Microcrystal. gyp	0.708852	0.000013
Not applicable	LE65a	Upper Gypsum	5.4450 - 4	Granular gyp.	0.708824	0.000016
Not applicable	LE62	Upper Gypsum	5.4455 - 4	Balatino gypsum	0.708819	0.000012
Not applicable	LE52	Upper Gypsum	5.4680 - 3	Balatino gypsum	0.708835	0.000011
Not applicable	LE41	Upper Gypsum	5.4945 - 2	Selenitic gypsum	0.708805	0.000007
Not applicable	LE39	Upper Gypsum	5.4949 - 2	Selenitic gypsum	0.708802	0.000012
Not applicable	LE36	Upper Gypsum	5.4953 - 2	Selenitic gypsum	0.708816	0.000010
Not applicable	LE33	Upper Gypsum	5.4957 - 2	Selenitic gypsum	0.708833	0.000012
Not applicable	LE26	Upper Gypsum	5.5130 - 1	Selenitic gypsum	0.708926	0.000007
Not applicable	LE22	Upper Gypsum	5.5120 - 1	Selenitic gypsum	0.708827	0.000009
Not applicable	LE17	Upper Gypsum	5.5130 - 1	Selenitic gypsum	0.708817	0.000008
Not applicable	LE11	Upper Gypsum	5.5142 - 1	Balatino gypsum	0.708827	0.000005

* *The total height of the Polemi section cannot be evaluated due to its composite nature.*

Locality: Pissouri
Basin - Section: Pissouri - Pissouri "gas station"
Coordinates: 34°40′54.9″N, 32°42′06.3″E
Data source: Appendix II, unpublished data

Strat. height (m)	Sample	Unit	Age (Ma)-Cycle	Material	$^{87}Sr/^{86}Sr$	2σ (*10^{-6})
4	PG10	Upper Gypsum	5.3510 - 7	*Cyprideis sp.*	0.708715	0.000006
3	PG07	Upper Gypsum	5.3525 - 7	*Cyprideis sp.*	0.708751	0.000014
1.05	PG01	Upper Gypsum	5.3540 - 7	*Cyprideis sp.*	0.708735	0.000009

Table A2. Compilation of the $^{87}Sr/^{86}Sr$ ratios measured in this work for Stage 3 deposits offhore. The age and cycle number are assigned based on the stratigraphic correlation with the Eraclea Minoa section (Fig. 6.2) and the chronostratigraphic scheme in the Epilogue (Fig. E.1; see for explanations).

Western (975B) and Central (654A) Mediterranean

Locality: South Balearic Margin (975B); upper Sardinia margin (654A)
Basin (Well site): Balearic Basin (975B); Tyrrhenian Basin (654A)
Seismostratigraphic unit: Upper Unit
Coordinates: 38°53.786'N, 4°30.596'E (975B); 40°34.76'N, 10°41.80'E (654A)
Data source: Chapter 6, unpublished data

Strat. depth (mbsl)	Sample	Age (Ma)-Cycle	Material	$^{87}Sr/^{86}Sr$	2σ ($*10^{-6}$)
305.50	975B-33X-3, 49-51	5.3340 - 7	Mixed Parat. ostr.	0.708753	0.000007
311.45	975B-34X-1, 142-145	5.3475 - 7	Balatino gypsum	0.708725	0.000002
312.45	975B-34X-2, 90-93	5.3480 - 7	Balatino gypsum	0.708722	0.000004
312.95	975B-34X-2, 144-147	5.3485 - 7	Balatino gypsum	0.708697	0.000005
313.60	975B-34X-3, 82-84	5.3490 - 7	Balatino gypsum	0.708705	0.000005
256.60	654A-28R-4, 12-14	5.4170 - 5	*Cyprideis sp.*	0.708718	0.000008
262.00	654A-29R-1, 30-32	5.4120 - 5	*Cyprideis sp.*	0.708690	0.000007
263.30	654A-29R-2, 32-34	5.4340 - 4	*Cyprideis sp.*	0.708713	0.000006
288.20	654A-33R-1, 60-62	5.5040 - 1	*Cyprideis sp.*	0.708753	0.000007
291.20	654A-34R-1, 56-58	5.5115 - 1	Balatino gypsum	0.708792	0.000005
292.80	654A-34R-2, 63-65	5.5120 - 1	Balatino gypsum	0.708805	0.000007
294.40	654A-34R-3, 82-84	5.5130 - 1	Balatino gypsum	0.708814	0.000009
295.40	654A-34R-4, 26-27	5.5142 - 1	Balatino gypsum	0.708789	0.000004

A

ACKNOWLEDGMENTS

An immense thank you to my supervisors, Wout Krijgsman and Rachel Flecker. The support, advices and guidance throughout the project from you all has been invaluable. I also could not have undertaken this journey without my defense committee, who generously provided knowledge and expertise. Thank you to all the academics who helped me get to this stage and to Vanni Aloisi, without whom I would have never achieved what I did. Your SALTGIANT project and the way you led it have been amazing. Thank you, of course, to the Saltgiant fellow I've worked so closely on this project with: Fadl, Jimmy, Hanneke, Francesca, Ronja, Simon (x2), Beatriz, Laetitia, Athina, Mariam, Gaia, Maria, Michael…it's been great fun working with you all! Lastly, I would be remiss in not mentioning my family, especially my parents, Eline and friends for their belief in me, encouragement and support during this adventure.

CV

ABOUT THE AUTHOR

Federico Andreetto completed a bachelor's degree (2012-2015) and a master's degree (cum laude; 2015-2017) in Geology at the University of Turin.

In the early 2018, Federico received an Erasmus Traineeship scholarship to continue at the University of Barcelona the master's thesis project on the Lorca Basin (SE Spain) started with the Spanish colleagues. In the spring of 2018, Federico was selected as one of the Early Stage Researchers in the European Union's Horizon 2020 SALTGIANT (Understanding the Mediterranean Salt Giant) project. His position was based at the Department of Geoscience of the Utrecht University, the Netherlands. In this position, Federico organised and/or assisted numerous fieldworks in Spain (Malaga, Sorbas, Nijar and Lorca), Italy (Piedmont, Northern-Central Apennines and Sicily), Northern Greece (Akropotamos) and Cyprus, where he was mainly responsible for paleomagnetic, stratigraphic and sedimentological studies. Over the course of the PhD, Federico took part to numerous staying in Bristol (United Kingdom) as part of the secondment planning, where he was trained in the laboratory activities to successfully measure radiogenic strontium isotopes on carbonate material and gypsum.

Over the course of his PhD, Federico has been actively involved in teaching activities that included assistance in class courses in such disciplines as sedimentology and stratigraphy and in field works in the Pyrenees (May 2019), in Limburg (June 2021) and SE Spain (June 2022).

PEER REVIEWED PUBLICATIONS

Contents lists available at ScienceDirect

Earth and Planetary Science Letters

www.elsevier.com/locate/epsl

High-amplitude water-level fluctuations at the end of the Mediterranean Messinian Salinity Crisis: Implications for gypsum formation, connectivity and global climate

F. Andreetto [a,*], R. Flecker [b], G. Aloisi [c], A.M. Mancini [d], L. Guibourdenche [c], S. de Villiers [e], W. Krijgsman [a]

Contents lists available at ScienceDirect

Palaeogeography, Palaeoclimatology, Palaeoecology

journal homepage: www.elsevier.com/locate/palaeo

Multi-proxy investigation of the post-evaporitic succession of the Piedmont Basin (Pollenzo section, NW Italy): A new piece in the Stage 3 puzzle of the Messinian Salinity Crisis

F. Andreetto [a,*], A.M. Mancini [b], R. Flecker [c], R. Gennari [b], J. Lewis [d], F. Lozar [b], M. Natalicchio [b], F. Sangiorgi [a], M. Stoica [e], F. Dela Pierre [b], W. Krijgsman [a]

Contents lists available at ScienceDirect

Earth-Science Reviews

journal homepage: www.elsevier.com/locate/earscirev

Freshening of the Mediterranean Salt Giant: controversies and certainties around the terminal (Upper Gypsum and Lago-Mare) phases of the Messinian Salinity Crisis

F. Andreetto [a,*], G. Aloisi [b], F. Raad [c], H. Heida [d], R. Flecker [e], K. Agiadi [f], J. Lofi [c], S. Blondel [g], F. Bulian [h], A. Camerlenghi [g], A. Caruso [i], R. Ebner [j], D. Garcia-Castellanos [d], V. Gaullier [k], L. Guibourdenche [b], Z. Gvirtzman [l,m], T.M. Hoyle [a,n], P.T. Meijer [j], J. Moneron [l,m], F.J. Sierro [h], G. Travan [k], A. Tzevahirtzian [i], I. Vasiliev [o], W. Krijgsman [a]

Contents lists available at ScienceDirect

Palaeogeography, Palaeoclimatology, Palaeoecology

journal homepage: www.elsevier.com/locate/palaeo

High Mediterranean water-level during the Lago-Mare phase of the Messinian Salinity Crisis: insights from the Sr isotope records of Spanish marginal basins (SE Spain)

F. Andreetto [a,*], K. Matsubara [b], C.J. Beets [b], A.R. Fortuin [b], R. Flecker [c], W. Krijgsman [a]

Contents lists available at ScienceDirect

Earth-Science Reviews

journal homepage: www.elsevier.com/locate/earscirev

Review Article

Changing seas in the late Miocene Northern Aegean: A Paratethyan approach to Mediterranean basin evolution

Wout Krijgsman[a,*], Dan V. Palcu[b], Federico Andreetto[a], Marius Stoica[c], Oleg Mandic[d]

Contents lists available at ScienceDirect

Earth and Planetary Science Letters

www.elsevier.com/locate/epsl

Paratethys pacing of the Messinian Salinity Crisis: Low salinity waters contributing to gypsum precipitation?

Arjen Grothe [a], Federico Andreetto [a], Gert-Jan Reichart [a,b], Mariette Wolthers [a], Christiaan G.C. Van Baak [a,c], Iuliana Vasiliev [d], Marius Stoica [e], Francesca Sangiorgi [a], Jack J. Middelburg [a], Gareth R. Davies [f], Wout Krijgsman [a,*]

frontiers in Microbiology

ORIGINAL RESEARCH
published: 21 May 2019
doi: 10.3389/fmicb.2019.01031

Potential Fossilized Sulfide-Oxidizing Bacteria in the Upper Miocene Sulfur-Bearing Limestones From the Lorca Basin (SE Spain): Paleoenvironmental Implications

Federico Andreetto[1], Francesco Dela Pierre[1], Luis Gibert[2], Marcello Natalicchio[1] and Simona Ferrando[1]*

Ref.

LIST OF REFERENCES

Abdel Aal, A., El Barkooky, A., Gerrits, M., Meyer, H., et al., 2000. Tectonic evolution of the eastern Mediterranean Basin and its significance for hydrocarbon prospectivity in the ultradeepwater of the Nile Delta. The Leading Edge 19, 1086-1102.

Abdel-Fattah, M. I., 2014. Petrophysical characteristics of the messinian abu madi formation in the baltim east and north fields, offshore Nile delta, Egypt. Journal of Petroleum Geology, 37(2), 183-195.

Albarède, F., Michard, A., 1987. Evidence for slowly changing $^{87}Sr/^{86}Sr$ in runoff from freshwater limestones of southern France.

Agiadi, K., Antonarakou, A., Kontakiotis, G., Kafousia, N., Moissette, P., Cornée, J.-J., Manoutsoglou, E., Karakitsios, V., 2017. Connectivity controls on the late Miocene eastern Mediterranean fish fauna. Int. J. Earth Sci. 106, 1147-1159.

Agnini, C., Monechi, S., Raffi, I., 2017. Calcareous nannofossil biostratigraphy: historical background and alication in Cenozoic chronostratigraphy. Lethaia 50(3), 447-463.

Aguirre, J., 1998. El Plioceno del SE de la Peninsula Iberica (provincia de Almeria). Sintesis estratigrafica, sedimentaria, bioestratigrafica y paleogeografica. Rev. Soc. Geol. Esp. 11, 295-315.

Aguirre, J., Sánchez-Almazo, I.M., 2004. The Messinian post-evaporitic deposits of the Gafares area (Almeria-Nijar basin, SE Spain). A new view of the "Lago-Mare" facies. Sedimentary Geology 168, 71-95.

Albarède, F., Michard, A., 1987. Evidence for slowly changing $^{87}Sr/^{86}Sr$ in runoff from freshwater limestones of southern France, Chem. Geol., 64, 55-65.

Aloisi, G., Guibourdenche, L., Natalicchio, M., Caruso, A., Haffert, L., El Kilany, A., Pierre, F.D., 2022. The geochemical riddle of "low-salinity gypsum" deposits. Geochimica et Cosmochimica Acta, 327, 247-275.

Amadori, C., Garcia-Castellanos, D., Toscani, G., Sternai, P., Fantoni, R., Ghielmi, M., Di Giulio, A., 2018. Restored topography of the Po Plain-Northern Adriatic region during the Messinian base level drop-Implications for the physiography and compartmentalization of the paleo-Mediterranean basin. Basin Research, 30(6), 1247-1263.

Amarathunga, U., Hogg, A.M., Rohling, E.J., Roberts, A.P., Grant, K.M., et al., 2022. Sill-controlled salinity contrasts followed post-Messinian flooding of the Mediterranean. Nature Geoscience, 1-6.

Andersen, N., Paul, H.A., Bernasconi, S.M., McKenzie, J.A., Behrens, A., et al., 2001. Large and rapid climate variability during the Messinian salinity crisis: evidence from deuterium concentrations of individual biomarkers. Geology 29, 799-802.

Andreetto, F., Aloisi, G., Raad, F., Heida, H., Flecker, R., Agiadi, K., Lofi, J., Blondel, S., et al., 2021a. Freshening of the Mediterranean Salt Giant: controversies and certainties around the terminal (Upper Gypsum and Lago-Mare) phases of the Messinian salinity crisis. Earth Sc. Rev. 216, 1–47.

Andreetto, F., Matsubara, K, Beets, C.J, Fortuin, A.R, Flecker, R., Krijgsman, W., 2021b. High Mediterranean water-level during the Lago-Mare phase of the Messinian Salinity Crisis: Insights from the Sr isotope records of Spanish marginal basins (SE Spain). Paleogeography, Paleoclimatology, Paleoecology, 562.

Andreetto, F., Flecker, R., Aloisi, G., Mancini, A.M., Guibourdenche, L., deVilliers, S., Krijgsman, W., 2022a. High-amplitude water-level fluctuations at the end of the Mediterranean Messinian Salinity Crisis: implications for gypsum formation, connectivity and global climate. Earth and Planetary Science Letters, 595, 117767.

Andreetto, F., Mancini, A.M., Flecker, R., Gennari, R., Lewis, J, Lozar, F., Natalicchio, M., Sangiorgi, F., Stoica, M., Dela Pierre, F., Krijgsman, W., 2022b. Multi-proxy investigation of the post-evaporitic succession of the Piedmont Basin (Pollenzo section, NW Italy): a new piece in the Stage 3 puzzle of the Messinian Salinity Crisis. Paleogeography, Paleoclimatology, Paleoecology, 594.

Andrusov, D., 1890. Les Dreissenidae fossiles et actuelles d'Eurasie. Geol. Min. 25, 1-683 (in Russian).

Angelone, C., Colombero, S., Esu, D., Giuntelli, P., Marcolini, F., et al., 2011. Moncucco Torinese, a new post-evaporitic Messinian fossiliferous site from Piedmont (NW Italy). Neues Jahrbuch für Geologie und Pal¨aontologie-Abhandlungen 259, 89–104.

Arribas Jr., A., Cunnningham, C.G., McKee, E.H., Rye, R.O., Rytuba, et al., 1995. Compilation of sample preparation and analytical method and results of chemicals, isotopic, and fluid inclusion annalyses, Rodalquilar Ar alunite deposit Spain. U.S. Geological Survey Open-File Report 95-221 (33 pp.).

Arab, M., Rabineau, M., Déverchère, J., Bracene, R., Belhai, D., Roure, F., et al., 2016. Tectonostratigraphic evolution of the eastern Algerian margin and basin from seismic data and onshore-offshore correlation. Mar. Pet. Geol. 77, 1355-1375.

Arenas, C., Pomar, L., 2010. Microbial deposits in upper Miocene carbonates, Mallorca, Spain. Paleogeography, Paleoclimatology, Paleoecology, 297(2), 465-485.

Artiaga, D., García-Veigas, J., Gibert, L., Soria Mingorance, J.M., 2020. The late Miocene Campo Coy gypsum (Eastern Betics, Spain). Geogaceta 67, 64-67.

Auer, G., Piller, W.E., Mathias Harzhauser, M., 2014. High-resolution calcareous nannoplankton palaeoecology as a proxy for small-scale environmental changes in the Early Miocene. Mar. Micropaleontol. 111, 53–65.

Aureli, A., Ganoulis, J., Margat, J., 2008. Groundwater resources in the Mediterranean region: importance, uses and sharing. Water Mediterr, 96-105.

Aufgebauer, A., McCann, T., 2010. Messinian to Pliocene transition in the deep part of the Sorbas Basin, SE Spain-a new description of the depositional environment during the Messinian Salinity Crisis. Neues Jahrbuch für Geologie und Paläontologie-Abhandlungen, 259(2), 177-195.

Aureli, A., Ganoulis, J., Margat, J., 2008. Groundwater resources in the Mediterranean region: importance, uses and sharing. Water in the Mediterranean, 96-105.

Avanzinelli, R., Boari, E., Conticelli, S., Francalanci, L., et al., 2005. "High Precision Sr, Nd and Pb Isotopic Analyses Using the New Generation Thermal Ionisation Mass Spectometer ThermoFinnigan Triton- Ti." Periodico Di Mineralogia 74: 147–66.

Avnaim-Katav, S., Milker, Y., Schmiedl, G., Sivan, D., Hyams-Kaphzan, O., Sandler, A., Almogi-Labin, A., 2016. Impact of eustatic and tectonic processes on the southeastern Mediterranean shelf during the last one million years: Quantitative reconstructions using a foraminiferal transfer function. Marine Geology, 376: 26-38.

Azdimousa, A., Poupeau, G., Rezqi, H., Asebriy, L., Bourgois, J., Ait Brahim, L., 2006. Geodynamique des bordures meridionales de la mer d'Alboran; alication de la stratigraphie sequentielle dans le bassin neogene de Boudinar Rif oriental. Maroc. Bull. Inst. Sci. Rabat 28, 9-18.

Bache, F., Olivet, J.-L., Gorini, C., Rabineau, M., Baztan, J., Aslanian, D., Suc, J.-P., 2009. Messinian erosional and salinity crisis: view from the Provence basin (Gulf of Lions, western Mediterranean). Earth and Planetary Science Letters 286, 139-157.

Bache, F., Popescu, S.-M., Rabineau, M., Gorini, C., Suc, J.-P., Clauzon, G., et al., 2012. A two-step process for the reflooding of the Mediterranean after the Messinian Salinity Crisis. Basin Research 24, 125-153.

Backman, J., Raffi, I., Rio, D., Fornaciari, E. Pälike, H., 2012. Biozonation and biochronol-ogy of Miocene through Pleistocene calcareous nannofossils from low and middle latitudes. News-letters on Stratigraphy 45, 221-244.

Baddouh, M.B., Meyers, S.R., Carroll, A.R., Beard, B.L., Johnson, C.M. 2016. Lacustrine $^{87}Sr/^{86}Sr$ as a tracer to reconstruct Milankovitch forcing of the Eocene hydrologic cycle. Earth and Planetary Science Letters 448, 62-68.

Bannikov A.F., Schwarzhans W. Carnevale G., 2018. Neogene Paratethyan croakers (Te-leostei, Sciaenidae). Rivista Italiana di Paleontologia e Stratigrafia 124, 535-571.

Barra, D., Bonaduce, G., Sgarrella, E., 1998. Paleoenvironmental bottom water conditions in the early Zanclean of the Capo Rossello area (Agrigento, Sicily). Bollettino della Società Pa-leontologica Italiana 37, 61-88.

Bassetti, M.A., Ricci Lucchi, F., Roveri, M., 1994. Physical stratigraphy of the Messinian post-evaporitic deposits in Central-Southern Marche area (Appennines, Central Italy). Mem. Soc. Geol. Ital. 48, 275±288.

Bassetti, M.A., Miculan, P., Lucchi, F.R., 2003. Ostracod faunas and brackish-water envi-ronments of the late Messinian Sapigno section (northern Apennines, Italy). Paleogeography, Pa-leoclimatology, Paleoecology, 198(3-4), 335-352.

Bassetti, M. A., Manzi, V., Lugli, S., Roveri, M., Longinelli, A., Lucchi, F. R., Barbieri, M., 2004. Paleoenvironmental significance of Messinian post-evaporitic lacustrine carbonates in the northern Apennines, Italy. Sedimentary Geology, 172(1-2), 1-18.

Bassetti, M.A., Miculan, P., Sierro, F.J., 2006. Evolution of depositional environments after the end of Messinian Salinity Crisis in Nijar basin (SE Betic Cordillera). Sedimentary Geology 188-189, 279-295.

Bataille, C. P., Laffoon, J., Bowen, G.J. 2012. Mapping multiple source effects on the stron-tium isotopic signatures of ecosystems from the circum-Caribbean region. Ecosphere, 3(12), 1-24.

Beets, C.J., 1991. $^{87}Sr/^{86}Sr$ dating of coralline algal limestones and its implications for the tectono-stratigraphic evolution of the eastern Prebetic (Spain). Sedimentary Geology 78, 233-250.

Beltrando, M., Compagnoni, R., Lombardo, B., 2010. (Ultra-) High-pressure metamorphism and orogenesis: an Alpine perspective. Gondwana Research, 18(1), 147-166.

Ben-Gal, Y., Ben-Avraham, Z., Buchbinder, B., Kendall, C.G.S.C., 2005. Post-Messinian evolution of the Southeastern Levant Basin based on two-dimensional stratigraphic simulation. Mar. Geol. 221 (1-4), 359-379.

Ben Moshe, L., Ben-Avraham, Z., Enzel, Y., Schattner, U., 2020. Estimating drawdown magnitudes of the Mediterranean Sea in the Levant basin during the Lago Mare stage of the Mes-sinian Salinity Crisis. Marine Geology, 106215.

Benison, K.C., and Karmanocky, F.J., 2014, Could microorganisms be preserved in Mars gypsum? Insights from terrestrial examples: Geology, v. 42, p. 615–618.

Benito, M.I., Suarez-Gonzalez, P., Quijada, I. E., Campos-Soto, S., Rodriguez-Martinez, M., 2021. Constraints of applying strontium isotope stratigraphy in coastal and shallow marine environments: insights from Lower Cretaceous carbonates deposited in an active tectonic setting (N Iberian Basin, Spain). Journal of Iberian Geology, 47(1), 151-169.

Bennett, C. E., Williams, M., Leng, M. J., Siveter, D. J., Davies, S. J., Sloane, H. J., Wil-kinson, I.P., 2011. Diagenesis of fossil ostracods: Implications for stable isotope based palaeoenvi-ronmental reconstruction. Palaeogeography, Palaeoclimatology, Palaeoecology, 305(1-4), 150-161.

Benson, R.H., 1978. The paleoecology of the ostracods of DSDP Leg 42A. In: Hsu¨, K., Montadert, L., Eds.), Initial Reports of the Deep-Sea Drilling Project 42. U.S. Government Printing Office, Washington, 777-787.

Benson, R.H., Rakic-El Bied, K., 1991. The Messinian parastratotype at Cuevas de Alman-zora, Vera Basin, SE Spain; refutation of the deep-basin, shallow-water hypothesis?. Micropaleon-tology, 37(3), 289-302.

Benson, R.H., Rakic-El Bied, K., Bonaduce, G., 1991. An important current reversal (in-flux) in the Rifian Corridor (Morocco) at the Tortonian-Messinian boundary: The end of Tethys Ocean. Paleoceanography, 6(1), 165-192.

Berner, R.A., 1991. A model for atmospheric CO sub 2 over phanerozoic time. American Journal of Science;(United States), 291(4).

Berner, R.A., 1999. Atmospheric oxygen over Phanerozoic time. Proceedings of the Na-tional Academy of Sciences 96, 10955.

Bertini, A., 1992. Palinologia ed Aspetti Ambientali del Versante Adriatico Dell'Appennino Centro-Settentrionale Durante il Messiniano e lo Zancleano. PhD Thesis, Univer-sity of Florence, Florence.

Bertini, A., 2006. The Northern Apennines palynological record as a contribute for the re-construction of the Messinian paleoenvironments. Sedimentary Geology, 188, 235-258.

Bertini, A., Corradini, D., 1998. Biostratigraphic and paleoecological significance of Ga-leacysta etrusca in the "Lago-Mare" facies from the Mediterranean area (Neogene). Dino NTNU Vitensk. Mus. Rapp. Bot. ser., vol. 6, pp. 15–16. Abstract.

Bertoni, C., Cartwright, J., 2007. Major erosion at the end of the Messinian Salinity Crisis: evidence from the Levant Basin, Eastern Mediterranean. Basin Research 19, 1-18.

Bessis, F., 1986. Some remarks on the study of subsidence of sedimentary basins. Applica-tion to the Gulf of Lions margin (Western Mediterranean) Mar. Pet. Geol., 3, 37-63.

Bialik, O.M., Frank, M., Betzler, C., Zammit, R., Waldmann, N.D., 2019. Two-step closure of the Miocene Indian Ocean Gateway to the Mediterranean. Scientific reports, 9(1), 1-10.

Bickle, M.J., Harris, N.B.W., Bunbury, J.M., Chapman, H.J., Fairchild, I.J., Ahmad, T. 2001. Controls on the $^{87}Sr/^{86}Sr$ ratio of carbonates in the Garhwal Himalaya, headwaters of the Ganges. The Journal of Geology, 109(6), 737-753.

Bigi, D., Lugli, S., Manzi, V., Roveri, M., 2022. Are fluid inclusions in gypsum reliable paleoenvironmental indicators? An assessment of the evidence from the Messinian evaporites. Geology, 50, 454-459.

Birck, J.L., 1986. Precision K-Rb-Sr isotopic analysis: application to Rb-Sr chronology. Chem. Geol. 56, 73-83.

Biscaye, P.E., Ryan, W.B.F., Wezel, F.C., 1972. Age and nature of the Pan-Mediterranean subbottom reflector M. The Mediterranean Sea, 83-90.

Bista, D., Hoyle, T.M., Simon, D., Sangiorgi, F., Richards, D.A., Flecker, R., 2021. Sr iso-tope-salinity modelling constraints on Quaternary Black Sea connectivity. Quaternary Science Reviews, 273, 107254.

Blanc, P.L., 2002. The opening of the Plio-Quaternary Gibraltar Strait: assessing the size of a cataclysm. Geodin. Acta 15, 303-317.

Blanc-Valleron, M.-M., Rouchy, J.-M., Pierre, C., Badaut-Trauth, D. Schuler, M., 1998. Evidence of Messinian nonmarine deposition at site 968 (Cyprus lower slope). ODP Sci. Results 160, Texas, USA, 43-445.

Boccaletti, M., Ciaranfi, N., Cosentino, D., Deiana, G., Gelati, R., Lentini, F., Massari, F., Moratti, G., Pescatore, T., Ricci Lucchi, F., Tortorici, L., 1990. Palinspastic restoration and paleo-geographic reconstruction of the peri-Tyrrhenian area during the Neogene. Palaeogeography, Pal-aeoclimatology, Palaeoecology 77, 41–50.

Bonaduce, G., Sgarrella, F., 1999. Paleoecological interpretation of the latest Messinian sediments from southern Sicily (Italy). Soc. Geol. Ital. Mem., 54, 83-91.

Booth-Rea, G., Ranero, R., Grevemeyer, I.C., 2018. The Alboran volcanic-arc modulated the Messinian faunal exchange and salinity crisis. Sci. Rep. 8.

Borsetti, A.M., Carloni, G.C., Cati, F., Ceretti, E., Cremonini, G., Elmi, C. and Ricci Luc-chi, F., 1975. Paleogeografia del Messiniano dei bacini periadriatici dell' Italia settentrionale e centrale. Giorn. Geol. 40, 21-72.

Borsetti, A.M., Curzi, P.V., Landuzzi, V., Mutti, M., Ricci Lucchi, F., et al., 1990. Messinian and pre-Messinian sediments from ODP Leg 107 Sites 652 and 654 in the Tyrrhenian Sea: sedimentologic and petrographic study and possible comparisons with Italian sequences. In: Kastens, K.A., Mascle, J., et al., Eds.), ODP Sci. Results, 107, 169-186.

Bossio, A., Esteban, M., Giannelli, L., Longinelli, A., Mazzanti, R., Mazzei, R., Ricci Luc-chi, F., Salvatorini, G., 1978. Some aspects of the upper Miocene in Tuscany. In: Messinian Semi-nar, vol. 4, Pacini, Pisa, 88 pp.

Bossio, A., Costantini, A., Lazzarotto, A., Liotta, D., Mazzanti, R., 1993. Rassegna delle conoscenze sulla stratigrafia del Neoautoctono toscano. Memorie della società Geologica italiana, 49, 17-98.

Bosworth, W., Huchon, P., Mc Clay, K., 2005. The Red Sea and Gulf of Aden Basins. J. Afr. Earth Sci. 43, 334-378.

Bourillot, R., Vennin, E., Rouchy, J. M., Blanc-Valleron, M. M., Caruso, A., Durlet, C. 2010. The end of the Messinian Salinity Crisis in the western Mediterranean: Insights from the carbonate platforms of south-eastern Spain. Sedimentary Geology 229(4), 224-253.

Bowman, S.A., 2012. A comprehensive review of the MSC facies and their origins in the offshore Sirt Basin, Libya. Petroleum Geoscience 18, 457-469.

Bown, P.R., Gibbs, S.J., Sheward, R., O'Dea, S. A., Higgins, D., 2014. Searching for cells: The potential of fossil coccospheres in coccolithophore research. J. Nannoplankt. Res, 34, 5-21.

Brachert, T.C., Krautworst, U.M.R., Steuckrad, O.M., 2002. Tectono-climatic evolution of a Neogene intramontane basin (Late Miocene Carboneras subbasin, southeast Spain): revelations from basin mapping and biofacies analysis. Basin Res. 14, 503-521

Braga, J.C., Martín, J.M., Riding, R., Aguirre, J., Sanchez-Almazo, I.M., Dinares-Turell, J., 2006. Testing models for the Messinian salinity crisis: the Messinian record in Almería, SE Spain. Sediment. Geol. 188-189, 131-154.

Brass, G.W., 1976. The variation of the marine $^{87}Sr/^{86}Sr$ ratio during Phanerozonic time: interpretation using a flux model. Geochimica et Cosmochimica Acta 40(7), 721-730.

Brenot, A., 2006. Origine de l'eau et Des éléments Dissous Par traçage Isotopique (H, O, S,Mg, Sr) Sur le Bassin Amont de La Moselle PhD thesis INPL - ENSG - CRPG (360 pp.).

Brenot, A., Cloquet, C., Vigier, N., Carignan, J., France-Lanord, C., 2008. Magnesium iso-tope systematics of the lithologically varied Moselle river basin, France. Geochimica et Cosmo-chimica Acta, 72(20), 5070-5089.

Bright, J., Cohen, A.S., Starratt, S.W., 2018. Distinguishing brackish lacustrine from brack-ish marine deposits in the stratigraphic record: A case study from the late Miocene and early Plio-cene Bouse Formation, Arizona and California, USA. Earth-Science Reviews, 185, 974-1003.

Bright, J., Cohen, A. S., Dettman, D. L., Pearthree, P.A. 2018. Freshwater plumes and brackish lakes: Integrated microfossil and OC-Sr isotopic evidence from the late Miocene and ear-ly Pliocene Bouse Formation (California-Arizona) supports a lake overflow model for the integra-tion of the lower Colorado River corridor. Geosphere, 14(4), 1875-1911.

Brolsma, M.J., 1975. Lithostratigraphy and Foraminiferal assemblages of the Mio-cene/Pliocene transitional strata at Capo Rossello and Eraclea Minoa (Sicily, Italy): Kon. Ned. Akad. Wetensch. Amsterdam Proc, v. 78, p. 1-40.

Brunner, B., Bernasconi, S.M., 2005. A revised isotope fractionation model for dissimilato-ry sulfate reduction in sulfate reducing bacteria. Geochimica et Cosmochimica Acta 69, 4759-4771.

Brunner, B., Bernasconi, S.M., Kleikemper, J., Schroth, M.H., 2005. A model for oxygen and sulfur isotope fractionation in sulfate during bacterial sulfate reduction processes. Geochimica et Cosmochimica Acta 69, 4773-4785.

Bulian, F., Sierro, F.J., Santiago, L., Jiménez-Espejo, F.J., Bassetti, M.A., 2021. Messinian West Alboran Sea record in the proximity 1 of Gibraltar: early signs of Atlantic-Mediterranean gateway restriction. Marine Geology.

Burke, A., Present, T.M., Paris, G., Rae, E.C.M., Sandilands, B.H., Gaillardet, J., Peucker-Ehrenbrink, B., Fischer, W.W., McClelland, J.W., Spencer, R.G.M., Voss, B.M., Adkins, J.F., 2018. Sulfur isotopes in rivers: Insights into global weathering budgets, pyrite oxidation, and the modern sulfur cycle. Earth and Planetary Science Letters 496, 168-177.

Butler, R.W.H., Likhorish, W.H., Grasso, M., Pedley, H.M., Ramberti, L., 1995. Tectonics and sequence stratigraphy in Messinian Basins, Sicily: constraints on the initiation and termination of the Mediterranean salinity crisis. Geological Society of America Bulletin 107, 425-439.

Butler, R.W.H., Maniscalco, R., Sturiale, G., Grasso, M., 2015. Stratigraphic variations control deformation patterns in evaporite basins: Messinian examples, onshore and offshore Sicily (Italy). Journal of the Geological Society 172, 113-124.

Calvert, S.E., Pedersen, T.F., 2007. Elemental proxies for palaeoclimatic and palaeoceano-graphic variability in marine sediments: interpretation and application. In: Hillaire-Marcel, C., De Vernal, A. (Eds.), Proxies in Late Cenozoic Paleoceanography, Developments in Marine Geology. vol. 1. Elsevier, pp. 567-644.

Camerlenghi, A., Aloisi, V., 2020. Uncovering the Mediterranean Salt Giant (MEDSALT)-Scientific Networking as Incubator of Cross-disciplinary Research in Earth Sciences. European Review, 28(1), 40-61.

Camerlenghi, A., Accettella, D., Costa, S., Lastras, G., Acosta, J., Canals, M., Wardell, N., 2009. Morphogenesis of the SW Balearic continental slope and adjacent abyssal plain, Western Mediterranean Sea. International Journal of Earth Sciences, 98, 735–750.

Camerlenghi, A., Del Ben, A., Hübscher, C., Forlin, E., Geletti, R., Brancatelli, G., Mi-callef, A., Saule, M., Facchin, L., 2019. Seismic markers of the Messinian salinity crisis in the deep Ionian Basin. Basin Res bre.12392.

Cameselle, A.L., Urgeles, R., 2017. Large-scale margin collapse during Messinian early sea-level drawdown: the SW Valencia trough, NW Mediterranean. Basin Research, 29, 576-595.

Cameselle, A.L., Urgeles, R., De Mol, B., Camerlenghi, A., Canning, J.C., 2014. Late Mio-cene sedimentary architecture of the Ebro Continental Margin (Western Mediterranean): implica-tions to the Messinian Salinity Crisis. International Journal of Earth Sciences, 103(2), 423-440.

Campillo, A.C., Maldonado, A., Mauffret, A., 1992. Stratigraphic and Tectonic evolution of the Western Alboran Sea late Miocene to recent. Geo-Mar. Lett. 12, 165-172.

Capella, W., Matenco, L., Dmitrieva, E., Roest, W.M., Hessels, S., Hssain, M., Chakor-Alami, A., Sierro, F.J., Krijgsman, W., 2017. Thick-skinned tectonics closing the Rifian Corridor. Tectonophysics 710, 249-265.

Capella, W., Barhoun, N., Flecker, R., Hilgen, F.J., Kouwenhoven, T.E., Matenco, L., Sier-ro, F.J., Tulbure, M., Yousfi, Z., Krijgsman, W., 2018. Paleogeographic evolution of the Late Mio-cene Rifian Corridor (Morocco): reconstructions from surface and subsurface data. Earth-Sci. Rev. 180, 37-59.

Capella, W., Flecker, R., Hernández-Molina, F. J., Simon, D., Meijer, P. T., Rogerson, M., Sierro, F.J., Krijgsman, W., 2019. Mediterranean isolation preconditioning the Earth System for late Miocene climate cooling. Scientific reports, 9(1), 1-8.

Capella, W., Spakman, W., van Hinsbergen, D.J., Chertova, M.V., Krijgsman, W., 2020. Mantle resistance against Gibraltar slab dragging as a key cause of the Messinian Salinity Crisis. Terra Nova, 32(2), 141-150.

Capellini, G., 1880. Gli strati a Congerie o la formazione gessoso solfifera nella provincia di Pisa e nei dintorni di Livorno. Mem. R. Accad. Lincei., Cl. Sci. Fis. Mat. Nat. 5, 1-64.

Carbonnel, G., 1978. La zone à Loxoconcha djaffarovi Schneider (ostracodes, Miocène su-périeur) ou le Messinien de la vallée du Rhône. Rev. Micropal. 21 (3), 106-118.

Carnevale, G., Schwarzhans, W., 2022. Marine life in the Mediterranean during the Mes-sinian Salinity Crisis: a paleoichthyological perspective. Rivista Italiana di Paleontologia e Stratigrafia, 128(2), 283-324.

Carnevale, G., Landini, W., Sarti, G., 2006a. Mare versus Lago-mare: marine fishes and the Mediterranean environment at the end of the Messinian Salinity Crisis. Journal of the Geological Society, 163(1), 75-80.

Carnevale, G., Caputo, D., Landini, W., 2006b. Late Miocene fish otoliths from the Colom-bacci Formation (Northern Apennines, Italy): implications for the Messinian 'Lago-mare'event. Geological Journal, 41(5), 537-555.

Carnevale, G., Longinelli, A., Caputo, D., Barbieri, M., Landini, W., 2008. Did the Mediter-ranean marine reflooding precede the Miocene/Pliocene boundary? Paleontological and geochem-ical evidence from upper Messinian sequences of Tuscany, Italy. Paleogeography, Paleoclimatolo-gy, Paleoecology 257, 81-105.

Carnevale, G., Dela Pierre, F., Natalicchio, M., Landini, W., 2018. Fossil marine fishes and the "Lago Mare" event: Has the Mediterranean ever transformed into a brackish lake? Newsletters on Stratigraphy 51, 57-72.

Carnevale, G., Gennari, R., Lozar, F., Natalicchio, M., Pellegrino, L., Dela Pierre, F., 2019. Living in a deep desiccated Mediterranean Sea: An overview of the Italian fossil record of the Messinian salinity crisis. Bolletino della Societa Paleontologica Italiana 58, 109-140.

Carrapa, B., Garcia-Castellanos, D., 2005. Western Alpine back-thrusting as subsidence mechanism in the Tertiary Piedmont Basin (western Po Plain, NW Italy). Tectonophysics, 406(3-4), 197-212.

Cartwright, J.A., Jackson, M.P.A., 2008. Initiation of gravitational collapse of an evaporitic basin margin: the Messinian saline giant, Levant Basin, eastern Mediterranean. Geological Society of America Bulletin 120, 399-413.

Caruso, A., Rouchy, J.M., 2006. The Upper Gypsum unit. In: Roveri, M. (Ed.), Post-Congress FieldTrip of the RCMNS Interim Colloquium (Parma, 2006, Acta Naturalia de "L'Ateneo Parmense" 42. pp. 157–168.

Caruso, A., Pierre, C., Blanc-Valleron, M. M., Rouchy, J.M., 2015. Carbonate deposition and diagenesis in evaporitic environments: The evaporative and sulphur-bearing limestones during the settlement of the Messinian Salinity Crisis in Sicily and Calabria. Palaeogeography, Palaeo-climatology, Palaeoecology, 429, 136-162.

Caruso, A., Blanc-Valleron, M.M., Da Prato, S., Pierre, C., Rouchy, J.M., 2020. The late Messinian "Lago-Mare" event and the Zanclean Reflooding in the Mediterranean Sea: New in-sights from the Cuevas del Almanzora section (Vera Basin, South-Eastern Spain). Earth-Science Reviews, 200, 102993.

Casati, P., Bertozzi, P., Cita, M.B., Longinelli, A., Damiani, V., 1976. Stratigraphy and paleoenvironment of the Messinian "Colombacci" Formation in the periadriatic trough. A pilot study. Memorie della Società Geologica Italiana 16, 173-195.

Castradori, D., 1998. Calcareous nannofossils in the basal Zanclean of the Eastern Mediter-ranean Sea: remarks on paleoceanography and sapropel formation. In: Robertson, A.H.F., Emeis, K.C., Richter, C., Camerlenghi, A., Eds.), Proceedings of the Ocean Drilling Program, Scientific Results 160. US Government Printing Office, Washington, 113-123.

Catalano, R., Valenti, V., Albanese, C., Accaino, F., Sulli, A., Tinivella, U., Morticelli, M.G., Zanolla, C., Giustiniani, M., 2013. Sicily's fold–thrust belt and slab roll-back: the SI. RI. PRO. seismic crustal transect. Journal of the Geological Society, 170(3), 451-464.

Cazzini, F.F., Amadori, C., Bosino, A., Fantoni, R., 2020. New seismic evidence of the Messinian paleomorphology beneath Lake Maggiore area (Italy). Italian Journal of Geosciences, 139(2), 195-211.

Chang, L., Vasiliev, I., van Baak, C.G.C., Krijgsman, W., Dekkers, M.J., Roberts, A.P.R., Fitz Gerald, J.D., van Hoesel, A., Winklhofer, M., 2014. Identification and environmental interpre-tation of diagenetic and biogenic greigite in sediments: a lesson from the Messinian Black Sea, Geochem. Geophys, Geosys.

Chumakov, I.S., 1973. Pliocene and Pleistocene deposits of the Nile valley in Nubia and upper Egypt. In W. B. F. Ryan K. J. Hsu, et al. (Eds), Initial Reports of the Deep Sea Drilling Pro-ject, 13, 1242-1243. Washington, DC: US Govern. Print. Office

Cicchella, D., Albanese, S., De Vivo, B., Dinelli, E., Giaccio, et al., 2010. Trace elements and ions in Italian bottled mineral waters: Identification of anomalous values and human health related effects. Journal of Geochem. Expl. 107(3), 336-349.

Cipollari, P., Cosentino, D., Gliozzi, E., 1999. Extension-and compression-related basins in central Italy during the Messinian Lago-Mare event. Tectonophysics, 315(1-4), 163-185.

Cipollari, P., Cosentino, D., Radeff, G., Schildgen, T. F., Faranda, C., Grossi, F., Gliozzi, E., Smedile, A., Gennari, R., Darbas, G., Dudas, F.Ö., Gürbüz, K., Nazik, A., Echtler, H., 2013. Easternmost Mediterranean evidence of the Zanclean flooding event and subsequent surface uplift: Adana Basin, southern Turkey. Geological Society, London, Special Publications, 372(1), 473-494.

Cita, M.B., 1973. Inventory of biostratigraphical findings and problems. Init. Rep. Deep-Sea Drill. Proj., 13 (2), 1045-1065.

Cita, M.B., Colombo, L., 1979. Sedimentation in the latest Messinian at Capo Rossello (Sicily). Sedimentology 26, 497-522.

Cita, M.B., Wright, R.C., Ryan, W.B.F., Longinelli, A., 1978. Messinian paleoenviron-ments, In: Hsü, K.J., Montadert, L. et al., Eds.), Initial Reports of the Deep Sea Drilling Project 42. U.S. Government Printing Office, Washington D.C, 1003-1035.

Cita, M. B., Santambrogio, S., Melillo, B., Rogate, F., 1990. Messinian Paleoenvironments: New Evidence from the Tyrrhenian Sea (ODP LEG 107)". In Proceedings of the Ocean Drilling Program, Scientific Results 107, 211-227.

Clauzon, G., 1982. Le canyon messinien du Rhoˆne: Une preuve decisive du "dessicated deep basin model" (Hsu¨ , Cita et Ryan, 1973). Bulletin de la Societe Geologique de France, 24, 231-246.

Clauzon, G., Suc, J.-P., Gautier, F., Berger, A., Loutre, M.F., 1996. Alternate interpretation of the Messinian salinity crisis, controversy resolved? Geology 24, 363-366.

Clauzon, G., Suc, J. P., Popescu, S. M., Marunteanu, M., Rubino, J. L., Marinescu, F., Melinte, M. C., 2005. Influence of Mediterranean sea-level changes on the Dacic Basin (Eastern Paratethys) during the late Neogene: the Mediterranean Lago Mare facies deciphered. Basin Re-search, 17(3), 437-462.

Clauzon, G., Suc, J.-P., Do Couto, D., Jouannic, G., Melinte-Dobrinescu, M.C., Jolivet, L., Quillévéré, F., Lebret, N., Mocochain, L., Popescu, S.-M., Martinell, J., Doménech, R., Rubino, J.-L., Gumiaux, C., Warny, S., Bellas, S.M., Gorini, C., Bache, F., Rabineau, M., Estrada, F., 2015. New insights on the Sorbas Basin (SE Spain): the onshore reference of the Messinian salinity cri-sis. Mar. Pet. Geol. 66, 71-100.

Claypool, G.E., Holser, W.T., Kaplan, I.R., Sakai, H. and Zak, I., 1980. The age curves of sulfur and oxygen isotopes in marine sulfate and their mutual interpretation. Chemical Geology 28, 199-260.

Colalongo, M.L., Cremonini, G., Farabegoli, E., Sartori, R., Tampieri, R., Tomadin, L., 1976. Paleoenvironmental study of the "Colombacci" Formation in Romagna (Italy): the cella section. Memorie della Società Geologica Italiana 16, 197-216.

Colalongo, M.L., Cremonini, G., Farabegoli, E., Sartori, R., Tampieri, R. and Tomadin, L, 1978. Evoluzione paleoambientale della formazione a "Colombacci" in Romagna. Rend. Soc. Geol. ltal. 1, 37-40.

Colombero, S., Bonelli, E., Kotsakis, T., Pavia, G., Pavia, M., Carnevale, G., 2013. Late Messinian rodents from Verduno (Piedmont, NW Italy): biochronological, palaeoecological and palaeobiogeographic implications. Geobios 46, 111-125

Colombero, S., Angelone, C., Bonelli, E., Carnevale, G, Cavallo, O., Delfino, M., Giuntelli P., Pavia, G., Pavia, M., Repetto, G., Mazza, P., 2014. The upper Messinian assemblages of fossil vertebrate remains of Verduno (NW Italy): Another brick for a latest Miocene bridge across the Mediterranean. Neues Jahrbuch für Geolog. und Paläontolog., Abhandlungen 272, 287-324.

Colombero, S., Alba, D.M., D'Amico, C., Delfino, M., Esu, D., Giuntelli, P., Harzhauser, M., Mazza, P.P.A., Mosca, M., Neubauer, T.A., Pavia, G., Pavia, M., Villa, A. Carnevale, G., 2017. Late Messinian mollusks and vertebrates from Moncucco Torinese, north-western Italy. Paleoeco-logical and paleoclimatological implications. Palaeontologia Electronica, 20.1.10A, 1-66.

Comas, M.C. , Zahn , R. , Klaus , A., et al., 1996. Proceedings of the Ocean Drilling Pro-gram, Initial Reports, v. 161: College Station, Texas , Ocean Drilling Program.

Comas, M.C., Platt, J.P., Soto, J.I., Watts, A.B., 1999. 44. The origin and tectonic history of the Alboran Basin: Insights from leg 161 results: Proceedings of the Ocean Drilling Program, Sci-entific Results, v. 161, p. 555–580.

Consorti, L., Sabbatino, M., Parente, M., 2020. Insights on the paleoecology of Ammonia (Foraminifera, Rotalioidea) from Miocene carbonates of central and southern Apennines (Italy). Palaeogeography, Palaeoclimatology, Palaeoecology, 110105.

Conticelli, S., Guarnieri, L., Farinelli, A., Mattei, M., Avanzinelli, R., Bianchini, G., Boari, E., Tommasini, S., Tiepolo, M., Prelevic, D., Venturelli, G., 2009. Trace elements and Sr-Nd-Pb isotopes of K-rich, shoshonitic, and calc-alkaline magmatism of the Western Mediterranean Re-gion: genesis of ultrapotassic to calc-alkaline magmatic associations in a post-collisional geody-namic setting. Lithos 107(1-2), 68-92.

Corbí, H., Soria J.M., 2016. Late Miocene-early Pliocene planktonic foraminifer event-stratigraphy of the Bajo Segura basin: a complete record of the western Mediterranean. Mar Pet Geol 77, 1010-1027.

Corbí, H., Lancis, C., García-García, F., Pina, J.A., Soria, J.M., Tent-Manclús, J.E., Viseras, C., 2012. Updating the marine biostratigraphy of the Granada Basin (central Betic Cordillera). Insight for the Late Miocene palaeogeographic evolution of the Atlantic–Mediterranean seaway. Geobios, 45(3), 249-263.

Corbí, H., Soria, J. M., Lancis, C., Giannetti, A., Tent-Manclús, J. E., Dinarès-Turell, J., 2016. Sedimentological and paleoenvironmental scenario before, during, and after the Messinian Salinity Crisis: The San Miguel de Salinas composite section (western Mediterranean). Marine Geology, 379, 246-266.

Corbí, H., Soria, J. M., Giannetti, A., Yébenes, A., 2020. The step-by-step restriction of the Mediterranean (start, amplification, and consolidation phases) preceding the Messinian Salinity Crisis (climax phase) in the Bajo Segura basin. Geo-Marine Letters, 1-21.

Cornée, J.J., Munch, P., Achalhi, M., Merzeraud, G., Azdimousa, A., Quillevere, F., Melinte-Dobrinescu, M., Chaix, C., Ben Moussa, A., Lofi, J., Seranne, A., Moissette, P., 2016. The Messinian erosional surface and early Pliocene reflooding in the Alboran Sea: New insights from the Boudinar basin, Morocco. Sediment. Geol. 333, 115-129.

Cornet, C., 1968. Le graben médian (zone A) de laMéditerranée occidentale pourrait être pontien. Sommaire Societé Géologique de France 149.

Corradini, D., Biffi, U., 1988. Etude des dinokystes a la limite Messinien-Pliocene dans la coupe Cava Serredi, Tos cane, Italie. Bulletin des Centres de Recherche Exploration-Production Elf-Aquitaine 12, 1, 221-236.

Cosentino, D., Cipollari, P., Mastro, S. L., Giampaolo, C., 2005. High-frequency cyclicity in the latest Messinian Adriatic foreland basin: Insight into paleoclimate and paleoenvironments of the Mediterranean Lago-Mare episode. Sedim. Geol., 178, 31-53.

Cosentino, D., Federici, I., Cipollari, P., Gliozzi, E., 2006. Environments and tectonic in-stability in central Italy (Garigliano Basin) during the late Messinian Lago-Mare episode: new data from the onshore Mondragone 1 well. Sedimentary Geology, 188, 297-317.

Cosentino, D., Gliozzi, E., Pionzi, G., 2007. The late Messinian Lago-Mare episode in the Mediterranean Basin: preliminary report on the occurrence of Paratethyan ostracod fauna from central Crete (Greece). Geobios, 40(3), 339-349.

Cosentino, D., Cipollari, P., Faranda, C., Florindo, F., Gennari, R., Gliozzi, E., Grossi, F., Laurenzi, M.A., Lo Mastro, S., Sampalmieri, G., Sprovieri, M., 2009. Integrated analyses of the Maccarone section (northern Apennines, Italy). 13th Congress RCMNS, 2nd-6th September 2009, Naples, Italy. Acta Natur. Aten.-Parm., 45, 338-339.

Cosentino, D., Darbaş, G., Gürbüz, K., 2010a. The Messinian salinity crisis in the marginal basins of the peri-Mediterranean orogenic systems: examples from the central Apennines (Italy) and the Adana Basin (Turkey). EGUGA, 2462.

Cosentino, D., Cipollari, P., Marsili, P., Scrocca, D., 2010b. Geology of the central Apen-nines: a regional review. Journal of the Virtual Explorer, Electronic Edition, ISSN 1441-8142, vol-ume 36, paper 11. In: (Eds.) Marco Beltrando, Angelo Peccerillo, Massimo Mattei, Sandro Conti-celli and Carlo Doglioni, The Geology of Italy, 2010.

Cosentino, D., Bertini, A., Cipollari, P., Florindo, F., Gliozzi, E., Grossi, F., Lo Mastro, S., Sprovieri, M., 2012. Orbitally forced paleoenvironmental and paleoclimate changes in the late postevaporitic Messinian of the central Mediterranean Basin. GSA Bulletin, 124(3-4), 499-516.

Cosentino, D., Buchwaldt, R., Sampalmieri, G., Iadanza, A., Cipollari, P., Schildgen, T.F., Hinnov, L.A., Ramezani, J., Bowring, S.A., 2013. Refining the Mediterranean "Messinian gap" with high-precision U-Pb zircon geochronology, central and northern Italy. Geology 41, 323-326.

Cosentino, D., Bracone, V., D'Amico, C., Cipollari, P., Esu, D., Faranda, C., Frezza, V., Gliozzi, E., Grossi, F., Gupperrieri, P., Iadanza, A., Kotsakis, D., Soulié-Märsche, I. 2018. The rec-ord of the Messinian salinity crisis in mobile belts: Insights from the Molise allochthonous units (southern Apennines, Italy). Paleogeography, Paleoclimatology, Paleoecology, 503, 112-130.

Coulson, S., Pico, T., Austermann, J., Powell, E., Moucha, R., Mitrovica, J.X., 2019. The role of isostatic adjustment and gravitational effects on the dynamics of the Messinian salinity cri-sis. Earth and Planetary Science Letters, 525, 115760.

Cziczer, I., Magyar, I., Pipík, R., Böhme, M., Ćorić, S., Bakrač, K., et al., 2009. Life in the sublittoral zone of long-lived Lake Pannon: paleontological analysis of the Upper Miocene Szák Formation, Hungary. International Journal of Earth Sciences, 98(7), 1741-1766.

Dal Cin, M., Del Ben, A., Mocnik, A., Accaino, F., Geletti, R., Wardell, N., Zgur, F., Cam-erlenghi, A., 2016. Seismic imaging of late Miocene (Messinian) evaporites from western Mediter-ranean back-arc basins. Petrol. Geosci. 22, 297-308.

Dal Piaz, G.V., 2010. The Italian Alps: a journey across two centuries of Alpine geology. Journal of the Virtual Explorer, 36(8), 77-106.

De Deckker, P., Lord, A., 2017. Cyprideis torosa: a model organism for the Ostracoda?. Journal of Micropalaeontology, 36(1), 3-6.

de la Chapelle, G., Gaudant, J., 1987. Decouverte de deux nouveaux gisements de poissons fossiles messiniens dans le bassin de Nijar-Carboneras (Andalousie Orientale): Signification pa-leoecologique et implications paleogeographiques.

De Benedetti, A., 1982. The problem of the origin of the salt deposits in the Mediterranean and of their relations to other salt occurrences in the Neogene formations of the contiguous re-gions. Marine Geology 49, 91-114.

de la Peña, L.G., Ranero, C. R., Gràcia, E., Booth-Rea, G., 2020. The evolution of the west-ernmost Mediterranean basins. Earth-Science Reviews, 103445.

Decima, A., 1964. Ostracodi del Gen. Cyprideis JONES del Neogene e del Quaternario ita-liani. Paleont. Italica. 57, 81.

Decima, A. Sprovieri, R., 1973. Comments on late Messinian microfaunas in several sec-tions from Sicily. In: Messinian Events in the Mediterranean (Ed. C.W. Drooger), 229-234. North-Holland Pub. Co, Amsterdam.

Decima, A., Wezel, F.C., 1971. Osservazioni sulle evaporiti Messiniane della Sicilia cen-tro-meridionale. Rivista Mineraria Siciliana, 130-134, 172-187.

Decima, A., Wezel, F.C., 1973. Late Miocene evaporites of the Central Sicilian Basin. In: Initial Reports of the Deep Sea Drilling Project, (Eds W.B.F. Ryan, K.J. Hsu), vol. 13, 1234-1240, U.S. Gov. Print. Off., Washington, DC.

Decima, A., Schreiber, B.C. McKenzie, J.A., 1988. The origin of "evaporative" lime-stones: an example from the Messinian of Sicily (Italy). J. Sed. Petrol., 58-2, 256-272.

De Feyter, A.J., Molenaar, N., 1984. Messinian fanconglomerates: the Colombacci For-mation in the Pietrarubbia Basin, Italy. Journal of Sedimentary Petrology 54, 746-758.

De Leeuw, A., Bukowski, K., Krijgsman, W., Kuiper, K.F., 2010. Age of the Badenian sa-linity crisis; Impact of Miocene climate variability on the circum-mediterranean region. Geology 38(8), 715-718.

Del Olmo, W.M., 2011. The Messinian in the Gulf of Valencia and Alboran Sea (Spain): paleogeography and paleoceanography implications. Revista de la Sociedad Geológica de España 24, 1–22.

Del Olmo, W.M., Martín, D., 2016. The Messinian record of Spanish onshore and offshore data (Atlantic Ocean and Western Mediterranean Sea). Petroleum Geoscience, 22(4), 291-296.

Dela Pierre, F., Clari, P., Cavagna, S., Bicchi, E., 2002. The Parona chaotic complex: a puzzling record of the Messinian (Late Miocene) events in Monferrato (NW Italy). Sedimentary Geology 152, 289–311.

Dela Pierre, F., Festa, A., Irace, A., 2007. Interaction of tectonic, sedimentary and diapiric processes in the origin of chaotic sediments: an example from the Messinian of Torino Hill (Tertiary Piedmont Basin, northwestern Italy). Geological Society of America Bulletin 119, 1107–1119.

Dela Pierre, F., Bernardi, E., Cavagna, S., Clari, P., Gennari, R., Irace, A., Lozar, F., et al.., 2011. The record of the Messinian salinity crisis in the Tertiary Piedmont Basin (NW Italy): The Alba section revisited. Paleog., Paleoclim., Paleoec. 310, 238-255.

Dela Pierre, F., Clari, P., Bernardi, E., Natalicchio, M., Costa, M., Cavagna, S., Lozar, F., Lugli, S., Manzi, V., Roveri, M., Violanti, D., 2012. Messinian carbonate-rich beds of the Tertiary Piedmont Basin (NW Italy): microbially-mediated products straddling the onset of the salinity crisis. Palaeogeogr. Palaeoclimatol. Palaeoecol. 34, 78–93.

Dela Pierre, F., Clari, P., Natalicchio, M., Ferrando, S., Giustetto, R., Lozar, F., Lugli, S., Manzi, V., Roveri, M., Violanti, D., 2014. Flocculent layers and bacterial mats in the mudstone interbeds of the Primary Lower Gypsum unit (Tertiary Piedmont Basin, NW Italy): archives of paleoenvironmental changes during the Messinian salinity crisis. Mar. Geol. 335, 71–87.

Dela Pierre, F., Natalicchio, M., Ferrando, S., Giustetto, R., Birgel, D., Carnevale, G., Gier, S., Lozar, F., Marabello, D., Peckmann, J., 2015. Are the large filamentous microfossils preserved in Messinian gypsum colorless sulfide-oxidizing bacteria?. Geology, 43(10), 855-858.

Dela Pierre, F., Natalicchio, M., Lozar, F., Bonetto, S., Carnevale, G., Cavagna, S., Clari, P., Colombero, S., Violanti, D., 2016. The northermost record of the Messinian salinity crisis (Piedmont Basin, NW Italy). Geol. F. Trips 8, 1-58.

Delrieu, B., Rouchy, J.M., Foucault, A., 1993. La surface d'erosion finimessinienne en Crète centrale (Grèce) et sur le pourtour méditerranéen: Rapports avec la crise de salinité méditer-ranéenne. Comptes rendus de l'Académie des sciences. Série 2, Mécanique, Physique, Chimie, Sciences de l'univers, Sciences de la Terre 316, no. 4, 527-533.

Dettman, D.L., Flessa, K.W., Roopnarine, P.D., Schöne, B.R., Goodwin, D.H., 2004. The use of oxygen isotope variation in shells of estuarine mollusks as a quantitative record of seasonal and annual Colorado River discharge. Geochimica et Cosmochimica Acta, 68(6), 1253-1263.

Di Stefano, A., Sturiale, G., 2010. Refinements of calcareous nannofossil biostratigraphy at the Miocene/Pliocene Boundary in the Mediterranean region. Geobios, 43(1), 5-20.

Dimiza, M.D., Koukousioura, O., Michailidis, I., Dimou, V.G., Navrozidou, V., Aligizaki, K., Seferlis, M., 2020. Seasonal living coccolithophore distribution in the enclosed coastal envi-ronments of the Thessaloniki Bay (Thermaikos Gulf, NW Aegean Sea). Revue de Micropaléontol-ogie, 69, 100449.

Do Couto, D., Popescu, S.-M., Suc, J.-P., Melinte-Dobrinescu, M.C., Barhoun, N., Gorini, C., et al., 2014. Lago Mare and the Messinian salinity crisis: evidences from the Alboran Sea (S. Spain). Mar. Pet. Geol. 52, 57-76.

Doebbert, A. C., Johnson, C. M., Carroll, A. R., Beard, B. L., Pietras, J. T., Carson, M. R., Norsted, B., Throckmorton, L.A. 2014. Controls on Sr isotopic evolution in lacustrine systems: Eocene green river formation, Wyoming. Chem. Geol. 380, 172-189.

Dominici, S., Danise, S., Benvenuti, M., 2018. Pliocene stratigraphic paleobiology in Tus-cany and the fossil record of marine megafauna. Earth-Science Reviews 176, 277-310.

Driussi, O., Maillard, A., Ochoa, D., Lofi, J., Chanier, F., Gaullier, V., et al.., 2015. Messinian Salinity Crisis deposits widespread over the Balearic Promontory: insights from new high-resolution seismic data. Mar. Petrol. Geol. 66, 41–54.

Dronkert, H., 1976. Late Miocene evaporites in the Sorbas Basin and adjoining areas. Mem. Soc. Geol. Ital. 16, 341-361.

Druckman, Y., Buchbinder, B., Martinotti, G. M., Tov, R. S., Aharon, P., 1995. The buried Afiq Canyon (eastern Mediterranean, Israel): a case study of a Tertiary submarine canyon exposed in Late Messinian times. Marine Geology, 123(3-4), 167-185.

Drury, A.J., Westerhold, T., Hodell, D., Röhl, U., 2018. Reinforcing the North Atlantic backbone: revision and extension of the composite splice at ODP Site 982. Climate of the Past, 14(3), 321-338.

Dypvik, H., Harris, N.B., 2001. Geochemical facies analysis of fine-grained siliciclastics using Th/U, Zr/Rb and (Zr+Rb)/Sr ratios. Chemical Geology 181, 131-146.

Emeis, K.-C, Robertson, A.H.F., Richter, C, et al., 1996. Proc. ODP, Initial Reports, 160: College Station, TX (ODP).

Englebrecht, A.C., Sachs, J.P., 2005. Determination of sediment provenance at drift sites using hydrogen isotopes and unsaturation ratios in alkenones. Geochim. Cosmochim. Acta 69, 4253-4265.

Estrada, F., Ercilla, G., Gorini, C., Alonso, B., Vazquez, J.T., García-Castellanos, D., et al., 2011. Impact of pulsed Atlantic water inflow into the Alboran Basin at the time of the Zanclean flooding. GeoMar. Lett. 31, 361-376.

Esu, D., 2007. Latest Messinian "Lago-Mare" Lymnocardiinae from Italy: close relations with the Pontian fauna from the Dacic Basin. Geobios, 40(3), 291-302.

Esu, D., Popov, S.V., 2012. Revision of late Messinian Lymnocardiinae (Bivalvia) from Piedmont (NW Italy). Rivista Italiana di Paleontologia e Stratigrafia, 118(2).

Evans, N.P., Turchyn, A.V., Gázquez, F., Bontognali, R.R., Chapman, H.J., Hodell, D.A., 2015. Coupled measurements of $\delta^{18}O$ and δD of hydration water and salinity of fluid inclusions in gypsum from the Messinian Yesares Member, Sorbas Basin (SE Spain). Earth and Planetary Science Letters. 430, 499-510.

Faranda, C., Gliozzi, E., Cipollari, P., Grossi, F., Darbaş, G., Gürbüz, K., ... Cosentino, D., 2013. Messinian paleoenvironmental changes in the easternmost Mediterranean Basin: Adana Ba-sin, southern Turkey. Turkish Journal of Earth Sciences, 22(5), 839-863.

Feng, Y.E., Yankelzon, A., Steinberg, J., Reshef, M., 2016. Lithology and characteristics of the Messinian evaporite sequence of the deep Levant Basin, Eastern Mediterranean. Mar. Geol. 376, 118-131.

Feng, Y.E., Steinberg, J., Reshef, M., 2017. Intra-salt deformation: implications for the evolution of the Messinian evaporites in the levant basin, eastern Mediterranean. Mar. Petrol. Geol. 88, 251-267.

Fiduk, J.C., 2009. Evaporites, petroleum exploration, and the Cenozoic evolution of the Libyan shelf margin, central North Africa. Marine and Petroleum Geology, 26(8), 1513-1527.

Flecker, R., Ellam, R.M., 1999. Distinguishing climatic and tectonic signals in the sedimentary successions of marginal basins using Sr isotopes: an example from the Messinian salinity cri-sis, Eastern Mediterranean. Journal of the Geological Society 156(4), 847-854.

Flecker, R., Ellam, R.M., 2006. Identifying Late Miocene episodes of connection and isola-tion in the Mediterranean-Paratethyan realm using Sr isotopes. Sediment. Geol. 188-189, 189-203.

Flecker, R., de Villiers, S., Ellam, R.M., 2002. Modelling the effect of evaporation on the salinity-$^{87}Sr/^{86}Sr$ relationship in modern and ancient marginal-marine systems: the Mediterranean Messinian Salinity Crisis. EPSL 203, 221-233.

Flecker, R., Krijgsman, W., Capella, W., de Castro Martíns, C., Dmitrieva, E., Mayser, J.P., Marzocchi, A., et al., 2015. Evolution of the late Miocene Mediterranean-Atlantic gateways and their impact on regional and global environmental change. Earth Sci. Rev. 150, 365-392.

Foeken, J.P.T., Dunai, T.J., Bertotti, G., Andriessen, P.A.M., 2003. Late Miocene to present exhumation in the Ligurian Alps (southwest Alps) with evidence for accelerated denudation during the Messinian salinity crisis. Geology 31, 707–800.

Fontes, J.-C., Letolle, R., Nesteroff, D., Ryan, W.B.F., 1973. Oxygen, Carbon, Sulfur and Hydrogen stable isotopes in carbonate and sulfate mineral phases of Neogene evaporites, sedi-ments and in interstitial waters, in: Texas A.M University, O.D.P.C.S., TX, United States (Ed.), Initial reports of the Deep Sea Drilling Project, covering Leg 13 of the cruises of the drilling vessel Glomar Challenger Lisbon, Portugal to Lisbon, Portugal, August-October 1970., United States 788-796.

Fortuin, A.R., Krijgsman, W., 2003. The Messinian of the Nijar basin (SE Spain): sedimen-tation, depositional environments and paleogeographic evolution. Sedimentary Geology 160, 213-242.

Fortuin, A.R., Dabrio, C.J., 2008. Evidence for Late Messinian seismites, Nijar Basin, south-east Spain. Sediment. 55, 1595-1622.

Fortuin, A.R., Kelling, J.M.D., Roep, T.B., 1995. The enigmatic Messinian -Pliocene sec-tion of Cuevas del Almanzora (Vera Basin, SE Spain) revisited-erosional features and strontium isotope ages. Sedimentary Geology 97, 177-201.

Frey-Martinez, J.F., Cartwright, J. A., Burgess, P. M., Bravo, J.V., 2004. 3D seismic inter-pretation of the Messinian Unconformity in the Valencia Basin, Spain. Geological Society, Lon-don, Memoirs, 29(1), 91-100.

Friedman, G.M., 1973. Petrographic data and comments on the depositional environment of the Miocene sulfates and dolomites at Sites 124, 132, and 134, western Mediterranean Sea. In: Ryan, W.B.F., Hsü, K.J., et al. (Eds.), Initial Reports of the Deep Sea Drilling Project 13. U. S. Government Printing Office,Washington, pp. 695–708.

Frigola, A., Prange, M., Schulz, M., 2018. Boundary conditions for the middle Miocene climate transition (MMCT v1. 0). Geoscientific Model Development, 11(4), 1607-1626.

Frigui, M., Youssef, M. B., Ouaja, M., 2016. Evidences of "Lago-Mare" episode around the Messinian-Pliocene boundary in eastern Tunisia (central Mediterranean). Journal of African Earth Sciences, 123, 57-74.

Fritz, P., Basharmal, G.M., Drimmie, R.J., Ibsen, J., Qureshi, R.M. 1989. Oxygen isotope exchange between sulphate and water during bacterial reduction of sulphate. Chemical Geology: Isotope Geoscience section 79, 99-105.

Fritz, M., Unkel, I., Lenz, J., Gajewski, K., Frenzel, P., Paquette, N., Lantuit, H., Körte, L., Wetterich, S., 2018. Regional environmental change versus local signal preservation in Holocene thermokarst lake sediments: A case study from Herschel Island, Yukon (Canada). J Paleolimnol 60, 77-96.

Gaillardet, J., Dupré, B., Louvat, P., Allegre, C.J., 1999. Global silicate weathering and CO2 consumption rates deduced from the chemistry of large rivers. Chemical geology, 159(1-4), 3-30.

Gallais, F., Gutscher, M.A., Graindorge, D., Klaeschen, D., 2018. - 12.B&E- Ionian Basin. In J. Lofi (Ed.), Seismic Atlas of the Messinian salinity crisis markers in the Mediterranean sea. Volume 2. - Mémoires de la Société géologique de France, n.s., 2018, t. 181, and Commission for the Geological Map of the World, p. 41-44.

García-Alix, A., Minwer-Barakat, R., Martín Suárez, E., Freudenthal, M., Aguirre, J., Kaya, F., 2016. Updating the Europe-Africa small mammal exchange during the late Messinian. Journal of Biogeography, 43(7), 1336-1348.

Garcia-Castellanos, D., Villaseñor, A., 2011. Messinian salinity crisis regulated by compet-ing tectonics and erosion at the Gibraltar arc. Nature 480, 359-363.

Garcia-Castellanos, D., Estrada, F., Jiménez-Munt, I., Gorini, C., Fernàndez, M., Vergés, J., De Vicente, R., 2009. Catastrophic flood of the Mediterranean after the Messinian salinity crisis. Nature 462, 10.

Garcia-Castellanos, D., Micallef, A., Estrada, F., Camerlenghi, A., Ercilla, G., Periáñez, R., Abril, J.M., 2020. The Zanclean megaflood of the Mediterranean-Searching for independent evi-dence. Earth-Science Reviews 201, 103061.

García-García, F., Corbí, H., Soria, J.M., Viseras, C., 2011. Architecture analysis of a river flood-dominated delta during an overall sea-level rise (Early Pliocene, SE Spain). Sediment Geol 237, 102-113.

García-Veigas, J., Orti, F., Rosell, L., Ayora, C., Rouchy, J.M., Lugli, S., 1995. The Mes-sinian salt of the Mediterranean: geochemical study of the salt from the Central Sicily Basin and comparison with the Lorca Basin (Spain). Bull. Soc. Géol. Fr., 166, 699-710. Gignoux, M., 1936. Géologie stratigraphique, 2°édition. Masson, Paris.

García-Veigas, J., Cendón, D.I., Gibert, L., Lowenstein, T.K. Artiaga, D. 2018. Geochemi-cal indicators in Western Mediterranean Messinian evaporites: Implications for the salinity crisis. Marine Geology 403, 197-214.

García-Veigas, J., Gibert, L., Cendon, D.I., Artiaga, D., Corbi, H., Soria, J.M., Lowenstein, T.K., Sanz, E., 2019. Late Miocene evaporite geochemistry of Lorca and Fortuna basins (Eastern Betics, SE Spain): Evidences of restriction and continentalization. Basin Res.

García-Veigas, J., Gibert Beotas, L., Cendón, D.I., Dela Pierre, F., Natalicchio, M., Artiaga, D., 2021. Sulfate isotope composition of Messinian evaporites in the Piedmont basin (Italy). Ge-ogaceta 70, 19-22.

Gargani, J., Moretti, I., Letouzey, J., 2008. Evaporite accumulation during the Messinian Salinity Crisis: the Suez rift case. Geophysical Research Letters, 35(2).

Gaullier, V., Chanier, F., Lymer, G., Vendeville, B., Maillard, A., Thinon, I., Lofi, J., Sage, F., Loncke, L., 2014. Salt tectonics and crustal tectonics along the Eastern Sardinian margin, Western Tyrrhenian: new insights from the «METYSS 1» cruise. Tectonophysics.

Geletti, R., Zgur, F., Del Ben, A., Buriola, F., Fais, S., Fedi, M., Forte, E., Mocknik, A., Paoletti, V., Pipan, M., Ramella, R., Romeo, R., Romi, A., 2014. The Messinian Salinity Crisis: new seismic evidence in the West-Sardinian Margin and Eastern Sardo-Provençal basin (West Mediterranean Sea). Mar. Geol. 351, 76–90.

Gennari, R., Iaccarino, S.M., Di Stefano, A., Sturiale, G., Cipollari, P., Manzi, V., Roveri, M., Cosentino, D., 2008. The Messinian–Zanclean boundary in the Northern Apennine. Strati-graphy 5, 307–322.

Gennari, R., Manzi, V., Angeletti, L., Bertini, A., Biffi, U., Ceregato, A., Rosso, A., 2013. A shallow water record of the onset of the Messinian salinity crisis in the Adriatic foredeep (Legnag-none section, Northern Apennines). Paleogeography, Paleoclimatology, Paleoecology, 386, 145-164.

Gennari, R., Lozar, F., Natalicchio, M., Zanella, E., Carnevale, G., Dela Pierre F., 2020. Chronology of the Messinian events in the northernmost part of the Mediterranean: the Govone section (Piedmont Basin, NW Italy). Rivista Italiana di Paleontologia e Stratigrafia 126, 517–60.

Ghibaudo, G., Clari, P., Perello, M., 1985. Litostratigrafia, sedimentologia ed evoluzione tettonico-sedimentaria dei depositi miocenici del margine sud-orientale del bacino terziario ligure-piemontese (Valli Borbera, Scrivia e Lemme). In memoria di Carlo Sturani. Bollettino della Società Geologica Italiana, 104(3), 349-397.

Ghielmi, M., Minervini, M., Nini, C., Rogledi, S., Rossi, M., Vignolo, A., 2010. Sedimen-tary and tectonic evolution in the eastern Po-Plain and northern Adriatic Sea area from Messinian to Middle Pleistocene (Italy). Rendiconti Lincei, 21(1), 131-166.

Ghielmi, M., Minervini, M., Nini, C., Rogledi, S., Rossi, M., 2013. Late Miocene-Middle Pleistocene sequences in the Po Plain-Northern Adriatic Sea (Italy): The stratigraphic record of modification phases affecting a complex foreland basin. Marine and Petroleum Geology, Special Issue: The Geology of the Periadriatic Basin and of the Adriatic Sea 42, 50-81.

Ghielmi, M., Rogledi, S., Vigna, B., Violanti, D. 2019. La successione messiniana e pliopleistocenica del Bacino di Savigliano (Settore occidentale del Bacino Terziario Piemontese). Geologia Insubrica, 13(1), 140 pp.

Gignoux, M., 1936. Géologie stratigraphique, 2°édition. Masson, Paris.

Gillet, S., 1932. Essai de classification du Miocène superieur et du Pliocene inferieur de Roumanie. La Transylvanie et le Banat. Comptes Rendus Hebdomadaires des séances de l'Acadé-mie des sciences. Paris: Académie des Sciences.

Gillet, S., 1933. Essai de classification du Miòcene supérieur et du Pliocène inférieur de Roumanie. Le bassin dacique. Comptes Rendus Hebdomadaires des séances de l'Académie des sciences. 01/1933. Paris: Académie des Sciences.

Giunta, S., Negri, A., Maffioli, P., Sangiorgi, F., Capotondi, L., Morigi, C., Principato, M.S., Corselli, C., 2006. Phytoplankton dynamics in the eastern Mediterranean Sea during marine isotopic stage 5e. Palaeog., Palaeoclim., Palaeoec., 235(1-3), 28-47.

Gladstone, R., Flecker, R., Valdes, P., Lunt, D., Markwick, P., 2007. The Mediterranean hydrologic budget from a Late Miocene global climate simulation. Paleogeography, Paleoclima-tology, Paleoecology, 251(2), 254-267.

Gliozzi, E., 1999. A late Messinian brackish water ostracod fauna of Paratethyan aspect from Le Vicenne Basin (Abruzzi, central Apennines, Italy). Paleogeography, Paleoclimatology, Paleoecology, 151(1-3), 191-208.

Gliozzi, E., Grossi, F., 2008. Late Messinian lago-mare ostracod paleoecology: A corre-spondence analysis aroach. Paleogeography, Paleoclimatology, Paleoecology, 264(3-4), 288-295.

Gliozzi, E., Ceci, M. E., Grossi, F., Ligios, S., 2007. Paratethyan ostracod immigrants in Italy during the Late Miocene. Geobios, 40(3), 325-337.

Gliozzi, E., Rodriguez-Lazaro, J., Pipik, R., 2017. The Neogene Mediterranean origin of Cyprideis torosa (Jones, 1850). Journal of Micropalaeontology, 36(1), 80-93.

Glok-Galli, M., Vadillo-Pérez, I., Jiménez-Gavilán, P., Ojeda, L., Urresti-Estala, B., Mar-tínez, D.E., 2022. Application of hydrochemical and multi-isotopic ($^{87}Sr/^{86}Sr$, $\delta^{13}C$-DIC, $\delta^{2}H$-H_2O, $\delta^{18}O$-H_2O) tools to determine contamination sources and processes in the Guadalhorce Riv-er Basin, southern Spain. Science of The Total Environment, 828, 154424.

Golovina, L.A., Radionova, E.P., van Baak, C.G., Krijgsman, W., Palcu, D.V., 2019. A Late Maeotian age (6.7-6.3 Ma) for the enigmatic "Pebbly Breccia" unit in DSDP Hole 380A of the Black Sea. Paleog., Paleoclimatology, Paleoecology, 533, 109269.

Gomes, M.L., Johnston, D.T., 2017. Oxygen and sulfur isotopes in sulfate in modern eux-inic systems with implications for evaluating the extent of euxinia in ancient oceans. Geochimica et Cosmochimica Acta 205, 331-359.

Gorini, C., Lofi, J., Duvail, C., Dos Reis, A.T., Guennoc, P., Lestrat, P., Mauffret, A., 2005. The Late Messinian salinity crisis and Late Miocene Tectonism: interaction and consequence on the physiography and post-rift evolution of the gulf of Lions margin. Marine and Petroleum Geolo-gy 22, 695-712.

Goudie, A., 2005. The drainage of Africa since the Cretaceous, Geomorphology, 67, 437–456.

Govers, R., 2009. Choking the Mediterranean to dehydration: the Messinian salinity crisis. Geology, 37(2), 167-170.

Grande, L., Nelson, G.J., 1985. Interrelationships of fossil and recent anchovies (Teleostei, Engrauloidea) and description of a new species from the Miocene of Cyprus. American Museum of Natural History.

Griffin, D.L., 2002. Aridity and humidity: two aspects of the late Miocene climate of North Africa and the Mediterranean. Paleogeography, Paleoclimatology, Paleoecology, 182(1-2), 65-91.

Griffin, D., 2006. The late Neogene Sahabi rivers of the Sahara and their climatic and environmental implications for the Chad basin, J. Geol. Soc., 163, 905–921

Grinsted, A., Moore, J.C., Jevrejeva, S., 2004. Application of the cross wavelet transform and wavelet coherence to geophysical time series. Nonlinear processes in geophysics, 11(5/6), 561-566.

Grossi, F., Cosentino, D., Gliozzi, E., 2008. Late Messinian Lago-Mare ostracods and pale-oenvironments of the central and eastern Mediterranean Basin. Bollettino della Società Paleontologica Italiana, 47(2), 131-146.

Grossi, F., Gliozzi, E., Cosentino, D., 2011. Paratethyan ostracod immigrants mark the bio-stratigraphy of the Messinian Salinity Crisis. Joannea Geologie und Paleontologie 11, 66-68.

Grossi, F., Gliozzi, E., Anadón, P., Castorina, F., Voltaggio, M., 2015. Is Cyprideis agrigen-tina Decima a good paleosalinometer for the Messinian Salinity Crisis? Morphometrical and geo-chemical analyses from the Eraclea Minoa section (Sicily). Paleogeography, Paleoclimatology, Paleoecology 419, 75-89.

Grothe, A., Sangiorgi, F., Mulders, Y. R., Vasiliev, I., Reichart, G.-J., Brinkhuis, H., Stoica, M., Krijgsman, W., 2014. Black Sea desiccation during the Messinian Salinity Crisis: Fact or fic-tion? Geology 42, 7, 563-566.

Grothe, A., Sangiorgi, F., Brinkhuis, H., Stoica, M., Krijgsman, W., 2018. Migration of the dinoflagellate Galeacysta etrusca and its implications for the Messinian Salinity Crisis. Newslet-ters on Stratigraphy, 51(1), 73-91.

Grothe, A., Andreetto, F., Reichart, G. J., Wolthers, M., Van Baak, C. G., Vasiliev, I., Stoi-ca, M., Sangiorgi, F., Middelburg, J.J., Davies G.R., Krijgsman, W., 2020. Paratethys pacing of the Messinian Salinity Crisis: Low salinity waters contributing to gypsum precipitation?. Earth and Planetary Science Letters, 532, 116029.

Grunert, P., Harzhauser, M., Rosenthal, Y., Carnevale, G., 2016. Estuarine Lago Mare fauna from the Tertiary Piedmont Basin indicates episodic Atlantic/Mediterranean exchange during the final stage of the Mediterranean Salinity Crisis. Paleogeography, Paleoclimatology, Paleoecology 457, 70-79.

Guennoc, P., Réhault, J.P., Thinon, I., 2011. West-Corsica Margin: MSC basinal units. In: Lofi, J., et al. (Eds.), Mémoires de la Société géologique de France and World Geological Map Commission ed, pp. 1-72.

Guerra-Merchán, A., Serrano, F., Garcés, M., Gofas, S., et al., 2008. Caracterización de la sedimentación Lago Mare (Messiniense terminal) y de la transgresión del comienzo del Plioceno en la cuenca de Málaga (Cordillera Bética). Geogaceta 44, 207–210.

Guerra-Merchán, A., Serrano, F., Garcés, M., Gofas, S., Esu, D., Gliozzi, E., Grossi, F., 2010. Messinian Lago-Mare deposits near the strait of Gibraltar (Malaga basin, S Spain). Paleo-geography, Paleoclimatology, Paleoecology 285(3-4), 264-276.

Guerra-Merchán, A., Serrano, F., Hlila, R., El Kadiri, K., de Galdeano, C. S., Garcés, M., 2014. Tectono-sedimentary evolution of the peripheral basins of the Alboran Sea in the arc of Gi-braltar during the latest Messinian-Pliocene. Journal of Geodynamics, 77, 158-170.

Guibourdenche, L., Cartigny, P., Dela Pierre, F., Natalicchio, M., Aloisi, G., 2022. Cryptic sulfur cycling during the formation of giant gypsum deposits. Earth and Planetary Science Letters 593.

Gülyüz, E., Durak, H., Özkaptan, M., Krijgsman, W., 2020. Paleomagnetic constraints on the early Miocene closure of the southern Neo-Tethys (Van region; East Anatolia): Inferences for the timing of Eurasia-Arabia collision, Global Planetary Change, 185, 103089.

Güneş, P., Aksu, A.E., Hall, J., 2018. Internal seismic stratigraphy of the Messinian evapo-rites across the northern sector of the eastern Mediterranean Sea. Marine and Petroleum Geology, 91, 297-320.

Gustavson, T.C., Smpkins, W.W., Alhades, A., Hoadley, A., 1982. Evaporite dissolution and development of karst features on the Rolling Plains of the Texas Panhandle. Earth Surface Processes and Landforms, 7(6), 545-563.

Gvirtzman, Z., Reshef, M., Buch-Leviatan, O., Ben-Avraham, Z., 2013. Intense salt defor-mation in the Levant Basin in the middle of the Messinian salinity crisis. Earth Planet Sci. Lett. 379, 108-119.

Gvirtzman, Z., Reshef, M., Buch-Leviatan, O., Groves-Gidney, G., Karcz, Z., Makovsky, Y., and Ben-Avraham, Z., 2015. Bathymetry of the Levant basin: Interaction of salt-tectonics and surficial mass movements. Marine Geology, 360, 25-39.

Gvirtzman, Z., Manzi, V., Calvo, R., Gavrieli, I., Gennari, R., Lugli, S., Reghizzi, M., Ro-veri, M., 2017. Intra-Messinian truncation surface in the Levant Basin explained by subaqueous dissolution. Geology 45(10), 915-918.

Hajj, F., Poszwa, A., Bouchez, J., Guérold, F., 2017. Radiogenic and "stable" strontium isotopes in provenance studies: A review and first results on archaeological wood from shipwrecks. Journal of Archaeological Science, 86, 24-49.

Hajós, M., 1973. 34.5. The Mediterranean diatoms. Proceedings of the Ocean Drilling Pro-gram: Initial report. Part A, 944.

Hallett, D. 2002. Petroleum Geology of Libya. Elsevier Inc., New York, 503 pp.

Hällfors, G., 2004. Checklist of Baltic Sea phytoplankton species (including some hetero-trophic protistan groups). Baltic Sea Environment Proceedings 95: [1]-208.

Han, S., Zhang, Y., Huang, J., Rui, Y., Tang, Z., 2020. Elemental Geochemical Characteri-zation of Sedimentary Conditions and Organic Matter Enrichment for Lower Cambrian Shale Formations in Northern Guizhou, South China. Minerals 10, 793, 1-21.

Haq, B., Gorini, C., Baur, J., Moneron, J., Rubino, J.L. 2020. Deep Mediterranean's Mes-sinian evaporite giant: How much salt?. Global and Planetary Change, 184, 103052.

Hardie, L.A., Lowenstein, T.K., 2004. Did the Mediterranean Sea dry out during the Mio-cene? A reassessment of the evaporite evidence from DSDP Legs 13 and 42A cores. J. Sediment. Res. 74, 453–461.

Hart, W., Quade, J., Madsen, D., Kaufman, D., Oviatt, C., 2004. The $^{87}Sr/^{86}Sr$ ratios of la-custrine carbonates and lake-level history of the Bonneville paleolake system. Geol. Soc. Am. Bull. 116 (9), 1107-1119.

Harzhauser, M., Neubaupper, T.A., Georgopoulou, E., Esu, D., D'Amico, C., Pavia, G., Giuntelli, P., Carnevale, G., 2015. Late Messinian continental and Lago-Mare gastropods from the Tertiary Piedmont Basin, NW Italy. Boll. Soc. Pal.. Ital. 54, 1-53.

Heida, H., Raad, F., Garcia-Castellanos, D., Jiménez-Munt, I., Maillard, A., Lofi, J., 2022. Flexural-isostatic reconstruction of the Western Mediterranean during the Messinian Salinity Cri-sis: implications for water level and basin connectivity. Basin Research 34(1), 50-80.

Herbert, T.D., Lawrence, K.T., Tzanova, A., Peterson, L.C., Caballero-Gill, R., Kelly, C.S., 2016. Late Miocene global cooling and the rise of modern ecosystems. Nat. Geosci. 9, 843-847.

Hersey, J.B., 1965. Sedimentary basins of the Mediterranean Sea. In: Whittard, W.F., Brad-shaw, R. (Eds.), Submarine Geology and Geophysics. Proceedings 17th Symposium Colston Res. Soc. April 5–9, 1965. Butterworths, London, pp. 75–91.

Heymann, C., Nelle, O., Dörfler, W., Zagana, H., Nowaczyk, N., Xue, J., Unkel, I., 2009. Late Glacial to mid-Holocene palaeoclimate development of Southern Greece inferred from the sediment sequence of Lake Stymphalia (NE-Peloponnese). Quaternary International 302, 42-60.

Hilgen, F.J., 1991. Astronomical calibration of Gauss to Matuyama sapropels in the Medi-terranean and implication for the geomagnetic polarity time scale. Earth and planetary science letters, 104(2-4), 226-244.

Hilgen, F.J., Krijgsman, W., Langereis, C. G., Lourens, L.J., Santarelli, A., Zachariasse, W.J. 1995. Extending the astronomical (polarity) time scale into the Miocene. Earth and Planetary Science Letters, 136, 495-510.

Hilgen, F.J., Krijgsman, W., Raffi, I., Turco, E., Zachariasse, W.J., 2000. Integrated stratig-raphy and astronomical calibration of the Serravallian/Tortonian boundary section at Monte Gib-liscemi (Sicily, Italy). Marine Micropaleontology, 38(3-4), 181-211.

Hilgen, F., Kuiper, K., Krijgsman, W., Snel, E., van der Laan, E., 2007. Astronomical tun-ing as the basis for high resolution chronostratigraphy: the intricate history of the Messinian Salini-ty Crisis. Stratigraphy, 4(2-3), 231-238.

Hodell, D.A., Benson, R.H., Kent, D.V., Boersma, A., Rakic-el Bied, K., 1994. Magneto-stratigraphic, biostratigraphic, and stable isotope stratigraphy of an Upper Miocene drill core from the Salé Briqueterie (northwest Morocco): A high-resolution chronology for the Messinian stage. Paleoceanography, 9, 835-855.

Hodell, D.A., Curtis, J.H., Sierro, F.J., Raymo, M.E., 2001. Correlation of late Miocene to early Pliocene sequences between the Mediterranean and North Atlantic, Paleoceanography, 16, 164-178.

Horwitz, E., Chiarizia, R., Dietz, M.L., 1992. A novel strontium-selective extraction chro-matographic resin. Solvent Extr Ion Exc 10:313–336

Hohenegger, J., Andersen, N., Baldi, K., Coric, S., Pervesler, P., Rupp, C., Wagreich, M., 2008. Paleoenvironment of the Early Badenian (Middle Miocene) in the southern Vienna Basin (Austria)-multivariate analysis of the Baden-Sooss section. Geologica Carpathica, 59(5): 461-488.

Hoyle, T.M., Leroy, S.A.G., López-Merino, L., Richards, K., 2018. Using fluorescence mi-croscopy to discern in situ from reworked palynomorphs in dynamic depositional environments-An example from sediments of the late Miocene to early Pleistocene Caspian Sea. Review of Palaeo-botany and Palynology 256, 32-49.

Hsü, K.J., 1972. Origin of Saline Giants: a critical review after the discovery of the Medi-terranean evaporite. Earth-Sci. Rev., 8, 371-396.

Hsü, K.J., Ryan, W.B.F., Cita, M., 1973a. Late Miocene desiccation of the Mediterranean. Nature 242, 240.

Hsü, K.J., Cita, M.B., Ryan, W.B.F., 1973b. The origin of the Mediterranean evaporites. In: Ryan, W.B.F., Hsü, K.J., et al. (Eds.), Initial Reports of the Deep Sea Drilling Project 13. U. S. Government Printing Office, Washington, pp. 1203-1231.

Hsü, K.J., Schreiber, B.C., 1973c. Petrography of a halite sample from Hole 134-Balearic Abyssal Plain. In: Ryan, W.B.F., Hsü, K.J., et al. (Eds.), Initial Reports of the Deep Sea Drilling Project 13. U. S. Government Printing Office, Washington, pp. 708-711.

Hsü, K.J., Montadert, L., Bernouilli, D., Cita, M.B., Erikson, A., Garrison, R.G., Kidd, R.B., Mélières, F., Müller, C., Wright, R., 1978a. History of the Mediterranean salinity crisis. In: Hsü, K.J., Montadert, L., et al. (Eds.), Initial Reports of the Deep Sea Drilling Project. U.S. Government Printing Office, Washington, DC.

Hsü, K.J., Montadert, L., Bernoulli, D., Bizon, G., Cita, M., Erickson, A., Fabricius, F., Gar-rison, R.E., Kidd, R.B., Mélières, F., Müller, C., Wright, R.C., 1978b. Initial reports of the deep sea drilling project: DSDP volume XLII Part 1.

Hull, P.M., Norris, R.D., 2011. Diverse patterns of ocean export productivity change across the Cretaceous-Paleogene boundary: New insights from biogenic barium. Paleoceanography 26, 1-10.

Iaccarino, S., Bossio, A., 1999. Paleoenvironment of uppermost Messinian sequences in the western Mediterranean (Sites 974, 975, and 978). In Proceedings of the Ocean Drilling Program, Scientific Results (Vol. 161, 529-541). College Station, TX: Ocean Drilling Program.

Iaccarino, S.M., Cita, M.B., Gaboardi, S., Gruppini, G.M., 1999. 15. High-Resolution Bio-stratigraphy at the Miocene/Pliocene boundary in Holes 974B and 975B, Western Mediterranean. In Proceedings of the ODP: Scientific Results (Vol. 161, p. 197).

Iaccarino, S.M., Bertini, A., Di Stefano, A., Ferraro, L., Gennari, R., Grossi, F., Lirer, F., Manzi, V., Menichetti, E., Ricci Lucchi, M., Taviani, M., Sturiale, G., and Angeletti, L., 2008. The Trave section (Monte dei Corvi, Ancona, central Italy): An integrated paleontological study of the Messinian deposits: Stratigraphy, v. 5, no. 3–4, p. 281-306.

Ingram, B.L., Sloan, D., 1992. Strontium isotopic composition of estuarine sediments as paleosalinity-paleoclimate indicator. Science 255, 68-72.

Irace, A., Dela Pierre, F., Clari, P., 2005. "Normal" and "chaotic" deposits in the Messinian Gessoso-Solfifera Fm. at the North-Eastern border of the Langhe domain (Tertiary Piedmont Basin). Bol. Società Geol. Italiana, Special Publication 4, 77–85.

Irace, A., Clemente, P., Natalicchio, M., Ossella, L., Trenkwalder, S., De Luca, D., Mosca, P., Piana, F., Polino, R., Violanti, D., 2009. Geologia e idrostratigrafia profonda della Pianura Pa-dana occidentale (Regione Piemonte).

Izumi, K., Haneda, Y., Suganuma, Y., Okada, M., Kubota, Y., Nishida, N., Kawamata, M., Matsuzaki, T., 2021. Multiproxy sedimentological and geochemical analyses across the Lower–Middle Pleistocene boundary: chemostratigraphy and paleoenvironment of the Chiba composite section, central Japan. Progress in Earth and Planetary Science 8:10, 2-19.

Jagger, L.J., Bevan, T.G., McClay, K.R., 2020. Tectono-stratigraphic evolution of the SE Mediterranean passive margin, offshore Egypt and Libya. Geological Society, London, Special Publications, 476(1), 365-401.

Johnston, D.T., Gill, B.C., Masterson, A., Beirne, E., Casciotti, K.L., Kna, A.N. Berelson, W., 2014. Placing an upper limit on cryptic marine sulphur cycling. Nature 513, 530-533.

Jolivet, L., Augier, R., Robin, C., Suc, J.-P., Rouchy, J.-M., 2006. Lithospheric-scale geo-dynamic context of the Messinian Salinity Crisis. Sediment. Geol. 188-189, 9-33.

Jonk, R., Biermann, C., 2002. Deformation in Neogene sediments of the Sorbas and Vera basins (SE Spain): constraints on simpleshear deformation and rigid body rotation along major strike-slip faults. J. Struct. Geol. 24, 963- 977.

Just, J., Hübscher, C., Betzler, C., Lüdmann, T., Reicherter, K., 2011. Erosion of continen-tal margins in the Western Mediterranean due to sea-level stagnancy during the Messinian Salinity Crisis. Geo-Marine Letters, 31(1), 51-64.

Kaplan, I.R., Rittenberg, S.C., 1964. Microbiological Fractionation of Sulphur Isotopes. Microbiology 34, 195-212.

Karakitsios, V., Cornée, J., Tsourou, T., Moissette, P., Kontakiotis, G., Agiadi, K., Manout-soglou, E., Triantaphyllou, M., Koskeridou, E., 2017a. Messinian salinity crisis record under strong freshwater input in marginal, intermediate, and deep environments: the case of the North Aegean. Paleogr. Paleoclimatol. Paleoecol. 485, 316-335.

Karakitsios, V., Roveri, M., Lugli, S., Manzi, V., Gennari, R., Antonarakou, A., Tri-antaphyllou, M., Agiadi, K., Kontakiotis, G., Kafousia, N., de Rafelis, M., 2017b. A record of the Messinian salinity crisis in the eastern Ionian tectonically active domain (Greece, eastern Mediter-ranean). Basin Res, 29, 203-233.

Kartveit, K. H., Ulsund, H. B., Johansen, S. E., 2019. Evidence of sea level drawdown at the end of the Messinian salinity crisis and seismic investigation of the Nahr Menashe unit in the northern Levant Basin, offshore Lebanon. Basin Res., 31(5), 827-840.

Kastens, K.A., Mascle, J., 1990. The geological evolution of the Tyrrhenian Sea: An intro-duction to the scientific results of ODP Leg 107. In Proceedings of the Ocean Drilling Program, Scientific Results (Vol. 107, No. 3, p. 26). College Station, TX (Ocean Drilling Program).

Kastens, K.A., Mascle, J., Auroux, C., et al., 1987. Proc. ODP, Init. Repts., 107. College Station, TX (Ocean Drilling Program).

Keller, G., Abramovich, S., 2009. Lilliput effect in late Maastrichtian planktic foraminif-era: Response to environmental stress: Paleogeography, Paleoclimatology, Paleoecology, 284, 47-62.

Keogh, S.M., Butler, R.W.H., 1999. The Mediterranean water body in the late Messinian: interpreting the record from marginal basins on Sicily. Journal of the Geological Society, 156(4), 837-846.

Kennet, J.P., Srinivasan, M.S., 1983. Neogene planktonic foraminifera. A phylogenetic at-las. Hutchinson Ross Pub. Co., 265.

Kirchner, K.L., Behr, W.M., Loewy, S., Stockli, D.F. 2016. Early Miocene subduction in the western Mediterranean: Constraints from Rb-Sr multimineral isochron geochronology. Geo-chemistry, Geophysics, Geosystems, 17(5), 1842-1860.

Kirkham, C., Bertoni, C., Cartwright, J., Lensky, N. G., Sirota, I., Rodriguez, K., Hodgson, N., 2020. The demise of a 'salt giant' driven by uplift and thermal dissolution. Earth and Planetary Science Letters, 531, 115933.

Kochhann, M.V.L., Savian, J.F., Tori, F., Catanzariti, R., Coccioni, R., Frontalini, F., Jo-vane, L., Florindo, F., Monechi, S., 2018. Orbital tuning for the middle Eocene to early Oligocene Monte Cagnero Section (Central Italy): Paleoenvironmental and paleoclimatic implications.

Kouwenhoven, T.J., Seidenkrantz, M.S., Van der Zwaan, G.J., 1999. Deepwater changes: the near-synchronous disappearance of a group of benthic foraminifera from the Late Miocene Mediterranean. Palaeogeogr Palaeoclimatol Palaeoecol 152(3):259–281

Kouwenhoven, T.J., Hilgen, F.J., Van der Zwaan, G.J., 2003. Late Tortonian–early Mes-sinian stepwise disruption of the Mediterranean–Atlantic connections: constraints from benthic foraminiferal and geochemical data. Palaeogeogr Palaeoclimatol Palaeoecol 198(3):303–319

Kováč, M., Andreyeva-grigorovich, A., Bajraktarević, Z., Brzobohatý, R., Filipescu, S., Fodor, L., Harzhauser, M., Nagymarosy, A., Oszczypko, N., Pavelić, D., Rögl, F., Saftić, B., Sliva, U., Studencka, B., 2007. Badenian evolution of the Central Paratethys Sea : paleogeography, cli-mate and eustatic sea-level changes. Geol. Carpathica 58, 579-606.

Krijgsman, W., Meijer, P. T., 2008. Depositional environments of the Mediterranean "Low-er Evaporites" of the Messinian salinity crisis: Constraints from quantitative analyses. Marine Ge-ology, 253(3-4), 73-81.

Krijgsman, W., Hilgen, F.J., Raffi, I., Sierro, F.J., Wilson, D.S., 1999a. Chronology, causes, and progression of the Messinian salinity crisis. Nature 400, 652-655.

Krijgsman, W., Hilgen, F.J., Marabini, S., Vai, G.B., 1999b. New paleomagnetic and cy-clostratigraphic age constraints on the Messinian of the Northern Apennines (Vena del Gesso Ba-sin, Italy). Memorie della Società Geologica Italiana 54, 25-33.

Krijgsman, W., Garcés, M., Agustı, J., Raffi, I., Taberner, C., Zachariasse, W.J., 2000. The 'Tortonian salinity crisis' of the eastern Betics (Spain). Earth and Planetary Science Letters, 181(4), 497-511.

Krijgsman, W., Fortuin, A.R., Hilgen, F.J., Sierro, F.J., 2001. Astrochronology for the Mes-sinian Sorbas basin (SE Spain) and orbital (precessional) forcing for evaporite cyclicity. Sedimen-tary Geology 140, 43-60.

Krijgsman, W., Gaboardi, S., Hilgen, F.J., Iaccarino, S., Kaenel, E.D., Laan, E.V.D., 2004. Revised astrochronology for the Ain el Beida section (Atlantic Morocco): no glacio-eustatic con-trol for the onset of the Messinian Salinity Crisis. Stratigr, 1, 87-101.

Krijgsman, W., Leewis, M.E., Garcés, M., Kouwenhoven, T.J., Kuiper, K.F., Sierro, F.J., 2006. Tectonic control for evaporite formation in the Eastern Betics (Tortonian; Spain). Sedimentary Geology 188/189, 155-170.

Krijgsman, W., Stoica, M., Vasiliev, I., Popov, V.V., 2010. Rise and fall of the Paratethys Sea during the Messinian Salinity Crisis. Earth and Planetary Science Letters, 290(1-2), 183-191.

Krijgsman, W., Capella, W., Simon, D., Hilgen, F.J., Kouwenhoven, T.J., Meijer, P.Th., Sierro, F.J., Tulbure, M.A., van den Berg, B.C.J., van der Schee, M., Flecker, R., 2018. The Gibraltar Corridor: watergate of the Messinian Salinity Crisis. Mar. Geol. 403, 238–246.

Krijgsman, W., Palcu, D., Andreetto, F., Stoica, M., Mandic, O., 2020a. Changing seas in the late Miocene Northern Aegean: A Paratethyan approach to Mediterranean basin evolution. Earth-Science Reviews, 103386.

Krijgsman, W., Stoica, M., Hoyle, T.M., Jorissen, E.L., Lazarev, S., et al., 2020b. The myth of the Messinian Dardanelles: Late Mio-cene stratigraphy and paleogeography of the ancient Aegean-Black Sea gateway. Paleogeography, Paleoclimatology, Paleoecology, 110033.

Kuznetsov, A.B., Semikhatov, M.A., Gorokhov, I.M., 2012. The Sr isotope composition of the world ocean, marginal and inland seas: Implications for the Sr isotope stratigraphy. Stratigra-phy and Geological Correlation, 20(6), 501-515.

Ladegaard-Pedersen, P., Achilleos, M., Dörflinger, G., Frei, R., Kristiansen, K., Frei, K.M., 2020. A strontium isotope baseline of Cyprus. Assessing the use of soil leachates, plants, ground-water and surface water as proxies for the local range of bioavailable strontium isotope composi-tion. Science of The Total Environment, 708, 134714.

Laskar, L.J., Robutel, P., Joutel, F., Gastineau, M., Correia, A.C.M., Levrard, B., 2004. A long term numerical solution for the insolation quantities of thQe Earth. Astron. Astrophys. 428, 261-285.

Lazarev, S., de Leeuw, A., Stoica, M., Mandic, O., van Baak, C.G.C., Vasiliev, I., Krijgs-man, W., 2020. From Khersonian drying to Pontian "flooding": Late Miocene stratigraphy and paleoenvironmental evolution of the Dacian Basin (Eastern Paratethys). Global and Planetary Change, 103224.

Leavitt, W.D., Halevy, I., Bradley, A.S., Johnston, D.T., 2013. Influence of sulfate reduction rates on the Phanerozoic sulfur isotope record. Proceedings of the National Academy of Sciences 110, 11244.

Leila, M., Moscariello, A., Šegvić, B., 2018. Depositional facies controls on the diagenesis and reservoir quality of the Messinian Qawasim and Abu Madi formations, onshore Nile Delta, Egypt. Geological Journal, 54(3), 1797-1813.

Lenton, T.M., Daines, S.J., Mills, B.J., 2018. COPSE reloaded: An improved model of biogeochemical cycling over Phanerozoic time. Earth-Science Reviews, 178, 1-28.

Lewis, J,, Pike, AWG,, Coath, C., Evershed, R., 2017. 'Strontium concentration, radiogenic ($^{87}Sr/^{86}Sr$) and stable ($\delta^{88}Sr$) strontium isotope systematics in a controlled feeding study.' Science and Technology of Archaeological Research 3, 53-65

Li, X.S., Berger, A., Loutre, M.-F., Maslin, M.A., Haug, G.H., Tiedemann, R., 1998. Simulating late Pliocene Northern Hemisphere climate with the LLN-2D model. Geophys. Res. Lett., 25, 915–918.

Ligios, S., Gliozzi, E., 2012. The genus Cyprideis Jones, 1857 (Crustacea, Ostracoda) in the Neogene of Italy: a geometric morphometric approach. Revue de Micropaleontologie, 55, 171–207.

Lirer, F., Foresi, L. M., Iaccarino, S. M., Salvatorini, G., Turco, E., Cosentino, C., Sierro, F.J., Caruso, A., 2019. Mediterranean Neogene planktonic foraminifer biozonation and biochro-nology. Earth-Science Reviews, 196, 102869.

Liu, J., Li, S., Zhong, J., Zhu, X., Guo, Q., Lang, Y., Han, X., 2017. Sulfate sources constrained by sulfur and oxygen isotopic compositions in the upper reaches of the Xijiang River, China. Acta Geochimica 36, 611-618.

Lloyd, R.M., 1968. Oxygen isotope behavior in the Sulfate-Water System. Journal of Geophys. Res. (1896-1977) 73, 6099-6110.

Lofi, J., 2018. Seismic Atlas of the Messinian salinity crisis markers in the Mediterranean sea. Volume 2 - Mémoires de la Société géologique de France, n.s., 2018, t. 181, and Commission for the Geological Map of the World, 72 p. + DVD.

Lofi, J., Gorini, C., Berne, S., Clauzon, G., Dos Reis, A.T., Ryan, W.B.F., Steckler, M.S., 2005. Erosional processes and paleo-environmental changes in the Western Gulf of Lions (SW France) during the Messinian Salinity Crisis. Mar. Geol. 217, 1–30.

Lofi, J., Sage, F., Déverchère, J., Loncke, L., Maillard, A., Gaullier, V., Thinon, I., Gillet, H., Guennoc, P., Gorini, C., 2011a. Refining our knowledge of the Messinian salinity crisis records in the offshore domain through multi-site seismic analysis. Bulletin de la Société géologique de France, 182(2), 163-180.

Lofi, J., Déverchère, J., Gaullier, V., Gillet, H., Gorini, C., Guennoc, P., Loncke, L., Mail-lard, A., Sage, F., Thinon, I., 2011b. Seismic atlas of the "Messinian Salinity Crisis" markers in the Mediterranean and Black seas. Commission for the Geological Map of the World and Memoires de la Société Géologique de France, Nouvelle Série, p. 72.

Loget, N., Davy, P., Van Den Driessche, J., 2006. Mesoscale fluvial erosion parameters de-duced from modelling the Mediterranean sea-level drop during the Messinian (late Miocene). Journal of Geophysical Research, 111, F03005.

Loncke, L., Gaullier, V., Mascle, J., Vendeville, B., Camera, L., 2006. The Nile deep-sea fan: An example of interacting sedimentation, salt tectonics, and inherited subsalt paleotopograph-ic features. Marine and Petroleum Geology, 23, 297-315.

Londeix, L., Benzakour, M., Suc, J.P., Turon, J.L., 2007. Messinian paleoenvironments and hydrology in Sicily (Italy): the dinoflagellate cyst record. Geobios, 40(3), 233-250.

Longinelli, A., 1979. Isotope geochemistry of some Messinian evaporates: paleoenviron-mental implications. Paleogeography, Paleoclimatology, Paleoecology 29, 95-123.

Longinelli, A., Craig, H., 1967. Oxygen-18 variations in sulfate ions in sea water and saline lakes. Science, 156(3771), 56-59.

López-Garrido, A.C., Sanz de Galdeano, C., 1999. Neogene sedimentation and tectonic-eustatic control of the Malaga basin, South Spain. J. Petrol. Geol. 22 (1), 81-96.

Loreto, M. F., Zitellini, N., Ranero, C. R., Palmiotto, C., Prada, M., 2020. Extensional tec-tonics during the Tyrrhenian back-arc basin formation and a new morpho-tectonic map. Basin Re-search, 33(1), 138-158.

Lourens, L.J., Antonarakou, A., Hilgen, F.J., Van Hoof, A.A.M., Vergnaud-Grazzini, C., Zachariasse, W., 1996. Evaluation of the Plio-Pleistocene astronomical timescale: Paleoceanogra-phy, v. 11, pp. 391-413.

Lourens, L., Hilgen, F., Shackleton, N.J., Laskar, J., Wilson, D., 2004. The Neogene period. In: Gradstein, F. M., J. G.Ogg & A. G. Smith (eds.): A geologic time scale 2004. – Cambridge Univ. Press: 409–440, Cambridge.

Lowenstein, T.K., 1988. Origin of depositional cycles in a Permian" saline giant": The Salado (McNutt zone) evaporites of New Mexico and Texas. Geological Society of America Bulletin, 100(4), 592-608.

Lozano, D.O., 2016. Astrobiochronological Constraints on Margin to deep basin correla-tions across the Balearic Promontory and the Valencia basin (Doctoral dissertation, Universidad de Salamanca).

Lozar, F., Violanti, D., Dela Pierre, F., Bernardi, E., Cavagna, S., Clari, P., Irace, A., Marti-netto, E., Trenkwalder, S., 2010. Calcareous nannofossils and foraminifers herald the Messinian salinity crisis: the Pollenzo section (Alba, Cuneo; NW Italy). Geobios 43, 21–32.

Lozar, F., Violanti, D., Bernardi, E., Dela Pierre, F., Natalicchio, M., 2018. Identifying the onset of the Messinian salinity crisis: a reassessment of the biochronostratigraphic tools (Piedmont Basin, NW Italy). Newsl. Stratigr. 51 (1), 11–31.

Lu, F.H., 2006. Lithofacies and water-body record of Messinian evaporites in Nijar Basin, SE Spain. Sedim. geology, 188, 115-130.

Lu, F.H., Meyers, W.J. Schoonen, M.A., 2001. S and O (SO_4) isotopes, simultaneous mod-eling, and environmental significance of the Nijar Messinian gypsum, Spain. Geochimica et Co-smochimica Acta 65, 3081-3092.

Lugli, S., Schreiber, B.C., Triberti, B., 1999. Giant polygons in the Realmonte mine (Agri-gento, Sicily): evidence for the desiccation of a Messinian halite basin. J. Sediment. Res. 69, 764–771.

Lugli, S., Bassetti, M.A., Manzi, V., Barbieri, M., Longinelli, A., Roveri, M., 2007. The Messinian "Vena del Gesso" evaporites revisited: characterization of isotopic composition and organic matter. In: Schreiber, B.C., Lugli, S., Bąbel, M. (Eds.), Evaporites through Space and Time. Special Publications, 285. Geological Society, London, pp. 143–154.

Lugli, S., Manzi, V., Roveri, M., Schreiber, B.C., 2010. The Primary Lower Gypsum in the Mediterranean: a newfacies interpretation for the first stage of the Messinian salinity crisis. Paleo-geography, Paleoclimatology, Paleoecology, 297, 83-99.

Lugli, S., Gennari, R., Gvirtzman, Z., Manzi, V., Roveri, M., Schreiber, B.C., 2013. Evi-dence of clastic evaporites in the canyons of the Levant Basin (Israel): implications for the Mes-sinian Salinity Crisis. Journal of Sedimentary Research 83, 942-954.

Lugli, S., Manzi, V., Roveri, M., Schreiber, B.C., 2015. The deep record of the Messinian salinity crisis: Evidence of a non-desiccated Mediterranean Sea. Paleogeography, Paleoclimatolo-gy, Paleoecology 433, 201-218.

Lymer, G., Lofi, J., Gaullier, V., Maillard, A., Thinon, I., Sage, F., Chanier, F., Vendeville, B.C., 2018. The Western Tyrrhenian Sea revisited: New evidence for a rifted basin during the Messinian Salinity Crisis. Marine Geology, 398, 1-21.

Madof, A.S., Connell, S.D., 2018. Northern Levant Basin. In: Lofi, et al. (Eds.), Atlas of the Messinian Salinity Crisis markers in the Mediterranean and Black Seas. Mémoires de la Société géologique de France 179. World Geol. Map Commission, pp. 60-62.

Madof, A.S., Bertoni, C., Lofi, J., 2019. Discovery of vast fluvial deposits provides evi-dence for drawdown during the late Miocene Messinian salinity crisis. Geology 47(2), 171-174.

Madof, A.S., Ryan, W.B., Bertoni, C., Laugier, F.J., Zaki, A.S., Baumgardner, S.E., 2022. Time-probabilistic approach to the late Miocene Messinian salinity crisis: Implications for a dis-connected Paratethys. Terra Nova.

Magyar, I., Geary, D.H., Lantos, M., Müller, P., Süto-Szentai, M., 1999a. Integrated bio-stratigraphic, magnetostratigraphic and chronostratigraphic correlations of the Late Miocene Lake Pannon deposits. Acta Geologica Hungarica, 42(1), 5-31.

Magyar, I., Geary, D. H., Müller, P., 1999b. Paleogeographic evolution of the late miocene Lake Pannon in Central Europe. Paleogeography, Paleoclimatology, Paleoecology, 147(3-4), 151-167.

Maillard, A., Mauffret, A., 2006. Relationship between erosion surfaces and Late Miocene Salinity Crisis deposits in the Valencia Basin (northwestern Mediterranean): Evidence for an early sea-level fall. Terra Nova, 18(5), 321-329.

Maillard, A., Mauffret, A., 2013. Structure and present-day compression in the offshore ar-ea between Alicante and Ibiza Island (Eastern Iberian Margin). Tectonophysics 591, 116–130.

Maillard, A., Mauffret, A., 2011. Valencia through. In: Lofi, et al. (Eds.), Atlas of the Mes-sinian Salinity Crisis markers in the Mediterranean and Black SeasMémoires de la Société géologique de France 179. World Geological Map Commission (72 pp.).

Maillard, A., Gorini, C., Mauffret, A., Sage, F., Lofi, J., Gaullier, V., 2006. Offshore evi-dence of polyphase erosion in the Valencia Basin (Northwestern Mediterranean): scenario for the Messinian Salinity Crisis. Sedimentary Geology 188–189, 69–91.

Maillard, A., Hübscher, C., Benkhelil, J., Tahchi, E., 2011a. Deformed Messinian markers in the Cyprus Arc: tectonic and/or Messinian Salinity Crisis indicators? Basin Res.23, 146-170.

Maillard, A., Lofi, J., Déverchère, J., Gaullier, V., et al., 2011b. Synthesis. In : J. LOFI, J. DÉVERCHÈRE et al., Eds., Seis-mic atlas of the Messinian salinity crisis markers in the offshore Mediterranean domain. – CCGM & Mém. Soc. géol. Fr., n.s., 179, 72 p.

Maillard, A., Driussi, O., Lofi, J., Briais, A., Chanier, F., Hübscher, C., Gaullier, V., 2014. Record of the Messinian Salinity Crisis in the SW Mallorca area (Balearic Promontory, Spain). Marine Geology, 357, 304-320.

Maillard, A., Gaullier, V., Lézin, C., Chanier, F., Odonne, F., Lofi, J., 2020. New onshore/offshore evidence of the Messinian Erosion Surface from key areas: The Ibiza-Balearic Promontory and the Orosei-Eastern Sardinian margin. Découverte de la surface d'érosion messi-nienne onshore/offshore dans deux lieux clés: le Promontoire Baléares (Ibiza) et la marge est-sarde (Orosei). Bulletin de la Société Géologique de France, 191(1).

Mancini, A. M., Gennari, R., Natalicchio, M., Pierre, F. D., Carnevale, G., Pastero, L., Pelle-grino, L., Pilade, F., Lozar, F., 2022. Taphonomic bias on calcareous micro and nannofossils and paleoenvironmental evolution across the Messinian Salinity Crisis onset: Insights from the Sorbas Basin (SE Spain). Palaeogeography, Palaeoclimatology, Palaeoecology, 111056.

Maniscalco, R., Casciano, C. I., Distefano, S., Grossi, F., Di Stefano, A., 2019. Facies anal-ysis in the Second Cycle Messinian evaporites predating the early Pliocene reflooding: the Balza Soletta section (Corvillo Basin, central Sicily). Italian Journal of Geosciences, 138(3), 301-316.

Manzi, V., Lugli, S., Ricci Lucchi, F., Roveri, M., 2005. Deep-water clastic evaporites dep-osition in the Messinian Adriatic foredeep (northern Apennines, Italy): did the Mediterranean ever dry out? Sedimentology 52, 875-902.

Manzi, V., Roveri, M., Gennari, R., Bertini, A., Biffi, U., Giunta, S., Iaccarino, S.M., Lanci, L., Lugli, S., Negri, A., Riva, A., Rossi, M.E., Taviani, M., 2007. The deep-water counterpart of the messinian lower evaporites in the apennine foredeep: the fanantello section (northern Apennines, Italy). Paleogeogr. Paleoclimatol. Paleoecol. 251, 470-499.

Manzi, V., Lugli, S., Roveri, M., Schreiber, B.C. 2009. A new facies model for the Upper Gypsum of Sicily (Italy): chronological and paleoenvironmental constraits for the Messinian salin-ity crisis in the Mediterranean. Sedimentology 56, 1937-1960.

Manzi, V., Lugli, S., Roveri, M., Schreiber, B.C., Gennari, R., 2011. The Messinian CdB (Sicily, Italy) revisited. Geol. Soc. Am. Bull. 123, 347–370.

Manzi, V., Gennari, R., Hilgen, F., Krijgsman, W., Lugli, S., Roveri, M., Sierro, F.J., 2013. Age refinement of the Messinian salinity crisis onset in the Mediterranean: Terra Nova 25 (4), 315-322.

Manzi, V., Lugli, S., Roveri, M., Dela, Pierre F., Gennari, R., Lozar, F., Natalicchio, M., Schreiber, B.C., Taviani, M., Turco, E., 2016a. The Messinian salinity crisis in Cyprus: A further step towards a new stratigraphic framework for Eastern Mediterranean. Basin Research 28, 207-236.

Manzi, V., Gennari, R., Lugli, S., Minelli, N., Reghizzi, M., et al., 2016b. Comment on "Carbonate deposition and diagenesis in evaporitic environments: the evapo-rative and sulphur-bearing limestones during the settlement of the Messinian Salinity Crisis in Sicily and Calabria" by Caruso et al., 2015. Palaeo3, 429, 136e162. Palaeog. Palaeocl. Palaeoec. 459, 585-596.

Manzi, V., Gennari, R., Lugli, S., Persico, D., Reghizzi, M., Roveri, M., Schreiber, B.C., Calvo, R., Gavrieli, I., Gvirtzman, Z., 2018. The onset of the Messinian salinity crisis in the deep Eastern Mediterranean basin. Terra Nova 30(3), 189-198.

Manzi, V., Argnani, A., Corcagnani, A., Lugli, S., Roveri, M., 2020. The Messinian salinity crisis in the Adriatic foredeep: Evolution of the largest evaporitic marginal basin in the Mediterra-nean. Marine and Petroleum Geology, 115, 104288.

Manzi, V., Roveri, M., Argnani, A., Cowan, D., Lugli, S., 2021. Large-scale mass-transport deposits recording the collapse of an evaporitic platform during the Messinian salinity crisis (Cal-tanissetta basin, Sicily). Sedimentary Geology 424, 106003.

Marcano, M. C., Frank, T. D., Mukasa, S. B., Lohmann, K.C., Taviani, M., 2015. Diagenet-ic incorporation of Sr into aragonitic bivalve shells: Implications for chronostratigraphic and pale-oenvironmental interpretations. The Depositional Record, 1(1), 38-52.

Marchina, C., Natali, C., Fahnestock, M.F., Pennisi, M., Brycec, J., Bianchini, G., 2018. Strontium isotopic composition of the Po river dissolved load: Insights into rock weathering in Northern Italy. Applied Geochemistry 97, 187-196.

Markovic, S., Paytan, A., Li, H., Wortmann, U.G., 2016. A revised seawater sulfate oxygen isotope record for the last 4Myr. Geochimica et Cosmochimica Acta 175, 239-251.

Marsaglia, K.M., Tribble, J.S., 1999. Petrography and mineralogy of the uppermost Mes-sinian section and the Pliocene/Miocene boundary at Site 975, Western Mediterranean Sea. In Proc. ODP, Sci. Results (Vol. 161, pp. 3-20).

Martín, J.M., Puga-Bernabéu, A., Aguirre, J., Braga, J.C. 2014. Miocene Atlantic-Mediterranean seaways in the Betic Cordillera (Southern Spain). Revista de la sociedad geológica de España, 27(1), 175-186.

Martinez-Diaz, J., Hernandez-Enrile, J.N., 2004. Neotectonics and morphotectonics of the southern Almeria region (Betic Cordillera-Spain) kinematic implications. Int. J. Earth Sci 93, 189-206.

Martín-Suárez, E., Freudenthal, M., Krijgsman, W., Fortuin, R., 2000. On the age of the continental deposits of the Zorreras Member (Sorbas Basin, SE Spain). Géobios, 33, 505-512.

Marzocchi, A., Lunt, D.J., Flecker, R., Bradshaw, C.D., Farnsworth, A., Hilgen, F.J., 2015. Orbital control on late Miocene climate and the North African monsoon: insight from an ensemble of sub-precessional simulations. Climate of the Past, 11(10), 1271-1295.

Marzocchi, A., Flecker, R., Van Baak, C.G.C., Lunt, D.J., Krijgsman, W., 2016. Mediterra-nean outflow pump: an alternative mechanism for the Lago-mare and the end of the Messinian Salinity Crisis. Geology 44, 523-526.

Marzocchi, A., Flecker, R., Lunt, D.J., Krijgsman, W., Hilgen, F.J. 2019. Precessional driv-ers of late Miocene Mediterranean sedimentary sequences: African summer monsoon and Atlantic winter storm tracks. Paleoceanography and Paleoclimatology, 34(12), 1980-1994.

Mas, G., 2013. Definició i caracterització de la Formació ses Olles (Lago mare, messinià terminal) a l'Illa de Mallorca (illes balears, mediterrània Occidental). Bolletí de la Societat d'Història Natural de Balears 56, 209–231.

Mas, G., 2015. El registre estratigr`afic del Messini`a terminal i del Pliocè a l'illa de Mallorca. Relacions amb la crisi de salinitat de la Mediterrània. PhD Tesis. Universitat de les Iles Balears. http://www.tdx.cat/handle/10803/375904.

Mas, G., Fornós, J.J., 2020. The messinian salinity crisis in Mallorca: New insights for a western mediterranean stratigraphic scenario. Marine and Petroleum Geology, 104656.

Mas, G., Bisconti, M., Torres-Roig, E., Juárez, J., Sacarès, J., 2018a. The last whale of the Messinian. First record of a mysticete cetacean from the Mediterranean Messinian Salinity Crisis. In 1st paleontological virtual congress. Book of Abstracts—paleontology in the virtual era (Vol. 97).

Mas, G., Maillard, A., Alcover, J. A., Fornós, J. J., Bover, P., Torres-Roig, E., 2018b. Terrestrial colonization of the Balearic Islands: New evidence for the Mediterranean sea-level drawdown during the Messinian Salinity Crisis. Geology, 46(6), 527-530.

Masterson, A.L., Wing, B.A., Paytan, A., Farquhar, J., Johnston, D.T., 2016. The minor sulfur isotope composition of Cretaceous and Cenozoic seawater sulfate. Paleoceanography 31, 779-788.

Mather, A., Martín, J.M., Harvey, A.M., Braga, J.C., 2001. A field guide to the Neogene sedimentary basins of the Almería Province, South-East Spain., 186-189). Oxford:Blackwell Sci-ence.

Mayser, J.P., Flecker, R., Marzocchi, A., Kouwenhoven, T.J., Lunt, D.J., Pancost, R.D., 2017. Precession driven changes in terrestrial organic matter input to the Eastern Mediterranean leading up to the Messinian Salinity Crisis. Earth Planet. Sci. Lett. 462, 199-211.

McArthur, J. M., Howarth, R. J., Shields, G.A., 2012. Strontium isotope stratigraphy. In F. M. Gradstein, J. G. Ogg, M. D. Schmitz, and G. M. Ogg (Eds.), The Geological Time Scale 2012 (127-144). Oxford: Elsevier B.V.

McCulloch, M.T., De Deckker, P., 1989. Sr isotope constraints on the Mediterranean envi-ronment at the end of the Messinian salinity crisis. Nature 342, 62-65.

McKenzie, J.A., 1999. From desert to deluge in the Mediterranean. Nature, 400, 613-614.

McKenzie, J.A., Hodell, D. A., Mueller, P. A., Mueller, D.W., 1988. Application of stronti-um isotopes to late Miocene-early Pliocene stratigraphy. Geology 16(11), 1022-1025.

McKenzie, J.A., Evans, N., Hodell, D., Aloisi, G., Vasconcelos, C., 2017. Subsurface dolomite formation during post-depositional flow of sulphate-bearing fluids from underlying salt giants: Early Pliocene example at DSDP Leg 42A, Site 374, Ionian Abyssal Plain. EGUGA, 10166.

Medaouri, M., Déverchère, J., Graindorge, D., Bracene, R., Badji, R., Ouabadi, A., Yelles, K., Bendib, F., 2014. The transition from Alboran to Algerian basins (Western Mediterranean Sea): chronostratigraphy, deep crustal structure and tectonic evolution at the rear of a narrow slab rollback system, J. Geodyn., 77, 186-205.

Meijer, P.T., Krijgsman, W., 2005. A quantitative analysis of the desiccation and re-filling of the Mediterranean during the Messinian Salinity Crisis. Earth and Planetary Science Letters, 240(2), 510-520.

Meilijson, A., Steinberg, J., Hilgen, F., Bialik, O. M., Waldmann, N. D., Makovsky, Y., 2018. Deep-basin evidence resolves a 50-year-old debate and demonstrates synchronous onset of Messinian evaporite deposition in a non-desiccated Mediterranean. Geology, 46(3), 243-246.

Meilijson, A., Hilgen, F., Sepúlveda, J., Steinberg, J., Fairbank, V., Flecker, R., Waldmann, N.D., Spaulding, S.A., Bialik, O.M., Boudinot, F.G., Illner, P., Makovsky, Y., 2019. Chronology with a pinch of salt: integrated stratigraphy of Messinian evaporites in the deep Eastern Mediterra-nean reveals long-lasting halite deposition during Atlantic connectivity. Earth-Sci. Rev. 194, 374–398.

Meisch, C., 2000. Freshwater Ostracoda of Western and Central Europe. Spektrum Aakad-emischer Verlag, Berlin, pp. 1–522.

Melinte-Dobrinescu, M.C., Suc, J.-P., Clauzon, G., Popescu, S.-M., Armijo, R., et al., 2009. The Mes-sinian salinity crisis in the Dardanelles region: Chronostratigraphic constraints. Paleogeogr. Paleo-climatol. Paleoecol. 278, 24-39.

Merzeraud, G., Achalhi, M., Cornee, J.J., Münch, P., Azdimousa, A., Moussa, A.B., 2019. Sedimentology and sequence stratigraphy of the late-Messinian-Early pliocene continental to ma-rine deposits of the Boudinar basin (North Morocco). Journal of African Earth Sciences, 150, 205-223.

Meulenkamp, J.E., Sissingh, W., 2003. Tertiary paleogeography and tectonostratigraphic evolution of the Northern and Southern Peri-Tethys platforms and the intermediate domains of the African-Eurasian convergent plate boundary zone. Paleogeography, Paleoclimatology, Paleoecol-ogy, 196(1-2), 209-228.

Meulenkamp, J.E., Dermitzakis, M., Georgiades-Dikeoulia, E., Jonkers, H.A., Boger, A., 1979. Field Guide to the Neogene of Crete. Publication of the Department of Geology and Paleon-tology, University of Athens, A, 32. pp. 1–32.

Meyer, J., Wrozyna, C., Gross, M., Leis, A., Piller, W.E., 2017. Morphological and geo-chemical variations of Cyprideis (Ostracoda) from modern waters of the northern Neotropics. Lim-nology, 18(3), 251-273.

Micallef, A., Camerlenghi, A., Garcia-Castellanos, D., Cunarro Otero, D., Gutscher, M.- A.M.A., Barreca, G., Spatola, D., Facchin, L., Geletti, R., Krastel, S., Gross, F., Urlaub, M., Sulli, A., Basilone, L., Basilone, G., 2018. Evidence of the Zanclean megaflood in the eastern Mediterra-nean Basin. Sci. Rep. 8, 1–8.

Milker, Y., Schmiedl, G., 2012. A taxonomic guide to modern benthic shelf foraminifera of the western Mediterranean Sea. Palaeontologia electronica, 15(2), 1-134.

Mocnik, A., Camerlenghi, A., Del Ben, A., Geletti, R., Wardell, N., Zgur, F., 2014. The Messinian Salinity Crisis in the West-Mediterranean Basins: comparison between two rifted mar-gins. In Proceedings of the 33rd GNGTS Conference, Bologna (Vol. 1, pp. 156-163).

Mocnik, A., Del Ben, A., Camerlenghi, A., Geletti, R., Saule, M., 2018. - 12. Ionian Basin. In J. Lofi (Ed.), Seismic Atlas of the Messinian salinity crisis markers in the Mediterranean sea. Volume 2. - Mémoires de la Société géologique de France, n.s., 2018, t. 181, and Commission for the Geological Map of the World, p. 41-44.

Modestou, S., Simon, D., Gutjahr, M., Marzocchi, A., Kouwenhoven, T.J., Ellam, R.M., Flecker, R., 2017. Precessional variability of $^{87}Sr/^{86}Sr$ in the late miocene sorbas basin: An inter-disciplinary study of drivers of interbasin exchange. Paleoceanography 32 (6), 531-552.

Molenaar, N., De Feyter, A.J., 1985. Carbonates associated with alluvial fans: an example from the Messinian Colombacci Formation of the Pietrarubbia Basin, Northern Marche, Italy. Sed-imentary Geology 42, 1-23.

Montadert, L., Letouzey, J., Mauffret, A., 1978. Messinian event: seismic evidence. In: Hsü, K.J. and Montadert, L. et al. (eds) Initial Reports of the Deep Sea Drilling Project, 1. US Government Printing Office, Washington, DC, 1037-1050.

Montenat, C., Bizon, G., 1976. A propos de l'évolution géodynamique Mio-Pliocène en Méditerranée occidentale. L'example du bassin de Vera (Cordillères béthiques. Espagne méridio-nale). C.R. Somm. Soc. Géol. Fr. 1, 15-16.

Montenat, C., Ott d'Estevou, Ph., 1999. The diversity of Late Neogene sedimentary basins generated by wrench faulting in the eastern Betic cordillera, SE Spain. J. Pet. Geol. 22, 61- 80.

Mosca, P., Polino, R., Rogledi, S., Rossi, M., 2009. New data for the kinematic interpreta-tion of the Alps–Apennines junction (Northwestern Italy). International Journal of Earth Sciences.

Mudie, P.J., Marret, F., Mertens, K.N., Shumilovskikh, L., Leroy, S.A., 2017. Atlas of mod-ern dinoflagellate cyst distributions in the Black Sea Corridor: from Aegean to Aral Seas, includ-ing Marmara, Black, Azov and Caspian Seas. Marine Micropaleontology, 134, 1-152.

Mueller, M., Igbokwe, O.A., Walter, B., Pederson, C.L., Riechelmann, S., et al., 2020. Testing the preservation potential of early diagenetic dolomites as geochemical archives. Sedimentology 67 (2), 849-881.

Müller, D.W., Mueller, P.A., 1991. Origin and age of the Mediterranean Messinian evapo-rites: implications from Sr isotopes. Earth and Planetary Science Letters, 107(1), 1-12.

Müller, D.W., Mueller, P.A., McKenzie, J.A., 1990. Strontium isotopic ratios as fluid trac-ers in Messinian evaporites of the Tyrrhenian Sea (western Mediterranean Sea). In Proceedings of the Ocean Drilling Program, Scientific Results (Vol. 107, 603-614). College Station, Tex.: Ocean Drill. Program.

Murillo-Barroso, M., Montero-Ruiz, I., Nieto, J.M., Camalich Massieu, M.D., Martín Socas, D., Martinón Torres, M., 2019. Trace elements and lead isotopic composition of copper deposits from the eastern part of the Internal Zone of the Betic Cordillera (SE Iberia): application to prove-nance of archaeological materials. J. Iber. Geol. 45 (4), 585-608.

Myrow, P.M., 1995. Thalassinoides and the enigma of Early Paleozoic open-framework burrow systems. Palaios, 58-74.

Natalicchio, M., Dela Pierre, F., Lugli, S., Lowenstein, T.K., Feiner, S.J., Ferrando, S., Manzi, V., Roveri, M., Clari, P., 2014. Did late Miocene (Messinian) gypsum precipitate from evaporated marine brines? Insights from the Piedmont Basin (Italy). Geology 42, 179–182.

Natalicchio, M., Birgel, D., Peckmann, J., Lozar, F., Carnevale, G., Liu, X., Hinrichs, K.-U., Dela Pierre, F., 2017. An archaeal biomarker record of paleoenvironmental change across the onset of the Messinian salinity crisis in the absence of evaporites (Piedmont Basin, Italy). Org. Geochem. 113, 242-253.

Natalicchio, M., Dela Pierre, F., Birgel, D., Brumsack, H., Carnevale, G., Gennari, R., Gier, S., Lozar, F., Pellegrino, L., Sabino, M., Schnetger, B., Peckmann, J., 2019. Paleoenvironmental change in a precession-paced succession across the onset of the Messinian salinity crisis: insight from element geochemistry and molecular fossils. Paleogeogr. Paleoclimatol. Paleoecol. 518, 45-61.

Natalicchio, M., Pellegrino, L., Clari, P., Pastero, L., Pierre, F.D., 2021. Gypsum lithofacies and stratigraphic architecture of a Messinian marginal basin (Piedmont Basin, NW Italy). Sedi-mentary Geology 42, 106009.

Neale, J.W., 1988. Ostracods and palaeosalinity reconstruction. In: De Deckker, P., Colin, J.-P., Peypouquet, J.P. (Eds.), Ostracoda in the Earth Science. Elsevier, Amsterdam, pp. 125–155.

Nesteroff, W.D., 1973. Un modéle pour les évaporites messinienne en Méditerranée, bas-sins peu profonds avec dépot d'évaporites lagunaires. In: Drooger, C.W., Ed.), Messinian Events in the Mediterranean. North-Holland Publ. Co., Amsterdam, 68-81.

Netzeband, G., Hübscher, C., Gajewski, G., 2006. The structural evolution of the Messinian evaporites in the Levantine Basin. Mar. Geol. 230, 249-273.

Nichols, G., Williams, E., Paola, C. (Eds.)., 2009. Sedimentary processes, environments and basins: a tribute to Peter Friend. John Wiley & Sons.

Nier, A.O., 1938. "The Isotopic Constitution of Strontium, Barium, Bismuth, Thallium and Mercury." Physical Review 54 (4): 275–78.

Nieto, J.M., Puga, E., Díaz de Federico, A. 2000. Late Variscan pyroclastic rocks from the Mulhacén Complex (Betic Cordillera, Spain), 217-24. In Volcaniclastic Rocks, from Magmas to Sediments; Leyrit, H., Montenat, C., Eds.; Gordon and Breach Science Publishers: Philadelphia, PA, USA, 2000; p. 265.

Ochoa, D., Sierro, F.J., Lofi, J., Maillard, A., Flores, J.A., Suárez, M., 2015. Synchronous onset of the Messinian evaporite precipitation: First Mediterranean offshore evidence. Earth and Planetary Science Letters, 427, 112-124.

Ochoa, D., Sierro, F.J., Hilgen, F.J., Cortina, A., Lofi, J., Kouwenhoven, T., Flores, J.A., 2018. Origin and implications of orbital-induced sedimentary cyclicity in Pliocene well-logs of the Western Mediterranean. Marine Geology, 403, 150-164.

Odin, G.S., Vai, G.B., Cosca, M., Tateo, F., Hunziker, J.C., 1997. Integrated stratigraphy of the Maccarone section, in Montanari, A., Odin, G.S., and Coccioni, R., eds., Miocene Stratigraphy: An Integrated Approach: Developments in Paleontology and Stratigraphy, Amsterdam, Nether-lands, Elsevier Science B.V., v. 15, p. 531-545.

Ogniben, L., 1955. Le argille scagliose del Crotonese. Memorie e Note dell'Istituto di Geo-logia Alicata di Napoli, 6, 1-72.

Omodeo-Salé, S., Gennari, R., Lugli, S., Manzi, V., Roveri, M., 2012. Tectonic and climat-ic control on the Late Messinian sedimentary evolution of the Nijar Basin (Betic Cordillera, Southern Spain). Basin Research 24, 314-337.

Orszag-Sperber, F., 2006. Changing perspectives in the concept of "Lago-Mare" in Medi-terranean Late Miocene evolution. Sedimentary Geology, 188, 259-277.

Orszag-Sperber F., Rouchy J.M., 1979. Le Miocène terminal et le Pliocène inférieur au sud de Chypre, livret-guide, 5e séminaire sur le Messinien, Chypre, 60 p.

Orszag-Sperber, F., Rouchy, J.-M., Bizon, G., Bizon, J.-J., Cravatte, J., Müller, C., 1980. La sédimentation messinienne dans le bassin de Polémi (Chypre). Géol. Méditerr. VII, 91–102.

Orszag-Sperber, F., Rouchy, J. M., Blanc-Valleron, M.M., 2000. La transition Messinien-Pliocène en Méditerranée orientale (Chypre): la période du Lago-Mare et sa signification. Comptes Rendus de l'Académie des Sciences-Series IIA-Earth and Planetary Science, 331(7), 483-490.

Orszag-Sperber, F., Caruso, A., Blanc-Valleron, M.M., Merle, D., Rouchy, J.M., 2009. The onset of the Messinian salinity crisis: insights from Cyprus sections. Sedimentary Geology, 217(1-4), 52-64.

Ortí, F., Pérez-López, A., García-Veigas, J., Rosell, L., Céndon, D.I. Pérez-Valera, F., 2014a. Sulfate isotope compositions ($\delta^{34}S$, $\delta^{18}O$) and strontium isotopic ratios ($^{87}Sr/^{86}Sr$) of Triassic evaporites in the Betic Cordillera (SE Spain). Rev. Soc. Geol. España, 27(1), 79-89.

Ortí, F., Rosell, L., Gibert, L., Moragas, M., Playà, E., Inglès, et al., 2014b. Evaporite sedimentation in a tectonically active basin: the lacustrine Las Minas Gypsum unit (Late Tortonian, SE Spain). Sedim.Geol., 311, 17-42.

Ott d'Estevou, P., Montenat, C., Alvado, J.C., 1990. Le basin de Vera-Garrucha. In: In: Montenat, C. (Ed.), Doc. et Trav. Vols. 12–13. IGAL, pp. 165-187.

Paillard, D., Labeyrie, L. D., Yiou, P., 1996. AnalySeries 1.0: a Macintosh software for the analysis of geophysical time-series. Eos, 77(39), 379.

Palcu, D.V., Golovina, L.A., Vernyhorova, Y.V., Popov, S.V., Krijgsman, W., 2017. Middle Miocene paleoenvironmental crises in Central Eurasia caused by changes in marine gateway con-figuration. Global Planetary Change 158, 57-71.

Palcu, D.V., Patina, I.S., Şandric, I., Lazarev, S., Vasiliev, I., Stoica, M., Krijgsman, W., 2021. Late Miocene megalake regressions in Eurasia. Scientific reports, 11(1), 1-12.

Palmer, M.R., Edmond, J.M., 1992. Controls over the strontium isotope composition of river water. Geochimica et Cosmochimica Acta, 56(5), 2099-2111.

Paytan, A., 1996. Marine barite: A recorder of oceanic chemistry, productivity and circulation, Ph.D. thesis, Univ. of Calif., San Diego, La Jolla.

Pełechaty, M., Pukacz, A., Apolinarska, K., Pełechata, A., Siepak, M., 2013. The signifi-cance of Chara vegetation in the precipitation of lacustrine calcium carbonate. Sedimentology, 60(4), 1017-1035.

Pellegrino, L., Natalicchio, M., Abe, K., Jordan, R.W., Longo, S.E.F., Ferrando, S., Carneva-le, G., Dela Pierre, F., 2021. Tiny, glassy, and rapidly trapped: The nano-sized planktic diatoms in Messinian (late Miocene) gypsum. Geology, 49(11), 1369-1374.

Pellen, R., Popescu, S.-M., Suc, J.-P., Melinte-Dobrinescu, M.C., Rubino, J.-L., Rabineau, M., Marabini, S., Loget, N., Casero, P., Cavazza, W., Head, M.J., Aslanian, D., 2017. The Apen-nine foredeep (Italy) during the latest Messinian: Lago Mare reflects competing brackish and ma-rine conditions based on calcareous nannofossils and dinoflagellate cysts. Geobios 50, 237–257.

Pellen, R., Aslanian, D., Rabineau, M., Suc, J.P., Gorini, C., Leroux, E., Blanpied, C., Si-lenziario, C., Popescu, S.M., Rubino, J.L., 2019. The Messinian Ebro River incision. Glob. Planet. Chang. 181, 102988.

Pellen, R., Aslanian, D., Rabineau, M., Suc, J. P., Cavazza, W., Popescu, S. M., Rubino, J.L., 2022. Structural and sedimentary origin of the Gargano-Pelagosa gateway and impact on sed-imentary evolution during the Messinian Salinity Crisis. Earth-Science Reviews, 104114.

Pellerin, A., Antler, G., Holm, S.A., Findlay, A.J., Crockford, P.W., Turchyn, A.V., Jørgen-sen, B.B., Finster, K., 2019. Large sulfur isotope fractionation by bacterial sulfide oxidation. Sci Adv 5, eaaw1480-eaaw1480.

Pérez-Asensio, J. N., Aguirre, J., Schmiedl, G., Civis, J., 2012. Impact of restriction of the Atlantic-Mediterranean gateway on the Mediterranean Outflow Water and eastern Atlantic circula-tion during the Messinian. Paleoceanography, 27(3).

Pérez-Asensio, J.N., Rodríguez-Tovar, F.J., Łaska, W., Uchman, A., 2021. Palaeoenvironmental changes after the Messinian Salinity Crisis in the Mediterranean Almería-Níjar Basin (SE Spain) recorded by benthic foraminifera. Palaeogeography, Palaeoclimatology, Palaeoecology, 577, 110536.

Peryt, T.M., 2006. The beginning, development and termination of the Middle Miocene Badenian salinity crisis in Central Paratethys. Sedimentary Geology 188-189, 379-396.

Peucker-Ehrenbrink, B., Fiske, G.J., 2019. A continental perspective of the seawater $^{87}Sr/^{86}Sr$ record: A review. Chem. Geol, 510, 140-165.

Peucker-Ehrenbrink, B., Miller, M.W., Arsouze, T., Jeandel, C., 2010. Continental bedrock and riverine fluxes of strontium and neodymium isotopes to the oceans. Geochemistry, Geophy-sics, Geosystems, 11(3).

Pierre, C., 1974. Contribution ~ l'Jtude sgdimentologique et isotopique des evaporites messiniennes de la Mediterrane; implications geodynamiques. Thesis, University of Paris.

Pierre, C., 1982 Teneurs en isotopes stables (^{18}O,^{2}H,^{13}C,^{34}S) et conditions de génèse des évaporites marines : Alication à quelques milieux actuels et au Messinien de la Mediterrannée, Ecole Normale Supérieure. Université Paris Sud Orsay, p. 262.

Pierre, C., Fontes, J.-C., 1978. Isotope Composition of Messinian sediments from the Mediterranean Sea as indicators of paleoenvironments and diagenesis, in: Texas A M University, O.D.P.C.S., TX, United States (Ed.), Initial reports of the Deep Sea Drilling, covering Leg 42 of the cruises of the drilling Vessel Glomar Challenger Malaga Spain to Itanbul Turkey. April-May 1975. University of California. Scris Institution of Oceanography, National Science Foundation.

Pierre, C., Rouchy, J.M., 1990. Stable isotope composition of carbonates in the Tyrrhenian Sea, Sulement to: Pierre, C; Rouchy, JM (1990): Sedimentary and diagenetic evolution of Messinian evaporites in the Tyrrhenian Sea (ODP Leg 107, Sites 652, 653, and 654): petrographic, mineralogical, and stable isotope records. In: Kastens, KA; Mascle, J; et al., eds.), Proceedings of the Ocean Drilling Program, Scientific Results, College Station, TX (Ocean Drilling Program), 107, 187-210.

Pierre, C., Rouchy, J.M., Blanc-Valleron, M.-M., 1998. Sedimentological and stable isotope changes at the Messinian-Pliocene boundary in the eastern Mediterranean. In: Robertson, A.H.F., Emeis, K.-C., Richter, C., Camerlenghi, A. (Eds.), Proc. O.D.P., Sci. Res., vol. 160. Ocean Drilling Program, College Station, TX, pp. 3-8.

Pierre, C., Caruso, A., Blanc-Valleron, M.M., Rouchy, J.M., Orzsag-Sperber, F., 2006. Reconstruction of the paleoenvironmental changes around the Miocene-Pliocene boundary along a West-East transect across the Med. Sedim. Geol., 188, 319-340.

Placzek, C.J., Quade, J., Patchett, P.J., 2011. Isotopic tracers of paleohydrologic change in large lakes of the Bolivian Altiplano. Quaternary Research, 75(1), 231-244.

Polonia, A., Torelli, L., Mussoni, P., Gasperini, L., Artoni, A., Klaeschen, D., 2011. The Calabrian Arc subduction complex in the Ionian Sea: Regional architecture, active deformation, and seismic hazard. Tectonics, 30(5).

Popescu, S.M., Melinte, M.C., Suc, J.P., Clauzon, G., Quillévéré, F., Süto-Szentai, M., 2007. Earliest Zanclean age for the Colombacci and uppermost Di Tetto formations of the "latest Messinian" northern Apennines: New paleoenvironmental data from the Maccarone section (Marche Province, Italy). Geobios, 40(3), 359-373.

Popescu, S.-M., Melinte, M.-C., Suc, J.-P., Clauzon, G., Quillévéré, F., Süto-Szentai, M., 2008. Marine reflooding of the Mediterranean after the Messinian Salinity Crisis predates the Zan-clean GSSP. Reply to the "Comment on 'Earliest Zanclean age for the Colombacci and uppermost Di Tetto formations of the "latest Messinian" northern Apennines: new paleoenvironmental data from the Maccarone section (Marche Province, Italy)' by Popescu et al. (2007) Geobios 40 (359-373)" authored by Roveri et al. Geobios 41, 657-660.

Popescu, S.M., Dalesme, F., Jouannic, G., Escarguel, G., Head, M.J., Melinte-Dobrinescu, M.C., Sütö-Szentai, M., Bakrac, K., Clauzon, G., Suc, J.P., 2009. Galeacysta etrusca complex: di-noflagellate cyst marker of Paratethyan influxes to the Mediterranean Sea before and after the peak of the Messinian Salinity Crisis. Palynology, 33(2), 105-134.

Popescu, S.-M., Dalibard, M., Suc, J.-P., Barhoun, N., Melinte-Dobrinescu, M.C., Bassetti, M.A., et al., 2015. Lago Mare episodes around the Messinian-Zanclean boundary in the deep southwestern Mediterranean. Marine and Petrol. Geology 66, 55–70.

Popescu, S.M., Melinte-Dobrinescu, M.C., Suc, J.P., Do Couto, D., 2017. Ceratolithus acutus (= C. armatus), calcareous nannofossil marker of the marine reflooding that terminated the Messinian salinity crisis: Comment on "Paratethyan ostracods in the Spanish Lago-Mare: More evidence for interbasinal exchange at high Mediterranean sea level" by. Paleogeogr., Paleoclimatol., Paleoecol. 441, 854-870. Paleogeography, Paleoclimatology, Paleoecology, 485, 986-989.

Popescu, S.M., Cavazza, W., Suc, J.P., Melinte-Dobrinescu, M.C., Barhoun, N., Gorini, C., 2021. Pre-Zanclean end of the Messinian Salinity Crisis: new evidence from central Mediterranean reference sections. Journal of the Geological Society.

Popov, S. V., Rögl, F., Rozanov, A. Y., Steininger, F. F., Shcherba, I. G., Kovac, M., 2004. Lithological-paleogeographic maps of Paratethys-10 maps late Eocene to pliocene.

Popov, S.V., Shcherba, I.G., Ilyina, L.B., Nevesskaya, L.A., Paramonova, N.P., et al., 2006. Late Miocene to Pliocene paleogeography of the Paratethys and its relation to the Mediterranean. Paleogeog. Paleoclim., Paleoecol., 238(1-4), 91-106.

Pross, J., Brinkhuis, H., 2005. Organic-walled dinoflagellate cysts as paleoenvironmental indicators in the Paleogene; a synopsis of concepts. Paläontologische Zeitschrift, 79(1), 53-59.

Puga, E., De Federico, A.D., Nieto, J.M. 2002. Tectonostratigraphic subdivision and petrological characterisation of the deepest complexes of the Betic zone: a review. Geodinamica Acta, 15(1), 23-43.

Raad, F., Lofi, J., Maillard, A., Tzevahirtzian, A., Caruso, A., 2021. The Messinian Salinity Crisis deposits in the Balearic Promontory: an undeformed analog of the MSC Sicilian basins?? Mar. Pet. Geol. 104777.

Rabbi E., Ricci Lucchi, F., 1968. Stritigrafia e sedimentologia del Messiniano forlivese (dintorni di Predappio). Giorn. Geol., s. 2, XXXIV, II, Bologna.

Radeff, G., Cosentino, D., Cipollari, P., Schildgen, T.F., Iadanza, A., Strecker, M.R., Darbas, G., Gurbuz, K., 2016. Stratigraphic architecture of the upper Messinian deposits of the Adana Basin (southern Turkey): implications for the Messinian salinity crisis and the Taurus petroleum system. Ital. J. Geosci. 135, 408–424.

Radeff, G., Schildgen, T.F., Cosentino, D., Strecker, M.R., Cipollari, P., Darbaş, G., Gürbüz, K., 2017. Sedimentary evidence for late Messinian uplift of the SE margin of the Central Anatolian Plateau: Adana Basin, southern Turkey: Basin Res., 29, 488-514.

Rausch, L., Stoica, M., Lazarev, S., 2020. A late Miocene–early Pliocene Paratethyan type ostracod fauna from the Denizli basin (SW Anatolia) and its palaeogeographic implications. Acta Palaeontologica Romaniae, 16(2), 3-56.

Reghizzi, M., Gennari, R., Douville, E., Lugli, S., Manzi, V., Montagna, P., Roveri, M., Sierro, F.J., Taviani, M., 2017. Isotope stratigraphy ($^{87}Sr/^{86}Sr$, $\delta^{18}O$, $\delta^{13}C$) of the Sorbas basin (Betic Cordillera, Spain): Paleoceanographic evolution across the onset of the Messinian salinity crisis. Paleogeography, Paleoclimatology, Paleoecology 469, 60-73.

Reghizzi, M., Lugli, S., Manzi, V., Rossi, F.P., Roveri, M., 2018. Orbitally forced hydrological balance during the Messinian Salinity Crisis: insights from Strontium Isotopes ($^{87}Sr/^{86}Sr$) in the Vena del Gesso Basin (Northern Apennines, Italy). Paleoceanogr. Paleoclimatol. 33 (7), 716–731.

Reiche, S., Hübscher, C., Ehrhardt, A., 2016. The impact of salt on the late Messinian to re-cent tectonostratigraphic evolution of the Cyprus subduction zone. Basin Research, 28(5), 569-597.

Ricchiuto, T.E. McKenzie, J.A., 1978. Stable Isotopic investigation of Messinian sulfate samples from DSDP. LEG 42. Eastern Mediterranean Sea, in: Texas A M University, O.D.P.C.S., TX, United States (Ed.), Initial reports of the DSDP Leg 42 of the cruises of the drilling vessel Glomar Challenger. Malaga, Spain to Istanbul, Turkey. April-May 1975. University of California. Scris Institution of Oceanography, National Science Foundation. National Ocen Sediment Coring Program, 657-660.

Ricci Lucchi, F., 1986. The Oligocene to Holocene foreland basins of the northern Apennines, in Allen, P.A., and Homewood, P., eds., Foreland basins: International Association of Sedimentologists Special Publication 8, p. 105–139.

Rio, D., Negri, A., 1988. Calcareous nannofossils (Monticino Quarry, Faenza). In: De Giuli, C.,Vai, G.B., Eds.), Fossil Vertebrates in the Lamone Valley, Romagna Apennines. Field Trip Guidebook of the International Workshop "Continental faunas at the Miocene/Pliocene boundary", Faenza, 55-57.

Robertson, A.H.F., Eaton, S., Follows, E.J. Payne, A.S. 1995. Depositional processes and basin analysis of Messinian evaporites in Cyprus. Terra Nova, 7, 233-253.

Robertson, A.H.F., 1998a. Late Miocene paleoenvironments and tectonic settings of the southern margin of Cyprus and the Eratosthenes Seamount. In: Robertson, A.H.F., Emeis, K.C., Richter, C., Camerlenghi, A., Eds.), Proc. ODP, Sci. Res., vol. 160. Ocean Drilling Program, College Station, TX, 453-463.

Robertson, A.H., 1998b. Tectonic significance of the Eratosthenes Seamount: a continental fragment in the process of collision with a subduction zone in the eastern Mediterranean (Ocean Drilling Program Leg 160). Tectonophysics, 298(1-3), 63-82.

Roca, E., Guimera, J., 1992. The Neogene structure of the eastern iberian margin: structural constraints on the crustal evolution of the Valencia trough (western mediterranean). Tectonophysics 203, 203–218.

Roep, Th.B., Van Harten, D., 1979. Sedimentological and ostracodological observations on Messinian post-evaporite deposits in some southeastern Spanish basins. Annales Géologiques des Pays Helleniques 3, 1037-1044.

Roep, T.B., Dabrio, C.J., Fortuin, A.R., Polo, M.D., 1998. Late highstand patterns of shift-ing and steing coastal barriers and washover-fans (Late Messinian, Sorbas Basina, SE Spain). Sed-iment. Geol. 116, 27-56.

Rögl, F., 1998. Paleogeographic considerations for Mediterranean and Paratethys seaways (Oligocène to Miocene). Annalen des Naturhistorischen Museums in Wien, 9 9 A : 279310.

Rogl, F., 1999. Mediterranean and Paratethys. Facts and hypotheses of an Oligocene to Mi-ocene Paleogeography (short overview). Geologica Carpathica 50(4): 339-349.

Rosenfeld, A., 1977. The sieve pores of Cyprideis torosa (Jones, 1850) from the Messinian Mavqi'im Formation in the coastal plain and continental shelf of Israel as an indicator of paleoen-vironment. Isr. J. Earth Sci., 26: 89993.

Rossi, M., 2017. Outcrop and seismic expression of stratigraphic patterns driven by ac-commodation and sediment suly turnarounds: Implications on the meaning and variability of un-conformities in syn-orogenic basins. Marine and Petroleum Geology, 87, 112-127.

Rossi, M., Rogledi, S., 1988. Relative sea-level changes, local tectonic setting and basin margin sedimentation in the interference zone between two orogenic belts: seismic stratigraphic examples from Padan foreland basin, northern Italy, in: Fan Deltas: Sedimentology and Tectonic Settings. 368-384.

Rossi, M., Minervini, M., Ghielmi, M., Rogledi, S., 2015a. Messinian and Pliocene erosion-al surfaces in the Po Plain-Adriatic Basin: Insights from allostratigraphy and sequence stratigraphy in assessing play concepts related to accommodation and gateway turnarounds in tectonically ac-tive margins. Marine and Petroleum Geology, The Messinian events and hydrocarbon exploration in the Mediterranean 66, 192-216.

Rossi, C., Vilas, L., Arias, C., 2015b. The Messinian marine to nonmarine gypsums of Ju-milla (Northern Betic Cordillera, SE Spain): Isotopic and Sr concentration constraints on the origin of parent brines. Sedimentary Geology, 328, 96-114.

Rouchy, J.M., 1982. La crise evaporitique messinienne de Mediterranee: nouvelles proposi-tions pour une interpretation genetique. Thesis, Mem, p. 280. Mus. Natn. Hist. Nat, Paris.

Rouchy, J.M., Martin, J.P.S., 1992. Late Miocene events in the Mediterranean as recorded by carbonate-evaporite relations. Geology, 20(7), 629-632.

Rouchy, J.M., Caruso, A., 2006. The Messinian salinity crisis in the Mediterranean basin: a reassessment of the data and an integrated scenario. Sedimentary Geology 188, 35-67.

Rouchy, J.M., Orszag-Sperber, F., Blanc-Valleron, M.M., Pierre, C., Rivière, M., Com-bourieu-Nebout, N., Panayides, I., 2001. Paleoenvironmental changes at the Messinian-Pliocene boundary in the eastern Mediterranean (southern Cyprus basins): significance of the Messinian Lago-Mare. Sedimentary Geology, 145(1-2), 93-117.

Rouchy, J.M., Pierre, C., Et-Touhami, M., Kerzazi, K., Caruso, A., Blanc-Valleron, M.M., 2003. Late Messinian to Early Pliocene paleoenvironmental changes in the Melilla Basin (NE Mo-rocco) and their relation to Mediterranean evolution. Sedimentary Geology, 163(1-2), 1-27.

Rouchy, J. M., Caruso, A., Pierre, C., Blanc-Valleron, M.M., Bassetti, M.A., 2007. The end of the Messinian salinity crisis: evidences from the Chelif Basin (Algeria). Paleogeography, Paleo-climatology, Paleoecology, 254(3-4), 386-417.

Roveri, M., Manzi, V., Bassetti, M.A., Merini, M., Ricci Lucchi, F., 1998. Stratigraphy of the Messinian post-evaporitic stage in eastern-Romagna (northern Apennines, Italy). G. Geol. 60, 119-142.

Roveri, M., Bassetti, M.A., Ricci Lucchi, F., 2001. The Mediterranean Messinian salinity crisis: an Apennines foredeep perspective. Sedimentary Geology 140, 201-214.

Roveri, M., Ricci Lucchi, F., Lucente, C.C., Manzi, V., Mutti, E., 2002. Stratigraphy, facies and basin fill history of the Marnoso-arenacea Formation. In: Revisiting Turbidites of the Marno-so-arenacea Formation and their Basin-margin Equivalents: Problems with Classic Models. 64th EAGE Conference and Exhibition. Excursion Guidebook (Eds E. Mutti, F. Ricci Lucchi and M. Roveri), pp. 1–26, Parma University and ENI – AGIP Division, Parma.

Roveri, M., Manzi, V., Ricci Lucchi, F., Rogledi, S., 2003. Sedimentary and tectonic evolu-tion of the Vena del Gesso Basin (Northern Apennines, Italy): implications for the onset of the Messinian Salinity Crisis. Geol. Soc. Am. Bull., 115/4, 387-405.

Roveri, M., Boscolo Gallo, A., Rossi, M., Gennari, R., Iaccarino, S. M., Lugli, S., et al., 2005. The Adriatic foreland record of Messinian events (central Adriatic sea, Italy). GeoActa, 4(139), 158.

Roveri, M., Bertini, A., Cosentino, D., Di Stefano, A., Gennari, R., Gliozzi, E., et al., 2008a. A high-resolution stratigraphic framework for the latest Messinian events in the Mediterra-nean area. Stratigraphy 5(3-4), 323-342.

Roveri, M., Lugli, S., Manzi, V., Schreiber, B.C., 2008b. The Messinian Sicilian stratigra-phy revisited: new insights for the Messinian salinity crisis. Terra Nova 20(6), 483-488.

Roveri, M., Bertini, A., Cipollari, P., Cosentino, D., Di Stefano, A., Florindo, F., et al., 2008c. Comment on "Earliest Zanclean age for the Colombacci and uppermost Di Tetto formations of the "latest Messinian" northern Apennines: new palaeoenvironmental data from the Maccarone sec-tion (Marche Province, Italy)" by Popescu et al. (2007) Geobios 40 (359–373). Geobios 41, 669-675.

Roveri, M., Lugli, S., Manzi, V., Schreiber, B.C., 2008d. The Messinian salinity crisis: a se-quence-stratigraphic approach. GeoActa, 1, 169-190.

Roveri, M., Manzi, V., Gennari, R., Iaccarino, S.M., Lugli, S., 2008e. Recent advancements in the Messinian stratigraphy of Italy and their Mediterranean-scale implications. Bollettino della Società Paleontologica Italiana, 47(2), 71-85.

Roveri, M., Gennari, R., Lugli, S., Manzi, V. 2009. The Terminal Carbonate Complex: the record of sea-level changes during the Messinian salinity crisis. GeoActa, 8(63), 63-77.

Roveri, M., Flecker, R., Krijgsman, W., Lofi, J., Lugli, S., Manzi, V., Sierro, F.J., et al., 2014a. The Messinian salinity crisis: Past and future of a great challenge for marine sciences. Ma-rine Geology 349, 113-125.

Roveri, M., Lugli, S., Manzi, V., Gennari, R., Schreiber, B.C., 2014b. High resolution stron-tium isotope stratigraphy of the Messinian deep Mediterranean basins: implications for marginal to central basins correlation. Marine Geology 349, 113-125.

Roveri, M., Manzi, V., Bergamasco, A., Falcieri, F., Gennari, R. and Lugli, S. 2014c. Dense shelf water cascading and Messinian canyons: a new scenario for the Mediterranean salinity crisis. American Journal of Science 314, 751-784.

Roveri, M., Gennari, R., Persico, D., Rossi, F.P., Lugli, S., Manzi, V., Reghizzi, M., Tavia-ni, M., 2019a. A new chronostratigraphic and paleoenvironmental framework for the end of the Messinian salinity crisis in the Sorbas Basin (Betic Cordillera, southern Spain). Geological Jour-nal, 54(3), 1617-1637.

Roveri, M., Gennari, R., Ligi, M., Lugli, S., Manzi, V., Reghizzi, M., 2019b. The synthetic seismic expression of the Messinian salinity crisis from onshore records: implications for shallow-to deep-water correlations. Basin Res. 31 (6), 1121–1152.

Roveri, M., Lugli, S., Manzi, V., Reghizzi, M., Rossi, F.P., 2020. Stratigraphic relationships between shallow-water carbonates and primary gypsum: insights from the Messinian succession of the Sorbas Basin (Betic Cordillera, Southern Spain). Sedimentary Geology, 105678.

Ruggieri, G., 1962. La serie marine pliocenica e quaternaria della Val Marecchia: Atti Accad. Sci. Lett. Arti Palermo, v. 19, p. 1-169.

Ruggieri, G., 1967. The Miocene and later evolution of the Mediterranean sea. In Adams and Ager (Eds.), Aspects of Tethyan Biogeography: Syst. Ass. Publ. 7, p. 238.

Russell, W., Papanastassiou, D., Tombrello, T., 1978. "Ca Isotope Fractionation on the Earth and Other Solar System Materials." Geochimica et Cosmochimica Acta 42: 1075–90.

Ryan, W.B.F., 1973. Geodynamic implications of the Messinian crisis of salinity. In: Mes-sinian Events in the Mediterranean (Ed. C.W. Drooger), North-Holland Publ. Co., Amsterdam, Netherlands, 26–38.

Ryan, W.B.F., 1976. Quantitative evaluation of the depth of the western Mediterranean be-fore, during and after the late Miocene salinity crisis. Sedimentology 23, 791-813.

Ryan, W.B.F., 1978. Messinian badlands on the southeastern margin of the Mediterranean Sea. Marine Geology 27, 349-363.

Ryan, W.B.F., 2008. Modeling the magnitude and timing of evaporative drawdown during the Messinian salinity crisis. Stratigraphy 5, 227-243.

Ryan, W.B.F., 2009. Decoding the Mediterranean salinity crisis. Sedimentology, 56(1), 95-136.

Ryan, W.B.F., Stanley, D.J., Hersey, J.B., Fahlquist, D.A., Allan, T.D., 1971. The tectonics and geology of the Mediterranean Sea. In Maxwell, A. (Ed.), The sea: New York (John Wiley & Sons), v. 4, p. 387.

Ryan, W.B.F., Hsü, K.J., Cita, M.B., Dumitrica, P., Lort, P., Maync, W., Nesteroff, W.D., et al., 1973. Initial Reports of the Deep Sea Drilling Project (Eds W.B.F. Ryan and K.J. Hsü), Vol. 13, pp. 1447. U.S. Government Printing Office, Washington, DC.

Rydberg, J., Lindborg, T., Sohlenius, G., Reuss, N., Olsen, J., Laudon, H., 2016. The importance of eolian input on lake-sediment geochemical composition in the dry proglacial land-scape of western Greenland. Arctic, Antarctic, and Alpine Research 48, 93-109.

Sabat, F., Gelabert, B., Rodriguez-Perea, A., Giménez, J., 2011. Geological structure and evolution of Majorca: implications for the origin of the Western Mediterranean. Tectonophysics 510, 217-238.

Sabato Ceraldi, T., Kamel, M., Mason, T., Poole, A., Hossack, J., Slack, J. Fraser, A., 2010. Messinian seismic facies in offshore Sirt Basin Libya and implications for sub-Messinian seismic imaging. Paper presented at TOG 2008-Technology of Oil and Gas, Forum and Exhibition, 21-23 October, Tripoli.

Sabino, M., Schefuß, E., Natalicchio, M., Dela Pierre, F., Birgel, D., Bortels, D., Schnetger, B., Peckmann, J., 2020. Climatic and hydrologic variability in the northern Mediterranean across the onset of the Messinian salinity crisis. Palaeogeography, Palaeoclimatology, Palaeoecology, 545, 109632.

Sabino, M., Dela Pierre, F., Natalicchio, M., Birgel, D., Gier, S., Peckmann, J., 2021. The response of water column and sedimentary environments to the advent of the Messinian salinity crisis: insights from an onshore deep-water section (Govone, NW Italy). Geological Magazine, 158(5), 825-841.

Sachse, D., Radke, J., Gleixner, G., 2006. δD values of individual n-alkanes from terrestrial plants along a climatic gradient - implications for the sedimentary biomarker record. Org. Geo-chem. 37, 469-483.

Sage, F., Von Gronefeld, G., Déverchère, J., Gaullier, V., Maillard, A., Gorini, C., 2005. A record of the Messinian salinity crisis on the western Sardinia margin, northwestern Mediterrane-an. Mar. Petrol. Geol, 22, 757-773.

Sampalmieri, G., Iadanza, A., Cipollari, P., Cosentino, D., Lo Mastro, S., 2010. Paleoenvi-ronments of the Mediterranean Basin at the Messinian hypersaline/hyposaline transition: evidence from natural radioactivity and microfacies of post-evaporitic successions of the Adriatic sub-basin. Terra Nova, 22(4), 239-250.

Sant, K., V. Palcu, D., Mandic, O., Krijgsman, W., 2017. Changing seas in the Early-Middle Miocene of Central Europe: a Mediterranean approach to Paratethyan stratigraphy. Terra Nova, 29(5), 273-281.

Sanz De Galdeano, C., Vera, J.A., 1991a. Una propuesta de clasificaciòn de las cuencas neógenas beticas. Acta Geologica Hispanica 26, 205-227.

Sanz de Galdeano, C., López Garrido, A.C., 1991b. Tectonic evolution of the Málaga Basin (Betic Cordillera). Regional implications. Geodin. Acta 5, 173–186.

Sanz De Galdeano, C., Vera, J.A., 1992. Stratigraphic record and paleogeographic context of the Neogene basins in the Betic Cordillera, Spain. Basin Research 4, 21-36.

Sanz de Galdeano, C.S., Santamaría-López, Á., 2019. The lithological sequence of the Ne-vado-Filábride Complex (Betic Internal Zone) in the sierras Nevada and Filabres. Revista de la Sociedad Geológica de España, 32(1), 113-126.

Sardella, R., 2008. Remarks on the Messinian carnivores (Mammalia) of Italy. Bollet. della Società Paleontol. Ital., 47(2), 195-202.

Schildgen, T.F., Cosentino, D., Frijia, G., Castorina, F., Dudas, F.Ö., Iadanza, A., Sampal-mieri, G., Cipollari, P., Caruso, A., Bowring, S.A., Strecker, M.R., 2014. Sea level and climate forcing of the Sr isotope composition of Late Miocene Mediterranean marine basins. Geochemis-try, Geophysics, Geosystems 15, 2964-2983.

Schmalz, R.F., 1969. Deep-water evaporite deposition, a genetic model. American Associa-tion of Petroleum Geologists Bulletin 53, 798-823.

Schmid, S.M., Kissling, E., 2000. The arc of the Western Alps in the light of geophysical data on deep crustal structure. Tectonics 19, 62– 85.

Schreiber, B.C., 1997. Field trip to Eraclea Minoa: Upper Messinian. "Neogene Mediterra-nean Paleoceanography", Excursion Guide Book Palermo-Caltanissetta-Agrigento-Erice (Sicily), 24-27 September 1997, 72-80.

Schoepfer, S.-D., Shen, J., Wei, H., Tyson, R.W., Ingall, E., Algeo, T.J., 2015. Total organ-ic carbon, organic phosphorous, and biogenic barium fluxes as proxies for paleomarine productivi-ty. Earth Sci. Rev. 149, 23-52.

Schütz, K.I., 1994. Structure and stratigraphy of the Gulf of Suez, Egypt, in Interior Rift Basins, edited by S. M. Landon, AAPG Mem., 59, 57--96.

Schwarzhans, W., Agiadi, K., Carnevale, G., 2020. Late Miocene-Early Pliocene evolution of Mediterranean gobies and their environmental and biogeographic significance. Rivista italiana di paleontologia e stratigrafia, 126(3).

Sciuto, F., Baldanza, A., 2020. Full restoration of marine conditions after the late Messinian Mediterranean Lago-Mare phase in Licodia Eubea and Villafranca Tirrena areas (east Sicily). Car-nets de géologie.

Sciuto, F., Baldanza, A., Temani, R., Privitera, G., 2018. New reports of Paratethyan ostra-cods affinity from the Mediterranean Basin (Sicily, Italy). Paleontologia Electronica 21(1), 1.

Scotese, C.R., Song, H., Mills, B.J.W., van der Meer, D.G., 2021. Phanerozoic paleotempe-ratures: The earth's changing climate during the last 540 million years. Earth-Science Reviews, 215, 103503.

Segev, A., Avni, Y., Shahar, J., Wald, R., 2017. Late Oligocene and Miocene different seaways to the Red Sea-Gulf of Suez rift and the Gulf of Aqaba-Dead Sea basins. Earth-science reviews, 171, 196-219.

Selli, R., 1954. Il Bacino del Metauro. Giornale di Geologia 24, 1-294.

Selli, R., 1960. Il Messiniano Mayer-Eymar 1867. Proposta di un neostratotipo. Giornale di Geologia 28, 1-33.

Selli, R., 1973. An outline of the Italian Messinian. In Drooger, C. W. (Ed.), Messinian events in the Mediterranean: Amsterdam (Kon. Nedl. Akad. Wetensch.), p. 150-171.

Serrano, F., Guerra-Merchán, A., El Kadiri, Kh., Sanz de Galdeano, C., López-Garrido, A.C., et al., 2006. Oligocene–early Miocene transgressive cover of the Be-tic-Rif Internal Zone. Revision of its geologic significance. Eclogae Geol. Helv. 99, 237–253.

Sgarrella, F., Sprovieri, R., Di Stefano, E., Caruso, A., 1997. Paleoceanographic conditions at the base of the Pliocene in the Southern Mediterranean Basin. Riv. Ital. Paleont. Strat. 103, 207-220.

Sgarrella, F., Sprovieri, R., Di Stefano, E., Caruso, A., Sprovieri, M., Bonaduce, G., 1999. The Capo Rossello Bore-Hole (Agrigento, Sicily): cyclostratigraphic and paleoceanographic re-constructions from quantitative analyses of the Zanclean foraminiferal assemblages. Riv. Ital. Paleont. Strat. 105, 303-322.

Shields G.A., Mills B.J.W., 2020. Evaporite weathering and deposition as a long-term climate forcing mechanism. Geology 49, 299-303.

Sierro, F.J., Flores, J.A., Civis, J., Gonza, J.A., France, G., 1993. Late Miocene globorotali-id event-stratigraphy and biogeography in the NE-Atlantic and Mediterranean. Marine Micropale-ontology, 21(1-3), 143-167.

Sierro, F.J., Hilgen, F.J., Krijgsman, W., Flores, J.A., 2001. The Abad composite (SE Spain): a Messinian reference section for the Mediterranean and the APTS. Paleogeogr. Paleocli-matol. Paleoecol. 168, 141- 169.

Sim, M.S., Bosak, T., Ono, S., 2011. Large sulfur isotope fractionation does not require disproportionation. Science 333, 74-77.

Simon, D., Meijer, P.T., 2017. Salinity stratification of the Mediterranean Sea during the Messinian crisis: A first model analysis. Earth and Planetary Science Letters, 479, 366-376.

Simon, D., Marzocchi, A., Flecker, R., Lunt, D.J., Hilgen, F.J., Meijer, P.T., 2017. Quantifying the Mediterranean freshwater budget throughout the late Miocene: New implications for sapropel formation and the Messinian Salinity Crisis. Earth and Planetary Science Letters, 472, 25-37.

Sinninghe Damsté, J.S., Frewin, N.L., Kenig, F., De Leeuw, J.W., 1995. Molecular indicators for palaeoenvironmental changes in a

Messinian evaporitic sequence (Vena del Gesso, Italy). I: Variations in extractable organic matter of ten cyclically deposited marl beds. Org. Geochem. 23, 471-483.

Sirota, I., Enzel, Y., Mor, Z., Ben Moshe, L., Eyal, H., Lowenstein, T.K., Lensky, N.G., 2021. Sedimentology and stratigraphy of a modern halite sequence formed under Dead Sea level fall. Sedimentology, 68(3), 1-20.

Sissingh, W., 1976. Aspects of late Cenozoic evolution of the South Aegean ostracode fauna: Paleog., Paleocl.., Paleoec., 20, 131-146.

Skejić, S., Arapov, J., Bužančić, M., Ninčević Gladan, Ž., Bakrač, A., Straka, M., Mandić, J., 2021. First evidence of an intensive bloom of the coccolithophore Syracosphaera halldalii in a highly variable estuarine environment (Krka River, Adriatic sea). Marine Ecology, 42(2), e12641.

Skliris, N., Zika, J. D., Herold, L., Josey, S. A., Marsh, R., 2018. Mediterranean sea water budget long-term trend inferred from salinity observations. Climate Dynamics, 51(7), 2857-2876.

Snel, E., Mărunţeanu, M., Meulenkamp, J.E., 2006. Calcareous nannofossil biostratigraphy and magnetostratigraphy of the upper Miocene and lower Pliocene of the Northern Aegean (Or-phanic Gulf-Strimon Basin areas), Greece. Paleogeography, Paleoclimatology, Paleoecolo-gy, 238(1-4).

Soria J.M., Caracuel, J.E., Yébenes, A., Fernández, J., Viseras, C., 2005. The stratigraphic record of the Messinian salinity crisis in the northern margin of the Bajo Segura basin (SE Spain). Sediment Geol 179(3), 225-247.

Soria J.M., Caracuel, J.E., Corbí, H., Dinarès-Turell, J., Lancis, C., Tent-Manclús, J.E., Yé-benes, A,. 2007. Estratigrafía y biomagnetoestratigrafía del Messiniense en la sección del Garru-chal (Cuenca del Bajo Segura). Implicaciones para la Crisis de Salinidad del Mediterráneo. Geo-gaceta 41, 215-218.

Soria, J.M., Caracuel, J.E., Corbí, H., Dinarès-Turell, J., Lancis, C., Tent-Manclús, J.E., Yébenes, A. 2008a. The Bajo Segura basin (SE Spain): implications for the Messinian Salinity Crisis in the Mediterranean margins. Stratigraphy 5:259-265

Soria, J.M., Caracuel, J.E., Corbí, H., Dinarès-Turell, J., Lancis, C., Tent-Manclús, J.E., Viseras, C., Yébenes, A., 2008b. The Messinian-Early Pliocene stratigraphic record in the southern Bajo Segura basin (Betic Cordillera, Spain). Implications for the Mediterranean salinity crisis. Sediment Geol 203:267-288

Spatola, D., del Moral-Erencia, J.D., Micallef, A., Camerlenghi, A., Garcia-Castellanos, D., Gupta, S., Bohorquez, P., Gutscher, M.A., Bertoni, C., 2020. A single-stage megaflood at the ter-mination of the Messinian salinity crisis: Geophysical and modelling evidence from the eastern Mediterranean Basin. Marine Geology, 106337.

Spezzaferri, S., Cita, M.B., McKenzie, J.A., 1998. The Miocene-Pliocene boundary in the Eastern Mediterranean: results from ODP Leg 160, Sites 967 and 969. In: Robertson, A.H.F., Emeis, K.-C., Richter, C., Camerlenghi, A. (Eds.), Proc. ODP, Sci. Results, vol. 160. Ocean Drill-ing Program, College Station, TX, pp. 9-28.

Stampfli, J., Höcker, C.F.W., 1989. Messinian paleorelief from a 3D seismic survey in the Tarrasco concession area (Spanish Mediterranean Sea). Geologie in Minjbouw 68, 201–210.

Steiger, R., Jäger, E., 1977. "Subcommission on Geochronology: Convention on the Use of Decay Constants in Geo-and Cosmochronology." Earth and Planetary Science Letters 36: 359–62.

Steinthorsdottir, M., Coxall, H. K., De Boer, A. M., Huber, M., Barbolini, N., Bradshaw, C. D., et al., 2021. The Miocene: The future of the past. Paleoceanography and Paleoclimatology, 36(4), e2020PA004037.

Stoica, M., Lazăr, I., Krijgsman, W., Vasiliev, I., Jipa, D., Floroiu, A., 2013. Paleoenvironmental evolution of the East Carpathian foredeep during the late Miocene-early Pliocene (Dacian Basin; Romania). Global and Planetary Change, 103, 135-148.

Stoica, M., Krijgsman, W., Fortuin, A., Gliozzi, E., 2016. Paratethyan ostracods in the Spanish Lago-Mare: More evidence for intra-basinal exchange at high Mediterranean sea level. Paleogeography, Paleoclimatology, Paleoecology 441, 854-870.

Strasser, A., Hilgen, F.J., Heckel, P.H., 2006. Cyclostratigraphy-concepts, definitions, and alications. Newsletters on Stratigraphy, 42(2), 75-114.

Sturani, C., 1973. A fossil eel (Anguilla sp.) from the Messinian of Alba (Tertiary Piedmon-tese Basin). Palaeoenvironmental and palaeogeographic implications. In: Drooger, C.W. Eds., Messinian events in the Mediterranean. K. Ned. Ak. Wetensch, Amsterdam, 243-255.

Sturani, C., 1976. Messinian facies in the Piedmont basin. Mem. Soc. Geol. It., 16, 11-25.

Suárez-González, P., Arenas, C., Benito, M.I., Pomar, L., 2019. Interplay between biotic and environmental conditions in presalt Messinian microbialites of the western Mediterranean (Upper Miocene, Mallorca, Spain). Palaeogeogr. Palaeoclimatol. Palaeoecol. 533, 109–242.

Suc, J.-P., Do Couto, D., Melinte-Dobrinescu, M.C., Macaleț, R., Quillévéré, F., et al., 2011. The Messinian salinity crisis in the Dacic Basin (SW Romania) and early Zanclean Mediter-ranean-Paratethys high sea-level connection. Paleoecol. 310, 256-272.

Suc, J.-P., Popescu, S.-M., Do Couto, D., Clauzon, G., Rubino, J.-L., et al., 2015. Marine gateway vs. fluvial stream within the Balkans from 6 to 5 Ma. Mar. Pet. Geol. 66 (1), 231-245.

Temani, R., Sciuto, F., Ammar, H.K., 2020. Messinian Lago-Mare ostracods from Tunisia. Carnets Geol., 20(17), 315.

Thinon, I., Guennoc, P., Serrano, O., Maillard, A., Lasseur, E., Réhault, J.P., 2016. Seismic markers of the Messinian Salinity Crisis in an intermediate-depth basin: data for understanding the Neogene evolution of the Corsica Basin (Northern Tyrrhenian Sea). Mar. Pet. Geol. 77, 1274-1296. November 2016.

Thirlwall, M.F., 1991, Long-term reproducibility of multicollector Sr and Nd isotope ratio analysis, Chemical Geology, 94, 85-104

Thode, H.G., Monster, J., 1965. Sulfur-Isotope Geochemistry of Petroleum, Evaporites, and Ancient Seas1, in: Young, A., Galley, J.E., Eds.), Fluids in Subsurface Environments. American Association of Petroleum Geologists, p. 0.

Thomsen, H.A., 2016. Baltic Sea coccolithophores-an overview of insights into their taxon-omy and ecology from the last 40 years. Journal of Nannoplankton Research, 36(2), 97-119.

Topper, R.P.M., Meijer, P.T., 2015. The precessional phase lag of Messinian gypsum depo-sition in Mediterranean marginal basins. Palaeogeography, Palaeoclimatology, Palaeoecology, 417, 6-16.

Topper, R.P.M., Flecker, R., Meijer, P.T., Wortel, M.J.R., 2011. A box model of the Late Miocene Mediterranean Sea: implications from combined $^{87}Sr/^{86}Sr$ and salinity data. Paleocean-ography 26, PA3223.

Topper, R.P.M., Lugli, S., Manzi, V., Roveri, M., Meijer, P.T., 2014. Precessional control of Sr ratios in marginal basins during the Messinian salinity crisis? Geochem. Geophys. Geosyst. 15-5, 1926-1944.

Toscani, L., Venturelli, G., Barbieri, M., Capedri, S., Soler, J.F., Oddone, M., 1990. Geo-chemistry and petrogenesis of two-pyroxene andesites from Sierra de Gata (SE Spain). Mineralogy and Petrology 41(2-4), 199-213.

Trenkwalder, S., Violanti, D., D'Atri, A., Lozar, F., Dela Pierre, F., Irace, A., 2008. The Miocene/Pliocene boundary in the Early Pliocene micropaleontological record: new data from the Tertiary Piedmont Basin (Moncucco quarry, Torino Hill, northwestern Italy). Boll. Soc. Paleontol. Ital. 47, 87-103.

Tsimplis, M.N., Bryden, H.L., 2000. Estimation of the transports through the Strait of Gi-braltar. Deep Sea Research Part I: Oceanographic Research Papers, 47(12), 2219-2242.

Turchyn, A.V., Schrag, D.P., 2004. Oxygen Isotope Constraints on the Sulfur Cycle over the Past 10 Million Years. Science 303.

Turchyn, A.V., Sivan, O., Schrag, D.P., 2006. Oxygen isotopic composition of sulfate in deep sea pore fluid: evidence for rapid sulfur cycling. Geobiology 4, 191-201.

Turchyn, A.V., Schrag, D.P., Coccioni, R., Montanari, A., 2009. Stable isotope analysis of the Cretaceous sulfur cycle. Earth and Planetary Science Letters 285, 115-123.

Tzanova, A., Herbert, T.D., Peterson, L., 2015. Cooling Mediterranean Sea surface temper-atures during the Late Miocene provide a climate context for evolutionary transitions in Africa and Eurasia. Earth Planet. Sci. Lett. 419, 71-80.

Urgeles, R., Camerlenghi, A., Garcia-Castellanos, D., De Mol, B., Garces, M., Verges, J., Haslam, I., Hardman, M., 2011. New constraints on the Messinian sealevel drawdown from 3D seismic data of the Ebro margin, western Mediterranean. Basin Res. 23, 123-145.

Usiglio, M.J., 1849. Etudes sur la composition de l'eau de la Mediterranee et sur l'exploitation des sel quy'elle conteint: Ann. Chim. Phys., v. 27, p. 172–191.

Utrilla, R., Pierre, C., Orti, F., Pueyo, J.J., 1992. Oxygen and sulphur isotope compositions as indicators of the origin of Mesozoic and Cenozoic evaporites from Spain. Chemical Geology 102, 229-244.

Vai, G.B., 1997. Chapter E3 Cyclostratigraphic estimate of the messinian stage duration. In: Montanari, A., Odin, G.S., Coccioni, R. (Eds.), Miocene Stratigraphy: An Integrated Approach. Developments in Paleontology and Stratigraphy, 15, pp. 463–476.

Vai, G.B., 2016. Over half a century of Messinian salinity crisis. Boletín geológico y minero, 127(2), 625-641.

an Baak, C.G.C., Radionova, E.P., Golovina, L.A., Raffi, I., Kuiper, K.F., Vasiliev, I., Krijgsman, W., 2015. Messinian events in the Black Sea. Terra Nova 27, 433-441.

van Baak, C.G., Stoica, M., Grothe, A., Aliyeva, E., Krijgsman, W., 2016. Mediterranean-Paratethys connectivity during the Messinian salinity crisis: The Pontian of Azerbaijan. Global and Planetary Change, 141, 63-81.

Van Baak, C.G., Krijgsman, W., Magyar, I., Sztanó, O., Golovina, L.A., Grothe, A., Hoyle, T.M., Mandic, O., Patina, I.S., Popov, S.V., Radionova, E.P., Stoica, M., Vasiliev, I. 2017. Parate-thys response to the Messinian salinity crisis. Earth-Science Reviews, 172, 193-223.

Van Couvering, J. A., Berggren, W. A., Drake, R. E., Aguirre, E., Curtis, G.H., 1976. The terminal Miocene event. Marine Micropaleontology, 1, 263-286.

van Couvering, J.A., Castradori, D., Cita, M.B., Hilgen, F.J., Rio, D., 2000. The base of the Zanclean Stage and of the Pliocene Series. Episodes 23, 179-187.

van de Poel, H.M. 1991. Messinian stratigraphy of the Nijar Basin (S.E. Spain) and the origin of its gypsum-ghost limestones. Geol. Mijnb. 70, 215- 234.

van de Poel, H.M., 1992. Foraminiferal biostratigraphy and palaeoenvironments of the Mi-ocene-Pliocene Carboneras-Nijar basin (SE Spain). Scripta Geologica, 102, 1-32.

Van der Zwaan, G., Duijnstee, I., Den Dulk, M., Ernst, S., Jannink, N., Kouwenhoven, T., 1999. Benthic foraminifers: proxies or problems?: a review of paleocological concepts. Earth-Science Reviews, 46(1-4): 213-236.

Van Hinsbergen, D.J.J., Kouwenhoven, T.J., Van Der Zwaan, G.J., 2005. Paleobathymetry in the backstripping procedure: Correction for oxygenation effects on depth estimates. 221(3-4): 245-265.

van Hinsbergen, D.J., Meulenkamp, J.E., 2006. Neogene supradetachment basin develop-ment on Crete (Greece) during exhumation of the South Aegean core complex. Basin Research, 18(1), 103-124.

van Hinsbergen, D.J., Torsvik, T.H., Schmid, S.M., Matenco, L.C., Maffione, M., Vissers, R.L.M., Gürer, D., Spakman, W., 2020. Orogenic architecture of the Mediterranean region and kinematic reconstruction of its tectonic evolution since the Triassic. Gondwana Research 81, 79-229.

van den Berg, B.C.J., Sierro, F.J., Hilgen, F.J., Flecker, R., Larrasoaña, J.C., Krijgsman, W., Flores, J.A., Mata, M.P., Martín, E.B., Civis, J., González-Delgado, J.A., 2015. Astronomical tun-ing for the upper Messinian Spanish Atlantic margin: disentangling basin evolution, climate cy-clicity and MOW. Glob. Planet. Chang. 135, 89-103.

van der Laan, E., Gaboardi, S., Hilgen, F.J., Lourens, L.J., 2005. Regional climate and gla-cial control on high-resolution oxygen isotope records from Ain El Beida (latest Miocene, NW Morocco): a cyclostratigraphic analysis in the depth and time domain. Paleoceanography 20, PA1001.

van der Laan, E., Snel, E., de Kaenel, E., Hilgen, F.J., Krijgsman, W., 2006. No major de-glaciation across the Miocene-Pliocene boundary: integrated stratigraphy and astronomical tuning of the Loulja sections (Bou Regreg area, NW Morocco). Paleoceanography 21, PA3011.

van der Meer, M.T.J., Baas, M., Rijpstra, I.C., Marino, G., Rohling, E.J., Sinninghe Damsté, J.S., Schouten, S., 2007. Hydrogen isotopic compositions of long-chain alkenones record freshwa-ter flooding of the Eastern Mediterranean at the onset of sapropel deposition. Earth Planet. Sci. Lett. 262, 594-600.

Varas-Reus, M. I., Garrido, C. J., Marchesi, C., Bosch, D., Acosta-Vigil, A., Hidas, K., et al., 2017. Sr-Nd-Pb isotopic systematics of crustal rocks from the western Betics (S. Spain): Impli-cations for crustal recycling in the lithospheric mantle beneath the westernmost Mediterranean. Lithos, 276, 45-61.

Vasiliev, I., Reichart, G.-J., Davies, G.R., Krijgsman, W., Stoica, M., 2010. Strontium iso-tope ratios of the Eastern Paratethys during the Miocene/Pliocene transition; Implications for in-terbasinal connectivity. Earth Planet. Sci. Lett. 292, 123-131.

Vasiliev, I., Reichart, G.J., Krijgsman, W., 2013. Impact of the Messinian Salinity Crisis on Black Sea hydrology - insights from hydrogen isotopes on molecular biomarkers. Earth Planet. Sci. Lett. 362, 272-282.

Vasiliev, I., Reichart, G.-J., Grothe, A., Sinninghe Damsté, J.S., Krijgsman, W., Sangiorgi, F., Weijers, J.W.H., van Roij, L., 2015. Recurrent phases of drought in the upper Miocene of the Black Sea region. Paleogeogr. Paleoclimatol. Paleoecol. 423, 18-31.

Vasiliev, I., Mezger, E.M., Lugli, S., Reichart, G.J., Manzi, V., Roveri, M., 2017. How dry was the Mediterranean during the Messinian salinity crisis?. Paleogeography, Paleoclimatology, Paleoecology 471, 120-133.

Vasiliev, I., Karakitsios, V., Bouloubassi, I., Agiadi, K., Kontakiotis, G., Antonarakou, A., et al., 2019. Large sea surface temperature, salinity, and productivity preservation changes preceding the onset of the Messinian Salinity Crisis in the eastern Mediterranean Sea. Paleoceanogr. Paleoclimatology 34, 182–202.

Vasiliev, I., Stoica, M., Grothe, A., Lazarev, S., Palcu, D.V., Van Baak, C., De Leeuw, A., et al., 2021. Hydrological Changes in Re-stricted Basins: Insights From Strontium Isotopes on Late Miocene-Pliocene Connectivity of the Eastern Paratethys (Dacian Basin, Romania). Geochemistry, Geophysics, Geosystems, 22, e2020GC009369.

Veizer, J., 1989. Strontium isotopes in seawater through time. Annual Review of Earth and Planetary Sciences 17(1), 141-167.

Vera, J.A., 2000. El terciario de la Cordillera Bética: estado actual de conocimientos. Revista Sociedad Geologica de Espana, 13, 345-373.

Vera, J.A., 2001. Evolution of the South Iberian continental margin. In: Peri-Tethys Memoir 6: Peri-Tethyian Rift/Wrench Basins and Passive Margins (Ed. by Ziegler P.A., Cavazza W., Robertson A.H.F. and Crasquin-Soleau S.) Mem. Mus. Natn. Hist. Nat. 186, 109-143.

Violanti, D., Trenkwalder, S., Lozar, F., Gallo, L.M., 2009. Micropaleontological analyses of the Narzole core: biostratigraphy and paleoenvironment of the late Messinian and early Zan-clean of Piedmont (Northwestern Italy). Bollettino della Società Paleontologica Italiana 48, 167-181.

Violanti, D., Dela Pierre, F., Trenkwalder, S., Lozar, F., Clari, P., Irace, A., D'Atri, A., 2011. Biostratigraphic and palaeoenvironmental analyses of the Messinian/Zanclean boundary and Zanclean succession in the Moncucco quarry (Piedmont, northwestern Italy). Bulletin de la Société géologique de France, 182(2), 149-162.

Violanti, D., Lozar, F., Dela Pierre, F., Natalicchio, M., Bernardi, E., Clari, P., Cavagna, S., 2013. Stress tolerant microfossils of a Messinian succession from the northern Mediterranean basin (Pollenzo section, Piedmont, Northwestern Italy). Bollettino della Società Paleontologica Italiana 52, 45-54.

Völk, H.R., Rondeel, H.E., 1964. Zur Gliedenmg des Jungtertilrs im Becken von Vera. Sti-dostspanien. Geol. Mijnbouw 43, 310-315.

Vonhof, H.B., Wesselingh, F.P., Ganssen, G.M., 1998. Reconstruction of the Miocene west-ern Amazonian aquatic system using molluscan isotopic signatures. Paleogeogr. Paleoclimatol. Paleoecol. 141, 85-93.

Wade, B.S., Bown, P.R., 2006. Calcareous nannofossils in extreme environment: the Mes-sinian Salinity Crisis, Polemi Basin, Cyprus. Palaeogeogr. Palaeoclimatol. Palaeoecol. 233, 271–286.

Warren, J.K., 2016. Evaporites: A geological compendium. Springer.

Westerhold, T., Marwan, N., Drury, A.J., Liebrand, D., Agnini, C., Anagnostou, E., et al., 2020. An astronomically dated record of Earth's climate and its predictability over the last 66 mil-lion years. Science, 369(6509), 1383–1387.

Williams, G.L., Fensome, R.A. MacRae, R.A., 2017. The Lentin and Williams index of fos-sil dinoflagellates 2017 edition. American Association of Stratigraphic Palynologists Contributions Series no. 48., Dallas, TX

Winterberg, S., Picotti, V., Willett, S. D., 2020. Messinian or Pleistocene valley incision within the Southern Alps. Swiss Journal of Geosciences, 113(1), 1-14.

Wortmann, U.G., Chernyavsky, B., Bernasconi, S.M., Brunner, B., Böttcher, M.E., Swart, P.K., 2007. Oxygen isotope biogeochemistry of pore water sulfate in the deep biosphere: Domi-nance of isotope exchange reactions with ambient water during microbial sulfate reduction (ODP Site 1130). Geochimica et Cosmochimica Acta 71, 4221-4232.

Wu, L., Wilson, D. J., Wang, R., Yin, X., Chen, Z., Xiao, W., Huang, M., 2020. Evaluating Zr/Rb Ratio From XRF Scanning as an Indicator of Grain-Size Variations of Glaciomarine Sediments in the Southern Ocean. Geochem Geophys Geosyst, 21, e2020GC009350.

Yang H, Zhao Y, Cui Q, Ren W, Li Q. 2020. Paleoclimatic indication of X-ray fluorescence core-scanned Rb/Sr ratios: A case study in the Zoige Basin in the eastern Tibetan Plateau. Science China Earth Sciences, 63.

Zachariasse, W.J., van Hinsbergen, D.J.J., Fortuin, A.R., 2008. Mass wasting and uplift on Crete and Karpathos (Greece) during the Early Pliocene related to beginning of South Aegean left-lateral, strike slip tectonics. Geol. Soc. Am.Bull., 120, 976-993.

Zachariasse, W. J., van Hinsbergen, D. J., Fortuin, A.R., 2011. Formation and fragmenta-tion of a late Miocene supradetachment basin in central Crete: implications for exhumation mech-anisms of high-pressure rocks in the Aegean forearc. Basin Research, 23(6), 678-701.

Zeck, H.P., Kristensen, A.B., Williams, I.S. 1998. Post-collisional volcanism in a sinking slab setting-crustal anatectic origin of pyroxene-andesite magma, Caldear Volcanic Group, Neo-gene Alborán volcanic Province, southeastern Spain. Lithos, 45(1-4), 499-522.

Zevenboom, D., 1995, Dinoflagellate cysts from the Mediterranean Late Oligocene and Miocene. Ph.D. Thesis, University of Utrecht, 221 p., 9 pl.; Cip-Gegevens Koninklijke Biblio-theek, Den Haag, The Netherlands.

Zielinski, M., Dopieralska, J., Belka, Z., Walczak, A., Siepak, M., Jakubowicz, M. 2017. The strontium isotope budget of the Warta River (Poland): Between silicate and carbonate weath-ering, and anthropogenic pressure. Applied Geochemistry 81, 1-11.

Ziveri, P., Baumann, K.H., Bockel, B., Bollmann, J., Young, J., 2004. Present day cocco-lithophore-biogeography in the Atlantic Ocean. In Coccolithophores: From Molecular Processes to Global Impact (403-428). Springer Verlag.

Zonneveld, K.A., Marret, F., Versteegh, G.J., Bogus, K., Bonnet, S., Bouimetarhan, I., Crouch, I.E., Esper, O., 2013. Atlas of modern dinoflagellate cyst distribution based on 2405 data points. Review of Paleobotany and Palynology, 191, 1-197.